REACTOR SHIELDING DESIGN MANUAL

EDITOR

Theodore Rockwell III

Technical Director, Naval Reactors Branch,
Division of Reactor Development
United States Atomic Energy Commission

First Edition

This document is
PUBLICLY RELEASABLE
Larry E. Williams
Authorizing Official
Date: 08/01/2007

NAVAL REACTORS BRANCH, DIVISION OF REACTOR DEVELOPMENT
UNITED STATES ATOMIC ENERGY COMMISSION

DISCLAIMER

This report was prepared as an account of work sponsored by an agency of the United States Government. Neither the United States Government nor any agency Thereof, nor any of their employees, makes any warranty, express or implied, or assumes any legal liability or responsibility for the accuracy, completeness, or usefulness of any information, apparatus, product, or process disclosed, or represents that its use would not infringe privately owned rights. Reference herein to any specific commercial product, process, or service by trade name, trademark, manufacturer, or otherwise does not necessarily constitute or imply its endorsement, recommendation, or favoring by the United States Government or any agency thereof. The views and opinions of authors expressed herein do not necessarily state or reflect those of the United States Government or any agency thereof.

DISCLAIMER

Portions of this document may be illegible in electronic image products. Images are produced from the best available original document.

THIS MANUAL is one of a series sponsored by the Naval Reactors Branch of the Atomic Energy Commission to evaluate and put into systematic and intelligible form the technology being developed in the Naval Reactors Program and Pressurized Water Reactor Program.

This series includes:

Liquid Metals Handbook
First Edition: Edited by R. N. Lyon, June 1950
Second Edition: Edited by R. N. Lyon, June 1952
Third Edition: (Sodium–NaK Supplement): Edited by C. B. Jackson, First Printing, June 1955; Second Printing (Revised), November 1955

Metallurgy of Zirconium
Edited by B. Lustman and F. Kerze, Jr., July 1955

The Metal Beryllium
Edited by D. W. White and J. E. Burke, July 1955

Bibliography of Reactor Computer Codes, Report AECU-3078
Edited by R. S. Brodsky, December 1955

Reactor Shielding Design Manual
Edited by T. Rockwell III, March 1956

Corrosion and Wear Handbook for Water-cooled Reactors
Edited by D. J. De Paul, in preparation

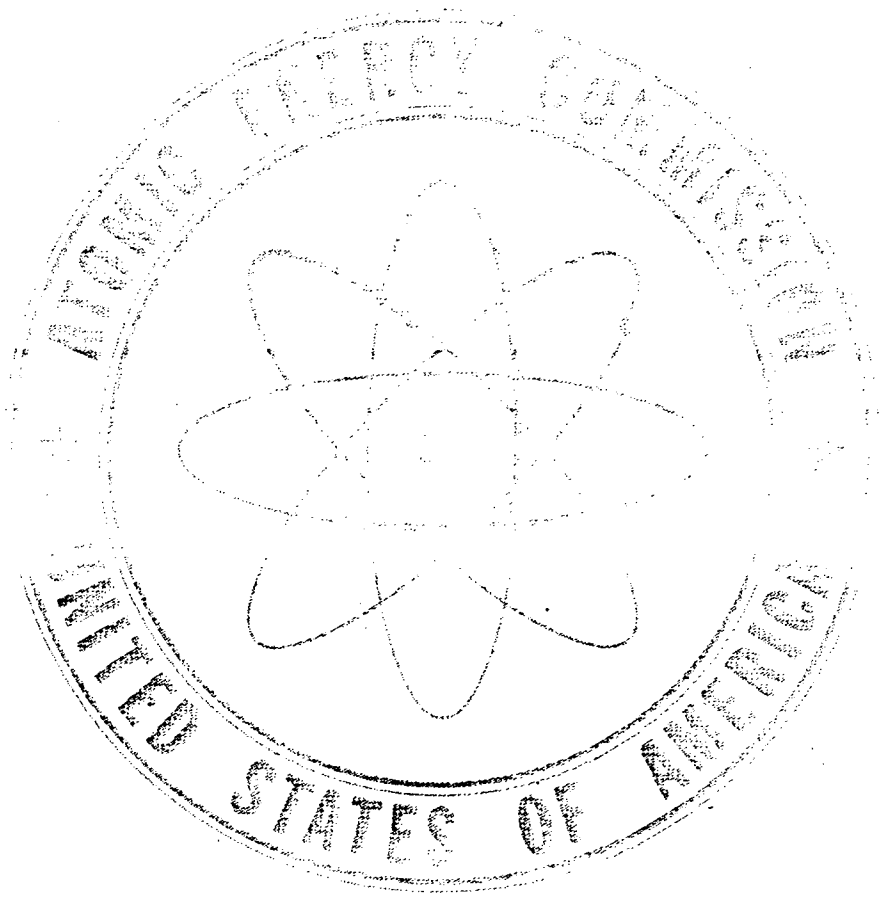
Naval Reactor Physics Design Manual
Edited by A. Radkowsky, in preparation

Reactor Core Design Manual
Edited by N. J. Palladino, in preparation

Hafnium Handbook
In preparation

Reactor Plant Piping Handbook
Edited by M. Shaw, in preparation

Reactor Heat Transfer Handbook
Edited by J. Zerbe, in preparation


UNITED STATES OF AMERICA

AUTHORS

E. L. Czapek
Electric Boat Division,
General Dynamics Corporation

T. A. Flynn
Naval Reactors Branch, AEC

A. Foderaro
Bettis Plant*

D. W. Johnson
Knolls Atomic Power Laboratory†

R. B. Minogue
Naval Reactors Branch, AEC

F. Obenshain
Bettis Plant*

C. J. Ranney
Knolls Atomic Power Laboratory†

K. Shure
Bettis Plant*

H. E. Stone
Knolls Atomic Power Laboratory†

J. J. Taylor
Bettis Plant*

CONTRIBUTORS

M. J. Abrams
Knolls Atomic Power Laboratory†
(now at Bettis Plant)

S. Bresticker
Bettis Plant*

R. S. Brodsky
Naval Reactors Branch, AEC

A. Cox
Newport News Shipbuilding
& Dry Dock Company

H. Endlund
Electric Boat Division,
General Dynamics Corporation

W. M. Haussler
Naval Reactors Branch, AEC

F. D. Judge
Knolls Atomic Power Laboratory†

B. O'Reilly
Bettis Plant*

M. A. Robkin
Bettis Plant*

J. Shapiro
Electric Boat Division,
General Dynamics Corporation

L. H. Weinberg
Knolls Atomic Power Laboratory†

*Operated by the Westinghouse Electric Corporation for AEC.
†Operated by the General Electric Company for AEC.

FOREWORD

"WATER HAS NO CRACKS . . ."

This manual describes the procedures and data which are used in the design, construction, and testing of shielding for the reactor plants of the Naval Reactors Program and for the Shippingport Pressurized Water Reactor (PWR). These procedures are quite different from those practiced on other projects.

The fact that these techniques—developed originally for naval reactor applications—apply so directly and so well to the PWR makes it apparent that this manual might be useful to other projects outside the Naval Reactors Program. It should not be assumed that careful shield design is important only for mobile reactor plants. Poor shield design in a stationary reactor can lead to high costs, poor maintenance accessibility, high radiation levels near shield penetrations or stiffeners, or excessive stresses due to nuclear heating in structures near the reactor core. Inadequate design of the reactor shield can result in activation of primary coolant equipment, decomposition of water in the heat exchanger (perhaps aggravating corrosion), or radiation damage to the material of the primary shield itself. The detectors upon which the reactor control system depends are designed around fluxes calculated by the shield designer; errors here can result in blind reactor start-ups or burned-out detectors.

The methods discussed in this manual have two salient features: (1) They have been actually used for, and tested on, real power reactor shields and (2) they form a basic approach rather than a mock-up approach and thus permit design of shields without expensive and time-consuming use of the reactor facilities in which full-scale shielding mock-ups can be made. This manual should simplify and lessen the time required for design of power reactor shields.

The quintessence of a great deal of practical experience is contained in this manual. Many theoretical methods that looked appealing on paper were found in practice to be of little practical value. Most of the difficulty in designing a practical shield comes from the layout, structure, and irregularities of an actual reactor plant and not in the mathematical analysis of an idealized reactor concept; these concepts never have any sharp corners, gaps, streaming paths, or clearances. In this regard a fact which

is important in practical shield design is that water, unlike more exotic shielding materials, has no cracks.

Particular credit for the preparation of this manual is due to Theodore Rockwell III. He has been in charge of designing the shielding used for naval vessel application and for the PWR. It was his ability, hard work, and leadership which made this manual possible.

H. G. RICKOVER
Chief, Naval Reactors Branch
Division of Reactor Development
United States Atomic Energy Commission

EDITOR'S PREFACE

It is the purpose of this manual to help an engineer or scientist to design a practical shield by making available to him the techniques and data developed by the Naval Reactors Program and Pressurized Water Reactor Program. The material is organized in the approximate order that the designer would have to accumulate it in developing a shield design of his own. Considerable thought has been given to the organization and relation of the material and to presenting it in the most usable and intelligible form.

Because of the effort spent in organizing the material and in cross-referencing within the text, no index has been provided. The serious reader is advised to study first the table of contents in the front of the book and then the more complete table of contents immediately preceding each chapter. Each of the major sections is also preceded by a summary, and facing pages are captioned with the chapter and section titles, respectively. It is felt that this method of presentation lends itself better to finding the information most pertinent to a given problem than an index indiscriminately listing all references, direct and oblique.

These shielding procedures were developed along somewhat different paths at different sites and were, in some cases, aimed originally only at a specific reactor application. Most of these procedures have not previously been written in a generally applicable form. A really cooperative effort was therefore required among the persons who worked on the manual. Long work sessions and many shorter discussions were organized to allow all the material originally written by persons at each of the naval reactors organizations to be combined and rewritten in a more cohesive form. The original authorship of each section has thus been sacrificed, and the manual is now a truly joint effort. Credit has been given to originators of all data and techniques whenever they were known; it is hoped that no omissions have been made in this regard.

At this stage of the reactor shielding art, this manual is necessarily somewhat unbalanced; it tells more about what is known than about what is not known. There will probably be a second edition within a year or so which will be more complete on (for example) thermal-shield design, disposition of insoluble fission products throughout a reactor system, selection of dose points for accurate shield contouring, shield geometry problems such as streaming and scattering, cheaper methods of fabricating

large lead shield sections, and perhaps better methods of analyzing the balance between reactor shielding and coolant shielding.

As this manual developed from a series of separate papers to the present form, it became increasingly apparent that, although these techniques were adequate to make possible the design, construction, testing, and operation of several power reactor shields, there are still aspects of the procedures which are unnecessarily tedious, overly conservative, or on somewhat shaky ground. For example, theoretical procedures have not been compared in all cases with experimental data that might be pertinent. Chapter 8 in particular is ripe for such scrutiny; further comparative analysis is invited. The best tribute the editor and authors can hope for is indications from readers that better methods or data are available. This will tell us that the manual is being used as intended and will lead to a better manual for the next edition and to an improved shielding art.

I want to express my appreciation to Admiral Rickover for first having the idea that such a manual should be prepared and for encouraging the authors and myself to do a thorough job even though the effort had necessarily to be made at the expense of urgent daily commitments. Special credit is also due the Technical Information Service and particularly the staff of the Oak Ridge Extension, whose help on this manual went considerably beyond normal editorial services and who converted rough copy into this book with intelligence and dispatch.

THEODORE ROCKWELL III

CONTENTS

Foreword v
Editor's Preface vii

CHAPTER 1 — INTRODUCTION AND OUTLINE OF BASIC SHIELDING THEORY 3
1 Summary of Shield-design Procedures 3
2 Neutron Attenuation 5
2.1 Basic Neutron-attenuation Processes. 2.2 The Fast-removal Theory.
3 Gamma-ray Attenuation 7
3.1 Sources. 3.2 Basic Gamma-attenuation Processes. 3.3 Build-up Factors.
References 11

CHAPTER 2 — SETTING ALLOWABLE RADIATION LEVELS . . 15
1 Radiation Specifications: The Problem 15
2 Basic Units of Radiation and Radioactivity 15
2.1 Definitions and Concepts. 2.2 Units of Measurement. 2.3 Some Useful Approximations.
3 Conversion Curves for Gamma and Neutron Fluxes and Dose Rates 18
4 Basic Radiation Specifications 18
5 Radiation Levels for Shield Design 24
5.1 Access to the Plant. 5.2 Average Power Level of Reactor Operation.
6 Special Problem of Local Radiation Streaming 27
References 27

CHAPTER 3 — SHIELDING THE REACTOR CORE 31
Introduction 31
1 Full-power Core Source Estimates 32
1.1 Fission Sources. 1.2 Secondary Sources in the Core. 1.3 Sources Outside the Core. 1.4 Relative Importance of the Various Sources.
2 After Shutdown of the Reactor 47
3 Attenuation Calculations 48
3.1 Fast-neutron Attenuation. 3.2 Thermal-neutron-flux Distribution. 3.3 Geometry for Fast-neutron Attenuation. 3.4 Sources of Error.

4 Heat Generation in Shields 76
4.1 Introduction. 4.2 Heat Generation by Core Gammas. 4.3 Heat Generation by Gammas from Neutron Capture and from Inelastically Scattered Neutrons. 4.4 Heat Generation by Elastically Scattered Neutrons.
References 83

CHAPTER 4—SHIELDING THE REACTOR COOLING SYSTEM . 87
1 Introduction 87
2 Calculation of Specific Activity in Coolant 88
2.1 Some Typical Activities. 2.2 Comparison of Various Coolants. 2.3 The Activation Equations. 2.4 Calculation of Effective Neutron Flux. 2.5 Equilibrium Gamma Activity. 2.6 Method for Approximating Coolant Activity with Changes in Core Time and Total Cycle Time. 2.7 Equilibrium Neutron Activity.
3 Gamma Shielding for the Reactor Cooling System . . . 108
3.1 Hand-calculation Procedure for Coolant Gamma Shield Thickness. 3.2 Attenuation of Gamma Rays at Oblique Incidence. 3.3 Experiments Using Cylindrical Sources. 3.4 Techniques for Isodose Calculation Varying Shield Thickness to Give Uniform Dose.
4 Neutron Shielding for the Reactor Cooling System . . . 141
4.1 Attenuation Kernel for N^{17} Neutrons. 4.2 Removal Cross Sections and Relaxation Lengths for N^{17} Neutrons. 4.3 Monte Carlo Results of the Transport of N^{17} Neutrons in a Water Medium.
5 Selection of Dose Points for Accurate Isodosing . . . 151
References 152
Bibliography 152

CHAPTER 5—PLANT LAYOUT AND OTHER FACTORS AFFECTING TOTAL SHIELD DESIGN 157
1 Introduction 157
2 Functional Requirements of Shield 158
2.1 Reactor (Primary) Shield. 2.2 Coolant (Secondary) Shield.
3 Reactor Plant Layout 159
3.1 Reactor Shield. 3.2 Coolant Shield. 3.3 Outside the Coolant Shield.
4 Specific Rules for Plant Layout 160
5 Distance Effect 161
6 Shield-design Optimization 164
7 Shadow Shielding 164
8 Weights and Weight Reporting as Applied to Ships . . . 165
Reference 166

CHAPTER 6—SHIELD ENGINEERING 169
1 Materials. 169
1.1 Introduction. 1.2 Iron. 1.3 Lead. 1.4 Water. 1.5 Polyethylene $(CH_2)_n$. 1.6 Concretes. 1.7 Lead Glass. 1.8 Boron-containing Materials.

2 Comparative Effectiveness of Various Materials for Gamma Radiation 190
3 Fabrication and Installation 196
3.1 Introduction. 3.2 Design Details of Composite Gamma and Neutron Shields. 3.3 Installation of Lead Shielding.
4 Operational Testing 214
4.1 Objectives. 4.2 Radiation Measuring Instruments. 4.3 Calibration of Instruments. 4.4 Planning and Performing the Shield Test. 4.5 Shield Test Experience.
References 224
Bibliography for Neutron Shielding Materials 225

CHAPTER 7—RADIOACTIVITY OF SHUTDOWN SYSTEM (THE ACCESSIBILITY PROBLEM) 229
Introduction 229
1 General Discussion of Significant Radiation Sources 229
1.1 Induced Activity of the Reactor Coolant Itself. 1.2 Induced Activity of Structural Material. 1.3 Photoneutron Production. 1.4 Fission Products in the Reactor Core. 1.5 Delayed Neutrons in the Reactor Core. 1.6 Activation of Impurities and Corrosion Products in the Coolant. 1.7 Fission Products in the Coolant System from Corrosion or Failure of Fuel Elements.
2 Aspects of Water Technology 233
2.1 Water Supply. 2.2 Corrosion of Plant Materials. 2.3 Purification Systems.
3 Activation of Impurities in the Coolant 235
3.1 Hypotheses. 3.2 Formulation of the Problem. 3.3 Solutions. 3.4 Determining Demineralizer Flow Rate. 3.5 Concentration of Radioactivity by Ion Exchangers and Filters. 3.6 Time-dependent Neutron Flux.
4 Fission Products in the Coolant System 249
4.1 Distribution of Fission-product Gases in Water-cooled Reactor Systems. 4.2 Continuous Release of Fission-product Gases. 4.3 Noncontinuous Release of Fission Products. 4.4 Alternate Approach to Case of Continuous Release of Fission-product Gases.

CHAPTER 8—EFFECT OF IRREGULARITIES IN SHIELD . . 261
1 Introduction 261
1.1 General. 1.2 Résumé of Formulas.
2 Neutrons 264
2.1 Transmission Through Rectangular Slots. 2.2 Transmission Through Cylindrical Ducts. 2.3 Transmission Through Annuli. 2.4 Effect of Small Voids in Shield. 2.5 Streaming Along Steel Paths.

3 Gammas 288
3.1 Source Geometries. 3.2 Rectangular Slots. 3.3 Cylindrical Ducts. 3.4 Annular Ducts. 3.5 Verification with Experimental Results. 3.6 Effect of Voids in Shield. 3.7 Gamma Streaming Along Steel Paths.
4 Radiation Scattering Around Shield Edge 316
4.1 Introduction. 4.2 Gamma Scattering. 4.3 Neutron Scattering.
References 342

CHAPTER 9—EFFECT OF GEOMETRY OF RADIATION SOURCE 347
Nomenclature 346
Introduction 347
1 Equations for the Flux 347
1.1 Point Source. 1.2 Line Source. 1.3 Disk Source. 1.4 Infinite-slab Source. 1.5 Truncated Right-circular Cone Source. 1.6 Cylindrical Source. 1.7 Spherical Source. 1.8 e^{-b}, $E_1(b)$, and $E_2(b)$. 1.9 The Function $F(\theta,b)$.
2 Derivations 391
2.1 Point Source. 2.2 Line Source. 2.3 Disk Source. 2.4 Infinite-slab Source. 2.5 Truncated Right-circular Cone Source. 2.6 Cylindrical Source. 2.7 Spherical Source. 2.8 The Functions $E_n(b)$, $F_n(t,a)$, $F(\theta,b)$, and $G(\mu_s h,b)$.
3 Asymptotic Approximations 409
3.1 Line Source. 3.2 Disk Source. 3.3 Truncated Right-circular Cone Source.
4 Effect of Scattered Radiation 412
4.1 Build-up in an Infinite Medium. 4.2 Build-up Within a Source. 4.3 Build-up Through Laminations.
5 Build-up Factors for Iron, Water, Lead, and Concrete 415
6 Transformation From One Geometry to Another . . . 424
6.1 Disk-source to Point-source Transformation. 6.2 Plane to Sphere Transformation. 6.3 Plane to Cylinder Transformation. 6.4 Disk to Infinite-plane Transformation.
References 425

CHAPTER 10—BASIC DATA 429
Curves of Build-up and Differential Energy Spectrums for Lead, Iron, and Water 430
Curves of Energy Absorption and Mass Absorption Coefficients Vs. Energy 447
Radiation Damage Summary Tables for Shielding Engineers . 451
Tables and Nomograms for Build-up and Decay 456
Thermal-neutron Cross Sections and Related Data . . . 462
Chart of the Nuclides 467

Chapter 1

INTRODUCTION AND OUTLINE OF BASIC SHIELDING THEORY

1 SUMMARY OF SHIELD-DESIGN PROCEDURES 3

2 NEUTRON ATTENUATION 5
- 2.1 Basic Neutron-attenuation Processes 5
- 2.2 The Fast-removal Theory . . . 6

3 GAMMA-RAY ATTENUATION 7
- 3.1 Sources 7
- 3.2 Basic Gamma-attenuation Processes 7
- 3.3 Build-up Factors 8
  - (a) Shields of One Material . . 9
  - (b) Several Slabs of Different Materials 9
  - (c) Homogeneous Mixtures . . 9

REFERENCES 11

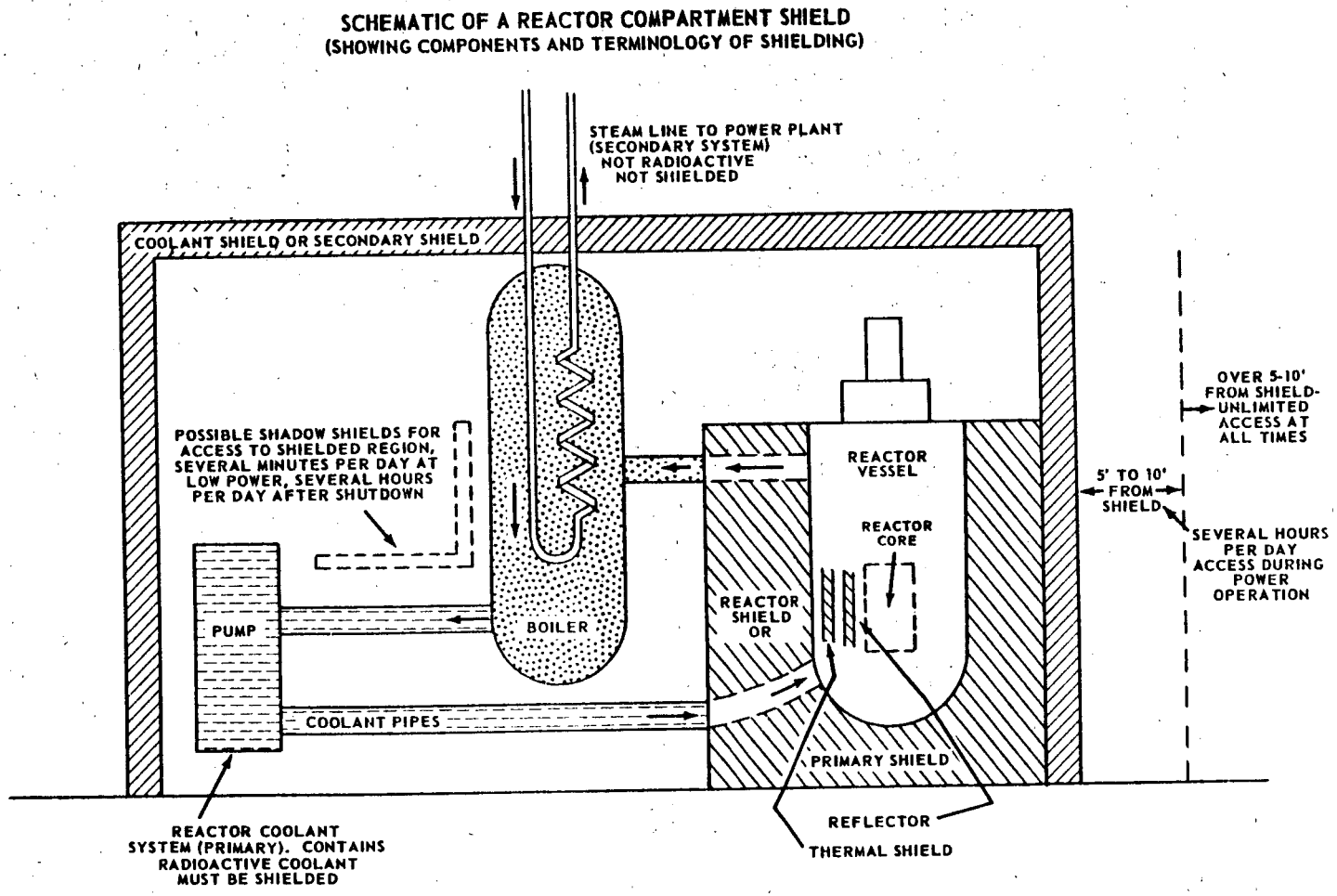

SCHEMATIC OF A REACTOR COMPARTMENT SHIELD
(SHOWING COMPONENTS AND TERMINOLOGY OF SHIELDING)
STEAM LINE TO POWER PLANT
(SECONDARY SYSTEM)
NOT RADIOACTIVE
NOT SHIELDED
COOLANT SHIELD OR SECONDARY SHIELD
POSSIBLE SHADOW SHIELDS FOR
ACCESS TO SHIELDED REGION,
SEVERAL MINUTES PER DAY AT
LOW POWER, SEVERAL HOURS
PER DAY AFTER SHUTDOWN
PUMP
BOILER
REACTOR
VESSEL
REACTOR
CORE
REACTOR
SHIELD
OR
COOLANT PIPES
PRIMARY SHIELD
REFLECTOR
THERMAL SHIELD
OVER 5-10'
FROM SHIELD-
UNLIMITED
ACCESS AT
ALL TIMES
5' TO 10'
FROM
SHIELD
SEVERAL HOURS
PER DAY
ACCESS DURING
POWER
OPERATION
REACTOR COOLANT
SYSTEM (PRIMARY). CONTAINS
RADIOACTIVE COOLANT
MUST BE SHIELDED

Figure 1.1

Chapter 1

INTRODUCTION AND OUTLINE OF BASIC SHIELDING THEORY

Personnel must be protected within reasonable limits of cost, weight, and space against the ionizing radiation emitted from reactors and their components. It is the purpose of this manual to provide the shielding engineer with some tools and data to accomplish this. This chapter summarizes the approach taken in this manual and discusses briefly the basic processes by which reactor radiations are attenuated.

1 SUMMARY OF SHIELD-DESIGN PROCEDURES

The following steps are generally followed in developing a shield design:

1. Decide which *type shield* best suits the purpose.
   a. A unit shield compactly surrounding the reactor and all its components.
   b. A compartment shield in which the reactor is partially shielded and the radioactive-coolant system is separately enclosed in a shielded room, with limited access to the equipment possible when the reactor is not operating.
   c. A shadow shield in which certain chosen regions are shielded by the shadow of a shield of limited area; the chosen region may be a passageway, a control station, or special maintenance regions. A "divided shield" extends this concept to the point of wrapping some of the shielding completely around a given region.

Generally the best design combines these features; Fig. 1.1 illustrates this point. Chapter 5 discusses some of the factors in distributing shielding between the reactor shield and the coolant-system shield.

2. The *allowable radiation levels* in various regions outside the shield must be established for both power operation and shutdown conditions. This is covered in Chap. 2. It should be noted that the dose rate is the sum total of the dose rates from all the various radiations leaving the shield.

3. The location, energy, and intensity of the *radiation sources* to be shielded must be determined; there are many, and not all of them originate directly in the reactor.
   a. Chapter 3 discusses those sources originating in the reactor.
   b. Chapter 4 discusses those sources originating in the reactor coolant.
   c. Chapter 7 discusses those which are important when the reactor is shut down.

4. The designer is now ready to *calculate required shield thicknesses*. He may use either of two approaches. He may consider the complex coolant loop as a series of radioactive cylinders, disks, cones, spheres, and other simplified shapes and calculate the contribution to each of several given points outside the shield from each of these sources; or he may choose to consider the source as a series of points, note the shielding along the path from source to receiver, and calculate by machine each of these miniature point-source shielding problems. The required attenuation can be obtained in equivalent iron thickness; the structure, tankage, and other iron is subtracted, and the remaining thickness is converted

to the desired shield materials. Only experience will minimize these calculations. The basic techniques, with data and sample calculations, are discussed in Chap. 3 for the reactor shield and in Chap. 4 for the coolant shield.

5. The *arrangement* of the piping and heat-exchange system inside the shield and of the regions accessible and inaccessible outside the shield plays an important part in minimizing shield cost and weight; this problem is covered in Chap. 5.

6. The *selection of materials* depends on the physical and shielding properties, availability, and cost (installed). This is covered in Chap. 6.

7. *Design and fabrication details* are also discussed in Chap. 6. Suggested methods for bonding lead to steel, for treating water and other shielding fluids, and for selecting and handling heavy concretes are discussed.

8. The problem of *inspecting and testing* these materials prior to and after installation is more complicated than might at first be assumed. The planning of an inspection and test program, selection of instruments, rejection criteria and test curves, and typical test forms and results are included in Chap. 6.

9. The problem of *radioactivity of the shutdown system* is discussed in Chap. 7. The build-up and decay of radioactivity in various places in the loop, the relative magnitude of the different activities, the sizing of the purification system to maintain a required radioactivity level, and the effect of coolant chemistry are treated analytically and compared with actual operating data.

10. *Streaming of radiation* through gaps, thermal insulation, structural members, and shield penetrations is another serious problem that requires continuous attention throughout the shield design. Some pertinent data and formulas are presented in Chap. 8.

11. The *geometry of the radiation sources* can be very complex, and the calculation of the geometrical effects can be very tedious. Chapter 9 presents curves from which the radiation dose from various source geometries can be derived.

12. Chapter 10 contains several miscellaneous curves, tables, nomographs, and other reference material found to be generally useful in shield design.

13. A part of the responsibility belonging to the shield designer is to calculate *radiation heating* in the structure near the reactor. These parts must be designed to prevent excessive thermal stresses caused by nuclear heating; this design in turn affects the shielding properties of the entire structure. This problem is considered briefly in Chap. 3.

These techniques have been developed for, and described in terms of, power reactor installations. They are also applicable in part to shielding of *hot laboratories, fuel handling coffins, source holders, fuel storage and shipping casks,* etc.

Each shield designer must choose his own *design criteria* or objectives; no handbook can do this for him. All shields cost money, occupy space, have weight, and interfere with access, observation, maintenance, and experimentation. The shield designer must decide how far he will go to minimize these interferences at the cost of money, radiation level, or complexity. Anyone can shield a reactor and make the emergent radiation level as low as he chooses; shield engineering is the art of doing this within specified limits of weight, volume, or cost.

Designing a reactor shield requires considering only two types of radiation: neutrons and gamma rays. These may react in many ways with materials, but a simplified concept of these processes is generally adequate for the shield designer. The rest of this chapter presents this simplified picture of how neutrons and gamma rays are attenuated by passing through materials. This approach has permitted the design of many very complex reactor shields to be successfully based on a few key experiments and an interlacing theoretical correlation, rather than on mock-ups of actual rapidly changing shield-design concepts.

Three types of experiments were done to develop this approach:

1. Bulk shielding experiments were run in the Oak Ridge National Laboratory (ORNL) Lid Tank in early 1950. Slabs of iron, lead, and water were placed between a fission source and detectors. This was originally conceived as a mock-up test, but changes in the design and the development of the Albert-Welton fast-removal theory, described in Sec. 2.2, made the mock-up and scale-up approach obsolete for naval and stationary reactor shield design.

2. Streaming and leakage experiments performed at Brookhaven National Laboratory and ORNL during 1951 and 1952 developed simple formulas for approximating the effect of gaps and weak spots in shields.

3. Miscellaneous experiments with N^{17} neutrons, N^{16} gammas, and Co^{60} gammas performed at Bettis, Knolls Atomic Power Laboratory, and the Naval Research Laboratory and the Westinghouse Atomic Power Division experiments in the Materials Testing Reactor and the Naval Reactor Testing Facility, Arco, Idaho, filled in some gaps in the picture.

2 NEUTRON ATTENUATION

It should first be understood that in an actual shield design the neutron- and gamma-shielding problems are inherently related; like two mischievous children, one cannot long be safely ignored while the other is being taken care of. In particular, the production of gamma rays by neutron attenuation is the major factor which complicates the design of reactor shields. This chapter, however, discusses the basic attenuation processes separately; the rest of the manual covers the practical problems of shield design.

2.1 Basic Neutron-attenuation Processes[1]

The processes which a neutron can undergo in being captured in a shield are:

1. It may make a collision with hydrogen; this will reduce its energy by an amount anywhere from zero to its total energy and change its direction from zero to 90°.
2. It may make elastic (or billiard ball) collisions with oxygen or heavy elements.
3. It may also make inelastic (or putty ball) collisions with oxygen or heavy elements.
4. The neutrons are finally removed by capture in either hydrogen or metal, the capture generally occurring at essentially thermal energies.

Each of these processes will be discussed, and an attempt will be made to approximate each one in a simple way.

A *collision with hydrogen* usually has nearly the effect (from a shielding standpoint) of absorption. Qualitatively, this is true because of the degradation in energy and lengthening of shield path which accompanies the collision, combined with the rapid increase of the hydrogen total cross section* as the neutron energy decreases. The stopping of neutrons in hydrogen is a rapidly convergent process in which most of the distance required for slowing the neutron to thermal energy is that required to make a first collision. A small number of the initial collisions with hydrogen will degrade and deflect the neutrons very little. These slightly scattered neutrons will penetrate nearly as well as uncollided neutrons and will cause the law of penetration to depart slightly from the exponential form which would be valid were all the neutrons removed completely by their first collision. *This effect, the so-called "build-up," will be ignored for the time being, and the distribution of first collisions in hydrogen will be taken as a simple exponential.*

Since the slowing down of neutrons in hydrogen after the first collision is a rapidly convergent process, it seems a reasonable assumption to neglect the distance traveled after the first collision. *This means that the resulting spatial distribution of captures at thermal energy will be taken, for the time being, as proportional to the spatial distribution of first collisions in hydrogen.*

A neutron may also collide *with oxygen or a heavy element.* The emergent neutron may come off in any direction with an energy spectrum that depends on the energy of the incident neutron and the scattering angle. For a neutron below about 1 Mev, the scattering will usually be *elastic*, whereas inelastic scattering becomes increasingly probable as the energy rises.

---

*Cross section measures the probability of a particle interacting with the element in question. Crudely, if a particle encounters an element of large cross section, it is apt to collide with it. For fast-neutron scattering these cross sections approximate the actual theoretical area of the nucleus (about $10^{-25}\ A^{\frac{2}{3}}\ cm^2$, where A = atomic weight); for special reactions (e.g., capture of thermal neutrons) the cross sections can be factors of 10 larger.

It may be expected that in lead or iron a neutron with energy higher than 2 or 3 Mev will be reduced to an energy of something like 1 Mev with a cross section which is approximately one-half the total cross section of the heavy element. Such a neutron of reduced energy will be stopped very quickly by hydrogen since the hydrogen cross section increases rapidly at low energies; the assumption is therefore made that such an *inelastic collision is equivalent to an absorption.* The spatial displacement is also neglected between the inelastic collision and the subsequent capture at thermal.

At low energies isotropic elastic scattering is common. Such a collision changes the direction of the neutron effectively so that it has little chance of escaping from the shield. For reactor plant shields of practical compositions and thicknesses, it is easily shown that isotropic *elastic deflection is also equivalent to absorption.*

At the higher neutron energies of interest in the shield (5 to 15 Mev), about one-half the total cross section of the heavy element corresponds to small-angle elastic deflections. These deflections are associated with the neutron shadow cast by the opaque nucleus. At low energies (1 or 2 Mev) this cross section due to shadow scattering is probably most easily treated as isotropic and therefore included as an absorption. At higher energies the total shadow scattering is included in a small angular range and is probably to a large extent ineffective in removing neutrons. As a simple prescription *assume that an energy-independent cross section describes the removal of neutrons by the heavy element.* Make a similar assumption for the oxygen scattering, and these two constants will be left as parameters that will be adjusted to obtain a best fit with bulk-shielding data.

2.2 The Fast-removal Theory

This theory was evolved by Albert and Welton[1] for the immediate purpose of systematizing and applying bulk-shielding data. The method is quite simple in structure, and, when applied under the proper conditions, it gives very dependable results. It was constructed by a careful examination of the neutron interactions that occur in a shield and by delineating only those which strongly determine the deep penetration of neutrons. It gives the *average* penetration characteristics of neutrons in a shield composed of water and other elements when these elements range from 0 to 50 per cent of the shield by volume. Like any phenomenological theory it applies in only a certain range of cases and answers only certain limited questions.

In spite of its limitations the theory makes it possible to design a practical reactor-core shield on the basis of a few fundamental bulk-shielding experiments. It bridges the gap between a simple bulk-shielding experiment and the many complications and details (including continual design changes) which enter into a practical core shield.

Neutron level generally decreases nearly exponentially through a shield, i.e., it decreases a certain percentage per inch of shielding; it follows a straight line on semilog paper, and it obeys an equation of the kind

$$\text{Neutron flux} = \text{constant} \times e^{-\Sigma x} \text{ or, for a point source: flux} = \frac{\text{constant}}{4\pi r^2} e^{-\Sigma x}$$

where x = shield thickness, Σ = a constant, and r = distance from source to point x.

Thus, when such an approximation is adequate, a single characteristic, Σ, describes the rate of neutron removal through a given material. This constant Σ_R is called the "removal cross section" and has the dimensions cm^2/cm^3, or cm^{-1}. It is sometimes expressed as σ_R in barns (10^{-24} cm^2) per atom, in which case the number of atoms per cubic centimeter must be factored in separately. To determine whether the removal cross-section concept is valid and, if so, what values should be used, the various processes considered above were, in effect, all lumped as a single absorption process, and data from bulk-shielding tests were analyzed to see whether one cross section would adequately correlate them. The validity and limitations of this approach are covered more fully in Chap. 3. It is sufficient here to note that a single cross section does appear reasonable for shielding purposes. (Except for hydrogen, which is treated specially; see Chap. 3.)

The effective removal cross sections of a fairly large number of materials have been measured at ORNL over the past few years. The most recent values are tabulated in Table 1.1.

The values are derived from an analysis of the attenuation measurements as described above. The data follow quite closely the shape of the curve for total cross sections for 8-Mev neutrons (compare with Report LA-1655) vs. atomic weight and lie about 40 per cent below the

Table 1.1 — EFFECTIVE REMOVAL CROSS SECTIONS FOR FISSION NEUTRONS[6]

Material*	Cross section,† barns/atom	Material	Cross section,† barns/molecule
Aluminum	1.31	C_7F_{16}	26.3
(Boron)	0.97	C_2F_3Cl	6.6
Beryllium	1.07	CH_2	2.8
Bismuth	3.49	B_4C	4.3
Carbon	0.81	$C_{30}H_{62}$	80.0
(Chlorine)	1.2	D_2O	2.8
Copper	2.04		
(Fluorine)	1.29		
Iron	1.98		
Lithium	1.01		
Nickel	1.89		
(Oxygen)	0.99		
Lead	3.5		
Tungsten	2.5		

*The effective removal cross sections for the materials in parentheses were derived from analysis of compounds containing these elements.

†These removal cross sections are for a source of neutrons with a fission spectrum. Some experimental data of removal cross sections from a source of 1-Mev neutrons from N^{17} are given in Chap. 4.

total cross-section data. An approximation of $\Sigma_R/\rho = 0.085A^{-1/3}$ (where ρ = density and A = atomic weight) is fairly good for atomic weights above 10 (reference 6).

3 GAMMA-RAY ATTENUATION

3.1 Sources

Basic information on the production processes of gamma rays can be obtained from any good textbook of nuclear physics (e.g., David Halliday, *Elementary Nuclear Physics*). The gamma-ray sources arising in the reactor core are outlined in Chap. 3; those originating in the reactor coolant are covered in Chap. 4. Information concerning the decay scheme of an activated nucleus is obtainable in NBS Circular 499 or from Table of Isotopes, Hollander, Pearlman, and Seaborg, Reactor Handbook, Report AECD-3645. This decay information and the amount of the element present determines the total source strength of a particular isotope under question.

3.2 Basic Gamma-attenuation Processes

The reduction of gamma flux is accomplished by two mechanisms: (1) pure distance from source to receptor and (2) interaction of the gamma-ray photons with matter that lies between the source and the receptor. The first effect is useful when small sources ("point sources") are under consideration and space is not a limiting factor in the design. Where it is impractical to remain physically removed from the source, the interaction of the photons with material is the prime attenuation mechanism. As is shown in Chap. 9, all the formulas for

various source geometries can be derived from the following equation for the attenuation of gamma rays from a point source. (Note the similarity of this process, from a shielding standpoint, with the simplified process that describes the attenuation of neutrons in Sec. 2 of this chapter.)

$$D = \frac{S_0 B e^{-\mu x}}{K 4\pi r^2} \tag{1}$$

where D = dose rate (units of dose rate)
S_0 = point source of gamma rays (photons/sec)
B = build-up factor (dimensionless) (see below)
μ = linear absorption coefficient (units of reciprocal length)
x = thickness of shield passed through in going from source to receptor (units of length)
K = conversion from gamma-ray flux to dose rate (see Chap. 2)
r = the distance from source to receptor (units of length)

The symbols μ and B warrant further discussion. The linear absorption coefficient, μ, is a function of energy and material. The magnitudes are given in Chap. 10. G. R. White's review of the available data (NBS Report 1003) shows that most of the important gamma-ray cross-section data are known to better than ± 2 per cent.

For a theoretical discussion of this absorption, reference is again made to any standard text. The articles by U. Fano in the August and September issues of *Nucleonics*, Volume 8, 1953, are particularly lucid and complete. Suffice it to say at this point that the attenuation is made up of three distinct processes commonly called photoelectric capture, pair production, and Compton scattering. The first two of these are an annihilation process in which the gamma ray is destroyed. In the third process the gamma photon interacts with an electron and is deflected to another direction, losing only part of its original energy. As a result of this, some gammas that were counted as lost in evaluating μ do penetrate the shield, and thus the net reduction is not as great as predicted by the exponential term of $e^{-\mu x}$. This gives rise to the use of a build-up factor, B, in Eq. 1 and throughout Chap. 9.

3.3 Build-up Factors

The build-up factor is defined as the ratio of the actual gamma flux to that which would be calculated using a simple exponential attenuation with the linear absorption coefficient. This gives a number build-up factor; however, the same definition may be used in terms of dose rate, giving a dose build-up factor; in terms of energy transmitted, giving an energy build-up factor; or in terms of energy absorbed, giving an energy-absorption build-up factor.

A technique of numerical solution of the transport equation for gamma penetration in its fully accurate form has been developed by Spencer and Fano.[2] This technique involves solution of a set of coupled integral equations for the spatial moments and the inversion of the moments to obtain the spatial distribution. With the aid of a large-scale computer at the Bureau of Standards (the SEAC), a series of calculations have been completed of the full-penetration characteristics of gamma rays over a range of initial gamma-ray energies (0.5 to 10 Mev) and a series of eight different shield mediums which covers the range of atomic number. These data are compiled in reference 7 along with computed curves for the build-up factors for a point isotropic source; some of these are reproduced in Chap. 10.

These curves are given in terms of only one medium surrounding the source. When the shield is made up of several materials, the total number of relaxation lengths (distance in a material for which $\mu x = 1$ and thus which attenuates the radiation by a factor of e, or 2.7) is the sum of the relaxation lengths of the various components. A "best method" of handling the build-up factor for every situation is not yet agreed upon. The situation is given essentially in the following sections.

(a) Shields of One Material. The best data for gamma build-up factors for a point isotropic source in an infinite medium are those of the NBS-NDA calculations given in Report NYO-3075 and in Chap. 10 of this manual.

Form 1: Data are presented in Report WAPD-TN-217 whereby the NBS-NDA calculations are fitted by a function of the form of the sum of two simple exponentials,

$$B_{mst}(\mu_0 x, E_0) = A_1(E_0)\exp[-\alpha_1(E_0)\mu_0 x] + A_2(E_0)\exp[-\alpha_2(E_0)\mu_0 x]$$

where $B(\mu_0 x, E_0)$ = build-up factor (ratio of scattered gamma radiation to uncollided gamma radiation at the point $\mu_0 x$)
subscript m = attenuating medium
subscript s = source geometry
subscript t = type of build-up (type refers to number flux, energy flux, or dose rate)
μ_0 = linear coefficient at energy E_0 (from the definition of B_{mst}, $A_1 + A_2 = 1$)

Curves of the parameters α_1, α_2, and A_1 as a function of energy for a point isotropic source are presented in Chap. 9. Curves are presented for dose build-up, energy build-up, and energy absorption build-up for four materials (where available): iron, lead, water, and concrete.

Form 2: In a limited region (i.e., for small variations of μx), the build-up factor may be expressed by either $B = 1 + \beta\mu x$ or form 3.

Form 3: $B = \beta(\mu x)^{\alpha}$, where β and a are constants depending on material and energy.

All three of these forms are useful for analytical expressions, and integrations for determining the effects of other geometries are given in Chap. 9.

The effect of gamma rays penetrating a slab shield is generally handled by form 1, assuming that the build-up for such a geometry is the same as for an infinite medium. In this case the use of extra shielding, resulting from penetration at an oblique angle, is generally considered valid. However, experimental data taken by Wyckoff et al.[3] indicate that the extra shielding at oblique angles can be utilized only up to angles of 30°. Calculations supporting this and giving build-up factors for oblique penetrations have been made by Peebles.[4] Unfortunately Peebles's calculations do not exactly agree with the NBS-NDA data for "straight-through" geometries. As a result it has been suggested that Peebles's data be normalized to the NBS-NDA data for the straight-through condition for calculating oblique penetrations (see Chap. 4, Sec. 3.2).

(b) Several Slabs of Different Materials. Several methods of treating the build-up factor for composite shields have been suggested. Some of these are as follows:

1. For a light material followed by a heavy material, use the build-up factor of the heavy material only.
2. For a heavy material followed by a light material, use the product of the individual build-up factors. This has also been suggested for more than two materials, but in many cases this may lead to a very conservative answer.
3. The build-up factors may be weighted according to the number of relaxation lengths of each of the shield materials present.
4. The shield may be converted to an equivalent shield of one material using the curves given in Chap. 6 (Figs. 6.4 to 6.6). The B for that material is then used.

(c) Homogeneous Mixtures. If the shielding mediums form a homogeneous mixture such as concrete, the build-up factor may be calculated by a method suggested by Goldstein and calculated for concrete by Obenshain.[5] This presentation will be summarized here. To find the build-up factor for the mixture, an effective atomic number, "Z," must be found. Build-up factors for various elements may be plotted as a function of the atomic number Z for a particular value of E_0 with the number of mean free paths ($\mu_0 x$) as parameter.

The problem now is to find some element that has the same properties as the mixture in so far as the scattering and absorption of the gamma rays are concerned. The characteristics of a material for gamma absorption and scattering are determined by the fraction of the total

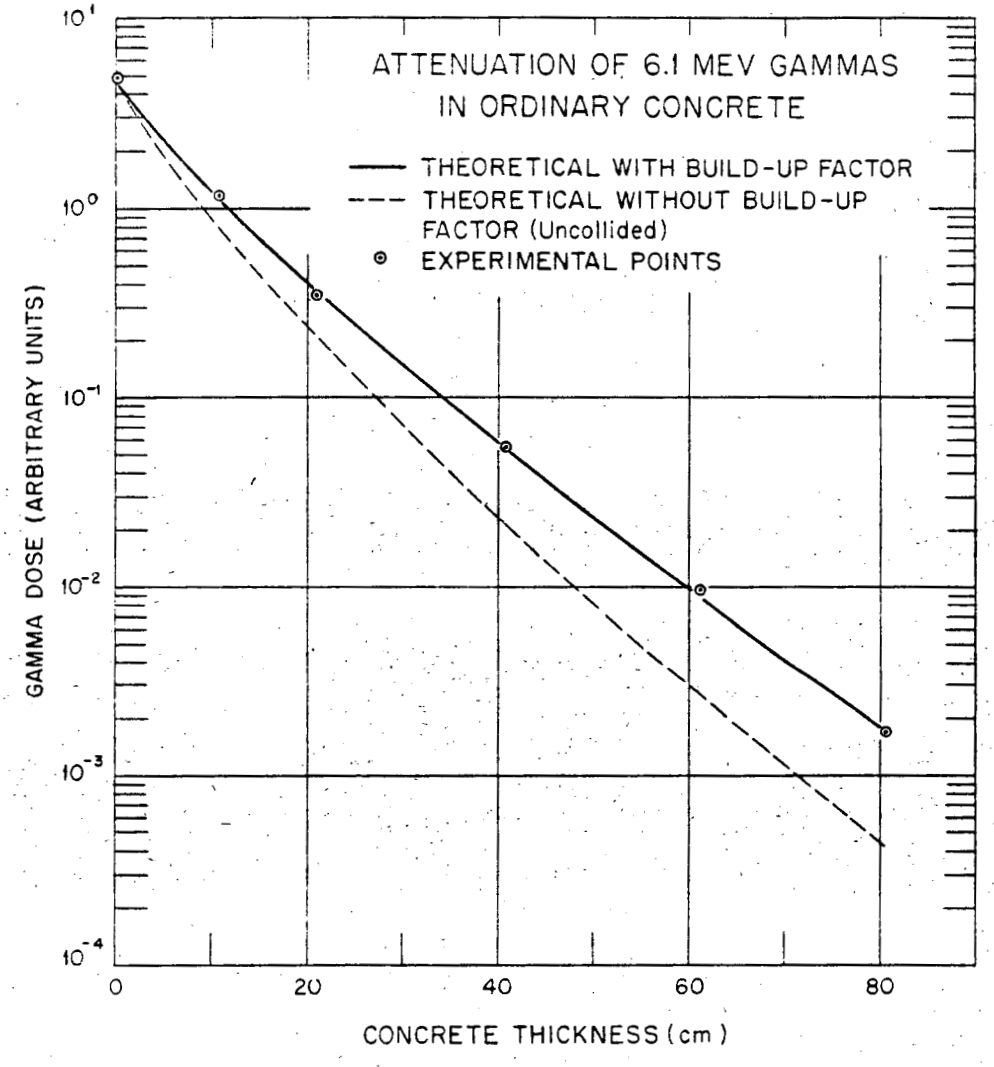


Figure 1.2

number of electrons associated with each nucleus. The electronic fraction may be determined by

$$\beta_i = \frac{a_i Z_i / A_i}{\sum_{i=1}^{n} a_i Z_i / A_i}$$

where a_i is the fraction by weight of the element i of the total, Z_i is the atomic number, and A_i is the atomic or molecular weight.

The absorption coefficient per electron is μ_i; then the total absorption coefficient of the material is

$$\mu(E) = \sum_i \beta_i \mu_i(E)$$

The first criterion for computing Z is that the shape of the curve of absorption coefficients must match the element absorption coefficients. In order to do this, the mass-absorption coefficients vs. energy for several elements were normalized at 2 Mev. Compari-

son between this curve and the coefficients for the mixture was made, and the effective Z was found to be 18.

The second criterion is that the ratio of the scattering cross section to the total cross section for the mixture must vary with energy in the same way as the natural element. The scattering cross section, σ_s, may be obtained in the same way as the total absorption cross section.

$$\sigma_s(E) = \sum_{i=1}^{n} \beta_i \sigma_{si}(E)$$

The ratio $\sigma_s(E_0)/\mu(E_0)$ is then plotted as a function of Z for the known elements for various energies, and the same ratio for the mixture is plotted on the graph. This was done for concrete, and the average Z was 18.

Since the two conditions have approximately the same atomic number, the NBS-NDA results for this atomic number were used. This theoretical method was verified by experiments with 6.1-Mev gammas through concrete, and the results are plotted in Fig. 1.2.

This treatment can be used in laminated shields if the laminations are small enough and sufficiently well distributed that it can be reasonably considered as a homogeneous mixture, i.e., when the relaxation lengths for the metal and water are about equal. If the shield laminations are few and quite large, the homogeneous method suggested above is not suitable.

REFERENCES

1. R. D. Albert and T. A. Welton, Report WAPD-15, Nov. 30, 1950 (Classified).
2. L. V. Spencer and U. Fano, J. Research Natl. Bur. Standards, 46: 446 (1951).
3. F. S. Kirn, R. J. Kennedy, and H. O. Wyckoff, The Attenuation of Gamma Rays at Oblique Incidents, Radiology, 63(1): 94-104 (1954).
4. G. H. Peebles, Gamma-ray Transmission Through Finite Slabs, RAND Report R-240, Dec. 1, 1952.
5. F. E. Obenshain, Report WAPD-P-646.
6. E. P. Blizard, paper given at the Nuclear Engineering Congress at Cleveland, Ohio, Dec. 12 through 16, 1955.
7. Herbert Goldstein and J. Ernest Wilkins, Jr., Calculations of the Penetration of Gamma Rays, Report NYO-3075, June 30, 1054.

12

1S

BLANK

FRONT 1S

PG - 11

14
IS
BLANK

FRONT-
PG 13

Chapter 2

SETTING ALLOWABLE RADIATION LEVELS

1 RADIATION SPECIFICATIONS: THE PROBLEM 15

2 BASIC UNITS OF RADIATION AND RADIOACTIVITY 15
- 2.1 Definitions and Concepts 15
  - (a) Source Strength 15
  - (b) Flux or Field Strength 15
  - (c) Dose and Dose Rate 16
  - (d) Biological Damage and RBE 16
- 2.2 Units of Measurement 16
  - (a) Source Strength 16
  - (b) Flux 16
  - (c) Dose and Dose Rate 17
- 2.3 Some Useful Approximations 18

3 CONVERSION CURVES FOR GAMMA AND NEUTRON FLUXES AND DOSE RATES . . 18

4 BASIC RADIATION SPECIFICATIONS 18

5 RADIATION LEVELS FOR SHIELD DESIGN 24
- 5.1 Access to the Plant 26
- 5.2 Average Power Level of Reactor Operation 27

6 SPECIAL PROBLEM OF LOCAL RADIATION STREAMING 27

REFERENCES 27

Chapter 2

SETTING ALLOWABLE RADIATION LEVELS

1 RADIATION SPECIFICATIONS: THE PROBLEM

The aim of the shield designer is to protect operating personnel. In order to do this, he must convert radiation standards establishing maximum permissible radiation doses for human beings into specifications that can be used for practical shield design.

The purpose of this chapter is to describe a method for arriving at design specifications for shielding. The remainder of this chapter is divided into five parts devoted to:

1. A definition of the basic units of radiation and radioactivity.
2. Conversion curves for dose rate and flux of neutrons and gamma radiation.
3. A statement of the maximum permissible doses of radiation normally allowed in Atomic Energy Commission laboratories.
4. A description of the method for applying these basic AEC standards to shield design.
5. The special problem of local radiation streaming.

Problems of shield design reduce to protection of personnel from *gamma and neutron radiation*. These are the most penetrating types of radiation produced by an operating nuclear reactor. A shield design for protection against gammas and neutrons normally provides adequate protection from all other forms of radiation.

2 BASIC UNITS OF RADIATION AND RADIOACTIVITY

2.1 Definitions and Concepts

(a) Source Strength. A quantity of radioactive material emits particles or rays of a certain energy and at a certain rate. The *rate* of emission (that is, the number of particles emitted per second) measures the *strength* of the radiation source; the *energy* of each particle is a separate matter. For example, a certain radiation source, such as a piece of irradiated steel, may have an intensity of 10^7 gammas emitted each second, some with an energy of 1.3 Mev, some with an energy of 1.1 Mev, etc.

(b) Flux or Field Strength. This is the rate of flow of particles, or of energy, through a unit area. Neutron flux, for example, is expressed as so many neutrons per square centimeter per second. Gamma flux is measured in gamma photons per square centimeter per second. Either may be multiplied by the particle energy to give million electron volts per square centimeter per second, an energy flux. (*Beware* when a reactor engineer speaks of "thermal flux"; he may refer to a flux of thermal neutrons or to a flux of thermal energy, i.e., a heat flux measured in British thermal units per hour per square foot.)

The relation of flux to source strength depends on the distance from the source at which the flux is being measured and whether any radiation is being absorbed or scattered in between.

(c) Dose and Dose Rate. Dose is the term for the actual radiation energy absorbed per unit mass by an absorbing medium, such as a radiation detector or a human being. A *flux* produces a *dose rate*; after a period of time at a given dose rate, an "integrated dose rate" or *dose* is accumulated. Either dose or dose rate can be measured directly by a suitable detector. To determine the damage to a human being from a given dose, account must be taken of the fact that absorption of a given amount of energy from one kind of radiation may be more harmful than from another. This *relative biological effectiveness*, RBE, is discussed further below.

(d) Biological Damage and RBE. Note then that the biological damage from a given radiation source depends upon the following factors: (1) The *flux* must be determined from the *source strength* by considering distance, geometry, and intervening material. (2) Flux × energy × absorption in body × RBE = biological damage.

2.2 Units of Measurement

Let us now consider some typical units used to measure the quantities we have discussed.

(a) Source Strength. Source strength is measured in *curies*. A curie was originally defined as the radioactivity associated with 1 g of radium in equilibrium with its decomposition products. This gives approximately 3.7×10^{10} dis/sec; later this rate of disintegration was defined as a curie for beta and gamma emitters.* For (α,n) or (γ,n) neutron sources, such as polonium-beryllium, a curie refers to the emission rate of alphas or gammas; the rate of neutron emission is considerably less, for example, a 1-curie polonium–beryllium neutron source generates about 2×10^6 neutrons/sec.

A *millicurie* (mc) is equal to 1 one-thousandth of a curie; a *microcurie* (μc) is equal to 1 one-millionth of a curie.

Source strengths are often expressed in the following ways:

1. Particles per second or million electron volts per second.
2. Disintegrations per minute (dis/min, dpm, or d/m). This is directly obtainable from the half life, but it is useless to the shield engineer until he determines how many particles, of what energy, are emitted per disintegration. The latest detailed information on decay schemes for each isotope is given in NBS Circular 499 and Supplements 1 to 3.[1]
3. Counts per minute (cpm or c/m). This is the number that a given radiation counter reads when a particular radioactive sample is brought near it. Such information is of comparative value only, unless the counter is calibrated with a known sample of nearly equal energy, of known disintegration rate, and in the same position.

It is apparent that curie* or particles per second accurately express the radioactivity of a source, whereas disintegrations per minute or counts per minute alone do not.

4. The *rutherford* has been defined as 10^6 dis/sec (i.e., 1 curie = 3.7×10^4 rutherfords); the rutherford is seldom used in shielding work.
5. The *rhm or rhf value* (roentgens per hour at 1 meter or at 1 foot) is also sometimes used to define the effective strength of a source of unknown characteristics.
6. *Distributed sources* are defined in terms of curies per cubic centimeter (for volumes), curies per milliliter (for fluids), curies per centimeter (for line sources), etc.

(b) Flux. Flux is expressed as particles (or radiation photons) per square centimeter per second, or, multiplying by the energy of the particle, it is expressed as million electron volts per square centimeter per second. For heat-generation calculations flux is sometimes given as watts per square centimeter.

---

*A source strength of 3.7×10^{10} particles/sec is often considered as a curie, which implies that one particle is emitted per disintegration. This does not coincide with the official definition of a curie but is common practice in radioisotope and shielding work.

(c) Dose and Dose Rate. The following units of radiation dosage are used to measure the effects of radiation on an instrument or on the human body.

1. The *roentgen* (r) is used to measure quantities of radiation in terms of its ionization of air.
2. The *roentgen equivalent physical* (rep) is used to measure the radiation energy absorbed in the body.
3. The *roentgen equivalent man* (rem) is used to measure the biological effects of radiation on the body.

(1) The *roentgen:* The roentgen is the basic unit of radiation-dose measurement. It is a physical unit and is primarily used to express dosages of gamma or X radiation. One roentgen is defined as the quantity of gamma radiation which will produce, by ionization, one electrostatic unit of electricity of either sign (i.e., 2×10^9 ion pairs) in 1 cm^3 of dry air, measured at standard conditions of temperature and pressure. A flux of about 10^6 1- or 2-Mev gammas equals 1r/hr (see Figs. 2.1 and 2.2).

(2) The *roentgen equivalent physical:* The rep measures the energy absorbed by the human body rather than the energy absorbed by the air. It is therefore applicable to any form of radiation, unlike the roentgen which applies only to gammas and X rays. One rep is defined as that radiation dosage which produces energy absorption in human tissue equal to 93 ergs per gram of tissue. This is roughly equal to the energy absorption in tissue caused by 1 r of gamma radiation.

(3) The *roentgen equivalent man:* Specifications for maximum permissible exposure to radiation are usually expressed in rem. The rem is not a *directly* measurable physical quantity as are the roentgen and the rep, but, rather, it is an index of the damage effects produced in the human body by the various types of radiation. The varying biological effects of the various types of radiation are frequently correlated by a coefficient called the *relative biological effectiveness* (RBE). The RBE is defined as the ratio of the body damage from a given type of radiation to that caused by the same dose of gammas. The rem is defined as the dosage in rep multiplied by the RBE for the type of radiation involved* (see Table 2.1).

Table 2.1—RELATIVE BIOLOGICAL EFFECTIVENESS OF RADIATION[2]

Type of radiation	RBE
X and gamma	1
Beta	1
Fast-neutron	10
Alpha particle (internal)	10

Roentgens, rep, and rem refer to doses; the dose rates are given, respectively, as roentgens per hour, rep per hour, or rem per hour. Workers in the field often refer to doses and roentgens, when dose rates and roentgens per hour are intended. These units are often too large for convenience, and *milliroentgens* (mr) or thousandths of a roentgen, mrep, or mrem are used.

* Compare the tolerable dose from nuclear radiation with that from sunlight. The 300 mr/week tolerance for X and gamma radiation is about $\frac{1}{20}$ microwatt of energy. By contrast, a person can absorb about 100 watts of sunlight, or a flux of over 10^{20} photons/cm^2-sec, for quite a while, and the "lifetime tolerance" is at least 1 watt continuously. In other words, the body can tolerate 20 million times as much radiation dosage in the form of sunlight as it can of the similar but higher energy photon we call gamma rays. This extreme example emphasizes that dose (i.e., absorbed energy) alone is not enough to define biological damage and that tolerance must account for the way in which the absorbed energy affects the body.

4. The *rad* is a unit of dose useful for correlating radiation damage in various materials; it is not used much for total human dosage. A rad is defined as an absorbed dose of 100 ergs/g. One rad is received by a material exposed to about 1 r of gamma radiation or to roughly 10^9 thermal neutrons per square centimeter with accompanying fast neutrons and reactor gammas. Different materials exposed to the same radiation flux for the same period of time will absorb different amounts of energy per gram and thus will have a different exposure expressed in rads but the same exposure expressed in reps.

2.3 Some Useful Approximations

1. The dose rate D at 1 ft from a point source in roentgens per hour is:
   $D = 6CE$ (C = curies*; E = Mev)
2. $D = 1.5NE \times 10^{-10}$ (N = gammas/sec; E = Mev)
3. $D = W \times 10^3$ (W = watts of gamma energy)
4. The dose rate D′ from a gamma flux is:
   $D' = 2\phi E \times 10^{-6}$ (ϕ = gamma flux in photons/cm^2-sec; E = Mev)
5. $D' = 1.1Q \times 10^7$ (Q = watts gamma energy/cm^2)
6. $D' = 1.2Q' \times 10^4$ (Q′ = watts gamma energy/sq ft)
7. 1 curie* produces 1 r in 1 hr at 1 meter (when E = 2 Mev).
8. All the world's refined radium gives off ionizing radiation equivalent to only a few watts of reactor power.
9. An *operating* reactor = several hundred curies* per watt of reactor power.
10. A *shutdown* reactor (1 day after long operation) contains fission products = 1 curie*/watt.
11. 1 curie* of 1-Mev radiation releases energy at a rate of 6 milliwatts.
12. 1 watt of energy release = 167 curies* at 1 Mev.
13. If a flux = 10^x at 1 cm from a point source, it equals $10^x/d^2$ at d cm and 10^{x-3} at 1 ft (since 1 ft$^2 \approx 10^3$ cm^2).

3 CONVERSION CURVES FOR GAMMA AND NEUTRON FLUXES AND DOSE RATE

Figures 2.1 and 2.2 provide conversion between gamma flux in photons per square centimeter per second and dose rate in roentgens per hour for various gamma energies. Figures 2.3 and 2.4 provide a similar conversion for neutrons, connecting the points of Table 2.2 with straight lines.

4 BASIC RADIATION SPECIFICATIONS

The National Committee for Radiation Protection has established limits for maximum permissible exposure to radiation which are published in National Bureau of Standards handbooks.[2] These limits are based on a conservatively established radiation dose rate that is known to produce no measurable physical effect on human beings when received continuously over a lifetime of exposure. The established limit or standard dose rate is 0.3 rem (300 mrem) per week.

For comparison, Table 2.3 shows the radiation level from several common sources.

In certain cases the dose rate may be averaged over a period of 13 weeks; that is, a radiation dose in excess of 300 mrem may be taken during any given week so long as the *average radiation dose rate* at the end of the 13 weeks has not been greater than 300 mrem/week. In these cases, however, the radiation dose in any single week may not normally exceed 900 mrem.

---

*Where a curie is considered to be 3.7×10^{10} photons/sec.

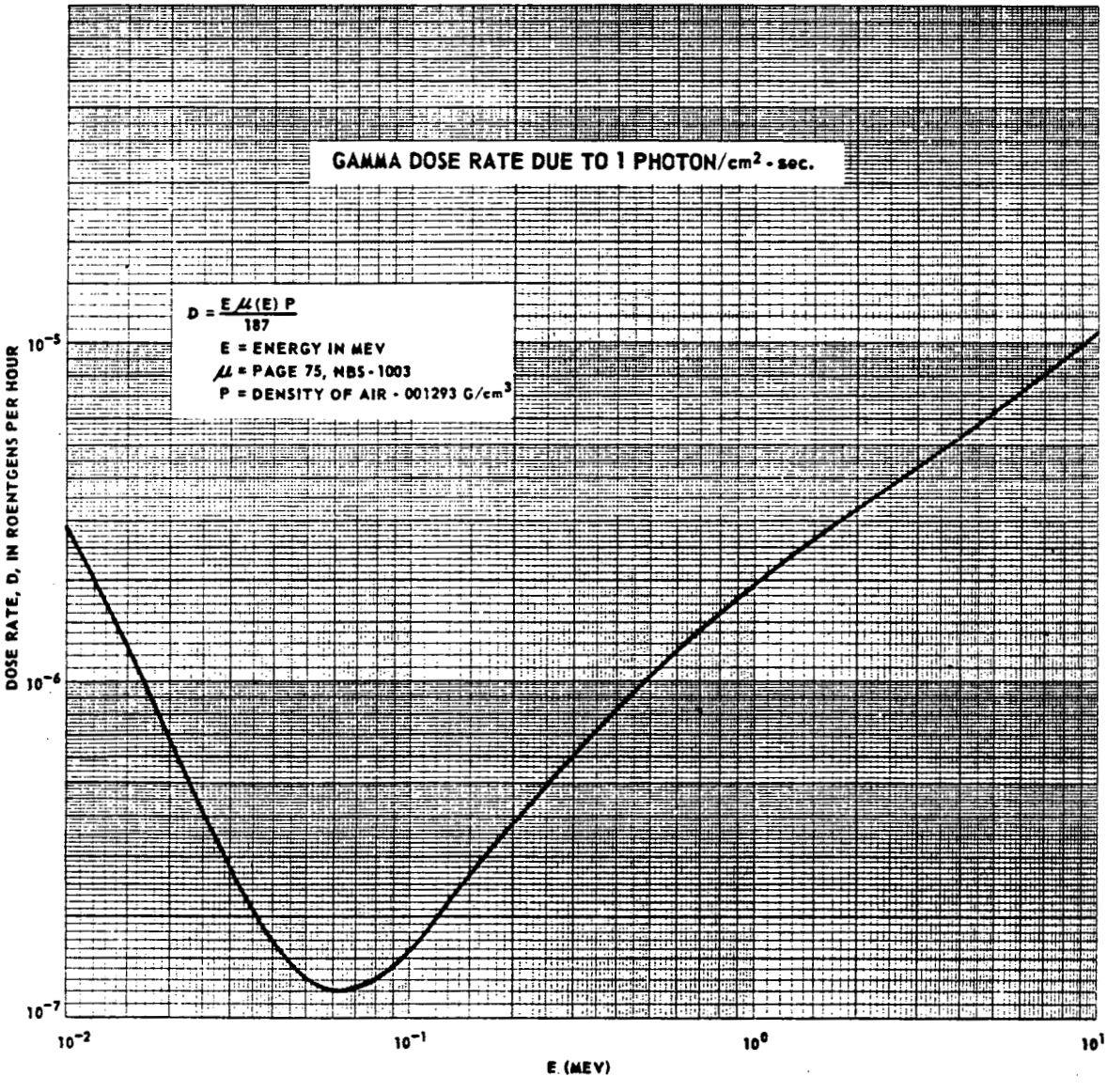

GAMMA DOSE RATE DUE TO 1 PHOTON/cm² - sec.
$D = \frac{E\,\mu(E)\,P}{187}$
E = ENERGY IN MEV
μ = PAGE 75, NBS - 1003
P = DENSITY OF AIR - 001293 G/cm³
DOSE RATE, D, IN ROENTGENS PER HOUR
10⁻⁵
10⁻⁶
10⁻⁷
10⁻²
10⁻¹
10⁰
10¹
E (MEV)

Figure 2.1

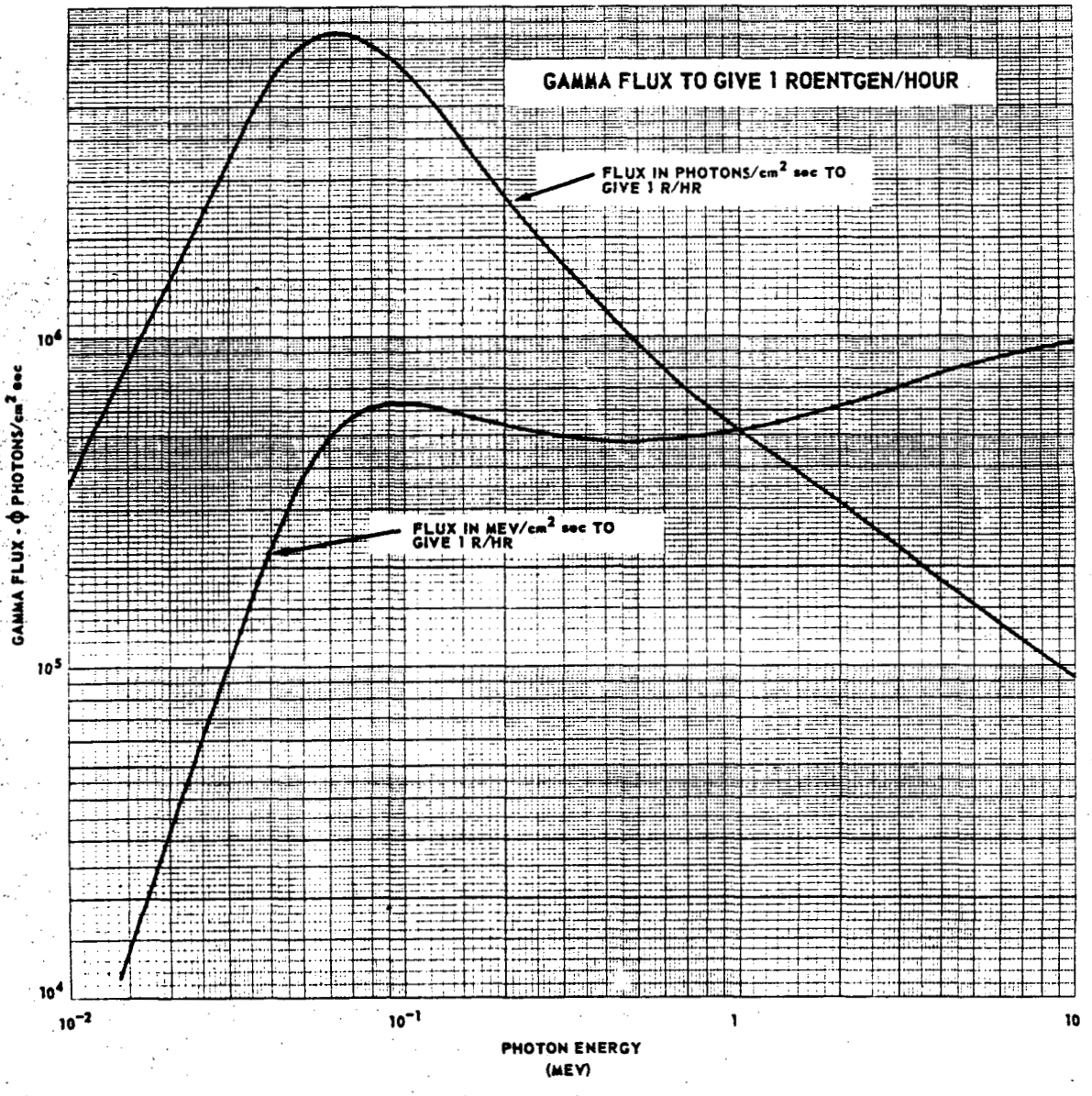

GAMMA FLUX TO GIVE 1 ROENTGEN/HOUR
FLUX IN PHOTONS/cm² sec TO GIVE 1 R/HR
FLUX IN MEV/cm² sec TO GIVE 1 R/HR
GAMMA FLUX - ϕ PHOTONS/cm² sec
10⁶
10⁵
10⁴
10⁻²
10⁻¹
1
10
PHOTON ENERGY (MEV)

Figure 2.2

CHART OF THE NUCLIDES

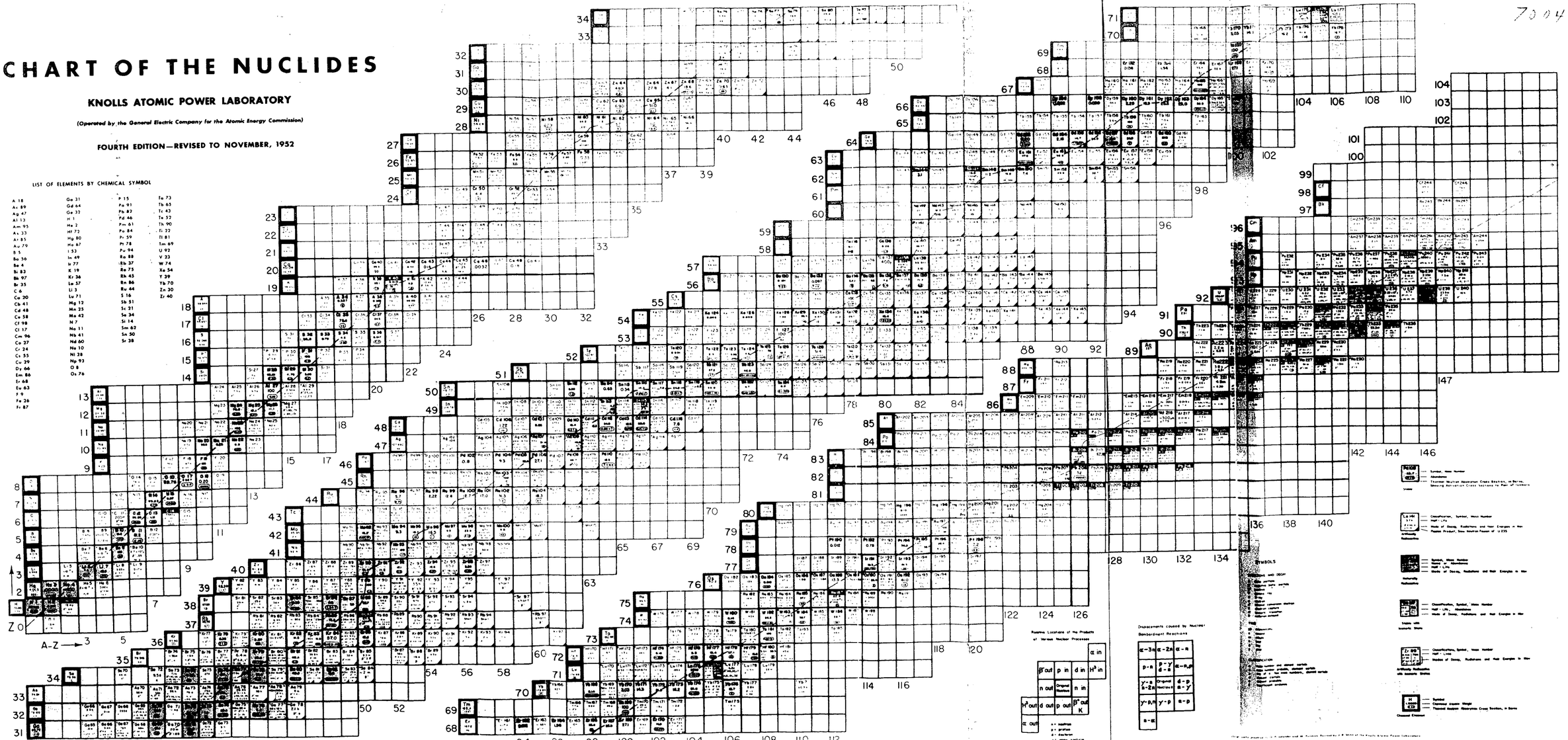
KNOLLS ATOMIC POWER LABORATORY

(Operated by the General Electric Company for the Atomic Energy Commission)

FOURTH EDITION—REVISED TO NOVEMBER, 1952

LIST OF ELEMENTS BY CHEMICAL SYMBOL

A 18	Ge 31	P 15	Te 73
As 89	Gd 64	Pa 91	Tb 65
Ag 47	Ga 32	Pb 82	Tc 43
Al 13	H 1	Pd 46	Te 52
Am 95	He 2	Pm 61	Th 90
As 33	Hf 72	Po 84	Ti 22
At 85	Hg 80	Pr 59	Tl 81
Au 79	Ho 67	Pt 78	Tm 69
B 5	I 53	Pu 94	U 92
Ba 56	In 49	Ra 88	V 23
Be 4	Ir 77	Rb 37	W 74
Bi 83	K 19	Re 75	Xe 54
Bk 97	Kr 36	Rh 45	Y 39
Br 35	La 57	Rn 86	Yb 70
C 6	Li 3	Ru 44	Zn 30
Ca 20	Lu 71	S 16	Zr 40
Cb 41	Mg 12	Sb 51	
Cd 48	Mn 25	Sc 21	
Ce 58	Mo 42	Se 34	
Cf 98	N 7	Si 14	
Cl 17	Na 11	Sm 62	
Cm 96	Nb 41	Sn 50	
Co 27	Nd 60	Sr 38	
Cr 24	Ne 10		
Cs 55	Ni 28		
Cu 29	Np 93		
Dy 66	O 8		
Em 86	Os 76		
Er 68			
Eu 63			
F 9			
Fe 26			
Fr 87			



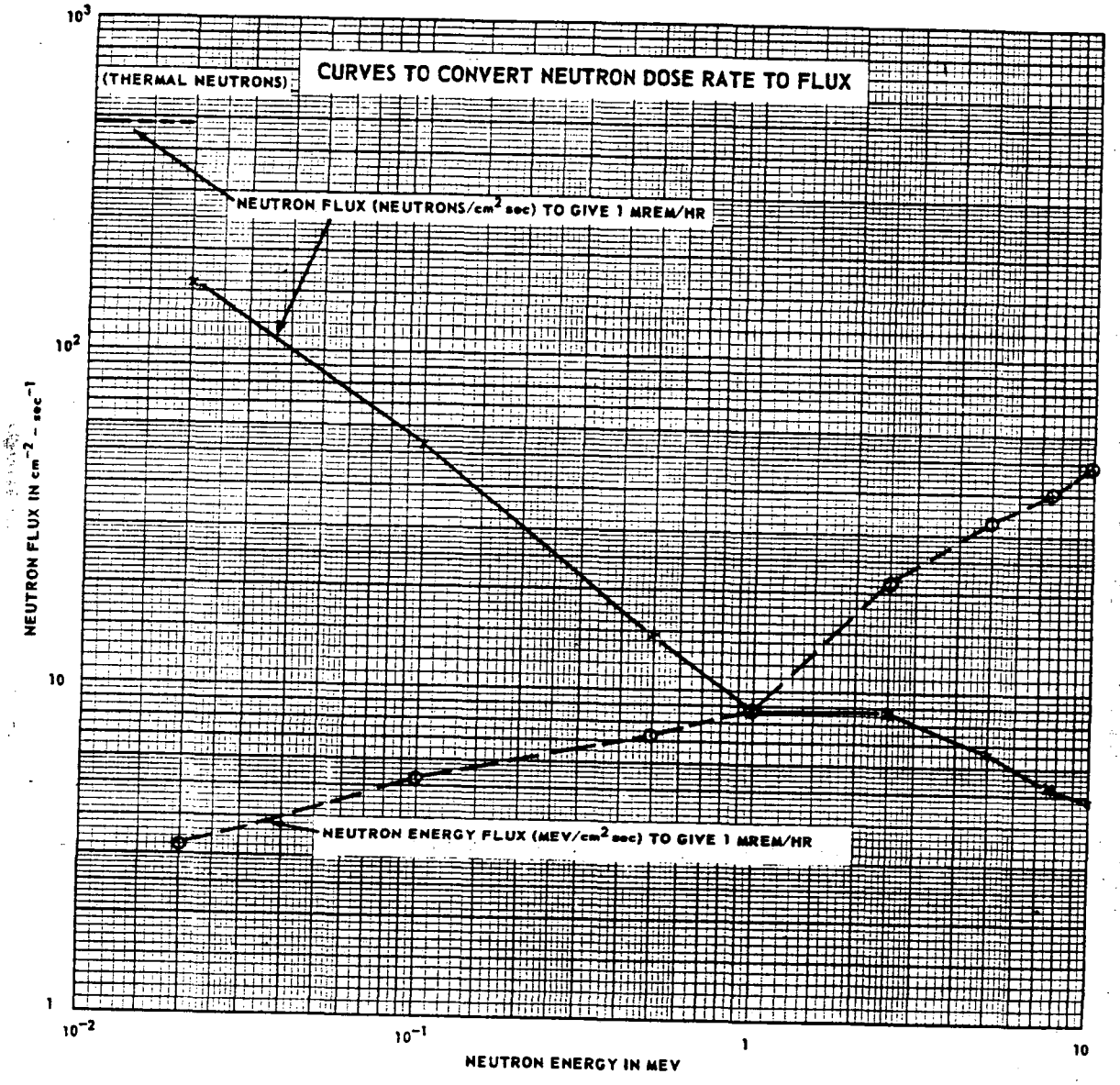

CURVES TO CONVERT NEUTRON DOSE RATE TO FLUX
(THERMAL NEUTRONS)
NEUTRON FLUX (NEUTRONS/cm² sec) TO GIVE 1 MREM/HR
NEUTRON ENERGY FLUX (MEV/cm² sec) TO GIVE 1 MREM/HR
NEUTRON FLUX IN cm⁻² - sec⁻¹
NEUTRON ENERGY IN MEV
10³
10²
10
1
10⁻²
10⁻¹
1
10

Figure 2.3

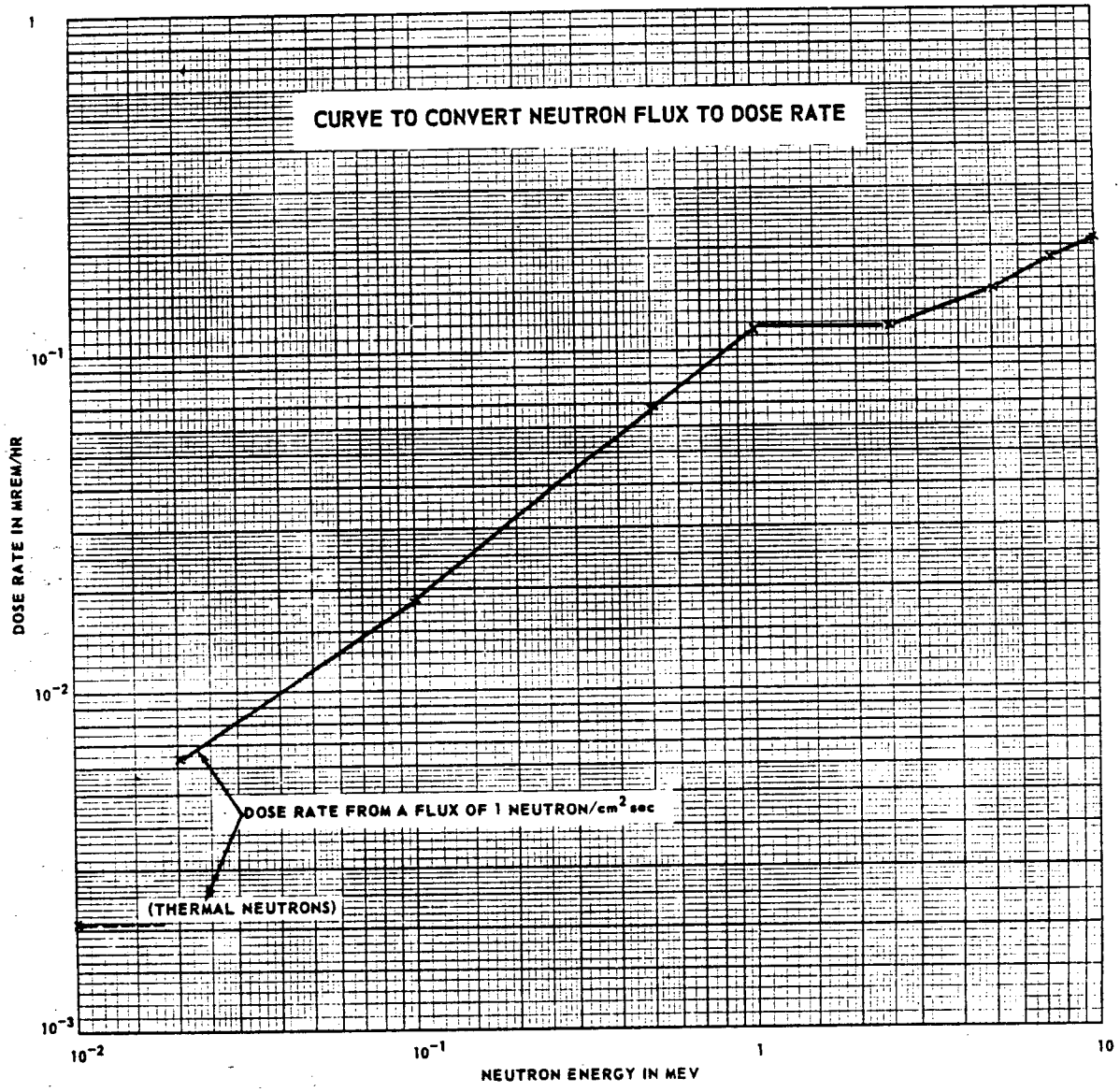

CURVE TO CONVERT NEUTRON FLUX TO DOSE RATE
DOSE RATE IN MREM/HR
1
10^{-1}
10^{-2}
10^{-3}
DOSE RATE FROM A FLUX OF 1 NEUTRON/cm^2 sec
(THERMAL NEUTRONS)
10^{-2}
10^{-1}
1
10
NEUTRON ENERGY IN MEV

Figure 2.4

Table 2.2 — FLUX OF NEUTRONS WHICH WILL PRODUCE 1 MREM/HR GIVEN AS A FUNCTION OF ENERGY*

Neutron energy, Mev	Neutrons/cm^2-sec
Thermal (0.02 ev)	480
0.0001	240
0.005	240
0.02	160
0.1	53
0.5	14.7
1.0	8.7
2.5	8.7
5.0	6.7
7.5	5.3
10.0	4.8

* This table was obtained from W. S. Snyder (ORNL) and is a proposed revision to the NBS handbooks.

Table 2.3 — RADIOACTIVITY AND RADIATION LEVELS OF SEVERAL COMMON SOURCES

Source	Rate
Cosmic rays (at sea level)	30 mr/year
K^{40} in blood	30 mr/year
Gammas from natural radioactivity of earth	30 to 100 mr/year
Gammas from a radium watch dial (locally, at wrist)	100 mr/day
Chest X ray (with film)	50 to 200 mr/exposure
Dental X ray (with film)	4 to 5 r/film
X-ray examination (fluoroscopic)	15 to 25 r/min
Radiation therapy (local, to destroy tissue)	500 to 10,000 r
Foot X-ray machines, shoe stores	1 r/min
Normal lifetime dose, without special exposures, for a person in the "prereactor era"	~10 to 40 r/lifetime
Dose expected to kill about one-half* of the persons exposed to it, if received in a short time	400 to 500 rem
Natural inland water radium content	0.4 to 4 $\mu\mu$c/liter
Maximum permissible concentration of radium in drinking water	40 $\mu\mu$c/liter
Spring water at Shimane, Japan, contains radium to the extent of	~1 μc/liter
Deposits near natural springs have been found as high as	1 to 3 mc/g
Luminous watch dial contains	~5 μc radium
The average human body contains natural C^{14} totaling	~0.01 μc
The average human body contains natural K^{40} totaling	~0.5 μc

* Known as "semilethal dose," SLD, or LD-50.

Because of the difficulty of accurately controlling personnel exposure under such conditions, it is advisable to restrict the total 13-week dose to 3.0 rem rather than 3.9 rem; NBS Handbook 59 recommends this limitation.

Higher permissible values have been set for very low energy gammas which do not penetrate beneath the skin and for exposure which can be definitely limited to the hands. These are discussed in NBS Handbook 59 but are not usually exploited in shield design.

During periods of emergency, radiation doses in excess of the above limits are permitted. In emergencies the total cumulative 13-week allowance may be taken as a single dose; that is, up to 3.9 rem may be taken in a single exposure if necessary. However, the total dosage received during any 13-week period should never exceed the established limit of 3.9 rem. In other words, if an emergency requires that an individual receive his entire 13-week allowance in one single exposure, then that individual should not be permitted to receive additional radiation until the 13-week period has elapsed. This concept is used for special high-level short-time maintenance work that cannot be avoided.

Operating within these limits, even those just described as "emergency," is believed to cause no biological damage, and such operation need not be reported outside the operating activity involved. It is only reasonable, however, that all unnecessary exposure to radiation be kept to an absolute minimum.

The above radiation standards are fully discussed in NBS Handbook 59, *Permissible Dose from External Sources of Ionizing Radiation.*

Some study has been made of the recovery of the body from minor radiation injury, and it has been shown that a dose received over a period of several weeks is less harmful than one received in minutes. The shield designer, however, is generally concerned with such low exposure levels that this factor does not apply.

In addition to the standards for external radiation, specific standards have been established for inhaled or ingested radiation. These standards are itemized by individual radionuclide and are included in NBS Handbook 52, *Maximum Permissible Amounts of Radioisotopes in the Human Body and Maximum Permissible Concentrations in Air and Water.* Table 2.4 summarizes these standards.

One must decide, in setting tolerances for a given plant, what fraction of the dose will be assigned to gamma radiation, what fraction to neutrons, and what fraction to miscellaneous sources, such as air-borne and water-borne activity. In the naval reactors and PWR programs, it has been decided to hold fluid-borne activity to less than 10 per cent of the lifetime tolerance values given in Table 2.4. This is an essentially negligible level and in many cases is near the minimum detectable concentration. The neutron contribution is also held to less than 10 per cent of the total dose. This allows the RBE for neutrons to fluctuate from one medical convention to the next without seriously affecting the shield design. It is also pertinent that a 10-fold reduction of gamma dose usually requires several times the weight of shielding that a similar reduction in neutron level requires.

5 RADIATION LEVELS FOR SHIELD DESIGN

One method of applying the standards set forth in Sec. 4 of this chapter to shield design would be to limit the radiation level in every area near the reactor plant to values such that *continuous exposure* with the reactor running continuously at full power would result in a dose of 300 mrem or less per week. This method, however, would be wasteful of shield weight, space, and cost since many such areas need not require continuous access by operating personnel. Sufficient shielding to provide continuous access to these areas would not be necessary.

Considerable reduction in shield cost, weight, and space may be achieved if careful consideration is given to two aspects of plant operation when setting shield specifications. These are: (1) The average amount of access time required to various regions near the reactor, and (2) the average power level at which the reactor will operate. These averages should be based on a long period of time, such as 13 weeks.

Table 2.4—MAXIMUM PERMISSIBLE CONCENTRATION IN AIR AND WATER FOR CONTINUOUS EXPOSURE*

Element	Microcuries per milliliter of water	Microcuries per milliliter of air
Common Radioisotopes That Are Alpha Emitters		
Po^{210}†	3×10^{-5}	2×10^{-10}
Po^{210}‡		7×10^{-11}
Rn^{222} + daughters	2×10^{-6}	10^{-8}
Ra^{226} + daughters	4×10^{-8}	8×10^{-12}
Natural uranium†	7×10^{-5}	1.7×10^{-11}
Natural uranium‡		1.7×10^{-11}
U^{233}†	1.5×10^{-4}	1×10^{-10}
U^{233}‡		1.6×10^{-11}
Pu^{239}†	1.5×10^{6}	2×10^{-12}
Pu^{239}‡		2×10^{-12}
Beta- and Gamma-emitting Radioisotopes That Are of Interest Because They are Common Body Elements		
H^3	0.2	2×10^{-5}
C^{14} (in bone)	4×10^{-3}	5×10^{-7}
Na^{24}	8×10^{-3}	2×10^{-6}
P^{32}	2×10^{-4}	1×10^{-7}
S^{35}	5×10^{-3}	10^{-6}
Cl^{36}	2×10^{-3}	4×10^{-7}
K^{42}	1×10^{-2}	2×10^{-6}
Ca^{45}	5×10^{-4}	3×10^{-8}
Mn^{56}	0.15	3×10^{-6}
Fe^{55}	4×10^{-3}	6×10^{-7}
Fe^{59}	1×10^{-4}	1.5×10^{-8}
Cu^{64}	8×10^{-2}	6×10^{-6}
Zn^{65}	6×10^{-2}	2×10^{-6}
I^{131}	3×10^{-5}	3×10^{-9}
Other Radioisotopes of Current Interest		
Be^{7}	1	4×10^{-6}
F^{18}	0.9	10^{-4}
A^{41}	5×10^{-4}	5×10^{-7}
Sc^{46}	0.4	7×10^{-8}
V^{48}	0.5	10^{-6}
Cr^{51}	0.5	8×10^{-6}
Co^{60}	2×10^{-2}	10^{-6}
Ni^{59}	0.25	2×10^{-5}
Ga^{72}	9	3×10^{-6}
Ge^{71}	9	4×10^{-5}
As^{76}	0.2	2×10^{-6}
Rb^{86}	3×10^{-3}	4×10^{-7}
Sr^{89}	7×10^{-5}	2×10^{-8}
Sr^{90} + Y^{90}	8×10^{-7}	2×10^{-10}
Y^{91}	0.2	4×10^{-8}

Table 2.4 — (Continued)

Element	Microcuries per milliliter of water	Microcuries per milliliter of air
Other Radioisotopes of Current Interest		
Nb^{95}	4×10^{-3}	4×10^{-7}
Mo^{99}	14	2×10^{-3}
Tc^{96}	3×10^{-2}	3×10^{-6}
$Ru^{106} + Rh^{106}$	0.1	3×10^{-8}
Rh^{105}	1.5×10^{-2}	10^{-6}
$Pd^{103} + Rh^{103}$	1×10^{-2}	7×10^{-7}
Ag^{105}	2	10^{-5}
Ag^{111}	4	3×10^{-5}
$Cd^{109} + Ag^{109}$	7×10^{-2}	7×10^{-6}
Sn^{113}	0.2	6×10^{-7}
Te^{127}	3×10^{-2}	10^{-7}
Te^{129}	10^{-2}	4×10^{-8}
Xe^{133}	4×10^{-3}	4×10^{-6}
Xe^{135}	1×10^{-3}	2×10^{-6}
$Cs^{137} + Ba^{137}$	1.5×10^{-3}	2×10^{-7}
$Ba^{140} + La^{140}$	2×10^{-3}	6×10^{-8}
La^{140}	1	10^{-6}
$Ce^{144} + Pr^{144}$	4×10^{-2}	7×10^{-9}
Pr^{143}	0.4	7.5×10^{-7}
Pm^{147}	1	2×10^{-7}
Sm^{151}	0.2	10^{-8}
Eu^{154}	3×10^{-2}	6×10^{-9}
Ho^{166}	23	3×10^{-6}
Tm^{170}	0.25×10^{-1}	5×10^{-8}
Lu^{177}	24	5×10^{-6}
Re^{183}	8×10^{-2} 0.2	8×10^{-6} 2×10^{-5}
Ir^{190}	10^{-2}	7×10^{-7}
Ir^{192}	9×10^{-4}	5×10^{-8}
Au^{198}	3×10^{-3}	1×10^{-7}
Au^{199}	7×10^{-3}	2.5×10^{-7}
Pb^{203}	0.1	6.5×10^{-6}
At^{211}	2×10^{-6}	3×10^{-10}
Th^{234}	3	6×10^{-7}
Am^{241}	10^{-4}	3×10^{-11}
Cm^{242}	9×10^{-4}	2×10^{-10}

* Derived from Table 3, NBS Handbook 52.
† Soluble.
‡ Insoluble.

5.1 Access to the Plant

Each piece of plant equipment, instrumentation, or control equipment required for use in the reactor plant should be considered in detail. The operational use of the equipment should be analyzed to determine the amount of time that operating personnel must spend in the area for operation, maintenance, and repair. On the basis of this analysis each area should be defined as requiring a certain average number of hours access per day, and the radiation level of that area should be set accordingly.

5.2 Average Power Level of Reactor Operation

Advantage can be taken of the fact that many reactors do not operate continuously at full power and that the radiation dosages can be averaged over a 13-week period. The anticipated operation of the reactor should be carefully analyzed to determine the average power level at which the reactor will operate. A conservative average power level, and not full power, should be used as a basis for shield-design specifications. It is important that this approach be applied in a realistic, and not an optimistic, manner. The shield should be designed so as not to place operational restrictions on the reactor plant. Personnel should be able to perform normal operational or maintenance duties with no concern about possible overirradiation.

The following example illustrates the application of the above principles: A reactor shield is being designed to protect personnel from radiation while they are working on associated steam-plant equipment. On the basis of an 8-hr working day, 7-day working week, and with the reactor continuously at full power, the radiation level at the surface of the shield should be 300 mrem/56 hr or 5.3 mrem/hr. However, after an analysis of the operational and maintenance requirements of specific equipment in an area near the shield, it is concluded that operating personnel require a conservative average of 4 hr access per day, 5 days a week, to the area. The shielding can be reduced therefore to permit an increase in radiation level in the area to 300 mrem/20 hr rather than 56 hr, or a level of 15 mrem/hr.

Further analysis of the operational use of the plant indicates that the reactor will run at an average power level of 50 per cent of full power. The full-power radiation level in the steam-plant area should therefore be increased by an additional factor of 2, to 30 mrem/hr. Considerable reduction in shielding requirements is thus achieved through use of these techniques, without increasing the danger of overirradiating operating personnel.

6 SPECIAL PROBLEM OF LOCAL RADIATION STREAMING

Frequently the structural requirements of the shield are such that structural members or other material causes streaming paths through the shield which produce isolated peaks of higher levels of radiation on the shield surface. The policy in the naval reactors program has been to ignore the local effect of streaming path if the peak of the radiation level is less than 7 times the surrounding field of radiation, providing the total area having such peaks does not exceed 1 per cent of the total shield surface. Levels above this factor of 7 require additional shielding in the form of shielding "blisters" or patches. This approach has been successful from the point of view of personnel exposure. Radiation streaming is discussed in further detail in Chap. 8.

REFERENCES

1. Nuclear Data, Natl. Bur. Standards, Circ. 499, Dept. of Commerce, U. S. Government Printing Office, 1950.
2. Natl. Bur. Standards Handbooks: No. 52, Maximum Permissible Amounts of Radioisotopes in the Human Body and Maximum Permissible Concentrations in Air and Water; No. 59, Permissible Dose from External Sources from Ionizing Radiation; No. 61, Regulation of Radiation Exposure by Legislative Means.

28
IS
BLANK

FRONT
IS -27-

Chapter 3

SHIELDING THE REACTOR CORE

INTRODUCTION 31

1 FULL-POWER CORE SOURCE ESTIMATES 32
- 1.1 Fission Sources 32
  - (a) Prompt Neutrons 32
  - (b) Delayed Neutrons 32
  - (c) Prompt-fission Gammas . . 33
  - (d) Fission-product (Delayed) Gammas 34
- 1.2 Secondary Sources in the Core . . 39
  - (a) Gamma Rays Resulting from the Capture of Thermal Neutrons 39
  - (b) Gammas from Inelastic Scattering of Fast Neutrons . . 41
  - (c) Gammas from Activated Materials 44
  - (d) Photoneutrons 44
- 1.3 Sources Outside the Core . . . 44
  - (a) Gammas from Capture of Thermal Neutrons . . . 44
  - (b) Gammas from Inelastic Scattering of Fast Neutrons . . . 45
  - (c) Gammas from Activated Materials 45
  - (d) Photoneutrons 46
- 1.4 Relative Importance of the Various Sources 47

2 AFTER SHUTDOWN OF THE REACTOR . 47

3 ATTENUATION CALCULATIONS . . 48
- 3.1 Fast-neutron Attenuation . . . 48
  - (a) Attenuation of Fast Neutrons in Water 48
  - (b) Attenuation of Fast Neutrons in Mixtures of Water and Other Materials 58
- 3.2 Thermal-neutron-flux Distribution . 62
- 3.3 Geometry for Fast-neutron Attenuation 65
  - (a) Spherical Core and Shield . . 65
  - (b) Cylindrical Core and Shield . . 69
  - (c) Exponential Expression for Fast-neutron Attenuation in Hydrogenous Shield . . . 69
  - (d) Scaling Up Experimental Data . 70
- 3.4 Sources of Error 71
  - (a) Removal Cross Section of Core Materials 71
  - (b) Removal Cross Section of Shield Materials 74
  - (c) Effect of Core Size . . . 74
  - (d) Power Distribution in the Core . 74
  - (e) Effect of Laminations in Shields . 75
  - (f) Misuse of Removal Cross Sections 75

4 HEAT GENERATION IN SHIELDS . . 76
- 4.1 Introduction 76
- 4.2 Heat Generation by Core Gammas . 78
  - (a) Geometry 78
  - (b) Source 78
  - (c) Calculation of Gamma Flux . . 78
  - (d) Build-up Included . . . 79
- 4.3 Heat Generation by Gammas from Neutron Capture and from Inelastically Scattered Neutrons . . . 79
- 4.4 Heat Generation by Elastically Scattered Neutrons 80
  - (a) General Equations . . . 80
  - (b) Water-moderated Fast Flux . . 82

REFERENCES 83

30

15

Chapter 3

SHIELDING THE REACTOR CORE

INTRODUCTION

The reactor core is the most intense single radiation source in the entire reactor system. This extremely high intensity of both gamma and neutron radiation makes the core-shield design a special problem in itself. On the other hand, the core shield cannot be isolated from the rest of the shield design. In fact, the attenuation requirements of the core shield are often determined (in order to achieve a balanced total shield design) by the intensities of other sources in the reactor system, particularly the coolant sources. This chapter discusses in detail the problems specific to the design of the core shield once the role of the core shield in relation to the complete shield has been established. The problem of establishing how much of the overall attenuation should be provided by the core shield is discussed in Chap. 5. Two conditions are examined below, namely, full-power operation and after shutdown. The areas of access are generally different for the two cases, and therefore the two problems are in most cases quite different. The shutdown case is discussed more thoroughly in Chap. 7.

The final design of the primary shield is based on the condition that is controlling. In the design of the Submarine Advanced Reactor (SAR) primary shield, for example, the after-shutdown condition has controlled the amount of gamma shielding on the primary shield. The general procedure that should be followed to establish the core-shield design is outlined as follows:

1. The *intensities* and *distribution* of the various sources arising in the core must be determined (Secs. 1.1 and 1.2).
2. The *secondary sources* that arise *outside the core* itself must be determined. In the case of the design of the primary shield of the Submarine Thermal Reactor (STR), the gamma rays due to thermal-neutron capture in the pressure vessel and inner wall of the neutron shield tank proved to be one of the main sources of gamma rays during power operations. This type of source is discussed in Sec. 1.3.
3. After all existing materials in the reactor, reflector, and structure are taken into account, the additional shield *material required outside the reactor* proper must be chosen. The configuration and thickness of these materials must be chosen with three (often conflicting) ideas in mind:
   a. The maximum attenuation of both neutrons and gamma rays must be achieved. At the same time the creation of secondary radiation sources must be kept low with regard to both intensity and energy.
   b. The shield weight, volume, and/or cost must be kept at a minimum.
   c. The configuration has to be something that can be constructed, for example, a large number of laminations would be abandoned for a simpler shield if the increased material requirement were reasonable.

4. The preceding three steps have to be *considered both for full-power operation* and its specifications and *for after shutdown* and the corresponding specifications. For example, in the design of the SAR shield, a dose-rate tolerance during full-power operation was specified outside the secondary shield, whereas the after-shutdown specification gave a required dose-rate tolerance on the surface of the primary shield. The final shield design will be based on the condition that is controlling.

The preceding stepwise description is somewhat oversimplified. In an actual design problem knowledge of at least the qualitative features of each step in the design is required before any effective solution of the problem can be started. Therefore an auxiliary purpose of the subsequent discussion is to establish these qualitative features of the core design as background for the more detailed quantitative design problem.

1 FULL-POWER CORE-SOURCE ESTIMATES

1.1 Fission Sources

(a) Prompt Neutrons. For each fission of a U^{235} nucleus, an average of 2.5 neutrons is given off. The spectrum of the fission neutrons has been measured quite completely. Figure 3.1 shows good analytical fit[1] to the experimental data, given by

$$N(E)\,dE = \sqrt{2/\pi e}\,\sinh\sqrt{2E}\,e^{-E}\,dE \quad \text{neutrons/fission neutron} \tag{1}$$

where N(E) is the number of neutrons per fission neutron in the energy range from E to E + dE. An approximate fit, useful in certain applications where only the high-energy neutrons are important, is

$$N(E)\,dE = \text{constant}\;e^{-0.72E}\,dE \qquad (\text{for } E = 4 \text{ to } 12 \text{ Mev}) \tag{2}$$

(b) Delayed Neutrons. Delayed neutrons are sufficiently few in number that they can be computed from the available yield data. Their intensity, as a function of time after fission, per fission per second is

$$N_{DN} = y_n \lambda_n e^{-\lambda_n t} \quad \text{neutrons/fission-sec}$$

where y_n is the total yield of neutrons with a disintegration constant of λ_n. Table 3.1 gives the yield, half life, and energy for each of the known delayed-neutron emitters for several fissionable materials. If allowance is made for minor groups not included in the table, the total percentage of fission neutrons which is delayed is about 0.25 per cent for U^{233}, 0.75 per cent for U^{235}, and 0.38 per cent for Pu^{239}.

Table 3.1—DELAYED NEUTRONS FROM THERMAL FISSION*

	Absolute yield, % of total fission neutrons			Half life, sec	Energy, kev
	U^{235}	U^{233}	Pu^{239}		
	0.025	0.018	0.014	55.6	250
	0.166	0.058	0.105	22.0	570
	0.213	0.086	0.126	4.51	412
	0.241	0.062		1.52	670
	0.085	0.018	0.119	0.43	400
Total	0.730	0.242	0.364		

*Data taken from Samuel Glasstone, "Principles of Nuclear Reactor Engineering," Table 2.11, p. 113, D. Van Nostrand Co., Inc., New York, 1955. (Geneva Paper 831 gives later 6-group data for U^{235} only.)

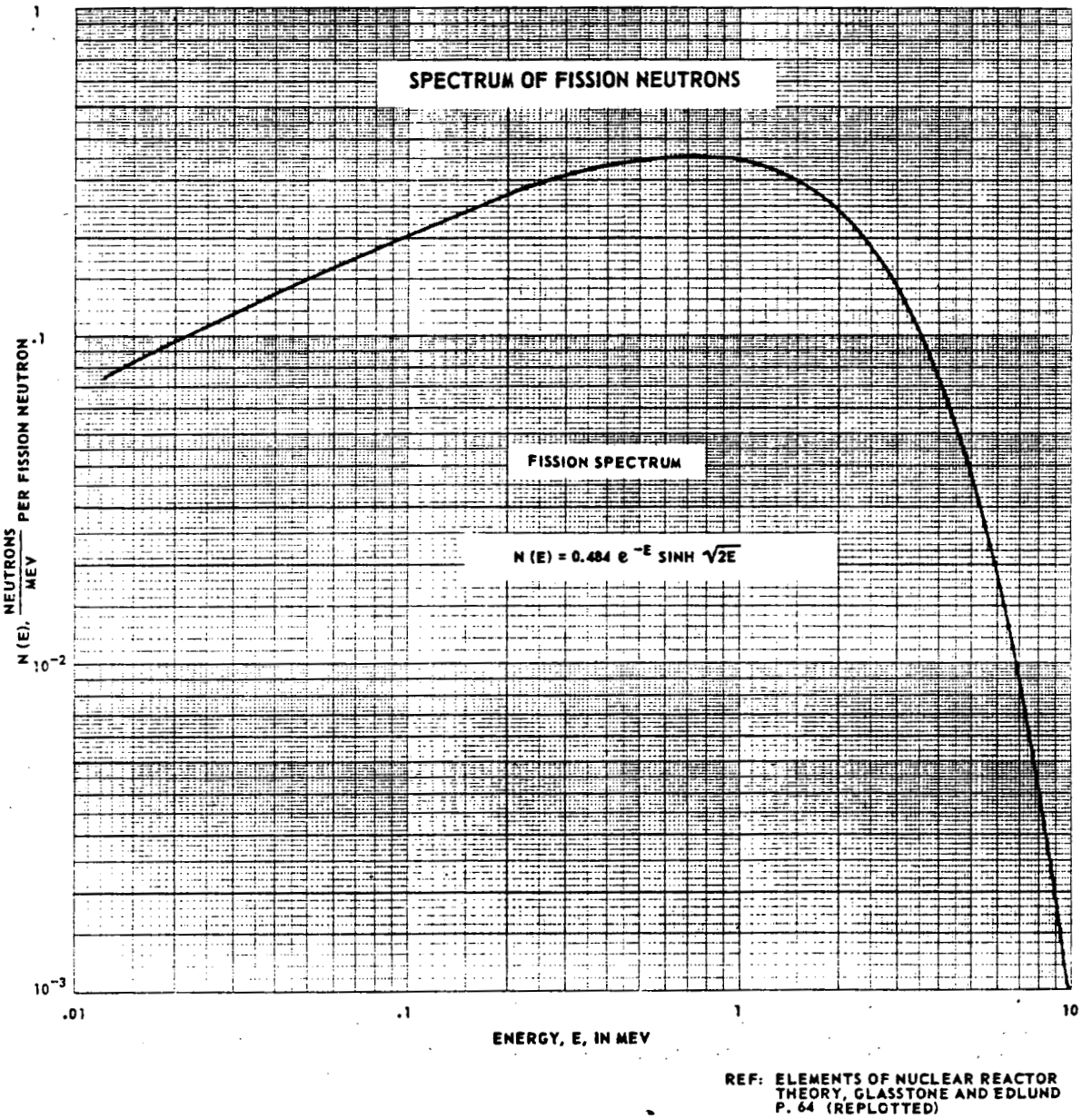


Figure 3.1

Since the half lives of the delayed-neutron emitters are so short, they reach equilibrium during any period of practical reactor operation, and thus their source strength in a U^{235} core is

$$N_{DN} = 7.5 \times 10^{-13}\, P(\vec{r})\, y_n e^{-\lambda_n t_s} \quad \text{neutrons/cm}^3\text{-sec}$$

where $P(\vec{r})$ is the power distribution in the reactor core in watts per cubic centimeter and t_s is time after reactor shutdown.

From a shielding standpoint, generally speaking, these neutrons are unimportant compared to the prompt-fission neutrons.

(c) Prompt-fission Gammas. The latest information on prompt gamma rays from the fission process is that reported by Gamble and Bell.[2] Table 3.2 summarizes the data in terms of gammas per fission in discrete energy ranges.

Table 3.2—GAMMAS PER FISSION IN VARIOUS ENERGY RANGES

Energy, Mev	Photons/fission in the ½-Mev range centered on this energy	N(E) photons/fission at E Mev/photon*
½	3.1	3.2 at 1 Mev
1	1.9	
1½	0.84	0.8 at 1.5 Mev
2	0.55	0.85 at 2.3 Mev
2½	0.29	
3	0.15	0.15 at 3 Mev
3½	0.062	0.2 at 5 Mev
4	0.065	
4½	0.024	
5	0.019	
5½	0.017	
6	0.007	
6½	0.004	
Total	7.0 photons/fission	
	7.8 Mev/fission	7.8 Mev/fission

*Possible grouping to reduce total number of sources considered.

Table 3.3—ENERGY GROUPS

Group	Energy range, Mev/photon
I	0.1–0.4
II	0.4–0.9
III	0.9–1.35
IV	1.35–1.8
V	1.8–2.2
VI	2.2–2.6
VII	2.8

The intensity of these radiations is estimated readily from the power-density distribution in the core. Thus, if the power density is $P(\vec{r})$ in watts per cubic centimeter, the intensity of the prompt-fission source radiation is (at 3.1×10^{10} fissions/watt-sec)

$$N_{PN} = 7.75 \times 10^{10}\ P(\vec{r})\ \text{prompt neutrons/cm}^3\text{-sec}$$

$$N_{P\gamma} = 3.1 \times 10^{10}\ N(E)\ P(\vec{r})\ \text{prompt gamma photons/cm}^3\text{-sec at energy E Mev/photon}$$

(d) Fission-product (Delayed) Gammas. The exact determination of the source of gamma rays presented by the fission products is rather complex. Owing to the extremely large number of isotopes formed by the fission process, it is impractical for the shield designer to consider a detailed determination of the gamma-ray sources considering each isotope and its decay scheme. However, this has been studied in detail, and the results have been presented in references 3, 4, 46, and 47. In these reports the fission products resulting after certain reactor operating times (10, 100, 1000, and ∞ hr of operation) have been grouped into the discrete energy groups given in Table 3.3.

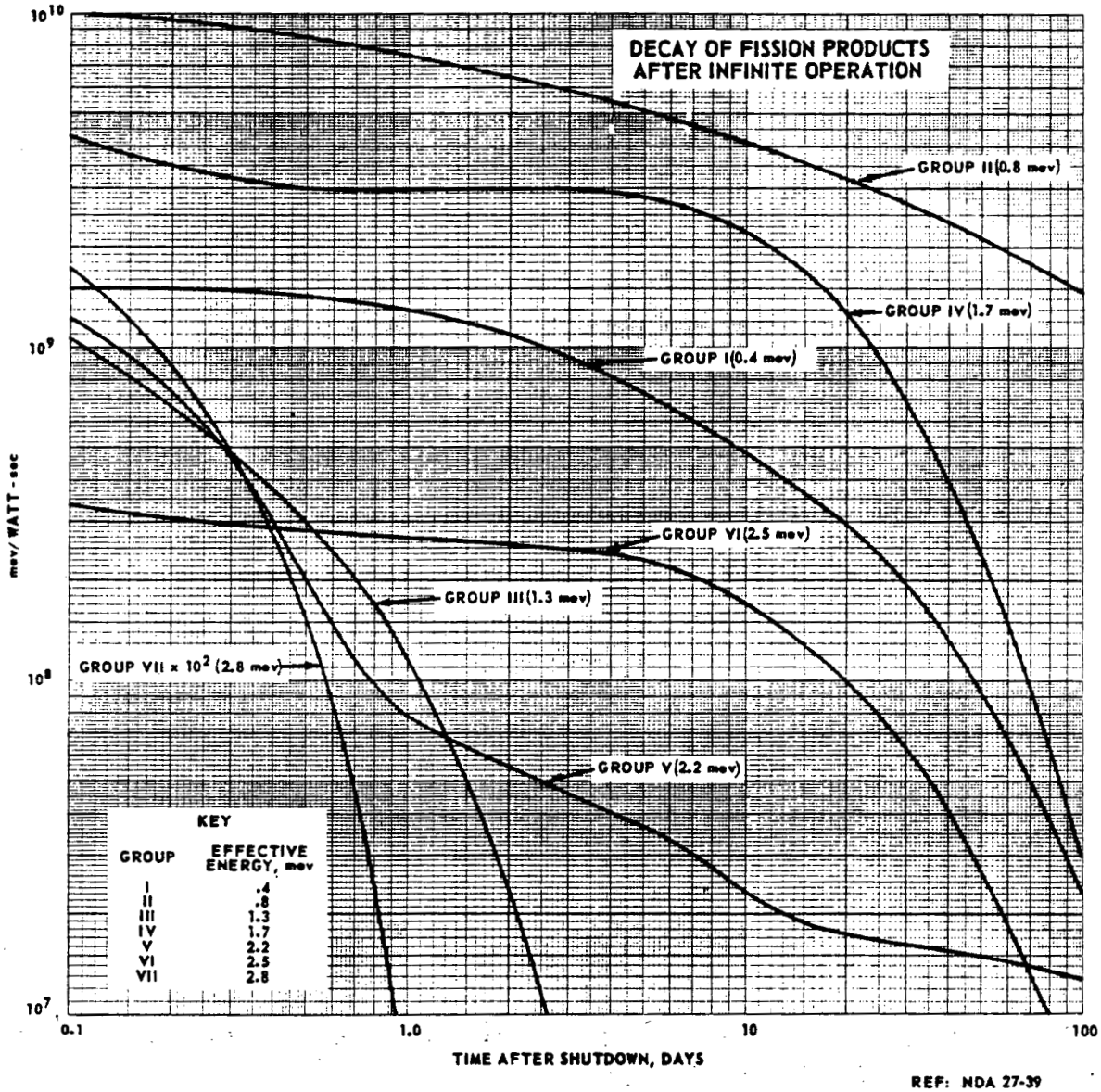


Figure 3.2a

The data are presented in terms of Mev/watt-sec as a function of time after shutdown. Figure 3.2a gives the curves for each of the energy groups for infinite reactor operation, along with a suggested effective energy to use with each group. Figure 3.2b gives the contribution of each group as a function of time after shutdown. Sources resulting from finite-time operation can be obtained from the curves for infinite power operation. A discussion of a method for doing this follows.

In references 5 and 6 the experimental curve of the rate of gamma-energy release per fission has been fitted by the following equation, for convenience in computation:

$$\Gamma(t) = \sum_{j=1}^{n} A_j e^{-\lambda_j t} \qquad (3)$$

where $\Gamma(t)$ is in Mev/sec-fission and t is the time after fission in seconds. A_j and λ_j are given in Table 3.4.

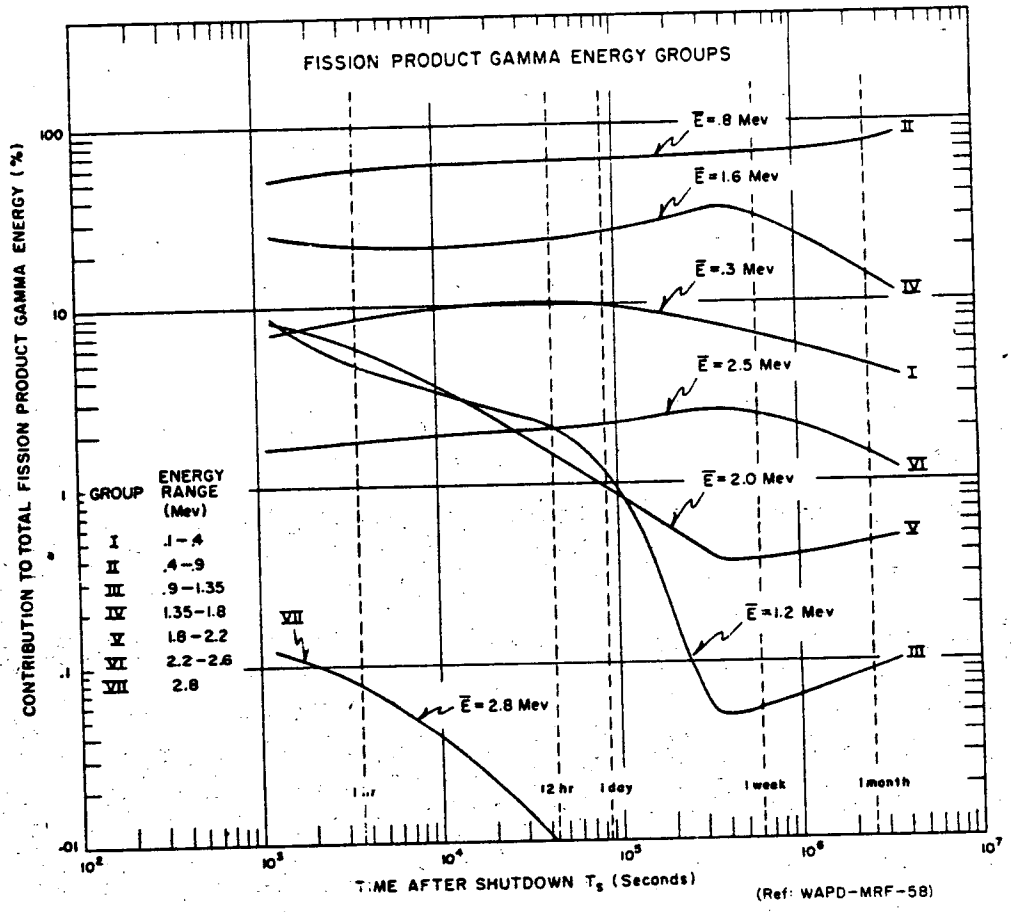


Figure 3.2b

Table 3.4—EXPONENTIAL FIT OF GAMMA FISSION PRODUCT ACTIVITY

j	A_j, Mev/sec-fission	λ_j, sec^{-1}	A_j/λ_j, Mev/fission
1	6.2×10^{-1}	7.55×10^{-1}	0.82
2	2.08×10^{-1}	1.17×10^{-1}	1.78
3	3.67×10^{-2}	2.43×10^{-2}	1.51
4	3.00×10^{-3}	4.19×10^{-3}	0.716
5	7.0×10^{-4}	1.12×10^{-3}	0.624
6	1.22×10^{-4}	2.03×10^{-4}	0.601
7	6.05×10^{-6}	1.59×10^{-5}	0.380
8	4.2×10^{-7}	2.29×10^{-6}	0.183
9	5.55×10^{-8}	5.63×10^{-7}	0.0986
10	1.50×10^{-8}	3.93×10^{-8}	0.382
		Total	7.095

If the reactor has been operating for a time T_0 (in seconds) at a constant fissioning rate, i.e., constant power level, the rate of gamma-energy release per unit volume of core may be found in the following way.

Let K be the number of fissions per cm^3-sec during operation.

$$K = 3.1 \times 10^{10} \frac{P}{V} \quad \text{fissions/cm}^3\text{-sec} \tag{4}$$

where P is the power of the core in watts and V is the active volume of the core in cubic centimeters.

Then the number of fissions per cubic centimeter occurring in a time dt is K dt. The rate of energy release at a time t after fission has occurred is

$$\Gamma(t)\, K\, dt \quad \text{Mev/cm}^3\text{-sec} \tag{5}$$

Integrating over the operating time, the total rate of gamma energy release, $E_\gamma(T_0,T_S)$, as a function of the operating time and the time after shutdown is

$$E_\gamma(T_0,T_S) = K \int_{T_S}^{T_0+T_S} \Gamma(t)\, dt \quad \text{Mev/cm}^3\text{-sec} \tag{6}$$

where t is greater than 10 sec, T_0 is the operating time in seconds, and T_S is the time after shutdown in seconds.

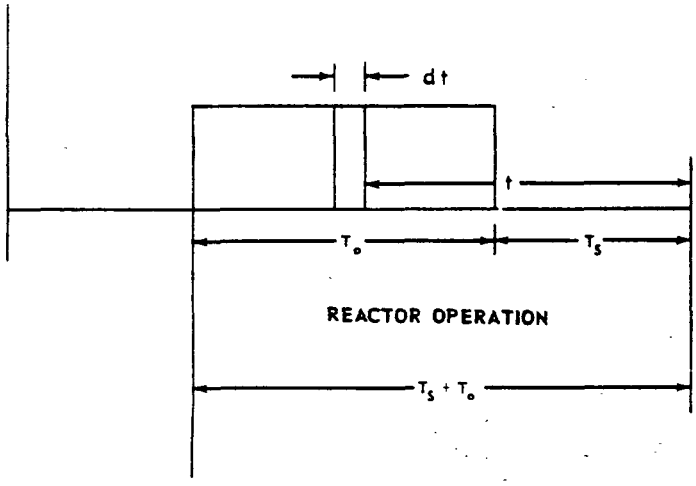


Figure 3.3

The region of integration is depicted in Fig. 3.3.

Integration of Eq. 6 gives

$$E_\gamma(T_0,T_S) = K \int_{T_S}^{T_0+T_S} \sum_{j=1}^{n} A_j e^{-\lambda_j t}\, dt$$

$$= K \sum_{j=1}^{n} \frac{A_j}{\lambda_j} \left[e^{-\lambda_j T_S} - e^{-\lambda_j (T_0+T_S)}\right] \tag{7}$$

In the limit for $T_0 \to \infty$,

$$E_\gamma(\infty,T_S) = K \sum_{j=1}^{n} \frac{A_j}{\lambda_j} e^{-\lambda_j T_S} \tag{7a}$$

Note that from Eqs. 7 and 7a the following results:

$$\boxed{E_\gamma(T_0,T_S) = E_\gamma(\infty,T_S) - E_\gamma(\infty,T_0 + T_S)} \tag{8}$$

Thus, having the curve of $E_\gamma(\infty,T_S)$ for fission-product decay after infinite operation (Fig. 3.2a), the sources after any finite time of reactor operation, T_0, can be found by Eq. 8.

The foregoing discussion deals predominantly with the fission products as a source of gamma rays after shutdown. However, it can be seen from Eq. 7 that during reactor operation, after operation for a time T_0 (greater than 10 sec), the contribution to the gamma-ray sources in the core from these is given by

$$E_\gamma(T_0,0) = K \sum_{j=1}^{n} \frac{A_j}{\lambda_j}(1 - e^{-\lambda_j T_0}) \tag{9}$$

In a manner similar to Eq. 8, this can be expressed as

$$E_\gamma(T_0,0) = E_\gamma(\infty,0) - E_\gamma(\infty,T_0) \tag{10}$$

or

$$\boxed{E_\gamma = 7.095K - E_\gamma(\infty,T_0) \quad \text{Mev/cm}^3\text{-sec}} \tag{10a}$$

The source strengths during operation resulting from fission products can be deduced from the curves in Fig. 3.2a by the use of Eq. 10a. These curves are not valid for short times. (less than 30 min) after reactor operation, and extrapolations are not too accurate. However, during operation other radiation sources are generally more important. Therefore an upper limit of the delayed-fission gammas during operation may be found by the method suggested below (see also nomograph in Chap. 10, Sec. 5).

Table 3.5 gives the extrapolated values of the $E_\gamma(\infty,0)$ taken from Fig. 3.2a. The sum of all groups adds up to

$$2.18 \times 10^{10} \quad \text{Mev/watt-sec}$$

as compared with

$$7.095 \times 3.1 \times 10^{10} = 2.2 \times 10^{11} \quad \text{Mev/watt-sec}$$

which the first term of Eq. 10a suggests as a total for all energy groups.

The Wigner-Way formula[7] gives the gamma power from fission products for times after 10 sec after shutdown. This is

$$\text{Gamma power} = 0.0315P\,[t^{-0.2} - (t + t_0)^{-0.2}] \qquad \text{for } t > 10 \text{ sec}$$

where P is the operating power of the reactor in the same units as the gamma power, t is time after shutdown in seconds, and t_0 is operating time in seconds.

For long operating times this yields a gamma power of 0.0199 watt per watt of reactor power at 10 sec after shutdown or, since 1 Mev = 1.6×10^{-13} watt-sec, 1.24×10^{11} Mev/watt-sec. This agrees well with that obtained from Eq. 8.

The dominant group of photons emitted is in the region near 0.75 Mev, although some are known to be emitted up to 3.0 Mev. These higher energy photons are probably relatively more prominent at short decay times (see Fig. 3.2b). With this information the extrapolations from Fig. 3.2a in Table 3.5 are increased to give a total of 2.2×10^{11} Mev/watt-sec. This gives

an idea of the energy distribution at zero decay time. Weighting this spectrum somewhat toward the higher energy gamma components, it can be used as a probably pessimistic source term for fission-product gammas during reactor operation.

Table 3.5 — FISSION PRODUCTS DURING OPERATION

Fission-product groups	$E_\gamma(\infty,0)$,* Mev/watt-sec	$E_\gamma(\infty,0)$,† Mev/watt-sec
I	1.8×10^9	2.0×10^{10}
II	1.2×10^{10}	1.2×10^{11}
III	2.2×10^9	2.0×10^{10}
IV	3.3×10^9	3.3×10^{10}
V	2.1×10^9	2.1×10^{10}
VI	4×10^8	9×10^9
VII	3×10^7	1×10^9
Totals	2.18×10^{10}	2.28×10^{11}

*Extrapolated from Fig. 3.2a.

†Adjusted values to be used as sources (arbitrary adjustment as discussed in text).

1.2 Secondary Sources in the Core

(a) Gamma Rays Resulting from the Capture of Neutrons. Determining the Neutron Flux. To determine the capture-gamma source distribution in the core, the following data must be known: the neutron-flux distribution throughout the reactor-core volume, $\phi(E',\vec{r})$, and the spectral distribution of these capture gamma rays, f(E). Thus the capture-gamma source distribution can be written

$$S_{\gamma c}(E,\vec{r}) = \int_0^\infty \Sigma(E')\,\phi(E',\vec{r})\,f(E)\,dE' \qquad (11)$$

where E is the gamma energy and E′ is the neutron energy.

The neutron-flux distribution is a characteristic of the specific core design. Figures 3.4 and 3.5 are typical radial thermal-neutron-flux plots in a water-cooled water-reflected core with uniformly distributed materials. The first plot shows the flux distribution in a region unaffected by absorbing control rods; the second shows the distribution in a region affected by rods. The plots reveal two aspects of the calculation of a secondary core source distribution:

1. The detailed source distribution in a core is generally quite complicated and rapidly varying. To take these variations into account, very cumbersome numerical procedures would have to be employed, but, as will be shown later, the self-absorption in the core makes it necessary to treat in detail only the region of the core near its surface.
2. The flux level in the region near the surface of a core is often significantly different from the average value in the core. Thus the average power level must often be weighted by a peak-to-average power factor, which characterizes the surface power density. In the typical case given in Fig. 3.5, this peak-to-average factor is approximately 2. In other core designs it is quite possible that the value would be much less than 1 for the core surface.

Thermal-neutron-capture Cross Sections and Spectrum. Table 3.6 contains a list of the common elements giving the cross section for thermal-neutron capture, along with the number and energy of gamma photons resulting.[8] For example, iron with a 2.43 barn/atom cross section has an average of 170 photons given off per 100 captures. The gamma spectrum is as follows:

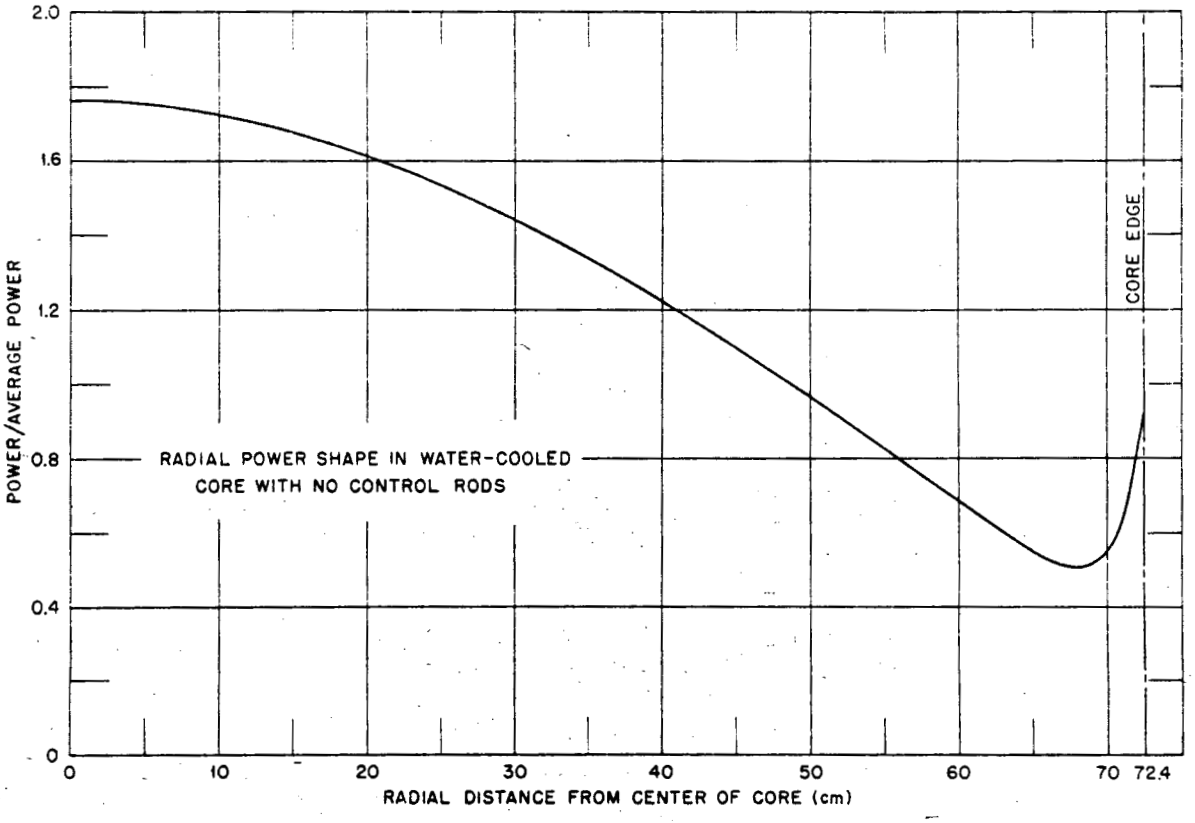


Figure 3.4

50 photons between 7 and 10.16 Mev
22 photons between 5 and 7 Mev
24 photons between 3 and 5 Mev
~10 photons between 1 and 3 Mev, and the rest, or approximately 64 photons, less than 1 Mev

The thermal-neutron capture-gamma spectrum is divided into three classes. These are referred to in Table 3.6 under spectral type. They are as follows:

1. The ground-state transition is dominant. Most of the de-excitation energy is carried off by gamma rays having energies of 6 to 8 Mev.
2. Gamma rays of many energies are present.
   a. A distinct line structure is evident.
   b. No distinct line structure is present except at energies above 4 to 5 Mev.
3. The gamma rays are weak or nonexistent owing to competing methods of de-excitation, i.e., particle emission.

The gamma-ray source is given by

$$S = N\sigma\phi$$

where S = the resulting source in photons/cm^3-sec
N = the number of nuclei per cubic centimeter of a particular element in the material in which the thermal-neutron capture is taking place
σ = the microscopic cross section in barns per nucleus, which gives the probability of the (n,γ) reaction which will give the gamma ray
ϕ = thermal-neutron flux in neutrons/cm^2-sec

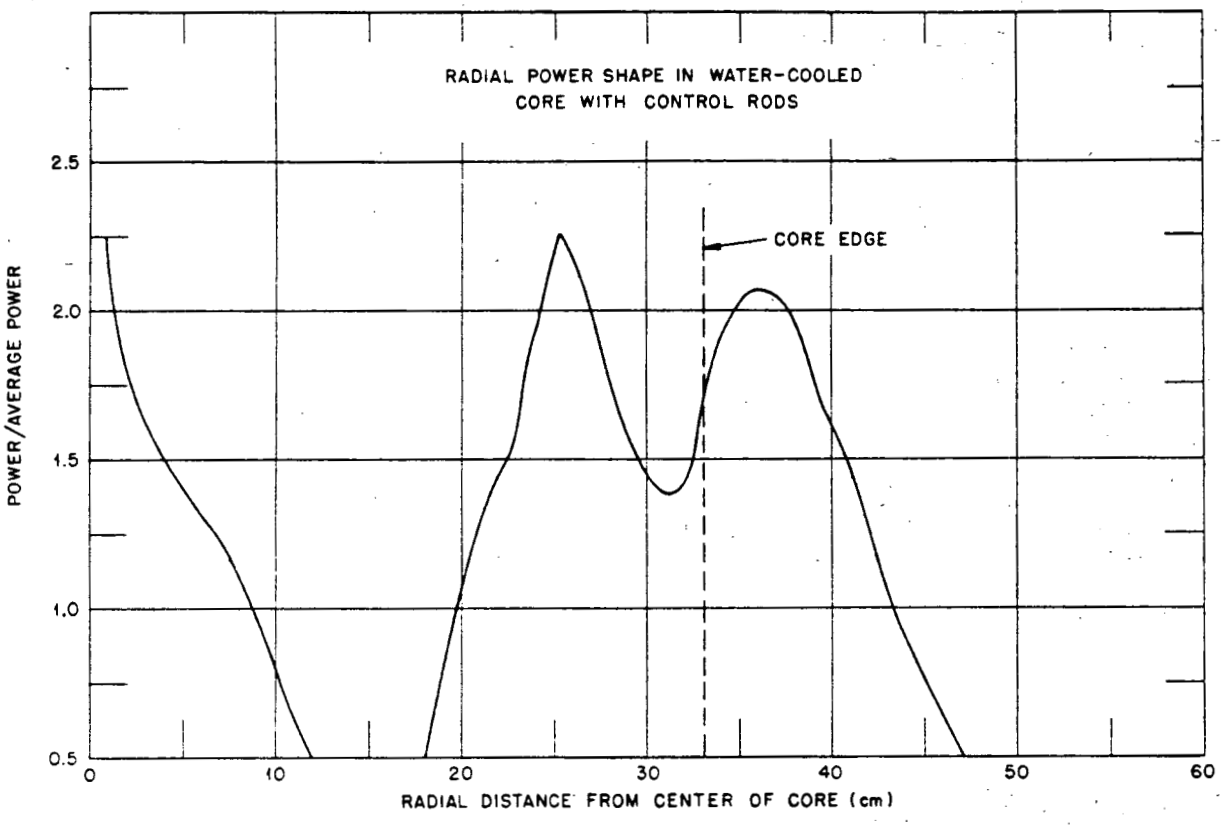


Figure 3.5

Thus the spatial distribution of the capture-gamma-ray source is the same as that of the thermal-neutron flux.

Various cross sections are encountered by the shield designer, and a word of clarification at this point may be helpful. The *capture cross section* gives the probability that a nucleus will capture a thermal neutron. This is often called the *absorption cross section*. On the other hand, an *activation cross section* gives the probability that a certain active nucleus will be formed. In most cases the activation cross section is the same as the absorption or capture cross section. However, in a few instances, such as that of Co^{59}, it is not; the capture or absorption cross section for the formation of Co^{60} is 34 barns. However, the activation cross section for the formation of the 11-min half-life form of Co^{60} is 14 barns, whereas that for the formation of the 5.2-year form is 20 barns.

(b) Gammas from Inelastic Scattering of Fast Neutrons. The *inelastic-scattering source* distributions require data similar to those needed for the capture of gamma ray determination, i.e., neutron-flux distribution, inelastic cross section, and emission spectrum. The inelastic gamma source distribution takes the same form as Eq. 11.

Flux Distribution. The flux distribution required is, of course, that for energies above the inelastic thresholds. This quantity is not a typical core characteristic as is the thermal flux or power density, and therefore it very often must be computed by the shield designer. Often the intensity of the gamma source from inelastic scattering of fast neutrons is not great enough, nor is the microscopic data good enough, to warrant detailed calculation of this flux distribution. High-energy-flux distributions are often needed for threshold activation estimates. A method of determining such a distribution is described in Chap. 4, Sec. 2.3 (see also reference 33).

Table 3.6—GAMMA RAYS RESULTING FROM NEUTRON CAPTURE

Target element	Thermal-neutron (n,γ) cross section, barns	Spectral type*	Number of photons emitted per 100 captures in the designated energy intervals†					Highest energy gamma ray	Av. no. of photons per capture[25]	Fraction S of available energy emitted by gamma rays[31] with energy >E_m		References	Remarks
			0–1 Mev	1–3 Mev	3–5 Mev	5–7 Mev	>7 Mev			E_m	S		
Al^{27}	0.215	1	?	>13	77	21	35	7.724	~2	2.5	0.78	12	In addition, the decay of Al^{28} (2.3min) yields one 1.80-Mev photon/capture
Be^{9}	9.0‡	1	0	0	50	75	0	6.814					
B^{10}	3390	3	0	0	0	0	0	0.478				28	The decay of B^{11} (fast) yields ninety-four 0.478-Mev gammas/100 B^{10} captures
Bi^{209}	15‡	1	0	0	100 (4.17 Mev)	0	0	4.17				20	
Calcium	0.406	2a	?	50	60	101	2.4	7.83		2.6	0.80	11, 19	
C^{12}	4.5‡	1	?	<30	100	0	0	4.95	1.3	3.68	0.93	13, 29	
(Cd^{113})	19,500	2b	>120	20	73	17	1	9.05	4.1			14, 23, 24, 26, 30, 32	
(Co^{59})	34.8	2a	?	?	36	49	8	7.486		2.5	0.67	10, 30	In addition, the decay of Co^{60} (5.3y) yields one 1.17-Mev and one 1.33-Mev gamma/capture
(Chromium)	2.9	1	>37	16	12	18	69	9.716	2	2.8	0.73	9, 19	
(Copper)	3.59	1	?	?	>23	22	42	7.914	2.6	3.4	0.67	10	
Chlorine	32	2a	?	20	13	18	21	8.56	3.1	3.3	0.26	11, 15, 21, 30	
F^{19}	9‡	1	?	?	?	35	0	6.63				9	In addition, the decay of F^{20} (12sec) yields one 1.63-Mev gamma/capture
H^{1}	0.330	1	0	100 (2.230 Mev)	0	0	0	2.230				27	
(Iron)	2.43	1	?	<10	24	22	50	10.16	1.7			9, 16	
Lead	0.17	1	0	0	0	7 (6.73 Mev)	93 (7.38 Mev)	7.38				20	
Li^{6}	910	3	0	0	0	0	0	0				28	
Magnesium	59‡	2a	?	>59	110	25	11	9.216		2.6	0.99	12, 19	In addition, the decay of Mg^{27} (9.58min) yields ten 0.84-Mev and two 1.01-Mev/100 captures

(Mn^{55})	12.6	2a	?	?	>27	30	27	7.261	2.6	3.5	0.64	10, 17, 18	In addition, the decay of Mn^{56} yields, per 100 captures, one-hundred 0.845-Mev gammas; twenty-five 1.81-Mev gammas; and fifteen 2.13-Mev gammas
Mercury	380	2b	?	?	82	40	0	6.4	3.3			32	
(Molybdenum)	2.4	2b	?	?	84	26	3	9.0				32	
Nickel	4.8	1	?	?	>14	30	72	8.997		3.4	0.95	9	
Niobium	1.1	2b	?	?	54	14	0	7.0	2.6			32	
N^{14}	0.1	2a	?	<5	<35	90	39	10.8				29	
Potassium	1.89	2a	?	36	36	32	12	9.28		3.00	0.48	11, 19	
P^{31}	0.193	2a	?	?	115	43	11	7.94		2.5	0.66	11	
(Sc^{45})	22	2b	?	?	63	29	14	8.85				10	In addition, the decay of Sc^{46} (85d) yields one 1.12-Mev and one 0.89-Mev gamma/capture
Silicon	0.160	2a	?	>100	229	41	16	10.55		2.5	1.44	12, 19	
Na^{23}	0.47	2a	≈100	>50	61	29	0	6.41	.2			12, 21, 22	In addition, the decay of Na^{24} (14.9hr) yields one 2.758-Mev and one 1.380-Mev gamma/capture
Sulphur	0.49	2a	≈	>19	80	91	8	8.64		2.7	0.76	11	
(Tin)	0.65	2b	?	?	139	33	4	9.3				32	
(Titanium)	5.8	2a	50	100	33	99	10	9.39		2.4	1.02	9, 21	
(Tungsten)	19.2	2b	?	?	53	14.5	0.5	7.42				32	
(V^{51})	4.7	2b	?	?	24	54	18	7.305	2.5	2.6	0.82	10	In addition, the decay of V^{52} (3.74min) yields one 1.46-Mev photon/capture
(Zinc)	1.06	2a-b	?	?	48	29	17	9.51		2.8	0.60	9	In addition, the decay of Zn^{65} (250d) yields twenty-five 1.12-Mev photons/100 captures in natural Zn
(Zirconium)	0.18	2b	?	?	113	35	4	8.7				32	In addition, the decay of Zr^{95} (65d) yields ≈ ten 750-Mev gammas/100 captures in natural Zr. Capture-gamma intensities given for Zr may be off by 50%

• See Sec. 1.2a for discussion.

† Except for those elements and isotopes in parentheses in column 1, only the intensity of the resolved lines in the gamma-ray spectrum is included.

‡ Millibarns.

Cross Sections and Spectrums. Cross-section and spectral data are considerably more sketchy than those in the capture-gamma-ray case. The data available are comparatively new, but a good bibliography of cross-section and spectral information is given in reference 34. Most of the spectral data available are characteristic of multiple transitions from level to level, with relatively few direct transitions to the ground state. This feature, plus the fact that the maximum gamma-ray energy can be only the difference between the ground state and the kinetic energy of the colliding neutron, makes a typical inelastic gamma-ray spectral distribution shift toward relatively low energies (of the order of 1 Mev).

(c) Gammas from Activated Materials. Another source for core shielding is that arising from unstable nuclei formed in the core, in shield materials, and in the coolant, chiefly through neutron capture. These sources will not be included in this discussion of core sources since they are generally negligible in the core. During reactor operation the fission gammas and neutrons are far more important, and after shutdown the induced activities are generally secondary to the fission-product radiations. Induced activities are, of course, important in the coolant when they are transported from the core. They are also important in the core container after removal of the core, as well as in the shield after shutdown.

The problem of the calculation of induced activities in the structural steel of the shield is discussed in Sec. 1.3.

(d) Photoneutrons. Photoneutron sources are relatively unimportant in shield design during power operation. They enter the core-shield-design problem principally in evaluating the neutron flux during removal of the core (to determine the extent of neutron shielding required on the fuel-removal coffin) and after shutdown (to ascertain the lowest neutron level that start-up instruments must see). Actually, even in these cases, the neutrons that escape the core are fission neutrons that have been produced through multiplication of the photoneutrons. Thus a complete study of this source problem utilizes methods more proper to nuclear reactor core design than to shield design.

Only a review of the photoneutron source data will be given in this section. The photoneutron source distribution is

$$S_{PN}(\vec{r},E) = \int_{E_T}^{\infty} \Sigma_p(E')\ \phi_\gamma(\vec{r},E')\ f(E)\ dE' \tag{12}$$

where $\Sigma_p(E')$ is the cross section for a (γ,n) reaction as a function of gamma-ray energy E' in million electron volts per photon, $\phi_\gamma(\vec{r},E')$ is the gamma-ray flux as a function of energy and position, and $f(E)$ is the neutron spectrum. Thus, given the dependence of the cross section with energy and the energy threshold, the problem consists in determining the gamma-ray distribution in space and energy above the threshold E_T. The threshold energies for (γ,n) reactions in light materials are as follows:

Beryllium	1.67 Mev
Deuterium	2.23 Mev
O^{17}	4.14 Mev
C^{13}	4.95 Mev
Li^{6}	5.50 Mev

The problem is analogous to the inelastic gamma source problem discussed previously. Uncollided flux calculations, taking the same form as Eq. 11, yield fairly reasonable approximations for $\phi_\gamma(\vec{r},E')$. Correction for multiple scattering can be included by utilizing the gamma-ray build-up data to improve the approximations.

1.3 Sources Outside the Core

(a) Gammas from Capture of Thermal Neutrons. During full-power operation there are gamma sources originating outside the core. The prime source in this group consists of gammas from capture of thermal neutrons in the structural material, such as the steel of the

pressure-vessel wall, and the water of the primary shield. The intensity of the source depends on the thermal-neutron-flux distribution out from the core, the thermal-neutron-capture cross section of the material, and the capture-gamma spectrum of the material. The capture cross section and gamma spectrum for various elements, including hydrogen, are listed in Table 3.6. The thermal-neutron flux through the shield can be calculated according to methods listed in Sec. 3.

The gamma sources originating from the capture of thermal neutrons and the activation of materials must be determined at specific points in the shield outside the core. These points are determined by the location of certain materials that give rise to these sources. It is necessary to be able to calculate the source strength at the interface of particular materials.

The gamma source (photons/cm^3-sec) at a source plane due to gammas born in the material is calculated by Eqs. 13 or 14.

$$S_{x=0} = \frac{I_{x=0}}{-2\Sigma}\left\{\ln\left|\frac{\mu-\Sigma}{\mu}\right| - e^{-\Sigma L}\,E_1(\mu L) + E_1[(\mu-\Sigma)L] - B\frac{\Sigma}{\mu-\Sigma}\left[1-e^{-(\mu-\Sigma)L}\right]\right\} \tag{13}$$

where $I_{x=0}$ is the gamma flux at x = 0 and the variation of the gamma-ray flux in the material is assumed to be the same as the variation of the neutron flux.

$$I = I_{x=0}e^{\Sigma x}$$

If the variation of the gamma-ray source in the material is defined by

$$I = I'_{x=0}e^{-\Sigma x}$$

then Eq. 14 should be used to determine source strength.

$$S_{x=0} = \frac{I'_{x=0}}{2\Sigma}\left\{\ln\left|\frac{\mu+\Sigma}{\mu}\right| - e^{-\Sigma L}\,E_1(\mu L) + E_1[(\mu+\Sigma)L] + B\frac{\Sigma}{\mu+\Sigma}\left[1-e^{-(\mu+\Sigma)L}\right]\right\} \tag{14}$$

The nomenclature for Eqs. 13 and 14 is defined as follows:

Σ = the reciprocal of the thermal-neutron relaxation length in the material (It is obtained by fitting experimental curves.)
μ = the gamma absorption coefficient in the material
B = the build-up factor (See Sec. 3.3 of Chap. 1.)
L = the thickness of the material
$I_{x=0}$ = the gamma source strength equal to $\Sigma_a\ \phi_{th}(x)$, where Σ_a is the activation cross section

$$E_1 = \int_b^\infty \frac{e^{-t}}{t} \times dt \qquad \text{(See Chap. 9)}$$

(b) Gammas from Inelastic Scattering of Fast Neutrons. The second source originating outside the core consists of the gammas from inelastic scattering of fast neutrons. This type of gamma source has been discussed in Sec. 1.2. It will only be noted here that since the gamma-ray spectrum for inelastic scattering is of relatively low energies, the intensity of the source will usually be greatly outweighed by the capture gammas in the region.

(c) Gammas from Activated Materials. The induced activities in the core shield, although lower in specific intensity than the residual activities in the core, can become an important after-shutdown source because their location is often in the outer portions of the shield. The distribution of these induced activities in most cases depends on the thermal-neutron-flux distribution during operation of the reactor and therefore can be determined from an equation similar to

$$A_i = \Sigma_i \phi_{th}(\vec{r})(1 - e^{-\lambda_i t_0})e^{-\lambda_i t_s} \tag{15}$$

where Σ_i = the macroscopic cross section for production of unstable isotope i (cm^{-1})
A_i = the average number of disintegrations of isotope i (dis/cm^3-sec)
λ_i = the disintegration constant of isotope i (sec^{-1}) = 0.693/half life in sec
t_0 = time of reactor operation (sec)
t_s = time after shutdown (sec)
$\phi_{th}(\bar{r})$ = thermal flux at operating power level P

A typical source of important induced activities in a core shield is the structural steel of the shield and the core container. Table 3.7 has been prepared to indicate the more important specific equilibrium-induced activities that will arise in stainless-steel structural elements

Table 3.7—EQUILIBRIUM-INDUCED ACTIVITIES IN TYPE 347 STAINLESS STEEL IN REACTOR-CORE SHIELD FOR UNIT THERMAL-NEUTRON FLUX

Reaction	Cross section, barns	Half life	Saturated specific disintegration rate, dis/cm^3-sec, A_i	Saturated gamma activity, gammas/cm^3-sec, dis rate × f(γ/dis)
$Mn^{55}(n,\gamma)Mn^{56}$	13	2.6 hr	2.3×10^{-2}	2.3×10^{-2} at 0.845 Mev 5.7×10^{-3} at 1.81 Mev 3.4×10^{-3} at 2.13 Mev
$Cr^{50}(n,\gamma)Cr^{51}$	11	26.5 days	6.8×10^{-3}	1.4×10^{-4} at 0.32 Mev
$Fe^{58}(n,\gamma)Fe^{59}$	0.36	46 days	4.8×10^{-5}	2.4×10^{-5} at 1.1 Mev 2.4×10^{-5} at 1.3 Mev
$Ta^{181}(n,\gamma)Ta^{182}$	21	117 days	4.0×10^{-4}	1.5×10^{-4} at 1.13 Mev 2.3×10^{-4} at 1.22 Mev
$Co^{59}(n,\gamma)Co^{60}$	20	5.2 years	5.6×10^{-4}	5.6×10^{-4} at 1.33 Mev 5.6×10^{-4} at 1.17 Mev

in a core shield when exposed to unit neutron flux. This table can be used in conjunction with the knowledge of $\phi_{th}(\bar{r})$ at the operating power level to determine the actual induced source strengths in a given reactor-core shield. The decay after shutdown or the build-up to equilibrium during operation can be estimated easily by application of the time factors given in Eq. 15. Also, in Chap. 10, nomograms are presented for the calculation of radioisotope build-up and decay.

The composition of the steel is based on the analyses given in Chap. 6, Sec. 1.2. It should be noted in this regard that standard metallurgical analyses of the composition of steel or other metals or alloys are generally untrustworthy for purposes of evaluating the problem of induced activity. These standard analyses may be quite precise in treating elements that are important to the metallurgical properties of the materials. On the other hand, they often ignore elements that are important to the induced-radiation characteristics of the material. Cobalt and tantalum compositions in stainless steel are two important cases in point.

(d) Photoneutrons. The production of photoneutrons outside the core depends on the presence of gamma rays with energies higher than the threshold energy of the photoneutron emitters. The probability for a photoneutron reaction is very small, so small, in fact, that during power operation these photoneutrons may usually be neglected. After shutdown, however, if high-energy gamma rays with a fairly long half life are available like those from the barium-lanthanum decay, photoneutrons may be produced in materials with the lowest threshold energies like beryllium or heavy water. If these materials are present in the reactor or shield, an evaluation of photoneutrons after shutdown should be made. The threshold energies for photoneutron production are given in Sec. 1.2d.

1.4 Relative Importance of the Various Sources for Core Shielding

During operation the *prompt-fission neutrons* are the only neutrons of consequence arising directly in the core.

An analysis of the relative importance of the core gamma sources is somewhat more complicated. Again, the *prompt-fission gammas* are important; however, the total energy release of the *delayed gammas* from the fission products, as well as the *capture gammas*, can be of the same order of magnitude. The total energy release of prompt-fission gammas in a core is 1.5×10^{14} Mev/kw-sec. The total energy release of delayed gammas is 2.3×10^{14} $(0.93 - t_0^{-0.2})$ Mev/kw-sec, which at equilibrium is approximately equal to the prompt-gamma energy release. It should be noted also that two-thirds of the equilibrium is reached in a few minutes. On the other hand, although the total energy release is approximately equal, the average energy of the delayed gammas is 0.7 Mev, which is considerably lower than the frequently assumed value of 2.5 Mev for the prompt gammas. Thus the prompt gammas often predominate in the shield calculation.

A range of importance for the *core capture gammas* can be gained by considering the neutron balance. Of the 2.5 neutrons produced per fission in U^{235}, 1.5 are dissipated during steady-state operation in leakage and parasitic absorption. The maximum total number of captures, then, is 4.5×10^{13} captures/kw. With binding energies reaching as high as 8 Mev, the upper limit for capture-gamma production is higher than the prompt-fission gammas. In typical cases the average capture-gamma production is actually less than the prompt-fission gamma production; however, its energy and location may make it dominant.

Induced activities in the core structural material and coolant also have an upper limit that is the same order of magnitude as the capture-gamma-ray sources since the equilibrium activity level is equal to the number of captures per cubic centimeter in the medium. However, in a typical core a relatively small percentage of the absorbing nuclei are transmuted into gamma-emitting unstable nuclei, and therefore the induced activities are relatively small compared to the fission or capture gammas.

2 AFTER SHUTDOWN OF THE REACTOR (See Also Chap. 7)

The predominant sources in the reactor core after shutdown are as follows:

1. Fission-product gammas.
2. Gammas from the induced activity of the core structure and the coolant.
3. If certain materials such as beryllium or heavy water are used in the reactor, photoneutrons may be an important source of after-shutdown radiation.

Outside the core the sources of radiation are from the induced activities of the structural materials of the reflector, thermal shields, and reactor container and shield. If the design of the reactor is such that materials are used in which photoneutrons are formed, prompt-capture gamma-ray production will also have to be investigated.

All the above sources have been taken into consideration and discussed in terms of the sources during reactor operation. For consideration after shutdown no new concepts are involved. The time-decay characteristics of each of the sources must be examined, and different sources will present different magnitudes of importance, depending on the time after shutdown. This subject is treated in detail in Chap. 7 in connection with accessibility to the system as a whole.

From the point of view of the primary shield, the important sources after reactor shutdown are summarized as follows:

1. *Fission-product gammas* are the most important source of radiation after shutdown.
2. *Induced activities* in the core are usually of secondary importance, but *in the shield* they may become important considerations.
3. *Photoneutrons* are of consequence after the delayed neutrons have decayed. They could also be of consequence if the shield were greatly overbalanced in neutron attenuation, i.e., if the gamma to neutron ratio were permitted to reach too high a value. This ratio, however, would have to reach 10^6 or more, a condition hardly to be expected in most reactor-shield

Table 3.8—RADIATION SOURCE DATA OF A HYPOTHETICAL WATER-COOLED ZIRCONIUM POWER REACTOR WITH EQUAL VOLUMES OF WATER AND ZIRCONIUM

Kind of radiation	Origin	Source energy, Mev	Strength	Remarks
Neutron	Fission	Up to 15	3.7×10^{12} neutrons/cm^3-sec	Predominant neutron source during operation
Neutron	Fission after thermal capture of polonium-beryllium source neutrons or photoneutrons from D_2O	Up to 15	5×10^5 neutrons/cm^3-sec	Predominant neutron source a few minutes after shutdown
Gamma	Prompt gammas from fission	Up to 7	3×10^{12} gammas/cm^3-sec	Predominant gamma source escaping from core during operation
Gamma	Delayed gammas from fission products	0.1–3	1.0×10^{13} Mev/cm^3-sec	Predominant gamma source in core after shutdown
Gamma	Capture gammas in zirconium	1–8	2.8×10^{11} gammas/cm^3-sec	
Gamma	Inelastic-scattering gammas in zirconium	1–8	1.5×10^{11} gammas/cm^3-sec	
Gamma	Capture gammas in uranium, xenon, cadmium, and silver	1–8	2.3×10^{11} gammas/cm^3-sec (average in uranium) 7.5×10^{10} gammas/cm^3-sec (average in xenon) 4.5×10^3 gammas/cm^3-sec (average in control rod)	
Gamma	Capture gammas in water	2.2	5.5×10^{11} gammas/cm^3-sec (average)	

designs. In a shield consisting entirely of water, however, the neutron attenuation would show a break when this ratio was reached, and the neutron flux would then follow the gamma flux down, with a relaxation length of 30 to 36 cm, rather than 5 to 8 cm. In heavy water, where photoneutron production is much greater, this effect would be even more pronounced.

4. *Delayed neutrons* might be of importance for a brief period after shutdown or in a circulating-fuel system where they may be transported outside the core shield.

Reviewing the preceding statements and those made in Sec. 1.4, it is seen that during steady-state operation of the reactor, the prompt-fission gammas are always important, with the capture gamma rays, delayed-fission gammas, and induced gamma activities generally being subsidiary sources in the order stated. After shutdown the delayed-fission-product activities are predominant, and the induced gamma activities in the core structure and coolant are generally of secondary importance.

To give further substance to these remarks about the relative importance of the various core sources, Table 3.8 lists the source intensities of a hypothetical water-cooled zirconium core of equal volumes of water and zirconium with an operating temperature of 400°F.

3 ATTENUATION CALCULATIONS

3.1 Fast-neutron Attenuation[39]

(a) Attenuation of Fast Neutrons in Water. Derivation of Approximate Formula. The simple approach to the solution of the neutron-attenuation problem, discussed in Chap. 1, will now be applied to a particular example. A very simple case is chosen, that of an infinite-plane

source distribution emitting parallel neutron radiation. This will be referred to, henceforth, as a beam source of neutrons, and the ratio of the neutron flux at a distance x from the source to the flux at the source surface will be called the *beam collision kernel*.

The beam collision kernel is taken to be an absorption kernel e^{-Kx}, where K is the macroscopic neutron cross section. The value of K is related to the energy of the neutron source since K has an energy dependent part due to hydrogen scattering, as well as a part due to oxygen and heavy-element scattering, which is considered independent of energy. The latter is left an adjustable parameter to be determined by the best fit to experimental data [for example, neutron-attenuation curves obtained at the Lid Tank Shielding Facility (LTSF) at the Oak Ridge National Laboratory (ORNL)].

Several simplifying approximations can be applied to the derivation of the spectrum and neutron-attenuation curve. It will be shown that for thick shields an approximate saddle-point method for evaluating the integral suggested by the work of Wigner and Young[35] leads to results almost identical to those obtained by an exact integration. The use of the saddle-point method involves approximations for the hydrogen cross section and the fission spectrum which are close to the true expressions only in the energy region of 3 to 11 Mev (see Figs. 3.6a and b). It turns out, fortunately, as will be shown, that it is unnecessary to consider other energies since neutrons of lower energies are rapidly absorbed in the early part of the shield and neutrons of higher energies are relatively rare in the fission spectrum.

The theoretical hydrogen total cross section is given by the expression:[37]

$$\sigma_H = \frac{3\pi}{4}\left[k^2 + \left(-\frac{1}{a_t} + \frac{1}{2}r_t k^2\right)^2\right]^{-1} + \frac{\pi}{4}\left[k^2 + \left(-\frac{1}{a_s} + \frac{1}{2}r_s k^2\right)^2\right]^{-1} \quad \text{cm}^2 \tag{16}$$

where k is the wave number of the neutron in the center-of-mass system. The parameters used, which were chosen from the recent work of Bethe and Blatt and Jackson,[37] are the following:

$$a_t = 0.528 \times 10^{-12} \text{ cm} \qquad r_s = 1 \times 10^{-13} \text{ cm}$$
$$-a_s = 2.375 \times 10^{-12} \text{ cm} \qquad r_t = 1.56 \times 10^{-13} \text{ cm}$$
$$k = \frac{1}{\lambda_{\text{neutron}}} = \text{reciprocal of neutron wave length} \qquad \lambda = 2.86 \times 10^{-9}/\sqrt{E \text{ in ev}}$$

A fairly good approximation to this expression between 2 and 12 Mev is

$$\boxed{\sigma_H = 5.13/E^{0.725} \text{ barns (E in million electron volts)}}$$

The fission spectrum has been obtained by careful measurement at Los Alamos[38] and has been fitted quite accurately to the function $\sinh \sqrt{2E}\, e^{-E}$. A good approximation in the energy range 2 to 12 Mev is $\boxed{1.4 \times 10^3 e^{-0.72E}}$.

By the use of the approximations for the total hydrogen scattering cross section and the fission spectrum, the spectrum and attenuation of a neutron beam of source strength 2.5 neutrons/sec were derived by the saddle-point method for the case of a shield composed of water plus heavy element. Only the results of the derivation, which is carried out in detail in reference 39, will be recorded here.

The peak energy E_0 of the neutron spectrum at a distance x centimeters from the source is

$$E_0 = 0.541(\theta x)^{0.58} \tag{17}$$

where θ is the volume fraction of water in the shield and E_0 is expressed in million electron volt units.

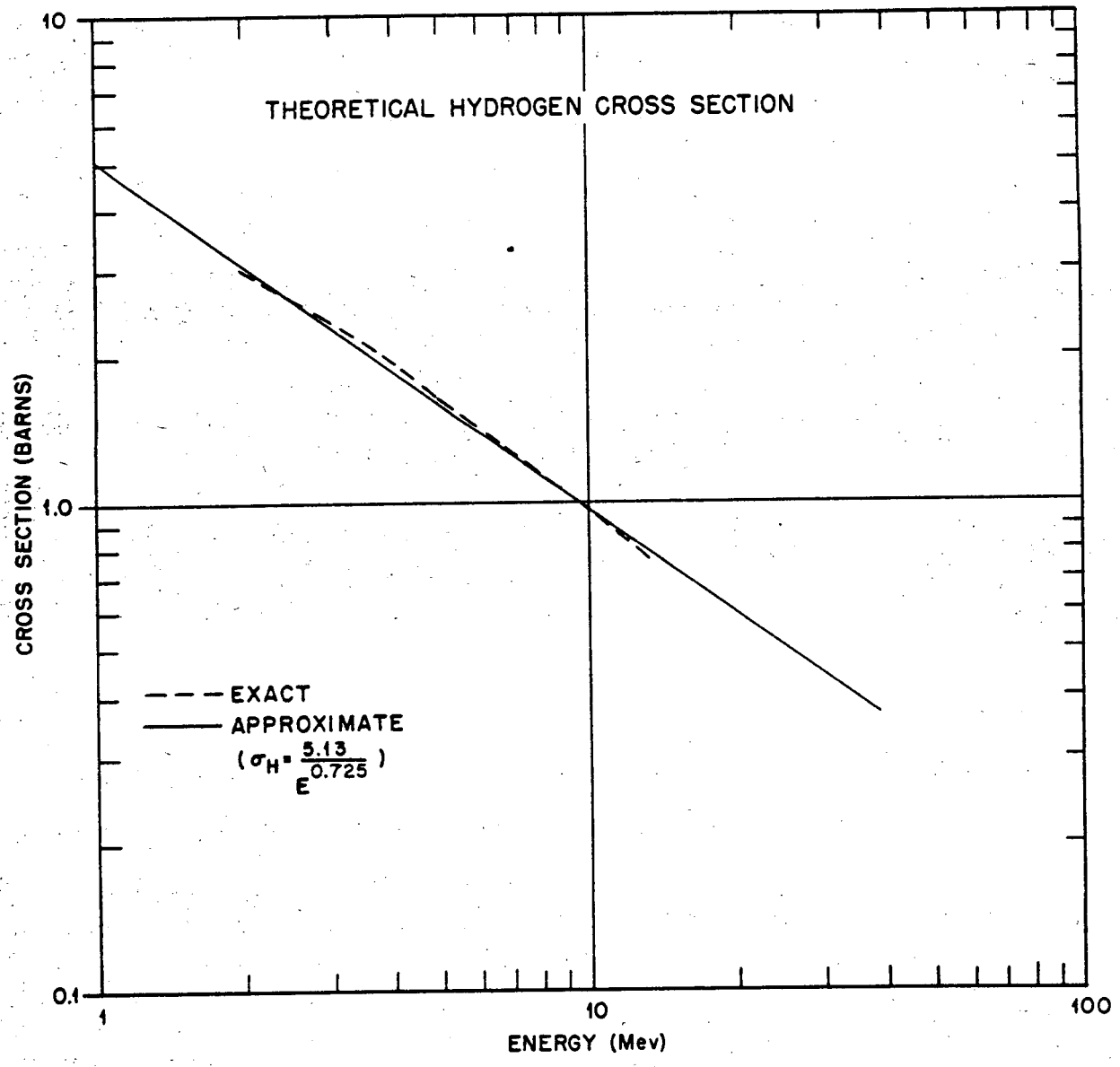

THEORETICAL HYDROGEN CROSS SECTION
CROSS SECTION (BARNS)
10
1.0
0.1
1
10
100
ENERGY (Mev)
EXACT
APPROXIMATE
$(\sigma_H = \frac{5.13}{E^{0.725}})$

Figure 3.6a

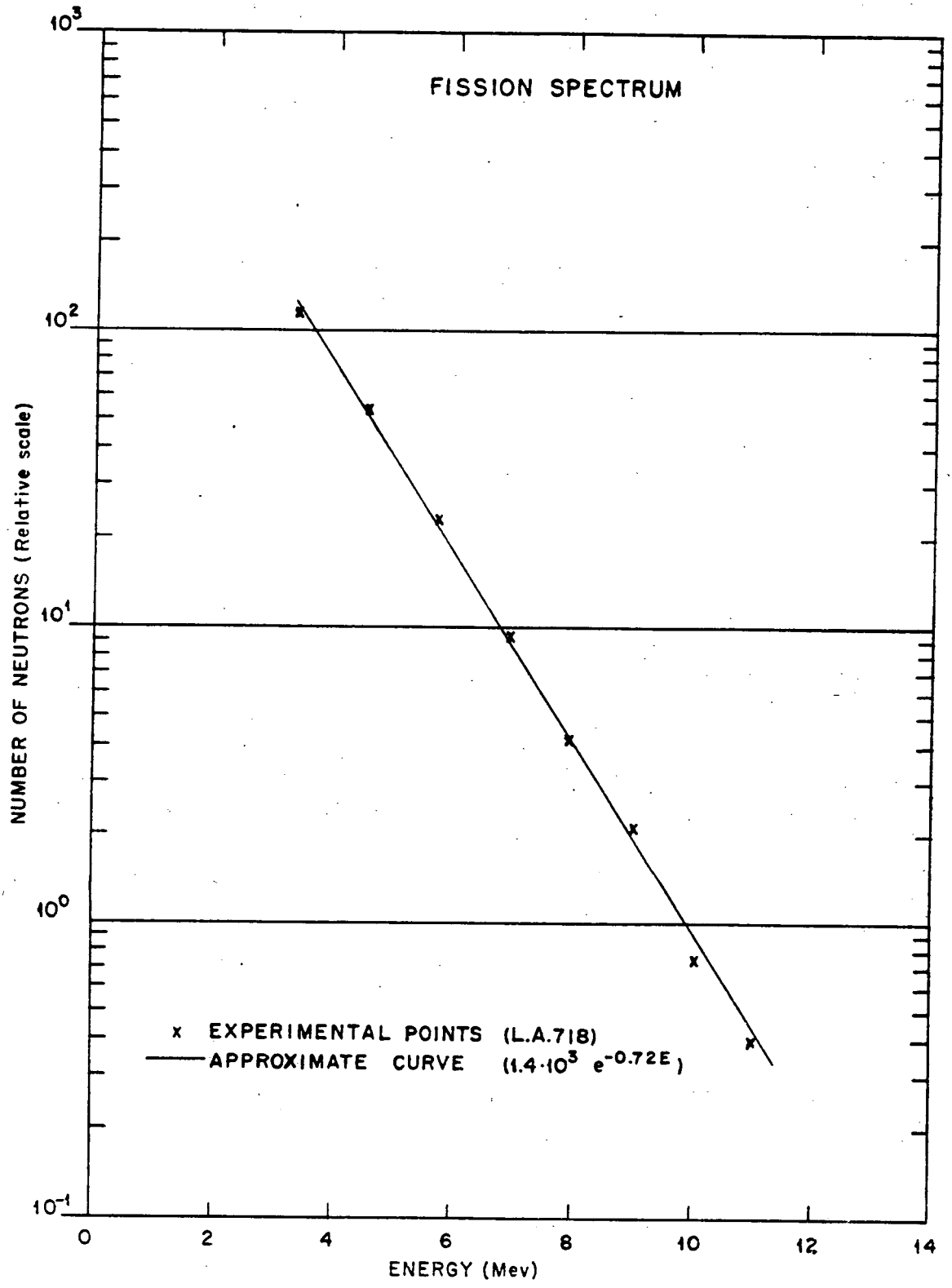

FISSION SPECTRUM
NUMBER OF NEUTRONS (Relative scale)
10^3
10^2
10^1
10^0
10^{-1}
x EXPERIMENTAL POINTS (L.A.718)
APPROXIMATE CURVE ($1.4 \cdot 10^3\ e^{-0.72E}$)
0
2
4
6
8
10
12
14
ENERGY (Mev)

Figure 3.6b

Further, for the half-width, ΔE (spectrum width at one-half maximum value) of the spectrum at x centimeters from the source, the following function is written:

$$\Delta E = 1.55(\theta x)^{0.29} \tag{18}$$

Finally, the result obtained for the attenuation of a beam of fission neutrons of initial strength 2.5 neutrons/sec is recorded.

$$\boxed{N(x) = 5.4(\theta x)^{0.29} e^{-0.928(\theta x)^{0.58}} e^{-\theta \Sigma_0 x} e^{-(1-\theta)\Sigma_r x}} \tag{19}$$

N(x) gives the neutron flux at x centimeters from an infinite-plane source emitting 2.5 neutrons/cm^2-sec in a parallel beam. The macroscopic oxygen scattering cross section is Σ_0, and the macroscopic scattering cross section of the heavy elements in the shield is Σ_r.

Comparison with Exact Formula. It will now be shown that these formulas, which are obtained using approximations to the hydrogen cross section and the fission spectrum, do not differ appreciably from those obtained when the exact expressions are used and when the integration is done by the numerical rather than the saddle-point method. If the exact form for the fission spectrum and the exact theoretical hydrogen cross section are used, the attenuation of a beam of fission neutrons of unit source strength exponentially absorbed in water becomes

$$N(x) = \frac{\int_0^{E_{max}} \sinh \sqrt{2E}\, e^{-E} e^{-(\Sigma_H + \Sigma_0)x}\, dE}{\int_0^{E_{max}} \sinh \sqrt{2E}\, e^{-E}\, dE} \tag{20}$$

This expression is the product of the probability that a fission neutron of energy E is produced and the probability that it has not been absorbed after traveling through x centimeters of water, averaged over the energy range of the fission spectrum (zero to E_{max}).

The close agreement between the saddle-point method and the more exact numerical method is demonstrated by the neutron-beam-attenuation curves of Fig. 3.7, which are a comparison of Eq. 20 normalized to 2.5 neutrons/sec with $\Sigma_0 = 0$ and the saddle-point results (Eq. 19) with $\Sigma_0 = 0$ and $\theta = 1$.

Comparison with Experiments. The following is an attempt to obtain agreement with measurements of neutron attenuation in water by making use of our previously stated assumption that an oxygen collision is equivalent to absorption. If Eq. 19 with $\theta = 1$ is transformed to spherical geometry, the following function can be written for the attenuation of a unit-point fission source:

$$\phi(r) = \frac{5.4 r^{0.29} e^{-0.928 r^{0.58}} e^{-\Sigma_0 r}}{4\pi r^2} \tag{21}$$

The factor containing Σ_0 (the effective removal cross section for oxygen) arises from the inclusion of oxygen scattering and is to be adjusted to obtain the best fit with experiment.

In the evaluation of the experimental data, the source has been idealized to be plane and isotropic. However, it is convenient to transform the experimental distribution to one that would arise from a point source, for comparison with the theory under discussion. This simplifies the determination of the adjustable parameter that produces the best theoretical fit.

The fitting procedure is as follows:

1. The experimental neutron distribution is first transformed to that which would result from a point fission source of neutrons by a method described below.
2. Equation 21 with $e^{-\Sigma_0 r}$ suppressed is then normalized to the experimental curve for some large value of r (r = a).
3. The value of the cross section is obtained by setting the logarithm of the ratio of the two curves at some smaller value of r (r = b) equal to $\Sigma_0(a - b)$ and solving for Σ_0.

The result thereby obtained for the experimental data on pure water is shown in Fig. 3.8. The experimental and theoretical curves were normalized at large distances, and the

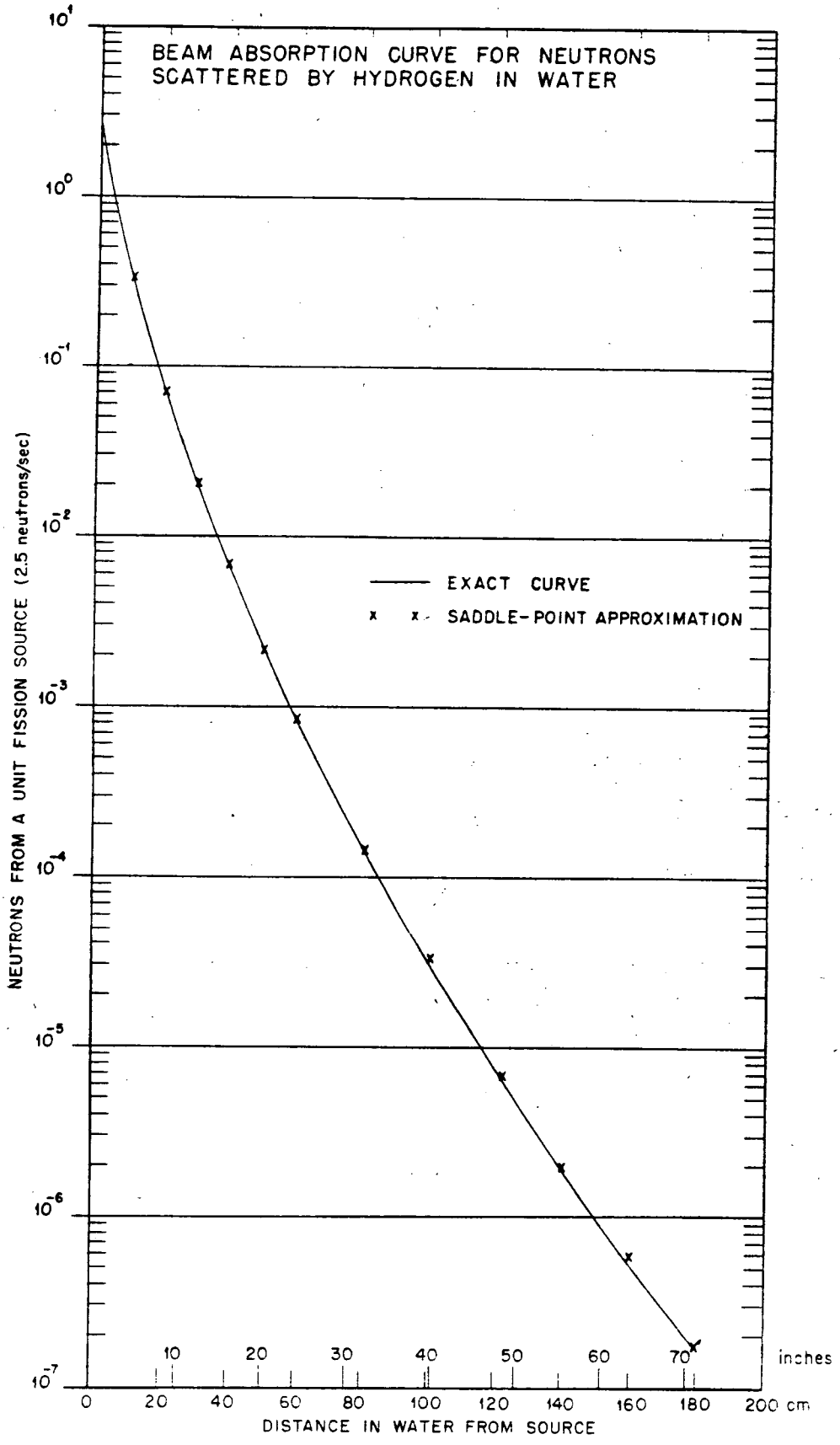

BEAM ABSORPTION CURVE FOR NEUTRONS
SCATTERED BY HYDROGEN IN WATER
EXACT CURVE
SADDLE-POINT APPROXIMATION
NEUTRONS FROM A UNIT FISSION SOURCE (2.5 neutrons/sec)
10^{1}
10^{0}
10^{-1}
10^{-2}
10^{-3}
10^{-4}
10^{-5}
10^{-6}
10^{-7}
10 20 30 40 50 60 70 inches
0 20 40 60 80 100 120 140 160 180 200 cm
DISTANCE IN WATER FROM SOURCE

Figure 3.7

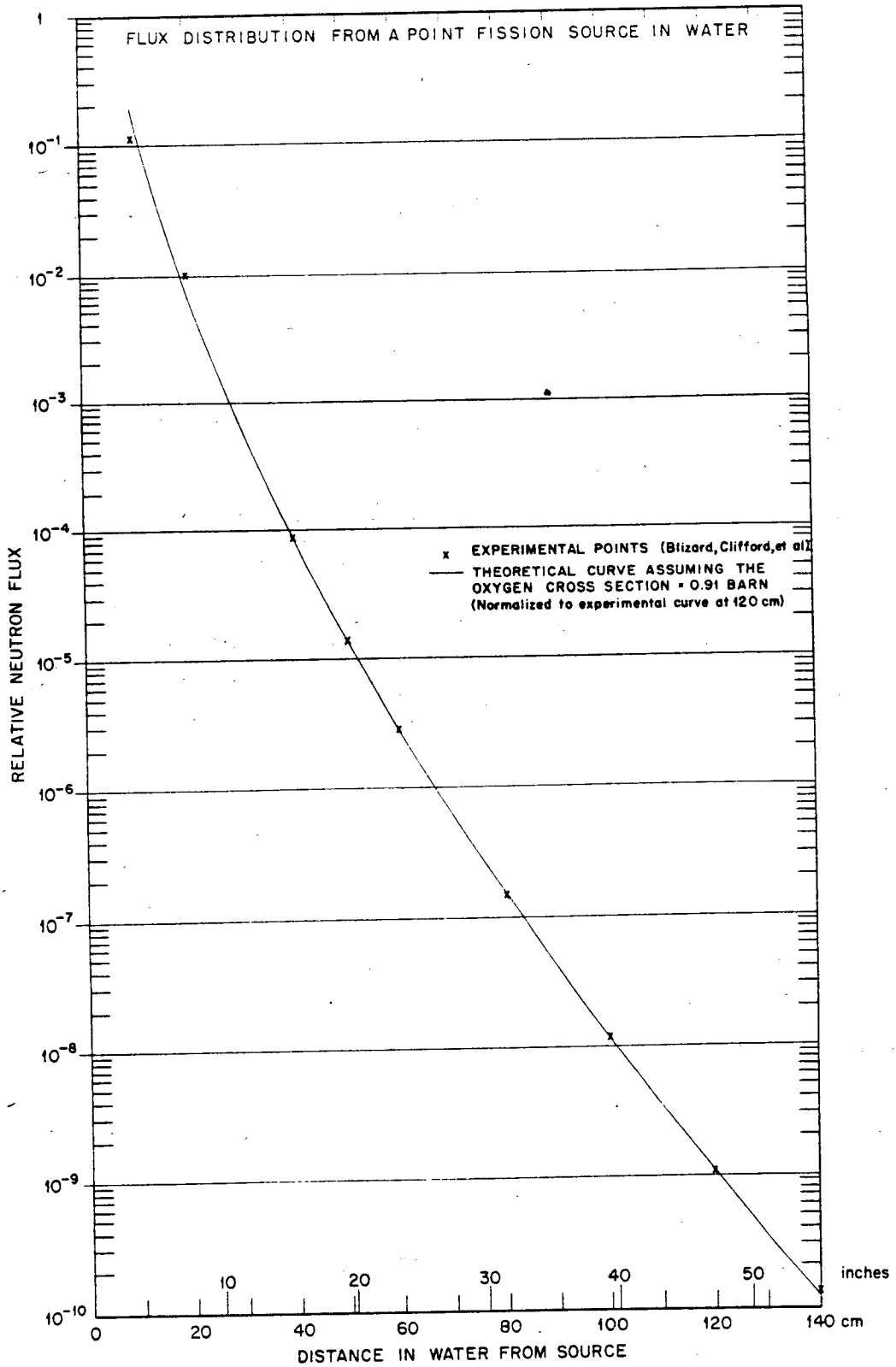
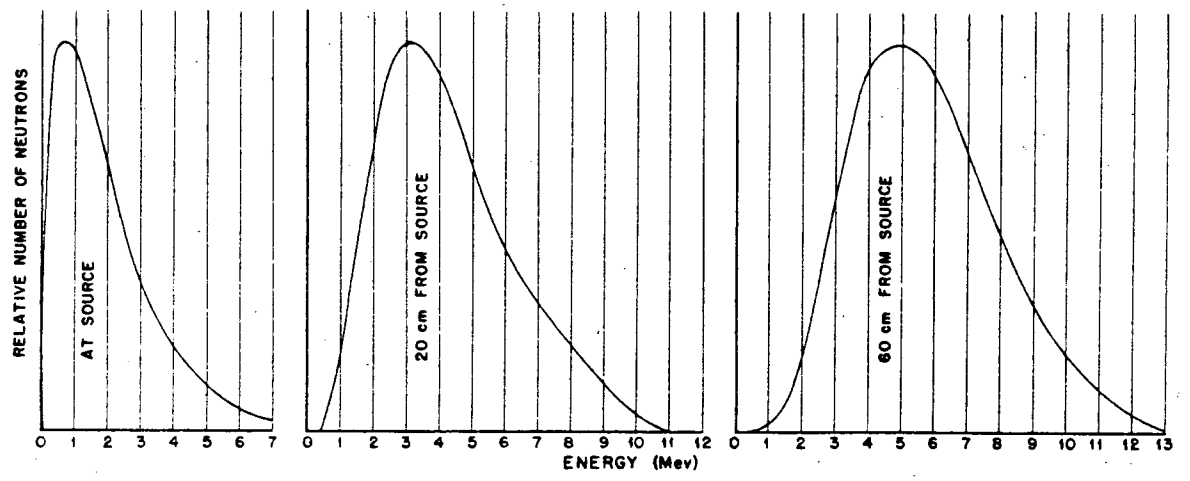

FLUX DISTRIBUTION FROM A POINT FISSION SOURCE IN WATER
RELATIVE NEUTRON FLUX
1
10^{-1}
10^{-2}
10^{-3}
10^{-4}
10^{-5}
10^{-6}
10^{-7}
10^{-8}
10^{-9}
10^{-10}
x EXPERIMENTAL POINTS (Blizard, Clifford, et al)
THEORETICAL CURVE ASSUMING THE OXYGEN CROSS SECTION = 0.91 BARN
(Normalized to experimental curve at 120 cm)
0
10
20
30
40
50
inches
0
20
40
60
80
100
120
140 cm
DISTANCE IN WATER FROM SOURCE

Figure 3.8



SPATIAL DEPENDENCE OF NEUTRON SPECTRUM (Based on assumption that a single collision is equivalent to absorption.)

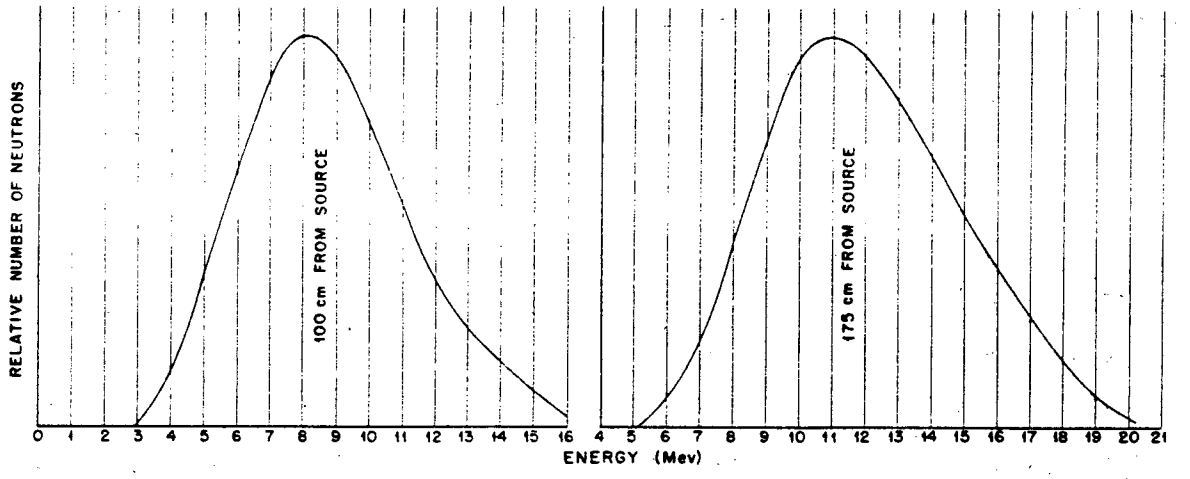


Figure 3.9a

fit was made using 0.91 barn for the oxygen cross section. It can be seen that the agreement in shape is excellent, substantiating the fact that a beam-removal concept does characterize the basic penetration of neutrons in a homogeneous hydrogenous medium.

Hardening of Spectrum with Penetration into Shield. The variation in the peak energy as a function of distance from the source can be obtained from the integrand of Eq. 20. The variation in the spectrum at various distances, x, from the source is shown by Figs. 3.9a, b, and c. In these figures are plotted the magnitude

$$\sinh \sqrt{2E}\, e^{-E} e^{-(\Sigma_H + \Sigma_0)x}$$

with an oxygen-removal cross section of 0.91 barn and with the magnitude of the peak energy arbitrarily made equal. The peak energy is observed to shift to higher energies as the distance from the source increases, increasing from less than 2 Mev to as high as 11 Mev at 175 cm from the source. This shift in energy, or "hardening of the spectrum," causes the gradual lengthening of the neutron relaxation length at greater distances and indicates the great importance that the high-energy portion of the source spectrum has at large penetration distances. It must be noted that this "uncollided" spectrum is only of use in revealing the penetration characteristics of the neutrons; the actual spectrum will include the multiply scattered

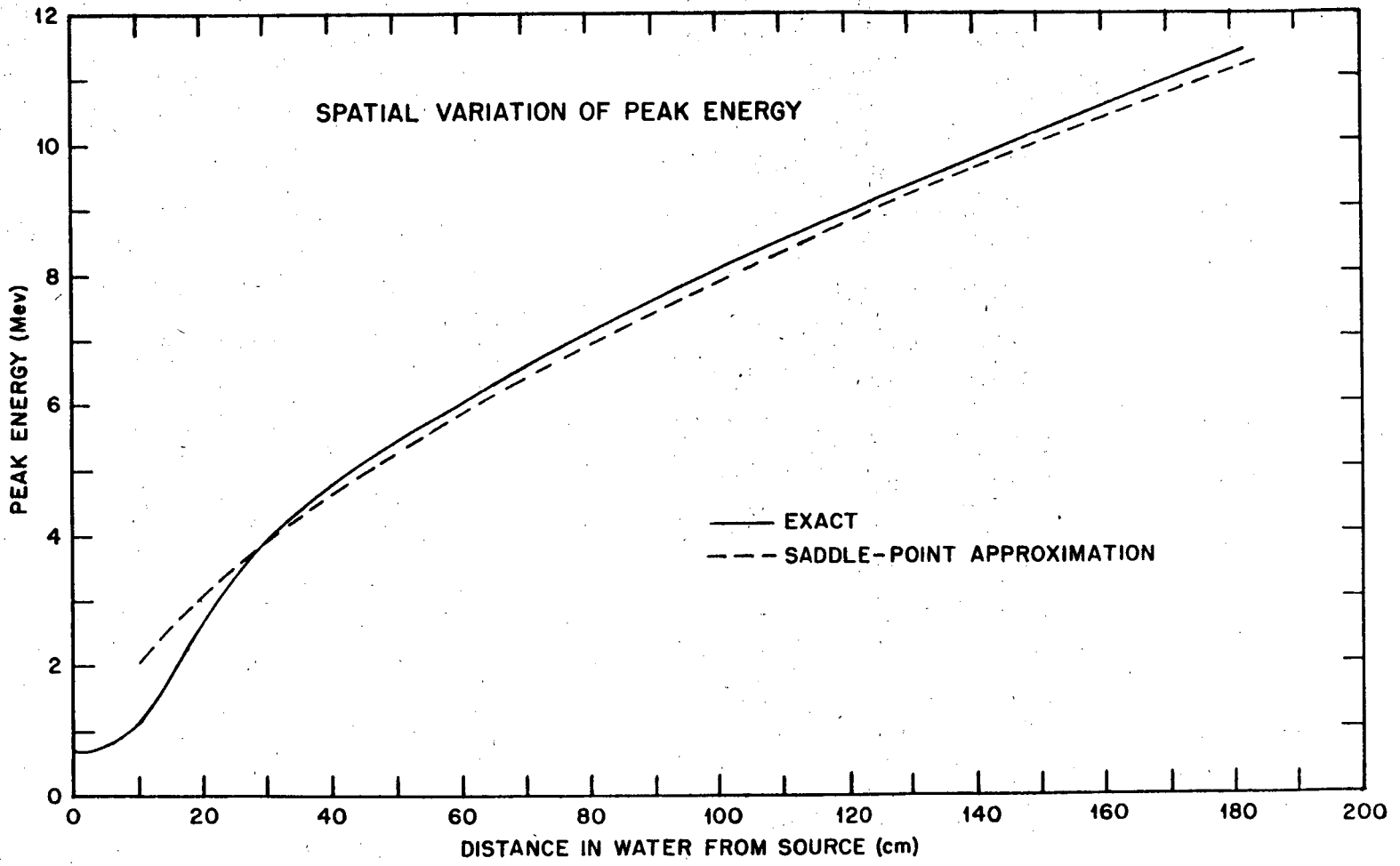

SPATIAL VARIATION OF PEAK ENERGY
PEAK ENERGY (Mev)
DISTANCE IN WATER FROM SOURCE (cm)
EXACT
SADDLE-POINT APPROXIMATION
0
2
4
6
8
10
12
0
20
40
60
80
100
120
140
160
180
200

Figure 3.9b

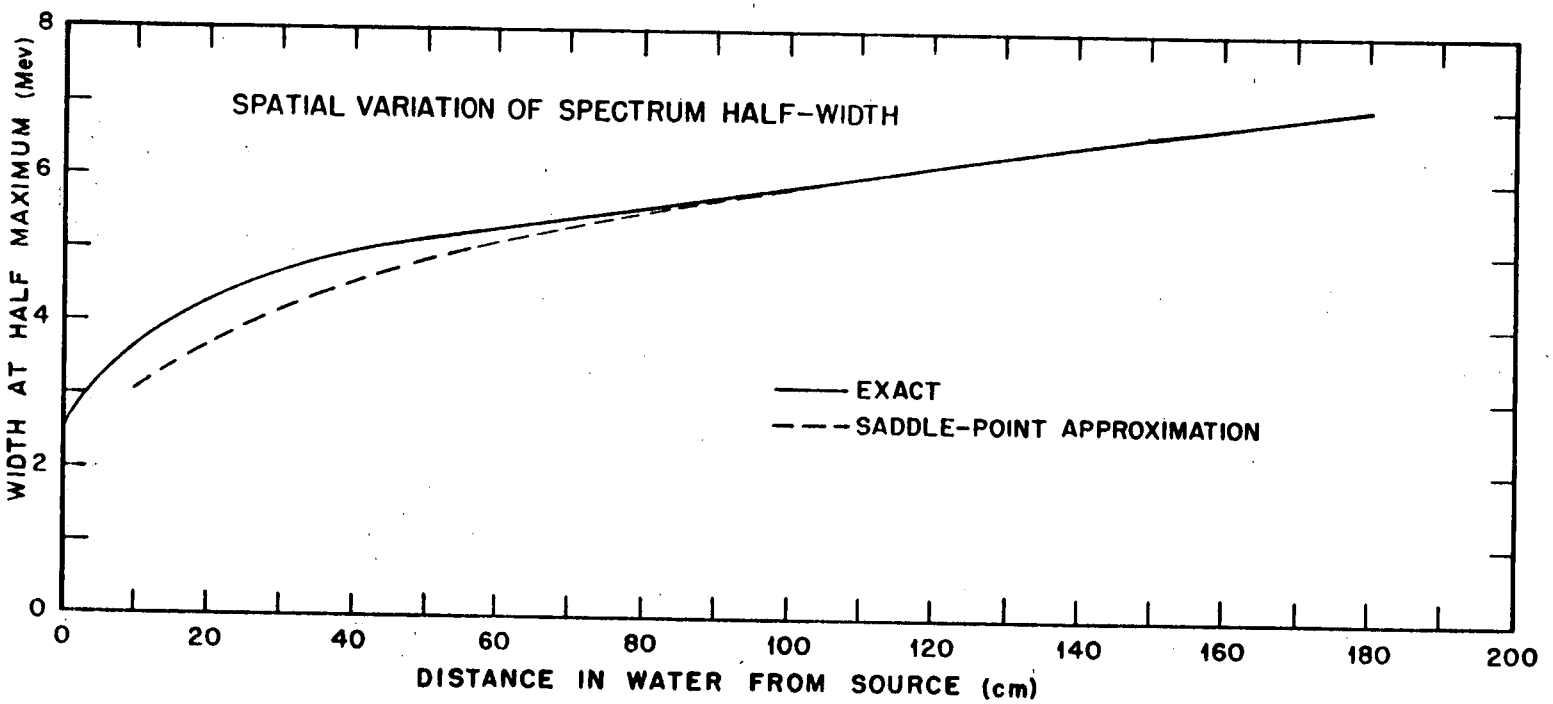

SPATIAL VARIATION OF SPECTRUM HALF-WIDTH
WIDTH AT HALF MAXIMUM (Mev)
DISTANCE IN WATER FROM SOURCE (cm)
EXACT
SADDLE-POINT APPROXIMATION
0
2
4
6
8
0
20
40
60
80
100
120
140
160
180
200

Figure 3.9c

neutrons and will have the characteristic distribution similar to that of a fission spectrum as shown in Fig. 3.6b, and at lower energies gives approximately a 1/E spectrum.

(b) Attenuation of Fast Neutrons in Mixtures of Water and Other Materials. Lead-Water and Iron-Water Mixtures. To determine the effect of other materials added to a water shield, tests have been performed at the LTSF of ORNL. Two mixtures of lead and water are presented here. They are for shields consisting of (1) 18 per cent lead and 82 per cent water and (2) 27 per cent lead and 73 per cent water. The results of these tests may be fitted quite closely by assuming an equivalent cross section of 3.6 barns for lead as shown in Figs. 3.10 and 3.11. Similar data exist for iron-water mixtures. The measurements on metal and water combinations are carried out by inserting the slabs into the lid tank one at a time and then obtaining flux data in the region behind the last slab only. The experimental points were systematically selected, for the purpose of this fit, at a distance of 10 cm behind each lead slab. This was done because of the likelihood that the measurements made near the slabs are affected by pile-up of the degraded neutrons produced from the inelastic neutron scattering in lead.

Effect of "Lumping." The types of shield compositions discussed so far have been homogeneous. However, a laminated shield can also be handled by tracing through the rays from the different points in the source. In this way the flux is obtained directly by use of this simple theory. The flux distribution for a nonuniform array of iron slabs[40] was derived in this manner and compared directly with measurements done at ORNL. The results are shown in Fig. 3.12, and the agreement is seen to be good except in the nonequilibrium region near the iron. The equilibrium is apparently restored at about 25 cm outside the last iron slab since the curves remain in good agreement thereafter.

Validity of the Removal Cross-section Concept. The phenomenological theory described above would have little practical value if it were limited to homogeneous mediums, as the assumptions, strictly adhered to, would indicate. Its use has, in fact, been extended to highly inhomogeneous mediums. This study is restricted to a basically hydrogenous medium in which has been inserted a slab of another material. With the uncollided flux model, a flux can be computed at a distance z in the medium, assuming that a "fast-removal" cross section and a simple exponential term is sufficient to describe the attenuation effect of the slab. If the saddle-point approximation mentioned above is used, the expression for the uncollided flux from a point source is

$$\phi(r,T) = \frac{5.4(r-T)^{0.29}}{4\pi r^2} \exp\left[-0.928(r-T)^{0.58} - \Sigma_0(r-T) - \Sigma_m T\right] \tag{22}$$

where Σ_m = the effective removal cross section of the material of which the slab is made (cm^{-1})
T = the thickness of the slab (cm)
r = the distance from source to point at which flux is calculated (cm)
Σ_0 = the effective removal cross section of oxygen (cm^{-1})

Similarly the expression for the uncollided flux if the slab is removed is

$$\phi(r,0) = \frac{5.4r^{0.29}}{4\pi r^2} \exp\left(-0.928r^{0.58} - \Sigma_0 r\right) \tag{23}$$

The effective removal cross section for the material of which the slab is composed can now be expressed in terms of the ratio of the flux without and with the slab.

$$\Sigma_m = \frac{1}{T} \ln\left\{\frac{\phi(r,0)}{\phi(r,T)} \frac{(r-T)^{0.29}\exp\left[-0.928(r-T)^{0.58} + \Sigma_0 T\right]}{r^{0.29}\exp\left(-0.928r^{0.58}\right)}\right\} \tag{24}$$

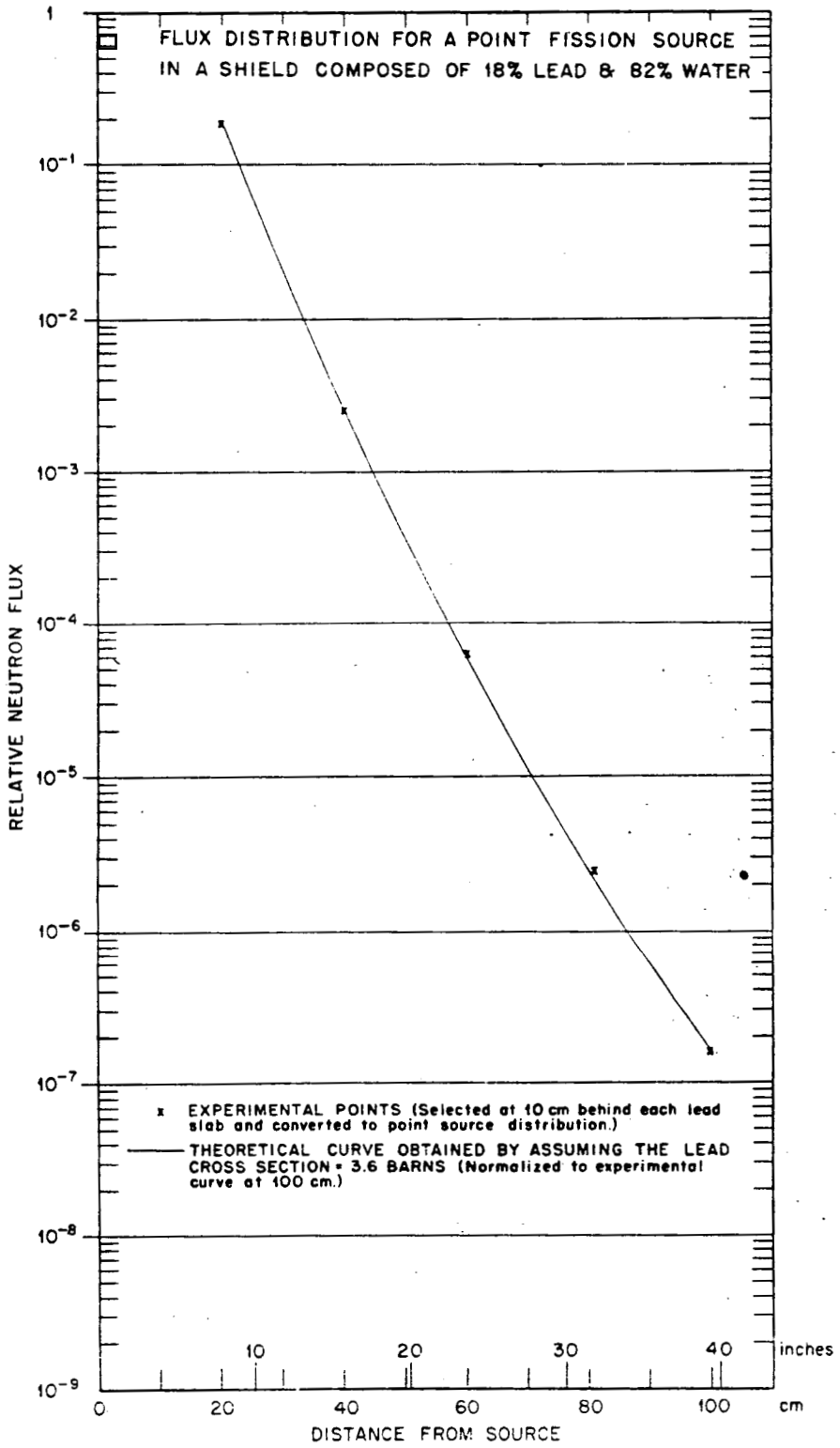

FLUX DISTRIBUTION FOR A POINT FISSION SOURCE
IN A SHIELD COMPOSED OF 18% LEAD & 82% WATER
RELATIVE NEUTRON FLUX
1
10^{-1}
10^{-2}
10^{-3}
10^{-4}
10^{-5}
10^{-6}
10^{-7}
10^{-8}
10^{-9}
x EXPERIMENTAL POINTS (Selected at 10 cm behind each lead slab and converted to point source distribution.)
THEORETICAL CURVE OBTAINED BY ASSUMING THE LEAD CROSS SECTION = 3.6 BARNS (Normalized to experimental curve at 100 cm.)
10
20
30
40
inches
0
20
40
60
80
100
cm
DISTANCE FROM SOURCE

Figure 3.10

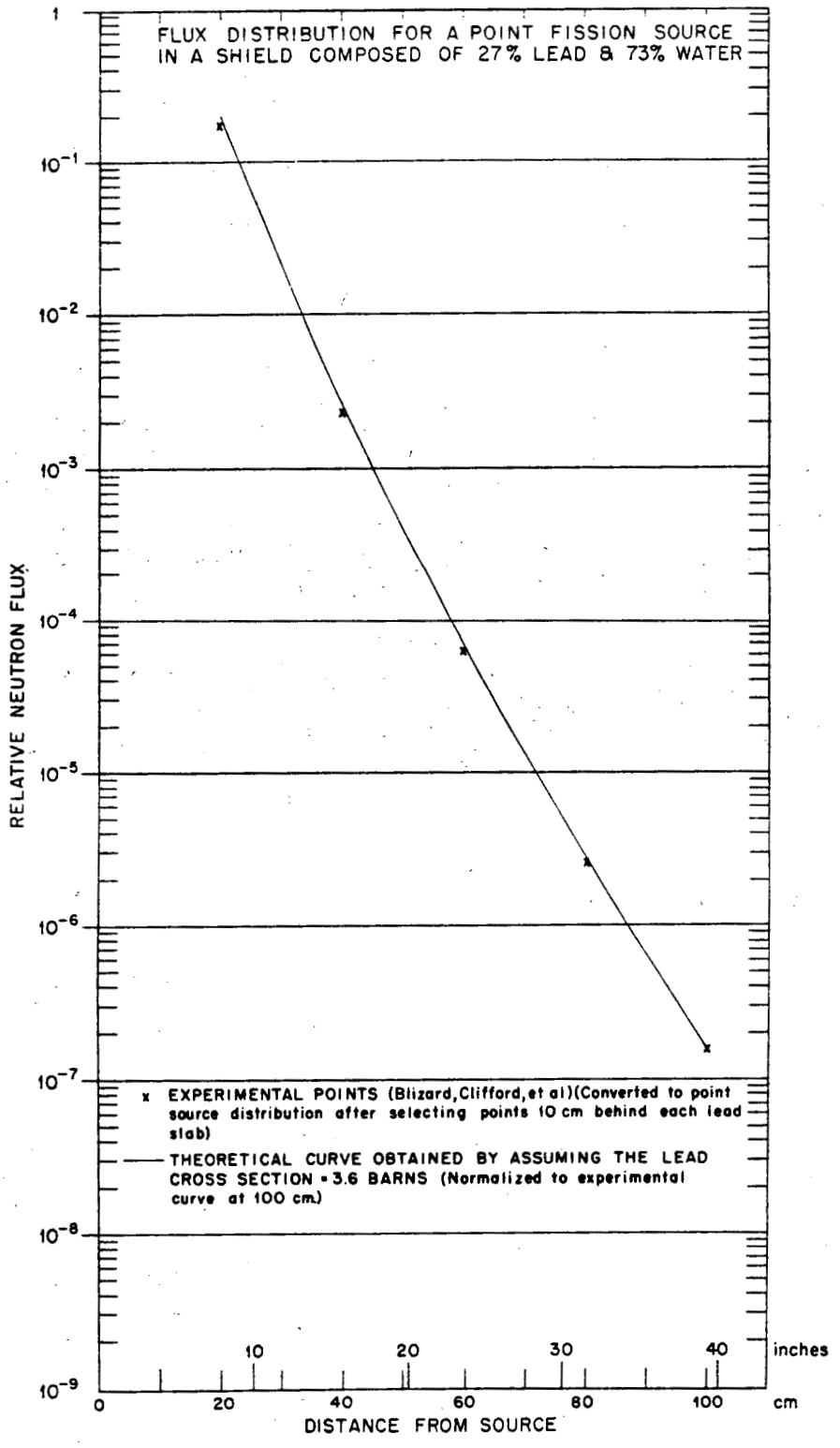

FLUX DISTRIBUTION FOR A POINT FISSION SOURCE
IN A SHIELD COMPOSED OF 27% LEAD & 73% WATER
RELATIVE NEUTRON FLUX
1
10^{-1}
10^{-2}
10^{-3}
10^{-4}
10^{-5}
10^{-6}
10^{-7}
10^{-8}
10^{-9}
x EXPERIMENTAL POINTS (Blizard, Clifford, et al)(Converted to point source distribution after selecting points 10 cm behind each lead slab)
THEORETICAL CURVE OBTAINED BY ASSUMING THE LEAD CROSS SECTION = 3.6 BARNS (Normalized to experimental curve at 100 cm.)
10
20
30
40
inches
0
20
40
60
80
100
cm
DISTANCE FROM SOURCE

Figure 3.11

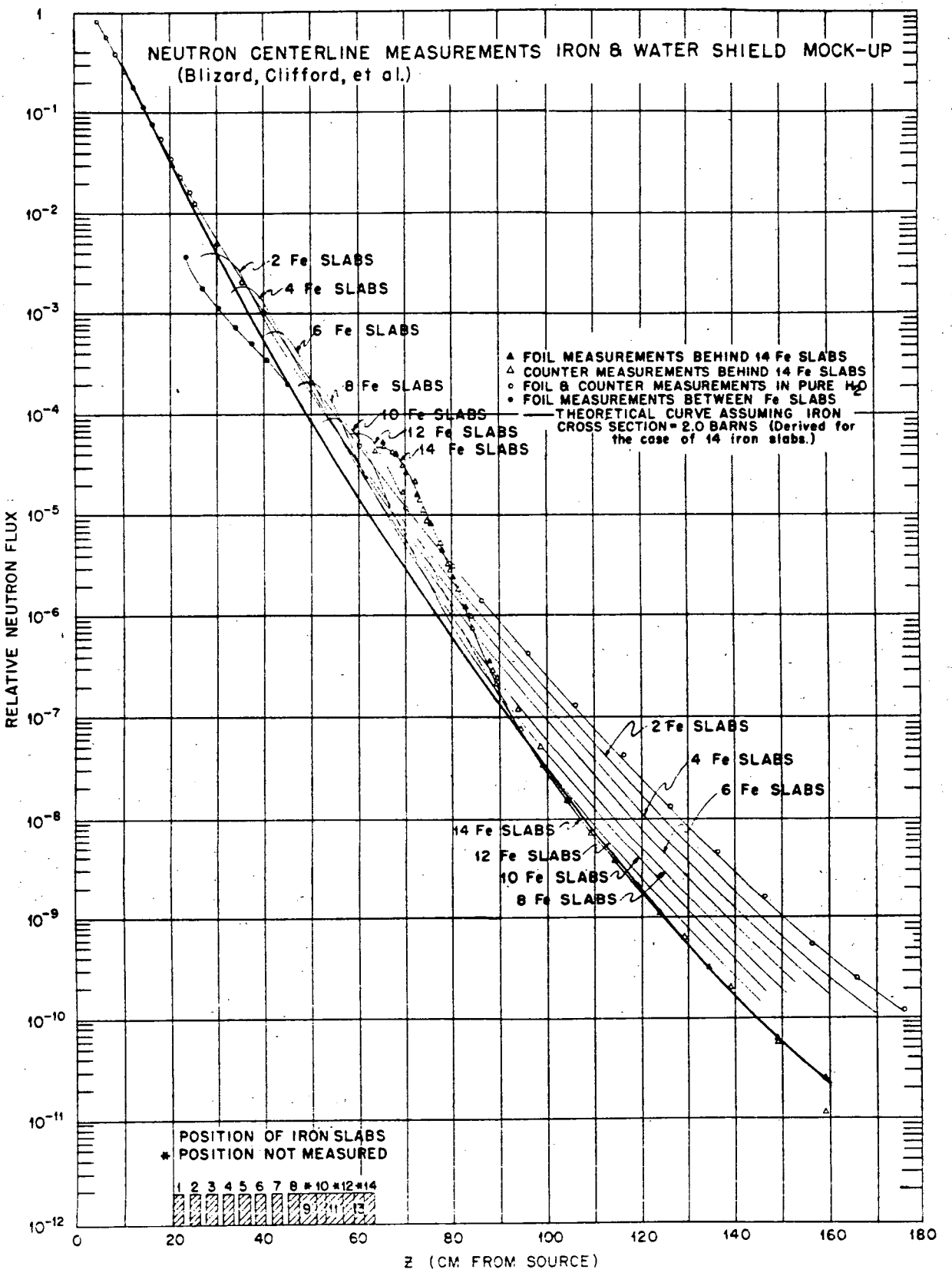

NEUTRON CENTERLINE MEASUREMENTS IRON & WATER SHIELD MOCK-UP
(Blizard, Clifford, et al.)
RELATIVE NEUTRON FLUX
Z (CM FROM SOURCE)
2 Fe SLABS
4 Fe SLABS
6 Fe SLABS
8 Fe SLABS
10 Fe SLABS
12 Fe SLABS
14 Fe SLABS
▲ FOIL MEASUREMENTS BEHIND 14 Fe SLABS
△ COUNTER MEASUREMENTS BEHIND 14 Fe SLABS
○ FOIL & COUNTER MEASUREMENTS IN PURE H2O
• FOIL MEASUREMENTS BETWEEN Fe SLABS
THEORETICAL CURVE ASSUMING IRON CROSS SECTION = 2.0 BARNS (Derived for the case of 14 iron slabs.)
POSITION OF IRON SLABS
* POSITION NOT MEASURED

Figure 3.12

The fast-removal cross section can now be determined if the ratio $\phi(r,0)/\phi(r,T)$ is assumed to be equal to the quantity measured in a bulk-shield experiment under the same conditions; that is, either the thermal-neutron flux or the fast-neutron dose is proportional to the uncollided flux in the region of validity. Let this ratio be designated R:

$$\boxed{R(r,T) \equiv \frac{\phi(r,0)}{\phi(r,T)} \text{ Definition}}$$

Thus the fast-removal cross section is

$$\boxed{\Sigma_m = \Sigma_0 + \frac{1}{T} \ln R(r,T) + \frac{0.29}{T} \ln\left(1 - \frac{T}{r}\right) + \frac{0.928}{T} r^{0.58}\left[1 - \left(1 - \frac{T}{r}\right)^{0.58}\right]} \qquad (25)$$

By an examination of this expression, it is seen that if a unique effective removal cross section is to be derived for the material in question, the expression

$$\frac{1}{T} \ln R(r,T) + 0.928\, r^{0.58}\left[1 - \left(1 - \frac{T}{r}\right)^{0.58}\right] + \frac{0.29}{T} \ln\left(1 - \frac{T}{r}\right)$$

must be practically independent of r and T. For this requirement to be true, the following subsidiary conditions are necessary:

1. R(r,T) should behave as a negative exponential in T.
2. R(r,T) should be practically independent of r.
3. T should be small compared to r.

Knowing the conditions that permit the determination of an effective removal cross section in turn tells us what information this phenomenological theory will reveal in an inhomogeneous-shield design. It will provide an estimate of the over-all attenuation of a slab in a hydrogenous shield at a distance in water far enough from the slab that equilibrium conditions have been restored.

In order to illustrate these limitations and the determination of an effective removal cross section, the iron-water flux data presented in Fig. 3.12 are plotted as R(r,T) for T varying from 0 to 28 cm and for r from 100 to 150 cm. These are shown in Figs. 3.13 and 3.14. R is exponential in T, and it is essentially independent of r. It is also observed that the remaining terms in r and T are insensitive to the large changes in r and T considered. The value of the fast-removal cross section derived from the point-source analysis is 2.1 barns.

A more exact analysis is possible by integrating over the plate-source geometry of the ORNL lid tank, where these tests were performed. Although straightforward in concept, such integration, performed exactly, leads to considerable numerical complications, as can be seen by examining the expression for the uncollided flux at a distance z centimeters along the central axis of a plate source of radius a.

$$\phi_u(z,T) = 2.7\left(1 - \frac{T}{z}\right)^{0.29} \int_z^{\sqrt{a^2+z^2}} \frac{\exp\left[-0.928 r^{0.58}\left(1 - \frac{T}{z}\right)^{0.58} - \Sigma_0 r\left(1 - \frac{T}{z}\right) - \Sigma_m \frac{Tr}{z}\right]}{r^{0.71}}\, dr \qquad (26)$$

The iron effective removal cross section was derived carrying out these numerical integrations and is reported in reference 39. The value so obtained was 2.0 barns (as compared with 2.1 barns, above), indicating that at the distances from the source being considered, the point-source description is adequate.

3.2 Thermal-neutron-flux Distribution

While the thermal-neutron flux itself does not contribute materially to dose rate, the capture gammas and activation caused by thermal-neutron capture require a detailed analysis of the thermal-neutron-flux distribution. Generally speaking, the thermal-neutron flux can be es-

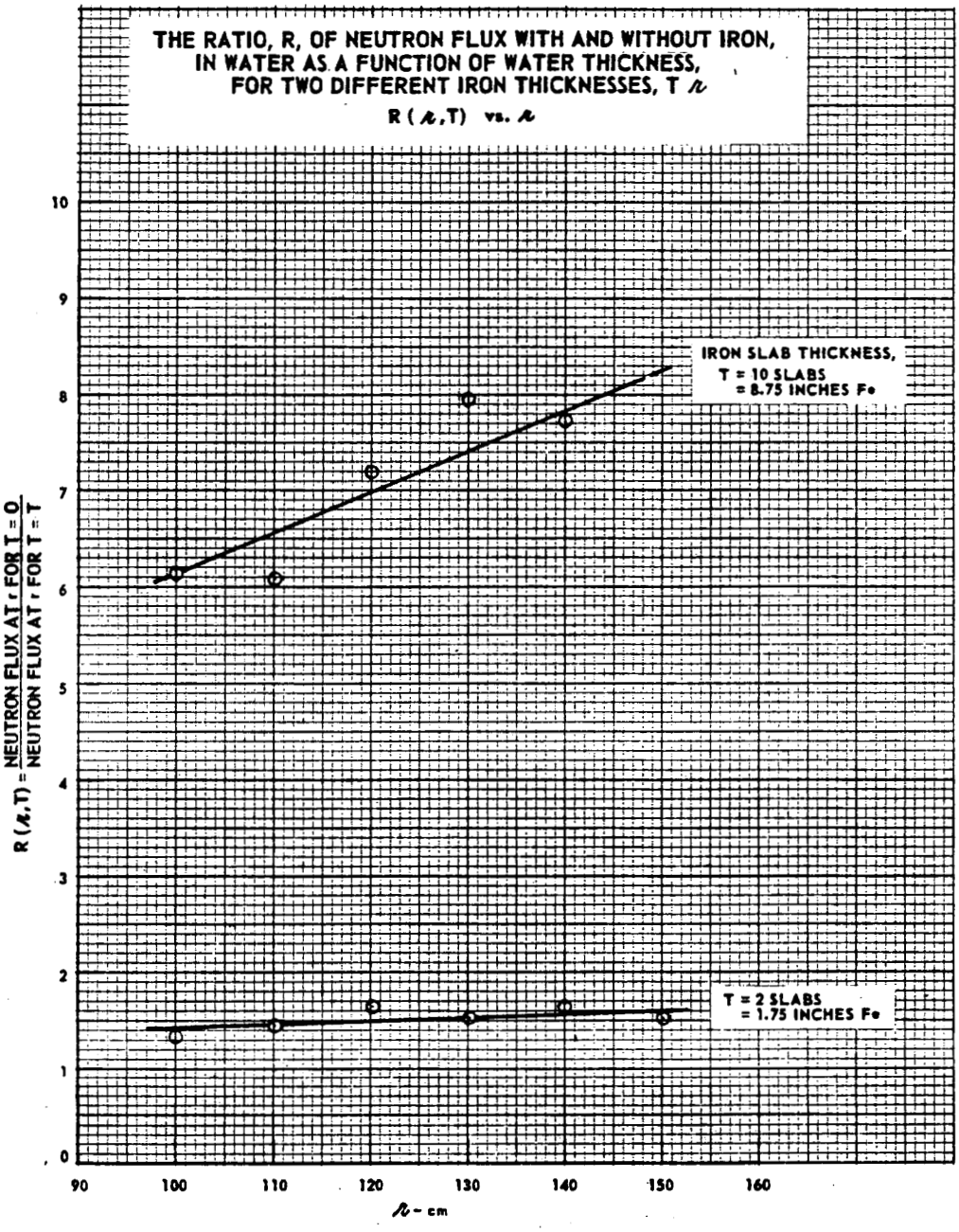


Figure 3.13

timated by scaling up experimental data at a few points in the shield, but the detailed distribution must be calculated or estimated by some other means.

For thermal neutrons a definite phenomenological theory similar to the fast-removal method is not available. The requirement of knowing the detailed thermal-flux distributions within and around the interfaces of shield laminations prevents any direct use of a removal method. Such a method is inherently an averaging process, and it is not able to give detailed information.

Bulk-shielding experiments will furnish an estimate of the thermal-neutron-flux distribution in the reactor shield. However, the shielding experiment will only provide data on a specific shield arrangement (usually not in detail like the reactor shield being designed), and, unless some knowledge is developed as to why the measured distributions appear as they do, the shield designer is faced with two serious problems:

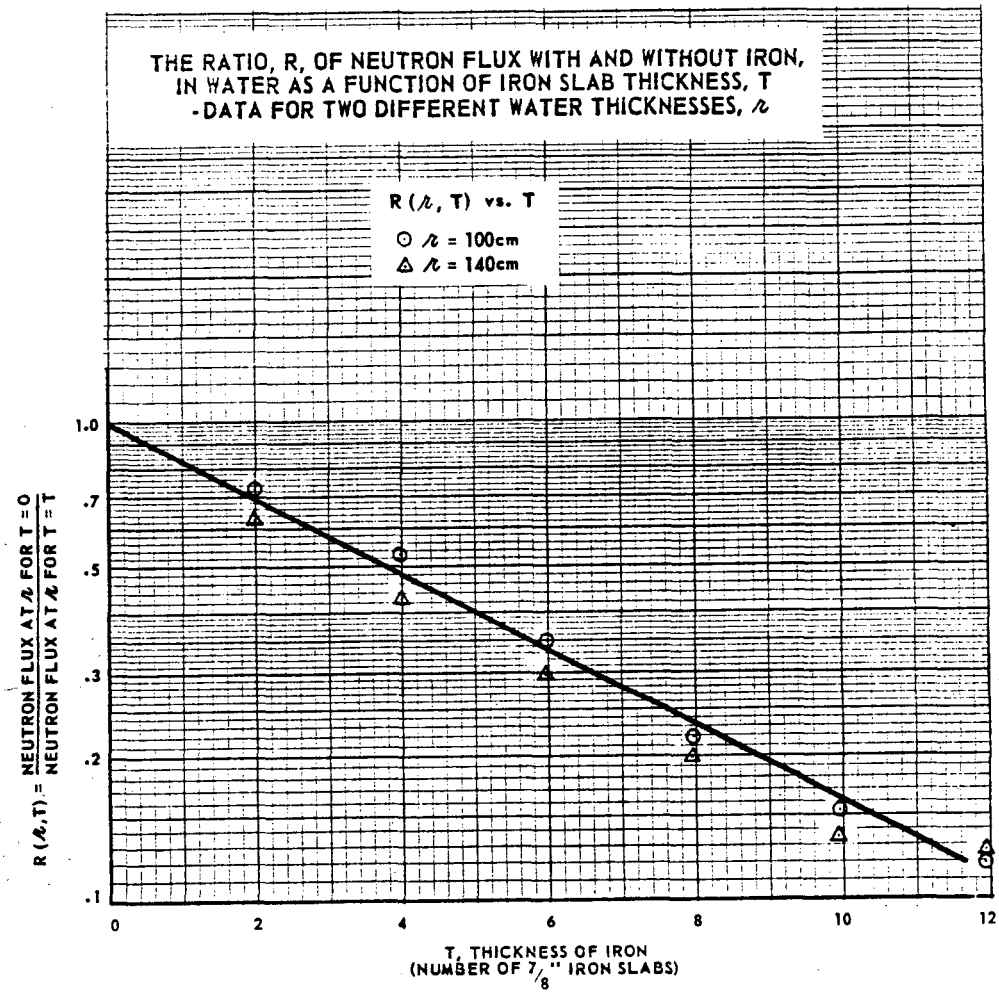


Figure 3.14

1. In applying the bulk-shielding data to the actual reactor, there is a lack of knowledge as to what the differences between the mock-up and the actual core shield mean quantitatively. Scale-up from bulk-shielding data to actual core design is made on the basis of the ratio of fast-neutron leakages because it is the fast-neutron attenuation that determines the thermal-neutron distributions. Scale-up is explained in Sec. 3.3.

2. During the evolution of the full reactor-plant design, many changes occur and detailed questions arise involving location of structural members, piping, instrumentation, etc., within the core shield. These questions cannot be answered except by more experiments unless some interpretation of the basic secondary-emission characteristics is known. It is usually impractical to run more experiments for each question; therefore a more basic understanding is essential.

One approach to gaining such knowledge is a parametric experimental study of certain basic core-shield mediums, such as iron-water and lead-water. The Navy shield test run in the lid tank in 1950 is an example of such a study, although the variations were restricted to a range of compositions of immediate interest. The neutron results for this test are shown in Fig. 3.12.

A method for calculating the thermal-flux distribution in the region of iron-water laminations in the shield has been carried out in reference 41. This involved the use of a three-group diffusion-theory model. The three-group equations are

$$\nabla^2\phi_f - K_f^2\phi_f = 0 \tag{27}$$

$$\nabla^2\phi_m - K_m^2\phi_m + (3\Sigma_{af/\lambda_m})\phi_f = 0$$

$$\nabla^2\phi_{th} - (1/L^2)\phi_{th} + (3\Sigma_{am/\lambda_{th}})\phi_m = 0$$

The fast group source is the calculated uncollided flux distribution.

The motivation of this particular choice is the following. The most basic features of the detailed neutron slowing-down picture in the laminated shield are three:

1. The high-energy neutrons, which characterize the over-all neutron penetration of the shield. (These are the neutrons treated in the fast-removal method.)

2. An intermediate-energy neutron group, which is supplied by degradation of the high-energy group by inelastic scattering in the heavy elements. The peak in the thermal flux in the water just beyond a slab of steel in a core shield is caused by the rapid thermalization of these neutrons produced in the steel slab.

3. The thermal group, which varies rapidly as a function of position because of large changes in the absorption cross sections of the various laminated mediums. It is this group that must be known because it furnishes the source for capture gammas in the shield.

This three-group calculation was applied to an idealization of the iron-water bulk-shielding experiments. The results are plotted in Fig. 3.15. The fast group, calculated on the basis of the fast-removal model, is shown, as well as the calculated thermal flux. The data from the iron-water experiment, scaled up to the same power level and geometry, are plotted for comparison. The qualitative success of this model is attributable to the fact that the fast-group and intermediate-group constants were determined largely from the bulk-shielding experiment itself. Group constants obtained in the normal manner, within the framework of group diffusion theory, would be expected to yield meaningful results only if the complete description of inelastic scattering were included.

The availability of adequate microscopic nuclear data throws open many possible theoretical approaches. The stochastic sampling technique (Monte Carlo method) with intelligent weighting methods seems particularly fruitful at this time with the availability of large-scale digital computers to carry out the burdensome calculations that are involved.

3.3 Geometry for Fast-neutron Attenuation

(a) Spherical Core and Shield. The theory and data presented in Sec. 3.1 give us a basis for computing the over-all fast-neutron attenuation in a reactor shield—one of the first characteristics of the shield which must be ascertained. There remains to apply this attenuation description to the source geometry and distribution of a specific reactor core and its shield configuration.

As in the removal cross section theory, the core and shield mediums are treated by simply computing the uncollided flux using an attenuation kernel. First, for simplicity, consider a core with a uniform power distribution of P watts per cubic centimeter and a spherical core of radius R_c. The fission-neutron-source density will be, from Sec. 1.1,

$$7.75 \times 10^{10}P \text{ neutrons/cm}^3\text{-sec}$$

If the point-source attenuation kernel is $G(\Sigma\rho)$ per unit source and the shield is uniform, the uncollided flux at distance R centimeters beyond the surface of the core is (see Fig. 3.16)

$$\phi_u(R) = 2\pi \times 7.75 \times 10^{10}P \int_{\sqrt{1-(R_c/a)^2}}^{1} d\mu \int_{a\mu-\sqrt{a^2\mu^2-b_c}}^{a\mu+\sqrt{a^2\mu^2-b_c}} \rho^2\, d\rho\; G(\Sigma_c\rho_c)\, G(\Sigma_s\rho_s) \tag{28}$$

where $a = R + R_c$ $\quad b_c = a^2 - R_c^2$ $\quad \mu = \cos\theta$

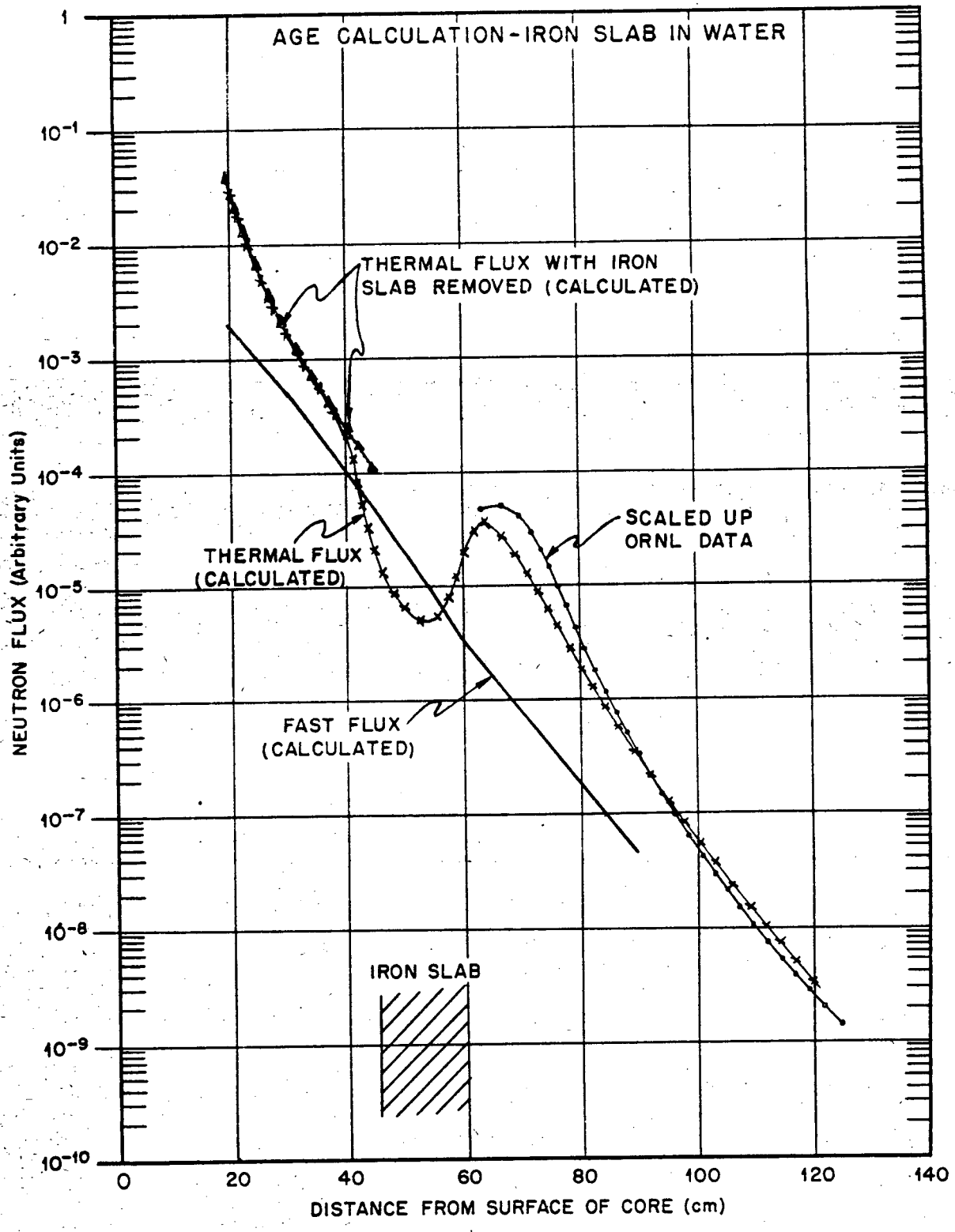
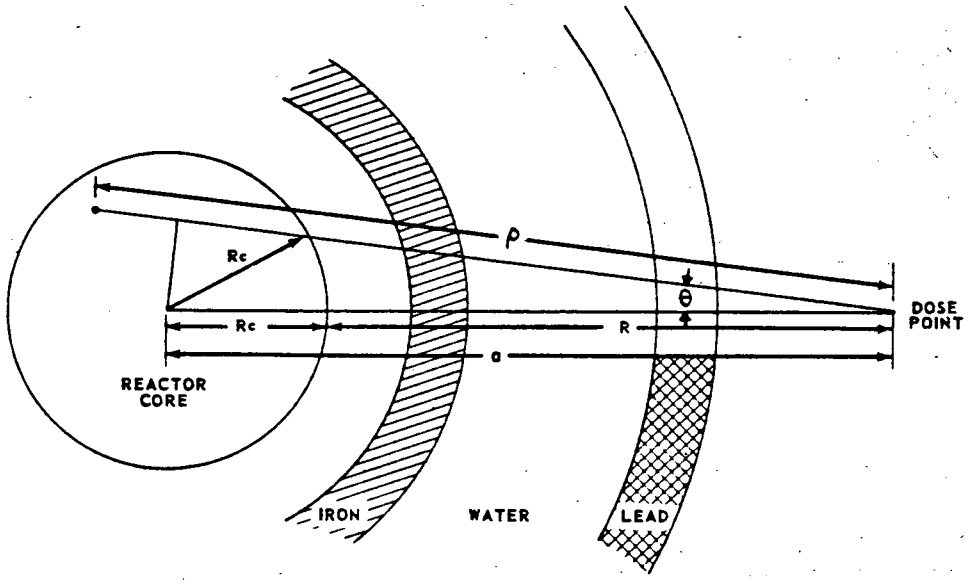

AGE CALCULATION-IRON SLAB IN WATER
THERMAL FLUX WITH IRON SLAB REMOVED (CALCULATED)
THERMAL FLUX (CALCULATED)
SCALED UP ORNL DATA
FAST FLUX (CALCULATED)
IRON SLAB
NEUTRON FLUX (Arbitrary Units)
DISTANCE FROM SURFACE OF CORE (cm)
1
10⁻¹
10⁻²
10⁻³
10⁻⁴
10⁻⁵
10⁻⁶
10⁻⁷
10⁻⁸
10⁻⁹
10⁻¹⁰
0
20
40
60
80
100
120
140

Figure 3.15



GEOMETRY OF SPHERICAL CORE AND SHIELD

Figure 3.16

There are two choices for $G(\Sigma\rho)$: Eq. 19 resulting from the saddle-point integration or an exponential fit to experimental distribution in water. Suppose that the latter form is

$$G(\Sigma\rho) = \frac{1}{4\pi\rho^2} \sum_{i=1}^{N} A_i e^{-\Sigma_i \rho} \qquad (29)$$

Suppose also that the volume fraction of metal, or materials other than water, in the core is f_c and that the fraction of metal in the shield is f_s. The attenuation of a point-source beam is then given by:

$$\text{Attenuation in the core} = e^{-f_c \Sigma_{mc} \rho_c} \sum_{i=1}^{N} A_i e^{-(1-f_c)\Sigma_{ic}\rho_c}$$

$$\text{Attenuation in the shield} = e^{-f_s \Sigma_{ms} \rho_s} \sum_{i=1}^{N} A_i e^{-(1-f_s)\Sigma_{is}\rho_s}$$

Equation 28 becomes

$$\phi_u(R) = 3.875 \times 10^{10} P \int_{\sqrt{1-(R_c/a)^2}}^{1} d\mu \int_{a\mu-\sqrt{a^2\mu^2-b_c}}^{a\mu+\sqrt{a^2\mu^2-b_c}} \exp\left(-f_c\Sigma_{mc}\rho_c - f_s\Sigma_{ms}\rho_s\right) \times \sum_{i=1}^{N} A_i \exp\left[-(1-f_c)\Sigma_{ic}\rho_c - (1-f_s)\Sigma_{is}\rho_s\right] d\rho \qquad (30)$$

This can be written in the following form:

$$\phi_u(R) = 3.875 \times 10^{10} P \int_{\sqrt{1-(R_c/a)^2}}^{1} d\mu \int_{a\mu-\sqrt{a^2\mu^2-b_c}}^{a\mu+\sqrt{a^2\mu^2-b_c}} \exp\left[-f_c\Sigma_{mc}\rho - (f_s\Sigma_{ms} - f_c\Sigma_{mc})(a\mu - \sqrt{a^2\mu^2 - b_c})\right] \sum A_i \exp\left\{-(1-f_c)\Sigma_{ic}\rho - \left[(1-f_s)\Sigma_{is} - (1-f_c)\Sigma_{ic}\right](a\mu - \sqrt{a^2\mu^2 - b_c})\right\} d\rho \qquad (31)$$

$\rho_c = \rho - \rho_s$ = the distance from unit-source volume to surface of sphere along line between unit source and the point R

$\rho_s = a\mu - \sqrt{a^2\mu^2 - b_c}$ = the distance in shield along line between unit-source volume and point R

Σ_{mc} = the effective removal cross section for nonhydrogenous materials in core (cm^{-1})

Σ_{ms} = the effective removal cross section for nonhydrogenous materials in shield

f_c = the volume fraction of nonhydrogenous materials in core

f_s = the volume fraction of nonhydrogenous materials in shield

The first integration can be carried out to give

$$\phi_u(R) = 3.875 \times 10^{10} P \int_{\sqrt{1-(R_c/a)^2}}^{1} d\mu \sum_{i=1}^{N} \frac{A_i}{f_c(\Sigma_{mc} - \Sigma_{ic}) + \Sigma_{ic}} \exp\left\{-\left(a\mu - \sqrt{a^2\mu^2 - b_c}\right)\right.$$

$$\left. \times \left[f_s(\Sigma_{ms} - \Sigma_{is}) + \Sigma_{is}\right]\right\}\left(1 - \exp\left\{-2\sqrt{a^2\mu^2 - b_c}\left[f_c(\Sigma_{mc} - \Sigma_{ic}) + \Sigma_{ic}\right]\right\}\right) \quad (32)$$

Several important characteristics of this part of the neutron-attenuation problem can be revealed by examining certain approximations to the above integral. The integral takes on simple forms if the flux is computed within or on the surface of the core, or at large distances from the core. Since the effective removal-cross-section theory is generally useful only at large distances from the source, the latter approximation is particularly useful.

At large distances from the core the angle subtended by the core surfaces is small; that is, the integration variable θ is restricted to sufficiently small values that the following approximation can be made:

$$\mu = \cos\theta \cong 1, \quad \sin\theta = \theta$$

Equation 32 reduces to

$$\phi_u(R) = 3.875 \times 10^{10} P \int_0^{R_c/(R_c+R)} \theta\, d\theta \sum_{i=1}^{N} \frac{A_i}{f_c(\Sigma_{mc} - \Sigma_{ic}) + \Sigma_{ic}} \exp\left\{-\left[f_s(\Sigma_{ms} - \Sigma_{is})\right.\right.$$

$$\left.\left. + \Sigma_{is}\right](a - R_c)\right\}\left(1 - \exp\left\{-2\left[f_c(\Sigma_{mc} - \Sigma_{ic}) + \Sigma_{ic}\right]R_c\right\}\right)$$

$$\phi_u(R) = 3.875 \times 10^{10} \frac{P}{2}\left(\frac{R_c}{R_c + R}\right)^2 \sum_{i=1}^{N} \frac{A_i}{f_c(\Sigma_{mc} - \Sigma_{ic}) + \Sigma_{ic}} \exp\left\{-\left[f_s(\Sigma_{ms} - \Sigma_{is})\right.\right.$$

$$\left.\left. + \Sigma_{is}\right]R\right\}\left(1 - \exp\left\{-2\left[f_c(\Sigma_{mc} - \Sigma_{ic}) + \Sigma_{ic}\right]R_c\right\}\right) \quad (33)$$

In the event the attenuation kernel (Eq. 29) is given by a simple exponential of one term (i = 1, A = 1)

$$G(\Sigma\rho) = \frac{1}{4\pi\rho^2} e^{-\Sigma_h \rho}$$

Eq. 32 further reduces to

$$\phi_u(R) = 3.875 \times 10^{10} \frac{P}{2}\left(\frac{R_c}{R_c + r}\right)^2 \frac{1}{f_c(\Sigma_{mc} - \Sigma_{hc}) + \Sigma_{hc}} \exp\left\{-\left[f_s(\Sigma_{ms} - \Sigma_{hs}) + \Sigma_{hs}\right]R\right\}$$

$$\times \left(1 - \exp\left\{-2\left[f_c(\Sigma_{mc} - \Sigma_{hc}) + \Sigma_{hc}\right]R_c\right\}\right) \quad (34)$$

These approximate relations can be used to answer several questions:

1. They provide a simple basis for the relative evaluation for over-all neutron attenuation of various shield mediums (assuming that the effective removal cross sections are known).
2. The effect of distance can be easily extracted. (The neutron flux varies inversely with the square of the distance measured from the center of the core.)
3. A fairly accurate description of the effects of some of the detailed characteristics of the core can be inferred. It is of value to delineate this last feature in more detail. This is done in Sec. 3.4 after other geometries are discussed.

(b) Cylindrical Core and Shield. The attenuation of fast neutrons in a shield surrounding a cylindrical core can be derived in a manner similar to that for the spherical core in Eq. 28. In this case the source distribution is assumed to be a function of length and radius of the following form:

$$S(r,z) = S_0 R(R) Z(Z) \tag{35}$$

The geometry is shown in Fig. 3.17. If the point-source attenuation kernel is G(R) per unit source and the shield is uniform, the uncollided flux at distance R centimeters beyond the surface of the core is

$$\phi(R) = \int_V \frac{S(r,z)}{4\pi\rho^2} G(R)\, dV \tag{36}$$

If cylindrical coordinates are used (see Fig. 3.17), this becomes

$$\phi = \frac{2}{4\pi} \int_{\psi=0}^{\pi} \int_{r=0}^{R_c} \int_z \frac{S(r,z)\, r\, d\psi\, dr\, dz}{\rho^2} G(R) \tag{37}$$

where $\rho^2 = z^2 + a^2 + r^2 - 2ar\cos\psi$

ψ = the azimuthal angle with respect to the transverse axis of the cylinder

a = the distance from the axis of the cylinder to the point at which the flux is being calculated

The solution of this equation has been carried out in reference 42. The approximation to the solution is given in Chap. 9. Both of these are for a source strength invariant in space. If a spatial distribution of the source is given, the integration is best obtained by numerical integration.

(c) Exponential Expression for Fast-neutron Attenuation in Hydrogenous Shield. In Sec. 3.3a the equations for the variation of fast-neutron flux in the core and shield have been developed in which the attenuation of fast neutrons in hydrogenous material are fitted by Eq. 29. Two sets of values for the constants in Eq. 29 are presented by approaching the problem from two directions. These are (1) an exponential fit to an infinite-plane source and (2) an exponential fit to a point-source attenuation curve. The actual experimental data taken in the LTSF at the ORNL are the attenuation in water of fast neutrons from a disk source.

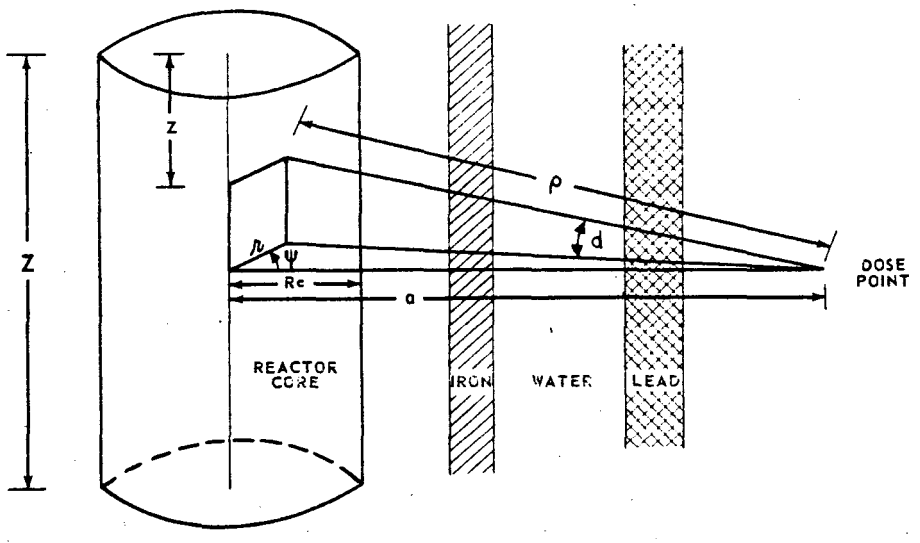
For the infinite-plane-source case the choice is a linear combination of two simple exponentials. This form will approximate the experimental curve quite closely over a wide range of distances from the source. It has the form

$$\phi(r) = A_1 e^{-\Sigma_1 r} + A_2 e^{-\Sigma_2 r} \tag{38}$$

where $\Sigma_1 = 0.14\ \text{cm}^{-1}$

$\Sigma_2 = 0.10\ \text{cm}^{-1}$

$A_2 / A_1 = 35$



GEOMETRY OF CYLINDRICAL CORE AND SHIELD

Figure 3.17

Using a plane-to-disk source transformation,

$$D_{pl}(r,a) = D_{pl}(r,\infty) - D_{pl}(\sqrt{r^2 + a^2},\infty)$$

Eq. 38 can be changed into a disk-source equation. The radius of the disk, a, is equal to the radius of the ORNL LTSF disk-source plate. Assuming a unit-source strength, the results are plotted on Fig. 3.18 with the experimental curve.

The proper point-source beam kernel g(r) was obtained by fitting the ORNL Lid Tank data after transformation to point-source geometry. If g(r) is set equal to $e^{-0.103r}$, where r is in centimeters, the flux as a function of distance from the lid-tank plate computed by using Eq. 39 agrees within 10 per cent with experimental data in the range of 10 to 140 cm.

Assuming each point of the ORNL disk source to radiate isotropically and the point-source beam kernel to be given by $g(r) = e^{-0.103r}$, the flux along the center line of the disk will be

$$\phi(r) = S_A \left[E_1(0.103r) - E_1(0.103\sqrt{r^2 + a^2})\right] \qquad G(r) = \frac{g(r)}{4\pi r^2} \tag{39}$$

Assuming unit-source strength, this equation is also plotted on Fig. 3.18. Figure 3.18 shows both approximations, and the choice of fit is left to the shield designer.

(d) Scaling Up Experimental Data. Much experimental work has been done at ORNL. The experimental facility is described in reference 43. The Lid Tank facility consists of a disk-source plate of fission neutrons placed in a water tank. Readings of fast-neutron dose rate, thermal-neutron flux, and gamma-ray dose rate are made as a function of the distance from the source plate with combinations of water and other materials between the source and detector.

In order to utilize these experimental data, a transformation must be made between the disk-source plate of the experimental facility and the (generally) cylindrical-source geometry of a reactor core.

Analytical Representation of the Flux from a Disk. The source is essentially a disk of radius R_p. It is assumed that the fast-neutron leakage from the surface of the disk has an isotropic angular distribution. If the point-source beam kernel, which represents the attenuation of fast neutrons in water and inherently takes into account the change in spectral distribution with penetration, is given by

$$g(r) = \sum_j A_j e^{-\Sigma_j r}$$

then the flux at a distance R in water along the axis of a disk of radius R_p of unit-source density is

$$I_p(R) = \tfrac{1}{2} \sum_j A_j \left[E_1(\Sigma_j R) - E_1(\Sigma_j \sqrt{R^2 + R_p^2})\right] \tag{40}$$

where R_p = the radius of the source disk
R = the distance from the surface of the disk

$$E_1(x) = \int_x^\infty \frac{e^{-u}}{u}\, du$$

j depends on the number of terms in the equation used to fit the curve of fast-neutron attenuation in wate-

Analytical Representation of the Flux from a Cylinder. Also the flux along the mid-plane of a cylinder of radius R_c at a distance R in water from its surface, assuming unit-source density, is (from Eq. 37)

$$I_c(R) = \int_0^{\cos^{-1}\left(\frac{R_c}{R+R_c}\right)} d\theta \sum_j \frac{R_c A_j}{\pi x} \int_0^{\arctan \frac{L}{2x}} e^{-\Sigma_j x \sec \phi}\, d\phi \tag{41}$$

where $x = \sqrt{(R_c)^2 + (R + R_c)^2 - 2(R + R_c)R_c \cos\theta}$
R_c = the radius of the cylinder
L = the length of the cylinder

Geometrical Conversion from Disk to Cylinder. The ratio of I_c/I_p is plotted in Fig. 3.19 as a function of the distance in water from the source surfaces for four different cylinder lengths.

3.4 Sources of Error

(a) Removal Cross Section of Core Materials. Very often the core materials are relatively esoteric as compared to typical shield materials, and experimental data are not available to provide removal cross sections. Is this lack of data a serious problem to the shield design? The average core removal cross section is Σ_{mc}, and this question can be answered by relating the variation of this cross section with the variation of flux. Differentiating Eq. 34 for the flux with respect to $f_c\Sigma_{mc}$, the following is obtained

$$\frac{\Delta\phi_u}{\phi_u} = -\frac{\Delta(f_c\Sigma_{mc})}{f_c\Sigma_{mc}} \left(\frac{1}{1 - \frac{\Sigma_{hc}}{\Sigma_{mc}} + \frac{\Sigma_{hc}}{f_c\Sigma_{mc}}} \right.$$

$$\left. + \frac{2(f_c\Sigma_{mc})\, R_c \exp\left\{-2[f_c(\Sigma_{mc} - \Sigma_{hc}) + \Sigma_{hc}]\, R_c\right\}}{\exp\left\{-2[f_c(\Sigma_{mc} - \Sigma_{hc}) + \Sigma_{hc}]\, R_c\right\} - 1} \right) \tag{42}$$

In typical practical cases the second term in the parentheses is small compared to the first. This is due to the negative exponential in the second term. The variation can therefore be written

$$\frac{\Delta\phi_u}{\phi_u} \cong -\frac{\Delta(f_c\Sigma_{mc})}{f_c\Sigma_{mc}} \frac{f_c\Sigma_{mc}}{f_c(\Sigma_{mc} - \Sigma_{hc}) + \Sigma_{hc}} \tag{43}$$

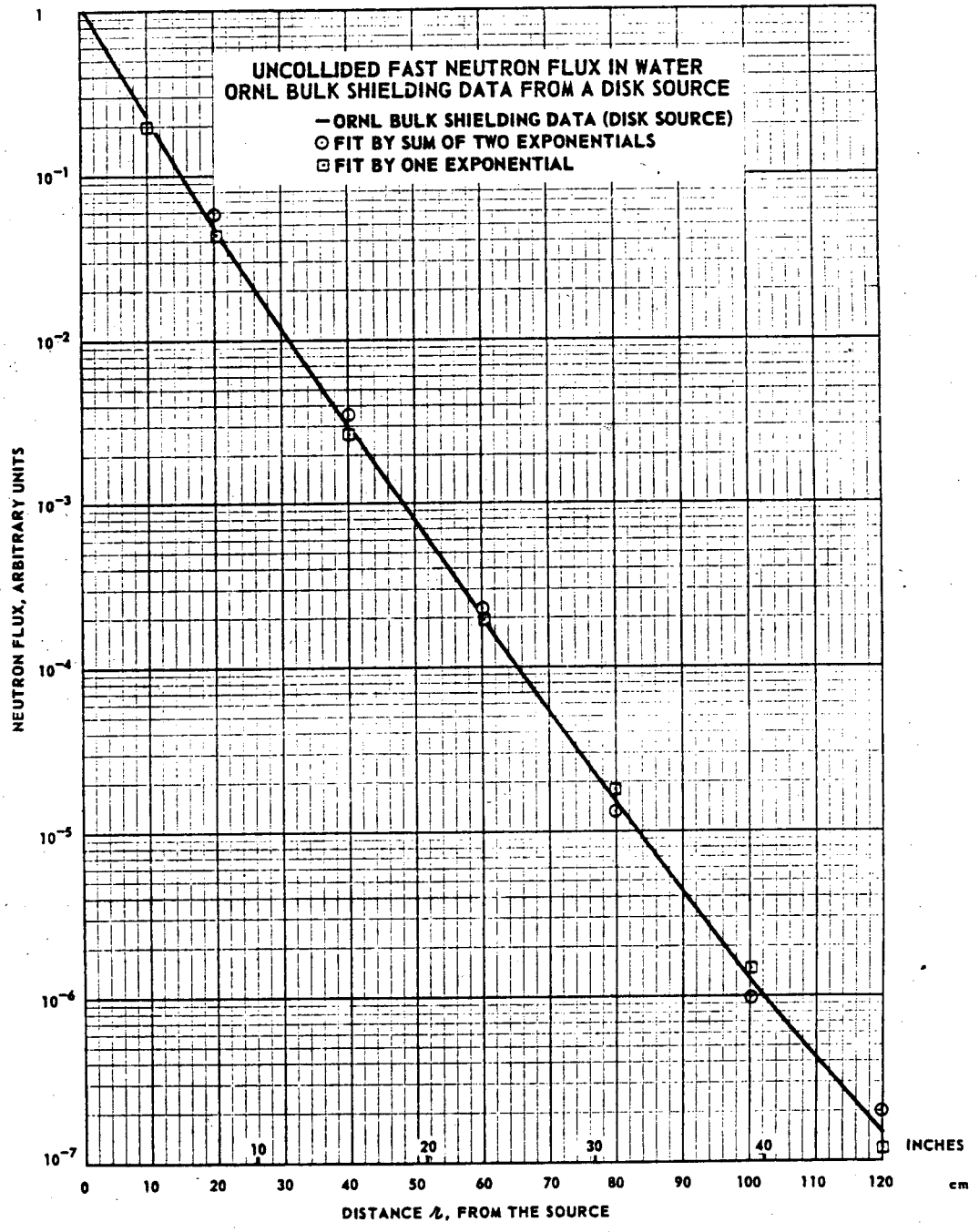

UNCOLLIDED FAST NEUTRON FLUX IN WATER
ORNL BULK SHIELDING DATA FROM A DISK SOURCE
—ORNL BULK SHIELDING DATA (DISK SOURCE)
⊙ FIT BY SUM OF TWO EXPONENTIALS
⊡ FIT BY ONE EXPONENTIAL
NEUTRON FLUX, ARBITRARY UNITS
1
10^{-1}
10^{-2}
10^{-3}
10^{-4}
10^{-5}
10^{-6}
10^{-7}
10
20
30
40
INCHES
0 10 20 30 40 50 60 70 80 90 100 110 120 cm
DISTANCE ℓ, FROM THE SOURCE

Figure 3.18

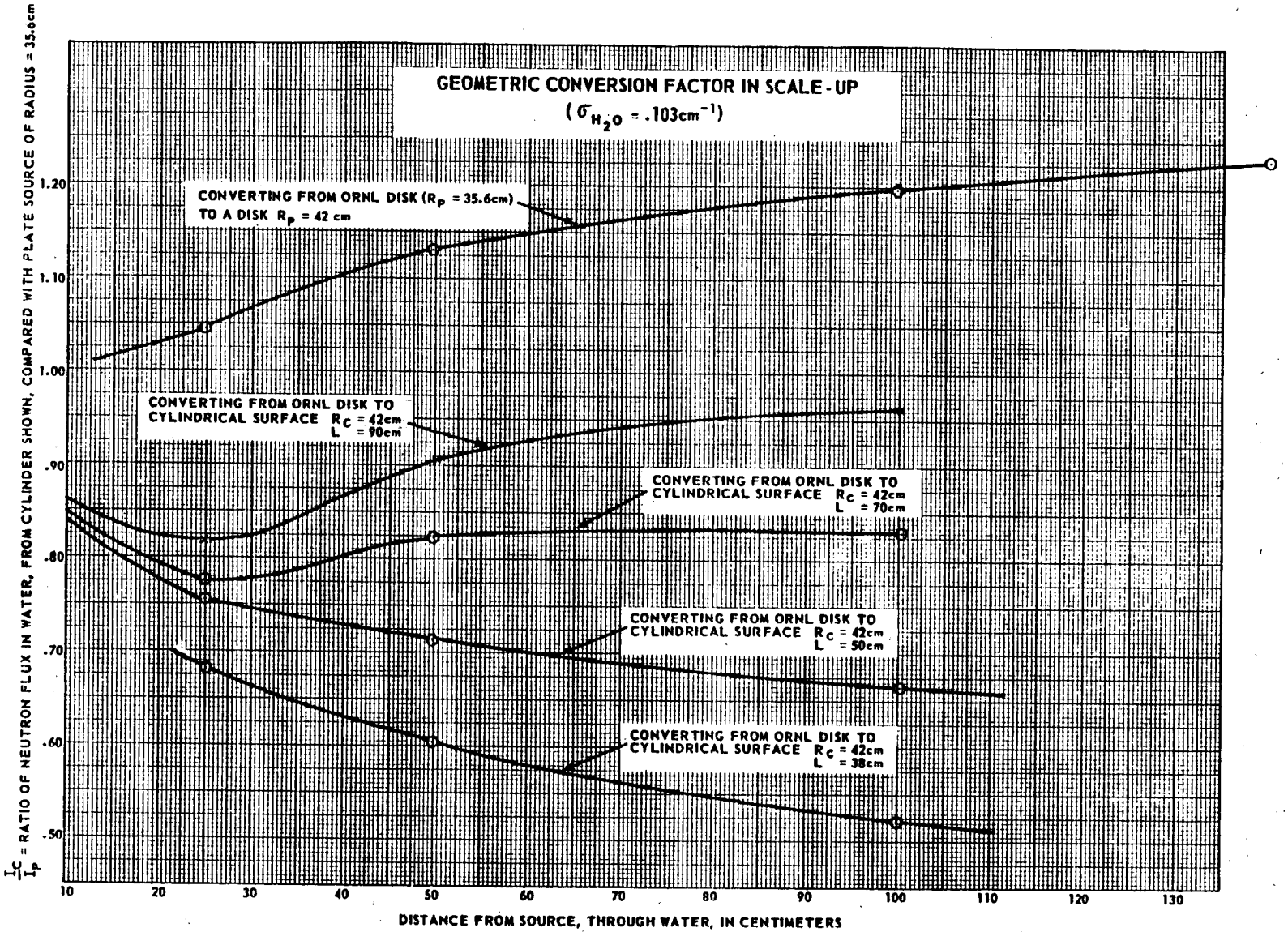

GEOMETRIC CONVERSION FACTOR IN SCALE-UP
(σ_{H_2O} = .103cm^{-1})
CONVERTING FROM ORNL DISK (R_p = 35.6cm) TO A DISK R_p = 42 cm
CONVERTING FROM ORNL DISK TO CYLINDRICAL SURFACE R_c = 42cm L = 90cm
CONVERTING FROM ORNL DISK TO CYLINDRICAL SURFACE R_c = 42cm L = 70cm
CONVERTING FROM ORNL DISK TO CYLINDRICAL SURFACE R_c = 42cm L = 50cm
CONVERTING FROM ORNL DISK TO CYLINDRICAL SURFACE R_c = 42cm L = 38cm
$\frac{I_c}{I_p}$ = RATIO OF NEUTRON FLUX IN WATER, FROM CYLINDER SHOWN, COMPARED WITH PLATE SOURCE OF RADIUS = 35.6cm
1.20
1.10
1.00
.90
.80
.70
.60
.50
10
20
30
40
50
60
70
80
90
100
110
120
130
DISTANCE FROM SOURCE, THROUGH WATER, IN CENTIMETERS

Figure 3.19

This relation shows that the flux estimate in the shield is relatively insensitive to the core removal cross section. In a typical water-cooled core the term

$$\frac{f_c \Sigma_{mc}}{f_c(\Sigma_{mc} - \Sigma_{hc}) + \Sigma_{hc}} \approx 0.5$$

where the individual terms may have the following magnitudes:

$$f_c = 0.5 \qquad \Sigma_{mc} = 0.12 \text{ cm}^{-1} \qquad \Sigma_{hc} = 0.103 \text{ cm}^{-1}$$

Thus an error in determination of Σ_{mc} of 50 per cent would give an error in ϕ of about 25 per cent.

(b) Removal Cross Section of Shield Materials. To determine the effect of errors in the shield removal cross section, again differentiate Eq. 34 with respect to $f_s\Sigma_{ms}$. The resulting relation similar to Eq. 43 is

$$\frac{\Delta\phi_u}{\phi_u} = -f_s\Sigma_{ms} R \frac{\Delta f_s \Sigma_{ms}}{f_s \Sigma_{ms}} \tag{44}$$

In typical core-shield designs $f_s\Sigma_{ms} R$ reaches values in the vicinity of 10. Here an error in the shield removal cross section is propagated in the flux estimate by a factor of 10.

(c) Effect of Core Size. Another question confronting the shield designer involves the care with which the core geometry should be described. A partial answer to this question can be given by examining the variation of Eq. 34 with the spherical-core radius. Thus

$$\frac{\Delta\phi_u}{\phi_u} = 2\left(\frac{R}{R_c + R} + \frac{[f_c(\Sigma_{mc} - \Sigma_{hc}) + \Sigma_{hc}] R_c \exp\{-2[f_c(\Sigma_{mc} - \Sigma_{hc}) + \Sigma_{hc}] R_c\}}{1 - \exp\{-2[f_c(\Sigma_{mc} - \Sigma_{hc}) + \Sigma_{hc}] R_c\}}\right)\frac{\Delta R_c}{R_c} \tag{45}$$

As in Eq. 42 the second term in Eq. 45 is negligible, and the flux varies as $2R/(R_c + R)$. A change in the core radius then tends to produce an equal change in flux, assuming that the power density remains the same. On the other hand, if the total power is kept constant, as is usually the case, the variation goes in the opposite direction because the power density (or source intensity) is a more sensitive parameter than the core radius. Here (where PR_c^3 in Eq. 34 remains constant)

$$\frac{\Delta\phi_u}{\phi_u} = -\frac{dR_c}{R_c}\left(\frac{3R_c + R}{R_c + R} + \frac{[f_c(\Sigma_{mc} - \Sigma_{hc}) + \Sigma_{hc}] R_c \exp\{-2[f_c(\Sigma_{mc} - \Sigma_{hc}) + \Sigma_{hc}] R_c\}}{\exp\{-2[f_c(\Sigma_{mc} - \Sigma_{hc}) + \Sigma_{hc}] R_c\}}\right) \tag{46}$$

$$\cong -\frac{dR_c}{R_c}\left(\frac{3R_c + R}{R_c + R}\right)$$

(d) Power Distribution in the Core. A final consideration is the importance of an accurate estimate of the over-all neutron attenuation of the actual power distribution in the core. Again, an examination of Eq. 34 will provide some insight. It is seen that the term that represents the self-attenuation of the core is

$$1 - \exp\{-2[f_c(\Sigma_{mc} - \Sigma_{hc}) + \Sigma_{hc}] R_c\}$$

This term reveals the fact that, for a uniform source density, the effective region of the core for neutrons penetrating the shield is within

$$[f_c(\Sigma_{mc} - \Sigma_{hc}) + \Sigma_{hc}]^{-1} \quad \text{centimeters}$$

of the surface of the core. For a typical water-cooled core this distance is only about 6 cm. Thus the important region in which an accurate power distribution should be provided is near the surface of the core. Of course, if the power distribution decreases rapidly as the surface of the core is approached, the region of influence increases in size. Comparatively simple calculations like the one above can, however, delineate the region of influence so that unnecessary detail is not included beyond that region.

(e) Effect of Laminations in Shields. In the previous discussion only a homogeneous shield was considered. In the case of laminated shields, which are more usually encountered, the same procedures are followed, except that a somewhat more cumbersome integral analogous to Eq. 32 arises. In the case of a spherical core and shield with n laminated regions, the resulting expression becomes

$$\phi_u = 3.875 \times 10^{10} P \int_{\sqrt{1-(R_c/a)^2}}^{1} d\mu \sum_{i=1}^{n} \frac{A_j}{f_c(\Sigma_{mc} - \Sigma_{ic}) + \Sigma_{ic}} \times \left(1 - \exp\left\{-2\sqrt{a^2\mu^2 - b_c}\,[f_c(\Sigma_{mc} - \Sigma_{ic})]\right\}\right) \exp\left[-\Sigma_i(\mu)\right] \qquad (47)$$

where $\Sigma_i(\mu) = [f_{s_1}(\Sigma_{m_1} - \Sigma_{i_1}) + \Sigma_{i_1}](\sqrt{a^2\mu^2 - b_1} - \sqrt{a^2\mu^2 - b_c})$

$+ [f_{s_2}(\Sigma_{m_2} - \Sigma_{i_2}) + \Sigma_{i_2}]\,(\sqrt{a^2\mu^2 - b_2} - \sqrt{a^2\mu^2 - b_1})$

$+ \ldots + [f_{s_n}(\Sigma_{m_n} - \Sigma_{i_n}) + \Sigma_{i_n}]\,(a\mu - \sqrt{a^2\mu^2 - b_{n-1}})$

$b_j = a^2 - R_j^2$

R_j = the radius of the outer boundary of the j*th* shield lamination surrounding the core

Σ_{m_j} = the effective removal cross section of the j*th* lamination

Σ_{i_j} = the constants in the exponential fit of the water attenuation curve, if any water exists in the j*th* lamination. If there is no water in the j*th* lamination, $\Sigma_{i_j} = 0$

It should be reemphasized that excessive detail in treating the lamination should be avoided since the removal-cross-section theory does not attempt to handle this kind of detail.

(f) Misuse of Removal Cross Sections. The question might be posed at this juncture as to the desirability of having this semiempirical neutron theory if simple curve fitting procedures can be used instead. The value of the theory is basically in the understanding it provides of the actual neutron penetration characteristics of the shield. The fact that such a simple theory yields a distribution shape that is close to that measured gives assurance that a few simple microscopic processes determine the penetration characteristics of the medium. This provides in turn a basis for interpretation of the attenuation experiments as well as interpolation of the data in a given shield design.

Thus far the limitations of applicability of the semiempirical approach have been delineated by pointing out the requirements on Eq. 25 for the effective removal cross section (see Sec. 3.1b). A more tangible basis must be established to avoid misapplication of the theory. If the neutron distributions in the iron-water experiment in Fig. 3.12 are examined, it is seen that there is an asymptotic behavior which occurs at large distances in the water which fits the removal-cross-section theory. It is in this region that the expression for the removal cross section has its proper behavior. Thus the range of application of the theory can be limited to that distance in water behind the heavy slab at which the equilibrium, or asymptotic, property appears, if thermal neutrons are used as a criterion for total neutron dose.

Table 3.9 lists this distance, d, for the various iron-slab thicknesses, T.

It can be seen from Table 3.9 that approximately 2 ft of water is required before spectral equilibrium of the neutrons is regained. These values should not be considered exact since it is difficult from the data to determine the exact point at which the asymptotic slope is reached and because varying amounts of water exist between the slabs. They do indicate, however, the magnitude of the limitation on the use of the removal-cross-section theory. Even a fast-neutron dosimeter cannot be relied on when no information exists on the dose from the large spectral region between thermal and the dosimeter threshold. A further indication of the

Table 3.9 —DISTANCE BEHIND IRON SHIELD AT WHICH EQUILIBRIUM IS REGAINED

T, cm	d, cm
4.44	29
8.88	29
13.3	29
17.8	34
22.2	35
26.2	36
31.1	37

Table 3.10 —MAXIMUM VALUES OF THE RATIO BETWEEN THE MEASURED AND UNCOLLIDED FLUX

Thickness of iron slabs, cm	$\frac{\phi_{peak}}{\phi_{unperturbed}}$
4.44	1.6
8.88	2.6
13.3	3.6
17.8	6.4
22.2	7.4
26.6	13.0
31.1	20.0

magnitude of the error that can result from indiscriminate use of the theory is given in Table 3.10, which lists the maximum values of the ratio between the peak thermal flux and the unperturbed flux in the Navy test (Fig. 3.12).

Although these maximum values are generally reached within 7 cm of the iron, they show the serious errors that can arise if the removal theory is applied without thought. The accuracy and range of application for other mediums used, of course, differ from iron. There is similar information available for lead which indicates that although the variation from the simple theory is not as great near the lead (as it is near iron), the equilibrium conditions set in at even further distances in water. Data of this type are generally sparse for other materials. It is necessary to depend either on rough theoretical estimates or on further experimentation to fill in this gap in the information.

4 HEAT GENERATION IN SHIELDS

4.1 Introduction

Interactions between radiation and material result in a transfer of energy which heats the material. Near a power reactor core the radiation levels are generally so high and changing so rapidly that severe local overheating can occur in structural parts. It is usually the re-

sponsibility of the shield designer to calculate this heating and to specify maximum permissible thicknesses and required provisions for cooling. Failure to do so properly can lead to excessive thermal stresses, surface boiling, or distortion of structural parts.

The radiation intensity at the edge of a reactor core is limited by the obtainable power density in the core and the allowable neutron leakage. These factors generally limit the fast-neutron-leakage flux to below 10^{14} neutrons/cm^2-sec. The thermal-neutron flux may tend to peak in a good reflector, and metal at that location could be in thermal-neutron fluxes as high as 10^{15} neutrons/cm^2-sec. Gamma fluxes resulting from neutron reactions will be of the same magnitude. This implies a total energy flux greater than 10^{15} Mev/cm^2-sec, or 500,000 Btu/hr/sq ft. Internal heat generation in steel can be as high as 10 watts/cm^3 or more.

From these values the radiation must be reduced so that the radiation damage and heating in the reactor-vessel walls will be tolerable. For heavy-walled pressure vessels a limit based on 50°F temperature difference across the wall has commonly been used. This is equivalent to an impinging flux of about 10^{11} Mev/cm^2-sec of gammas plus neutrons. For thinner walled vessels the flux can be somewhat higher. This reduction is usually accomplished by placing a series of shields between the reactor core and the vessel wall. These internal shields are called thermal shields. The required total thickness of shielding (which might be as much as 8 in.) is, in practice, divided into several layers with cooling in between to reduce thermal stress. The innermost shield may have to be limited to less than 1 in. in thickness. Each thermal shield shields the next one outward, and therefore the allowable shield thickness increases rapidly with distance from the core.

It must be remembered that the thermal shield will produce a large number of secondary gammas from neutron reactions and hence will influence the design of the biological shielding (i.e., the great bulk of the shielding, the purpose of which is to protect personnel.)

There are two main sources of heat generation in thermal shields, gammas and neutrons from the operating reactor (heat generation in the thermal shields after shutdown is not significant). The many possible sources of *gamma radiation in the reactor core* are discussed in Sec. 1, along with methods and data for estimating their magnitude. *Neutrons* from the reactor can generate heat in the thermal shields by *capture* or by *inelastic collisions;* in these cases the energies of the resulting gammas must be determined. Neutrons can also transfer energy by elastic collision with atoms in the thermal shields.

The required thermal shielding for a specific reactor vessel and core is calculated in the following manner:

1. If the temperature of the coolant inside the reactor vessel and the temperature at the reactor vessel–insulation interface outside and the thickness and physical properties of the reactor-vessel wall are known, a stress calculation can be made which determines the permissible upper limit for the heat generation in the vessel wall (e.g., in watts per cubic centimeter).

2. If the radiation sources (as discussed in Sec. 1) and the gamma- and neutron-energy-absorption cross sections and build-up factors (given in Chaps. 9 and 10) are known, the actual heat generation in the reactor-vessel wall can be calculated, assuming no thermal shielding.

3. By the use of normal shielding techniques (as discussed in this chapter), the amount of shielding required to reduce this radiation level to the permissible limit referred to in item 1 can be computed.

4. If the shape of the internal shields and their stress limitations are known, the total required thermal-shield thickness may be divided into several layers. The required cooling for each is calculated and provided for. The maximum permissible thickness of each shield is determined from calculations similar to those performed for the reactor-vessel wall.

The purpose of Secs. 4.2 to 4.4 is to present methods for calculating the magnitude of these internal heat sources as a function of core and shield designs. Each source of heat is treated separately; the heat generation of each is summed for design purposes. In general, a continuous energy spectrum is not assumed, but, instead, important average energies are considered.

It is seen that the problem of thermal-shield design is one of determining the absorption of radiation energy through the shield. As would be expected, the methods for doing this are

similar to those used for the design of biological shielding. Applicable material on this subject which appears elsewhere in this manual is not repeated in this section.

More elegant methods are now being worked out, and, if sufficient computer time can be made available, the next edition of this manual should have a rather complete treatment of heat generation and thermal-shield design.

4.2 Heat Generation by Core Gammas

(a) Geometry. The core is assumed cylindrical. The shield may take the form of a cylindrical shell around the core or a plane slab placed against the core. The equations presented in Chap. 9 permit the calculation of the gamma flux in the shield if it is assumed that the core is infinite and has a uniform distribution of isotropic gamma-ray sources. A correction can then be made for the finite height of the core.

Computationally, the plane-shield case is easier, especially when the problem involves an arrangement of laminations that cannot be treated as a homogeneous mixture. The use of a plane slab slightly overestimates the result. This error is small compared to other uncertainties—build-up and source spectrums, for example.

(b) Source. The source is considered to be made up of a discrete number of gamma-ray energies. Section 1 contains methods for evaluating the fission-gamma and fission-product-gamma sources. If the coolant, moderator, or structural material has a fairly large neutron-capture cross section, the capture gammas produced must also be considered as core gammas. Any gamma rays resulting from the decay of radioactive material in the core must also be considered.

Usually, however, only the gammas resulting directly from the fission process need be considered for thermal-shield design; all other gamma sources are generally negligible by comparison. This statement does *not* apply to gammas generated within the thermal shield by neutron reactions; these are discussed in Secs. 4.3 and 4.4.

(c) Calculation of the Gamma Flux. Build-up Neglected. Neglecting build-up gives a lower limit to the flux and hence to the energy absorption. The first step is to find the flux, $\phi(E_0,R)$ cm^{-2}-sec^{-1}, from a uniform distribution of point isotropic sources of energy E_0 and strength 1 photon/cm^3-sec. For an infinite cylindrical source the parameters that are needed are (in metric units):

R_0 = radius of cylinder (cm)

a = perpendicular distance from the axis of the cylinder to R, the point at which the flux is calculated (cm). $a = R_0 + R$

T_j = thickness of *jth* layer of shield (cm), the count starting from the cylinder surface. If the point R, at which the flux is to be determined, is in layer k, then T_k is the thickness of the material in that layer only up to the point R

$\nu(E_0)$ = energy-absorption coefficient of the cylinder treated as a homogeneous mixture (cm^{-1})

$\mu_j(E_0)$ = total absorption coefficient of the *jth* layer of the shield (cm^{-1})

$b(E_0) = \sum_{j=1} \mu_j T_j$, where the sum is taken only for the shielding material from the surface of the cylinder to R

The uncollided flux $\phi(E_0,R)$ is found from the equations presented in Chap. 9. If $\mu_k(E_0)$ is the energy-absorption coefficient of the k*th* material, then the energy absorbed per cubic centimeter per second at R, neglecting build-up, is found by multiplying the flux $\phi(E_0,R)$ by $\mu_k(E_0)\,E_0$ and the source strength ratio S_ν and then summing over the energies of the source gammas.

$$H(R)\ (\text{watts/cm}^3) = K \sum_{E_0} S_\nu(E_0)\ \mu_k(E_0)\ \phi(E_0,R)\ E_0 \tag{48}$$

where $K = 1.6 \times 10^{-13}$ watt-sec/Mev.

The finite height of the cylinder is corrected for by multiplying the ϕ found for the infinite case by the following correction factor:

$$\frac{F\left(\arctan\frac{h}{2R_0};\, b\right)}{F\left(\frac{\pi}{2};\, b\right)} \tag{49}$$

where h is the height of the cylinder

$$F(\arctan x, b) = \int_0^{\arctan x} e^{-b \sec\theta}\, d\theta$$

which is plotted in Chap. 9. The final result is the flux along the perpendicular to the midpoint of the axis of the cylinder.

(d) Build-up Included. The energy-absorption build-up factor B_A can be expressed as a sum of two exponentials, just as has been done for other types of build-up factors (see Chap. 1). Coefficients to calculate energy-absorption build-up factors in this way for iron and for water are plotted as a function of energy in Part 5 of Chap. 9. Alternatively, the values of B_A for several materials are plotted in Chap. 10 as functions of penetration and initial energy.

The first step in finding a B_A is to assume that the thermal shield and reactor container are a homogeneous mixture and to compute an effective atomic number Z (see Chap. 1). The same thing is done for the reactor core. In the case of an iron-water shield with a sizable metal to water volume ratio, the effective Z of the shield is that of iron.

At the present stage of the art, it is conjectured that the appropriate recipe is to use the build-up corresponding to the effective Z of the shield mixture. The penetration variable, however, takes cognizance of the actual layer construction.

This approximation improves for deeper penetrations into the shield, as more shield material is placed between R and the core surface. Near the core-shield interface an overestimate of the heating may be expected when the effective Z of the shield is less than that of the core. When the Z of the core is less than that of the shield, an underestimate is likely. The error at the interface seems to decrease with increasing gamma-ray energy. Thus, where the contribution of low-energy photons to the heating is small, the indicated procedure should provide a reasonably good approximation.

A typical case occurs when the core has an effective Z = 40 (zirconium) and the shield an effective Z = 26 (iron). Assume the core radius to be about 7 mean free paths. An examination of the point isotropic energy-absorption build-up factors for iron and zirconium* shows the following features, at $\mu_0 r \geq 7$:

1. At energies less than 1 Mev the B_A for iron is about 30 per cent greater than that for zirconium.
2. At moderate energies the percentage difference declines as $\mu_0 r$ gets larger.
3. For higher energies B_A for iron becomes less than the B_A for zirconium as $\mu_0 r$ increases.

As noted earlier, the farther the distance from the core surface the greater is the amount of iron present as absorbing medium. Hence the difference between the correct B_A and the iron B_A will actually be smaller than the differences between the zirconium and the iron build-ups. The over-all error in the heating contributed by the preceding build-up uncertainties is expected to be about 30 per cent.

4.3 Heat Generation by Gammas from Neutron Capture and from Inelastically Scattered Neutrons

Assume plane slab geometry and isotropic emission of gammas. Let the neutron flux (either thermal or fast) be represented by a sum of exponentials,

---

* The zirconium build-up factors were obtained from B_A vs. Z plots of the data in Report NYO-3075 (such as the curves given in Chap. 10).

$$\phi(z) = \sum_{i=0}^{m} \beta_i e^{-\sigma_i z}$$

where z is the distance from the inner face of the shield, $(\phi)_{z=0} = \sum_{i=0}^{m} \beta_i$ is the neutron flux at the inner face of the slab, and σ_i is the absorption coefficient for neutrons (cm^{-1}). The gamma source strength at z, i.e., the number of gammas of energy E_0 emitted at z per cubic centimeter per second, is then given by

$$S(z,E_0) = \nu\, f(E_0) \sum_{i=0}^{m} \beta_i e^{-\sigma_i z} \quad \frac{\text{gammas of energy } E_0}{cm^3\text{-sec}}$$

where ν cm^{-1} is the macroscopic cross section for gamma production, either capture cross section or inelastic scattering, and $f(E_0)$ is the number of gammas emitted per capture having energy E_0.

Because the source strength is given as a sum of exponentials, the formulas developed in Chap. 9 can be used.

The expression for the energy absorption per cubic centimeter per second from a gamma ray of energy E_0 is

$$H(z) = \frac{K}{2} \mu_A(E_0)\, E_0[\nu\, f(E_0)] \sum_{j=1}^{n} \frac{A_j}{\mu_j} \sum_{i=1}^{m} \beta_i e^{-\sigma_i z} \left\{F_1(\mu_j z,a) + F_1[\mu_j(h - z), -a]\right\}$$

where $K = 1.6 \times 10^{-13}$ watt-sec/Mev, $\mu_A(E_0)$ is the energy-absorption coefficient for the resultant gammas (cm^{-1}), $a = \sigma_i/\mu_j$, and A_j and μ_j are connected with the representation of the build-up factor as a sum of exponentials. The build-up factor (in this case, for energy absorption) for a point isotropic source is

$$B_A(\mu_0 r,E_0) = \sum_{j=1}^{n} A_j e^{-\alpha_j(\mu_0 r)}$$

The A_j's and α_j's are functions of energy only. Note that μ_0, the total absorption coefficient, should be used, not the energy absorption coefficient.

$$\mu_j = (1 + \alpha_j)\mu_0$$

The F_1 functions are defined and plotted in Chap. 9.

4.4 Heat Generation by Elastically Scattered Neutrons

(a) General Equations. If $\phi(E)$ is the scalar flux of neutrons at some point in the reactor system, the specific rate of heating at this point due to elastic scattering of neutrons is

$$H\ (watts/cm^3) = K \sum_i N_i \int_0^\infty \phi \sigma_i g_i E\, dE \tag{50}$$

where $K = 1.6 \times 10^{-13}$ watt-sec/Mev

N_i = the number density of the *ith* nuclear species at the point under consideration (cm^{-3})

$\phi(E)\, dE$ = the flux of neutrons with the energies in the range E to E + dE (neutrons/cm^2-sec)

$\sigma_i(E)$ = the elastic scattering cross section of the *ith* nuclear species (cm^2)

$g_i(E)$ = the average fractional energy loss of a neutron which scatters off the *ith* nuclear species

E = the energy of the neutrons (Mev)

Equation 50 follows from the fact that all the kinetic energy lost by the neutrons will be gained by the recoil nuclei, plus the assumption that the nuclei will deposit their kinetic energy so near the point of collision that the displacement may be ignored.

The average fractional energy loss in an elastic collision is, of course, a function of the differential cross section, i.e.,

$$g(E) = \left(\frac{E - E'}{E}\right)_{av} = 1 - \int_{-1}^{+1} \frac{E'}{E} \frac{d\sigma}{d\theta_c} (E,\theta_c)\, d\theta_c \tag{51}$$

where E = energy of the neutron entering the collision
E' = energy of the neutron leaving the collision
θ_c = the cosine of the scattering angle in the center-of-mass system
$d\sigma/d\theta_c$ = the differential cross section in the center-of-mass system

Through a somewhat lengthy argument, which will not be repeated here, it can be shown[44] that

$$\frac{E'}{E} = \left[1 - \frac{2A}{(A+1)^2}(1 - \theta_c)\right] \tag{52}$$

where A is the mass of the scattering nucleus in units of the neutron mass.

The differential cross section can be expressed as a sum of Legendre polynomials, $P_n(\theta_c)$.

$$\frac{d\sigma}{d\theta_c} (E,\theta_c) = \sum_n \frac{2n+1}{2} F_n(E)\, P_n(\theta_c) \tag{53}$$

After substituting Eqs. 52 and 53 into Eq. 51 and performing the integration, there results

$$g(E) = \frac{2A}{(A+1)^2} [1 - F_1(E)] \tag{54}$$

Thus the average fractional energy loss in an elastic collision depends only on the mass of the target nucleus and the coefficient of the first Legendre polynomial in the expansion of the differential cross section.

After substituting Eq. 54 into Eq. 50,

$$H = K \sum_i N_i \frac{2A_i}{(A_i+1)^2} \int_0^\infty \phi \sigma_i (1 - F_{1i}) E\, dE \tag{55}$$

where A_i is the mass of the *ith* nuclear species in atomic-mass units and $F_{1i}(E)$ is the first expansion coefficient of the *ith* nuclear species.

Since proton scattering is spherically symmetrical in the center-of-mass system up to at least 14 Mev, $F_1(E)$ for H^1 can be set equal to zero for all heating calculations. Values of F_1 have been calculated on the basis of the optical ("cloudy crystal ball") model of the nucleus for many elements.

To evaluate the integral in Eq. 55, it is necessary to determine the neutron flux [$\phi(E)$]. This problem, which is indeed *the* problem, is discussed in considerable detail in Sec. 3. Suppose, as is often the case in preliminary design, a two-group diffusion calculation has been made. Two numbers are available at each point of interest, the fast flux (ϕ_f) and the slow flux (ϕ_s), defined by

$$\phi_f \equiv \int_{E_c}^\infty \phi(E)\, dE \tag{56}$$

$$\phi_s \equiv \int_0^{E_c} \phi(E)\, dE \tag{57}$$

where E_c is the value of the energy that separates the groups. Usually the cutoff energy (E_c) is in the range 0.1 to 5 ev.

Because the cutoff energy is so low, the average energy carried by a neutron in the slow group will be less by a factor of 10^5 to 10^7 than that carried by a neutron in the fast group. Since ϕ_f and ϕ_s are almost invariably within a factor of 10^2 of one another, the kinetic energy carried by the slow group is always considerably less than 1 per cent of that carried by the fast group. This, coupled with the fact that the average scattering cross sections of the slow

Table 3.11—TOTAL CROSS SECTIONS

Element	σ, barns	Energy range, Mev
Hydrogen	$2.4 \exp\left(\frac{-E}{10.75}\right) + 5.3 \exp\left(\frac{-E}{1.2}\right)$	$0.1 \le E \le 8.0$
Oxygen	3	$0.1 \le E \le 2.6$
	2	$2.6 \le E \le 8.0$
Iron, nickel, and manganese	3	$0.1 \le E \le 8.0$

and fast groups seldom differ by more than 10, allows elastic heating by the slow group to be ignored. Thus the zero lower limit in Eq. 55 may be replaced by E_c.

$\phi(E)$ may be broken down into a magnitude and a shape

$$\phi(E) \equiv \phi_f W(E) \tag{58}$$

where ϕ_f (neutrons/cm^2-sec) is the fast flux and W(E) is the number spectrum of the fast flux. From Eqs. 56 and 58

$$\int_{E_c}^{\infty} W(E)\, dE = 1 \tag{59}$$

Substituting Eq. 58 into Eq. 55 yields

$$H = K\phi_f \sum_i N_i \frac{2A_i}{(A_i + 1)^2} G_i \tag{60}$$

in which, by definition,

$$G_i \equiv \int_{E_c}^{\infty} W\sigma_i(1 - F_{1i})E\, dE \tag{61}$$

In Eq. 61, $\sigma_i(E)$ is supposedly the *elastic scattering* cross section of the *ith* type nucleus for neutrons of energy E; however, the *total* cross section will be used in most practical problems. As shown in Sec. 4.4b, the energy region that contributes most to the heating is about 0.1 to 5 Mev. In this region the scattering is either all elastic, as in the cases of hydrogen, oxygen, and other light nuclei, or mostly elastic in the heavier nuclei.

The total cross sections given in Table 3.11 were obtained by fitting the data in the "Barn Book."[45] The roughness of these approximations to the cross sections is compatible with the grossness of the $F_1(E)$ values and the assumption that must be made about the spectrum.

(b) Water-moderated Fast Flux. The results obtained thus far, represented by Eqs. 60 and 61, are quite general. To illustrate the calculation of the numbers G_i, reference must be made to some particular reactor type so that the spectrum W(E) can be specified. One type of particular importance is the light-water-moderated reactor. In this reactor the slowing down is due almost entirely to collisions with hydrogen nuclei; the resulting spectrum, which has been studied in considerable detail,[33] is called the "proton-moderated spectrum."

In a proton-moderated region, approximately one-half the fast flux (i.e., that above 0.1 Mev) is in the energy range 0.1 to 5 Mev. Furthermore, E W(E) has an appreciable value only in the same region. In the energy region above 0.1 Mev, the spectrum is well represented by

$$W(E) = 0.63 \exp(-E/1.53) - 0.57 \exp(-E/1.20) \quad (62)$$

The normalization is such that $W(E)\,dE = \frac{1}{2}$.

On substituting Eq. 62 into Eq. 61, there results

$$G_i = \int_{0.1}^{\infty} [0.63 \exp(-E/1.53) - 0.57 \exp(-E/1.20)]\, E\sigma_i(1 - F_{1i})\, dE$$

which can be evaluated analytically by finding simple expressions for $\sigma_i(E)$ (see Table 3.11) and $F_{1i}(E)$ or, alternatively, which can be evaluated numerically.

REFERENCES

1. Samuel Glasstone and M. C. Edlund, "The Elements of Nuclear Reactor Theory," D. Van Nostrand Company, Inc., New York, 1952, p. 64.
2. Gamble and Bell, Report ORNL-1620.
3. John Moteff, Fission Product Decay Gamma Energy Spectrum, Report APEX-134, June 1953.
4. F. H. Clark, Decay of Fission Product Gammas, Report NDA-27-39, Dec. 30, 1954.
5. F. E. Obenshain and A. Foderaro, Report WAPD-P-652, January 1956.
6. J. J. Taylor, Report WAPD-RM-59, June 21, 1951 (Classified).
7. K. Way and E. P. Wigner, Phys. Rev., 70: 115 (1946).
8. P. S. Mittelman and R. A. Liedtke, Gamma Rays from Thermal-neutron Capture, Nucleonics, 13(5): 50 (1955).
9. B. B. Kinsey and G. A. Bartholomew, Phys. Rev., 89: 375 (1953).
10. G. A. Bartholomew and B. B. Kinsey, Phys. Rev., 89: 386 (1953).
11. B. B. Kinsey, G. A. Bartholomew, and W. H. Walker, Phys. Rev., 85: 1012 (1952).
12. B. B. Kinsey, G. A. Bartholomew, and W. H. Walker, Phys. Rev., 83: 519 (1951).
13. G. A. Bartholomew and B. B. Kinsey, Can. J. Phys., 31: 49 (1953).
14. W. Thornton et al., Phys. Rev., 86: 604A (1952).
15. B. Hamermesh and V. Hummel, Phys. Rev., 88: 916 (1952).
16. B. Hamermesh and V. Hummel, Phys. Rev., 84: 158 (1951).
17. B. Hamermesh and V. Hummel, Phys. Rev., 83: 663 (1951).
18. R. W. Pringle and G. Isford, Phys. Rev., 83: 467 (1951).
19. T. H. Braid, Bull. Am. Phys. Soc., 28(3): 13 (1953).
20. B. B. Kinsey, G. A. Bartholomew, and W. H. Walker, Phys. Rev., 82: 380 (1950).
21. J. T. Braid, NSA, 7(5): New Nuclear Data (1953).
22. H. T. Motz, NSA, 7(5): New Nuclear Data (1953).
23. G. A. Bartholomew and B. B. Kinsey, Bull. Am. Phys. Soc., 28(1): J6 (1953).
24. H. T. Motz, NSA, 7(6A): New Nuclear Data (1953).
25. C. O. Muehlhause, Phys. Rev., 79: 277 (1950).
26. R. W. Pringle, Phys. Rev., 87: 1016 (1952).
27. R. E. Bell and L. G. Elliot, Phys. Rev., 79: 282 (1950).
28. F. Ajzenberg and T. Lauritsen, Revs. Mod. Phys., 24: 231 (1952).
29. B. B. Kinsey, G. A. Bartholomew, and W. H. Walker, Can. J. Phys., 29: 1 (1951).
30. W. A. Reardon, R. W. Krone, and R. Stump, Phys. Rev., 91: 334 (1953).
31. B. B. Kinsey and G. A. Bartholomew, Can. J. Phys., 31: 537 (1953).
32. B. B. Kinsey and G. A. Bartholomew, Can. J. Phys., 31: 1025-1086 (1953).
33. F. C. Brooks and H. L. Glick, Report WAPD-45, November 1951 (Classified).
34. "Reactor Handbook," Chap. 2.1, AEC Technical Information Service, Oak Ridge (Classified).

35. E. P. Wigner and G. Young, Report MonP-283 (Classified).
36. "Reactor Handbook," Vol. 1, AEC Technical Information Service, Oak Ridge, 1953 (Classified).
37. J. M. Blatt and J. D. Jackson, On the Interpretation of Neutron-Proton Scattering Data by the Schwinger Variational Method, Phys. Rev., 76: 18 (1949).
38. B. E. Watt, D. Hill, T. W. Bonner, R. A. Ferrell, and N. C. Rinhart, Energy Spectrum of Neutrons from Fissions Induced by Thermal Neutrons, Report LA-718, Dec. 17, 1948.
39. R. D. Albert and T. A. Welton, Report WAPD-15, Nov. 30, 1950 (Classified).
40. M. J. Nielsen and C. B. Ellis, editors, Report ORNL-768, Aug. 14, 1950 (Classified).
41. J. J. Taylor, Report WAPD-23, January 1951 (Classified).
42. J. J. Taylor and F. E. Obenshain, Flux From Homogeneous Cylinders Containing Uniform Source Distributions, Report WAPD-RM-213, Dec. 7, 1953.
43. E. P. Blizard, Part II, Report ORNL-51-10-70, Mar. 7, 1952 (Classified).
44. S. Glasstone and M. C. Edlund, "The Elements of Nuclear Reactor Theory," D. Van Nostrand Co., Inc., New York, 1952.
45. D. J. Hughes and J. A. Harvey, Neutron Cross Sections, Report BNL-325, July 1, 1955.
46. H. F. Hunter and N. E. Ballou, Report ADC-65, 1949.
47. F. E. Obenshain, Report WAPD-RM-180, April 1953 (Classified).

Chapter 4

SHIELDING THE REACTOR COOLING SYSTEM

1 INTRODUCTION 87

2 CALCULATION OF SPECIFIC ACTIVITY IN COOLANT 88
- 2.1 Some Typical Activities . . . 88
  - (a) Activation Cross Section for $O^{16}(n,p)N^{16}$ Reaction . . . 88
  - (b) Activation Cross Section for $O^{17}(n,p)N^{17}$ Reaction . . . 89
  - (c) Other Reactions 89
- 2.2 Comparison of Various Coolants . . 89
- 2.3 The Activation Equations . . . 91
  - (a) General Expressions . . . 91
  - (b) Activation Equations for the Three Most Probable Flow Schemes 94
- 2.4 Calculation of Effective Neutron Flux 100
- 2.5 Equilibrium Gamma Activity . . 104
- 2.6 Method for Approximating Coolant Activity with Changes in Core Time and Total Cycle Time . . 107
- 2.7 Equilibrium Neutron Activity . . 108

3 GAMMA SHIELDING FOR THE REACTOR COOLING SYSTEM 108
- 3.1 Hand-calculation Procedure for Coolant Gamma Shield Thickness 108
  - (a) Procedure 111
  - (b) Sample Calculation . . . 113
- 3.2 Attenuation of Gamma Rays at Oblique Incidence 118
- 3.3 Experiments Using Cylindrical Sources 118
- 3.4 Techniques for Isodose Calculation Varying Shield Thickness To Give Uniform Dose 119
  - (a) Statement of the Problem . . 119
  - (b) Method of Designing the Shield . 119
  - (c) Source Geometries . . . 119
  - (d) Methods for Machine Calculations 121
  - (e) Geometrical Considerations: Reduction of Sources into Series of Point Sources 122
  - (f) Sample Calculation . . . 137

4 NEUTRON SHIELDING FOR THE REACTOR COOLING SYSTEM 141
- 4.1 Attenuation Kernel for N^{17} Neutrons 141
  - (a) Calculation of Thermal-neutron Flux 141
  - (b) Calculation of Fast-neutron Flux 143
- 4.2 Removal Cross Sections and Relaxation Lengths for N^{17} Neutrons . . . 144
- 4.3 Monte Carlo Results of the Transport of N^{17} Neutrons in a Water Medium . 144
  - (a) Introduction 144
  - (b) Transmission Through and Reflection from Water Slabs. . 145

5 SELECTION OF DOSE POINTS FOR ACCURATE ISODOSING 151

REFERENCES 152

BIBLIOGRAPHY 152

FRONT OF THIS PAGE IS [illegible] — NO NUMB ON ORI

Chapter 4

SHIELDING THE REACTOR COOLING SYSTEM

1 INTRODUCTION

When the coolant passes through a reactor, it is exposed to a high neutron flux, which may be as high as 10^{15} neutrons/cm^2-sec, depending on the reactor power. The coolant atoms will capture neutrons or will suffer some collisions which result in the formation of unstable isotopes. These tend to go to a more stable state by giving off alpha or beta particles, gamma rays, or neutrons. The rate of disintegration is governed by the half life of the particular isotope, the neutron flux, the cross section, and the time of exposure. Since the coolant usually passes to a heat exchanger, a complete loop containing radioactive coolant, including pipes, pumps, surge tanks, valves, and heat exchangers, must be shielded. In order to be able to calculate the shielding, the exact nature of the source (radioactive coolant) must be known, especially its specific activity (particle emission per unit volume and time) as a function of position and time and the type of radiation to be shielded.

The total activation of any coolant may be broken up into two major subdivisions: intrinsic activity and impurity activity.

The *intrinsic activity* is the radioactivity associated with the nuclear composition of the coolant itself. Thus, for a water-cooled system, the minimum activation possible would be the activity due to the $O^{16}(n,p)N^{16}$ and $O^{17}(n,p)N^{17}$ reactions taking place in the oxygen atoms of the water molecules (see Sec. 2.1). Demineralization or other coolant purification techniques can have no effect on this activity.

The *impurity activity* represents an additional source of radiation over and above that from the intrinsic activity and is due to the activation of impurities in the coolant from corrosion products or impure make-up water. Most of the activity can be attributed to metal nuclides that are corroded or fed into the system. Purification techniques can have a significant effect on the radiation level due to these activities. Even very small purification rates can markedly reduce the specific activities in the coolant.

As a general rule impurity activity does not affect the thickness of the coolant shield since it is negligible in comparison to the intrinsic activity of the coolant itself. For example:

For water $\quad \dfrac{\text{intrinsic activity}}{\text{impurity activity}} = \sim 300$

For sodium $\quad \dfrac{\text{intrinsic activity}}{\text{impurity activity}} = \sim 30{,}000$ (when the sodium activity is saturated)

A complete discussion of impurity levels in various coolants and of the methods of calculating impurity activity is given in Chap. 7. The intrinsic activity, upon which the coolant shield design is based, is discussed in this chapter.

Since the specific activity must be evaluated before the coolant system is shielded, procedures are described in Sec. 2 for evaluating the intrinsic specific activity. Prior to the evaluation of the activation equations, a knowledge is also required of the magnitude of the

Table 4.1—INDUCED ACTIVITIES FROM SOME POSSIBLE REACTOR COOLANTS

Target isotope	Target in natural element, %	Thermal cross section, barns	Radioactive product of reaction	Half life	Energy of radiation, Mev	Gammas/dis
Na^{23}	100	0.48	Na^{24}	14.9 hr	2.76, 1.38 (γ's)	1 each
K^{41}	6.8	1	K^{42}	12.4 hr	1.51 (γ)	0.25
Li^{7}	92.6	0.033	Li^{8}	0.88 sec	13.4-Mev beta and resulting bremsstrahlung	
Bismuth	(Intrinsic activity will be very low, but total activity will probably be determined by impurities and corrosion products)					
Lead						
O^{16}	99.8	fast n,p reactions	N^{16}	7.4 sec	6.13 and 7.10 (γ)	0.82
O^{17} from H_2O*	0.039		N^{17}	4.1 sec	1 (n)	1.0 (n)

* Only two induced activities are significant in water for water-cooled and -moderated reactors during operation: the N^{16} gamma activity and N^{17} neutron activity. The characteristics of each are given in Secs. 2.1a and b.

effective neutron flux (discussed in Sec. 2.4) as a function of position in the core, reflector, and other regions of the reactor through which the coolant flows. It is advantageous, at times, to have a procedure for approximating the specific activity; this is discussed in Sec. 2.6. In addition to the methods presented in this chapter using the activation equations, the specific activity of the coolant can also be obtained from reactor multigroup calculations.

Once the specific activity of coolant is known, the reactor coolant system (which consists of one or more loops including some or all of the following: pipes, heat exchangers, pumps, surge tanks, pressurizers, demineralizers, and valves) is subdivided into appropriate geometric configurations. Each source can then be approximated by either cylinders, lines, points, or disks, and hence the dose rate outside the shields may be calculated by definite formulas. These formulas are given in Chap. 9. The amount of shielding necessary to reduce the dose rate to specified tolerance at a chosen point outside the secondary shield is calculated to include the contribution from all the nearby sources. Thus the total dose rate outside the secondary shield is equal to the sum of all individual dose rates computed. Generally, it is convenient: *first*, to estimate a shield thickness including structural material; *second*, to compute the sum of the dose rates due to all sources; and *third*, to adjust the shield to produce the specified dose rates. Sections 3 and 4 discuss methods of calculation for the gamma and neutron shields, respectively.

2 CALCULATION OF SPECIFIC ACTIVITY IN COOLANT

2.1 Some Typical Activities*

Table 4.1 shows some of the important induced activities encountered in pure reactor coolants, their half lives, and types of radiation. Only the thermal-neutron-capture cross sections are given, and beta rays have been omitted since their energy is usually such as to produce no problems (except for the case of Li^{8}).

(a) Activation Cross Section for $O^{16}(n,p)N^{16}$ Reaction. The activation cross section for the $O^{16}(n,p)N^{16}$ reaction has been determined from the results of experiments conducted in the WAPD-10 water activation loop at the Materials Testing Reactor (MTR). The cross section has been calculated to be 46 millibarns per O^{16} atom for fission neutrons above 11.6 Mev. This

* P. A. Roys and K. Shure, report in preparation.

cross section is dependent on the value of the effective threshold for the $Al^{27}(n,\alpha)Na^{24}$ reaction, assumed to be 8.1 Mev, and on the value of the cross section for this reaction, assumed to be 135 millibarns and on the assumption that the irradiating flux had a fission spectrum. When the $O^{16}(n,p)N^{16}$ activation cross section is averaged over the fission spectrum, the result is 0.016 millibarns. The variation of this cross section with neutron energy is shown in Fig. 4.1 as found from data obtained by H. C. Martin, Los Alamos Scientific Laboratory. The cross section for the (O^{16}-N^{16}) reaction averaged over the entire fission spectrum as computed from this curve is 0.020 millibarns. The half life of the N^{16} product is 7.35 sec; the beta energies are 4 Mev (82 per cent) and 10 Mev (18 per cent). The gamma energies are 6.13 and 7.10 Mev in the ratio 12.5 to 1. Eighty-two per cent of the disintegrations are accompanied by a high-energy gamma.

(b) Activation Cross Section for $O^{17}(n,p)N^{17}$ Reaction. The activation cross section for the $O^{17}(n,p)N^{17}$ reaction was also determined from the results of experiments conducted in the WAPD-10 water activation loop at the MTR. The cross section has been calculated to be 5.9 millibarns per O^{17} atom for fission neutrons above 10.0 Mev. Once again, this cross section is dependent on the values of the effective threshold and cross section for the $Al^{27}(n,\alpha)Na^{24}$ reaction. When the $O^{17}(n,p)N^{17}$ activation cross section is averaged over the fission spectrum, the result is 0.0070 millibarn. The variation of this cross section with neutron energy is assumed to have the same form as that for the $O^{16}(n,p)N^{16}$ reaction but to be displaced by 1.5 Mev and reduced by the factor 0.130. That is,

$$\sigma_n(E) = 0.130\sigma_\gamma(E + 1.5)$$

This factor (0.130) gives an average cross section above 10 Mev of 6 millibarns. Using this assumption, the cross section for the (O^{17}-N^{17}) reaction averaged over the fission spectrum above 8.5 Mev is 2.3 millibarns. The half life is 4.14 sec, with the emission of a 3.7-Mev beta and a 1-Mev neutron. The natural abundance of O^{17} is 0.039 per cent.

(c) Other Reactions. Less important reactions in water are the $O^{18}(n,\gamma)O^{19}$ and the $H^2(n,\gamma)H^3$ reactions. The first results in a 1.6-Mev gamma emitter with a 29.4-sec half life (cross section, 22 millibarns), and the hydrogen emits only weak beta rays and no gamma rays. These reactions are not important in so far as shield thicknesses are concerned.

2.2 Comparison of Various Coolants

In order to compare various coolants on the basis of their shielding requirements, it must be realized that the energy of the radiation is an important factor. The lower the energy the more effective is the self-shielding by the equipment containing the coolant, and the more effective is the shielding material. Furthermore, the spectrum and, therefore, the number of neutrons captured or reacting with the coolant differ widely for various coolants. Assuming all these variables constant in order to compare, for example, sodium with potassium as a coolant with the same volume fraction in the core, the dose rate or energy flux as approximated by a semi-infinite sea of coolant can be estimated. The dose rate in milliroentgens per hour is

$$D = K_1AEl$$

where A = specific activity (dis/cm^3-sec)
K_1 = constant for flux-to-dose conversion (see Chap. 2) divided by 2
E = energy (Mev)
l = relaxation length for coolant gammas within the coolant (cm)

Thus

$$D_{Na} = K_1A_{Na}\ (2.76 \times 30.9 + 1.38 \times 21.4) = 114.8A_{Na}K_1 \qquad (1)$$

$$D_K = K_1A_K\left(\frac{1.51}{4} \times 22.4\right) = 8.46\,A_KK_1 \qquad (2)$$

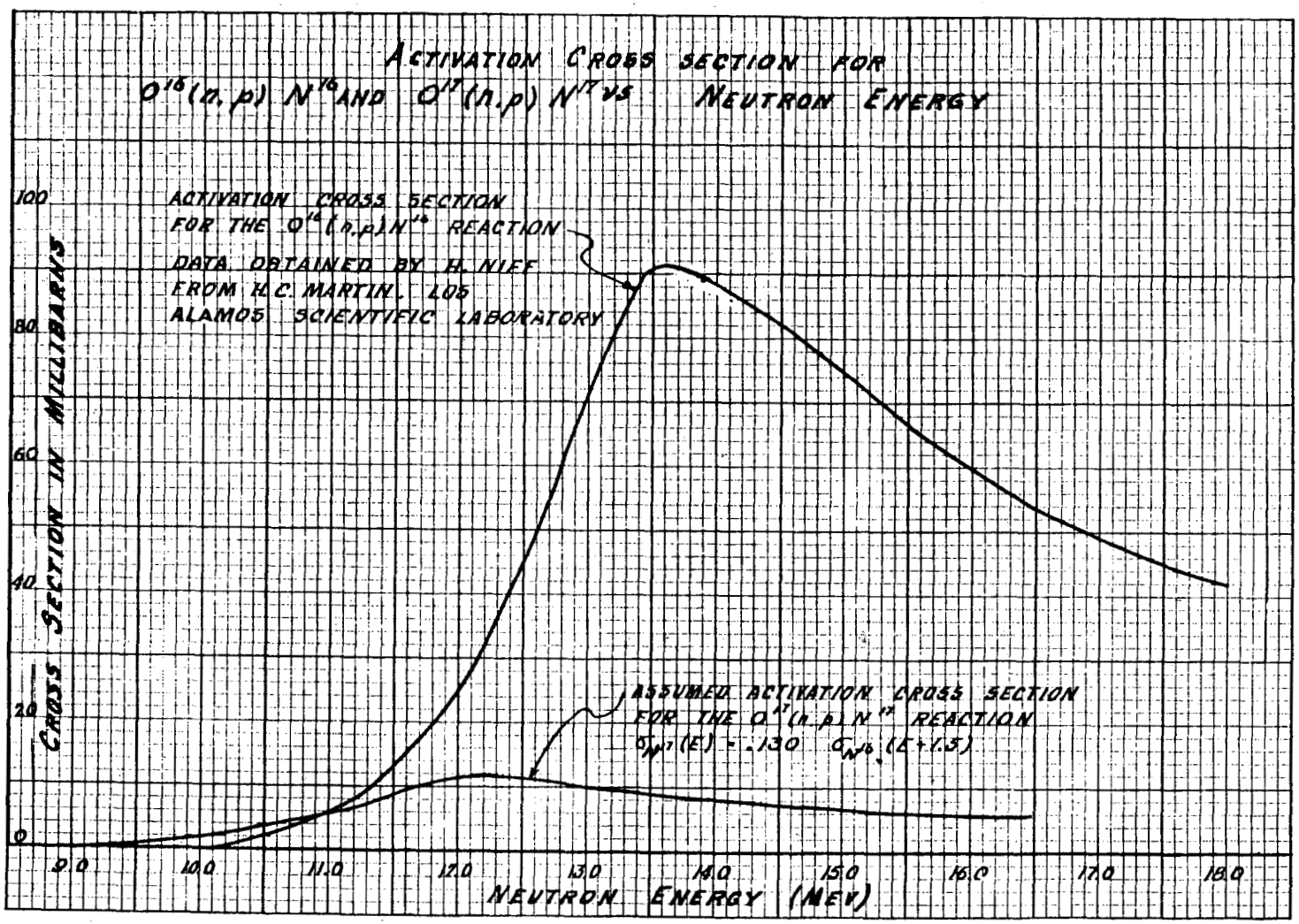

ACTIVATION CROSS SECTION FOR
O16(n,p) N16 AND O17(n,p) N17 VS NEUTRON ENERGY
ACTIVATION CROSS SECTION
FOR THE O16(n,p)N16 REACTION
DATA OBTAINED BY H. NIEF
FROM H.C. MARTIN, LOS
ALAMOS SCIENTIFIC LABORATORY
ASSUMED ACTIVATION CROSS SECTION
FOR THE O17(n,p) N17 REACTION
σN17(E) = .130 σN16(E+1.5)
CROSS SECTION IN MILLIBARNS
NEUTRON ENERGY (MEV)
100
80
60
40
20
0
9.0
10.0
11.0
12.0
13.0
14.0
15.0
16.0
17.0
18.0

Figure 4.1

(For the decay schemes of Na^{24} and K^{42} see NBS Circular 499, pages 19 and 36.)

From Table 4.1 the ratio of specific activities may be found as follows:

$$\frac{A_{Na}}{A_K} = \frac{0.48 \times 0.0233}{0.068 \times 1 \times 0.0121} = 13.6 \qquad (3)$$

where 0.0233 equals the number of sodium atoms/$cm^3/10^{24}$ and 0.0121 equals the number of potassium atoms/$cm^3/10^{24}$, all evaluated at 250°C (arbitrarily).

Substituting in Eq. 2, $A_K = A_{Na}/13.6$,

$$D_K = 8.46K_1 \frac{A_{Na}}{13.6}$$

and

$$\frac{D_{Na}}{D_K} = \frac{114.8}{8.46} \times 13.6 = 184$$

Thus the dose outside a large source containing sodium is 184 times the dose outside the same container full of potassium (at 250°C).

Table 4.2—SHIELDING REQUIREMENTS FOR VARIOUS COOLANTS
(For the Same Hypothetical Power Reactor)

Coolant	Lead, in.
Sodium	14
Potassium	8¾
Li^7*	8¾
H_2O	6

*Based on an estimate of bremsstrahlung from reference 1.

It is difficult to make shielding comparisons for the various coolants neglecting the variables mentioned above (spectrum, half life, circulation time, and volume fraction within the reactor at any one time), but a rough estimate can be made by assuming in each case that the number of neutrons captured by each coolant is the same; results of this calculation are shown in Table 4.2.

A comparatively simple method may be used to compute the gamma (bremsstrahlung) flux and spectrum produced when beta-decay electrons enter a metal absorber. The lead requirements for the lithium coolant were based on these results. Figure 4.2 shows the gamma spectrum due to the Li^8 electron per cubic centimeter of lithium (density 0.42 g/cm^3) leaving an iron absorber, such as a wall of a pipe or heat exchanger. This can, in turn, be used as the source of gamma rays to be shielded.

Usually beta particles may be neglected for shielding purposes; however, in the case of very high energy beta particles like those due to Li^8 (see Table 4.1), bremsstrahlung (similar to gamma rays) will result as the velocity of the electron decreases.

2.3 The Activation Equations

(a) General Expressions. General expressions can be derived for the specific activity of a fluid circulating through a neutron flux. These equations can be simplified under equilibrium

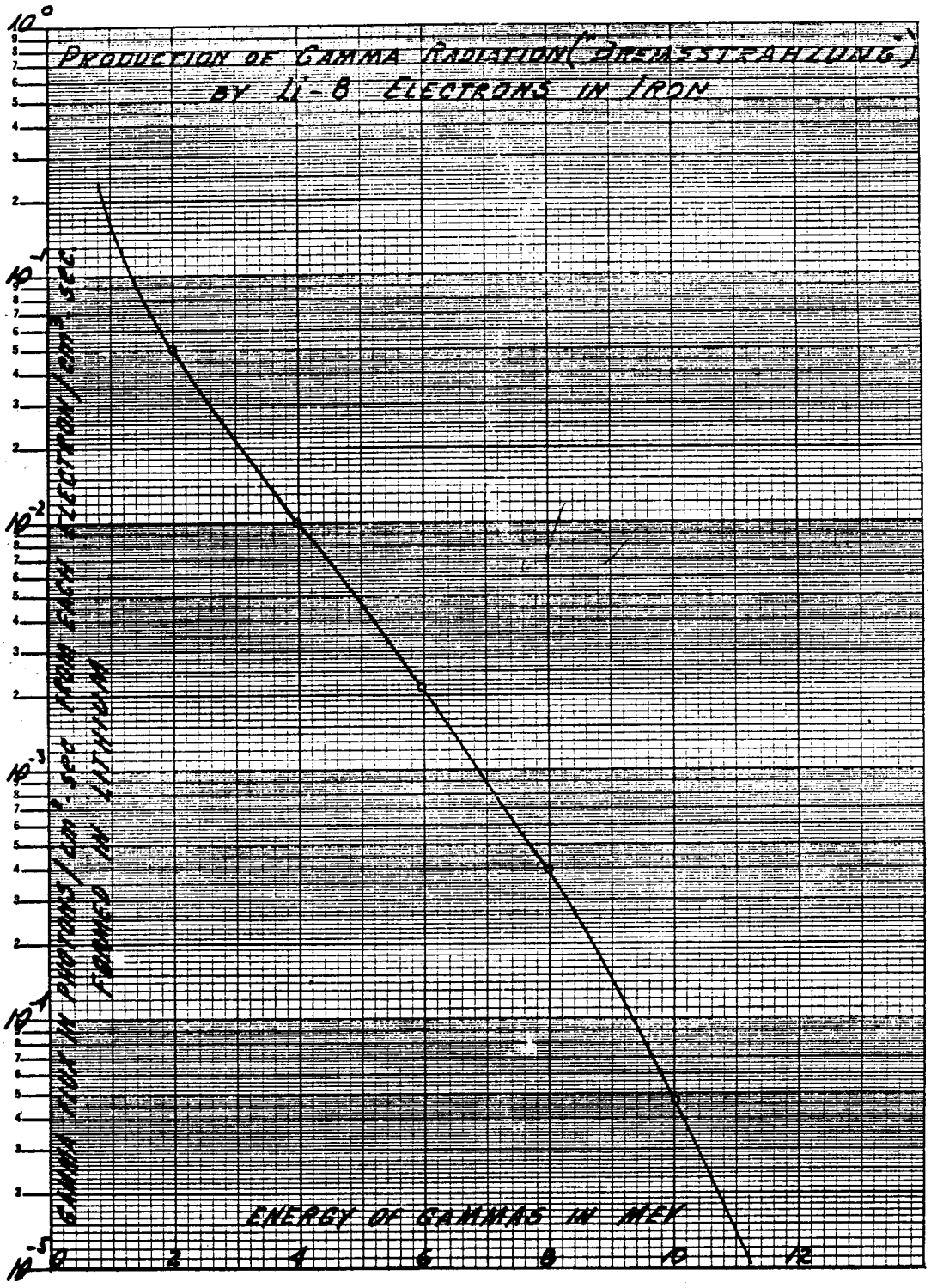

PRODUCTION OF GAMMA RADIATION ("BREMSSTRAHLUNG") BY Li-8 ELECTRONS IN IRON
GAMMA RAYS IN PHOTONS/cm² sec FROM 1 ELECTRON/cm² sec IN FERRITE IN MILLIMETERS
ENERGY OF GAMMAS IN MEV
10°
10⁻¹
10⁻²
10⁻³
10⁻⁴
10⁻⁵
0
2
4
6
8
10
12

Figure 4.2

conditions, i.e., when the rate at which atoms are being activated is equal to the rate of decaying atoms.

The definitions of the terms used in these expressions are as follows:

- A Specific activity (dis/sec-cm^3 of fluid)
- A(t) Value of A as a function of time outside the neutron flux
- A(t′) Value of A at the outlet from the neutron flux
- F Neutron flux in energy range under consideration (neutrons/cm^2-sec)
- k Number of circulation cycles undergone by the cubic centimeters of coolant under consideration
- N Total number of nuclei under study per cubic centimeter of fluid
- T Period of complete circulation cycle, i.e., time between two successive entrances of a particular nucleus into the neutron flux, assuming that all the nuclei circulate at the same rate (sec)
- t Time measured from the instant the cubic centimeter of fluid under consideration enters the neutron flux; t starts at zero again whenever the cubic centimeter of fluid reenters the flux
- t′ Time of exposure of each nucleus in neutron flux (sec)
- λ Disintegration constant of activated nuclei, λ = 1/mean life = 0.693/half life, (sec^{-1})
- σ Capture cross section of nuclei under consideration in energy range considered, where σ is assumed constant (cm^2)

In all cases

$$A(t) = A(t')\ e^{-\lambda(t-t')} \tag{4}$$

$$\frac{A(t')}{\lambda(T-t')}\ 1 - e^{-\lambda(T-t')} \tag{5}$$

For cyclic irradiation the general expressions, after k cycles, are

$$A_k(t') = \frac{\lambda NF\sigma\left\{1 - \exp\left[-(F\sigma + \lambda)t'\right]\right\}\left\{1 - \exp\left[-(k+1)(F\sigma t' + \lambda T)\right]\right\}}{(F\sigma + \lambda)\left\{1 - \exp\left[-(F\sigma t' + \lambda T)\right]\right\}} \tag{6}$$

and at equilibrium are

$$A_\infty(t') = \frac{(\lambda NF\sigma)}{(F\sigma + \lambda)}\left\{\frac{1 - \exp\left[-(F\sigma + \lambda)t'\right]}{1 - \exp\left[-(F\sigma t' + \lambda T)\right]}\right\} \tag{7}$$

For $F\sigma \ll \lambda$, after k cycles,

$$A_k(t') = NF\sigma\ \frac{(1 - e^{-\lambda t'})\left[1 - e^{-(k+1)\lambda T}\right]}{1 - e^{-\lambda T}} \tag{8}$$

and at equilibrium

$$A_\infty(t') = NF\sigma\left(\frac{1 - e^{-\lambda t'}}{1 - e^{-\lambda T}}\right) \tag{9}$$

For $F\sigma \ll \lambda$ and $\lambda T \ll 1$, after k cycles,

$$A_k(t') = NF\sigma\ \frac{t'}{T}\left[1 - e^{-(k+1)\lambda T}\right] \tag{10}$$

and at equilibrium

$$A_\infty(t') = NF\sigma \frac{t'}{T} \tag{11}$$

From these equations it can be seen that the activity of a coolant depends on the following variables:

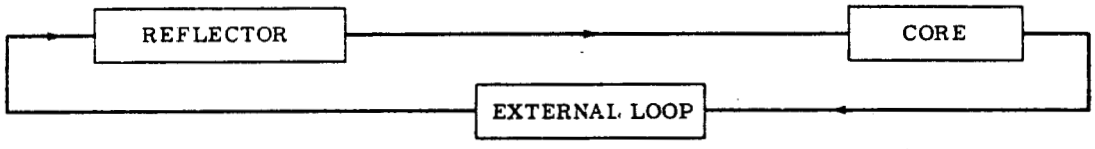
1. Macroscopic capture cross section, $N\sigma$ (nuclei per cubic centimeter × the cross section in square centimeters per nucleus), the probability of a neutron capture in the element; this is energy dependent.
2. Neutron flux and spectrum (as it affects the capture cross section).
3. Half life of the radioactive isotope; the longer the half life the longer it takes to arrive at the equilibrium condition. A longer half life also indicates a slower decay of the radioactive isotope.
4. Circulation time of the coolant.
5. Fraction of circulation time spent in the neutron flux.

These variables must be known in order to integrate over energy. This may be accomplished by using finite energy intervals, calculating the activation for each, and summing up the result. This will be shown below.

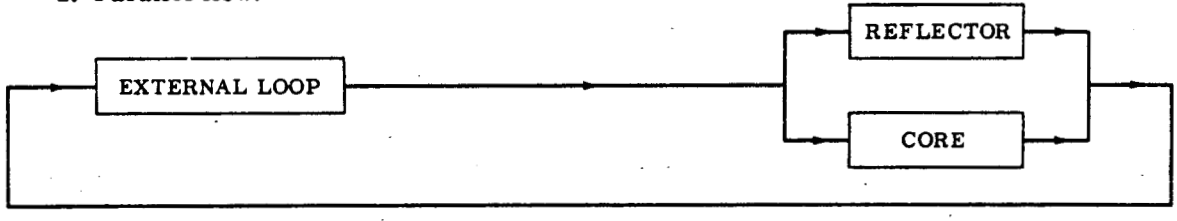
The specific activity of the coolant can also be obtained as a by-product from reactor multigroup calculations. In such a process the history of all neutrons is accounted for throughout the reactor, resulting in the total number of neutrons absorbed within the reactor and the total number of neutrons escaping as a function of energy and position. Thus the total number of neutrons absorbed in the coolant is calculated. Where the half life of the coolant is small compared to the circulation time, the decay while outside the reactor must also be calculated from the above equations.

(b) Activation Equations for the Three Most Probable Flow Schemes. There are only three likely flow schemes which can produce significantly different activations of the water: series flow, parallel flow, and series-parallel flow.

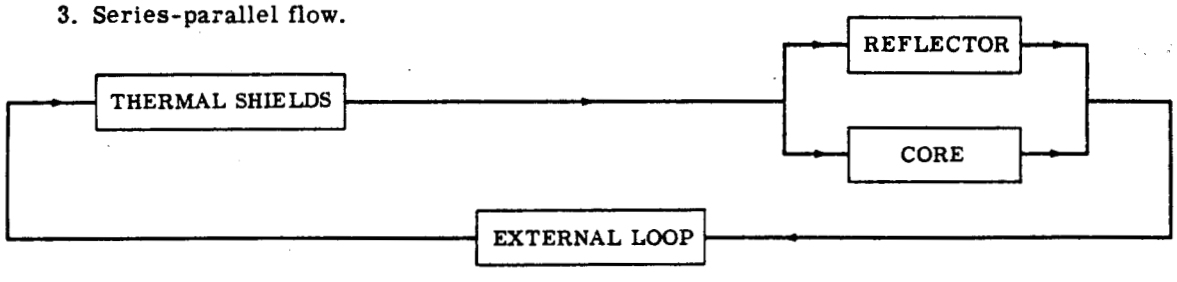
1. Series flow.



2. Parallel flow.



3. Series-parallel flow.



When the half lives of the intrinsic activities are short, e.g., 7.4 sec for N^{16} and 4.1 sec for N^{17}, an equilibrium calculation describes the activation sufficiently well for practical applications.

For all three modes of flow the equilibrium specific activity in the water as it enters the external loop is given by an equation of the form

$$S = N(\overline{\sigma\phi})_c \; F(\lambda t_j) \left\{ f_c \; G_c \left[\lambda t_i, \frac{\lambda t_j}{j}, \frac{(\overline{\sigma\phi})_j}{(\overline{\sigma\phi})_i} \right] + f_r \; G_r \left[\lambda t_i, \lambda t_j, \frac{(\overline{\sigma\phi})_j}{(\overline{\sigma\phi})_i} \right] \right\}$$

where S = equilibrium specific activity in water entering external loop
N = the number density of target atoms in the water = $\rho IA/M$
ρ = density of water (g/cm^3)
I = isotopic fraction of target atoms per molecule = 0.9976 for O^{16} and 3.7×10^{-4} for O^{17}
A = Avogadro's number 6.023×10^{23} atoms/mole
M = molecular weight of water = 18.02 g/mole
r,c,s = reflector, core, and thermal shield, respectively

For activation of O^{16} and O^{17}, high-energy neutrons are required, and the quantity

$(\overline{\sigma\phi})_{c_{i,j}}$ = the average activation probability over the range of the available spectrum above the threshold in events per atom per second (where i = c or r and j = r or s)
f_i = fraction of flow going through *ith* parallel region
$F(\lambda t_i)$ has a different form for each mode of flow as do G_c and G_r and is a dimensionless number representing the reduction in activity due to the time coolant spends out of the flux in the external part of the loop
G_c and G_r are similar to F but apply to the activating regions of the system (e.g., the core or reflector)

Series Flow

$$F(\lambda t) = \frac{1}{1 - e^{-\lambda t}}$$

$$G_c = (1 - e^{-\lambda t_c}) + \frac{(\overline{\sigma\phi})_r}{(\overline{\sigma\phi})_c} (1 - e^{-\lambda t_r}) \, e^{-\lambda t_c} \qquad (12)$$

$$G_r = 0$$

where λ = decay constant of nuclide under consideration (sec^{-1})
T = total cycle time (sec)
t_c = average time a unit volume spends in core per cycle (sec)
t_r = average time a unit volume spends in reflector per cycle (sec)

Parallel Flow

$$F(\lambda t) = \frac{1}{1 - f_c e^{-\lambda (t_c + t_e)} - f_r e^{-\lambda (t_r + t_e)}} \qquad (13)$$

where f_c = fraction of flow going through core
f_r = fraction of flow going through reflector
t_e = average time a unit volume spends in external loop per cycle (sec)

$$G_c = (1 - e^{-\lambda t_c}) + \frac{f_r}{f_c} \frac{(\overline{\sigma\phi})_r}{(\overline{\sigma\phi})_c} (1 - e^{-\lambda t_r})$$

$$G_r = 0$$

Series-Parallel Flow

$$F(\lambda t) = \frac{1}{1 - f_c \exp\left[-\lambda(t_c + t_s + t_e)\right] - f_r \exp\left[-\lambda(t_r + t_s + t_e)\right]} \tag{14}$$

where t_s = average time a unit volume of water spends in the thermal shield.

$$G_i = (1 - e^{-\lambda t_i}) + \frac{(\overline{\sigma\phi})_s}{(\overline{\sigma\phi})_i} (1 - e^{-\lambda t_s})\, e^{-\lambda t_i}$$

where i refers to core and reflector; that is, i = c,r.

Equations 12 to 14 may be obtained in similar ways. In particular, for Eq. 12 (series O^{16}, O^{17} activation),

let n = the number density of active (N^{16} or N^{17}) nuclei
n_a = the equilibrium number density of active (N^{16} or N^{17}) nuclei entering the reflector
n_b = the equilibrium number density of active (N^{16} or N^{17}) nuclei entering the core
n_c = the equilibrium number density of active (N^{16} or N^{17}) nuclei leaving the core

The rate equations which apply in the reflector, the core, and the external loop are, respectively:

$$(dn/dt)_r = (\overline{\sigma\phi})_r N - \lambda n \tag{15}$$

$$(dn/dt)_c = (\overline{\sigma\phi})_c N - \lambda n \tag{16}$$

$$(dn/dt)_e = -\lambda n \tag{17}$$

where N is the number density of target (O^{16} or O^{17}) nuclei; $(\overline{\sigma\phi})_c$ is the average activation probability in the core; and $(\overline{\sigma\phi})_r$ is the average activation probability in the reflector.

The integration of these equations is straightforward; consider Eq. 15:

$$\int_{n_a}^{n_b} \frac{dn}{(\overline{\sigma\phi})_r N - \lambda n} = \int_0^{t_r} dt$$

Integrating Eqs. 16 and 17 similarly and substituting the appropriate limits results in

$$\frac{(\overline{\sigma\phi})_r N - \lambda n_b}{(\overline{\sigma\phi})_r N - \lambda n_a} = e^{-\lambda t_r} \tag{18}$$

$$\frac{(\overline{\sigma\phi})_c N - \lambda n_c}{(\overline{\sigma\phi})_c N - \lambda n_b} = e^{-\lambda t_c} \tag{19}$$

$$\frac{n_a}{n_c} = e^{-\lambda t_e} \tag{20}$$

where t_r, t_c, and t_e are the average time a unit volume of water spends in the reflector, core, and external loop, respectively.

By straightforward algebra these equations are solved for n_c, the equilibrium specific activity as the water leaves the core.

$$S = \frac{(\overline{\sigma\phi})_c N(1 - e^{-\lambda t_c}) + (\overline{\sigma\phi})_r N(1 - e^{-\lambda t_r})\, e^{-\lambda t_c}}{1 - \exp\left[-\lambda(t_c + t_r + t_e)\right]}$$

or

$$S = \frac{N(\overline{\sigma\phi})_c}{1 - e^{-\lambda T}} \left[(1 - e^{-\lambda t_c}) + \frac{(\overline{\sigma\phi})_r}{(\overline{\sigma\phi})_c} (1 - e^{-\lambda t_r})\, e^{-\lambda t_c}\right] \tag{21}$$

where $T = t_c + t_r + t_e$ is the total cycle time.

It is to be noted that, for parallel and series-parallel flow through m parallel regions,

$$S = \frac{N \sum_{i=1}^{m} f_i(\overline{\sigma\phi})_i \, (1 - e^{-\lambda t_i})}{1 - \sum_{i=1}^{m} f_i \, e^{-\lambda (t_i + t_e)}} \qquad \text{(for parallel flow)} \tag{22}$$

$$S = \frac{N \sum_{i=1}^{m} f_i \, (\overline{\sigma\phi})_i \left[(1 - e^{-\lambda t_i}) + \dfrac{(\overline{\sigma\phi})_s}{(\overline{\sigma\phi})_i} (1 - e^{-\lambda t_s}) \, e^{-\lambda t_i} \right]}{1 - \sum_{i=1}^{m} f_i \exp\left[-\lambda (t_i + t_s + t_e)\right]} \qquad \text{(for series-parallel flow)}$$

Note: For series flow the equation for S is symmetric in c and r; that is, for reversed flow the activation may be computed by interchanging the subscripts c and r; however, the order of the subscripts as shown refers to the direction of flow as shown.

If the following definition is used for G, a single nomogram may be used as an aid for computing the G functions in all three cases.

$$G_i = (1 - e^{-\lambda t_a}) + f_i(m) \, (1 - e^{-\lambda t_b}) \, e^{-\lambda t_a} \tag{23}$$

where f(m) is a function of the mode of flow (m).

Series flow:

$$\begin{aligned} f_i(S) &= \frac{(\overline{\sigma\phi})_r}{(\overline{\sigma\phi})_c} \\ t_a &= t_c \\ t_b &= t_r \end{aligned} \tag{24}$$

Parallel flow:

$$\begin{aligned} f_i(P) &= \frac{f_r}{f_c} \frac{(\overline{\sigma\phi})_r}{(\overline{\sigma\phi})_c} \, e^{\lambda t_c} \\ t_a &= t_c \\ t_b &= t_r \end{aligned} \tag{25}$$

Series-parallel flow: Here G may be computed piecewise from the nomogram, each piece having an f(m) of

$$\begin{aligned} f_c(S\text{-}P) &= \frac{(\overline{\sigma\phi})_s}{(\overline{\sigma\phi})_c} \\ t_a &= t_c \\ t_b &= t_s \\ f_r(S\text{-}P) &= \frac{(\overline{\sigma\phi})_s}{(\overline{\sigma\phi})_r} \\ t_a &= t_r \\ t_b &= t_s \end{aligned} \tag{26}$$

G may be obtained from the nomogram in Fig. 4.3 or Fig. 4.4 as follows. Lay a straight edge across the f(m) and λt_r lines at known values of these quantities. Note the intersection of the straight edge with line P. Now align the straight edge with this value of P on the P line and with a known value of λt_c on the λt_c line. Read G at the intersection of the straight edge with the G line.

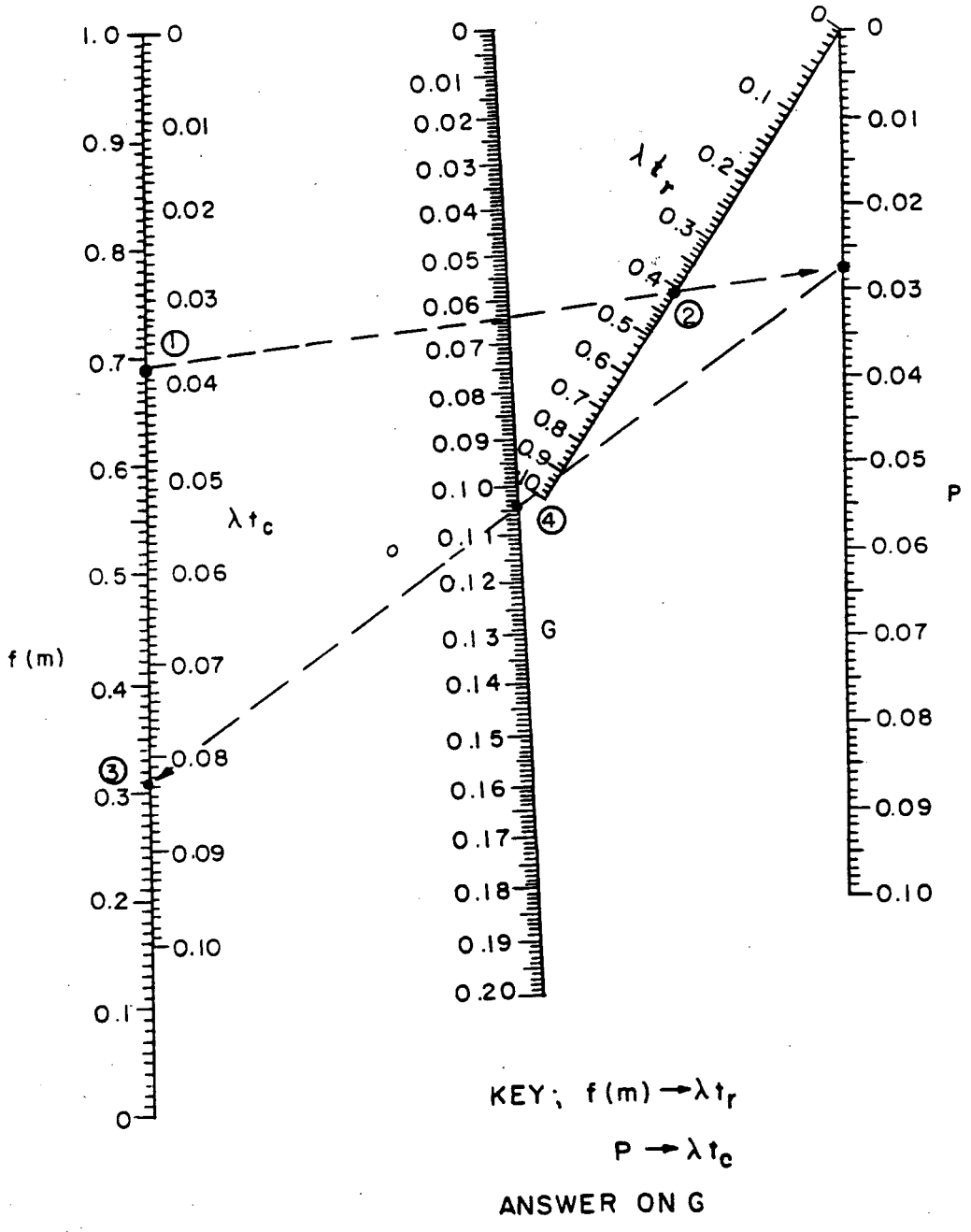

NOMOGRAM FOR ACTIVATION
OF
REACTOR COOLANT
f (m)
λ t c
G
P
λ t r
KEY; f (m) → λ t r
P → λ t c
ANSWER ON G

Figure 4.3

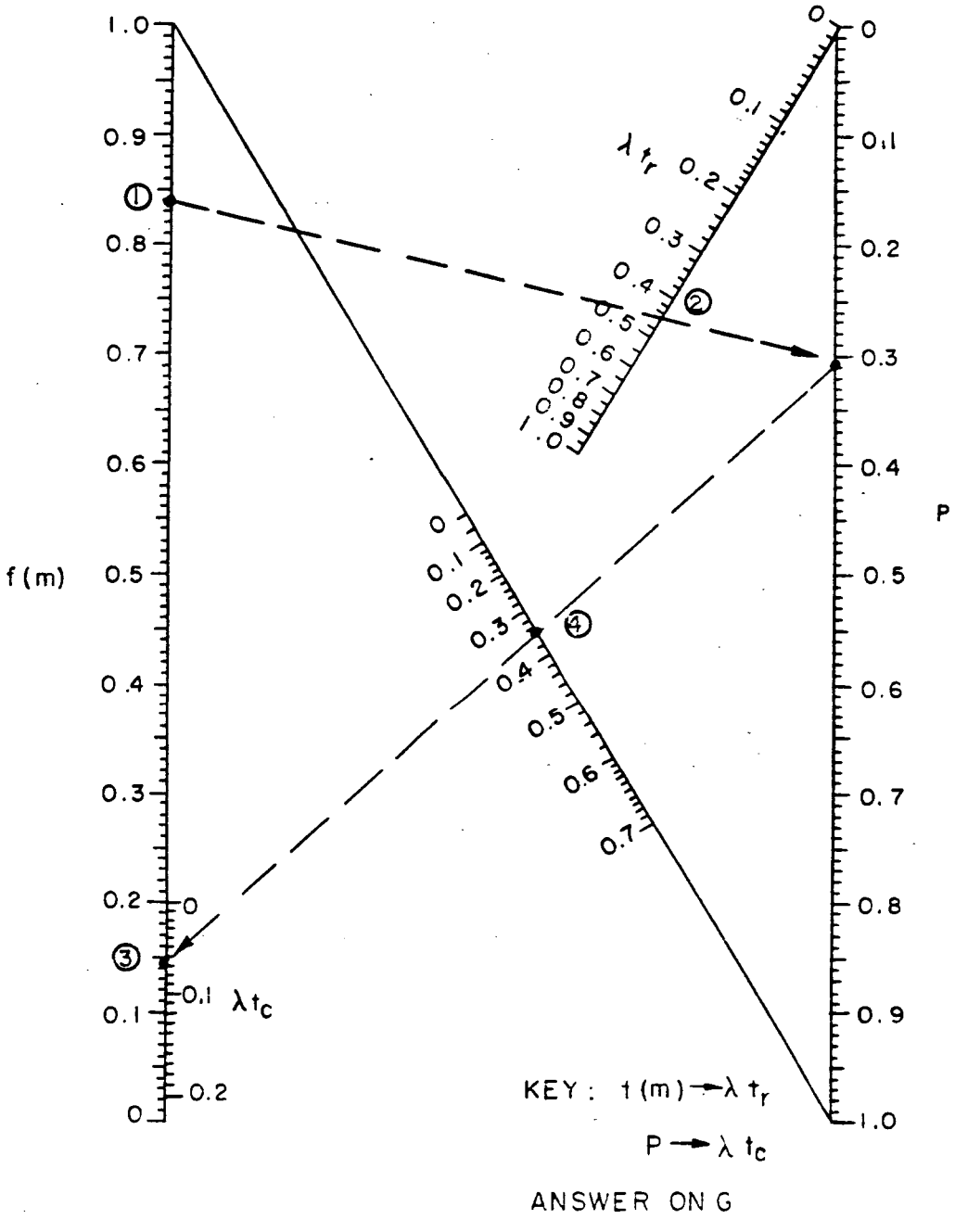

NOMOGRAM FOR ACTIVATION
OF
REACTOR COOLANT
f(m)
P
λ tr
λ tc
KEY : f(m) → λ tr
P → λ tc
ANSWER ON G

Figure 4.4

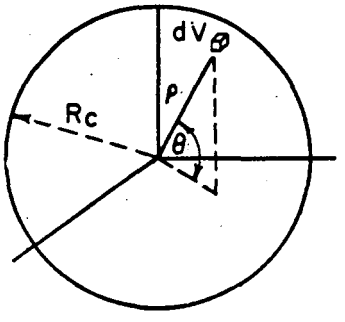
2.4 Calculation of Effective Neutron Flux

The method used in this section to determine the induced activity due to the $O^{16}(n,p)N^{16}$ reaction is essentially the same as the method used by Taylor.[2]

A knowledge of the fast flux above 10 Mev as a function of position in the reactor core, reflector, and upper and lower plenums is required to determine the induced activity level due to the $O^{16}(n,p)N^{16}$ reaction. Although the flux in the reflector and plenums is much lower than that in the core, a significant contribution is made to the gamma activity level by these regions since the coolant generally spends a much longer time there than in the core.

The fast spectrum (above 8.5 Mev) is calculated as a function of position in the reactor assembly by assuming an absorption kernel. This is effectively a single-collision calculation. The justification for the use of a single-collision calculation is good in this case since we are interested only in very fast neutrons. Because of the rapidly decreasing exponential "tail" of the fission spectrum, the majority of the core neutrons which remain above this energy are uncollided neutrons.

The spectrum of the neutron flux at the center of the core is determined by assuming the core to be a sphere and integrating the absorption kernel over the core with the origin chosen at the center of the core. The calculations following are made for an average fission-neutron source density of 1 neutron/cm^3-sec over the core. The accompanying sketch shows an element of volume dV of the core at a distance ρ from the center of the core. The radius of the core is R_c.



The fission spectrum (plotted in Fig. 4.5) is given by

$$n(E) = \sqrt{\frac{2}{\pi e}} \sinh \sqrt{2E}\, e^{-E} \approx \frac{1}{\sqrt{2\pi}\, e}\, e^{-(E-\sqrt{2E})}$$

The spectrum of the neutrons from dV will be

$$S_{dV}(E) \text{ (in neutrons/Mev-sec)} = dV\, n(E)$$

Since dV is a point source, the spectrum at C from dV is given by

$$N(E)_{dV} = dV\, n(E)\, \frac{e^{-\Sigma_T(E)\rho}}{4\pi\rho^2}$$

To find the spectrum of the neutron flux at C, the above expression must be integrated over the entire core. Since the core is assumed to be a sphere,

$$dV = 2\pi\rho^2 \sin\theta\, d\theta\, d\rho$$

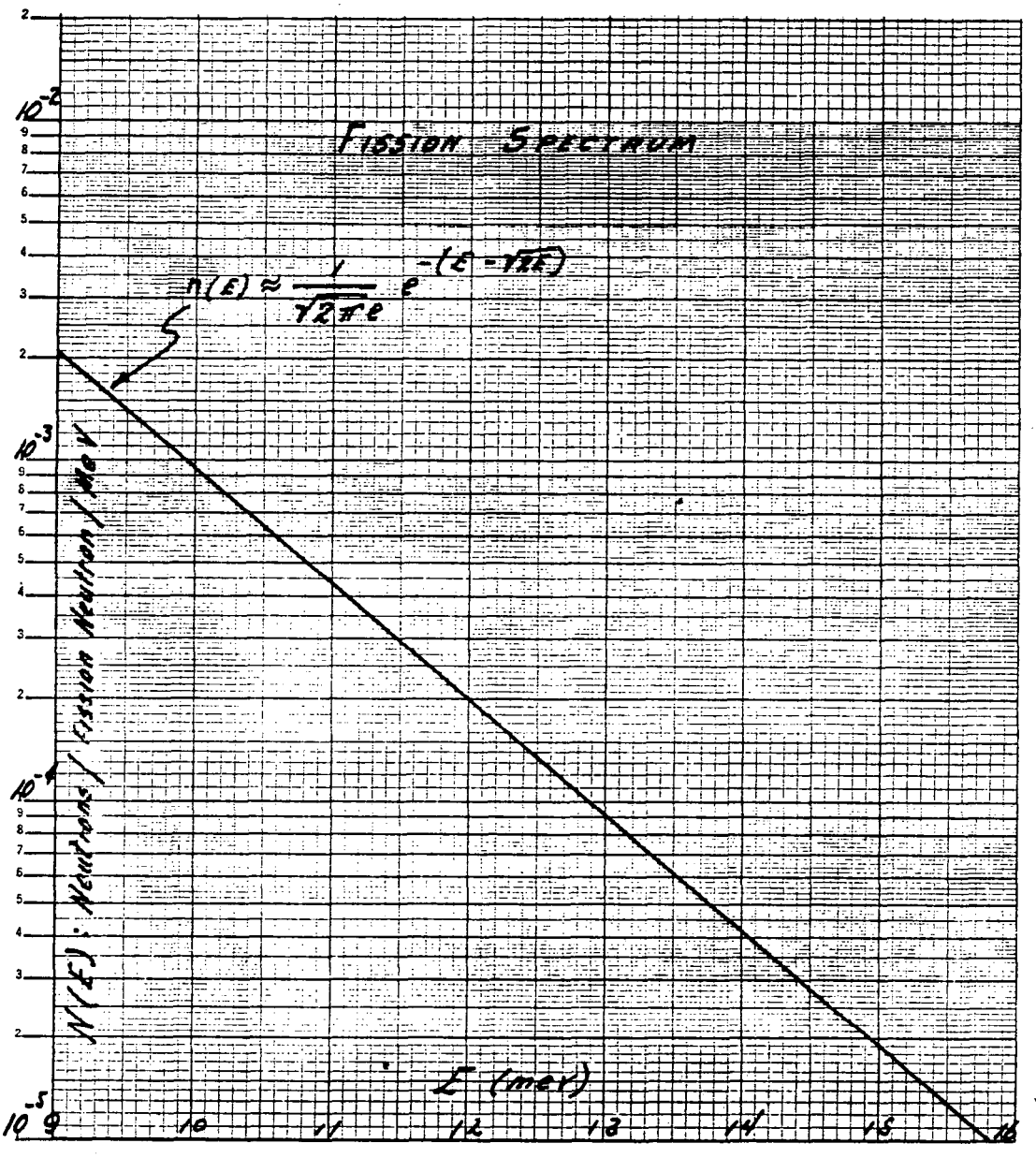


Figure 4.5

Therefore

$$N(E) = \frac{A \sinh \sqrt{2E}}{2} e^{-E} \int_0^{R_c} d\rho \int_{-1}^{1} d\mu \, e^{-\Sigma_T(E)\rho} \tag{27}$$

where μ is $\cos \theta$; R_c is the radius of core; and A is $\sqrt{2/\pi e}$.

In a water-moderated reactor

$$\Sigma_T(E) = f_{fuel}\Sigma_{fuel} + f_{water}\Sigma_{water} + f_{structure}\Sigma_{structure}$$

where f = volume fraction in the reactor

$$\Sigma_{water} = \Sigma_H(E) + \Sigma_O = \frac{N_H}{10^{24}}\left(\frac{11.1}{E + 4.2} + \frac{2.4}{E + 0.134}\right) + \Sigma_O$$

Σ_{fuel} = effective total macroscopic cross section for the fuel

$\Sigma_{structure}$ = total macroscopic cross section for the structural material in the core

Σ_H = total macroscopic cross section for the hydrogen in water

Σ_O = total macroscopic cross section for the oxygen

The hydrogen cross section, $\Sigma_H(E)$, is derived from the theoretical expression of J. M. Blatt and J. D. Jackson, Phys. Rev., 76: 18 (1949).

Integrating Eq. 27, the spectrum of the outer radius of the core is

$$N(E) = \frac{A \sinh \sqrt{2E}\, e^{-E}\left[1 - e^{-\Sigma_T(E) R_c}\right]}{\Sigma_T(E)} \tag{28}$$

The idealization to spherical geometry introduces a negligible error as can be seen from Eq. 28. For example, if R_c equals 45 cm, which is a reasonable value for some power reactors, $\exp[-\Sigma_T(E) R_c] \ll 1$. Even assuming the oxygen cross section to be zero, $\exp[-\Sigma_T(E) R_c] < 0.001$. Therefore the source density contributes to the integrated value only within a sphere of radius less than R_c.

A plot of the spectrum calculated for a specific case from Eq. 28 is shown in Fig. 4.6. $\Sigma_T(E)$ varies only slightly over the energy range; there is very little difference in the shape of the integrated spectral curve from the fission spectrum. For the plot of Eq. 28, $\Sigma_T(E)$ has been taken as a constant equal to $\Sigma_T = 0.107\ cm^{-1}$, but it could be plotted for any Σ_T.

The effective flux at core center for the $O^{16}(n,p)N^{16}$ reaction is obtained by integrating Eq. 28 above the effective energy, 10 Mev.

$$\phi(>10\ Mev) = \frac{A}{2}\int_{10}^{\infty} \frac{e^{\sqrt{2E}-E}}{\Sigma_T(E)}\, dE \tag{29}$$

where $\exp[-\Sigma_T(E) R_c]$ has been neglected and the $\sinh \sqrt{2E}\, e^{-E}$ is approximated by $e^{\sqrt{2E}-E}/2$.

The average fission-neutron source density must then be calculated in neutrons per cubic centimeter per second, and $\phi(>10)$ from Eq. 29 must be multiplied by this to arrive at the total effective neutron flux above 10 Mev at the core center.

It can be shown that the spectrum through the reflector can be approximated by

$$N(E,R) = \frac{A \sinh \sqrt{2E}\, e^{-E}}{4(R + R_c)\,\Sigma_R\,\Sigma_C}\left[\Sigma_R(R + 2R_c)E_2(\Sigma_R R) - e^{-\Sigma_R R}\right] \tag{30}$$

where subscript R = total macroscopic cross section of the reflector

subscript C = total macroscopic cross section of the core

R_c = core radius

$E_2(x) = \int_x^{\infty} e^{-\mu}/\mu^2\, d\mu$

R = distance from the surface of the core

Since $\Sigma_H(E)$ does not vary appreciably between 9 and 16 Mev, $\Sigma_H(E)$ was taken as a constant equal to $0.057\ cm^{-1}$ for purposes of plotting Fig. 4.6 where the spectrum at the core surface (R = 0) is plotted.

The effective flux for the N^{16} production at the core surface is given by

$$\phi_{core\ surface}\ (>10) = \int_{10}^{\infty} N(E,0)\, dE\ n_f = 5.1 \times 10^{-3} n_f \qquad (neutrons/cm^2\text{-}sec)$$

where n_f is the average fission-neutron source density, as used above, in neutrons per cubic centimeter per second.

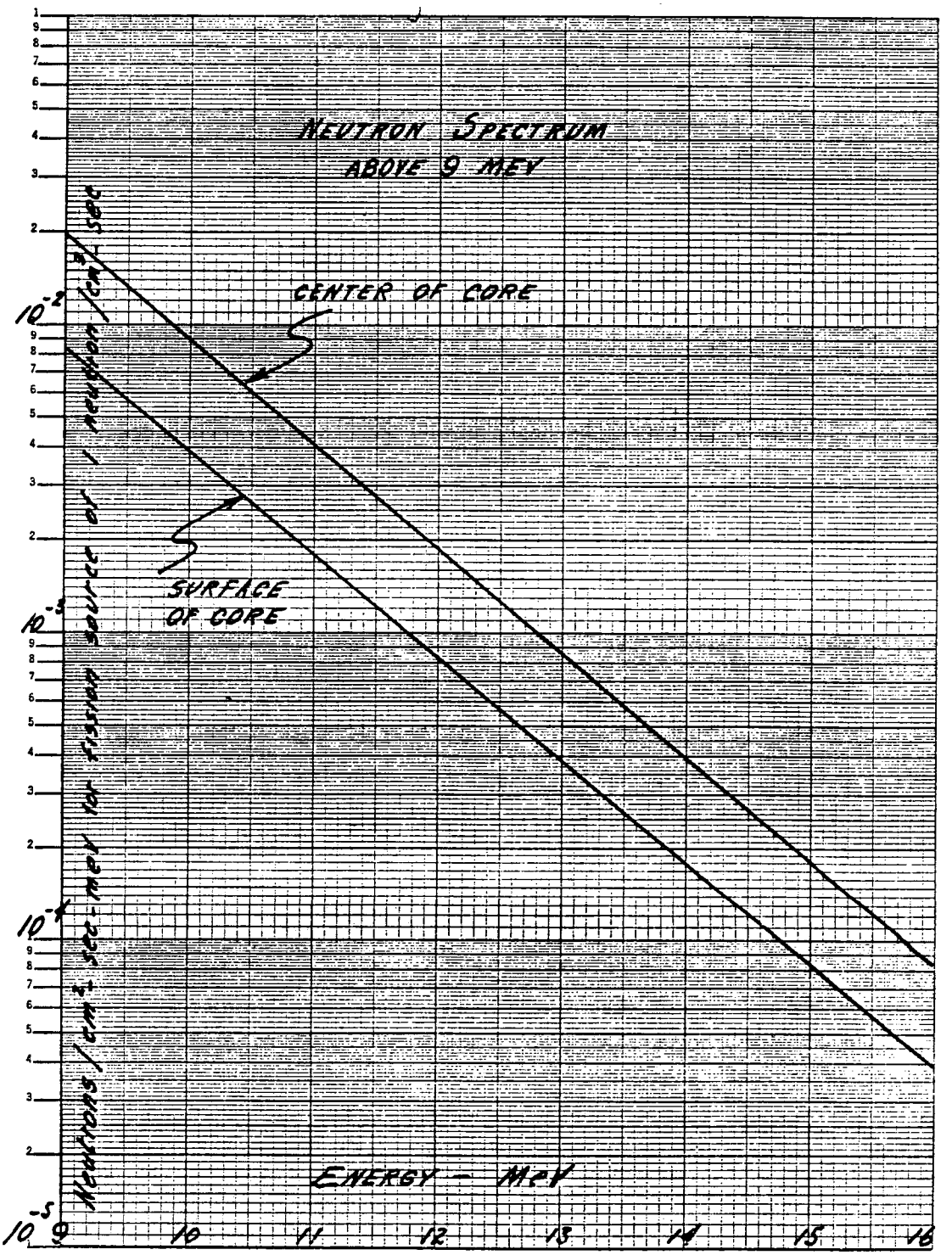

NEUTRON SPECTRUM
ABOVE 9 MEV
CENTER OF CORE
SURFACE
OF CORE
Neutrons / cm² sec - MeV for fission source on 1 sec scale
ENERGY - MeV
9
10
11
12
13
14
15
16

Figure 4.6

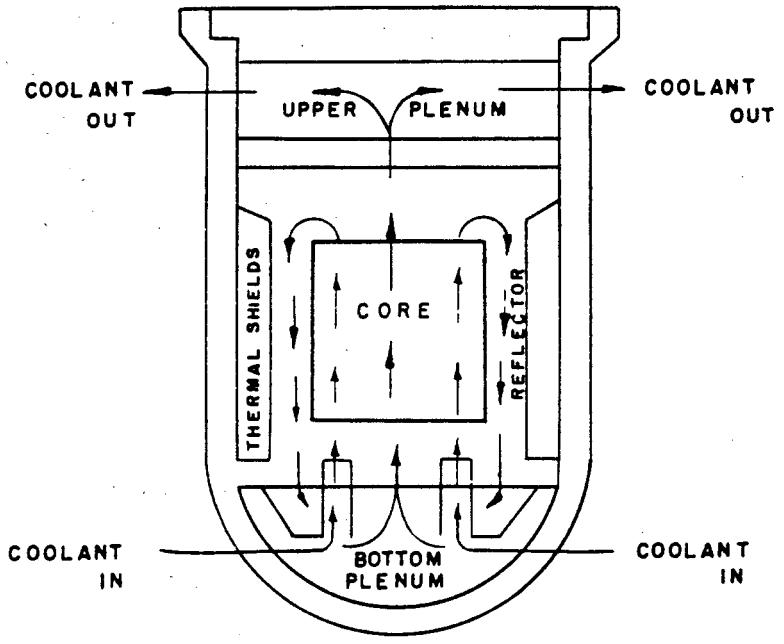
Since the reaction cross section averaged over the fission spectrum has been determined (see Sec. 2.1), the effective production rate, $\overline{\sigma\phi}$ (the number of N^{16} atoms formed per second per O^{16} atom), can now be determined by applying the fluxes previously calculated as follows:

$$\overline{\sigma\phi} = \overline{\sigma}\ \phi(R)_{>10}\ \frac{A}{A_{>10}} \tag{31}$$

when $\phi(R)_{>10}$ = calculated flux above 10 Mev at position R at full power
A = area of fission spectrum = 1 neutron/fission neutron
$A_{>10}$ = area of fission spectrum above 10 Mev = 1.24×10^{-3}
$\overline{\sigma}$ = reaction cross section = 0.020 millibarn (averaged over the fission spectrum)

2.5 Equilibrium Gamma Activity

Since the effective neutron flux for the N^{16} production is known, the induced N^{16} equilibrium activity level can be calculated from the flow diagram of the primary coolant. This diagram is shown in Fig. 4.7. In a two-pass system, as assumed here, the water passes through the bottom plenum and up through the outer part of the core; then it passes down through the reflector, up the center of the core, and through the upper plenum (see accompanying diagram). The two



FLOW IN A TYPICAL TWO-PASS CORE

time intervals in the core are considered as a single stage in the calculation. The total average times per unit volume of water in the various parts of the system are:

Time in reflector (t_r)	Time in upper plenum (t_u)
Time in lower plenum (t_l)	Total cycle time (T)
Time in core (t_c)	

FLOW DIAGRAM

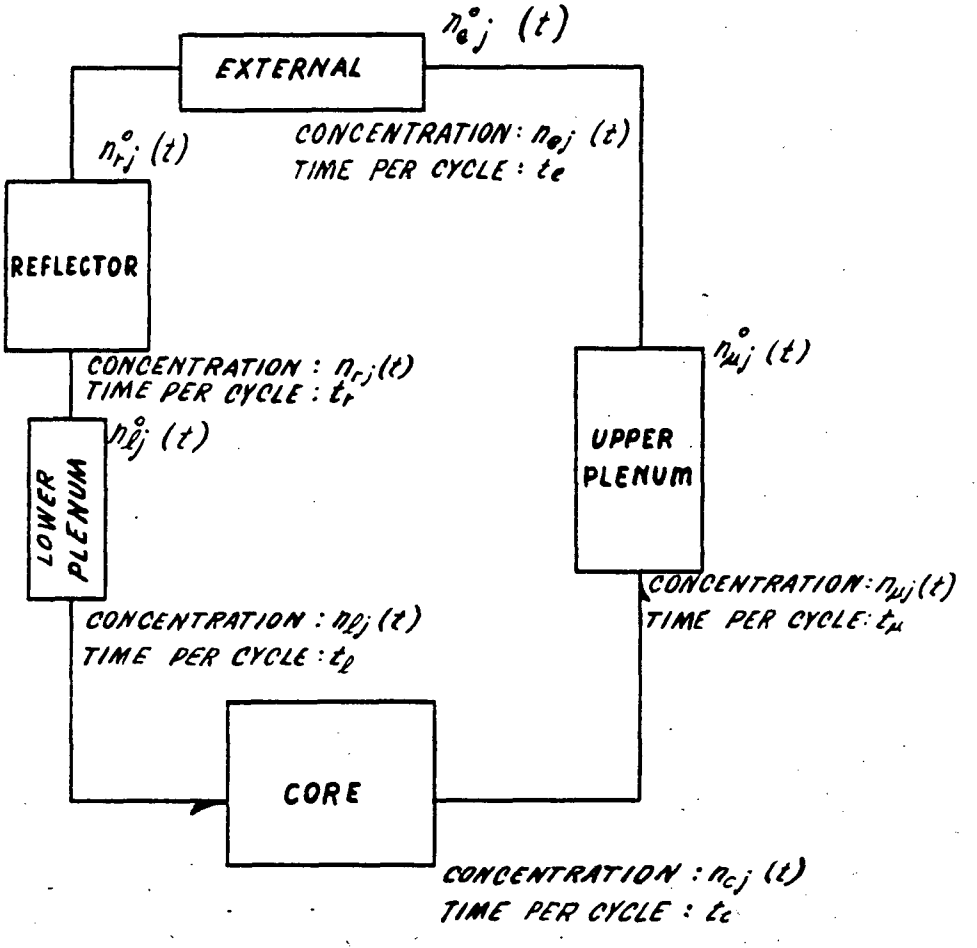


Figure 4.7

The induced activity per unit volume in each portion of the coolant circuit is given by the following expressions, each a particular solution of the basic differential equation for the N^{16} build-up and decay:

$$dn_i/dt = (\overline{\sigma\phi})_i\, C - \lambda_i \tag{32}$$

with the initial condition that the concentration of N^{16} atoms as the i*th* portion of the circuit is entered is $n_{0i}(t)$, that is,

$$n_i(0) = n_{0i}(t)$$

where n = number of N^{16} (atoms/cm^3)
C = concentration of O^{16} isotope (atoms/cm^3)
λ = disintegration constant of N^{16} (= 0.094 sec^{-1})
and the subscript i applies to the different portions of the circuit, i.e., c, core; r, reflector; *l*, lower plenum; u, upper plenum; and e, system external to reactor.

The model and symbolism shown in Fig. 4.7 are used for the mathematical description of the problem.

The solution of Eq. 32 is

$$n_i = \left[n_{0i} - \frac{(\overline{\sigma\phi})_i C}{\lambda}\right] e^{-\lambda t} + \frac{(\overline{\sigma\phi})_i C}{\lambda} \tag{33}$$

The following continuity conditions hold between the activity levels expressed in each particular solution.

$$n_{0r} = n_{0e} e^{-\lambda t_e} \tag{34}$$

$$n_{0l} = \left[n_{0r} - \frac{(\overline{\sigma\phi})_r C}{\lambda}\right] e^{-\lambda t_r} + \frac{(\overline{\sigma\phi})_r C}{\lambda} \tag{35}$$

$$n_{0c} = \left[n_{0l} - \frac{(\overline{\sigma\phi})_l C}{\lambda}\right] e^{-\lambda t_l} + \frac{(\overline{\sigma\phi})_l C}{\lambda} \tag{36}$$

$$n_{0u} = \left[n_{0c} - \frac{(\overline{\sigma\phi})_c C}{\lambda}\right] e^{-\lambda t_c} + \frac{(\overline{\sigma\phi})_c C}{\lambda} \tag{37}$$

$$n_{0e} = \left[n_{0u} - \frac{(\overline{\sigma\phi})_u C}{\lambda}\right] e^{-\lambda t_u} + \frac{(\overline{\sigma\phi})_u C}{\lambda} \tag{38}$$

The N^{16} activity at equilibrium will be of the form shown in Fig. 4.8. When equilibrium is reached, n_{0r}, n_{0c}, n_{0u}, n_{0l}, and n_{0e} will remain constant with time. By substituting Eqs. 34 to 37 into Eq. 38, a relation for the equilibrium activity of the coolant as it leaves the upper plenum is obtained:

$$\frac{\lambda}{n_{0e}} = \frac{C}{1 - e^{-\lambda T}} \left[(\overline{\sigma\phi})_r e^{-\lambda(t_l + t_c + t_u)} (1 - e^{-\lambda t_r}) + (\overline{\sigma\phi})_l e^{-\lambda(t_c + t_u)} (1 - e^{-\lambda t_l}) \right.$$

$$\left. + (\overline{\sigma\phi})_c e^{-\lambda t_u} (1 - e^{-\lambda t_c}) + (\overline{\sigma\phi})_u (1 - e^{-\lambda t_u})\right] \tag{39}$$

Appropriate average values of $(\overline{\sigma\phi})_i$ must be chosen for use in the above equation. Most of the coolant in the core will be acted on by $(\overline{\sigma\phi})_c$ equal to that at the center of the core. The reason for this can be seen from Eq. 28 and the paragraph following. The average $(\overline{\sigma\phi})_r$, $(\overline{\sigma\phi})_l$, and $(\overline{\sigma\phi})_u$ are found by expressing each as a simple exponential and averaging over the region thickness.

$$(\overline{\sigma\phi})_r = (\overline{\sigma\phi})_{|R|=0} e^{-kR}$$

where k is the relaxation length for the flux in that region. This value[3] is taken as 0.15 cm^{-1}. Therefore

$$(\overline{\sigma\phi})_{r_{av}} = \frac{(\overline{\sigma\phi})_{|R=0|} \int_{R=0}^{d_R} e^{-kR} R\, dR}{\int_0^{d_R} R\, dR}$$

where d_R is the distance from core surface to reflector.

The integration is taken from the core surface (R = 0) to the assumed outer part of the reflector d_R. In the case of the lower plenum

$$(\overline{\sigma\phi})_{l_{av}} = \frac{(\overline{\sigma\phi})_{|R=0|} \int_0^{d_l} e^{-kR} R\, dR}{\int_0^{d_l} R\, dR}$$

where d_l is the distance of the lower plenum.

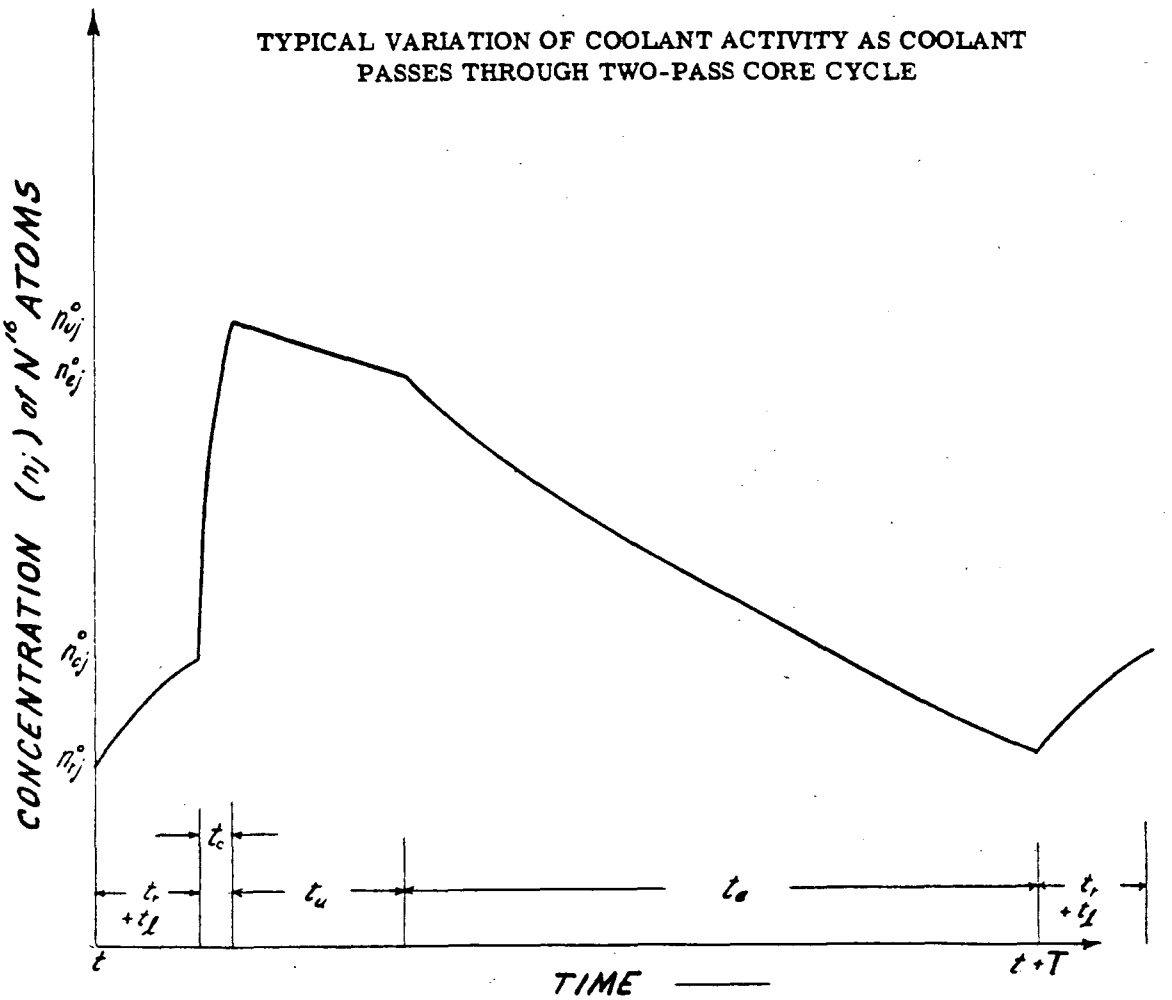


Figure 4.8

For the upper plenum

$$(\overline{\sigma\phi})_{u_{av}} = \frac{(\overline{\sigma\phi})_{|R=0|} \int_0^{d_u} e^{-kR}\, R\, dR}{\int_0^{d_u} R\, dR}$$

where d_u is the distance of the upper plenum. Therefore the equilibrium coolant activity, as it leaves the upper plenum, can be obtained by solving Eq. 39.

Some explanation may be required as to why Fig. 4.8 has the shape it does. Under the conditions imposed in this problem, it turns out that the activity of the coolant on leaving the core is higher than $(\overline{\sigma\phi})_{u_{av}} C$, the equilibrium activity for coolant in the upper plenum after an infinite time. Therefore the activity of the coolant decreases as it passes through the upper plenum.

2.6 Method for Approximating Coolant Activity with Changes in Core Time and Total Cycle Time

When only rough values for the times in the various portions of the cycle are known, it is advantageous to have a simple method for approximating the primary coolant activity for any given core time and total cycle time. We should note that in a typical case the main contribu-

tion to primary coolant activity is from the core itself, with the reflector contribution being about one-fourth the total. That from the upper and lower plenums is generally small. If we keep t_r, t_l, t_c, and t_u constant and equal to the values given below, the activity of the primary coolant will vary with total cycle time as shown in Fig. 4.9. Figure 4.10 shows a plot of the ratio of the resultant activity to a reference activity as a function of the ratio of a given time in each portion of the cycle to a reference time. That is, we start with a given arbitrary set of times:

T_0 = 7 sec, total cycle time
T_{r_0} = 0.40 sec, time in reflector
T_{l_0} = 0.23 sec, time in lower plenum
t_{c_0} = 0.12 sec, time in core
t_{u_0} = 0.62 sec, time in upper plenum

The resultant activity A_0 can now be computed. Each time is changed by the ratio T/T_0, and the new activity A is computed. A/A_0 is then plotted against T/T_0. Four curves are given, all with t_{r_0}, t_{l_0}, t_{c_0}, and t_{u_0} the same but with different T_0 values.

From Figs. 4.9 and 4.10, an approximate value for the coolant activity for a given core time (t_c) and a total cycle time (T_1) can then be found. First, find $T_0 = (T_1/t_c)(0.12)$. From Fig. 4.9 the activity A_0 corresponding to T_0 is then found. From Fig. 4.10, using the curve for total cycle time T_0, A_1/A_0 is then determined. Finally, the unknown activity A_1 is $(A_1/A_0)\,A_0$.

Example. Find A_1 for T_1 = 6.6 sec and t_c = 0.29 sec.

$$T_0 = \frac{6.6}{0.29}\,(0.12) = 2.75 \text{ sec} \tag{40}$$

A_0 for T_0 = 2.75 sec (Fig. 4.9) = 2.0×10^6 gammas/cm^3-sec.

$$\frac{A_1}{A_0} \text{ (evaluated at) } \left(\frac{T_1}{T_0} = 2.4\right) \text{ (on the } T_0 = 2.75\text{-sec curve)} \approx 1.17 \tag{41}$$

$$A_1 = 1.17\,(2.0 \times 10^6) = 2.34 \times 10^6 \text{ gammas/cm}^3\text{-sec} \tag{42}$$

This method for approximating coolant activity assumes that the time in the reflector is about 3.4 times the time in the core. If this is not the case, the estimated activity will be in error. The coolant activity found by using Figs. 4.9 and 4.10 is good within 25 per cent for the conditions given.

2.7 Equilibrium Neutron Activity

Since the threshold for the $O^{17}(n,p)N^{17}$ reaction is high, the single collision theory can be applied as it has been demonstrated for the $O^{16}(n,p)N^{16}$ reaction.

The effective fluxes for this reaction are found by integrating Eqs. 28 and 30 from 8.5 Mev to infinity and multiplying by the fission-neutron source density. The effective production rate ($\overline{\sigma\phi}$) is then found by multiplying these values by the reaction cross section averaged over the fission spectrum above 8.5 Mev.

The average effective flux values in the various portions of the flow can be found as shown earlier for the N^{16} case.

With a disintegration constant (λ) of 0.168 sec^{-1} and using the proper flow times, the equilibrium neutron activity as the coolant leaves the upper plenum can be calculated by Eq. 39.

3 GAMMA SHIELDING FOR THE REACTOR COOLING SYSTEM

3.1 Hand-calculation Procedure for Coolant Gamma Shield Thickness

A hand-calculation method using the curves presented in Chap. 9 was developed for "isodosing" the coolant gamma shield, i.e., calculating a shield thickness which varies over its

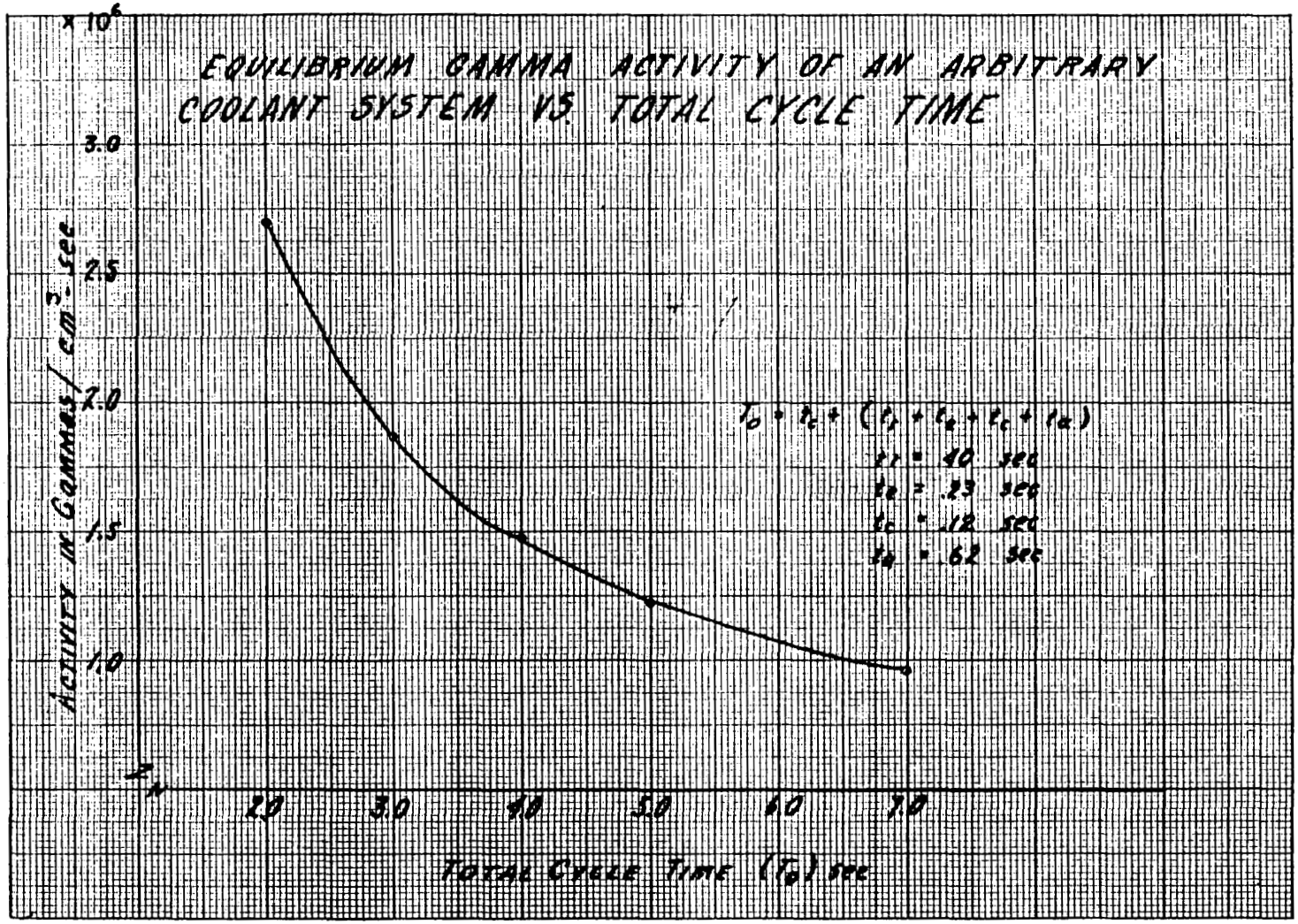

EQUILIBRIUM GAMMA ACTIVITY OF AN ARBITRARY COOLANT SYSTEM VS TOTAL CYCLE TIME
x 10^6
3.0
2.5
2.0
1.5
1.0
Activity in Gammas / cm³ - sec
$T_D = t_c + (t_1 + t_2 + t_3 + t_4)$
t_1 = 40 sec
t_2 = 23 sec
t_3 = 12 sec
t_4 = 62 sec
2.0
3.0
4.0
5.0
6.0
7.0
Total Cycle Time (T_D) sec

Figure 4.9

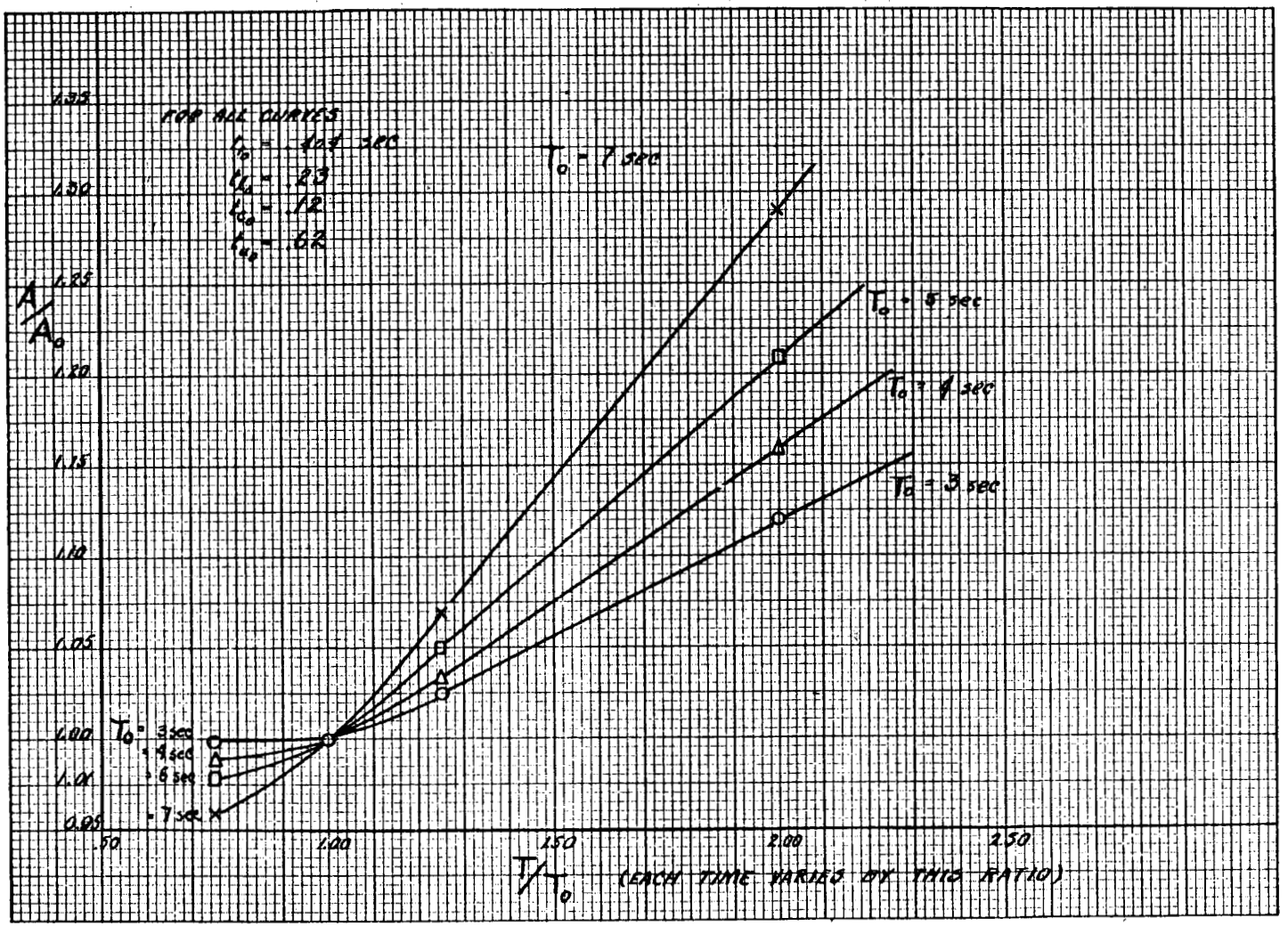

FOR ALL CURVES
t_o = .424 sec
t_{L_o} = .23
t_{c_o} = .12
t_{u_o} = .62
T_o = 7 sec
T_o = 5 sec
T_o = 4 sec
T_o = 3 sec
T_o = 3 sec
4 sec
5 sec
7 sec
A/A₀
T/T₀ (EACH TIME VARIED BY THIS RATIO)
1.35
1.30
1.25
1.20
1.15
1.10
1.05
1.00
.95
.50
1.00
1.50
2.00
2.50

Figure 4.10

surface to maintain a constant dose rate. The method uses the assumption that the gamma flux leaving the reactor shield has been reduced to a level where it will not contribute significantly to the required coolant shield thickness. The coolant shield (or secondary shield) is calculated in terms of an equivalent iron shield. The structure and other incidental shielding between the source and the shield is subtracted from the calculated shield thickness, and the remainder is converted to lead or other shielding material. The use of build-up factors for iron introduces a slight error in the calculated amount of other shielding. This error is conservative for denser material and optimistic for less dense material.

(a) Procedure. 1. A number of points are selected over the surface of the secondary shield. The procedure is to calculate the dose rate at each point for two arbitrary iron shield thicknesses, e.g., 4 in. and 8 in. of iron.

2. The primary coolant system is approximated by cylindrical and hemispherical sources having the same effective specific activity as the actual source.

3. The distances from the center line of each source to each dose point and the angles subtended by each source at each dose point are tabulated.

4. The dose rate at each point from each source must then be calculated. From the generalized cylindrical and spherical source data in Chap. 9, working curves are replotted in terms of dose rate (milliroentgens/hr), distance (feet), and equivalent iron shield thicknesses for specific parameters, as illustrated by Fig. 4.15. This is done to facilitate the calculation of the dose rate through a shield from an infinitely long cylinder located at various distances from the shield.

5. The dose rate for the infinitely long cylinder as obtained in item 4 must be corrected for its finite size. This is done by means of a general line-source geometric factor (GF) based on the definition: $GF = F(b,\phi)/F(b,\pi/2)$, where ϕ is the subtended angle of the extremities of the pipe and $b = \mu t$ = shield thickness in relaxation lengths (see Fig. 4.11).

To determine the angles, a plane is passed through the source and the dose point. Lines are drawn from the dose point to the extremities of the source in this plane. A line normal to the line of intersection of the source plane and the shield plane is drawn to the source. The angles thus formed at the dose point by the normal line and the lines to the extremities are those measured for the geometric factor (see Fig. 4.12). These specific geometric factors resolve into various cases as shown on Fig. 4.13.

6. A second correction is necessary to account for build-up. Ordinary build-up data are for normal incidence of gamma rays. The ordinary build-up data in Chap. 10 are modified by the method originated by G. H. Peebles, as described in Sec. 3.2 and Fig. 4.16. These data are for number build-up and are normalized to agree with the dose build-up at normal incidence. The secant of angle θ in Fig. 4.12 is used.

7. The actual dose rate is the product of the dose from the infinite pipe. The geometric factor, and the build-up. The actual dose rates at each dose point are summed for each assumed iron shield.

8. To determine the required shield thickness, the two dose rates at each dose point are plotted in a semilog plot of dose rate vs. iron thickness. The two points are connected by a straight line. The point at which allowable dose rate intersects the line has as its abscissa the required equivalent iron shield. The structural iron is subtracted from this value, and the remainder is converted to lead or other shielding material. The equivalent amount of lead is determined by the attenuation properties of lead and iron at the predominant decay energy of the primary coolant (see Chap. 6, Sec. 2).

9. Since the secondary shield is determined by the primary coolant in the coolant system without considering the reactor contribution, it is then necessary to check reactor dose rates to determine whether or not there is a sizable reactor contribution to the secondary shield.

It also becomes important to evaluate the prevalent gamma source within the primary shield for this check (see Chap. 3, Sec. 1.3). In one particular reactor and primary-shield complex, this prevalent gamma source was due to the capture of thermal neutrons within the reactor vessel walls. Subsequently, an equivalent point-source model was utilized to represent this gamma source for receptors located outside the primary shield. This equivalent point

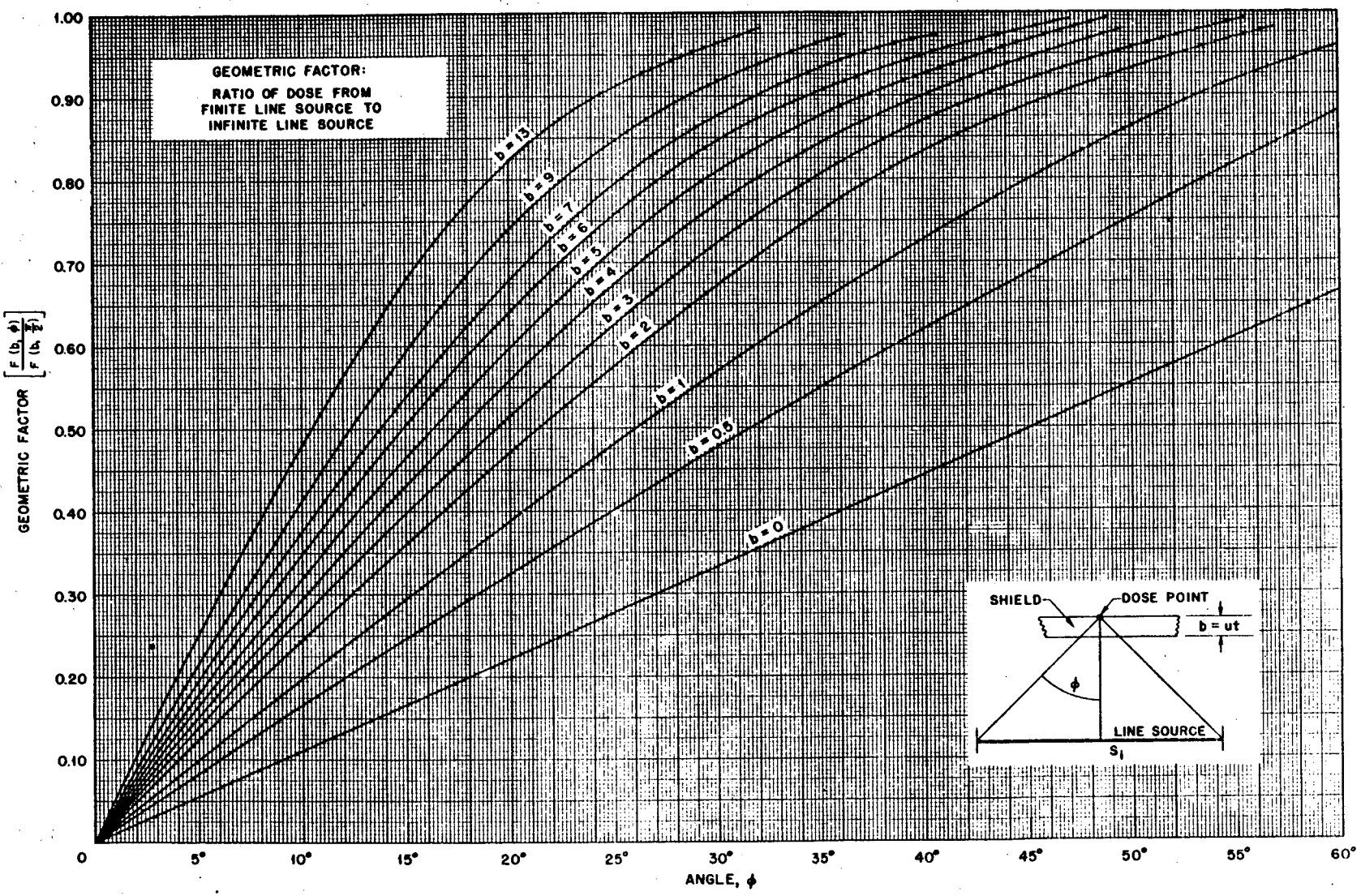
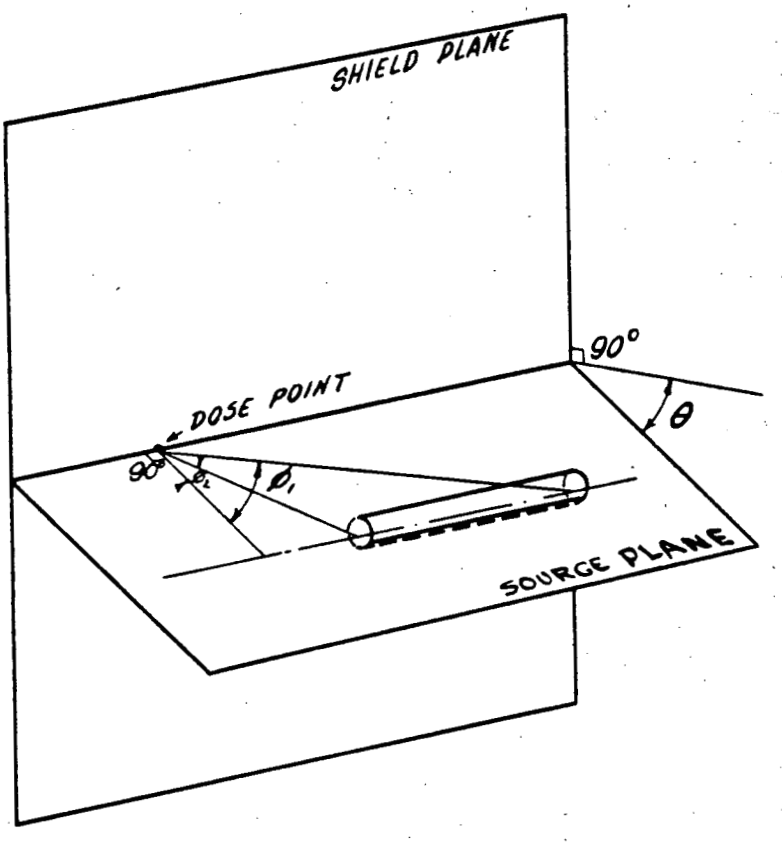

GEOMETRIC FACTOR:
RATIO OF DOSE FROM FINITE LINE SOURCE TO INFINITE LINE SOURCE
GEOMETRIC FACTOR $\left[\frac{F(b,\phi)}{F(b,\frac{\pi}{2})}\right]$
ANGLE, ϕ
b = 13
b = 9
b = 7
b = 6
b = 5
b = 4
b = 3
b = 2
b = 1
b = 0.5
b = 0
1.00
0.90
0.80
0.70
0.60
0.50
0.40
0.30
0.20
0.10
0
5°
10°
15°
20°
25°
30°
35°
40°
45°
50°
55°
60°
SHIELD
DOSE POINT
b = ut
ϕ
LINE SOURCE
S_l

Figure 4.11



GEOMETRIC FACTOR. METHOD FOR DETERMINING SUBTENDED ANGLES ϕ_1 AND ϕ_2. θ IS THE BUILD UP ANGLE.

Figure 4.12

source was located on the outside of the reactor vessel wall and at the core center height. Only the nearest equivalent point source to the receptor point was picked for the check calculation. The equivalent point-source model enabled a reasonable evaluation of the primary-shield gamma contribution to all regions of the secondary shield which were at a considerable distance from the reactor-core region.

(b) Sample Calculation. Consider the case of a cylindrical source that is offset from the dose point and whose direct radiation impinges obliquely on the dose point as illustrated in Fig. 4.14.

1. Assume a 10-in. schedule-120 pipe source with a wall thickness of 0.843 in. Assume an equivalent iron shield of 4 in.

$\theta = 36°$
$\phi_1 = 30°$
$\phi_2 = 15°$
a = 10 ft = the true distance from the source to the dose point
z = 8 ft = the horizontal distance from pipe center line to dose point plane
y = 6 ft = the vertical distance from pipe center line to dose point plane

2. To calculate the dose from an infinitely long pipe source (D_∞), enter curve on Fig. 4.15 with the distance a = 10 ft. Read the dose where the line for 4-in. equivalent iron shield crosses the distance line of a = 10 ft. The dose at the point is 49 mr/hr.

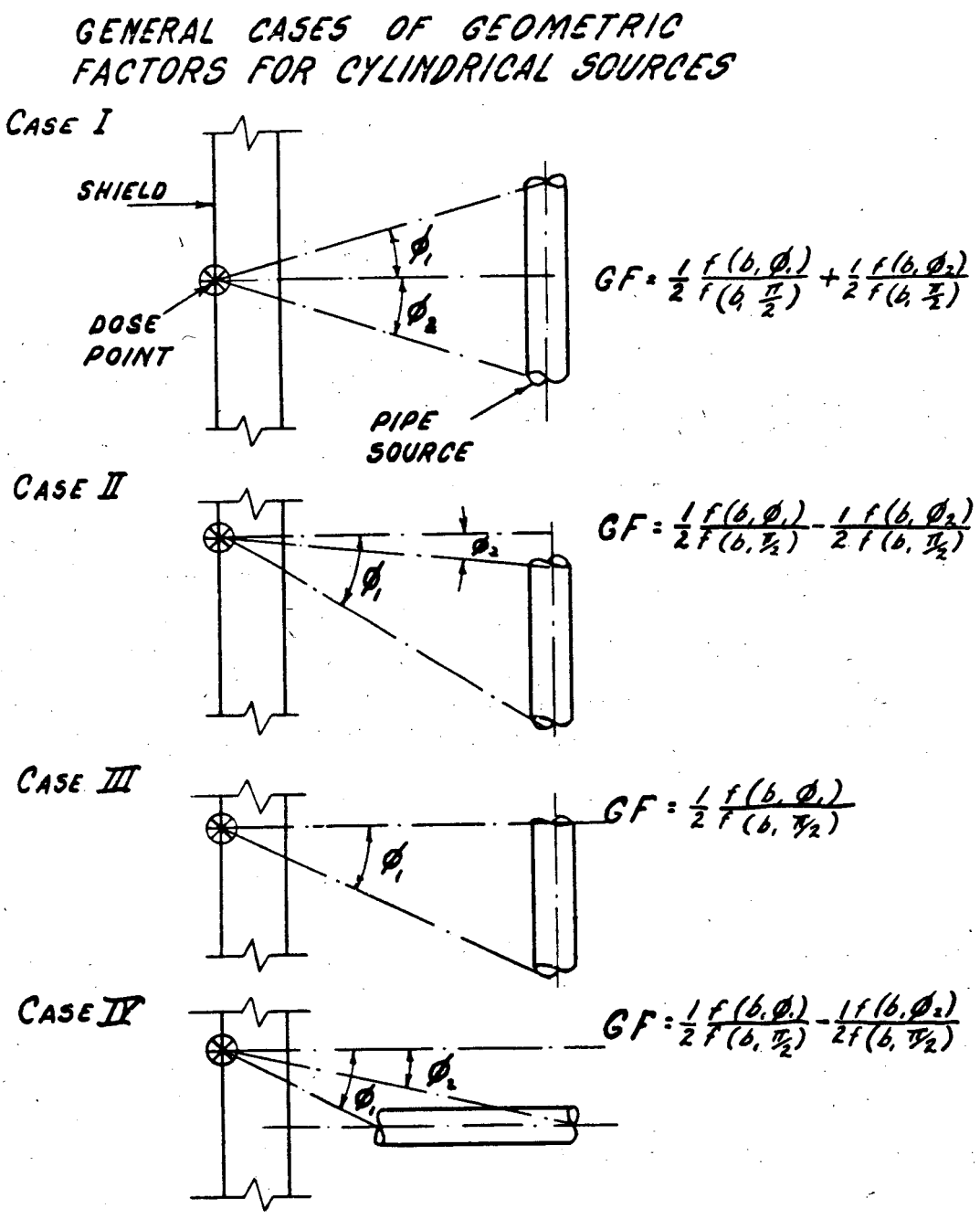

GENERAL CASES OF GEOMETRIC FACTORS FOR CYLINDRICAL SOURCES
CASE I
SHIELD
DOSE POINT
PIPE SOURCE
$GF = \frac{1}{2}\frac{f(b,\phi_1)}{f(b,\frac{\pi}{2})} + \frac{1}{2}\frac{f(b,\phi_2)}{f(b,\frac{\pi}{2})}$
CASE II
$GF = \frac{1}{2}\frac{f(b,\phi_1)}{f(b,\pi/2)} - \frac{1}{2}\frac{f(b,\phi_2)}{f(b,\pi/2)}$
CASE III
$GF = \frac{1}{2}\frac{f(b,\phi_1)}{f(b,\pi/2)}$
CASE IV
$GF = \frac{1}{2}\frac{f(b,\phi_1)}{f(b,\pi/2)} - \frac{1}{2}\frac{f(b,\phi_2)}{f(b,\pi/2)}$
NOTE: ALL VIEWS ARE IN THE PLANE OF THE SOURCE
SOURCES MAY BE SKEW. NOTE THAT CASE IV
IS SIMILAR TO CASE II

Figure 4.13

3. To find the build-up, B (Fig. 4.16), calculate the value of b and γ where

b = μt = (0.238 cm^{-1})(4 in.)(2.54 cm/in.) = 2.42 relaxation lengths (where μ = gamma absorption coefficient for iron = 0.238 cm^{-1} at 6 Mev and t = shield thickness = 4 in.)

γ = cos θ = cos 36° = 0.80

Enter curve on Fig. 4.16 with these values for b and γ. The build-up found is 1.3.

4. To calculate the geometric factors (GF), pass a plane A through the pipe-source center line and the dose point. Determine the angle ϕ_1 formed by the normal to the intersection of

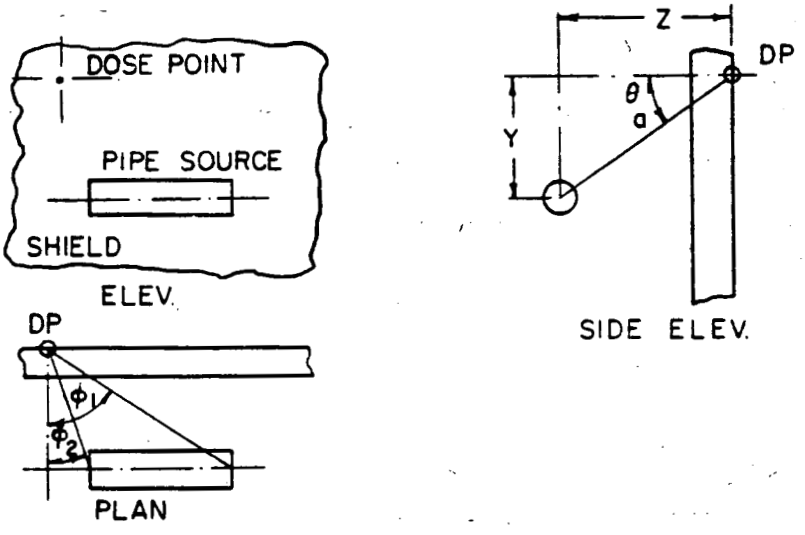


Figure 4.14

plane A and the dose point plane (plane B) which lies in the plane A. Determine the angle ϕ_2 formed by the lines connecting the dose point with the ends of the pipe.

Enter curve on Fig. 4.11 with the values of b and ϕ to find the value of $F(b,\phi)/F(b,\pi/2)$.

$$\phi_1 = 30° \qquad \frac{F(b,\phi)}{F\left(b,\frac{\pi}{2}\right)} = 0.69$$

$$\phi_2 = 15° \qquad \frac{F(b,\phi)}{F\left(b,\frac{\pi}{2}\right)} = 0.38$$

The geometric factor is typical of case II, Fig. 4.13.

$$GF = \frac{1}{2}\frac{F(b,\phi_1)}{F\left(b,\frac{\pi}{2}\right)} - \frac{1}{2}\frac{F(b,\phi_2)}{F\left(b,\frac{\pi}{2}\right)}$$

$$GF = \frac{1}{2}(0.69) - \frac{1}{2}(0.38)$$

$$GF = 0.16$$

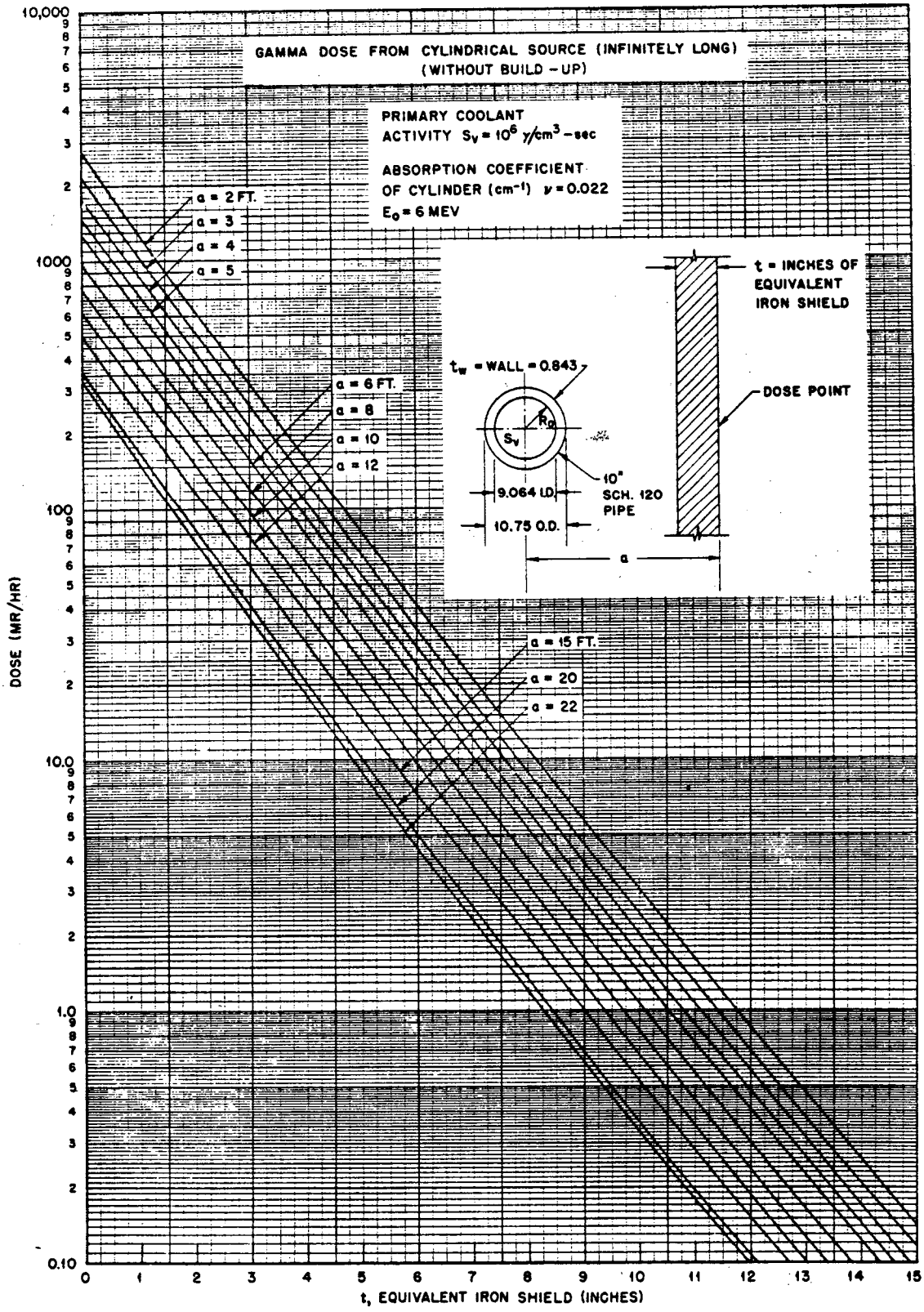

GAMMA DOSE FROM CYLINDRICAL SOURCE (INFINITELY LONG)
(WITHOUT BUILD – UP)
PRIMARY COOLANT
ACTIVITY $S_v = 10^6$ γ/cm³ – sec
ABSORPTION COEFFICIENT
OF CYLINDER (cm⁻¹) μ = 0.022
E_0 = 6 MEV
a = 2 FT.
a = 3
a = 4
a = 5
a = 6 FT.
a = 8
a = 10
a = 12
a = 15 FT.
a = 20
a = 22
t = INCHES OF EQUIVALENT IRON SHIELD
DOSE POINT
t_w = WALL = 0.843
R_0
S_v
10" SCH. 120 PIPE
9.064 I.D.
10.75 O.D.
a
DOSE (MR/HR)
10,000
1000
100
10.0
1.0
0.10
0 1 2 3 4 5 6 7 8 9 10 11 12 13 14 15
t, EQUIVALENT IRON SHIELD (INCHES)

Figure 4.15

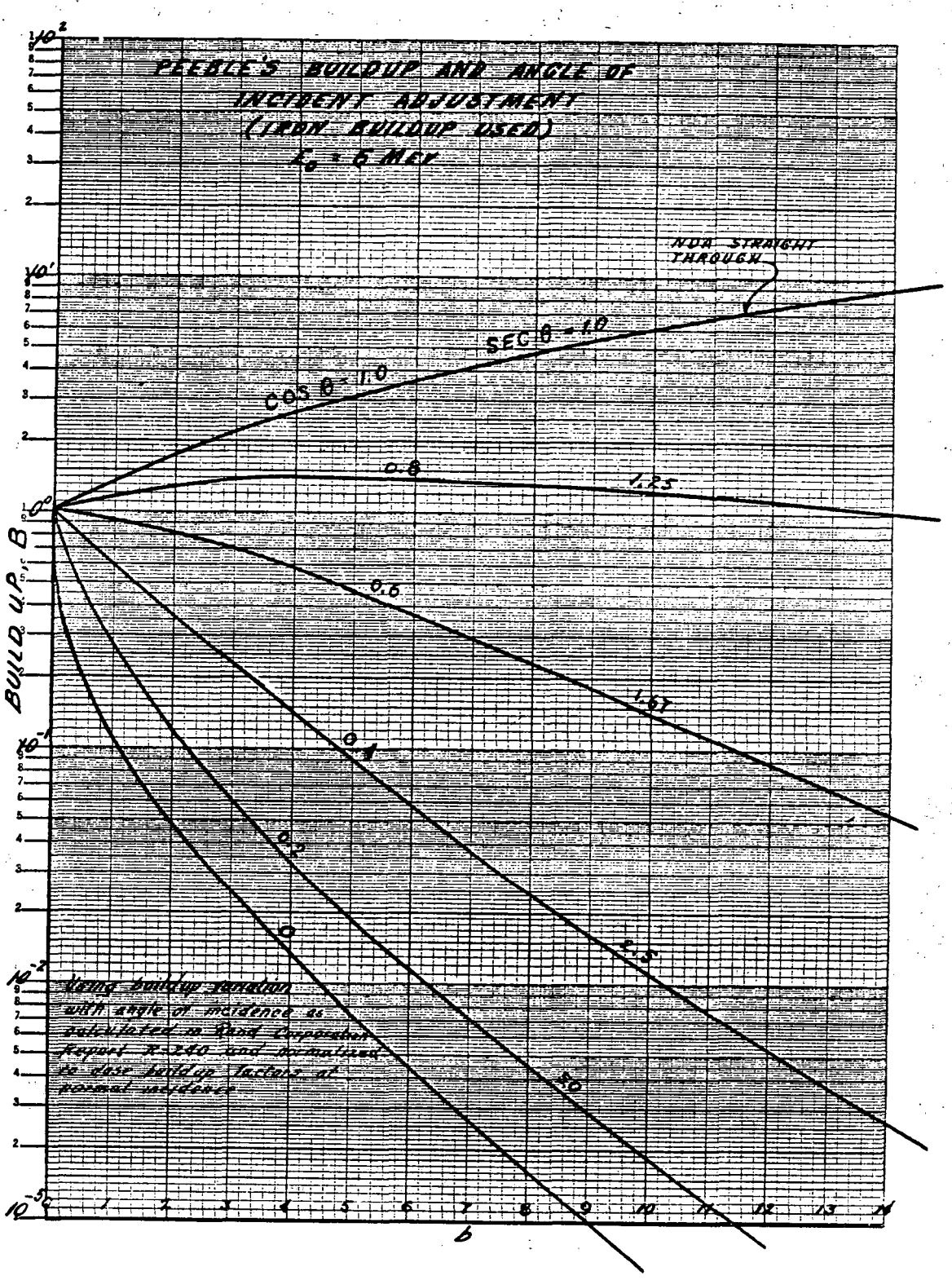

PEEBLE'S BUILDUP AND ANGLE OF INCIDENT ADJUSTMENT
(IRON BUILDUP USED)
E_0 = 6 MEV
NON STRAIGHT THROUGH
SEC θ = 1.0
COS θ = 1.0
0.8
1.25
0.6
1.67
0.1
0.2
0
2.5
5.0
BUILD UP B
b
Using buildup variation with angle of incidence as calculated in Rand Corporation Report R-240 and normalized to dose buildup factors at normal incidence

Figure 4.16

5. The actual dose rate then is:

$$\text{Actual dose rate} = (D_\infty)(B)(GF)$$
$$= (49)(1.3)(0.16)$$
$$= 10.2 \text{ mr/hr}$$

For the total dose rate at any one dose point, the procedure is repeated for all sources, and the dose rates are summed to give the total dose rate for the chosen shield thickness (see the general procedure outline, Sec. 3.10a).

3.2 Attenuation of Gamma Rays at Oblique Incidence

It has sometimes been assumed that radiation obliquely incident on a shield is attenuated to the same extent as it would be when it is normally incident on a shield whose thickness is equal to the slant distance through the oblique shield. This assumption may lead to a significant underestimate of the shield thickness required to produce a particular degree of attenuation. Scattered radiation can make an important contribution to the transmission through the shield in this case. When radiation impinges on a shield perpendicularly, any scattered radiation must travel a greater distance through the shield than the uncollided radiation. In oblique incidence, however, some of the scattered radiation travels a shorter distance than the uncollided radiation. Measurements[4] have been made with gamma rays from Co^{60}, Cs^{137}, and Au^{198} through concrete, lead, and polyethylene shields; these data may be applicable when such problems are encountered.

The following method is suggested to account for scattered gamma rays of higher energy and those through materials not as yet tested:

Peebles[5] using multiple scattering techniques calculated build-up factors for a monoenergetic monoangular beam of photons incident on a slab of finite thickness but infinite area. The build-up factor was defined as a number build-up

$$\sum_{k=0}^{\infty} \frac{N_k}{e^{-x}}$$

where N_k is the probability that a photon will be transmitted through a slab with exactly k scattering and e^{-x} is the uncollided flux. Hence, a reasonable representation of build-up and obliqueness (incident angle) that direct radiation from a cylindrical source makes with the normal at the dose point can be made by employing the Peebles's build-up variation with angle of incidence normalized at angle of incidence equal to zero to the dose build-up factors given in Chap. 10. A typical set of curves describing the variation of build-up with angle of incidence for an iron shield and 6-Mev gamma rays is shown in Fig. 4.16. Note that the perpendicular distance through the shield (not oblique) must now be used in calculations.

3.3 Experiments Using Cylindrical Sources

Experiments on dose rates from cylindrical sources are not extensive. One of the more interesting series of experiments was performed at the Naval Research Laboratory.[6] Cylindrical tanks with dimensions as indicated in Table 4.3 were filled with a water solution of a radioactive Co^{60} salt (average energy, 1.25 Mev). The cylindrical tanks were suspended vertically, and measurements were taken in a radial direction from the cylinders. There was no shield outside the cylindrical source.

The results, Fig. 4.17, show that, for small cylindrical source radius-to-length ratio (less than 1/15), cylindrical sources can be considered as line sources of corresponding length. For ratios greater than 1/15, correction should be applied to compensate for self-absorption, build-up, and geometric factors.

Table 4.3—CHARACTERISTICS OF CYLINDRICAL SOURCES

Source	Radius (a), cm	Length (L), cm	Wall thickness, cm	Specific activity, photons/cm^3-sec	Radius, mfp* of 1.25-Mev gammas in water
A	4	150	0.159	1295	0.25
B	8	150	0.317	515	0.51
C	20	150	0.635	260	1.27
D	20	250	0.635	260	1.27

* Mean free path.

3.4 Techniques for Isodose Calculation Varying Shield Thickness to Give Uniform Dose

(a) Statement of the Problem. In order to design an optimum secondary (coolant) shield, it is necessary to devise a method for calculating the required shield thickness at every point on the shield. In a compartment type shield the secondary shield encloses the heat-transfer equipment located outside the reactor, whereas the primary (reactor) shield encloses the reactor itself. The heat-transfer equipment requires shielding because it contains radioactive primary coolant from the reactor. The major portion of the neutron attenuation is in the primary shield in order to reduce the activation of the heat-transfer equipment and the secondary coolant. As a result the design of the secondary shield is primarily a problem of gamma-ray attenuation.

The pieces of equipment to be shielded are of different sizes and shapes and are located at varying distances from the shield; therefore each source gives a different contribution to the dose outside the shield. After the tolerance dose rate outside the coolant shield has been set by the methods of Chaps. 2 and 5, it is the object of the shield designer to meet this specification with a minimum of shielding. This means that, although the dose at any one point should not exceed the tolerance, there should also be no points where the dose is much less than the specified tolerance. A secondary shield, designed by the isodose calculation methods presented in this chapter, should require 15 to 25 per cent less shielding than a uniform shield sufficiently thick to attenuate the gamma rays in the worst region.

Generally, the secondary shield consists of structural steel, hydrogenous material (such as concrete, water, oil, or plastic) for neutron attenuation, and lead, iron, or concrete for gamma-ray attenuation. Where a liquid is used as a neutron shield, it is convenient to make the total shield of uniform thickness. In this case the thickness of the gamma shielding is varied from point to point to give the required gamma attenuation at each point, and the remaining shield thickness is made up of liquid. A similar argument applies when a box-like shield structure is used, such as that discussed in Chap. 6, Sec. 3.2.

(b) Method of Designing the Shield. In the actual design calculations a trial-and-error method is used. A uniform shield is initially assumed with a lead thickness at a magnitude near the expected average value. The dose is then calculated at points designated by a systematic grid on the outside of the shield. This results in an "isodose map." A functional relation between dose at a particular point and shield thickness may then be derived. This relation is then applied to correct the lead thickness thus obtaining the tolerance dose outside the shield at each point. (This is discussed in detail in the following sections.)

Lead is usually installed in slabs, the areas of which are determined by the structure of the shield; hence it is usually inconvenient to vary the lead thickness continuously. In this case, the thickness of each slab area will be determined by the point within the region requiring the maximum lead thickness.

(c) Source Geometries. For isodose calculations the heat-transfer equipment in the shielded compartment, such as evaporators, pipes, and pumps, may be idealized into geo-

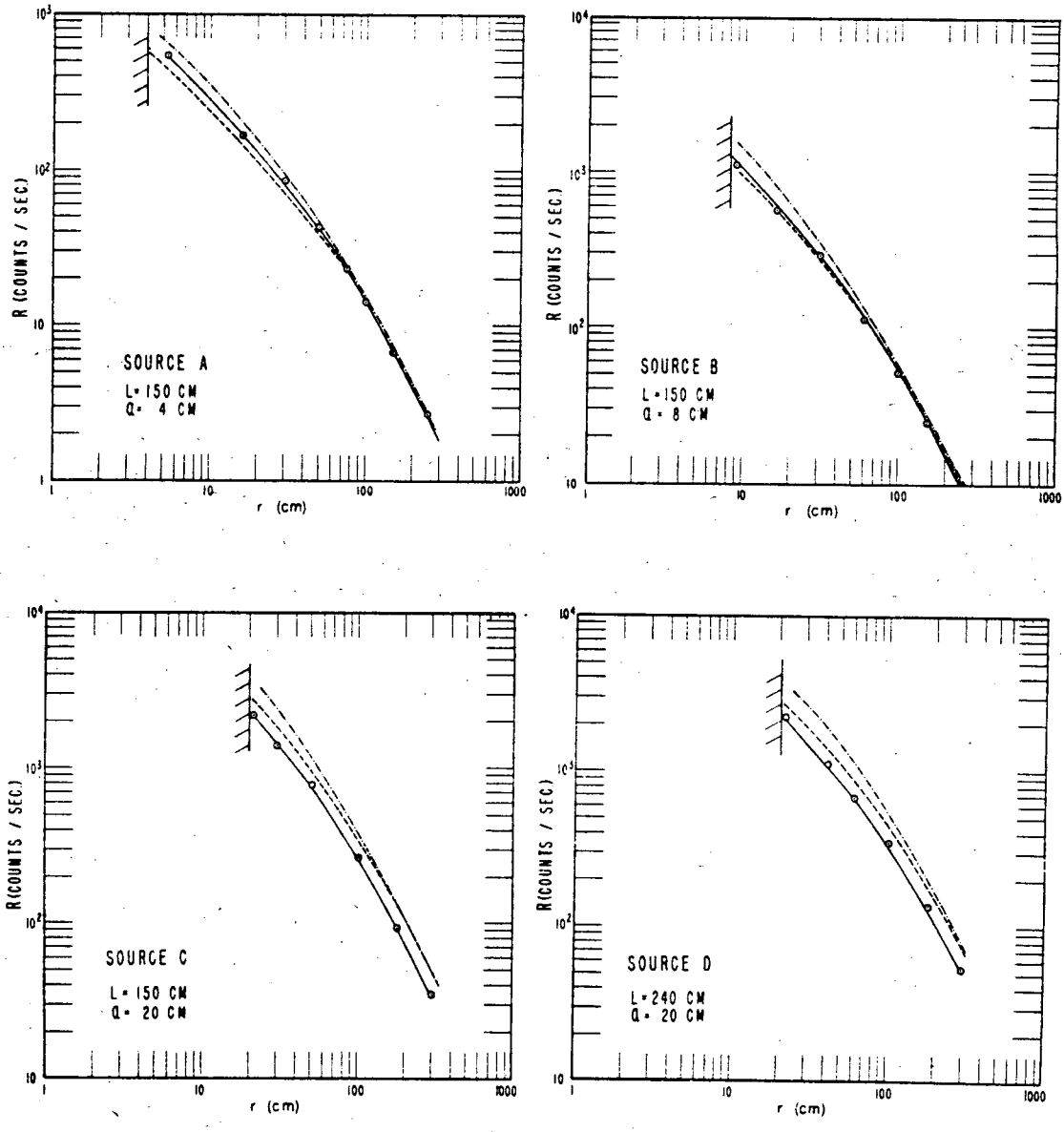


Fig. 4.17 —Counting rate data for various cylindrical sources in a plane perpendicular to, and bisecting, the source. ----, theoretical predictions. ——, experimental data.

metrical shapes such as points, lines, and cylinders. Formulas for determining the dose from such radioactive objects shielded by a slab shield have been compiled and tabulated in Chap. 9.

It can readily be seen that, if the shielded compartment is fairly large with extensive heat-transfer equipment to be shielded, the calculations required will be quite voluminous. Considerable saving in calculation time is afforded by use of the concept of a *cone of effectiveness*. The major contribution to the dose at a point outside the shield comes from sources which can be "seen" in a cone through the shield, the vertex of which is at the point and the axis of which is perpendicular to the shield. For sources uniformly distributed throughout the space, it can be shown that *90 per cent of the dose at a point comes from the sources that can be seen in a cone with a slant height through the shield of (t + 2l)*, where t is the perpendicular thickness of the shield and l the length in the shield necessary to reduce the gamma flux by a factor of e(= 2.718, base of the natural system of logarithms).

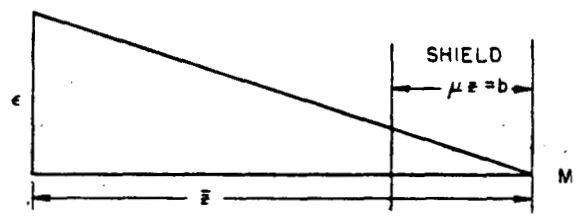


Figure 4.18

(d) Methods For Machine Calculations. Considerable simplification of the problem is obtained by setting it up for calculation by machine methods, such as on a Card Programmed Calculating (CPC) machine. In this case *all sources are subdivided into series of point sources*, and the dose at a dose point M outside the shield (see Fig. 4.18) is given by

$$D_M = \frac{1}{K} \sum_{i=1}^{N} \frac{E_0 S_i B_i \exp(-\mu z_i/\cos\theta_i)}{4\pi(\bar{z}_i/\cos\theta_i)^2} \tag{43}$$

where E_0 = the energy of the photons (Mev)
S_i = the source strength (photons/sec)
B_i = the appropriate build-up factor
$\bar{z}_i$ = the perpendicular distance from a source through the shield (cm or in.)
$\mu z_i = \Sigma \mu z$ various materials; μ is the attenuation coefficient (cm^{-1} or $in.^{-1}$) for each material, a function of E_0
$\theta_i = \tan^{-1}(\epsilon_i/\bar{z}_i)$ where ϵ_i is the eccentricity of the source relative to the dose point (cm or in.)
K = a dimensional constant to give the desired units to D_M
i = N = the total number of sources seen in the cone of effectiveness described in Sec. 3.4c.

Build-up factor data are available in Chaps. 9 and 10. Generally, for small changes in shield thickness the build-up factor can be approximated by $1 + \beta\mu z$, where β depends on the material and energy of the photons and varies in magnitude between zero and 1. The use of build-up factors is discussed more thoroughly in Chap. 1, Sec. 3.3.

The dose at point M having been computed by Eq. 43, the shield thickness can be adjusted to give the required dose, D_S, by the following equation:

$$\frac{D_S}{D_M} = \frac{B_2}{B_1} \exp - \left(\frac{\mu z_2 - \mu z_1}{\cos\theta_{av}}\right) \tag{44}$$

where subscript 1 indicates original conditions and subscript 2 indicates new conditions.

The use of Eq. 44 is somewhat a trial-and-error operation. Initially D_S/D_M is plotted vs. $(\mu z_2 - \mu z_1)$ for a θ average of approximately 15 to 20°. The correction is applied to a few typical dose points, and the dose is recomputed. A second correction may be necessary. When the desired dose, D_S, is obtained at each point, a new curve may be plotted of D_S/D_M vs. $(\mu z_2 - \mu z_1)$ which will incorporate the actual magnitude of θ average.

For example, for a shield made of iron, water, and lead, the total magnitude of μz is given by

$$\mu z = \mu z_{Fe} + \mu z_{H_2O} + \mu z_{Pb}$$

where

$$z_{Fe} + z_{H_2O} + z_{Pb} = \text{constant}$$
$$z_{Fe} = \text{constant} \tag{45}$$

(e) Geometrical Considerations: Reduction of Sources into Series of Point Sources. In the majority of cases the radioactive sources in the shielded compartment can easily be idealized into one of the following geometric forms: line, cylinder, infinite plane, or disk. Criteria will now be presented for the subdivision of the following: (1) line into points; (2) cylinder into set of parallel lines; (3) disk into point; (4) end of cylinder into a disk.

The details of the derivation of the dose rate from sources of different geometrical shapes are given in Chap. 9 along with various asymptotic approximations. The following four sections summarize the results obtained by calculating with these formulas.

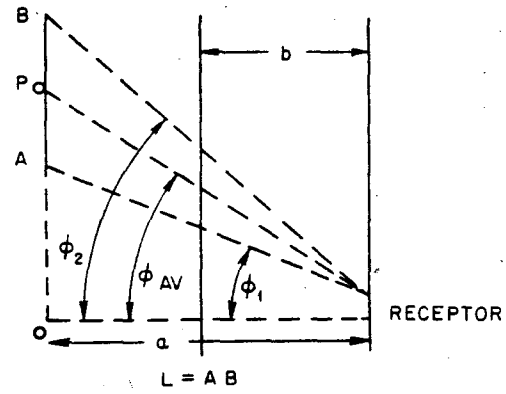


Figure 4.19

(1) Line Sources into Point Sources. Line Source Parallel to Slab Shield. The line source of length L = AB and strength S_L photons/cm-sec behind a slab shield of b relaxation lengths thick is assumed to be a point source of strength $S_P = LS_L$ located at point P midway between points A and B (see Fig. 4.19). The length of line which can be lumped into a point source such that the error in calculation of the dose rate is no greater than, say, 5 per cent is a function of three quantities: (1) the perpendicular distance a from line to receptor, (2) the shield thickness b in relaxation lengths, and (3) the average angle ϕ_{av}.

This is brought out in Figs. 4.20 through 4.23 which show the relation between D_L, the dose rate from a line source, and D_P, the dose rate from an equivalent point source.

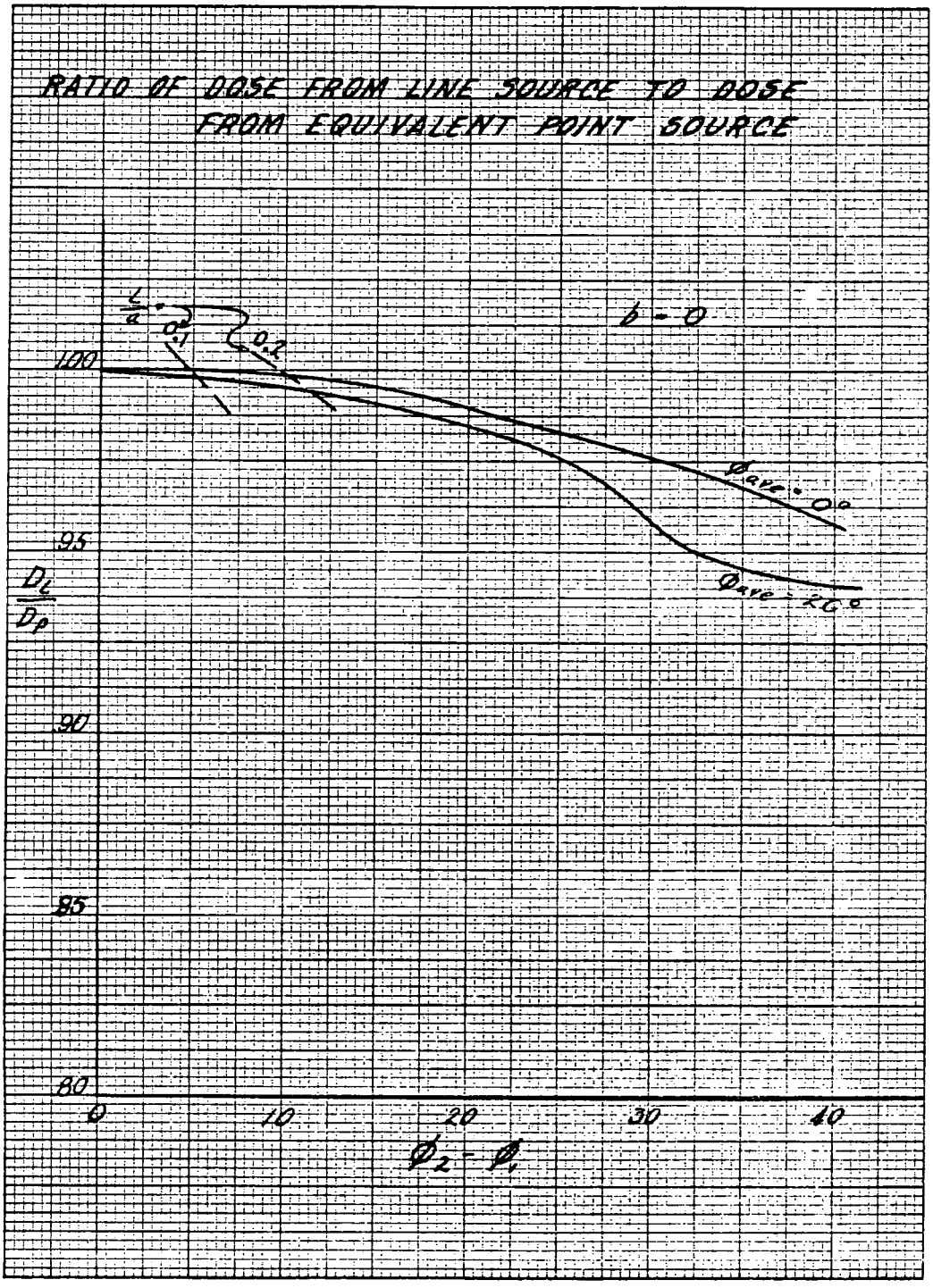

RATIO OF DOSE FROM LINE SOURCE TO DOSE FROM EQUIVALENT POINT SOURCE
L/a = 0.1
0.2
b = 0
100
95
90
85
80
D_L/D_P
$\phi_{ave} = 0.0$
$\phi_{ave} = 2.0$
0
10
20
30
40
$\phi_2 - \phi_1$

Figure 4.20

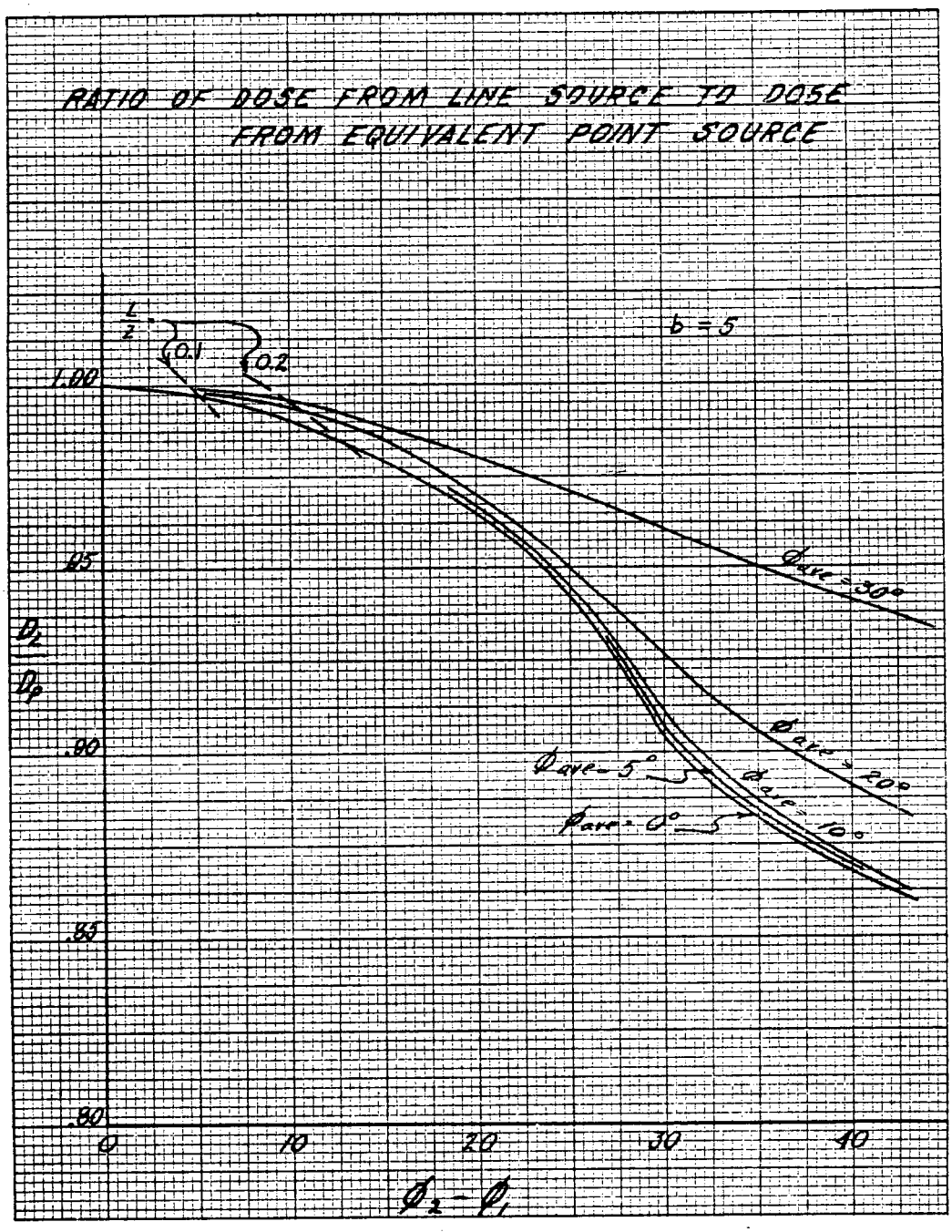

RATIO OF DOSE FROM LINE SOURCE TO DOSE FROM EQUIVALENT POINT SOURCE
L/z
0.1
0.2
b = 5
1.00
.95
D2/Dp
.90
.85
.80
0
10
20
30
40
Ø2 - Ø1
Øave = 30°
Øave = 20°
Øave = 10°
Øave = 5°
Øave = 0°

Figure 4.21

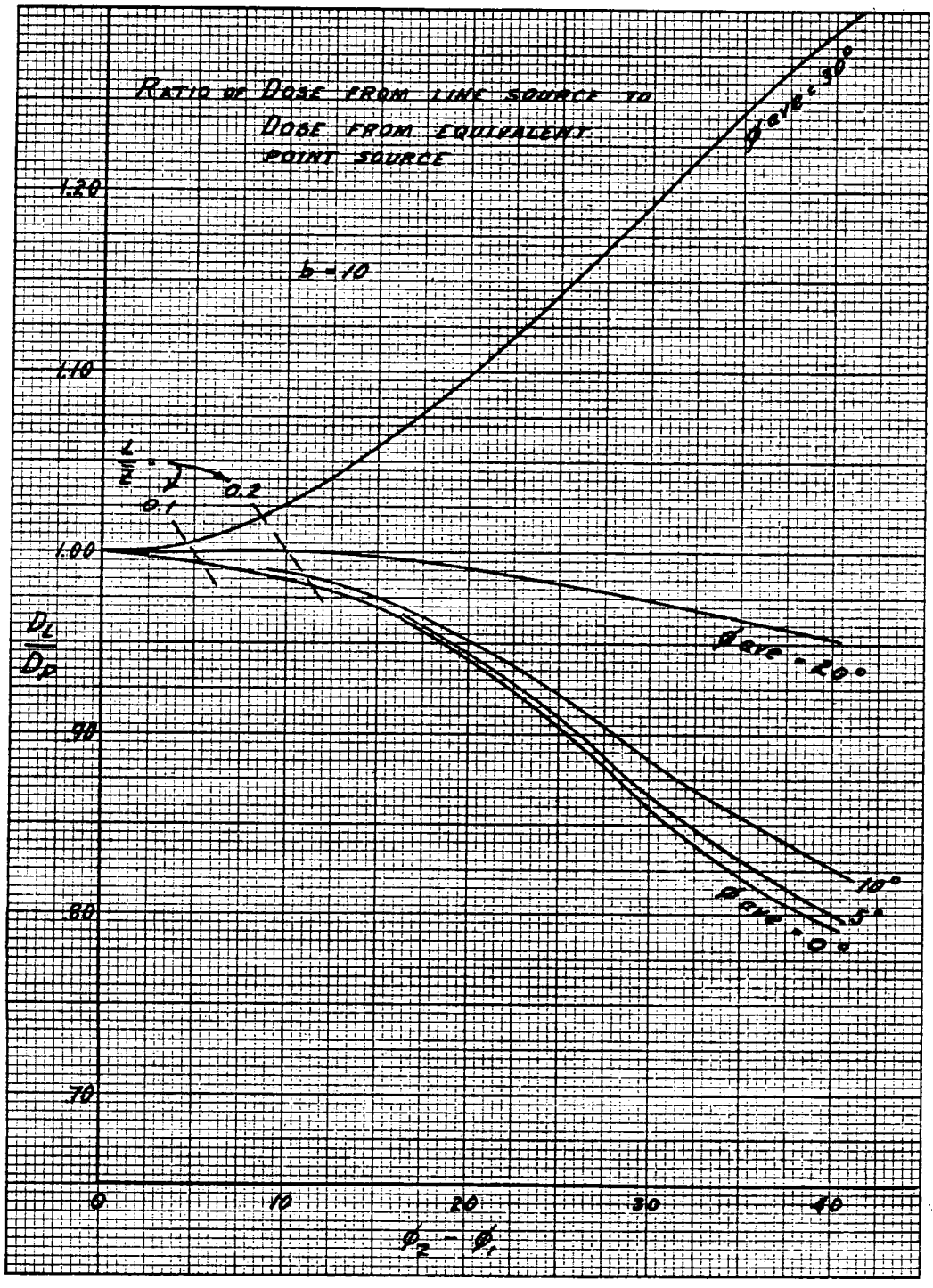

RATIO OF DOSE FROM LINE SOURCE TO DOSE FROM EQUIVALENT POINT SOURCE
b = 10
1.20
1.10
1.00
90
80
70
0
10
20
30
40
$\frac{D_L}{D_P}$
$\frac{L}{2}$
0.1
0.2
$\phi_2 - \phi_1$
$\phi_{arc} = 20°$
$\phi_{arc} = 10°$
$\phi_{arc} = 5°$
$\phi_{arc} = 0°$

Figure 4.22

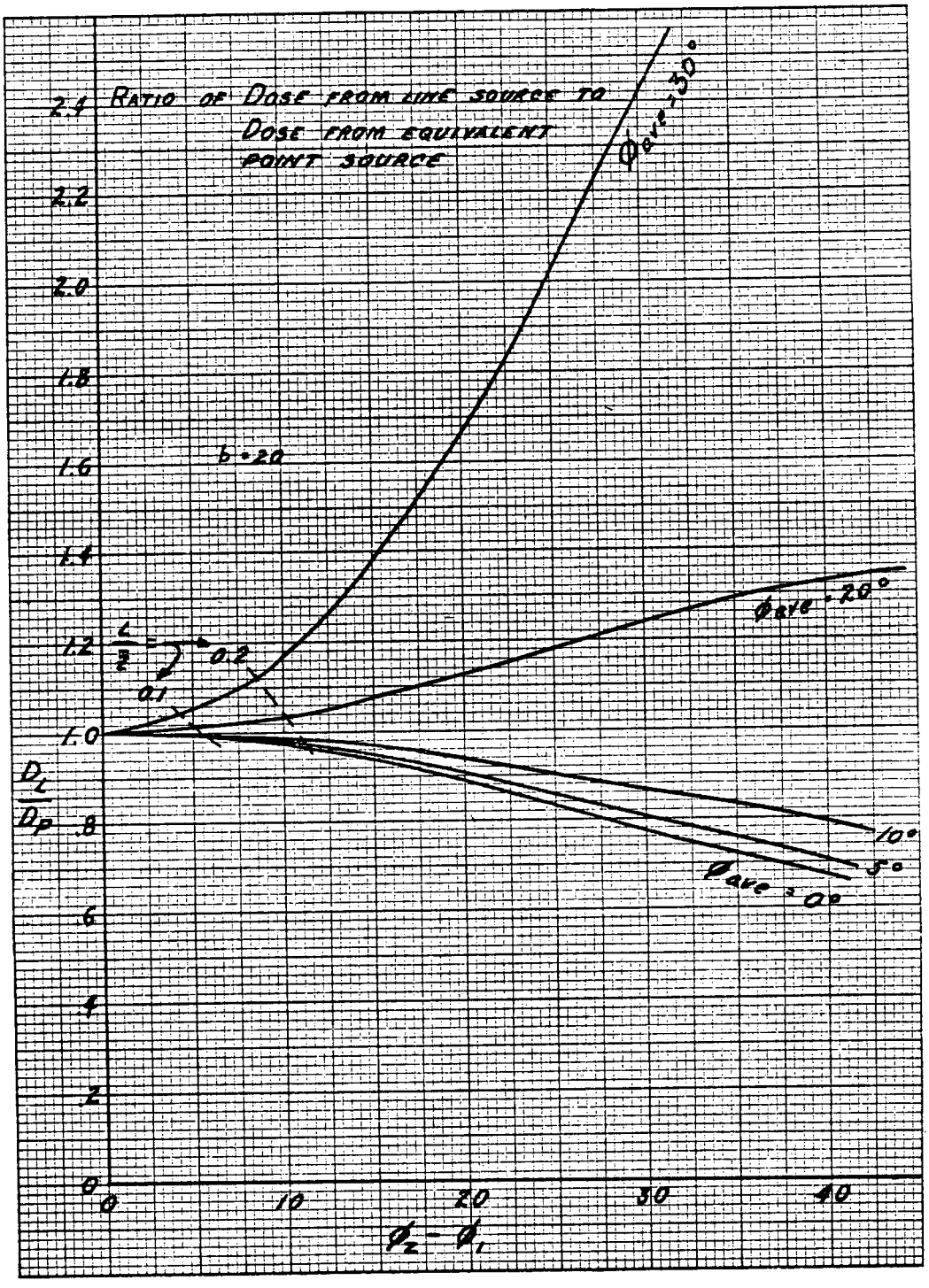
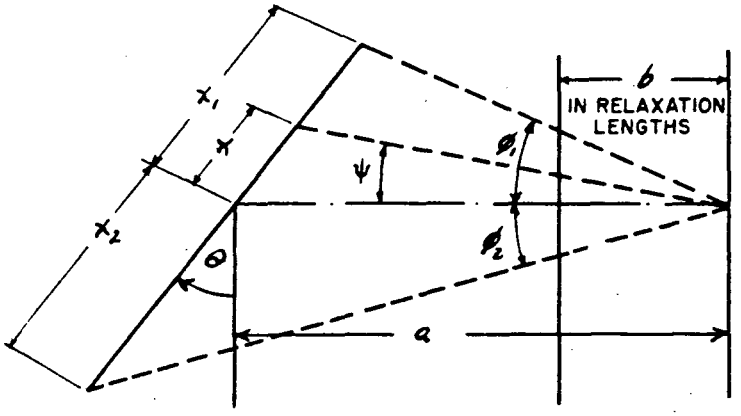

Ratio of Dose from line source to Dose from equivalent point source
2.4
2.2
2.0
1.8
1.6
1.4
1.2
1.0
.8
.6
.4
.2
0
$\frac{D_L}{D_P}$
b = 20
$\frac{L}{2}$ = 0.2
0.1
ϕ_{ave} = 20°
10°
5°
ϕ_{ave} = 0°
0
10
20
30
40
$\phi_2 - \phi_1$

Figure 4.23

Line Source Not Parallel to Shield. The geometry of a line source that is not parallel to the shield is shown in the accompanying diagram. The line makes an angle θ with the shield.

LINE SOURCE NOT PARALLEL TO SHIELD



The dose from the line source is given by

$$D_L = \frac{S_L E}{K4\pi} \int_{-x_2}^{x_1} \frac{e^{-b\sec\psi}}{(a - x \sin\theta)^2 \sec^2\psi} dx$$

where S_L is the source strength of the line in photons per centimeter per second of energy E in million electron volts per photon, and K converts from gamma flux to gamma dose rate. The equation above can be simplified to

$$D_L = \frac{S_L E}{K4\pi a \cos\theta} \int_{-\phi_2}^{\phi_1} e^{-b\sec\psi} d\psi$$

This indicates that the dose from a slant line is the same as that from a parallel line under the following conditions: (1) same value of "a" straight through the shield; (2) the parallel line subtends the same angles ϕ_1 and ϕ_2 as the slant line; and (3) the source strength of the parallel line is equal to $S_L/\cos\theta$.

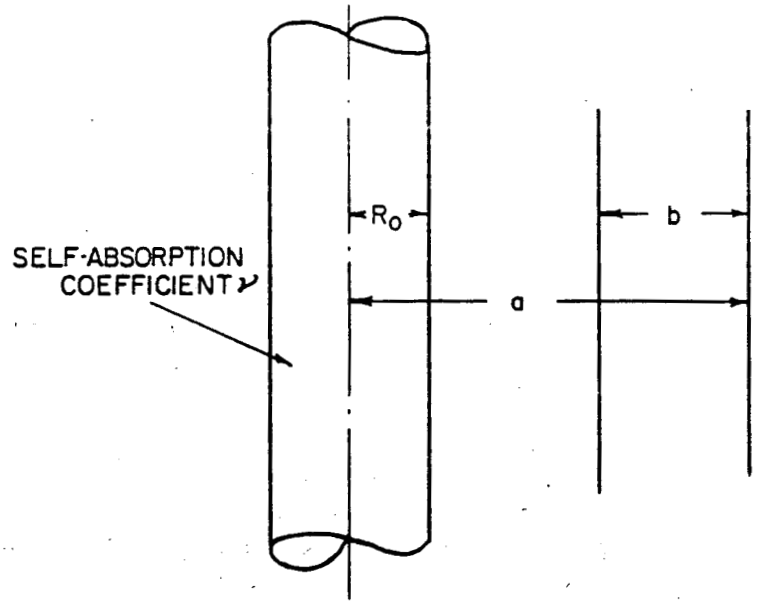
When the slant line has been replaced for calculation purposes by the parallel line, the latter may then be broken up into point sources as shown in the previous paragraph.

(2) Cylinder into Set of Parallel Lines. Equations for the dose rate from an infinitely long cylindrical source shielded by a slab shield are given in Chap. 9.

Calculations have been performed for infinite cylinders of unit source strength. These are tabulated and plotted in reference 7. Using these results the equation for a cylinder is

$$D_C = \frac{S_\nu E}{\pi K\gamma} P(b, \nu a, R_0/a) \qquad (46)$$

where S_ν = source strength ratio = actual source/unit source
ν = the self-absorption coefficient for the cylinder (cm^{-1})
P = the tabulated result of the computation of reference 7 (cm^{-3}-sec^{-1})
R_0 = radius of the cylinder (cm)
a = perpendicular distance from axis of cylinder to receptor (cm)



The dose calculated by Eq. 46 is compared with the dose from an equivalent line source (in terms of total source strength, neglecting self-absorption) by the ratio of D_C/D_L in Table 4.4, where

$$D_L = \frac{S_\nu \pi R_0^2}{4\pi a K} 2 \int_0^{\pi/2} e^{-b\sec\psi}\, d\psi \tag{47}$$

Equation 47 gives the dose from an infinite line with a total strength the same as that of the cylinder.

Table 4.4—MAGNITUDE OF a/R_0 FOR $D_C/D_L \geq 0.90$

νa	1	3	5	10
a/R_0	9	24	40	85

The magnitude of D_C/D_L from Eqs. 46 and 47 is insensitive to the shield thickness when it is expressed in relaxation lengths.

If a cylinder can be treated as a line source, the computations can further be simplified by dividing the line source into segments as suggested in Sec. 3.1.

For cylindrical sources that are finite in length, the result for infinitely long cylinders may be modified, as shown in Chap. 9, by the ratio

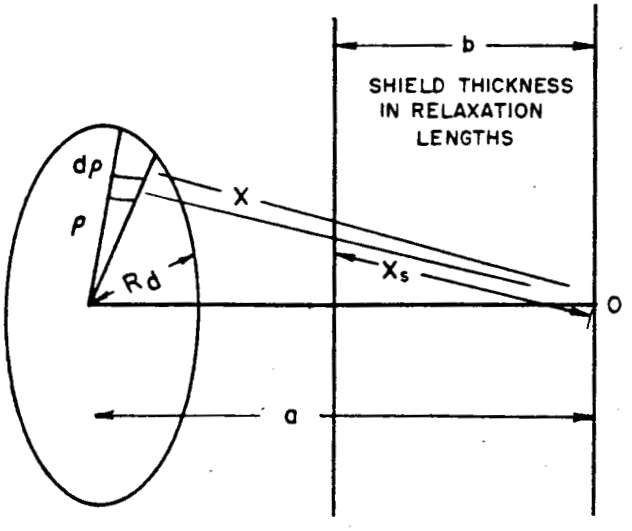
$$\frac{\int_{\phi_1}^{\phi_2} e^{-\mu z\sec\psi}\, d\psi}{\int_0^{\pi_2} e^{-\mu z\sec\psi}\, d\psi} = \frac{F(\phi_2,\mu z) - F(\phi_1,\mu z)}{2\, F\left(\frac{\pi}{2},\mu z\right)} \tag{48}$$

where

$$F(b,\phi) = \int_0^{\phi} e^{-b\sec\psi}\, d\psi$$

This function is plotted in Chap. 9.

(3) Disk into Point. In Chap. 9 the formula for a disk source behind a shield of thickness b relaxation lengths is derived.



The dose at point O opposite the center of the disk is given by

$$D_D = \frac{S_D}{K} \int_0^{R_d} B(\mu r, E_0) \frac{2\pi\rho \, d\rho}{2\pi x^2} e^{-\mu x_s} \tag{49}$$

where S_D is source strength (photons/cm^2-sec), from one side of the disk only; E is photon energy (Mev/photon); and K is a dimensional constant to change photons/cm^2-sec to mr/hr or similar change of units.

If the build-up factor is expressed as

$$B(\mu r, E_0) = \sum_i A_i e^{-\alpha_i \mu r}$$

Eq. 49 integrates to

$$D_D = \sum_i \frac{S_D A_i}{K} \left\{ E_1[(\alpha_i + 1)b_i] - E_1\left[(\alpha_i + 1)b_i \sqrt{\left(\frac{R_d}{a}\right)^2 + 1}\right] \right\} \tag{50}$$

If the build-up factor is expressed as $B = 1 + \beta\mu r$ (where B = 0 to 1), Eq. 49 results in

$$D_D = \frac{S_P}{K} \left\{ E_1(b_1) + \beta b_1 \exp(-b_1) - E_1\left[b_1 \sqrt{\left(\frac{R_d}{a}\right)^2 + 1}\right] - \beta \exp(-b_1) \sqrt{\left(\frac{R_d}{a}\right)^2 + 1} \, E_0\left[b_1 \sqrt{\left(\frac{R_d}{a}\right)^2 + 1}\right] \right\} \tag{50a}$$

where $E_n(b) = b^{n-1} \int_b^\infty (e^{-t}/t^n)dt$, as plotted in Chap. 9. The dose from an equivalent point source, where $S_P = \pi R_d^2 S_D$ (in photons/sec), is given by

$$D_P = \frac{S_P}{K 2\pi a^2} \sum_i A_i e^{-(\alpha_i + 1)b_i} \tag{51}$$

or

$$D_P = \frac{S_P}{K} \frac{1 + \beta b_i}{2\pi a^2} e^{-b_i} \tag{51a}$$

In both Eqs. 50 and 51 only those photons are considered which proceed in a forward direction, i.e., only those photons that have any possibility of going through the shield. The ratio of the dose from these two types of source is given for $B = \sum_i A_i e^{-\alpha_i \mu r}$

$$\frac{D_D}{D_P} = \frac{\sum_i A_i \{E_1[(\alpha_i + 1)b_1] - E_1[(\alpha_1 + 1)b_1\sqrt{(R_d/a)^2 + 1}]\}}{\sum_i A_i (R_d/a)^2 e^{-(\alpha_i+1)b_1}} \tag{52}$$

For $B = 1 + \beta\mu r$, D_D/D_P is equal to

$$\frac{E_1(b_1) + \beta \exp(-b_1) - E_1[b_1\sqrt{(R_d/a)^2 + 1}] - \beta \exp(-b_1)\sqrt{(R_d/a)^2 + 1}\ E_0[b_1\sqrt{(R_d/a)^2 + 1}]}{(R_d/a)^2 e^{-b_1}(1 + \beta b_1)} \tag{52a}$$

The limiting cases of the above equations can be expressed by $\beta = 0$ and $\beta = 1$ in Eq. 52a.

For the special case of build-up factor equal to unity ($\beta = 0$), Eq. 52a is plotted in Fig. 4.24 for various shield thicknesses. For $\beta = 1$, on Fig. 4.25, the curves are approximately the same.

From Fig. 4.24 it is seen that for disk sources such that $R_d/a = 0.1$, a point source assumption will overestimate the dose by no more than 5 per cent for shields of $b = 20$. Considering a disk source with $R_d/a = 0.2$, a point source assumption will give errors of 5 per cent or less for shields of $b = 4$.

These criteria may be compared to those suggested for breaking a line source into segments. Not as much liberty may be taken in the approximation of a disk source since a greater proportion of the total contribution to the dose comes from points removed from the point at which the simplified source is located.

The curves in Figs. 4.24 and 4.25 are drawn for the condition where the point of detection is opposite the center of the disk. The effects of moving off the axis of the disk may be derived from the curves in Chap. 9.

(4) End of Cylinder to Disk Source. To find the dose outside a shield opposite the end of a cylindrical source, it is convenient to consider the cylinder in terms of an equivalent disk source (see Fig. 4.26). The disk source may then be treated by the criteria suggested in Sec. 3.4e(3).

Curves are given in Figs. 4.27 to 4.29 which may be used to obtain the equivalent disk source strength for cylinders of various radii. The surface source strength of the disk is assumed to be given by the flux through the end of the cylinder.

In expressing the flux a double subscript notation is used. $F_{(a,l)}$ indicates the flux through the end of a cylinder of length l relaxation lengths and radius a relaxation lengths ($a = \nu r$). The limiting case of $F_{(\infty,\infty)}$ is the flux through the surface of a semi-infinite volume source.

For a volume source extending to infinity in the radial direction but of thickness l relaxation lengths ($l = \nu L$), the flux through the face is given by

$$F_{(\infty,l)} = \int_0^L I_0\, dz \int_z^\infty B(\mu r, E_0) \frac{e^{-\nu r}\, dr}{2r} \tag{53}$$

This may be expressed for $B = \sum_i A_i e^{-\alpha_i \mu r}$

$$F_{(\infty,l)} = \frac{I_0}{2\nu} \int_0^l \sum_i A_i E_1[(\alpha_i + 1)\ \nu z]\, d(\nu z) \tag{54}$$

or for $B = 1 + \beta\mu r$

$$F_{(\infty,l)} = \frac{I_0}{2\nu} \int_0^l [E_1(\nu z) + \beta \exp(-\nu z)]\, d(\nu z) \tag{54a}$$

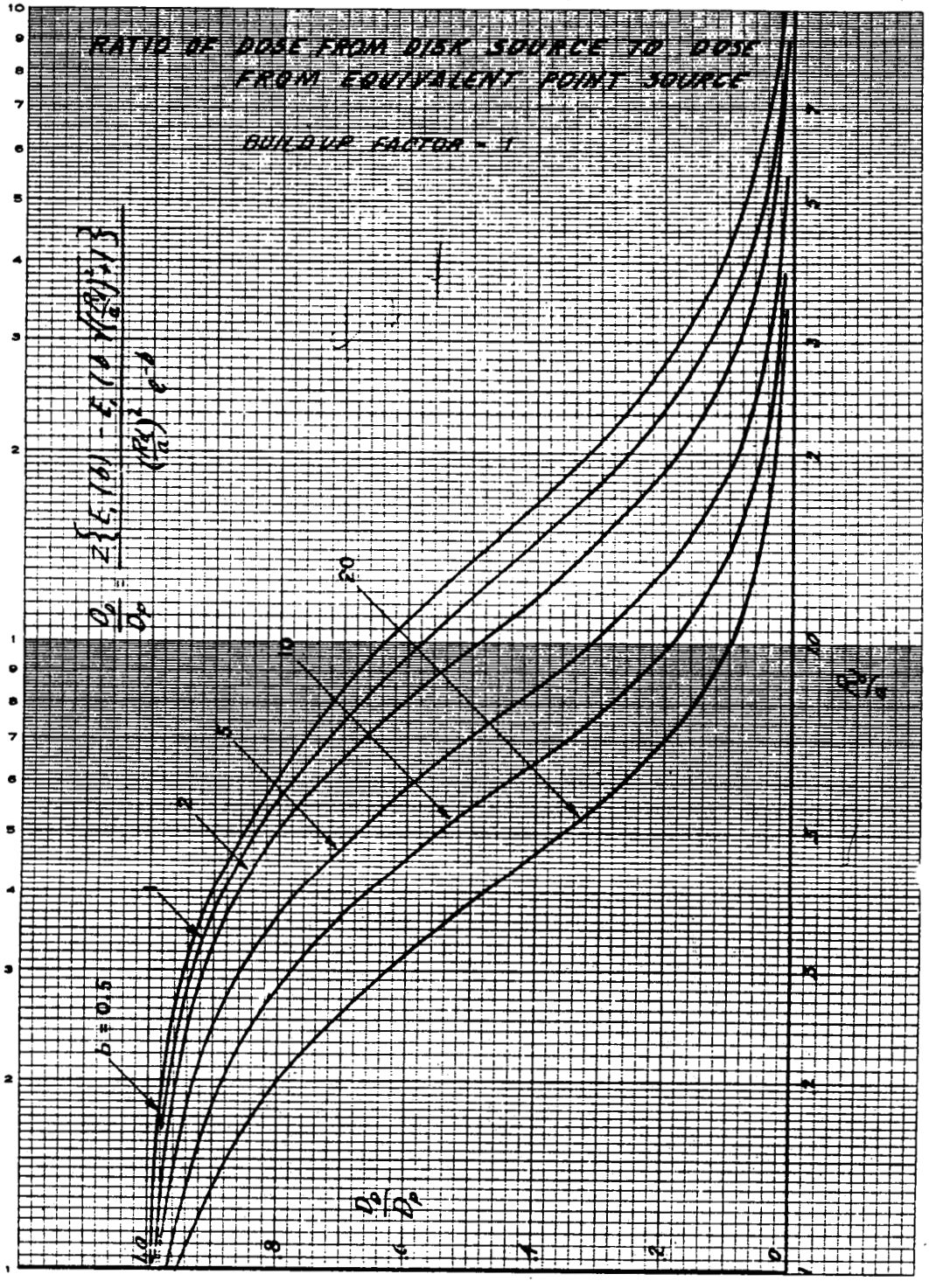

RATIO OF DOSE FROM DISK SOURCE TO DOSE FROM EQUIVALENT POINT SOURCE
BUILDUP FACTOR = 1
$\frac{D_2}{D_P} = \frac{2[E_1(\mu t) - E_1(\mu t\sqrt{(R/a)^2+1})]}{(R/a)^2 e^{-\mu t}}$
D_2/D_P
R/a
b = 0.5
0.7
1.0
2.0
3.0

Figure 4.24

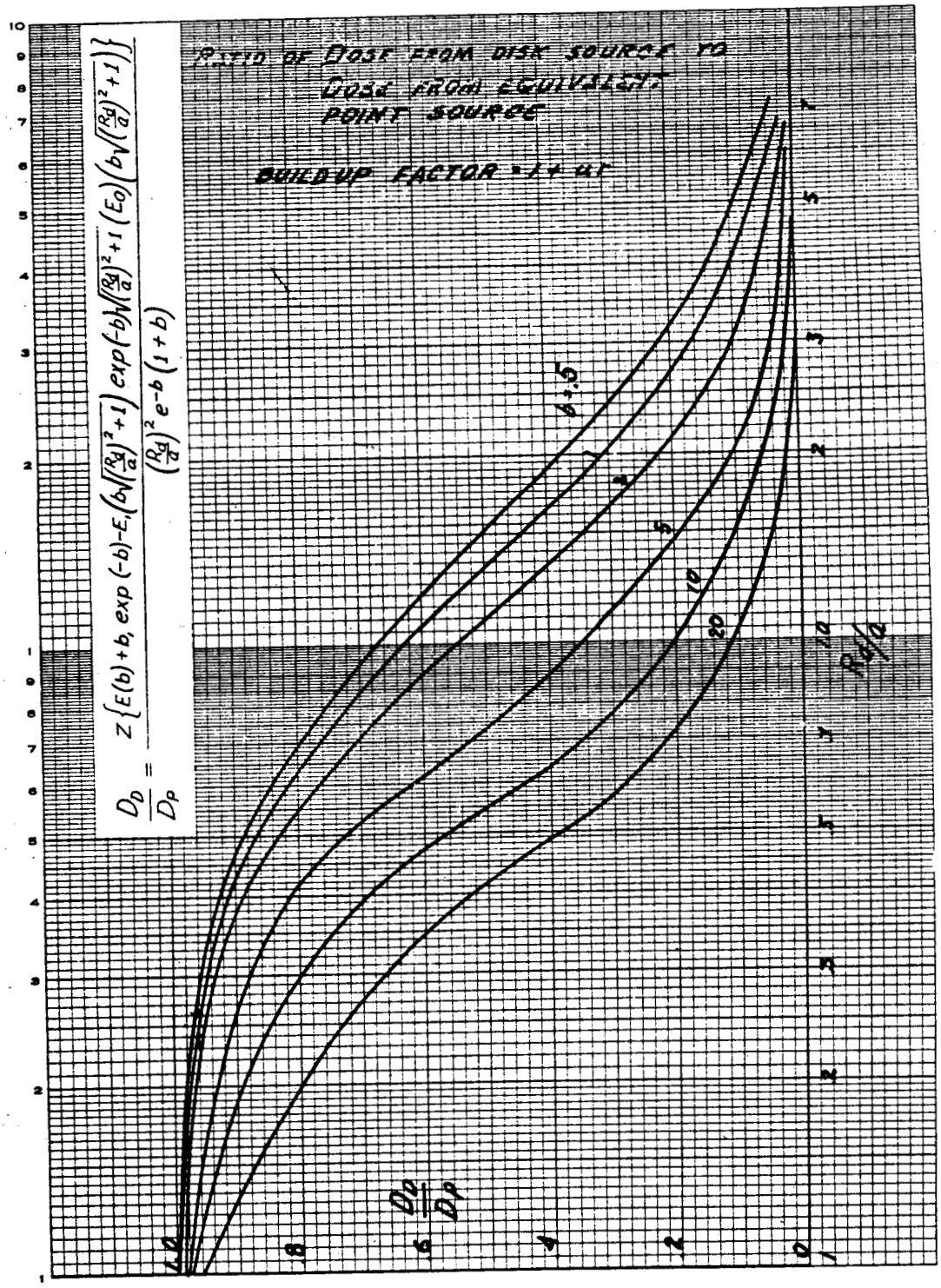

RATIO OF DOSE FROM DISK SOURCE TO DOSE FROM EQUIVALENT POINT SOURCE
BUILDUP FACTOR = 1 + ut
$\frac{D_D}{D_P} = \frac{2\{\varepsilon(b)+b,\ \exp(-b)-\varepsilon_1\left(b\sqrt{\left(\frac{R_d}{a}\right)^2+1}\right)\exp\left(-b\sqrt{\left(\frac{R_d}{a}\right)^2+1}\ (E_0)\left(b\sqrt{\left(\frac{R_d}{a}\right)^2+1}\right)\right\}}{\left(\frac{R_d}{a}\right)^2 e^{-b}\ (1+b)}$
b=0.5
1
2
3
5
10
20
R_d/a
$\frac{D_D}{D_P}$

Figure 4.25

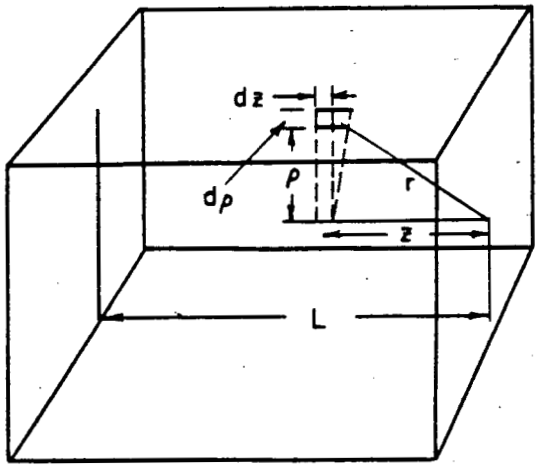


Figure 4.26

where

$$E_n(x) = x^{n-1} \int_x^\infty \frac{e^{-t}}{t^n} dt \qquad \text{(plotted in Chap. 9)}$$

Integration of Eq. 54 gives

$$F_{(\infty,l)} = \sum_i \frac{I_0}{2\nu(\alpha_i + 1)} \{[(\alpha_i + 1)l]\, E_1[(\alpha_i + 1)l] + [1 - e^{-(\alpha_i+1)l}]\} \tag{55}$$

and integrating Eq. 54a gives

$$F_{(\infty,l)} = \frac{I_0}{2\nu} [l\, E_1(l) + (1 + e^{-l})(1 + \beta)] \tag{55a}$$

For a semi-infinite volume source, where $l \to \infty$, Eq. 55 becomes

$$F_{(\infty,\infty)} = \sum_i \frac{I_0}{2\nu(\alpha_i + 1)} \tag{56}$$

Eq. 55a reduces to

$$F_{(\infty,\infty)} = \frac{I_0}{2\nu} (1 + \beta) \tag{56a}$$

Most cases of build-up factors fall between the cases for $\beta = 0$ and $\beta = 1$. From Eq. 56a these special cases give

$$F_{(\infty,\infty)} = \frac{I_0}{2\nu} \qquad \text{for } \beta = 0$$

$$F_{(\infty,\infty)} = \frac{I_0}{\nu} \qquad \text{for } \beta = 1$$

From Eqs. 54 and 54a it is seen that $F_{(\infty,l)}$ is made up of the sum of contributions from slabs of thicknesses $d(\nu z)$. The contribution of each slab is shielded through a length νz. For

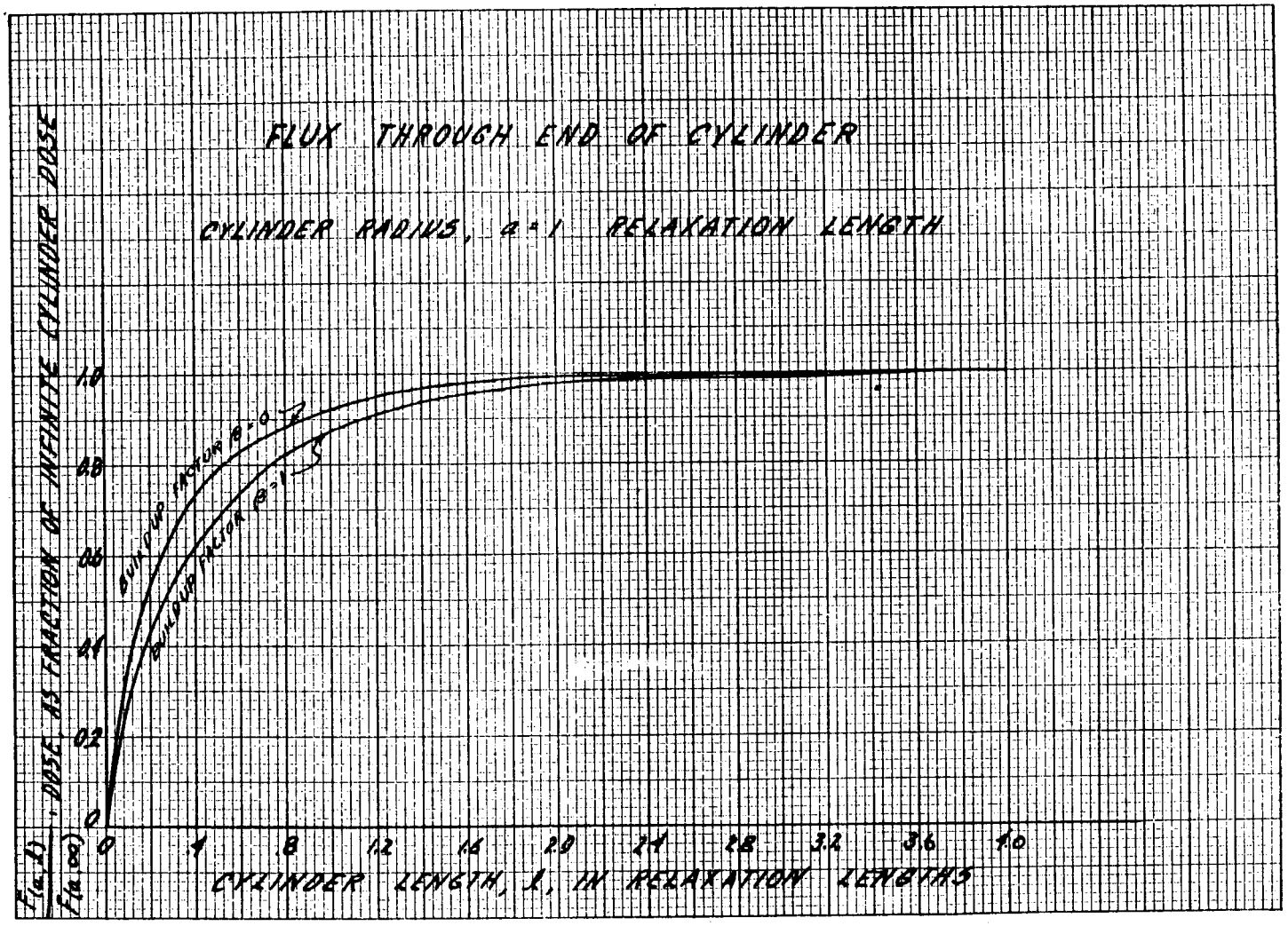

FLUX THROUGH END OF CYLINDER
CYLINDER RADIUS, a = 1 RELAXATION LENGTH
BUILDUP FACTOR B=0
BUILDUP FACTOR B=1
$\frac{F_{(a,l)}}{F_{(a,\infty)}}$ = DOSE AS FRACTION OF INFINITE CYLINDER DOSE
0
0.2
0.4
0.6
0.8
1.0
0
.4
.8
1.2
1.6
2.0
2.4
2.8
3.2
3.6
4.0
CYLINDER LENGTH, l, IN RELAXATION LENGTHS

Figure 4.27

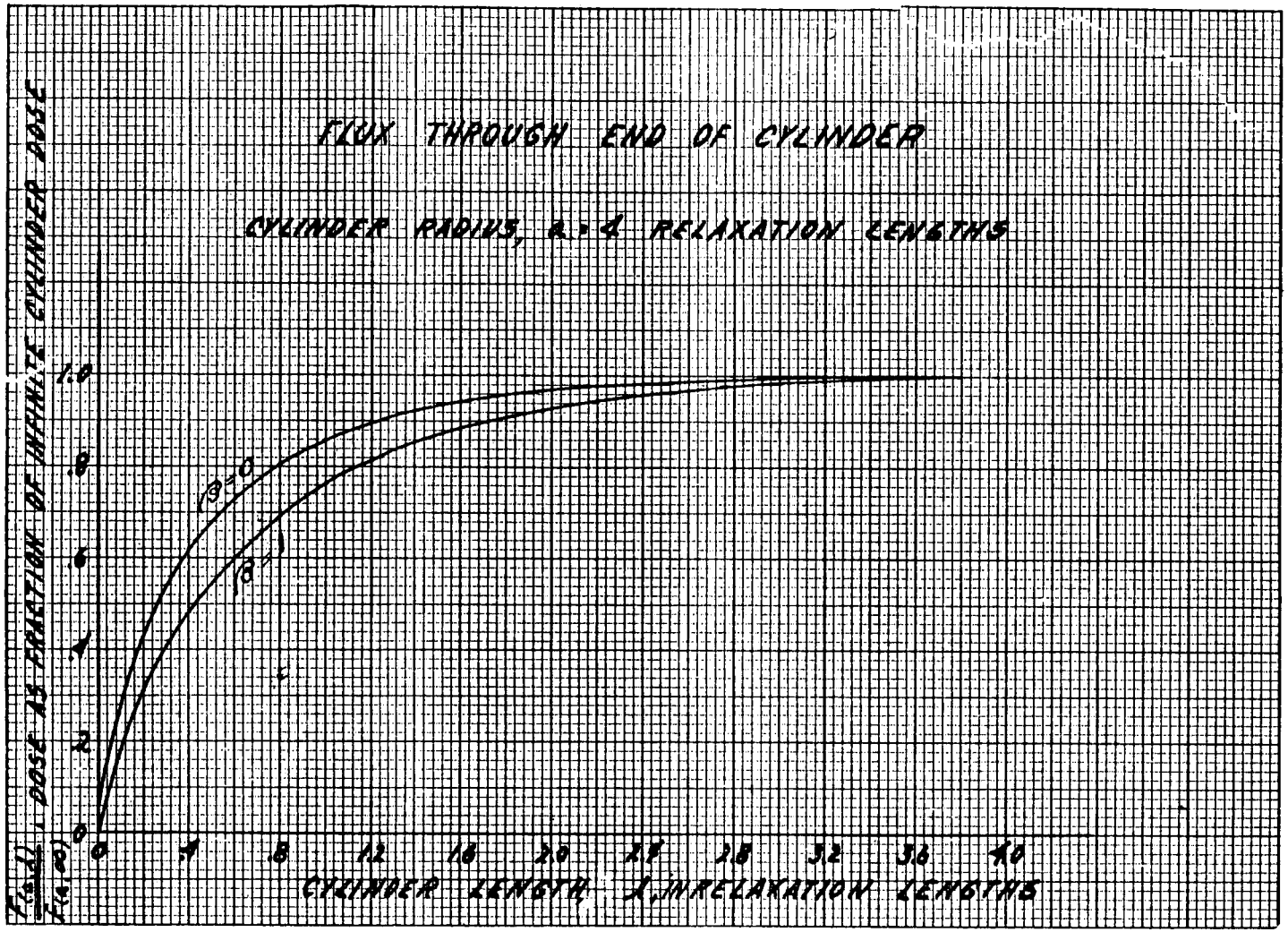

FLUX THROUGH END OF CYLINDER
CYLINDER RADIUS, R = 4 RELAXATION LENGTHS
RATIO, DOSE AS FRACTION OF INFINITE CYLINDER DOSE
1.0
.8
.6
.4
.2
0
0
.4
.8
1.2
1.6
2.0
2.4
2.8
3.2
3.6
4.0
CYLINDER LENGTH, L, MFP RELAXATION LENGTHS

Figure 4.28

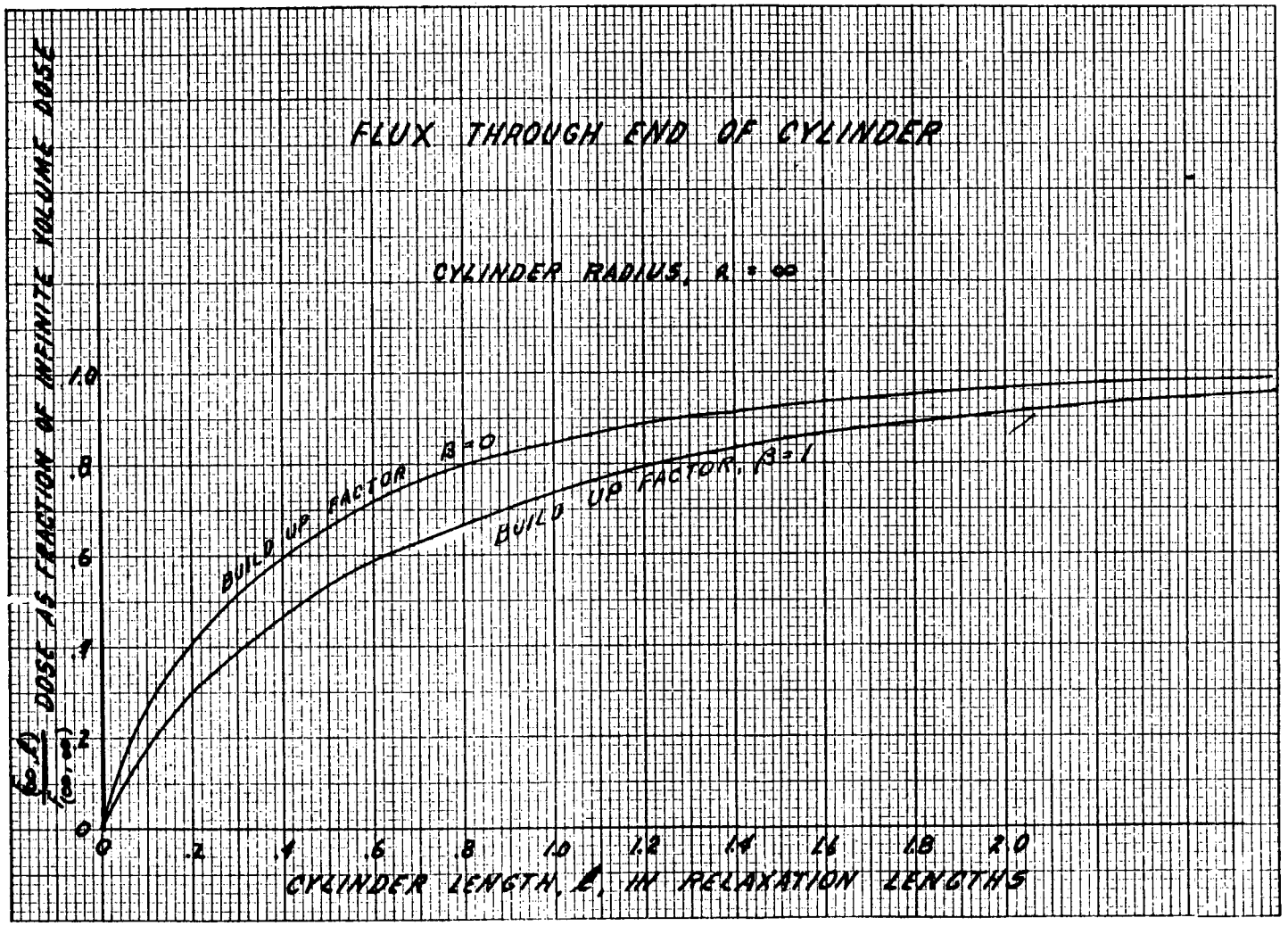

FLUX THROUGH END OF CYLINDER
CYLINDER RADIUS, R = ∞
BUILD UP FACTOR β=0
BUILD UP FACTOR, β=1
DOSE AS FRACTION OF INFINITE VOLUME DOSE
1.0
.8
.6
.4
.2
0
0
.2
.4
.6
.8
1.0
1.2
1.4
1.6
1.8
2.0
CYLINDER LENGTH, L, IN RELAXATION LENGTHS

Figure 4.29

a cylinder these slabs are finite in extent; thus the integrand must be multiplied by the factor D/D_∞. Equation 54a for a cylinder of radius a relaxation lengths then becomes

$$F_{(a,l)} = \frac{I_0}{2\nu} \int_0^l \frac{D}{D_\infty} (\nu z) \left[E_1(\nu z) + \beta E_0(\nu z)\right] d(\nu z) \tag{57}$$

This equation may be solved numerically for a particular cylinder of radius a after a curve of $D_{\nu z}/D_\infty$ vs. (νz) is obtained.

Data from computation of Eq. 57 are presented as a ratio to compare the flux from a finite cylinder (integration from 0 to l) to that from an infinite cylinder (integration from 0 to ∞). These are presented for cylinders of radii (in relaxation lengths) of 1, 4, and ∞ (Figs. 4.27 to 4.29). The lengths (in relaxation lengths) necessary to give $F_{(a,l)}/F_{(a,\infty)} = 0.95$ are given in Table 4.5 and plotted in Fig. 4.30.

Table 4.5

a, relaxation lengths	Relaxation lengths (l) to give $F_{(a,l)}/F_{(a,\infty)} = 0.95$	
	$\beta = 0$	$\beta = 1$
1	1.14	1.50
4	1.70	2.26
∞	1.72	2.48

Table 4.6

a, relaxation lengths	Magnitude of $\frac{F_{(a,\infty)}}{F_{(\infty,\infty)}}$	
	$\beta = 0$	$\beta = 1$
1	0.745	0.660
4	0.970	0.952
∞	1.00	1.00

Figure 4.31 compares the cylinder, $F_{(a,l)}$ to the semi-infinite volume source $F_{(\infty,\infty)}$ for two cylinders, a = 1 and 4. These are summarized in Table 4.6 when $l = \infty$ (asymptotic magnitudes).

The factor $F_{(a,l)}/F_{(a,\infty)}$ is useful when it is desirable to divide the volume source into point sources. This factor indicates, for example, that for a radius a = 4 and $\beta = 1$, only $2\frac{1}{4}$ relaxation lengths of the cylinder need be considered to give 95 per cent of the dose. This reduces the number of points which need be considered in calculating the total dose from the end of the cylinder.

(f) Sample Calculation. To show the use of some of the curves to subdivide a volume source into point sources (in preparation for performing the calculations on the CPC machine), consider a cylinder (Fig. 4.32) with the following dimensions:

Length: 18.6 ft
Diameter: 3.9 ft; a (radius): 3.9/2 = 1.95 ft
$\nu = 0.068\ cm^{-1} = 2.07\ ft^{-1}$
Build-up factor: $1 + 0.5\ \nu r$
Distance from dose point, M, to cylinder: 9.5 ft
Calculate $\nu a = (2.07)(1.95) \approx 4$

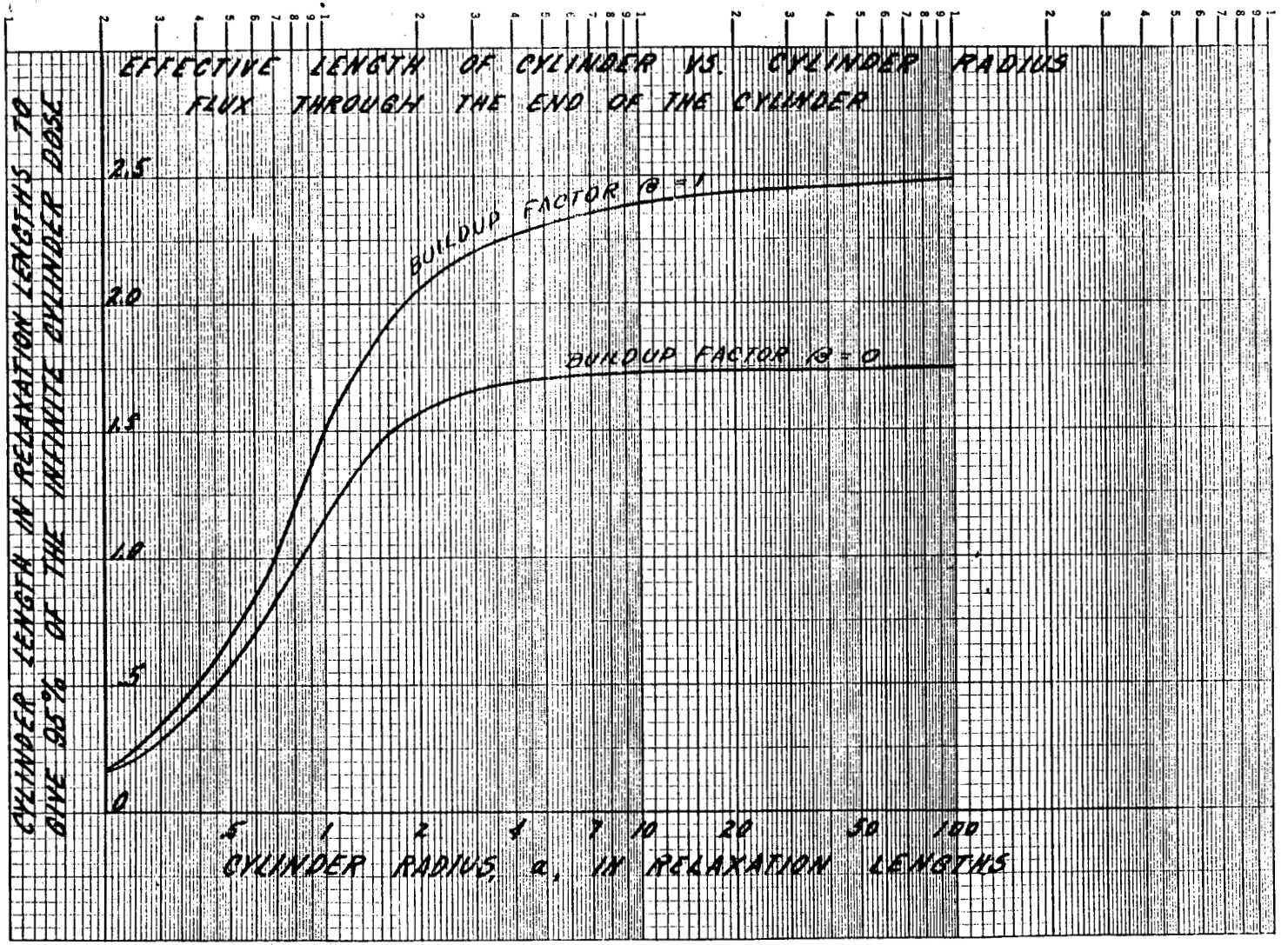

EFFECTIVE LENGTH OF CYLINDER VS. CYLINDER RADIUS
FLUX THROUGH THE END OF THE CYLINDER
BUILDUP FACTOR R = 1
BUILDUP FACTOR R = 0
CYLINDER LENGTH IN RELAXATION LENGTHS TO GIVE 95% OF THE INFINITE CYLINDER DOSE
2.5
2.0
1.5
1.0
.5
0
.5
1
2
4
7
10
20
50
100
CYLINDER RADIUS, a, IN RELAXATION LENGTHS

Figure 4.30

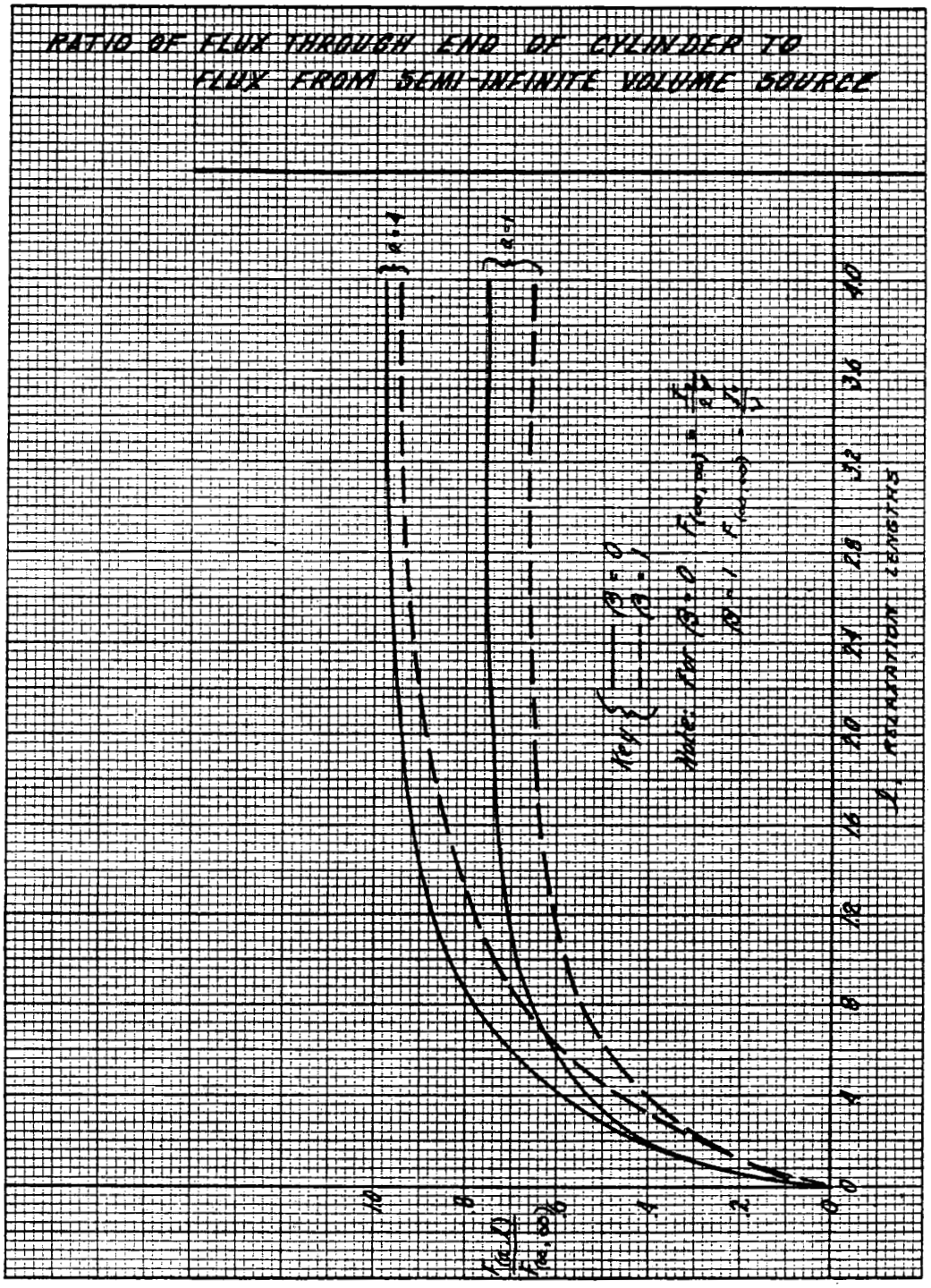

RATIO OF FLUX THROUGH END OF CYLINDER TO
FLUX FROM SEMI-INFINITE VOLUME SOURCE
μa=1
μa=0
μa=0
μa=1
μa=0
μa=1
0
2
4
6
8
10
12
16
20
24
28
32
36
40
λ, RELAXATION LENGTHS

Figure 4.31

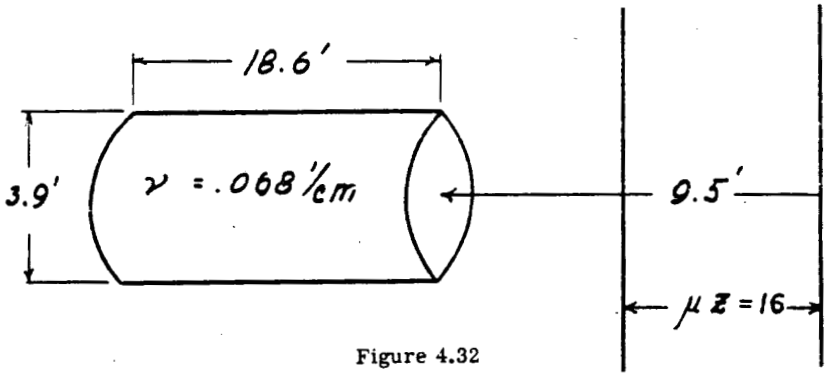


Figure 4.32

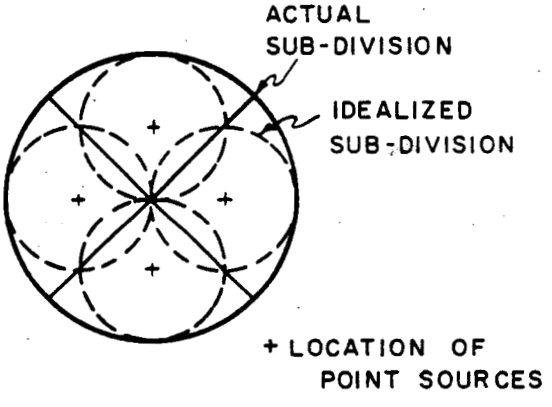


Figure 4.33

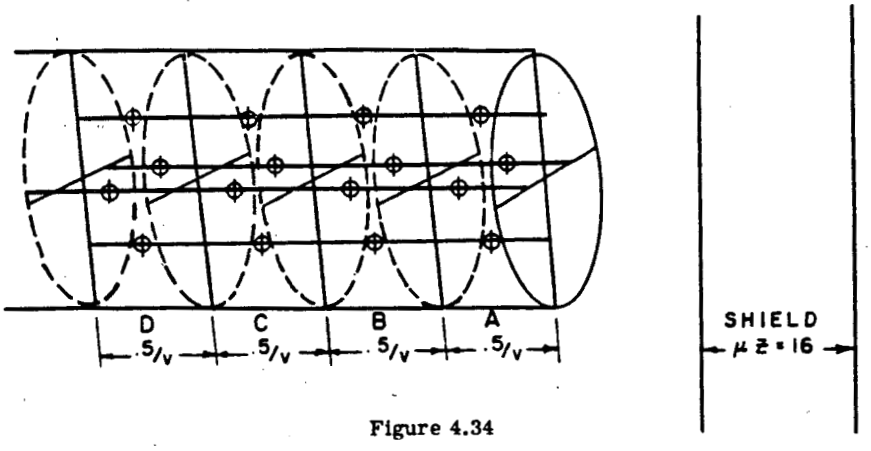


Figure 4.34

From Fig. 4.30 with $\beta = 0.5$ and $\nu a = 4$, two relaxation lengths or approximately 1 ft need be considered to give 95 per cent of the dose at M. For the end of the cylinder $a/\bar{z} = 0.2$. From Fig. 4.25 for $\mu z = 16$ and for $D_D/D_P = 0.95$; $a/\bar{z} = 0.1$.

This means that a disk source at the end of the cylinder, in order to be considered a point source, should have a radius of no more than one-half the cylinder radius.

Therefore, divide the end of the cylinder (Fig. 4.33) into four segments or consider the cylinder as four longitudinal elements, each being two relaxation lengths long.

To divide these sources into point sources, consider the two relaxation lengths determined above as four elements, each one 0.5 relaxation length long (Fig. 4.34).

The cylinder is now represented by 16 point sources which are shielded by the following total number of relaxation lengths:

4 sources of element A $\mu z = 16.25$
4 sources of element B $\mu z = 16.75$
4 sources of element C $\mu z = 17.25$
4 sources of element D $\mu z = 17.75$

If the source strength of the cylinder is S_ν photons/cu ft-sec, the strength of each of the points is given by

$$S_P = S_\nu \times \frac{1}{4}\pi \frac{(3.9)^2}{4} \times \frac{0.5}{2.07}$$

$$= 0.721\ S_\nu$$

This last breakdown is rather arbitrary, and greater accuracy can be obtained by using smaller elements.

4 NEUTRON SHIELDING FOR THE REACTOR COOLING SYSTEM

Some coolants (such as water) may be neutron emitters as well as gamma sources (Sec. 2.1). Then the *specific activity* of the neutron emitter must be calculated as a function of the position of the coolant as it circulates through the system. *Multigroup calculations*, mentioned in Sec. 1, are usually most reliable; however, in general, the neutron activation is due to very high energy neutrons, and cross sections for these reactions are not yet very reliable [e.g., the $O^{17}(n,p)N^{17}$ reaction]. A simpler method consists of a *single collision type calculation*, outlined below, resulting in a specific neutron activity of the coolant.

The minimum thickness of neutron shielding in the secondary shield is determined by the neutron activity of the coolant, but usually the neutron shielding requirements are larger than this owing to neutrons escaping the primary shield. The methods for calculating this shielding are discussed in Chap. 3; the question of balancing the distribution of shielding between the primary and secondary shields is discussed in Chap. 5.

The shielding requirements for neutrons (like the gamma shielding requirements) depend on the effective self-shielding properties of the sources, the geometry of the sources, the amount of structural material and lead in the secondary shield, and the distance between the source and the secondary shield. The geometric equations in Chap. 9 of course are as applicable to neutrons as to gammas; in this case the correct removal cross section is used in the equation where μ, the generic absorption term, is given.

4.1 Attenuation Kernel for N^{17} Neutrons*

The neutron shield thickness may be determined with the aid of experimental information if 0.9-Mev neutrons (from N^{17}) are involved.

(a) Calculation of Thermal-neutron Flux. The thermal-neutron flux can be calculated as follows: Fig. 4.35 is an experimentally determined graph of the thermal-neutron flux point-source strength from a point isotropic 0.9-Mev (N^{17}) source in water as a function of distance from the source. This is the function I.

$$I = G(r) = \frac{g(r)\ S}{4\pi\rho^2}$$

where g(r) is the thermalization function in water for 0.9-Mev neutrons; $1/4\pi\rho^2$ is the distance effect; and S is the source strength (neutrons/sec).

*K. Shure and P. A. Roys, Report WAPD-T-226, August 1955.

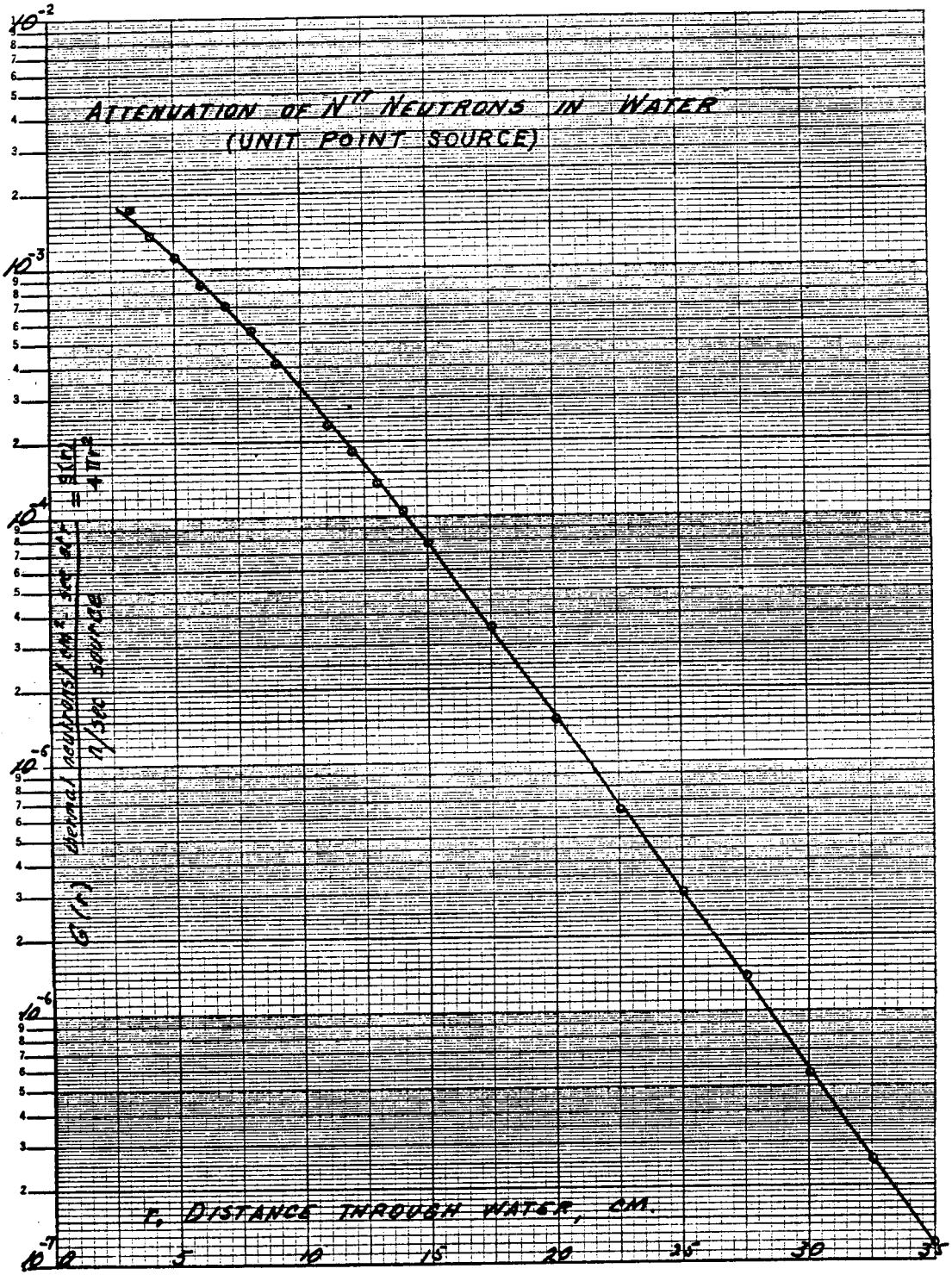

ATTENUATION OF N16 NEUTRONS IN WATER
(UNIT POINT SOURCE)
G(r) = thermal neutrons / cm² sec = S(r) / 4πr²
r, DISTANCE THROUGH WATER, CM.
0
5
10
15
20
25
30
35

Figure 4.35

Figure 4.36 shows a point P shielded by a water slab t centimeters thick from an N^{17} neutron source S. The thermal flux at P from S will be

$$I_{th} = \frac{g(t/\cos\theta)\, S}{4\pi\rho^2} \tag{58}$$

where ρ is the distance from S to P (cm); S is the source strength (neutrons/sec); and $[g(t/\cos\theta)]/4\pi$ is the value of $g(r)/4\pi$ from Fig. 4.35, where $r = t/\cos\theta$.

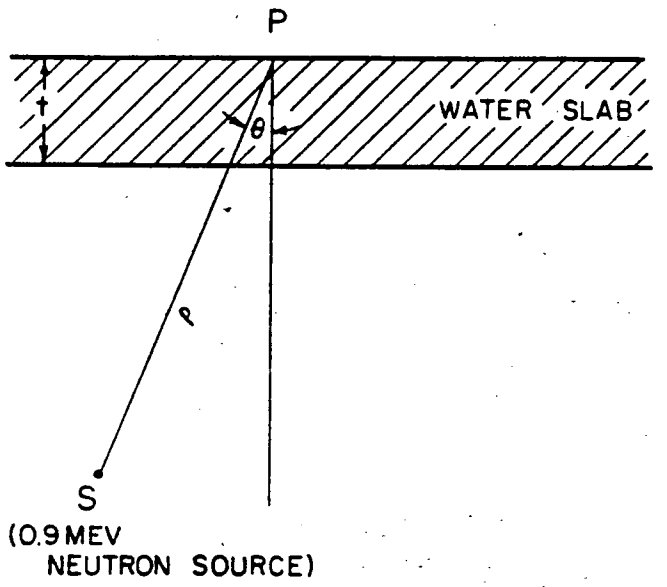


Figure 4.36

(b) Calculation of Fast-neutron Flux. The fast flux can be approximated from the thermal flux. It can be shown[8] that the relation between the fast flux and the thermal flux in water (or plastic) at a sufficiently large distance from the fast source is

$$I_f(z) = \lambda(z)\, \Sigma_a\, I_{th}(z)\, e^{-\tau/\lambda^2} \tag{59}$$

where z = distance from source (cm)
$\lambda(z)$ = relaxation length of the fast flux in the vicinity of z (cm)
Σ_a = macroscopic thermal absorption cross section in water (or plastic)(cm^{-1})
$I_f(z)$ = fast flux at z (neutrons/cm^2-sec)
$I_{th}(z)$ = thermal flux at z (neutrons/cm^2-sec)
τ = Fermi age for slowing down in water (or plastic)(cm^2)

The choice of λ is not difficult since it is clear that, if λ is not a rapidly varying function of z, the relaxation length of the observed thermal flux will give a very good estimate of the corresponding quantity for the fast flux.

Equation 59 is based on a concept of a collimated fast-neutron current which probably does not introduce serious errors since the most penetrating component is well collimated at large distances. The source of removed neutrons from which slowing down commences was assumed to be isotropic in the derivation of Eq. 59. This is definitely not the case. Collisions with hydrogen result in scattering through angles not over $\pi/2$. This effect results in an *overestimate* of the fast flux.

Another difficulty with Eq. 59 arises in the choice of neutron energy for the purpose of determining τ. The energy before collision is not appropriate since the removal collision introduces some moderation. The hydrogen collisions, which are usually the most frequent, result in energies which are distributed from zero to the initial energy. Choosing the initial energy for the determination of τ results in an *underestimate* of the fast flux, partially compensating for the error discussed in the preceding paragraph.

Also, although the penetration of the fast neutrons is determined by the very high energy beam, essentially uncollided, nevertheless, there is carried along with this beam a much larger flux of intermediate-energy neutrons. These neutrons, representing the build-up of fast-neutron dose, account for nearly all the measured dose but are not included in $I_f(z)$ as calculated.

To allow for these lower energy, less collimated neutrons, an age corresponding to an energy lower than the source energy should be used. Although this adjustment must be made to τ, no such treatment is required for λ, which comes from the observed flux distribution in a straightforward manner.

Sample Calculation. The fast flux at point P = $I_f(P) = \lambda\Sigma_a e^{-\tau/\lambda^2} I_{th}(P)$. For the 1-Mev source we use

$\tau(0.5\ \text{Mev}) = 11\ \text{cm}^2$

Σ_a for H_2O shield = $0.0252\ \text{cm}^{-1}$

$\lambda = 4.2$ cm [slope of the g(r) curve of Fig. 4.35]

$I_f(P) = 0.055 I_{th}(P) = {}^1/_{18} I_{th}(P)$

The contribution of each neutron point source in the shielded compartment to the fast-neutron flux outside the shield with a given water or plastic thickness can then be calculated. The fast-neutron dose and thermal-neutron dose can then be evaluated.

For the 0.9-Mev neutrons (see Chap. 2), ~8.7 neutrons/cm^2-sec = 1 mrem/hr.

For the thermal neutrons (see Chap. 2), 480 neutrons/cm^2-sec = 1 mrem/hr.

The total dose rate at point P from source S will be

$$D = \frac{I_{th}(P)}{18 \times 8.7} + \frac{I_{th}(P)}{480} \quad (\text{mrem/hr}) \tag{60}$$

This analysis points out the fact that for a 0.9-Mev monoenergetic neutron source the thermal-neutron dose at P is quite significant and must be taken into account when calculating the total dose rate.

4.2 Removal Cross Sections and Relaxation Lengths for N^{17} Neutrons

Thermal-neutron measurements have been taken in water behind several thicknesses of various materials using freshly irradiated water from the WAPD-10 loop in the MTR as a source. After correcting these data for the effect of the water and geometry, an exponential attenuation curve in the material is anticipated. When this technique is used, the results for iron indicate an effective removal cross section of 1.1 barns/atom for N^{17} neutrons. The relaxation length of N^{17} neutrons in ordinary concrete (density 2.25 g/cm^3) has been determined to be 14 cm. There are no reliable results for lead. The data for polyethylene indicate that polyethylene is equally as effective as water as an attenuator for N^{17} neutrons. The relaxation length for N^{17} neutrons in water at a distance of 25 cm from a point source is 4.3 cm, which corresponds to a σ_R of 7.0 barns/molecule.

4.3 Monte Carlo Results of the Transport of N^{17} Neutrons in a Water Medium

(a) Introduction. Neptune is the UNIVAC code name for an exploratory Monte Carlo (i.e., random scattering) study of the transport of N^{17} neutrons in water. Ten thousand neutron his-

tories were generated and stored on magnetic tape. Complete histories were made of the impacts of neutrons while they slowed down from 0.89 Mev to 1.0 ev in a water moderator. Both the differential cross section and the finite mass of the oxygen were treated exactly, but molecular scatterings in this range were ignored.

The history tapes were run through the computer under the control of several data processing routines to extract the results presented here.

(b) Transmission Through and Reflection from Water Slabs. As the coolant in a water-cooled reactor circulates through the core, the reaction $O^{17}(n,p)N^{17}$ takes place (Sec. 2.1). The N^{17} decays by emissions with a half life of 4.1 sec to O^{17} in an excited state which immediately decays by emitting a neutron. Alvarez[9] has determined the energy spectrum of the O^{17} neutrons by measuring the energies of the O^{16} recoils. He found a rather broad spectrum with a peak somewhere near 0.9 Mev.

Shielding for these neutrons in mobile reactor systems often takes the form of slabs of water or some hydrogenous plastic such as polyethylene. As basic information from which to compute the thickness of the water slab, the shield designer must know the dose attenuation of the neutrons as a function of angle of incidence and thickness of the slab. The Neptune histories were processed to yield this information. The medium was considered to be a slab of water of finite thickness bounded on both sides by vacuum. The shield thickness extended from $Z = 0$ to $Z = T$, and the angle θ defined the deviation from perpendicular. A 0.9-Mev neutron emitted into the slab from the semi-isotropic source plane could suffer one of three fates: (1) die within the slab, (2) be reflected, or (3) be transmitted. In the event of any of these fates, the rest of the history was skipped. If the neutron was reflected, the event was noted by adding unity to an appropriate counter. If the neutron was transmitted, unity was added to a counter that specified its lethargy (defined as the logarithm of E_0/E). Seven lethargy groups were considered:

Group No.	Lethargy, $u \equiv \ln(E_0/E)$	$f(u)$, $\frac{\text{rem/hr}}{\text{neutrons/cm}^2\text{-sec}}$
1	0.12 (uncollided)	12×10^{-5}
2	$0.12 < u \leq 1.12$	9.4×10^{-5}
3	$1.12 < u \leq 2.12$	5.0×10^{-5}
4	$2.12 < u \leq 3.12$	2.7×10^{-5}
5	$3.12 < u \leq 4.12$	1.4×10^{-5}
6	$4.12 < u \leq 5.12$	0.76×10^{-5}
7	$5.12 < u$	0.42×10^{-5}

The dose rate per unit neutron flux as a function of the lethargy of the neutrons is shown in the third column above.

The Neptune histories were generated for neutrons incident semi-isotropically on an infinite water medium. The analysis was carried out for three "directions" of incidence; 0 to 30° from the normal to the slab, 30 to 60°, 60 to 90°, as well as for a semi-isotropic source, 0 to 90°.

These "truncated isotropic sources" were chosen to show, at least roughly, the dependence of the transmitted dose and the albedo on the angle of incidence.

The results are summarized in Figs. 4.37 through 4.41. Figure 4.37 shows the number albedo as a function of water slab thickness and angle of incidence. The albedo reached its asymptotic value for a slab thickness of approximately 6 to 8 cm. This is about 3 to 4 mean free paths at the initial energy.

Figure 4.38 indicates the dose attenuation of 0.9-Mev neutrons as a function of water slab thickness and angle of incidence.

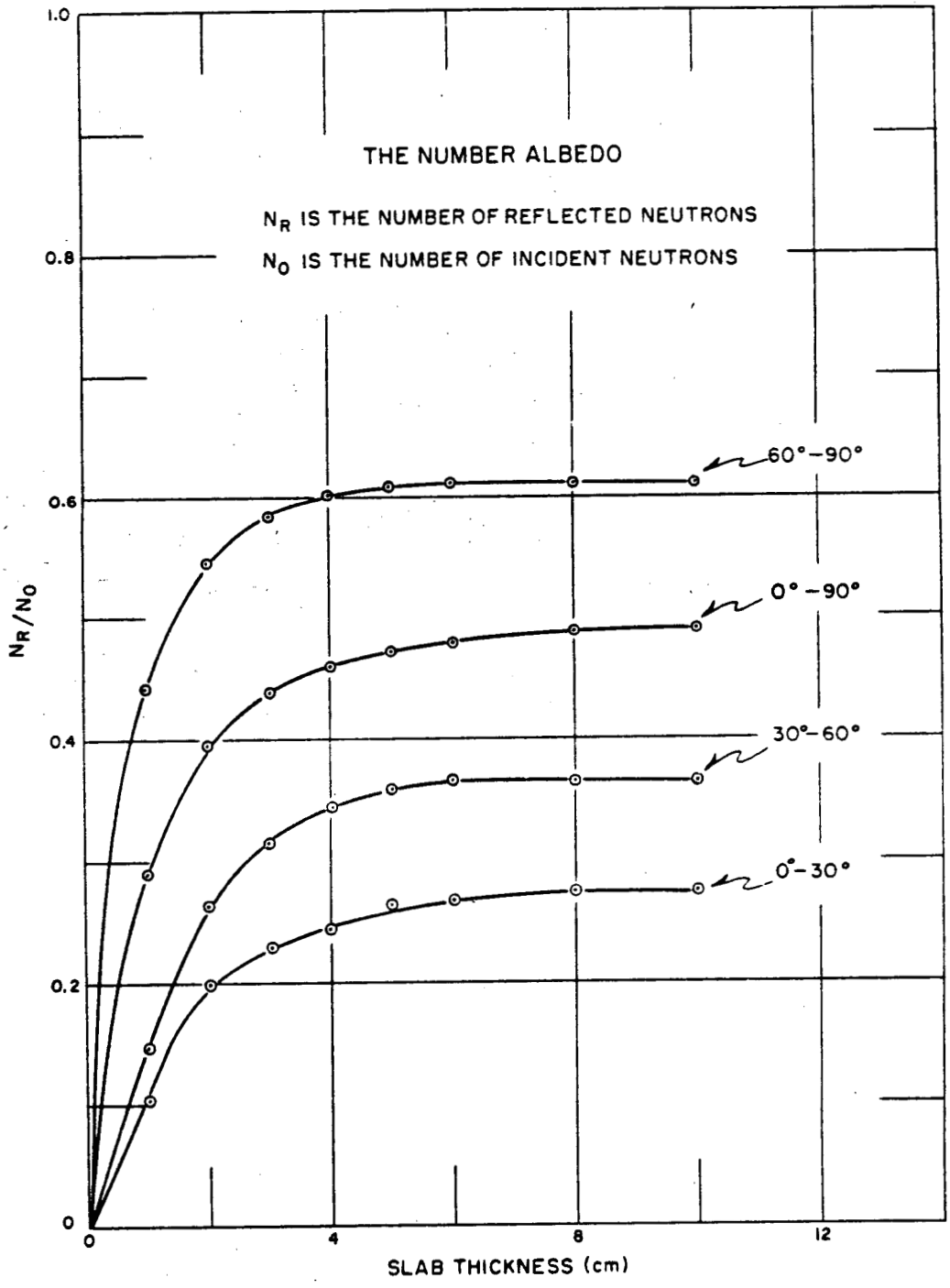

THE NUMBER ALBEDO
N_R IS THE NUMBER OF REFLECTED NEUTRONS
N_0 IS THE NUMBER OF INCIDENT NEUTRONS
60°-90°
0°-90°
30°-60°
0°-30°
N_R/N_0
SLAB THICKNESS (cm)
1.0
0.8
0.6
0.4
0.2
0
0
4
8
12

Figure 4.37

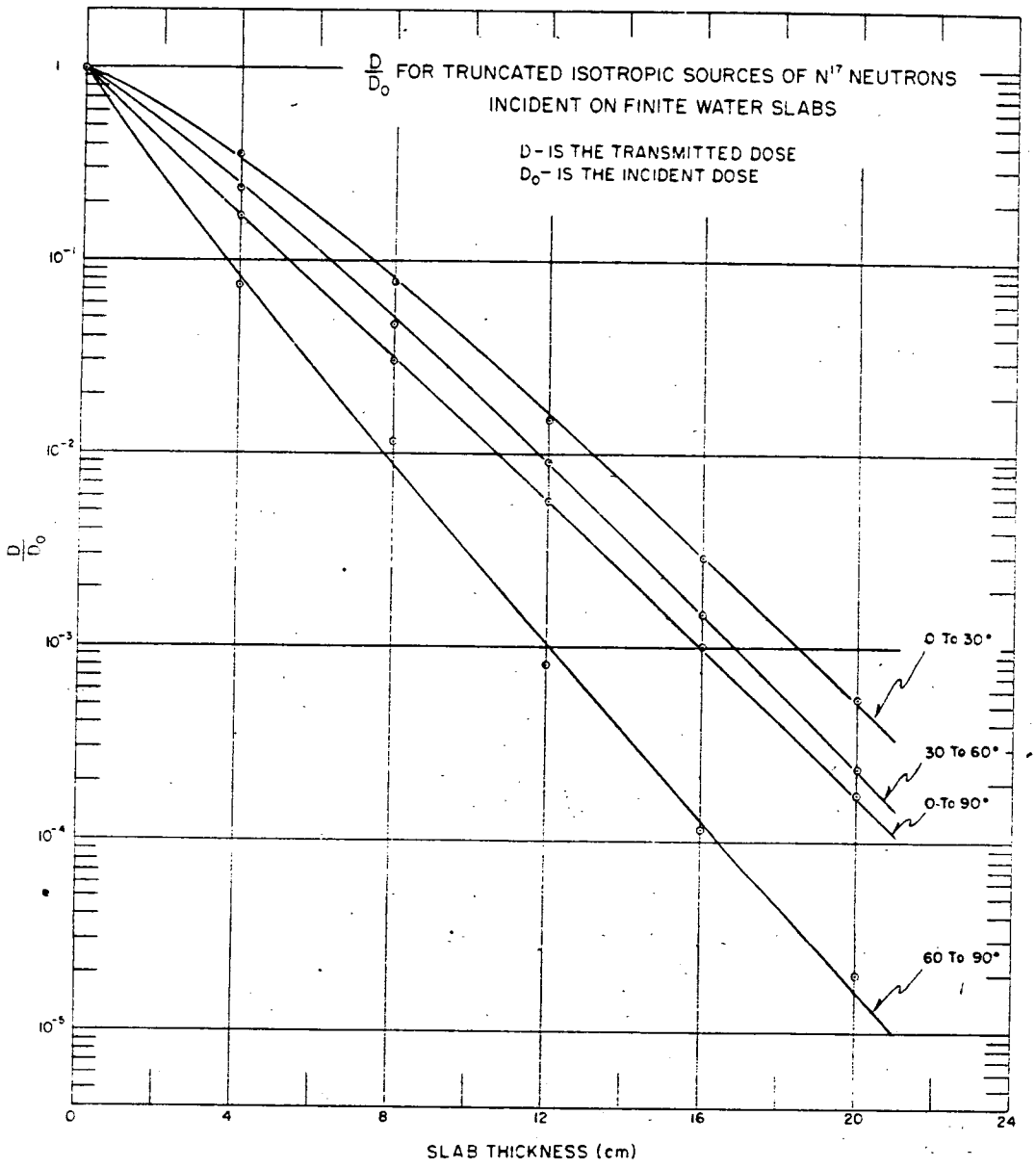

D/D0 FOR TRUNCATED ISOTROPIC SOURCES OF N17 NEUTRONS
INCIDENT ON FINITE WATER SLABS
D - IS THE TRANSMITTED DOSE
D0 - IS THE INCIDENT DOSE
D/D0
1
10-1
10-2
10-3
10-4
10-5
0 To 30°
30 To 60°
0-To 90°
60 To 90°
0
4
8
12
16
20
24
SLAB THICKNESS (cm)

Figure 4.38

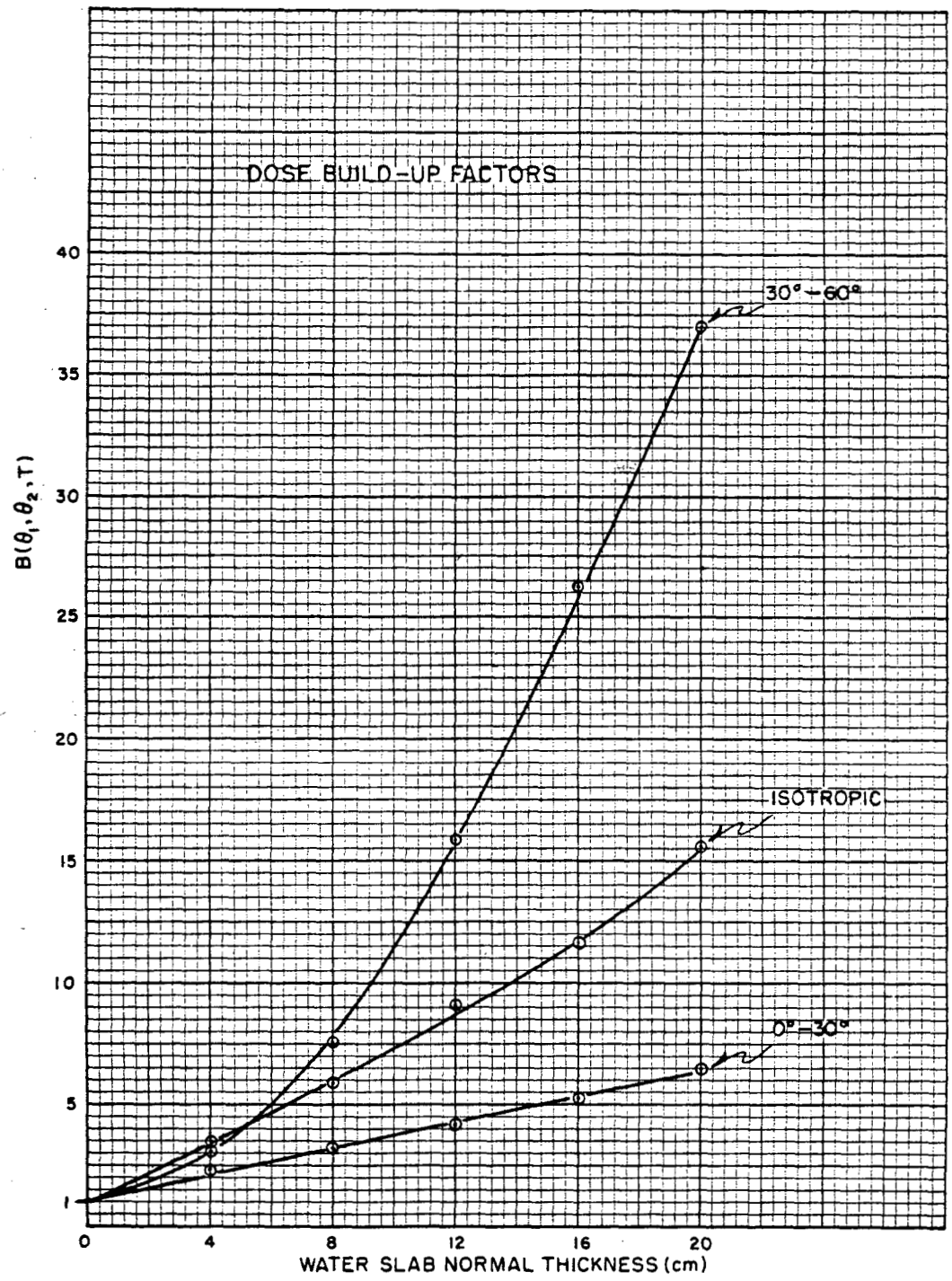

DOSE BUILD-UP FACTORS
$B(\theta_1, \theta_2, T)$
40
35
30
25
20
15
10
5
1
0
4
8
12
16
20
WATER SLAB NORMAL THICKNESS (cm)
30°-60°
ISOTROPIC
0°-30°

Figure 4.39

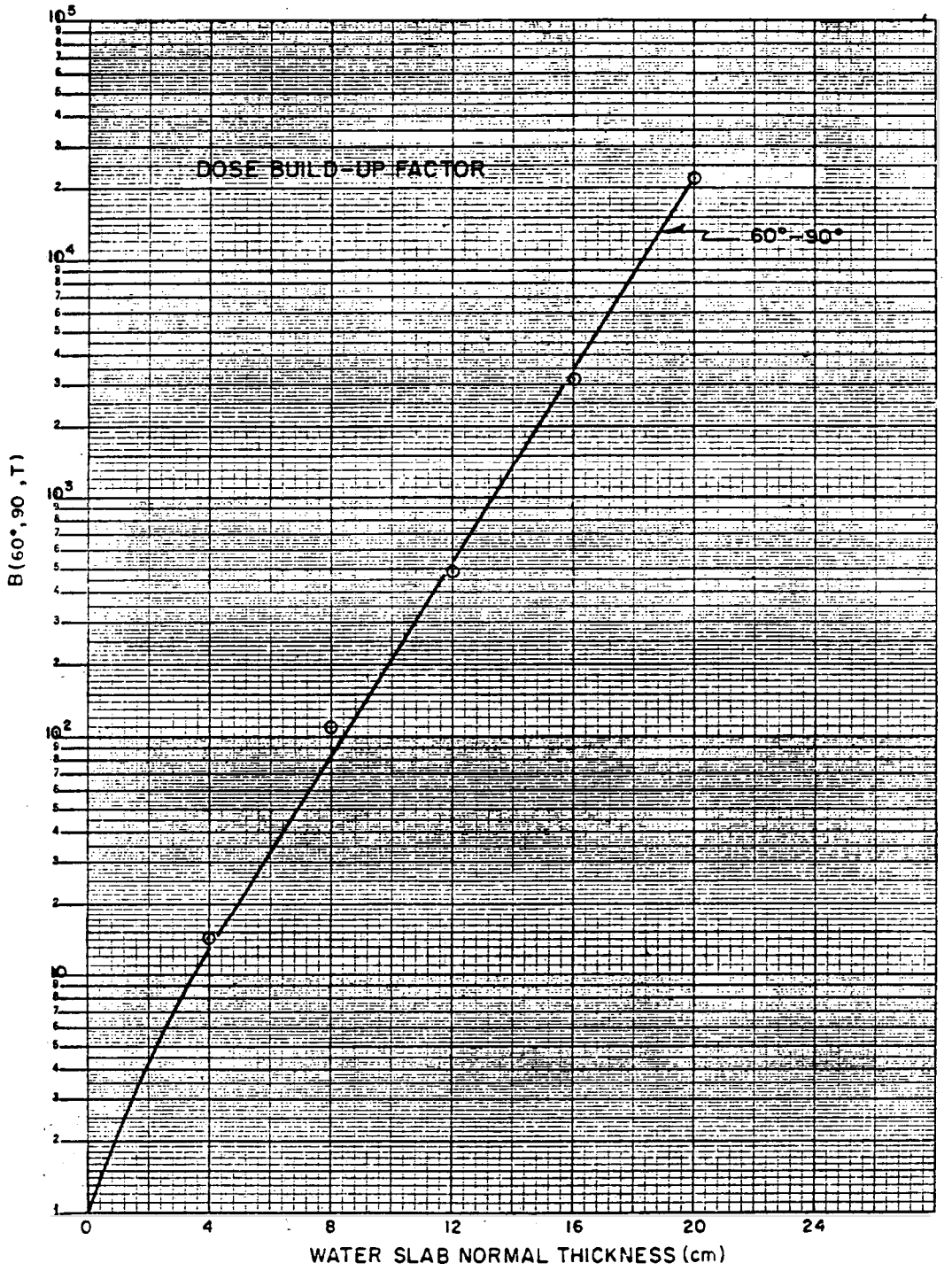

DOSE BUILD-UP FACTOR
60°-90°
B(60°,90,T)
WATER SLAB NORMAL THICKNESS (cm)
0
4
8
12
16
20
24

Figure 4.40

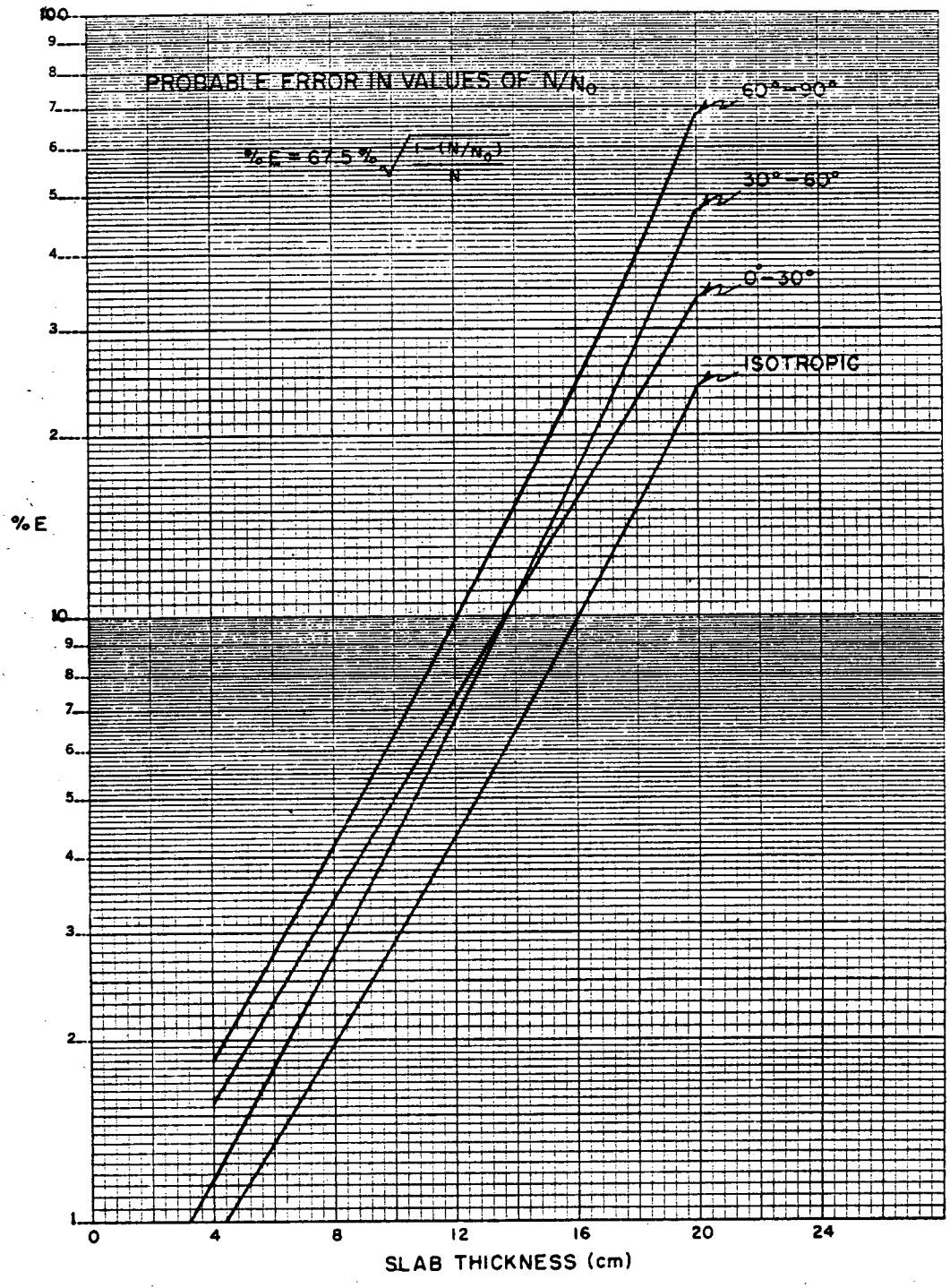

PROBABLE ERROR IN VALUES OF N/N0
%E = 67.5 % √((1−(N/N0))/N)
60°–90°
30°–60°
0°–30°
ISOTROPIC
%E
100
9
8
7
6
5
4
3
2
10
9
8
7
6
5
4
3
2
1
0
4
8
12
16
20
24
SLAB THICKNESS (cm)

Figure 4.41

Figures 4.39 and 4.40 present the same data as Fig. 4.38 but in the form of dose build-up factors, defined by

$$\text{Dose build-up factor} \equiv \frac{\text{total transmitted dose}}{\text{uncollided transmitted dose}}$$

The uncollided transmitted dose is readily calculated.

The average probability that a neutron in a truncated isotropic source incident between θ_1 and θ_2 on a water slab of normal thickness T will be transmitted without collision is

$$P(\theta_1,\theta_2,\Sigma_0 T) = \frac{\int_{\theta_1}^{\theta_2} e^{-\Sigma_0 T \sec\theta} \sin\theta \, d\theta}{\int_{\theta_1}^{\theta_2} \sin\theta \, d\theta} \tag{61}$$

where Σ_0 is the macroscopic cross section at the initial energy (in the case of Neptune, $\Sigma_0 = 0.448\ \text{cm}^{-1}$). After integrating,

$$P(\theta_1,\theta_2,\Sigma_0 T) = \frac{\cos\theta_1 \, E_2[\Sigma_0 T \sec\theta_1] - \cos\theta_2 \, E_2[\Sigma_0 T \sec\theta_2]}{\cos\theta_1 - \cos\theta_2} \tag{62}$$

where

$$E_2(b) \equiv b \int_b^\infty \frac{e^{-x}}{x^2} \, dx$$

and is plotted vs. b in Chap. 9.

Thus the uncollided transmitted dose is given by

$$D_0 P(\theta_1,\theta_2,T) \tag{63}$$

where D_0 is the dose incident between θ_1 and θ_2.

The dose build-up factor is then

$$B(\theta_1,\theta_2,T) \equiv \frac{D}{D_0 P(\theta_1,\theta_2,T)} = \frac{D/D_0}{P(\theta_1,\theta_2,T)} \tag{64}$$

Figure 4.41 shows the probable percentage error in the ratio of the number of transmitted neutrons to the number of incident neutrons. This may be taken as a rough estimate of the probable error in D/D_0 and in the build-up factors.

A production computer code is now being prepared which will determine the dose build-up factors for any incident energy or spectrum of energies and any incident angle or angular distribution.

5 SELECTION OF DOSE POINTS FOR ACCURATE ISODOSING

It is apparent that the selection of the points at which the secondary-shield thickness is calculated will have an effect on the accuracy of the final isodose plot. That is, if only obviously worst points are chosen, the shield will be overdesigned, perhaps by as much as 10 to 15 per cent. Yet the worst points must be adequately shielded too.

The number and location of the points selected will be determined by:

1. The time available and the accuracy desired for a given series of calculations.
2. The firmness of the design of the reactor system and external plant arrangement at the time.
3. The desired mesh fineness or thickness steps which the shield is to have; will it be varied by eighths of an inch? Halves of an inch?

Where weight and space are at a premium, the shield thickness should be varied in small increments. The best approach is to lay out the shield surface in a grid, the spacing of its points being set by the smallest size shield piece that it is desired to install (e.g., a 3-ft-square grid). The grid size may vary from one part of the shield to another. A fine grid calls for a great deal of calculation time and is possible only where good computing machines are available to do this work. If the calculation is to be done by hand, the assumed worst points must be chosen and contouring estimated by the random selection of a few average points in between.

The areas of the shield that see large amounts of reactor radiation can be handled by only one or two points in a large area since the variations in shield requirements are small. Where components block out large fractions of the incident radiation, many points should be taken.

The shadowing effect of components is not as sharp as would be expected from a point-source model since the areas not shadowed keep the required thickness fairly high. This is illustrated by tests done on the aircraft carrier, USS RANDOLPH, by the Naval Research Laboratory.[10] A single Co^{60} point source was moved to various locations, and measurements were taken to determine the attenuation of ship structure. The resulting gamma plot along a bulkhead showed clear-cut shadow pictures of structure between the source and the detector. However, when two sources were used, the shadowing of one was partially masked by the radiation from the other. In a reactor compartment where an infinity of sources is present, the blurring is even stronger.

A very fine grid calculation made by the Electric Boat Division, General Dynamics Corporation, to explore this point was compared with a more typical coarse-grid isodose. The fine-mesh calculation showed a much smaller variation from one area of the shield to the next, as compared with the coarse-mesh isodose plot. This effect has been further verified by measurements of the dose variations on actual operating plants. It has been found that accurate isodosing of shielding near components may save $\frac{1}{4}$ to $\frac{3}{4}$ in. of lead, which may be 5 to 20 per cent of the total thickness at that point in a typical case.

REFERENCES

1. L. H. Weinberg and H. E. Stone, Calculation of the Bremsstrahlung from Li^8 Electrons, Report KAPL-919, June 15, 1953.
2. John J. Taylor, Report WAPD-23, January 1951 (Classified).
3. D. K. Holmes and N. M. Smith, Jr., Report Y-F10-8 (Classified).
4. F. S. Kirn, R. J. Kennedy, and H. O. Wyckoff, The Attenuation of Gamma Rays at Oblique Incidence, Radiology, 63(1): 94-104 (1954).
5. G. H. Peebles, Gamma-ray Transmission Through Finite Slabs, Rand Report R-240, Dec. 1, 1952.
6. J. D. Plawchon, L. A. Beach, and W. R. Faust, Energy Flux Distributions Near Cylindrical Sources, Report NRL-4330, Mar. 10, 1954.
7. J. J. Taylor and F. E. Obenshain, Flux from Homogeneous Cylinders Containing Uniform Source Distributions, Report WAPD-RM-213, Dec. 7, 1953.
8. E. P. Blizard, Report ORNL CF-51-10-70, Part I, Jan. 30, 1952; Part II, Mar. 7, 1952 (Classified).
9. L. W. Alvarez, N^{17}, A Delayed Neutron Emitter, Phys. Rev., 75: 1127 (1949).
10. L. A. Beach, R. B. Theus, and W. R. Faust, Measurement of Penetration and Scattering of Radiation Aboard USS RANDOLPH, Report NRL-4146, Apr. 9, 1953.

BIBLIOGRAPHY

Allard, G. A., Activation of a Fluid Circulating Through a Neutron Flux, Report KAPL-665, Dec. 14, 1951.

Blizard, E. P., in "Reactor Handbook," 2d ed., Vol. 1, Chap. 2.5, p. 677, AEC Technical Information Service, Oak Ridge, 1955.

Grotenhuis, M., and J. W. Butler, in "Reactor Handbook," 1st ed., Vol. 2, Chap. 1.12, p. 257, AEC Technical Information Service, Oak Ridge, 1953 (Classified).

Smith, J. H., and M. L. Storm, Generalized Off-axis Effects from Disk Sources of Radiation, Report KAPL-918, June 1, 1953.

Stone, H. E., in "Reactor Handbook," 1st ed., Vol. 2, Chap. 2.4, p. 334, AEC Technical Information Service, Oak Ridge, 1953 (Classified).

Storm, M. L., and J. H. Smith, Numerical Studies of Nonaxial Distribution from Disk Sources of Radiation, Report KAPL-966, Aug. 1, 1953.

Taylor, J. J., Application of Gamma-ray Build-up Data to Shield Design, Report WAPD-RM-217, Jan. 25, 1954.

154
IS
BLANK

FRONT OF THIS PAGE 153

Chapter 5

PLANT LAYOUT AND OTHER FACTORS AFFECTING TOTAL SHIELD DESIGN

1 INTRODUCTION 157

2 FUNCTIONAL REQUIREMENTS OF SHIELD 158
- 2.1 Reactor (Primary) Shield . . . 158
- 2.2 Coolant (Secondary) Shield . . . 158

3 REACTOR PLANT LAYOUT . . . 159
- 3.1 Reactor Shield 159
- 3.2 Coolant Shield 159
- 3.3 Outside the Coolant Shield . . . 160

4 SPECIFIC RULES FOR PLANT LAYOUT . 160

5 DISTANCE EFFECT 161

6 SHIELD-DESIGN OPTIMIZATION . . 164

7 SHADOW SHIELDING 164

8 WEIGHTS AND WEIGHT REPORTING AS APPLIED TO SHIPS 165

REFERENCE 166

156

19

FRONT OF THIS PAGE IS 155 -

Chapter 5

PLANT LAYOUT AND OTHER FACTORS AFFECTING TOTAL SHIELD DESIGN

1 INTRODUCTION

In most reactors built to date the shielding designer has had little restriction placed upon him in providing the required radiation attenuation. The obvious exception is the mobile reactor, where it has been absolutely essential that shield weight and volume be minimized.

With the design of the Pressurized Water Reactor (PWR), it has become surprisingly apparent that the same kinds of requirements for minimum shielding and separate shield functions which are so important to naval reactors also apply to large-scale stationary plants. Although the reasons for the various shielding requirements have somewhat different roots in the mobile and the stationary plants, the resultant shield requirements are very similar.

There is a need to identify and deal separately with the several shielding problems in a reactor plant. Personnel must be shielded from radiation originating directly with the operating reactor. The irradiated coolant is also a source of radiation which must be shielded. Some of the equipment must be accessible for repairs after reactor shutdown, and the shield design must be evaluated from that standpoint. It is advantageous to have limited access to certain regions near the reactor during low power operation, and this possibility must be explored. It is usually desirable to specify a higher radiation level near the reactor than in operating and working spaces somewhat farther away. In summary, nearly all the problems associated with shipboard reactor design have reappeared in somewhat different form in the shielding design of the PWR and therefore presumably will appear in the design of shielding for other stationary reactors.

This chapter discusses the general problems of plant arrangement and shield location to balance best these different conflicting requirements.

In general, it has been found advantageous to deal separately with the reactor and with its coolant system. The reactor (or primary) shield reduces the radiation from the reactor to slightly lower than that of the activated coolant. The entire reactor coolant system is then surrounded with a coolant (or secondary) shield to reduce the radiation in operating regions to an acceptable radiation level. The best distribution of shielding between the primary and secondary shields is a subject of considerable engineering design. In addition, accessibility to the plant equipment under various conditions has to be explored and factored into the shield design.

It often appears desirable and feasible to utilize some "shadow shielding" between the major radiation sources and the secondary shield (see Fig. 1.1). A shadow shield, if judiciously designed, could allow brief intermittent access into the volume surrounded by the secondary shield. It could also nearly eliminate the direct radiation impinging upon the inner surface of the secondary shield and allow most of the shield to be designed for only soft scattered radiation. If such a concept is introduced into a shield design, then the whole balance between the primary and secondary shield must be reexamined.

This chapter also discusses the effect of reactor plant layout upon shield weight, both from the standpoint of minimizing the volume to be surrounded and also from the standpoint of getting the best arrangement of source and self-shielding within that volume. The effect upon shield weight of operating and working areas outside the shielded volume is also discussed. Some general rules are listed which have been developed from the experience of the naval reactors and PWR projects. The effect of distance from the shield, when that distance is traversed through regions containing miscellaneous machinery and other partially shielding structures, is explored with some examples and data from actual experience. Finally, this chapter discusses the problem of keeping track of what the shield actually weighs and how one shield design really compares with another, taking into account structure which may contribute to shielding effect or, conversely, structure which may weigh more than it would without a shielding requirement.

2 FUNCTIONAL REQUIREMENTS OF SHIELD

2.1 Reactor (Primary) Shield

The following specifications have to be met for the *reactor (primary) shield:*

a. The reactor shield must attenuate the neutron flux from the reactor sufficiently to prevent excessive *activation of the secondary coolant.* This is necessary to eliminate the need for shielding the secondary coolant and to prevent any inhalation problems produced by the leakage of secondary coolant into inhabited regions.

b. The reactor shield must attenuate the neutron flux from the reactor sufficiently to reduce the production of *capture gammas in the coolant shield* to a negligible level.

c. The reactor shield must reduce *residual radiation* from the core to levels allowing accessibility at a reasonable time after shutdown to the region between the coolant and reactor shields.

d. The reactor shield must attenuate the neutron flux from the reactor sufficiently to prevent the build-up of *induced activity in structure* and equipment to levels that would prevent the prescribed accessibility. The shielding necessary to fulfill this requirement is responsible for the major part of the volume of the primary shield.

2.2 Coolant (Secondary) Shield

The following specifications have to be met for the *coolant (secondary) shield:*

a. The coolant shield must reduce the gamma and neutron fluxes impinging on it to levels that will not cause *radiation injury to personnel* working near its surface (see Chap. 2).

b. The coolant shield must also prevent excessive *streaming of radiation* through shield penetrations such as steam lines. (The problem of shield penetrations can often be minimized by locating these penetrations in regions where only scattered radiation impinges on the coolant shield or where the direct radiation from important sources impinges obliquely on the region of the penetration. This topic is discussed more fully in Chap. 8.)

c. The coolant shield must sometimes act as a barrier against *air-borne contamination* originating in the vicinity of the reactor. This contamination could in some cases constitute an inhalation hazard if it were carried into inhabited areas. The coolant shield also serves to prevent direct access by personnel to regions of intense radioactivity during reactor operation.

Subject to fulfilling the requirements stated in Secs. 2.1 and 2.2, the distribution of shielding material between the primary and secondary shields is apportioned to obtain an optimum shield design. This is discussed in detail in Sec. 6.

3 REACTOR PLANT LAYOUT

3.1 Reactor Shield

When the characteristics of the reactor core, thermal shielding, and reactor vessel are known, the size of the reactor shield can be established. The establishment of the size of the reactor shield permits the arrangement work for the reactor compartment to proceed. Great care should be taken with the initial primary-shield size calculations. Later work on optimization of the total shield may affect the weight of the reactor shield, but it should not be permitted to change the volume appreciably since changing the size of the reactor shield affects the entire plant layout.

3.2 Coolant Shield

A common approach in the design of the coolant shield is to neglect initially the reactor as a gamma radiation source and to assume that all the radiation comes from the coolant. The reactor contribution to the dose is kept at an inappreciable fraction (e.g., less than 10 per cent) of the total dose by the addition, where necessary, of lead to the reactor shield. This procedure saves weight and incidentally simplifies the design of the coolant shield which often must proceed without final information on the radioactivity emerging from the reactor.

The question of whether to put lead for shielding reactor gamma radiation on the reactor shield or on the coolant shield often does not have a clear-cut answer. In many instances the weight of the total shield is minimized by placing some lead close to the reactor. However, placing all the lead on the coolant shield may be less costly because of savings in constructional costs. The final decision depends on the importance of the particular saving and may require fairly thorough optimization studies.

The weight of the coolant shield is very dependent upon the layout of the components inside the reactor compartment. Several suggestions to be followed in arranging the compartment and in designing the shield to obtain minimum shield weight can be listed. It should be recognized, however, that shield design involves many compromises between weight, cost, stability (in mobile plants), accessibility, etc. The following suggestions must be evaluated accordingly in the light of the requirements of the individual shielding problem:

a. If it is feasible from an engineering viewpoint, the most highly radioactive sources should be located in the center of the compartment, and components of lower source strength should be arranged progressively outward. This is the ideal arrangement and gives maximum self-shielding.

b. Equipment with little or no radioactivity should be located to serve a dual purpose as shielding material, where possible. As a rule, such equipment should be located near the coolant shield. (Measurements taken at the Naval Reactor Testing Facility in Idaho have shown that self-shielding by the components within the reactor compartment has been instrumental in attenuating the neutron leakage from the primary shield by approximately a factor of 20. This self-shielding can be exploited as a saving in the primary neutron shield thickness. The smaller primary-shield-tank diameter means either smaller compartment size or more maintenance accessibility around components for a given compartment size.)

c. The primary coolant pipe runs should be made as short as possible.

d. The primary coolant compartments should be kept as close together as possible, consistent with good maintenance accessibility.

e. For any given source the required shielding is minimum when the shield is closest to the source (assuming that the region to be shielded is larger than the source in question). It may be advantageous to provide some shielding directly adjacent to exceptionally radioactive sources in order to make them commensurate with the other sources. For example, when the reactor dominates as a gamma source, some lead shielding should be added to the reactor shield.

f. Considerable weight can be saved by contouring the coolant shield (i.e., varying its thickness over the surface) to give closer conformance with the specified permissible dose pattern. However, excessive contouring should be avoided; it indicates that local additional shielding should be installed near the strongest contribution to the dose.

g. In plants having more than one primary loop, a symmetrical arrangement of primary loops around the primary shield should be adopted. Such an arrangement minimizes the variation in the thickness of the secondary shield. Asymmetrical arrangement should be considered when advantage can be taken of equipment or structure as shielding, such as a large storage tank. In plant designs employing more than one reactor, a layout in which reactors are located adjacent to each other may permit the use of common shields, reducing primary- and secondary-shield requirements.

h. The area of the coolant-shield envelope should be made as small as possible because of the strong dependence of shield weight on the area of the envelope. To decrease the size of the envelope, the components within the reactor compartment should be arranged in the smallest possible volume. However, the arrangement must allow sufficient space for maintenance. Overexposure of maintenance personnel to radiation could occur if these personnel require too long a time to do their work because of poor accessibility to the equipment.

i. The coolant shield does not always need to surround the entire volume of the reactor compartment. Some of the radiation leaving the reactor compartment may be allowed to enter some unoccupied zone, such as the ocean or earth. There may be a limit imposed upon the total number of neutrons entering the unoccupied zone to avoid activation problems.

3.3 Outside the Coolant Shield

The arrangement of the working areas outside the secondary shield determines the level of radiation that can be tolerated on the shield surface. For example, it is extremely advantageous to locate equipment or areas requiring only limited access adjacent to the secondary shield, since this will permit higher radiation levels at the shield surface. Effectively advantage is being taken of the distance effect, which is discussed in more detail in Sec. 5.

The shield designer has an opportunity to effect shielding reductions through his ingenuity in locating equipment outside the secondary shield. He often must point out the possible savings to others charged with the actual plant layout. The relocation of a storeroom, a large water storage tank, a wireway, or a pipeway may prove beneficial. Access requirements should be realistic. Unduly conservative estimates (i.e., high daily access requirements) will be reflected in higher shield weights. Although a stationary reactor plant may operate at nearly full power most of the time, a mobile power plant will usually operate at a fairly low power level, averaged over several months. Inclusion of a power-load factor may thus offer additional shield savings. (See Chap. 2, Sec. 5.2.)

4 SPECIFIC RULES FOR PLANT LAYOUT

When the general criteria governing plant layout discussed in Sec. 3 is followed, suggestions for arrangements in specific instances may be itemized. It should be emphasized again that these suggestions are guides rather than rigid rules since shielding problems must generally be attacked by taking many factors into account.

a. Equipment containing large volumes of primary coolant activity should be grouped adjacent to the *reactor* shield (i.e., *away* from the *coolant* shield).

b. Equipment with little primary coolant radioactivity should be near the coolant shield in a position to shield areas of low permissible exposure from reactor radiation. This may apply to equipment that contains only a small amount of reactor coolant (e.g., a pump) or to equipment in which the primary coolant is short-lived and nearly stagnant and the radioactivity, therefore, is low (e.g., a surge tank).

c. Equipment whose emitted radiation has a directional preference should be oriented to obtain the best shield design. In general, this requires that dose points with the lowest permissible radiation level "see" the least source area.

d. Reactor pressure vessel inlet and outlet piping should be as far from the core as possible and should point out to the part of the secondary shield with the highest allowable radiation level in order to eliminate special shielding for these penetrations. This piping should not see the surface of the reactor core.

e. High-intensity sources containing primary coolant which are poorly located from a shielding standpoint should be partially shadow-shielded.

f. Equipment requiring little or no maintenance and which can provide shielding should be located around the outside of the secondary shield.

g. Equipment that requires more frequent maintenance should be located at the farthest distance possible from the outside of the shield.

h. If it becomes necessary to penetrate the coolant shield with sampling lines containing short half-lived primary coolant, such as water, the transport time from the primary coolant system to the outside of the shield should be made long enough, if practicable, to take advantage of the decay of the coolant activity.

i. Dual-purpose shielding can be obtained by arranging tanks and storage equipment against the secondary shield, if the arrangement is compatible with other design requirements. The tank should cover as much shield area as possible. The tanks arranged on the coolant shield, besides serving a dual purpose (shielding and storage), also increase the distance from the reactor compartment sources to the nearest accessible stations where radiation tolerances must be met. For tanks to be effective as shielding, they should be full at all times. If there are fluctuations in level, the pattern of the fluctuations should be known in order that they may be taken into account.

It may be useful to note some examples of the effects of plant arrangement in actual cases:*

a. Relocation of one primary coolant line from a high to a low position resulted in a 10 per cent saving in the secondary shield.

b. A redesign from a layout employing lengthy primary coolant lines with large expansion loops to one employing short pipe runs without expansion loops gave a saving of about 15 per cent in the secondary shield.

c. Detailed studies of partial shadow shielding of selected components indicate a significant weight saving.

5 DISTANCE EFFECT

The gamma dose rate may drop rapidly as one moves away from the shield. The drop-off with distance from a secondary shield has been measured at the Naval Reactor Testing Facility.[1] The drop-off from one point on the shield is shown in Fig. 5.1). This variation in dose rate with distance, the so-called "distance effect," should be utilized in the arrangement of control stations, maintenance regions, and passageways.

A detailed calculation of dosages at various distances from the shield can be very time consuming. In many instances it may be possible to use the concept of "effective distance" to provide a relatively rapid estimate of the variation in dose rate with distance from the shield.

The effective distance is based on the observation from experimental data and from calculations that the complex of gamma sources behind the reactor shield can often be replaced by a single point source at a fixed distance inside the shield for the purpose of roughly calculating

* Studies done at the Electric Boat Division, General Dynamics Corporation.

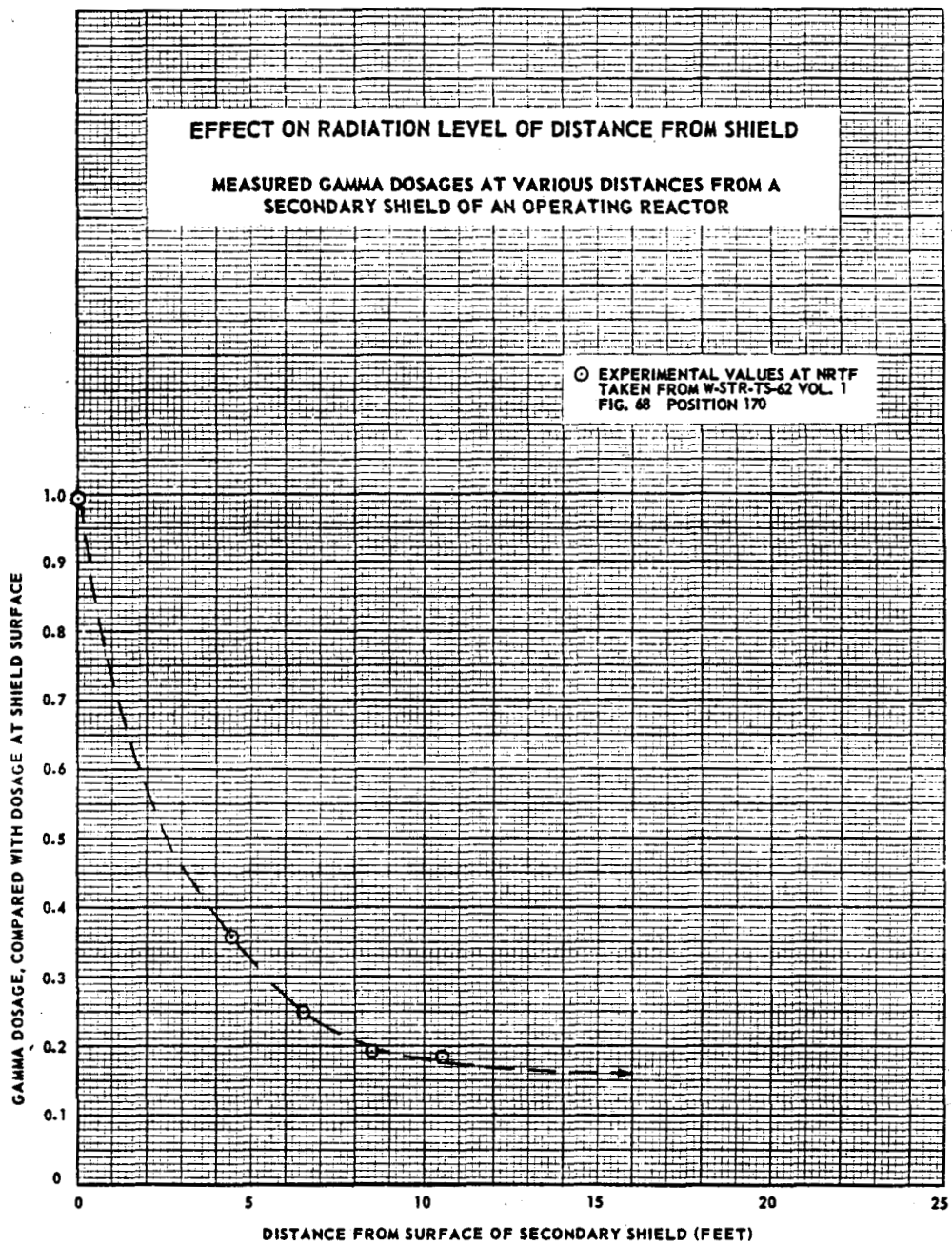

EFFECT ON RADIATION LEVEL OF DISTANCE FROM SHIELD
MEASURED GAMMA DOSAGES AT VARIOUS DISTANCES FROM A SECONDARY SHIELD OF AN OPERATING REACTOR
⊙ EXPERIMENTAL VALUES AT NRTF TAKEN FROM W-STR-TS-62 VOL. 1 FIG. 68 POSITION 170
GAMMA DOSAGE, COMPARED WITH DOSAGE AT SHIELD SURFACE
1.0
0.9
0.8
0.7
0.6
0.5
0.4
0.3
0.2
0.1
0
0
5
10
15
20
25
DISTANCE FROM SURFACE OF SECONDARY SHIELD (FEET)

Figure 5.1

the decrease in dosage with distance from the shield. The effective distance consists of two parts. One part is the actual distance of the dose point outside the shield surface, and the other is a weighted source distance inside the shield surface, determined as follows:

D_s = total dose rate at the secondary-shield surface
D_i = contribution to the dose rate D_s by component i
r_i = distance of component i from reference dose point on the shield surface
r_w = weighted distance
r_d = distance from dose point to shield

Then

$$r_w = r_1 \frac{D_1}{D_s} + \frac{r_2 D_2}{D_s} + \ldots \frac{r_i D_i}{D_s} + \ldots \frac{r_n D_n}{D_s}$$

The ratio of the dose rate at a selected dose point to that at the shield is obtained by first calculating r_w for the given shield. The inverse-square law is then used to obtain the fractional decrease in dosage between r_w and $(r_w + r_d)$. For example, assume that an r_w of 11 ft has been obtained and that it is desired to find the dose rate 15 ft away from a shield having a dose rate at the surface of D_s. Then the dose rate at the desired point is

$$\frac{(11)^2}{(26)^2} = 0.18\ D_s$$

A comparison* has been made between dosages predicted by the effective-distance method and by detailed computations. The calculations were made for points outside a bulkhead that shielded the reactor compartment of a nuclear submarine. The detailed calculation took into account shadow shielding by equipment.

The results were as follows:

Distance from shield, ft	Dosage by effective-distance method / Dosage by detailed calculation
5	0.91
10	0.91
15	0.78

The effective source distance from the shield was 16.6 ft. The shield thickness was 4 in. of iron.

It is important to recognize those situations where use of the effective distance could lead to considerable error. The largest errors arise when the major sources are close to the shield and far apart and when their radiations penetrate the shield at large slant incidences to the dose point used for obtaining the effective distance. Under these conditions the true dosage at locations away from the shield is considerably higher than the dosage calculated from the effective distance for two reasons: (1) the true distance increases more slowly than the effective distance as distance from the shield increases and (2) the effective-distance concept neglects the decrease in slant path through the shield as distance from the shield increases. In such cases the shape of the curve can be entirely different and the error, near the shield, very high.

* Study done at the Electric Boat Division, General Dynamics Corporation.

6 SHIELD-DESIGN OPTIMIZATION

Shield optimization as it shall be treated here is concerned with the distribution of low-density materials, such as water and polyethylene, and the distribution of high-density materials, such as lead, between the reactor shield and the coolant shield.

The major volume of the reactor shield consists of water or other low-density hydrogenous materials. Optimization of the reactor shield is directed to cutting down the volume of the hydrogenous component. Any reduction in volume results in reduction in size of the reactor compartment, and therefore of the heavy coolant shield, with accompanying appreciable weight savings. Several limitations exist on the minimum size of the primary shield. (See Sec. 2.1 and Chaps. 3 and 4).

The decrease in weight produced by a smaller compartment size, with its lighter gamma shield, is offset to some extent by an increase in weight resulting from having to spread a given thickness of neutron shielding material taken from the reactor shield over the much larger area covered by the coolant shield.

On the other hand, increasing the neutron shielding on the secondary shield provides added protection against scattered neutrons originating in the reactor compartment. Little information is available to evaluate for the purpose of shield design the magnitude of the scattered neutron flux.

As discussed in the preceding paragraphs, the reactor shield optimization is toward a smaller reactor-shield size. Decreasing the amount of water shielding results also in a greater gamma leakage from the reactor. Accessibility in the neighborhood of the reactor after shutdown may then require that the water shielding be replaced by some gamma shielding, thus increasing the weight of the shield.

The distribution of gamma shielding between the reactor and coolant shields requires a study of the specific application. Lead placed near the reactor to shield its radiation requires a much smaller area (and thus weight) than the same thickness of lead placed at the coolant shield. On the other hand, lead placed near the reactor does not participate in the shielding of the coolant sources. The incorporation of lead in the reactor shield is desirable when the reactor is the dominating gamma source. The lead should then be added to make the reactor contribution to the dosage commensurable with that from other sources. The amount of lead which should be incorporated in the reactor shield is a complex function of the arrangement and the strength of the other gamma sources. The addition of sufficient shielding to cut the reactor contribution to the dosage at a selected point even as little as from 50 to 10 per cent of the total dose may result in a significant weight saving.

The shield weight also depends on the division of the permissible dose between neutron dose and gamma dose. The weight of a shield decreases as the relative dosage apportioned to gamma radiation increases, up to a certain minimum. Naval reactor and PWR shield designs allow a maximum of 10 per cent of the total dosage to be from fast neutrons, the rest being from gammas. This ratio has been set from radiological considerations (see Chap. 2), but it is also in the right direction from weight and cost considerations. The best apportionment weightwise would depend on a study of the specific problem. Costwise, neutron shields are relatively inexpensive if they can consist primarily of water.

7 SHADOW SHIELDING

Current shielding practice is to contain the reactor and radioactive coolant within a shield envelope. The compartment containing the reactor cannot be entered during plant operation.

An alternate shielding arrangement makes use of the shadow-shield concept. This concept involves the individual shielding of the radioactive sources within the reactor compartment to allow access under reduced power to certain parts of the compartment. This arrangement has certain advantages from a maintenance viewpoint. It may allow some remotely operated valves to be replaced with manually operated valves. In a shipboard installation it is

also desirable from a stability point of view since the shields are placed low in the ship, close to the sources.

The shadow-shield concept has received little consideration to date because of the lack of data for calculating the scattering of radiation around the shields and the attenuation of the scattered radiation by the coolant shield. Data giving detailed analyses of gamma scattering from surfaces are becoming available, however, and such data should enable studies of the feasibility of shadow shields. Chapter 8 presents the results of Monte Carlo calculations of 6-Mev gamma-ray albedos (i.e., gamma reflection coefficients). These were made at the Naval Research Laboratory (NRL) with the NAREC high-speed computer there. An example of the type of analysis that can be performed with the aid of these albedos is also given in Chap. 8.

From the NRL data, a study has been made of the feasibility of using shadow shielding on a current reactor power plant design for shipboard use. This reactor used pressurized water, which emits predominantly 6-Mev gamma rays, as a coolant. The study concluded that shadow shielding was feasible from a radiological point of view for the arrangement in question. The shadow shield arrangement gave a lower center of gravity and about the same total weight compared conservatively with a standard shield arrangement.

8 WEIGHTS AND WEIGHT REPORTING AS APPLIED TO SHIPS

Weights and moments are very often the deciding factors in making an appraisal of a proposed shield for shipboard installation. The shield should be of minimum weight and should be low in the ship to keep the size of the ship within the accepted limits, to maintain satisfactory stability, and to minimize construction costs.

The reactor plant arrangement has a definite and far-reaching effect on the amount of shielding required. Shield weights must be computed for a variety of plant arrangements, and it is not uncommon to investigate as many as 25 different arrangements during a study series. If a thorough shield design were carried out for each arrangement, the amount of work required would be staggering. It is therefore necessary for the shield designer to use judgment, intuition, and experience in applying the methods of Chap. 4 to estimate shield thicknesses by considering simplified source configurations and a limited number of dose points.

Simplified calculations of shield thicknesses should be used only for comparing different arrangements since errors resulting from simplifications usually have a smaller effect on relative shield thickness than on absolute thicknesses.

Preliminary shield estimates to determine an absolute weight for the shield should be made in considerable detail. The accurate appraisal of shielding thicknesses (or shield weight) is very important at the preliminary phases of design since, once plant layout and shielding are established, many plant parameters are fixed and cannot be improved by further shield refinements. This is particularly true for marine propulsion plants, especially so for submarines, where total ship weight must remain fixed once the hull volume is set. Too much conservatism in shield weight at the outset results in unnecessary expenditure of material.

It may be useful to realize that the weights of power plant shields are not directly proportional to the plant power output. Actually a decrease in the power level of a reactor by a factor of 2 may result in only a 5 per cent decrease in the total shield weight.

In shield-weight accounting the weight of material used only for shielding is termed "parasitic," whereas other structural material and equipment that serve dual shielding functions are termed "nonparasitic" shield weight.

In a shipyard the system used for weight accounting should be so designed that weights of lead, plastic, liquids, or other materials used primarily for shielding can be readily segregated from other weights. Structures or equipment that are installed primarily for some other purpose are logically omitted from the shield weights even though they contribute to the shielding effect by attenuating radiation. Only in this way can a real knowledge of shield weights be acquired, and this knowledge is essential if weights are to be held down.

When a nonparasitic structure, e.g., a subdivision bulkhead, is made heavier to contribute to shielding, it is usually impractical to segregate the increment into a different weight account. Nevertheless such increments should be considered by the shield designer in comparing the merits of alternate arrangements.

The shield engineer segregates the weight items to fit into his pattern of plant-layout weight comparison. He includes in his weight analysis all material contained within an envelope which is defined by the external surface of the shield.

The end result will give the true effect of the nuclear plant arrangement on the weight and will also include the weight of shielding materials as a separate subtotal.

REFERENCE

1. Preliminary Report on Mark I STR High-powered Shield Test, Report W-STR-TS-62, Vol. 1, March 1954.

Chapter 6

SHIELD ENGINEERING

1 MATERIALS 169
1.1 Introduction 169
1.2 Iron 170
(a) Structural Steels 170
(b) Stainless Steels 171
1.3 Lead 172
1.4 Water 174
1.5 Polyethylene $(CH_2)_n$ 175
1.6 Concretes 177
(a) General 177
(b) Aggregates 178
(c) Cements 181
(d) Additives 181
(e) Forms and Placement . . . 181
1.7 Lead Glass 185
1.8 Boron-containing Materials . . 188
(a) Boral: An Aluminum–B_4C Mixture 189
(b) Boron-containing Steels . . 190
(c) Boron-containing Plastics . . 190

2 COMPARATIVE EFFECTIVENESS OF VARIOUS MATERIALS FOR GAMMA RADIATION 190

3 FABRICATION AND INSTALLATION . . 196
3.1 Introduction 196
3.2 Design Details of Composite Gamma and Neutron Shields 196
3.3 Installation of Lead Shielding . . 197
(a) Casting of Slabs 197
(b) Inspection of Lead Slabs for Voids 199
(c) Preparation of Steel Surfaces for Lead Bonding 204
(d) Bonding 206
(e) Installation of Sheathing Plates 207
(f) Inspection of Seams After Lead Installation 208

4 OPERATIONAL TESTING 214
4.1 Objectives 214
4.2 Radiation Measuring Instruments . 214
(a) Instruments for Measuring Dose Rates 214
(b) Instruments for Obtaining Design Data 214
4.3 Calibration of Instruments . . . 216
(a) Gamma-radiation Detectors . 216
(b) Fast-neutron Detectors . . 216
(c) Thermal-neutron Detectors . . 216
4.4 Planning and Performing the Shield Test 217
(a) Low- and High-power Tests . . 217
(b) Determination of Biological Adequacy of the Shield . . 218
(c) Obtaining Design and Operational Data 218
4.5 Shield Test Experience 219
(a) Summary of STR Mark I Shield Test 219
(b) General Conclusions from SIR Mark A Shield Tests . . . 221

REFERENCES 224

BIBLIOGRAPHY FOR NEUTRON SHIELDING MATERIALS 225

Chapter 6

SHIELD ENGINEERING

Nuclear calculations do not make a shield. This chapter discusses the problems of selecting commercial materials to provide the required radiation attenuation, designing these into a sound structure, inspecting the materials before and after installation, and planning and performing an operational shield test with the reactor in the completed installation. Material specifications, procedures, instrumentation, and test forms used in the naval-reactors and PWR programs are discussed.

1 MATERIALS

1.1 Introduction

There is generally not a large difference in weight between shields of the same design but of different materials (e.g., tungsten instead of lead). Therefore, wherever possible shield materials should be used which are readily available, inexpensive, and comparatively easy to work with. Other considerations are attenuation characteristics, structural strength, radiation damage, flammability, and creation of air-borne toxicity. The more common shielding materials are concrete, structural steel, lead, and water.

Gamma radiation will be most effectively attenuated by high-density materials. In mobile nuclear reactors the most usual of these materials are lead and steel; however, large thicknesses of light materials, e.g., water or plastic, also augment the attenuation of gammas when used in a composite shield.

Neutrons are most effectively attenuated by materials of low atomic number. Hydrogenous materials, such as water and most organic compounds, are useful in this respect. Where liquid neutron shielding cannot be used easily, plastic sheets can be used instead. Polyethylene, sometimes borated to about 1 wt. % boron, is the most common plastic used, but other plastics or elastomers, wood, concrete, and paraffin also find uses. General specifications for solid neutron shielding material will usually require the following:

1. The hydrogen content should be high, comparable to water.
2. Weight of the material should be kept to a minimum.
3. The material should conform to the following:
   a. The fire resistance should be high. If the material burns, the burning rate should be low, and it should be self-extinguishing when the heat source is removed.
   b. It should not be toxic, nor should any gases released by heating it be toxic.
   c. It should not have a disagreeable odor; preferably it should be odorless.
4. The material should be durable.
   a. It should be resistant to aging, heat, light, water, and spillage of oil or solvents.

b. It should present a smooth surface and have good abrasion resistance.
c. It should have no corrosive effects on steel, lead, aluminum, copper, etc.
d. It should be dimensionally stable.

5. The material should be easy to apply on horizontal, vertical, and irregular surfaces.
6. It should be possible for the material to be easily removed, replaced, or repaired.
7. The no-load distortion temperature should be above 150°F.
8. Good thermal insulating properties are desirable but are not a requirement.
9. Resistance to radiation damage is usually not a problem, although close to the reactor it could be.

The bibliography at the end of this chapter lists sources of information on possible neutron shielding materials. For stationary nuclear plants the use of concrete for shielding is generally the most economical (see Sec. 1.6).

1.2 Iron

Iron (as steel) generally appears in so many places around a reactor plant that its shielding properties must be known. First, the reactor container is usually steel, often quite thick. It is often protected by steel thermal shields. The structure that holds other shielding in place and the components that shield as well as contain primary coolant are also usually steel. Miscellaneous structures and machinery between the sources of radiation and the persons to be shielded must be considered. These pieces of steel must be checked for *bulk shielding effect*, for providing *streaming paths* through lead or water, for thermal stresses resulting from *nuclear heat generation*, and for production of *induced and secondary radiation*.

The shield engineer must decide whether a common or a special steel is justified in view of these requirements. He may wish to use a stainless steel to minimize build-up of radioactive corrosion products, and then he may find that long-lived activities not present in standard steels become a problem. The manganese, tantalum, and cobalt content in steel should be checked because these elements may cause a high induced gamma source after shutdown for structural members in a high neutron flux near the reactor. It is recommended that iron with manganese content no higher than 0.2 per cent be used in these areas. Similarly, as small a percentage as possible of cobalt and tantalum should be present. Tantalum is an impurity generally associated with niobium; cobalt comes with nickel. Therefore, changing from type 347 steel (niobium-stabilized) to type 304 or the equivalent eliminates tantalum; changing to a nickel-free steel eliminates cobalt. Most common steels have appreciable manganese. Low-manganese steels have been made and appear to have mechanical and corrosion properties essentially the same as their manganese-bearing counterparts. Their use may be justified sometimes. In any case, the specification of a special steel where a common steel would serve must be justified.

(a) Structural Steels. The physical properties of a typical (SAE-212) carbon steel are:

Composition	Maximum percentage
Manganese	0.9
Carbon	0.35
Silicon	0.15 to 0.30
Sulfur	0.05
Phosphorus	0.04
Iron	Remainder
Specific gravity	7.8
Young's modulus of elasticity, psi/in.	29×10^6
Coefficient of linear expansion/°F	6.3×10^{-6}
Tensile strength:	
Ultimate, psi	60,000 (approx.)
Yield, psi	30,000 (approx.)

The various grades of steel available are numerous; therefore the particular grade that suits the purpose best should be selected.

The excellent structural properties of steel make it ideal for use where good structural properties, as well as shielding, are required. On a weight basis steel is about 30 per cent or more heavier than an equivalent lead shield (see Sec. 1.3); however, its added structural advantage may sometimes override this weight difference. Where a steel structure supports a lead shield, steel plates normal to the radiation may be somewhat thicker than necessary, giving a negligible over-all increase in weight while providing an additional safety factor in the structural design. For neutrons steel is more effective than lead.

In areas where corrosion is likely, it should be noted that the corrosion attack may be accelerated in the presence of radiation if, for example, free oxygen is produced by the decomposition of water.

As a bulk shield there is no significant difference between ordinary carbon steel and stainless steel; hence, where possible, carbon steel should be employed because of its lower cost. There does seem to be some advantage in stainless steel where a long streaming path for neutrons occurs, but this factor will not, in general, be determining.

(b) Stainless Steels. Creep is not significant at temperatures below 1000°F; therefore stainless steel will maintain its dimensional stability at high temperatures. The corrosion resistance of stainless steel is good. Its tensile strength remains high at service temperatures, and its ductility is desirable in resisting shock forces. Its thermal conductivity is low compared to other steels, which is a disadvantage in some applications but is usually not objectionable from a shielding viewpoint. However, its high coefficient of expansion requires that special consideration be given to thermal stresses.

The physical properties of type 347 stainless steel are:

Composition	Maximum percentage	Composition	Maximum percentage
Chromium	17 to 19	Phosphorus	0.04
Nickel	9 to 12	Sulfur	0.01
Manganese	2	Tantalum	0.1
Silicon	1	Cobalt	0.04
Niobium	0.8	Iron	Remainder (65 to 70)
Copper	0.2		
Carbon	0.08		

Specific gravity		7.2	
Temperature, °F	400	600	1000
Young's modulus of elasticity,* million psi/in.	27.0	25.5	22.6
Coefficient of linear expansion/°F (mean above 70°F)	9.6×10^{-6}	9.7×10^{-6}	10.3×10^{-6}
Thermal conductivity, Btu/hr/sq ft/°F/in.	130	140	163
Tensile strength:			
Ultimate, psi	70,000	66,000	61,000
Yield, psi	32,000	32,000	30,000
Elongation in 2 in., %	48	39	37
Lattice		Face-centered cubic	

*Steels for Elevated-temperature Service, United States Steel Co., ADV-18566.

1.3 Lead

Because of its high density, good working qualities, lack of objectionable impurities, ability to withstand radiation without damage, and availability in large quantities, lead is a valuable gamma shield. It is particularly effective against low-energy gammas because of high photoelectric absorption and also against high-energy gammas because of its high pair-production cross section. Its minimum cross section occurs at about 3 Mev.

Because of the high density of lead, the volume required for a shield is low, resulting in a comparatively small, light shield. This makes it attractive for shielding mobile reactors, where space and weight are at a premium.

It has poor structural properties, especially at temperatures above 150°F, and is comparatively expensive. It also may be toxic if not handled properly.*

Lead has the following physical properties:

Atomic number	82
Atomic arrangement	Cubic face-centered
Length of lattice edge, angstroms	4.9389
Atomic weight (natural lead)	207.21
Atomic volume, cm^3/mole	18.27
Specific gravity	11.35
Melting point (chemical lead), °F	618
Casting temperature, °F	790 to 830
Mean linear coefficient of expansion (17 to 100°C)	29.3×10^{-6}/°C 16.3×10^{-6}/°F
Tensile strength, psi	
At 66°F	1920
At 300°F	710
At 500°F	280

Because of its poor structural properties, lead is usually bonded to steel. For this reason the bonding characteristics are important.

Of the various grades of lead listed in ASTM Spec. B29-43, corroding lead, chemical lead, acid lead, copper lead, common desilverized lead A, and soft undesilverized lead are all considered acceptable for bonding to steel, but common desilverized lead B is objectionable because of its high bismuth content. The high bismuth content is objectionable because it increases the amount of dross (i.e., slag) in the lead and increases the difficulty in obtaining a satisfactory bond when the lead is bonded to a structural support.

The acceptable grades all fall within the following composition:

Composition	Maximum percentage
Silver	0.020
Copper	0.080
Arsenic	0.0015
Antimony	0.0095
Tin	0.015
Zinc	0.002
Iron	0.002
Bismuth	0.150
Lead (by difference)	99.72 (min.)

* Lead in Modern Industry, Lead Industries Association, 420 Lexington Ave., New York 17, N. Y.

The lead fabricators melt down the same lead that is used for the main body of the shield for use as bonding lead; therefore the bond material will have the same composition.

The effects of the various impurities on the bonding qualities of the lead are:

1. Silver: Because of its financial value there is little chance of finding a detrimental amount of silver in any commercial lead. It has never been observed to have any effect on the bonding of lead.

2. Copper: Small amounts of copper are not known to have any effect on lead bonding. Copper increases the creep strength of lead, but this is important only when long thin sheets are hung, which sometimes occurs in chemical applications. More than 0.080 per cent copper would do no harm but would increase the cost unnecessarily for most shielding applications. Even in the relatively thick sections used for shielding, creep is not usually perceptible, except at high temperatures.

3. Arsenic: Small amounts of arsenic have a negligible effect on lead bonding and on the mechanical properties of lead. However, it reduces the grain size in castings and is used for this purpose in battery grids.

4. Antimony: Over 2 per cent antimony produces noticeable hardening of lead. It can cause segregation of hard spots in bonding. Reclaimed lead often contains enough antimony to be troublesome in bonding.

5. Zinc: Zinc makes lead brittle and porous. It causes segregations. Zinc is so detrimental to lead and vice versa that these two metals should not even be melted in the same room.

6. Iron: Although iron is known to be detrimental to lead in certain chemical applications, its effect on the mechanical properties of lead is uncertain.

7. Bismuth: Bismuth is also known to be detrimental chemically. For shield installation its disadvantage is increased dross.

8. Tin: In the small quantities found in commercial lead, tin produces no detrimental effects upon shield installation.

9. Other impurities: No other impurities are listed in ASTM Spec. B29-43. Thus any traces that might be found in any lead purchased under the ASTM specification would be negligible with respect to both radiation and mechanical properties.

For structural reasons the steel supporting structure will often penetrate the lead shield. The effects of such penetrations on shielding effectiveness are discussed in Chap. 8. It is important to eliminate voids in the lead slabs or in the bond to the structural support. The lead slabs used for the shield should be gamma-graphed (see Chap. 4, Sec. 3). To obtain a good bond, it is necessary to thoroughly clean and tin the area of the steel to be bonded.

Two types of bonded-lead construction are commonly used, the edge bond and the full bond. The details of these two types are discussed in Sec. 3. Both these methods have been found to be satisfactory when tested for shock.

If lead is used at temperatures in excess of 500°F, its creep properties must be considered. For example, lead hung fully bonded on a vertical surface at this temperature for a period of a year or two will sag to the lower part of the plate. Thus lead thickness will be reduced in the upper portions and increased in the lower portions.

For certain applications lead shot may be desirable. It can be packed to a density about 65 per cent of that of solid lead. It has the advantage that it may be moved with jets of air or industrial vacuum cleaners. Since it may compact further with time, the design of the shield must be such that this compacting will not form voids in the shield at its top surface.

At the time of writing it is considered prudent to keep lead out of contact with water, even at room temperature. This means, for example, that lead in a primary-shield tank must be sheathed with steel to prevent galvanic corrosion. This steel can become a secondary gamma source, which determines the primary-shield design. Work is now under way to determine whether aluminum, boron-containing aluminum (Boral), or boron-containing steel can be used in place of steel for this purpose (see Sec. 1.8).

1.4 Water

Because it contains a high density of hydrogen atoms, water is widely used as a neutron shield. Since hydrogen produces a large energy decrease for each scattering collision with a neutron, after a neutron is scattered once, it will be rapidly reduced to thermal energy and will be absorbed. The primary coolant of water-cooled reactors, of course, serves the purpose of attenuating the neutron flux within the container; in addition, a primary neutron shield outside the container composed of water is often used to lower the neutron flux escaping from the reactor. Water may also be used in the secondary shield for the further attenuation of neutrons to tolerance levels.

Water has the advantage that it is cheap and readily available. It is nonpoisonous and, for the most part, stable. Care should be taken when procuring the water that it does not contain dissolved salts that will assist the decomposition of the water into hydrogen and oxygen gas. For this reason distilled or demineralized water is often justified.

Surface and ground waters contain various dissolved salts that can cause gassing of shield water or the undesirable deposition of scale in the shield tank. Table 6.1 gives the impurities in fresh water from various parts of the United States.

Radiation can cause dissociation of water as a result of the radiation's breaking the chemical bonds holding the atoms together. Thus the products will be molecules or ions composed of various combinations of hydrogen and oxygen. When water decomposes, the yields will be (in molecules per 100 ev)*

$$H_2O \xrightarrow{100\ ev} 0.42H_2 + 0.75H_2O_2 + 2.78H + 2.12OH$$

The OH and H_2O_2 result in the evolution of O_2.

Back-reactions between these products will reduce the amount of gassing. The principal back-reactions are

$$H_2 + OH \rightarrow H_2O + H$$

$$H_2O_2 + H \rightarrow H_2O + H$$

These back-reactions increase with an increase in pressure. The net hydrogen production, namely, the difference between the generation and recombination of hydrogen, is reduced by increasing the pressure and decreasing the impurities.

The back-reaction is also influenced by the dynamic properties of the water. If the water is circulating rapidly or if steam or other gases are bubbling through it, the products of the decomposition reaction will be carried off, which will reduce the back-reaction and result in an increase in the net evolution rate of gas.

Pure degassed water does not evolve appreciable quantities of gas up to radiation intensities as high at 10^{19} ev/ml/min. However, the presence of ordinary impurities dissolved in the water will inhibit the back-reaction and may result in gassing. This was encountered in the Submarine Intermediate Reactor (SIR) Mark A reactor shield tank, where hydrogen evolution up to nearly 1 liter/min (2 cu ft/hr) took place in a maximum gamma flux of 10^{11} and neutron flux of 10^{10}.

Dissolved solutes, such as rust inhibitors, will further aggravate the problem. The use of lithium compounds as rust inhibitors is particularly objectionable because of the reaction $Li^6(n,\alpha)H^3$. The tritium in the evolved gases could create a health hazard. For instance, it was calculated that adding 1000 ppm of LiOH rust inhibitor to shield water of the reactor shield of a typical nuclear power plant would result in a sizable rate of tritium (H^3) evolution during a lengthy high-power operation.

The design of the shield tank should be such that all pockets are vented since gas pockets are, in effect, voids in the shield. These could be particularly troublesome if the pockets were

* C. Hochanadel, Chemistry Division, Oak Ridge National Laboratory.

Table 6.1—TYPICAL ANALYSES OF SURFACE AND GROUND WATERS IN THE UNITED STATES*

Material	Analyses of various types of water,† ppm				
	Type A	Type B	Type C	Type D	Type E
Silica	2.4	12	10	9.4	22
Iron	0.14	0.02	0.09	0.2	0.08
Calcium	5.8	36	92	96	3.0
Magnesium	1.4	8.1	34	27	2.4
Sodium	1.7	6.5	8.2	183	215
Potassium	0.7	1.2	1.4	18	9.8
Bicarbonate	14	119	339	334	549
Sulfate	9.7	22	84	121	11
Chloride	2.0	13	9.6	280	22
Nitrate	0.54	0.1	13	0.2	0.52
Total dissolved solids	31	165	434	983	564
Total hardness as $CaCO_3$	20	123	369	351	17

* This table was taken from the Handbook of Chemistry, N. A. Lange, ed., 7th ed., Handbook Publishers, Sandusky, Ohio, 1949.

† Type A: Natural soft water; contains around 30 ppm of dissolved solids; found in rivers and lakes of New England, New York, and mountainous regions of the United States; high corrosive action.

Type B: Intermediate hard water; contains well over 100 ppm of dissolved solids; typical of Great Lakes and St. Lawrence waterway; may need to be softened for industrial use.

Type C: Hard water from wells 30 to 60 ft deep; contains well over 300 ppm of dissolved solids; commonly used in the heart of the United States for public supplies; must be softened for domestic and industrial uses.

Type D: Hard water from wells 2000 ft deep; contains more chloride than type C and a high number of dissolved solids; not common; must be softened for industrial use.

Type E: Naturally softened water from wells 300 ft deep or more; high totality of dissolved solids but hardness very low; may be highly colored; common in the Atlantic and Gulf coastal plains.

to form between the reactor and its control-system neutron detectors or where they could create an explosion hazard.

Capture-gamma-ray production within water shields may be suppressed by the addition of small amounts of boron to the water. This efficiency of suppression is accomplished by virtue of the large thermal capture cross section of boron. The relatively soft gamma ray (½ Mev) subsequently emitted is more easily absorbed within the shield than the harder gammas that are characteristic of capture in most other material. However, in most shield designs it is the neutron capture in the steel tank walls, rather than in the water, that determines the shield design. In such cases, borating the water may not significantly reduce the emergent gamma flux.

1.5 Polyethylene $(CH_2)_n$

Polyethylene posesses most of the requirements for an ideal secondary neutron shielding material. Polyethylene is a thermoplastic sometimes sold as "Ethylene Polymer." Commercial polyethylene has a molecular weight of 18,000 to 22,000. Since polyethylene contains more hydrogen atoms per unit volume than water, its neutron-attenuation properties are slightly better than water.

Table 6.2—PROPERTIES OF COMMERCIAL POLYETHYLENE*

Properties	Polyethylene
General appearance	A solid material resembling paraffin in appearance but tough and flexible in thin sections
Coefficient of expansion, in./in./°F	9×10^{-5}
Hydrogen content compared to water	1.29
Chemical constituents	Hydrogen and carbon
Specific gravity	0.92
Thermal conductivity, Btu/hr/sq ft/°F/in.	2.2
Max. continuous service temp., °F	212
Softening temperature, °F	240
Burning rate	$\frac{1}{8}$-in. sheets, slow
Resistance to sunlight	Effect is slight
Resistance to aging	Good
Resistance to water	Good
Resistance to oil	Good
Resistance to acids	Good
Resistance to alkalies	Good
Effect of organic solvents	None below 50°C
Tensile strength, psi	1300 to 1860
Corrosive effect on metals	None
Abrasion resistance	Good at light loads
Toxicity	None
Odor	None
Cost per pound	~$1.50

* From Report WAPD-B(L)-456.

The virgin material is a tough, waxlike substance with a translucent white color. In very thin sections it is nearly transparent. Table 6.2 lists various properties of commercial polyethylene.

The softening point is between 220 and 240°F, which is well above the maximum operating temperature for most secondary shields. This characteristic is advantageous from the standpoint of field fabrication and allows the material to be heated and molded to a form. On cooling, it will take a permanent set and remain in the molded position. At normal room temperature the material has an elastic memory.

The material has no odor and is nontoxic. The combustion products are carbon dioxide and water. It is not affected by acids or alkalies, has good resistance to oil, and is resistant to most solvents. It can be cut with a knife, saw, or hot rod, successfully welded or flame sprayed, and easily worked with woodworking tools. It can be screwed, bolted, clamped, or cemented into place.

This material may be obtained in rod, sheet, strip, tape, and granular forms.

Laboratory tests of flammability show that polyethylene will burn. The rate of propagation is slow, and the gases emitted are invisible. The surface of the material remains smooth and waxy after the flame has been extinguished.

Polyethylene has a high coefficient of expansion, and this property must be considered at installation. The linear expansion of polyethylene is about 13 times that of iron. Difficulties are experienced when polyethylene is utilized as a neutron shield around thermally hot components because of (1) the large thermal expansion and (2) the low softening point, which causes distorted thicknesses (nonuniform shield). The greatest usefulness of polyethylene has

been in secondary-shield design, where the annoying thermal physical properties do not require special consideration.

Polyethylene loses strength as temperature increases and suffers radiation damage because its chain type molecule can be easily split by radiation. This, however, does not limit most shielding applications.

Some of the outstanding characteristics of polyethylene are as follows:

1. It is easily manufactured. Usually polyethylene is processed and molded in such a manner as to produce sheets that are solid, homogeneous, and reasonably free of entrapped gases or foreign material. The sheets are usually specified to a tolerance of $\pm 1/32$ in. of the nominal thickness.

2. Flaws are easily detected visually.

3. It is chemically stable for many years.

Some of the disadvantages of polyethylene are as follows:

1. It will burn. Various crude tests performed by cutting off thin sections and igniting them with a match show a small flame. Thick slabs were exposed to the flame from a bunsen burner; the material supported combustion but was self-extinguishing when the flame was removed.

2. Polyethylene is extremely inert, and it is thus generally not practical to use solvent cementing. Some cements are available to join it to itself and to other materials, but these are not completely reliable. Certain nonhardening mastic types of adhesives containing no halogens appear satisfactory except in shear.

When polyethylene is borated, the number of secondary gammas due to thermal-neutron capture in the hydrogen and carbon of the polyethylene is reduced considerably, and the thermal-neutron absorption characteristics are increased. When borated polyethylene is required, sufficient anhydrous boric oxide (B_2O_3) powder of 325-mesh particle size can be mixed into the base polyethylene material by the plastic manufacturer. Borated polyethylene usually contains 1 wt. % boron homogeneously distributed throughout the polyethylene. To indicate the presence of boron, a coloring agent is added during manufacture. Because boric oxide is hygroscopic and hence may produce steam bubbles in the polyethylene sheets during manufacture, the current practice is to use crude boron carbide (B_4C) instead of boric oxide. The resulting increase in cost is only a few cents per pound of polyethylene.

1.6 Concretes

(a) General. Concrete is a natural choice for shielding material; it is cheap, reliable, structurally useful, and versatile. A great deal of work has been done on conventional and special shielding concretes, and a wide variety of compositions are described in the literature. From a practical standpoint the following facts are important:

1. Gammas, rather than neutrons, generally determine shield thickness, even in high-density concretes.

2. Shield thickness can therefore usually be reduced proportionately to the increase in concrete density; composition is usually unimportant.

3. Determining the most economic shield density is thus a matter of savings in floor space and length of reach (through shield) of mechanisms, piping, etc., balanced against the increased cost of denser shielding concrete.

4. Neutron attenuation should be checked for adequacy; water content below 4 per cent may be insufficient.

5. Boron can be added but is generally not worth while.

6. Radiation stability is good enough so as not to present any problem in most applications.

7. Use of heavy concretes can result in significant cost savings in many applications, but costs for special concretes can be very high if special forms, placement techniques, aggregate handling and shipment, and other special provisions are not controlled.

J. A. Lane [Nucleonics, 13: 57 (1955)] states that, with the reactor cores of a size reasonable for industrial power production, the most economic densities range from 3.0 to 4.5. This is based on shielding only the reactor from a high flux (10^{11}) down to full-time biological

tolerance with no primary-loop shield considered. This would not be typical of most power installations, but the conclusion that the use of heavy aggregate is often economically justified is probably generally true.

Table 6.3 — SHIELDING THICKNESS*

Shield material	Specific gravity	Absorption,† cm^{-1}	Needed thickness for 10^8 attenuation, ft	Aggregate, tons/cu yard
Water	1.0	0.029	21	0
Standard concrete	2.3	0.067	9.1	1.65
Barytes concrete	3.5	0.100	6.0	2.66
Iron-aggregate concrete	5.6	0.162	3.8	4.45

* From J. A. Lane, Nucleonics, 13: 57 (1955).

† These absorption coefficients are for a gamma energy of 2 to 3 Mev.

Table 6.4 — BIOLOGICAL-SHIELD UNIT COSTS*

Concrete type	Cost		
	Aggregate, dollars/ton	Materials, dollars/cu yard	Installed cost,† dollars/cu yard
Standard	18	75	150
Barytes	36	140	250
Iron aggregate	125	600	800

* From J. A. Lane, Nucleonics, 13: 57 (1955).

† These costs include $5 per cubic yard for portland cement and $40 per cubic yard for forms and reinforcing materials. Installed costs estimated on this basis are costs for high-construction-cost areas rather than average costs. At ORNL the installed cost of ordinary-concrete reactor shields is $120 per cubic yard (including overhead), and the corresponding cost for barytes concrete is $175 per cubic yard.

Lane states that structural concrete should not be exposed to radiation exceeding a flux of about 2×10^{11} Mev/cm^2-sec in order to ensure acceptable thermal stresses (this flux is about 100 Btu/hr/sq ft and would cause about a 50°F rise in the shield). He then assumes that the shielding should reduce this radiation 10^8-fold to biological tolerance (taken here as approximately 4 mr/hr). The required shielding thicknesses are given in Table 6.3. Costs for shielding concretes are given in Table 6.4. From these two tables Lane has calculated the cost of shielding the reactor with different concretes (see Fig. 6.1). Similar calculations could be made with other assumptions of required attenuation or of cost.

(b) Aggregates. Selection. There are three general classes of aggregates, conventional, natural high-density ores, and special materials such as iron punchings or shot. An aggregate should not be selected from the literature and then shipped to the site regardless of the

locations of the site and the ore. Instead, locally available ores or slags should be investigated. Even then shipping costs may be several times the material cost at the mine. (In this regard it should be noted that heavy aggregate is still crushed rock, and freight rates should be so charged. The rates for ores are generally considerably higher.)

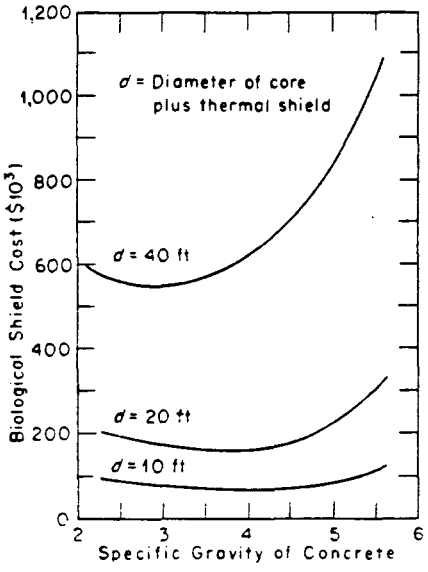


Fig. 6.1—Biological-shield cost vs. specific gravity of shielding concrete and size of reactor core plus thermal shield. Core is cylinder with height equal to diameter. Ordinary concrete has a specific gravity of 2.3; iron-aggregate concrete has a specific gravity of 5.6.

From a structural standpoint the normal specifications for good aggregates should be applied. Test batches can be made and tested if necessary. From a shielding standpoint the main criterion is density. Some aggregates, notably limonite, contain water of crystallization, and this is useful.

Table 6.5 gives information on some good typical aggregates.

Processing. The selection of aggregate size and gradation for maximum density is discussed* by C. C. Furnas and F. O. Anderegg [Ind. Eng. Chem., 23: 1052 (1931)]. They point out that maximum density requires a large ratio of coarse to fine aggregate diameters whereas optimum workability requires a continuous gradation of size. Graphs are included in the article showing the optimum number of components for different aggregates and minimum voids obtainable under various conditions. As an example, for minimum voids, if the cement particle diameter is assumed to be 0.001 in., the coarse aggregate should be 2.2 in. If a compromise to 1 in. is made, the fine aggregate should be 28 mesh. The volume ratio cement: fines: coarse should be $1 : 2\frac{1}{2} : 6\frac{1}{2}$. Refinements are then made to include the density of aggregates. This is admittedly a harsh mixture, and the second half of the article is devoted to reducing the mathematical results to working practice.

* Later work along similar lines is covered in: T. C. Powers, J. Am. Concrete Inst., 3: 419-448 (1932); C. A. G. Weymouth, Rock Products, 26-30 (Feb. 25, 1933); C. A. G. Weymouth, ASTM Proc., 38(2): 354-372 (1938); and C. T. Kennedy, J. Am. Concrete Inst., 11: 373-400 (1940).

Table 6.5—AGGREGATES*

Heavy aggregate	Source	Composition	Specific gravity†		Iron, wt. %	Fixed water, wt. %	F.O.B. source, dollars/ton	Processed at job,‡ dollars/ton
			Coarse pieces	Fine sand				
Limonite-goethite§	Michigan and Utah	$2Fe_2O_3 \cdot 3H_2O$	3.75	3.80	58	9	7	25–40
		$Fe_2O_3 \cdot H_2O$	3.45	3.70	55	11	11–20	40–50
Magnetite	Nevada	Fe_3O_4, etc.	4.62	4.68	64	1	9	20–30
Magnetite	Montana	Hydrous iron¶	4.30	4.34	60	2–5	7	18
Barite	Tennessee	> 92% $BaSO_4$	4.20	4.24	1–10	0	18	22–30
Barite	Nevada	> 90% $BaSO_4$	4.28	4.31	< 1	0	19	30–40
Ferrophosphorus	Tennessee and Missouri	Fe_3P, Fe_2P, FeP	6.30	6.28	70	0	80	90
Steel aggregate	Punchings, sheared bars		7.78		99	0	120	130
Steel shot	Chilled	SAE standard		7.50	98	0	120	130

* From H. S. Davis, Nucleonics, 13: 60 (1955).

† Material water saturated, with its surface dry.

‡ Processing charges include grinding and other operations to make the ore suitable for use in concrete. Freight charge of $10 per ton is included. Cost of grout sand is underscored.

§ This ore occurs as a mixture of the two minerals.

¶ This ore is primarily magnetite, with some hematite (Fe_2O_3) and limonite.

It is concluded that, to produce a maximum-density aggregate by screening, the ratio of the fraction of aggregate retained on any one sieve to that on the next smaller must be 1.1 for sieves differing in mesh dimensions by $\sqrt{2}$, and 1.2 for sieves differing by 2. This screening should be applied continuously from the coarsest aggregate to, and including, the cement powder. In practice most crushing processes tend to produce a product with approximately such a gradation so that crushed aggregates will generally produce a compact concrete. However, many contractors on conventional work have found that screening and grading aggregate can often pay for itself in cement saved, and, where density is an objective, the potential gains from correct grading should not be overlooked.

(c) Cements. Conventional portland cement is generally the best cement for shielding applications. Many special cements have been studied, usually with the object of increasing water content. These studies are summarized in Reports AECD-3352 by T. Rockwell, AECD-3007 by A. E. Pavlish and J. C. Wynd, and AECD-3004 by M. J. Snyder, C. A. Burkhart, and J. W. Clegg. Table 6.6 lists the properties of some of these special cements.

For small applications (portable sources, experimental equipment, etc.), some of these materials may be useful. In tonnage lots the lack of experience in handling the special materials will generally dictate the use of portland cement. Table 6.7 lists some heavy grouts made with portland cement and various fines.

(d) Additives. Additives may be used (1) to add boron to the mixture, (2) to increase the bound-water content, and (3) to improve the fluidity of the concrete. Table 6.8 lists several boron-containing materials. For most large-scale shielding boron is of doubtful value. Some boron additives (borax and, to a lesser extent, colemanite) retard the setting of portland cement. Where a borated concrete is desirable, 400 lb of colemanite per cubic yard of concrete is recommended. Boron frits, made by fritting borax with silica, can be used at 670 lb/cu yard. ORNL reports the material cost of this concrete to be 2 or 3 times the cost of material without boron.

Figure 6.2 shows the relation between the final concrete density and the density of its cement and its aggregate, for various cement to aggregate ratios.

Note: Since Fig. 6.2 portrays a simple composition equation, all scales can be multiplied by the same factor to cover different ranges; for example, the numbers can be used to show concrete materials cost as a function of the cost of cement and aggregate and the fraction of each.

Water is contained in some aggregates (e.g., limonite), in the special cements noted in Table 6.6, and in some additives, such as haydite. Colemanite is also quite high in bound water. No good correlation has been obtained between water content and neutron relaxation length, but 4 per cent is generally accepted as a lower limit. The best way to ensure adequate water content is to use sufficient cement (a 1 : 2 : 3 volume ratio of cement : fine aggregate : coarse aggregate) and to cure it well. The added cost of a richer cement content is generally unimportant for this application, where expensive forming and aggregate are used and where the penalty for voids is high. A good curing job may increase the water content of the cement from a normal 15 per cent to a well-cured 20 per cent or more. Some of the additives discussed below also help ensure highly cured cement.

Dense aggregates, complex forms, and a need to ensure lack of voids all increase the importance of fluidity of the concrete. Several commercial additives are available to do this. Plastiment (Sika Chemical Corporation, Passaic, N. J.) and Intrusion Aid (Prepakt Concrete Co., Cleveland, Ohio) are two which have been successfully used in large shield installations.

(e) Forms and Placement. Over half the cost of concrete shielding is generally tied up in the forms. On some jobs forming has cost as much as $600 per cubic yard. Mixing and placement may also run high. The only remedy for this is for the shield engineer to insist that the shielding requirements be tempered with good construction practice so that a reasonable procedure results. This sort of responsibility can seldom be successfully delegated. A few points to consider are:

Table 6.6—PROPERTIES OF CHEAP CEMENTS FOR SHIELDING*

Material	Density, g/cm^3	Grams of hydrogen/cm^3	Cents/lb	Dollars/cu ft	Compressive strength, psi	Remarks
Portland cement, wet, in special concrete	2.0	0.100	0.62	0.62	4000	50% H_2O
Portland cement, dry but well cured	1.8	0.060	0.62	0.62	4000	30% H_2O
Portland cement, poorly cured	1.6	0.018	0.62	0.62	2000	10% H_2O
Magnesium oxychloride	1.8	0.078	2.56	2.88	6000	39% H_2O
Lead glycerine	3.8	0.079	20.7	38.76	4500	
Plaster of paris	2.3	0.041	0.53	0.76	4000	
Lumnite + $CaSO_4$ (BMI)	1.9	0.06			5000	
$3CaO{\cdot}5Al_2O_3$ (BMI)	~1.8	0.07			3000	
Paraffin (~CH_2)	0.9	0.128	7.0	3.93		
Pitch	1.1	0.132	2.5	1.72		
Synthetic elastomers (~CH_2)	1.0	0.143	2.0	12.50		
Water (or silica gel)	1.0	0.111	0.13	0.082		Cost based on sodium silicate and boric acid
For comparison:						
Wood (oak; maple)	0.7	0.042	3.8	1.67	4500	
Masonite	1.3	0.078	10.0	8.10		

* From Report AECD-3352 by T. Rockwell (cost figures based on 1950 information).

Table 6.7—GROUTS*

Type†	Grout sand	Sand/cement ratio By wt.	Sand/cement ratio By vol.	Water/cement weight ratio	Wet weight, lb/cu ft
S-270	No. 110 steel shot	3.75	1.58	0.35	270
S-250	No. 110 steel shot	3.30	1.39	0.35	250
M-170	Magnetite	2.13	1.04	0.55	170
B-155	Barite	1.49	1.10	0.54	155
L-146	Limonite	1.28	1.09	0.55	146

* From H. S. Davis, Nucleonics, 13: 60 (1955).

† Grout sands processed from heavy ores should have a fineness modulus of 1.0 to 1.5; the heavier the sand the finer it must be to stay in suspension. Sands having 20 to 40 per cent finer than No. 200 screen may be used if tensile strength at high temperature is not important. Each of the grouts is pumpable; however, the metallic ones should not be pumped into large masses of aggregates. Grout S-250 may be pumped more easily than grout S-270.

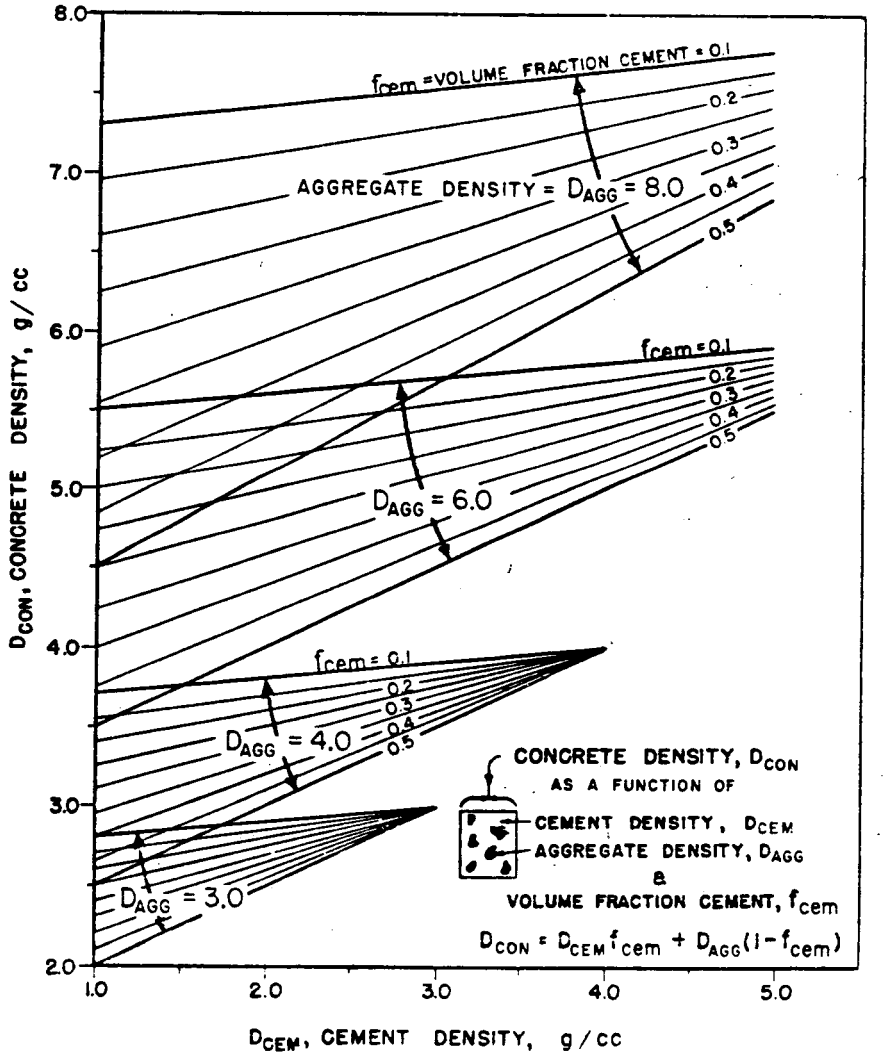


Figure 6.2

Table 6.8—PROPERTIES OF VARIOUS BORON VEHICLES*

Material	Grams of boron/cm³	Boron, wt.%	Total density	Dollars/lb of boron	Dollars/lb of total (large lots)	Other elements, g/cm³	Remarks
Crystalline boron, theoretical density and purity	2.33	100	2.33	150	150		Cost estimate for tonnage lots, 99% purity
Crystalline boron, hot-pressed with B_2O_3	2.00	98 max.	2.04				
Amorphous boron, hot-pressed with B_2O_3	1.8	80	2.3	20	15	Magnesium and carbon impurities	Quality could probably be improved
B_4C, Norton abrasive grade	2.0	80	2.5	~9	~7	<1% impurities. Some iron and carbon	Cost decreases with quantity
B_4C, Norton metallurgical grade	1.8	78	2.3	~6	~4.5		
$B_{10}H_{14}$ (a paraffin-like material)	0.83	88.4	0.94	High	High	0.108H	Only gram lots presently available
Boral (¼-in. sheet and aluminum wrapper)	1.012	40	2.5	7.50	~3	1.3Al; 0.25C	Can be made in 1000-sq ft lots
Boroxal (¼-in. sheet and aluminum wrapper)	0.305	15	2.0	1.33	~0.20	1.0Al; 0.7O	Still experimental, though easily fabricated
B_2O_3	0.575	31	1.85	0.485	~0.15	1.3O	Highly hygroscopic
Colemanite	0.0606	16	2.3	0.234	0.038	0.056H	
Ammonium pentaborate	0.40	20	2	0.530	0.106	0.074H	$(NH_4)_2B_{10}H_{16}\cdot 5H_2O$
Borax	0.197	11.4	1.73	0.155	0.018	0.092H	$Na_2B_4O_7\cdot 10H_2O$
Boroffin (20% B_2O_3)	0.062	6.2	1.0	1.39	0.086	0.089H	
Saturated H_3BO_3 solution in H_2O (3%)	0.0093	0.93	1.0	0.272	0.0014	0.119H	
M1 cement (magnesium oxychloride plus colemanite)	0.0845	4.45	1.90	0.655	0.0281	0.072H	
Ferroboron	1.0	~20	5.0	7.50	1.50	Iron and carbon	Density assumptions made; see Report HKF-3 (Classified) for boron steel
Boron steel	0.152	~2.0	7.6	8.00	0.16	Iron, carbon, and manganese	
Lead borate glass (assumed 60% PbB_2O_4 and 40% B_2O_3)	0.627	16.8	3.73				
Scrap pyrex glass	0.104	44.0	2.6	1.48	0.06		1947 price quotation from Corning Glass Works
Boron plastic, Monsanto	0.081	3.8	2.14			0.078H	Cellulose acetate and zinc borate
Boron plastic, ORNL (to be reported)	1.07	67	1.6			0.027H	Tygon and B_4C

* From Report AECD-3352 by T. Rockwell (cost figures based on 1950 information).

1. *Wooden forms* (preferably plywood) are nearly always adequate. Permanent steel forms can be very expensive, and the claimed advantages often do not materialize.

2. *Alignment tolerances* are often overemphasized. Oversized holes in plywood forms can be lined up in the field to within $\frac{1}{32}$ in. by use of a transit and wedges. This technique was very successfully used on the shield of the graphite reactor at ORNL. Penetrations were lined up, a layer of concrete was poured around the shield, and, when the round had been completed (24 hr later), the initial shrinkage and set had occurred. The second layer of penetrations was then lined up, and the process was continued.

Alignment to $\frac{1}{64}$ in. is claimed for steel forms, but, with problems of warpage from welding and distortion from rigging and shimming the heavy forms in the field, it is difficult to meet an actual $\pm\frac{1}{8}$ in.

3. *Special handling* of aggregate should be minimized. Degreasing, steam cleaning, crushing, sizing, removing fines, and special storage facilities have been used on various jobs, and all add to the cost. Standard crushing tests have shown that normal good construction practice is usually adequate.

4. Mixing may be troublesome. *Mixer loading* must be reduced not only by the density ratio of the special to the normal concrete but must be further reduced because of the greater moment arm of the small dense mix at the outside of the mixer drum. Mixers have been stalled and even overturned when this problem was not adequately considered.

5. The grinding action of hard dense aggregates (particularly steel punchings) may tend to expose the fresh surface on the cement particles and *accelerate setting.* There may also be trouble because the inside surfaces of a mixer tend to *coat with cement;* with the small loads this may be a significant fraction of the total cement in the mix. Both these problems are helped greatly by the use of additives and do not appear to be serious except when metallic iron is used as a coarse aggregate.

There are several placement techniques that give more assurance of complete filling than simply dumping the mixed concrete into a form. The various placement methods are:

1. *Conventional:* All ingredients are mixed together and dumped into forms. Vibration is important to ensure flow of the concrete into all corners, but excessive vibration may lead to the settling out of the aggregate. On the BNL shield this technique was used, inspection during pouring being done with a yoke holding a gamma source on one side of the shield and a detector on the other. Several hundred voids were spotted this way, and the vibrator moved in until the void was filled. The concrete can also be pumped into the forms with conventional concrete pumps.

2. *Puddling:* A shield of density 6.0 was poured in an Argonne National Laboratory hot lab by placing 6 in. of mortar (consisting of fine iron shot and portland cement) and then adding steel punchings while vibrating. When mortar stopped rising to the surface, another foot of mortar was placed, and the process was repeated. This method accepts aggregate segregation and exploits it. There were apparently no voids except for a thin gap under the viewing windows. Iron window sills compensated for this.

3. *Prepacked:* The coarse aggregate may be packed into forms dry, and then special grout may be pumped into the interstices. This method has been successfully used on several large installations, and those who have used it are enthusiastic. The shield designer must decide for himself whether the somewhat greater expense is warranted. A very uniform and void-free job should result from this method.

Tables 6.9 and 6.10 list properties of some recommended shielding concretes.

1.7 Lead Glass

It is important to be able to visually inspect the shielded portion of a reactor power plant while it is in operation and access is impossible. It is valuable not only to be able to observe a casualty after it has happened so that repairs may be planned but also to observe conditions that might lead to a casualty if they remain uncorrected.

Table 6.9 — CONCRETES*

Concrete type	Weight, lb/cu ft	Material cost, dollars/cu ft	Compressive strength,† psi	Cement, lb/cu ft	Heavy aggregate‡ (fine, lb/cu ft; coarse, lb/cu ft)	Admixture§	Mix water, lb/cu ft	Water content,¶ lb/cu ft		Grout type	Placement
								Min.	Max.		
A	410	25.40	3000 (3)	16.8	No. 110 shot, 63; punchings, 324	I.A.	5.9	2.5	5.9	S-270	Puddled
B	346	18.40	3000 (3)	20.6	Magnetite, 44; punchings, 270	I.A.	11.3	3.5	11.8	M-170	Prepacked
C	300	15.40	4700 (3)	M.O.**	Ferrophosphorus, 107; 161			~9.5	15.0		Conventional
D	300	12.05	3870 (4)	24.1	Ferrophosphorus, 92; 171		12.7	3.6	12.7		Conventional
E	300	11.90	5000 (3)	19.8	Magnetite, 42; magnetite + punchings, 67 + 160	I.A.	10.9	4.1	12.0	M-170	Prepacked
F	263	11.20	6000 (3)	22.2	Limonite,†† 28; limonite + punchings, 60 + 140	I.A.	12.2	13.0	21.9	L-146	Prepacked
G	262	11.30	7000 (3)	34.0	Limonite, 65; shot No. 330 + 1320, 49 + 100	Plast.	13.5	12.3	20.9	Mortar	Conventional
H	262	7.75	5350 (4)	23.7	Ferrophosphorus + barite, 70 + 35; 70 + 50		12.8	3.6	12.8		Conventional
I	262	5.75	4800 (3)	19.8	Magnetite, 42; magnetite + punchings, 122 + 67	I.A.	10.9	4.7	12.6	M-170	Prepacked
J	244	2.55	5000 (3)	17.5	Magnetite, 37; 180	I.A.	9.7	4.8	11.9	M-170	Prepacked
K	232	2.20	6500 (3)	24.3	Magnetite, 86; 110		11.5	5.7	13.5		Conventional
L	227	3.30	3500 (3)	19.3	Barite, 29; 168	I.A.	10.5	2.9	10.5	B-155	Prepacked
M	222	3.05	6000 (3)	19.3	Barite, 86; 105	I.A.	11.6	2.9	11.6		Conventional
N	219	2.10	6500 (3)	24.9	Hydrous iron ore, 82; 100	Plast.	12.0	9.2	17.5		Conventional
O	215	2.75	5000 (3)	22.7	Limonite, 29; limonite + magnetite, 28 + 122	I.A.	12.5	10.9	20.0	L-146	Prepacked
P	185	3.10	5800 (1)	31.3	Limonite, 62; 76	Plast.	15.4	17.1	27.8		Conventional
Q	154	0.50	8800 (1)	31.3	Local sand, 50; 61	Plast.	11.5	4.7	11.5		Conventional

* From H. S. Davis, Nucleonics, 13: 60 (1955).

† The number in parentheses indicates the age of the concrete in months.

‡ Where only one material is given, it is used for both fine and coarse aggregate.

§ Intrusion aid, 1.5 wt. % of the portland cement, is added where shown. I.A. (Intrusion Aid) is a special grout admixture designed and used by Prepakt Concrete Co., Cleveland, Ohio. Plast. (Plastiment) is a concrete densifier manufactured by Sika Chemical Corporation, Passaic, N. J.

¶ Maximum water content is the water weight when the concrete is wet. Minimum water content is the amount left after drying to constant weight at 85°C. The difference between the maximum water content and the amount of mix water added is the water of crystallization held by the aggregate. The difference between the minimum water content and the water of crystallization is the water retained by the hardened cement paste.

** This concrete is made using magnesium-oxychloride cement, made of 12.2 lb/cu ft of MgO powder and 19.8 lb of MgCl solution.

†† Utah limonite is used except for mix P, which uses Michigan limonite.

Table 6.10 — PROPERTIES OF CONCRETES*

Concrete†	Lb/cu ft	Bags/ cu yard	Compressive strength,‡ psi	Rupture modulus,‡ psi	Modulus of elasticity, $\times 10^{-6}$‡	Ultimate bond strength,‡ psi	Shrinkage, %	Expansion, in./in./°F	Specific heat, Btu/lb/°F	Conductivity, Btu/hr/ft/°F	Diffusivity, sq ft/hr
Conv.	153	~5.0	4960	630	4.6		0.041	5.5	0.23	1.50	0.042
Q	154	9.0	8870	1005	5.9	900	0.012				
P	185	9.0	5865	700	4.4	970	0.021				
O	210	6.55	4640	516	5.0	1396	0.023	5.6	0.20	1.20	0.030
M	226	5.1	6130	445	4.3		0.029	10	0.157	0.884	0.025
L	230	5.0	3340	630	3.7		0.029	10	0.146	0.867	0.026
K′	224	7.0	5780	684	4.3	1423	0.018	5.7	0.21	1.68	0.034
F	273	6.55	3180	406	5.4	1266	0.013	5.9	0.18	2.75	0.056

* From H. S. Davis, Nucleonics, 13: 60 (1955).

† Concrete composition is similar to that given in Table 6.9, except for K′, which has 46 lb of limonite and 0.6 lb of fixed water/cu ft. Conv. is Grand Coulee concrete. The placement method is given in Table 6.9. The limonite used was from Michigan, and the barite was from Nevada; the specific gravity of the magnetite was 4.4.

‡ Strength values are for moist cured specimens 28 days old.

Lead glass has proved to be a satisfactory shielding material for this application. Its properties* are:

Density (average), g/cm^3	6.2
Refractive index	1.95
Color	Yellow-green
White-light transmission per inch, %	80 to 90
Chemical composition (typical)	
Silica, %	27
Lead oxide, %	71
Potassium oxide, %	2
Gamma macroscopic cross section, cm^{-1}	0.244
Cost per cubic foot	$1000

The shielding ability of this glass for gamma radiation is about equal to that of steel. The neutron attenuation is negligible. For this reason, when used as a reactor shield it must be used in conjunction with lucite or plexiglass, which will provide the neutron attenuation while meeting the transparency requirements.

Lead glass will tend to darken or brown upon exposure to high beta or gamma fluxes. However, this will not usually be a problem when the glass is used in the secondary shield.

The high refractive index of the glass increases the width of the field of view, which is a distinct advantage for inspection ports since it helps the viewer see a greater area. A lead-glass viewing port 1 ft square and 10 in. thick would allow a field of view about 170 to 180° compared to the 100° view with only air in the port.

Owing to the reflection of light from the surfaces and absorption of light in the glass, there is some loss of light in the lead glass. Of this, reflection at normal incidence may account for about 10 per cent of the transmission loss. Therefore the fewer surfaces the light must penetrate the lower will be the losses. To minimize reflection loss, one thick pane, rather than laminations, is advisable. This reflection loss may be reduced by about half if the surfaces are coated with low-reflection coatings.

This lead glass will withstand the thermal shock that might be expected in a secondary shield, about 50°F/15 min on one surface.

Like all glass, lead glass is brittle and subject to damage from shock. It is necessary to exercise care in mounting it so that it is isolated from stresses that might be developed in the shield structure supporting it.

Lead glass is not chemically inert. It will react with sulfur compounds in the air or with vulcanized rubber since sulfur is employed in the vulcanizing process. Substances that react with lead or lead oxide will affect the glass. Weak acids can easily etch the surface. Therefore protecting the exposed surfaces with lucite will serve the purpose of protecting the glass, as well as attenuating neutrons.†

1.8 Boron-containing Materials

Gammas produced by the absorption of neutrons are one of the major headaches of the shielding engineer. Most materials will readily absorb thermal neutrons but only by producing one or more 5- to 10-Mev secondary gammas that are then a source requiring heat removal and further shielding. Boron is nearly unique in its ability to absorb thermal neutrons avidly, producing only a soft ($\frac{1}{2}$-Mev) gamma and an easily absorbed alpha particle in the process and leaving no significant residual induced radioactivity. Cadmium, by contrast, emits several hard gammas and leaves four radioactive isotopes after neutron irradiation.

---

*See Report WAPD-SFR-A-469.

†See Lead Glass Viewers, by J. M. Holeman, Hanford Works, Report HW-18206, and Radiation Shielding Window Glasses, by W. S. Rothwell, Corning Glass Works, Corning, N. Y.

(a) Boral: An Aluminum–B_4C Mixture. Boron carbide (B_4C), a dense, hard, highly inert material containing 80 per cent boron, can be suspended in aluminum up to 50 vol. %. The resulting ingot can be rolled into sheets, aluminum clad, and fabricated like aluminum. This material, and a suggested process for its manufacture, is described in Report AECD-3625, Boral: A New Thermal-neutron Shield, by V. L. McKinney and T. Rockwell III, Aug. 29, 1949, and by the supplemental report by A. S. Kitzes and W. Q. Hullings, also in Report AECD-3625. Boral is now available on a commercial scale (hundreds of square feet) from the Oak Ridge Operations Office, AEC. A sheet $\frac{1}{8}$ to $\frac{1}{4}$ in. thick, containing 35 per cent B_4C, will reduce thermal neutrons by 10^4 to 10^6. The removal of heat from such a thin aluminum sheet is considerably easier than from the conventional heavy steel thermal shields.

The physical properties of boral are as follows:

1. *Composition* (for a $\frac{1}{4}$-in.-thick sheet including aluminum cladding on each side):

	Wt. %	mg/cm²	
Boron	15.7	254	Sandwich material is
Carbon	4.3	71.6	35 wt. % B_4C
Aluminum	80.0	1303.0	

Borals with B_4C contents varying from 10 to 50 per cent in the core can be supplied.

2. *Density:* 2.53 g/cm³
   0.09 lb/cu in.
   $3\frac{1}{4}$ lb/sq ft for $\frac{1}{4}$-in.-thick sheet

3. *Strength:*
   a. Tensile. Tensile specimens containing 50 wt. % B_4C were exposed to radiations in the X-10 reactor for 14 months with no serious damage.

Weeks of exposure	Total nvt	Average tensile strength, psi
0	0	5000
6	3.1×10^{18}	6335
8	4.8×10^{18}	7500
30	1.2×10^{19}	5650
60	2.6×10^{19}	5500

   b. Elongation, 0.4 per cent.
   c. Shear, 8237 psi.
   d. Welded tensile specimens did not fail at weld.

4. *Thermal Properties* (50 wt. % B_4C):
   a. Thermal conductivity (Btu/hr/ft/°F):

Temperature, °F	200	450	500
k	25	19.2	19.0

   b. Heat content: 0.175 Btu/lb/°F.
   c. Softening point: Maintains some mechanical strength up to 1500°F (800°C), above which oxidation is excessive.
   d. Cooling required: Incident energy, plus 4.1×10^{-10} watt/sq ft per unit thermal neutron flux.

5. *Cost:* $5 to $15 per sq ft for $\frac{1}{4}$-in.-thick sheet containing 35 per cent B_4C in the core.

6. *Workability:* Boral can be sheared, sawed, welded, punched, drilled, tapped, rolled, hot-formed, and experimentally die-cast. Recommended methods for working boral are shearing and punching. Boral with 35 per cent B_4C can be sawed at low speeds with DoAll saws. All welding must be done with heliarc. Boral tubes can be hot-turned or -pressed.

(b) Boron-containing Steels. Development work has been and is being carried out on boron-containing stainless steel and carbon steel for reactor control rods and thermal shields. Work has been done on these alloys in compositions up to 5 wt. % boron. At present the cost of these materials runs about $3 per pound. Material can be obtained from Superior Steel Corporation, Pittsburgh, Pa., Universal-Cyclops Steel Corp., Pittsburgh, Pa., and Vacuum Metals Corporation, Syracuse, N. Y. From a forging and rolling standpoint an upper limit of approximately 2 per cent boron in both stainless steel and carbon steel can be tolerated before fabrication difficulties are encountered. If a higher B^{10} content is desired, presumably enriched boron could be used. Highly enriched boron is available from the Oak Ridge Operations Office, AEC, in pound lots, for about $15 per pound of B^{10} or about $100 per square foot for a ¼-in.-thick sheet containing 1 per cent B^{10}. Welding can be done using a filler of the matrix material under an inert atmosphere. Diffusion of boron within the weld area will occur, resulting in higher concentrations of boron in the weld. Corrosion studies indicate that these boron alloys have corrosion resistance in hot water approximately equivalent to the matrix material. In general, as boron content increases, the corrosion resistance decreases, the ductility decreases, and the ultimate strength increases slightly. Some irradiation tests have been run which indicate no significant damage; other tests indicate severe decrease in impact strength, but only after irradiation periods of 10^{20} nvt or more, beyond the range of shielding application.

(c) Boron-containing Plastics. Section 1.5 discusses polyethylene containing 1 per cent boron in the form of B_4C (recommended) or B_2O_3. Plastic sheets were produced by Rockwell and others at ORNL up to 20 sq ft each, containing over 70 per cent B_4C. These were cloth reinforced and handled about like leather. Presumably any B_4C content between 1 and 70 per cent could be made; probably 35 per cent would be a reasonable limit. Such sheets might find specialized application where suppression of potential secondary gammas is required and a life for the sheets of 10^{18} neutrons/cm^2 or 10^9 rep of gamma dose can be accepted. Adequate cooling must also be provided to remove the absorbed energy plus that from the high-energy particles which are produced by neutron absorption. The latter will produce about 4.1×10^{-10} watt/sq ft per unit thermal neutron flux, i.e., 4.1 watts/sq ft for a flux of 10^{10}.

2 COMPARATIVE EFFECTIVENESS OF VARIOUS MATERIALS FOR GAMMA RADIATION

It has become very expedient for a shield engineer to have for ready reference a set of thickness equivalents for gamma rays of various common structural material. These equivalents are useful whenever shield material substitutes are made. For example, detail structural changes can be readily adjusted with the use of these equivalents so as not to alter the effectiveness of the shield.

Comparisons are usually expressed in terms of lead because it represents the best practical gamma shield material for most applications. The equivalent ratios were calculated by considering a point source.

The gamma dose transmitted by a lead shield may be written as

$$D_{Pb} = D_0 B_{Pb} \exp(-\mu^0_{Pb} T_{Pb}) \tag{1}$$

where $\exp(\ ) \equiv e^{(\ )}$ and $e = 2.72$, the base of natural logarithms.

D_0 = the dose rate on the source side of the shield (assumed to be plane monodirectional)
B_{Pb} = the dose build-up factor for lead at the incident energy for the particular geometry involved and the particular ($\mu^0 T$) of the shield (see Chap. 1)
μ^0_{Pb} = the absorption coefficient for lead at the incident gamma energy
T_{Pb} = the thickness of the lead shield

The equivalent expression for a shield of any general material is

$$D = D_0 B \exp(-\mu^0 T) \tag{2}$$

We require that the total attenuation of the shield be the same as that of the lead shield, i.e., $D = D_{Pb}$. Equating,

$$D_0 B \exp(-\mu^0 T) = D_0 B_{Pb} \exp(-\mu^0_{Pb} T_{Pb}) \tag{3}$$

Dividing through by D_0 and operating on both sides of the equation by (ln) yields

$$(\ln B) - \mu^0 T = \ln B_{Pb} - \mu^0_{Pb} T_{Pb}$$

or

$$\mu^0_{Pb} T_{Pb} - \mu^0 T = \ln \frac{B_{Pb}}{B}$$

Multiplying and dividing the first term by the density of lead (ρ_{Pb}), the second term by ρ, and rearranging terms yields finally

$$\boxed{\rho T = \frac{(\mu^0/\rho)_{Pb}}{(\mu^0/\rho)} (\rho T)_{Pb} + \frac{1}{(\mu^0/\rho)} \ln \frac{B}{B_{Pb}}} \tag{4}$$

This expression is in terms of the quantity of interest and the areal density (ρT), in units of grams per square centimeter. The first term on the right is the first-order approximation; the second term is the correction due to build-up differences between lead and the material in question.

If we deal specifically with the predominant gamma energy emitted by water (6 Mev),* and the shield materials, iron and lead,

$$\left(\frac{\mu^0}{\rho}\right)_{Pb} = 0.0445 \text{ cm}^2/\text{g} \qquad \left(\frac{\mu^0}{\rho}\right)_{Fe} = 0.0305 \text{ cm}^2/\text{g}$$

$$(\rho T)_{Fe} = 1.46(\rho T)_{Pb} + 32.7 \ln \frac{B_{Fe}}{B_{Pb}} \tag{5}$$

At first glance this equation seems incapable of solution because one of the arguments of B_{Fe}, namely, $(\mu^0 T)_{Fe}$, is related to the unknown, $(\rho T)_{Fe}$. However, this expression is ideally suited to an iterative procedure. As a first approximation, use $(\mu^0 T)_{Fe} = (\mu^0 T)_{Pb}$ and solve for $(\rho T)_{Fe}$. Then, using this value of $(\rho^0 T)_{Fe}$ as the argument for B_{Fe}, solve for the second approximation $(\rho T)_{Fe}$, and so on. Because the second term in Eq. 5 is small compared with the first, this procedure converges rapidly; one rarely has to go beyond the second iteration.

Another question involved in the use of Eq. 5 is: What values are used for the build-up factors? Build-up factors have been tabulated only for infinite mediums. One may be quite sure that finite-slab build-up factors are smaller than the corresponding infinite-medium ones. In addition, one may guess that B_∞/B_{finite} is greater for iron than for lead because of the greater albedo (coefficient of gamma reflection) of iron. Comparisons (Report WAPD-T-170) have been made between finite-slab build-up factors and infinite-medium build-up factors for both lead and iron. The results indicated that $(B_{Fe}/B_{Pb})_{finite} = 0.95(B_{Fe}/B_{Pb})_\infty$. Thus very little error is made in using the tabulated infinite-medium build-up factors in Eq. 5.

Figure 6.3 shows the results of using Eq. 5. The ratio of areal densities is seen to be considerably above the first-order approximation (1.46) over the range of lead thicknesses

*A similar treatment can be made for other coolants emitting different energies of gammas.

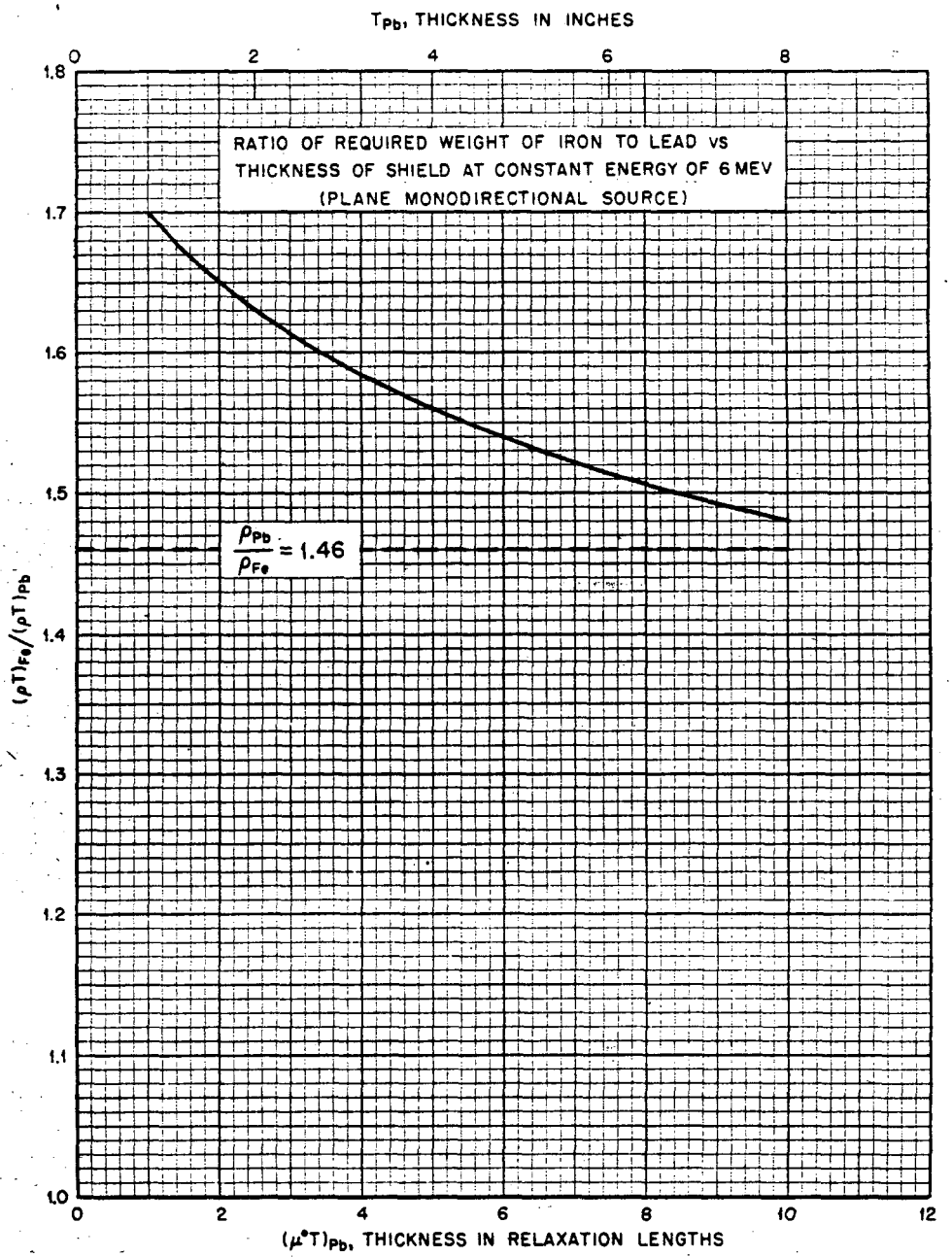


Figure 6.3

from 1 to 4 in. A graph of the same function for the case of a plane isotropic source yields essentially the same picture out to seven mean free paths.

The above analysis holds only for the N^{16} radiation from water (about 6 Mev). No general formula can be given which includes the actual energy spectrum of the radiation emitted from all the components containing primary coolant because this spectrum will differ from different components. For example, a small pipe will emit essentially 6-Mev gammas. A lead-shielded boiler will emit a spectrum with a large component at about 2 Mev, the lead absorption coefficient minimum, and so on.

Figures 6.4 to 6.6 show the results of using Eq. 4 for various materials—iron, water, and concrete—as a function of energy while keeping $\mu^{0}T$ constant. For organic materials the areal

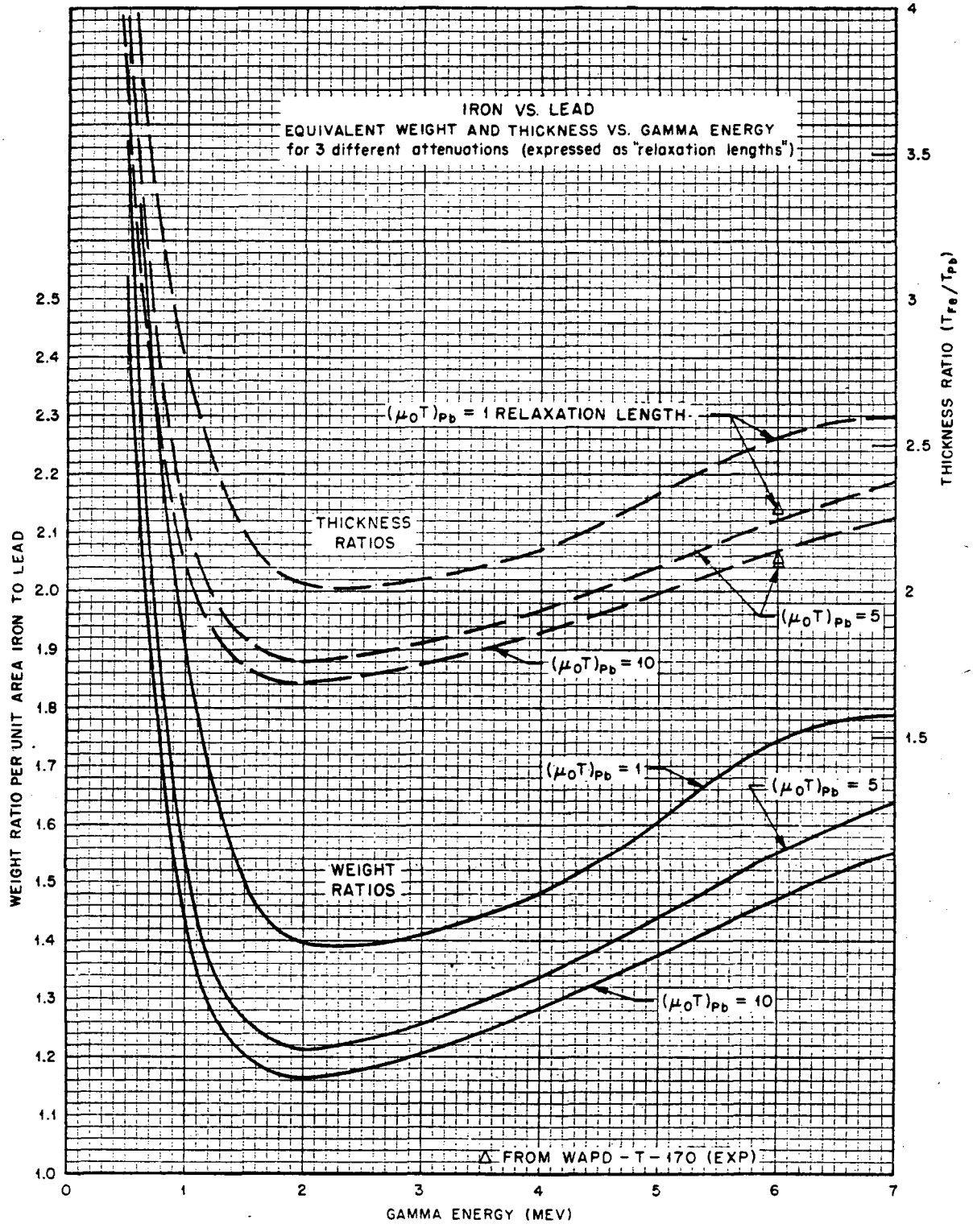

IRON VS. LEAD
EQUIVALENT WEIGHT AND THICKNESS VS. GAMMA ENERGY
for 3 different attenuations (expressed as "relaxation lengths")
$(\mu_0 T)_{Pb}$ = 1 RELAXATION LENGTH
THICKNESS RATIOS
$(\mu_0 T)_{Pb}$ = 5
$(\mu_0 T)_{Pb}$ = 10
$(\mu_0 T)_{Pb}$ = 1
$(\mu_0 T)_{Pb}$ = 5
WEIGHT RATIOS
$(\mu_0 T)_{Pb}$ = 10
Δ FROM WAPD - T - 170 (EXP)
WEIGHT RATIO PER UNIT AREA IRON TO LEAD
THICKNESS RATIO (T_{Fe}/T_{Pb})
GAMMA ENERGY (MEV)
1.0
1.1
1.2
1.3
1.4
1.5
1.6
1.7
1.8
1.9
2.0
2.1
2.2
2.3
2.4
2.5
1.5
2
2.5
3
3.5
4
0
1
2
3
4
5
6
7

Figure 6.4

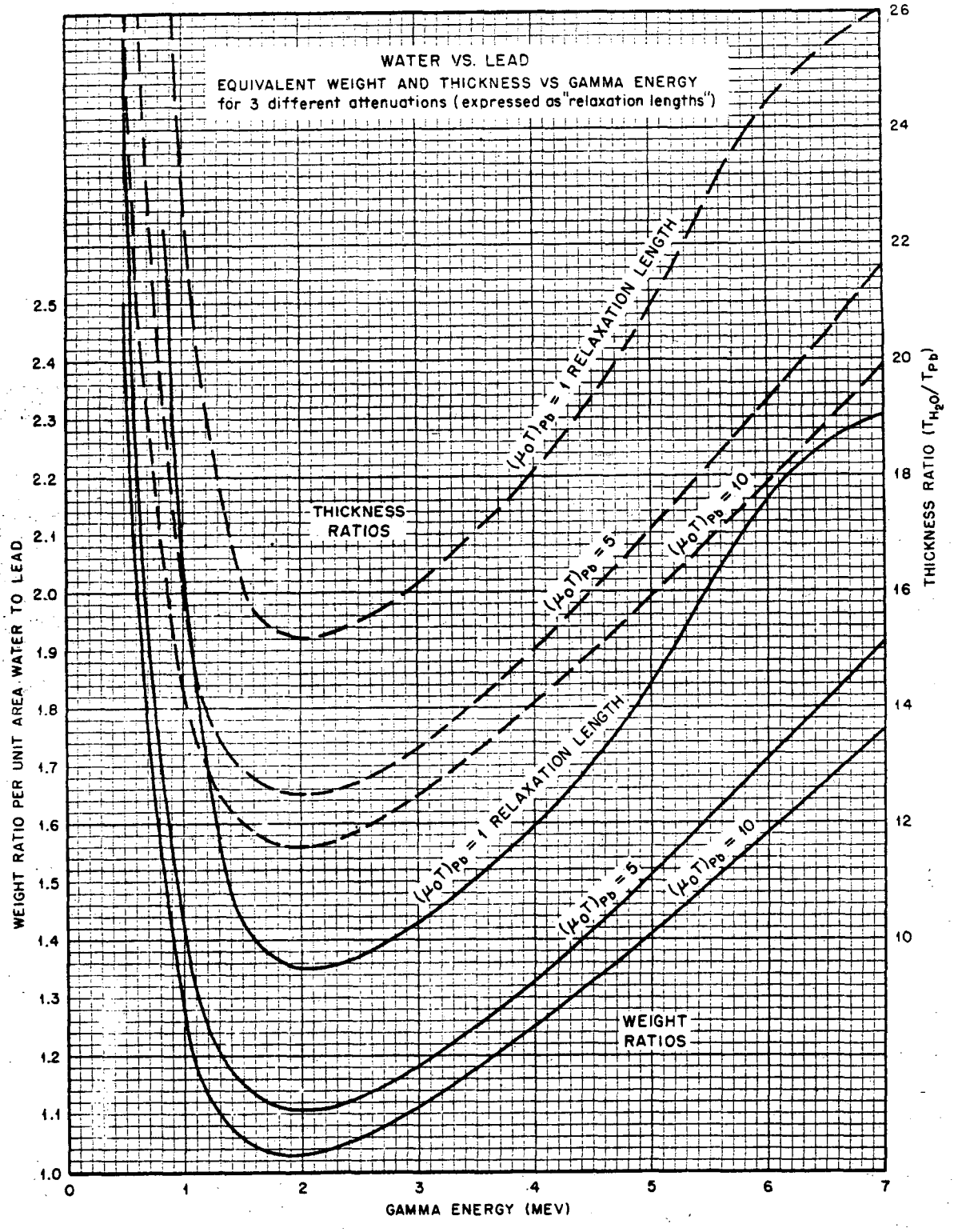

WATER VS. LEAD
EQUIVALENT WEIGHT AND THICKNESS VS GAMMA ENERGY
for 3 different attenuations (expressed as "relaxation lengths")
THICKNESS RATIOS
WEIGHT RATIOS
(μ0T)Pb = 1 RELAXATION LENGTH
(μ0T)Pb = 5
(μ0T)Pb = 10
WEIGHT RATIO PER UNIT AREA WATER TO LEAD
THICKNESS RATIO (TH2O/TPb)
GAMMA ENERGY (MEV)
2.5
2.4
2.3
2.2
2.1
2.0
1.9
1.8
1.7
1.6
1.5
1.4
1.3
1.2
1.1
1.0
26
24
22
20
18
16
14
12
10
0
1
2
3
4
5
6
7

Figure 6.5

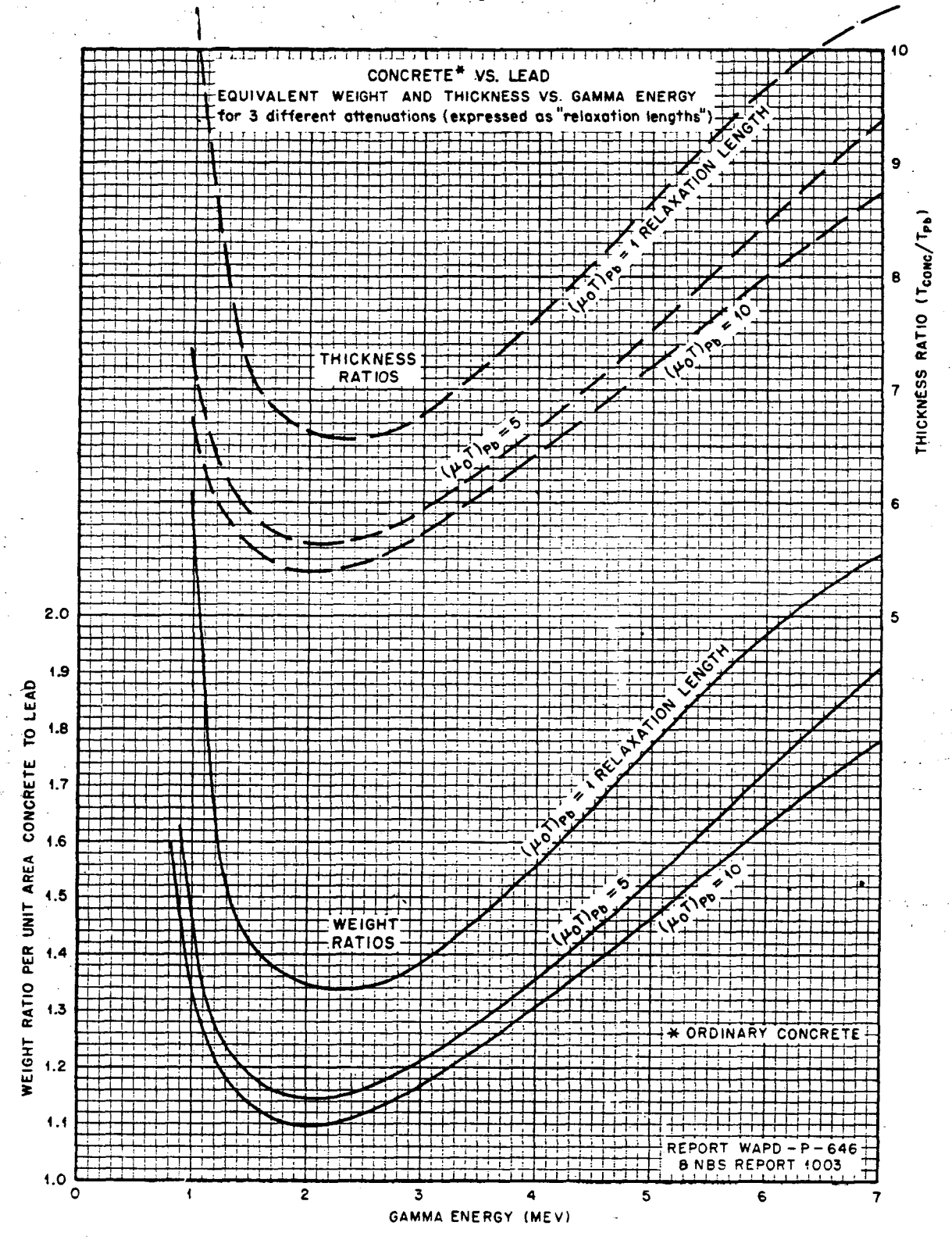

CONCRETE* VS. LEAD
EQUIVALENT WEIGHT AND THICKNESS VS. GAMMA ENERGY
for 3 different attenuations (expressed as "relaxation lengths")
THICKNESS RATIOS
WEIGHT RATIOS
(μ0T)Pb = 1 RELAXATION LENGTH
(μ0T)Pb = 5
(μ0T)Pb = 10
* ORDINARY CONCRETE
REPORT WAPD - P - 646
& NBS REPORT 1003
WEIGHT RATIO PER UNIT AREA CONCRETE TO LEAD
THICKNESS RATIO (TCONC/TPb)
GAMMA ENERGY (MEV)
1.0
1.1
1.2
1.3
1.4
1.5
1.6
1.7
1.8
1.9
2.0
5
6
7
8
9
10
0
1
2
3
4
5
6
7

Figure 6.6

density will be the same as for water since build-up and attenuation are the same. The thickness will increase by the density ratio.

As expected, the areal density ratio (wt./unit area) shows a minimum at about 2 Mev, where the absorption coefficient for lead assumes its lowest value. From Figs. 6.4 to 6.6 a table of thickness equivalents has been formulated (Table 6.11). It should be noted that for low-energy gamma rays, e.g., scattered radiation, lead is far superior to materials of low atomic number. At 0.1 Mev, for example, the iron-to-lead equivalent thickness is roughly 20; $\frac{1}{4}$ in. of lead equals 5 in. of steel! For this reason scatter shields should be made of lead.

Table 6.11 — EQUIVALENT THICKNESS (IN INCHES) OF VARIOUS MATERIALS PER 1-IN. THICKNESS OF LEAD FOR GAMMA RADIATION

	Iron		Water		Concrete	
Energy, Mev	$(\mu^0T)_{Pb} = 5$	$(\mu^0T)_{Pb} = 10$	$(\mu^0T)_{Pb} = 5$	$(\mu^0T)_{Pb} = 10$	$(\mu^0T)_{Pb} = 5$	$(\mu^0T)_{Pb} = 10$
0.10	21					
0.5	3.9	3.6	32.8	27.8		
1.0	2.2	2.1	16.0	14.3	7.2	6.6
2.0	1.8	1.7	12.5	11.6	5.6	5.4
3.0	1.8	1.8	13.3	12.5	5.9	5.7
4.0	1.9	1.9	15.0	14.2	6.7	6.4
5.0	2.1	2.0	17.1	15.9	7.5	7.2
6.0	2.3	2.1	19.3	17.9	8.5	8.0
7.0	2.4	2.3	21.6	19.9	9.4	8.8
8.0	2.5	2.3	23.8	21.9	10.0	9.4

3 FABRICATION AND INSTALLATION

3.1 Introduction

Where large attenuations of gamma-radiation intensities are desired, the use of lead instead of iron results in a weight saving of at least 30 per cent. If the shield must also serve as a neutron shield, some hydrogenous material, such as oil or water, may be an integral part thereof. In this case it is sometimes desirable to can the lead so that the liquid is in contact with only one metal. It is often important that the lead be bonded properly to structural supports by lead burning and that no voids exist between the lead and structural members. Lead may be installed in the form of castings of various thicknesses or in rolled layers to make up the design thickness. Where plastic is used as the neutron shield, the lead can be bonded to the structural materials in slabs with overlapping joints. The plastic can also be mounted as sheets, overlapping at the joints, and aluminum nails or fasteners may be used to minimize secondary high-energy gamma production.

In some rare instances bulky blisters of lead or steel can be avoided by placing a small amount of extra-heavy gamma shielding material into strategic locations. For this purpose tungsten, tungsten carbide, or some commercially available substitute may be used. The cost of these heavy materials must be balanced against the cost of the large blisters and the space they occupy. Some of the commercially available heavy materials are Mallory 1000 metal (P. R. Mallory & Co., Inc., Indianapolis 6, Ind.), Densalloy (Welded Carbide Tool Company, Clifton, N. J.), Fansteel 77 (Fansteel Metallurgical Corp., North Chicago, Ill.), and Hevimet (Carboloy Dept. of General Electric Co., Detroit 22, Mich.).

3.2 Design Details of Composite Gamma and Neutron Shields

A shield consists of several materials arranged to suit concurrent requirements for the following:

1. Structural support.
2. Liquid tightness and/or gas tightness.
3. Gamma-ray attenuation.
4. Neutron attenuation.

Material that is arranged for structural stability and for containment or exclusion of gas and liquids in the shield serves a dual purpose; in addition to its structural function, it is effective in attenuating gamma radiation and, to lesser extent, neutrons. Material used specifically for attenuation of nuclear radiation, e.g., lead for gammas and hydrogenous material for neutrons, must be joined to the structural material to form a unified structurally stable component of the plant.

Following are some concepts of shields that meet these requirements.

In Fig. 6.7 is shown a shield whose strength is contributed mainly by the steel structural support, a web plate, and, to a lesser extent, by a steel sheathing plate. The lead gamma shielding is bonded to the structure as shown in Figs. 6.8 and 6.9 (for further detail see the following sections) and is contained further by a sheathing plate which can be made tight if the adjacent hydrogenous material is a fluid. In the illustrations the hydrogenous neutron shielding is composed of polyethylene sheets which are secured to each other by a staggered arrangement of aluminum nails. Aluminum is recommended for the fastenings to minimize the effect of capture gammas. In placement of these sheets the butts and seams should be staggered to avoid gaps which create a direct path for radiation through the material. The polyethylene is covered by a light metal cover to protect against abrasion and hazards which may arise from flammability.

In Fig. 6.10 a later development is shown which has the sheathing plate outside the polyethylene instead of directly against the lead. This arrangement offers several advantages:

1. The sheathing plate serves as a flange on the beams or stiffeners. This makes the whole shield a very strong orthotropic plate which needs no external framing unless the span is very great. Thus weight is saved by distributing the structural material efficiently. The plate serves three ways: as shock support, flange, and part of shielding.
2. The sheathing plate is convenient for the attachment of wireways, pipe hangers, and miscellaneous foundations.
3. No sheet metal is required for fire prevention.
4. Water cannot seep around the polyethylene and corrode the structure.
5. Air tightness will be much easier to achieve because the side of the shield which is accessible when under test can be made tight.

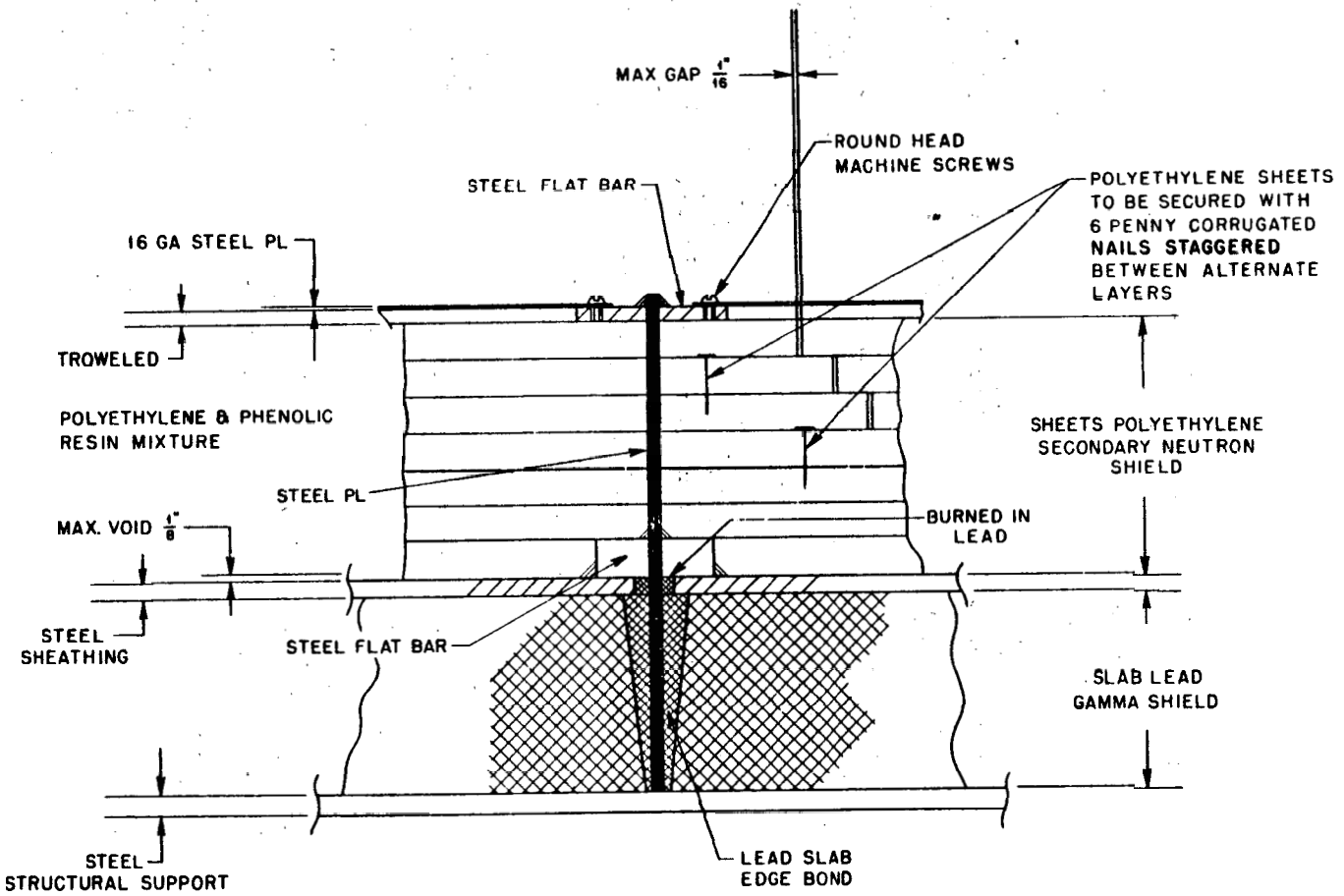
For these reasons, this type of design is generally preferable to that shown in Figs. 6.7 to 6.9.

Figure 6.11 shows an alternate method of installing lead shielding, which can be used economically in a limited number of locations where no polyethylene is required over the lead. It lacks some of the advantages described above (items 1 to 3) for the other method, but in some locations these features are not required. In such cases this alternate method offers the convenience of shop prefabrication. Adequate shock strength is obtained by full surface bonding of the lead to a thin steel backing plate. Edge bonding to steel in this case is not required. However, lead is burned to lead to seal all seams and butts and to patch around foundations or other penetrations.

The use of edge bonding is the most satisfactory method for eliminating gaps around the boundaries of slabs of lead. It also provides good resistance against impact loading. However, since tests have indicated that edge bonding alone is not completely dependable for shock support, the sheathing plate provides additional support.

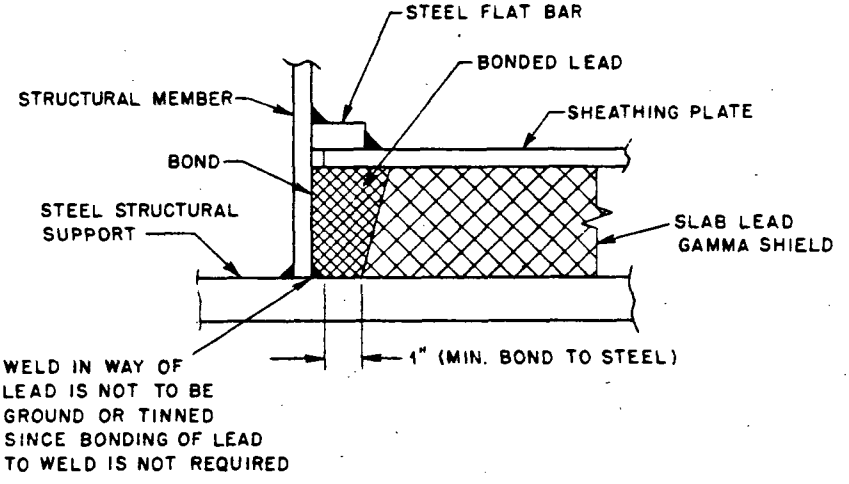
3.3 Installation of Lead Shielding

(a) Casting of Slabs. Lead slabs are cast to thicknesses required by the shield plans with a tolerance of plus $\frac{1}{16}$ in. minus zero. Lead slabs more than 1 in. thick are cast. Those slabs under 1 in. are full-bonded to steel backing plates; the required shield thicknesses are obtained



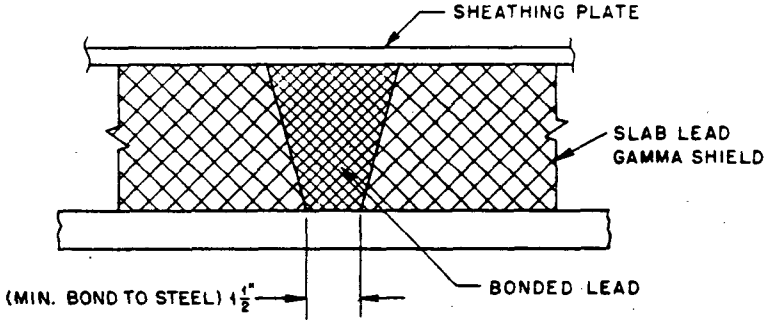
TYPICAL SHIELD SECTION

Figure 6.7



TYPICAL SHIELDING AT EDGE BOUNDARIES

Figure 6.8



TYPICAL SHIELDING AT PANEL SEAM

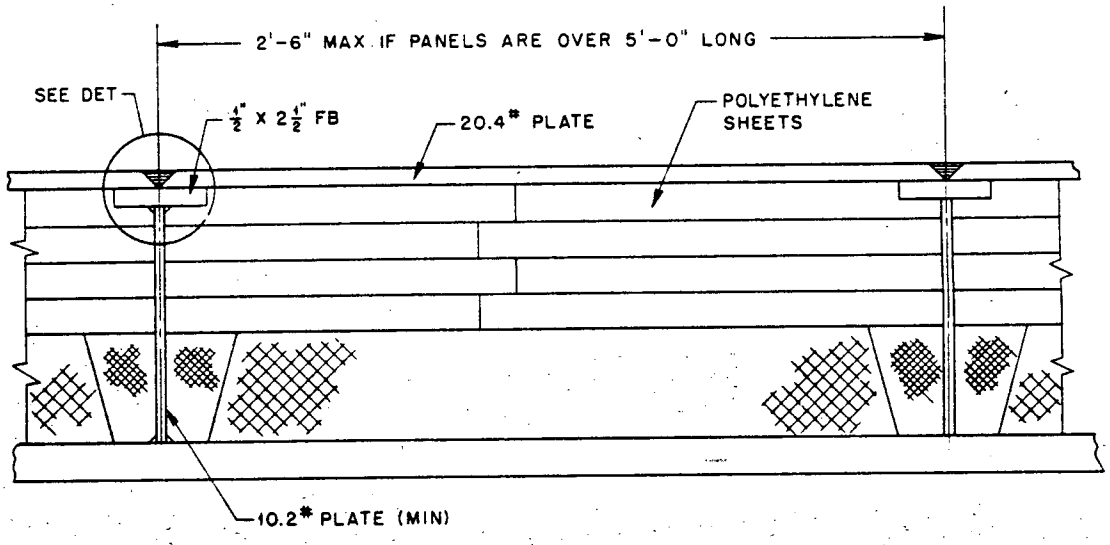
Figure 6.9

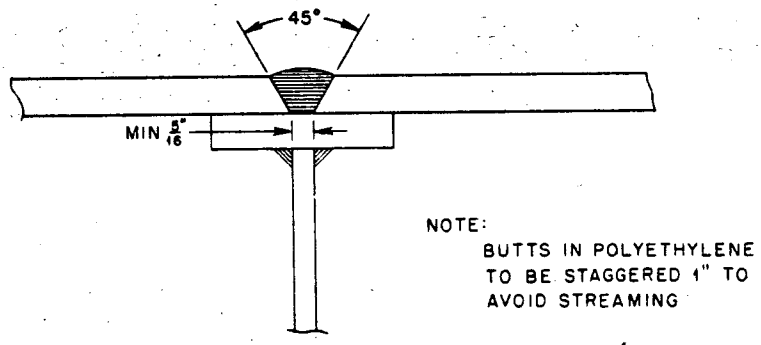
either by casting the lead on the backing plate or by building up the slab by hand or machine burning.

(b) Inspection of Lead Slabs for Voids.[8] Some of the lead slabs should undergo radiographic inspection. The number of lead slabs to be gamma-graphed should be sufficient to assure a good sampling of all slabs (at least 5 per cent of all slabs over 2 in. thick). Thinner slabs are harder to cast; therefore greater sampling should be used (a minimum of 15 per cent of the total number cast). The arrangement of lead slabs for radiographing is shown in Fig. 6.12. The exposure times are determined from the source strength, distance from source to slab, slab thickness, and type of film. As an aid in determining exposure times, a curve of gamma attenuation through lead for different source strengths for a Co^{60} source is shown in Fig. 6.13, and dose as a function of distance in air is plotted in Fig. 6.14. The gamma attenuation through the lead is given as dose rate in milliroentgens per hour; therefore, if we know the sensitivity of the film and the dose rate, we can determine the correct exposure time for each slab.

Standards should be set up in order to permit determination of the extent of a flaw by visual inspection of the radiograph. The standards should consist of Kodak 14 by 17 in. type K

TYPICAL DETAIL OF
DECK OR BULK HEAD SHIELDING
WITH LEAD & POLYETHYLENE





TYPICAL WELD DETAIL

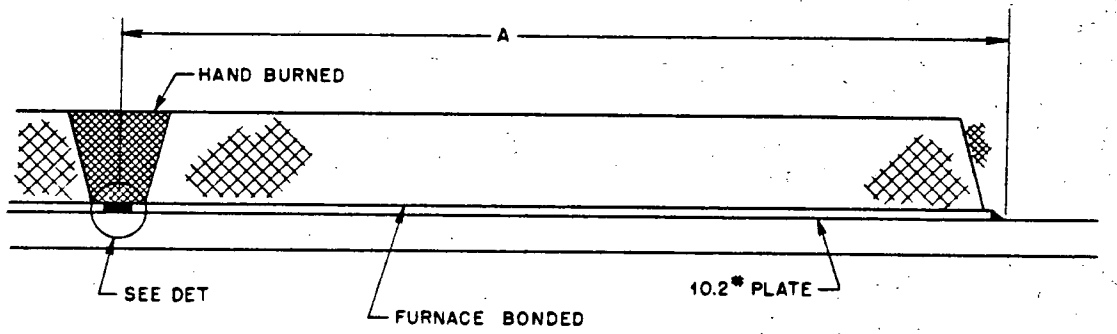
Figure 6.10

X-ray film, or equivalent, exposed through penetrameters. The penetrameter construction is shown in Fig. 6.15, and one should be constructed for each basic thickness of lead slab to be employed. From these standard radiographs of known size voids, the approximate volumes of voids found in radiographs of test slabs can be determined. Standard radiographs also serve as an aid in checking proper exposure times for desirable density and contrast. Figure 6.16 is a photograph of exposure through a typical penetrameter.

After the standards have been established, calculate what size flaws will be acceptable and prepare a list showing depth of flaw and maximum permissible areas. This can best be done by preparing a curve such as Fig. 8.30 in Chap. 8. This curve shows dose increase as a function of void area with flaw depth as parameter. A typical radiograph of a flaw is shown in Fig. 6.17. Figure 6.18 is a photograph of a flaw in a lead slab.

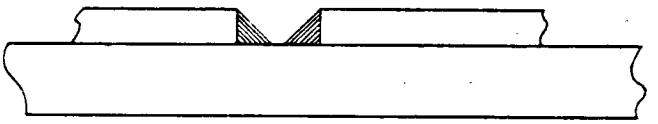
Spot checks of *full-bonded* steel-backed slabs are made by similar radiographic examination prior to being welded in place to ensure that a satisfactory bond has been obtained and flaws or voids are within the limits of acceptability.

TYPICAL DETAIL OF
BULKHEAD SHIELDING LEAD
ONLY



DIMENSION "A"	LEAD THICKNESS
24" MAX	0 – 2"
20" MAX	2" – 3"
18" MAX	3" – 4"

NOTE:
LEAD TO BE CUT TO SUIT NEAR FOUNDATIONS. HAND BURN LEAD TO REPAIR SHIELD NEAR FOUNDATIONS. CUT THRU BACKING PLATE FOR FOUNDATION ATTACHMENTS.



TYPICAL WELD DETAIL

Figure 6.11

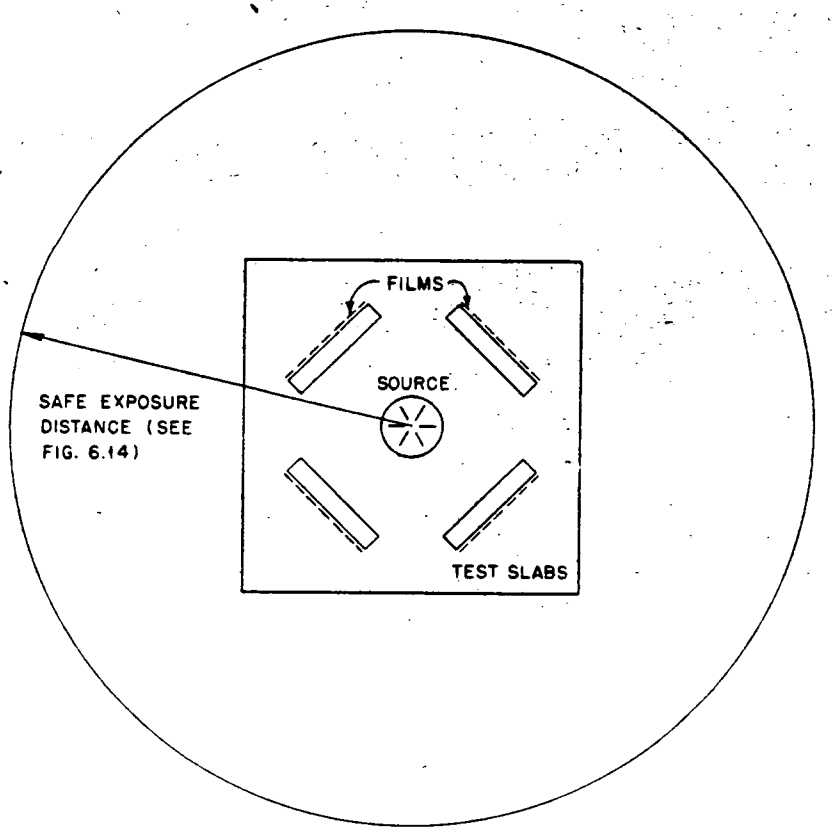


Figure 6.12

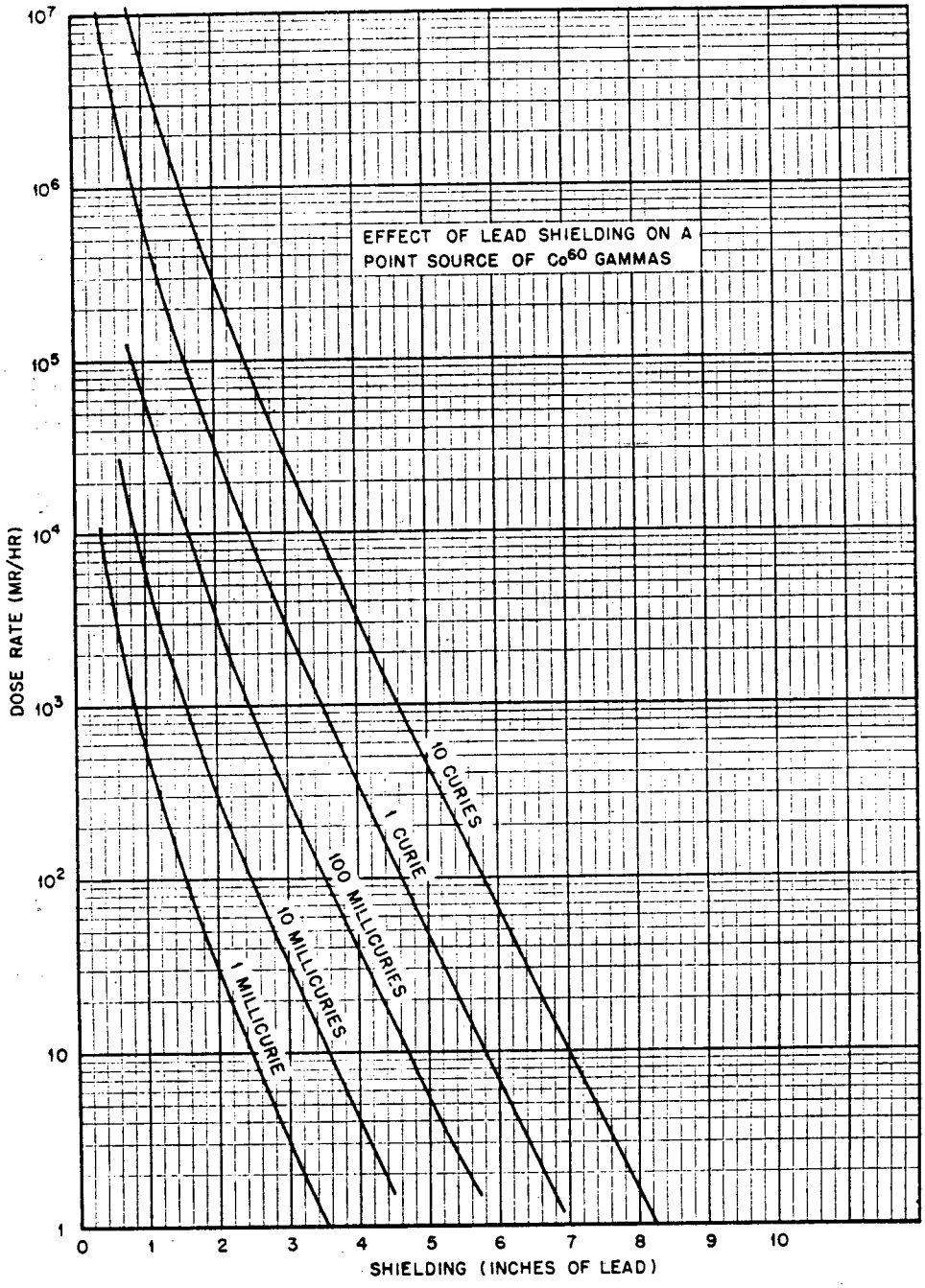

EFFECT OF LEAD SHIELDING ON A POINT SOURCE OF Co^{60} GAMMAS
DOSE RATE (MR/HR)
10^7
10^6
10^5
10^4
10^3
10^2
10
1
0 1 2 3 4 5 6 7 8 9 10
SHIELDING (INCHES OF LEAD)
10 CURIES
1 CURIE
100 MILLICURIES
10 MILLICURIES
1 MILLICURIE

Figure 6.13

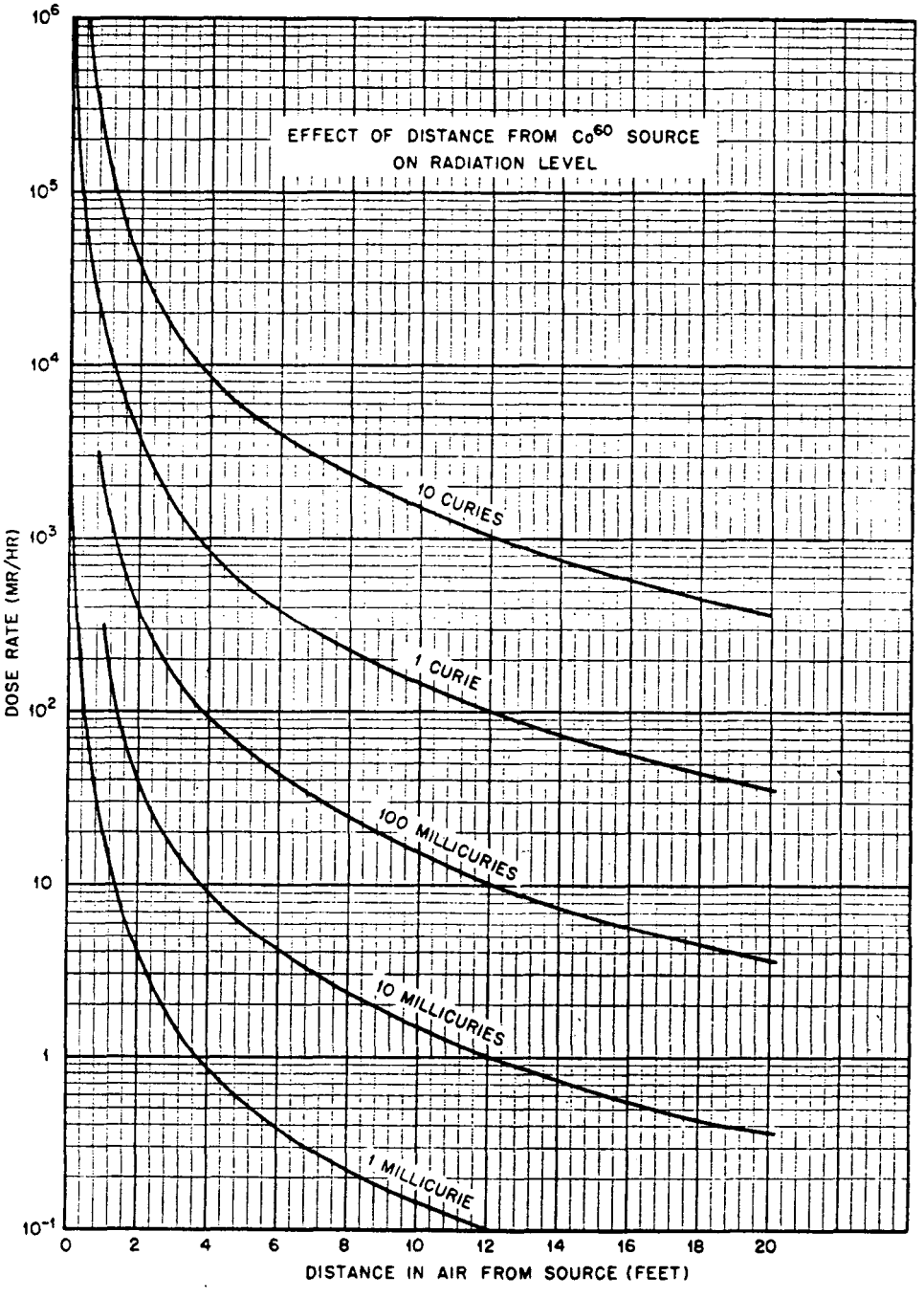
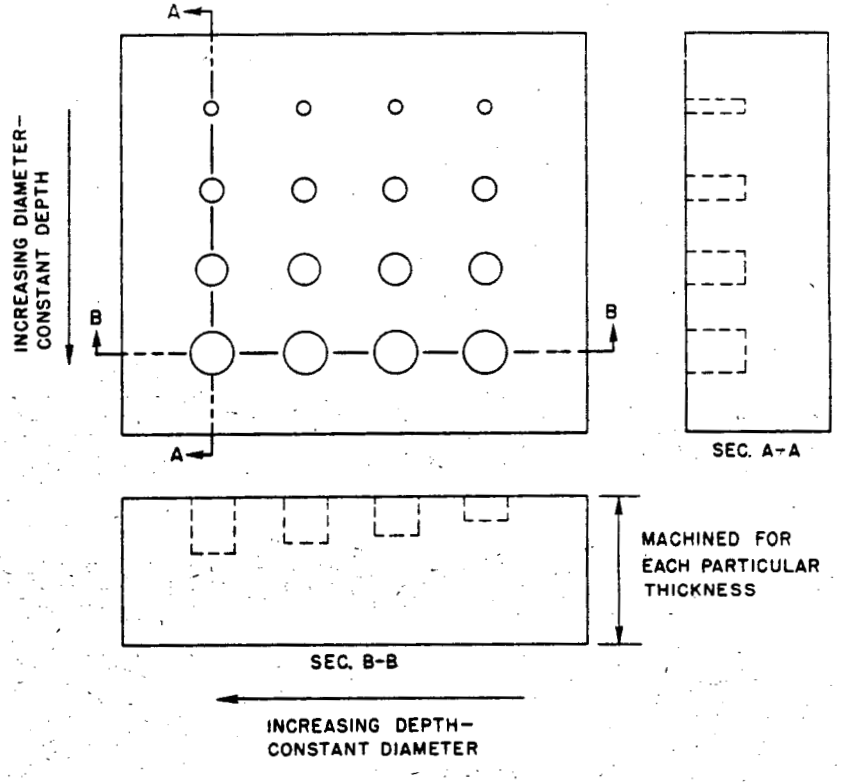

EFFECT OF DISTANCE FROM Co60 SOURCE
ON RADIATION LEVEL
DOSE RATE (MR/HR)
10^6
10^5
10^4
10^3
10^2
10
1
10^-1
10 CURIES
1 CURIE
100 MILLICURIES
10 MILLICURIES
1 MILLICURIE
0
2
4
6
8
10
12
14
16
18
20
DISTANCE IN AIR FROM SOURCE (FEET)

Figure 6.14

TYPICAL PENETRAMETER CONSTRUCTION
MATERIAL: LEAD



NOTE: DIMENSIONS MAY VARY BOTH IN DIAMETER AND DEPTH IN ANY SET OF INCREMENTS DESIRED, I.E., $\frac{1}{16}$", $\frac{1}{8}$", ETC. PREFERABLY, THE SMALLER THE INCREMENTS, THE MORE ACCURATE THE STANDARD, BUT THIS NECESSITATES A PENETRAMETER OF LARGER AREA.

Figure 6.15

The following equipment is necessary for the execution of the radiograph test:

1. A high-intensity gamma source; for some slabs the minimum source requirements will be as much as 50 curies for Co^{60}.
2. A shielded container for the source.
3. A positioning device for the source.
4. Film holders.
5. Film (type K X-ray film by Kodak, or equivalent, size 14 by 17 in.).
6. Densitometer.
7. Calibration pieces.
8. Film-developing facilities.

The cast lead slabs have proved to be relatively free of voids. Inspection of lead slabs for the *USS Nautilus* resulted in a rejection of 10 lead slabs from a total of 110 slabs tested, about 10 per cent.

(c) Preparation of Steel Surfaces for Lead Bonding. Steel surfaces to which lead will be bonded must be mechanically and chemically clean.

Mechanical cleaning is accomplished by scraping, scaling, grinding, and/or wire brushing; the best method is grinding. Surfaces should be tinned within 24 hr after cleaning. Sand blasting is particularly bad due to the deposition of a thin coating of silica which remains to

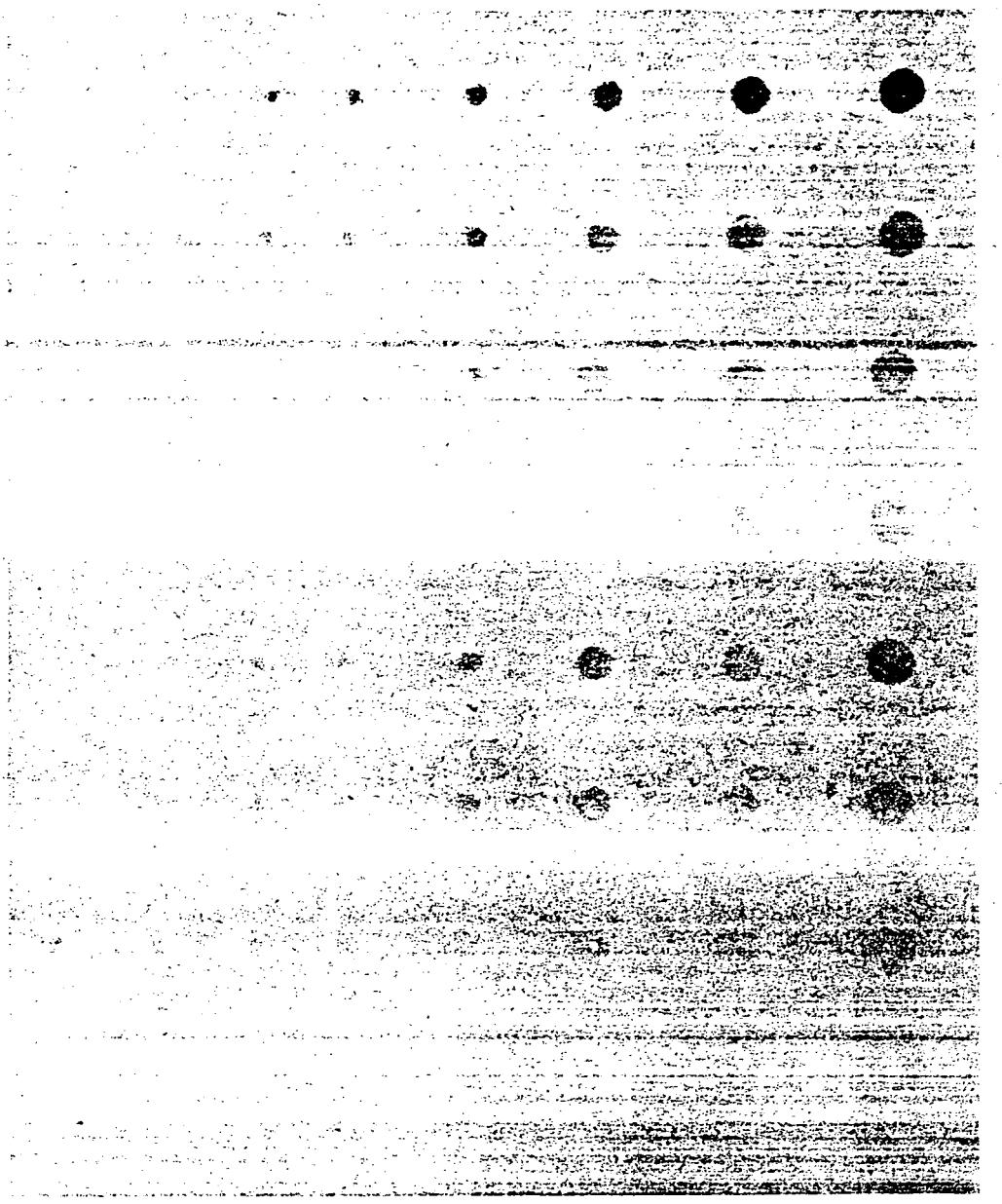


Fig. 6.16— Photograph of exposure through a typical penetrameter.

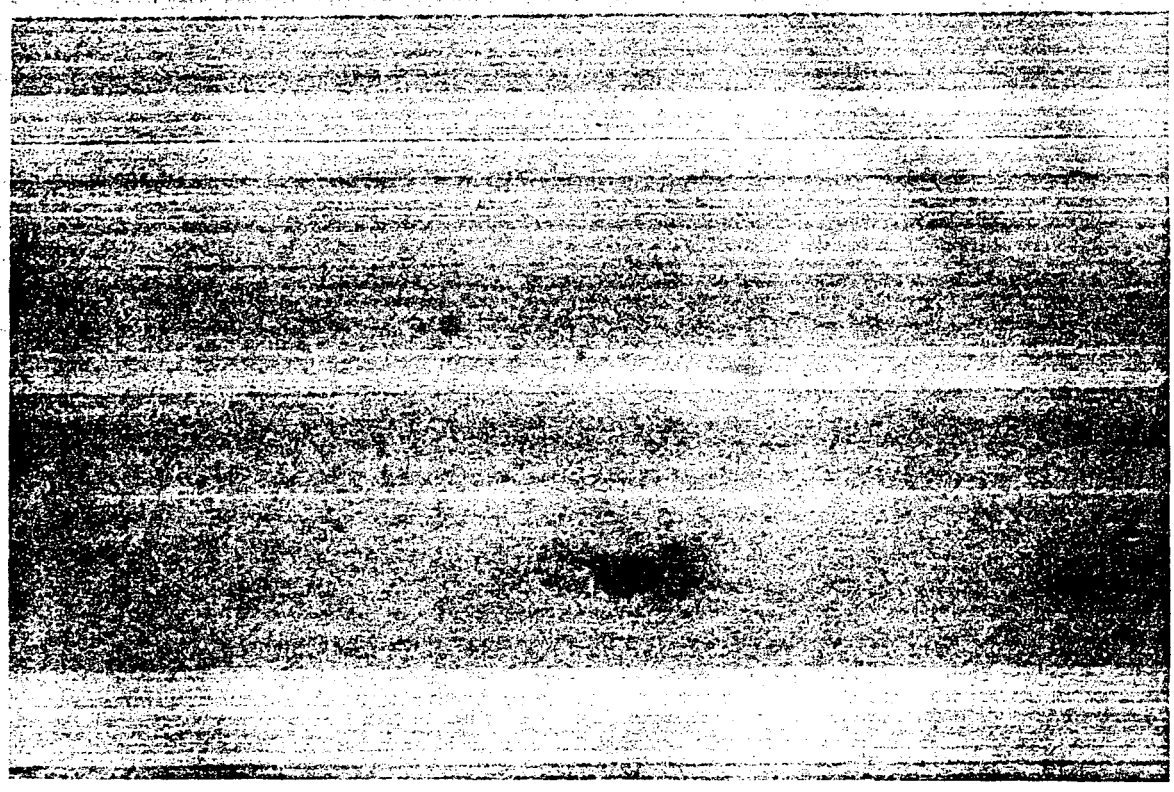


Fig. 6.17—Radiograph of flaw in lead slab.

hamper the tinning operation. Disk sanders leave a surface which is too smooth to receive the tinning lead satisfactorily.

Chemical cleaning of the surface is accomplished by washing with 50 per cent muriatic acid (HCl) and then with cold water.

Tinning consists of brushing the steel surface with 50 per cent zinc chloride solution, then heating the steel with a torch and flowing on a solder made with 50 per cent tin and 50 per cent commercial lead. After the tinning operation the surface should not be exposed to the weather for more than four days. Extreme care should be taken to apply the correct degree of heat. Since the fumes caused by the tinning operation are very toxic, each lead burner engaged in tinning should have the necessary equipment to protect him from these gases.

(d) Bonding. Bonding of the lead-to-steel surfaces extends the full length of the joint for all joints except in the weld-metal region; see Fig. 6.19 for positioning of lead slabs before bonding. Where the lead slabs are bounded by steel structure, the lead is bonded to the shielded steel surface for a distance of 1 in., measured from the edge of the weld metal and to the boundary structure for the full thickness of the lead except near weld metal (see Fig. 6.20). The thickness of the deposited filler metal is made equal to the thickness of the parent metal (lead slab). Figure 6.21 shows the deposited filler metal during one of the intermediate stages. After the lead has been burned into corners near welds, it is calked to ensure tightness.

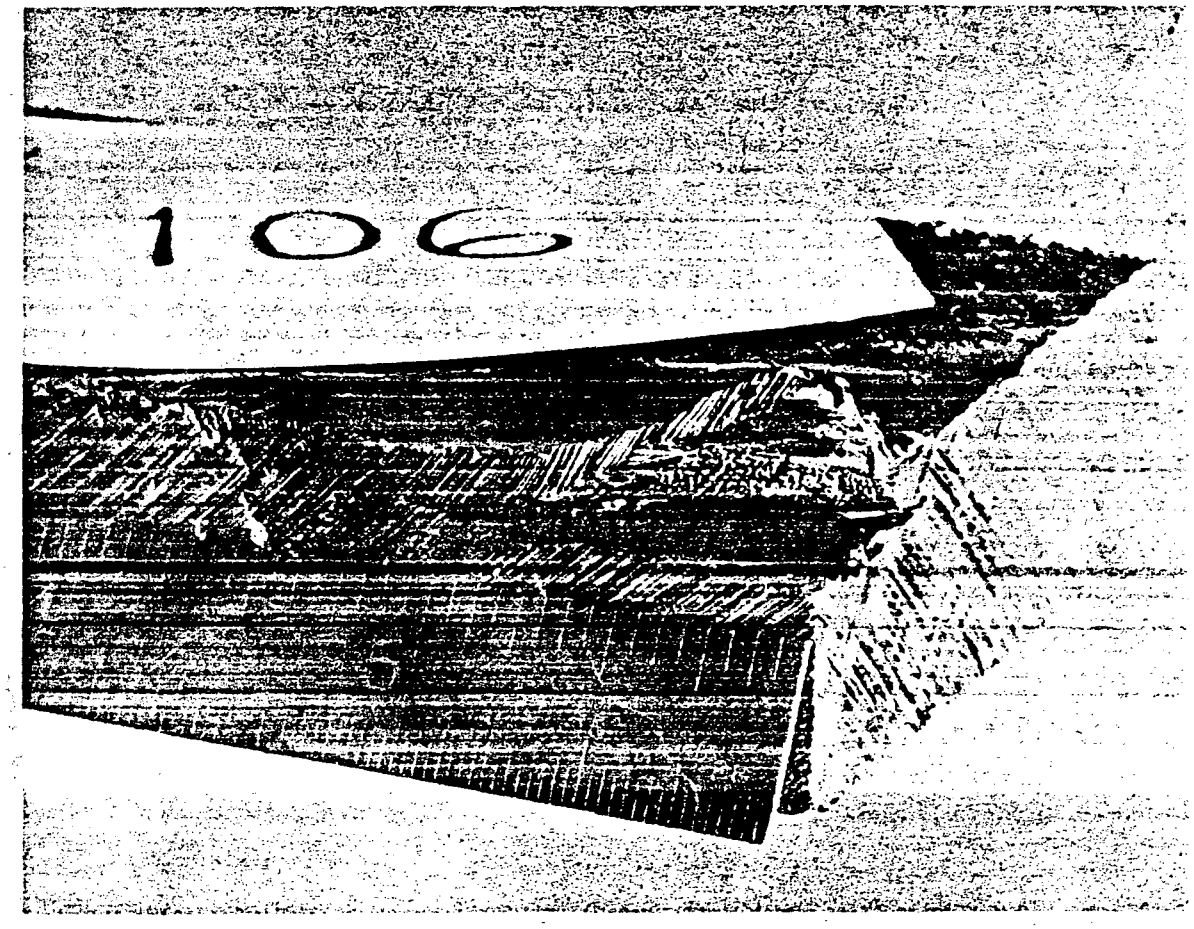


Fig. 6.18—Flaw in lead slab.

Excess filler metal is usually deposited at the corners during the burning process to provide calking material.

Butts between adjacent lead slabs not separated by steel structure are bonded to the shielded steel surface for a width of at least $1\frac{1}{2}$ in. along the full length of the joint except in the case of slabs or layers $\frac{3}{4}$ in. thick and under, which are bonded for a width of $\frac{3}{4}$ in. The thickness of the filler metal is equal to the thickness of the lead slabs with a tolerance of plus $\frac{1}{16}$ in. minus zero. These intermediate butt joints are spaced no more than 30 in. apart on vertical surfaces or more than 48 in. apart on horizontal surfaces.

When a full-bonded steel-backed slab is welded in place, the space between adjacent slab edges or between slab edges and steel structure is filled and bonded by hand burning.

Lead-wool calking, where required, is tightly and evenly packed to maximum density to eliminate all voids. However, a penetration through a lead slab which is calked rather than bonded will not stay tight because of the difference in the coefficients of thermal expansion of lead and steel; this will not be enough to cause gamma streaming, however.

(e) Installation of Sheathing Plates. It is not advisable to install any steel sheathing plates in a given area until lead burning is complete on all adjacent areas and until it is allowed to cool for at least three days. During this cooling period defective lead-to-steel bonding will be evidenced by shrinkage gaps. Experience shows that only fillet welds should be used on sheathing plates; lap joints are preferable, and a good welding procedure should be set up for each section of the shield. Extreme care should be taken to ensure that no welding is done on a tinned area so that lead inclusions will not impair the welding of the canning plate.

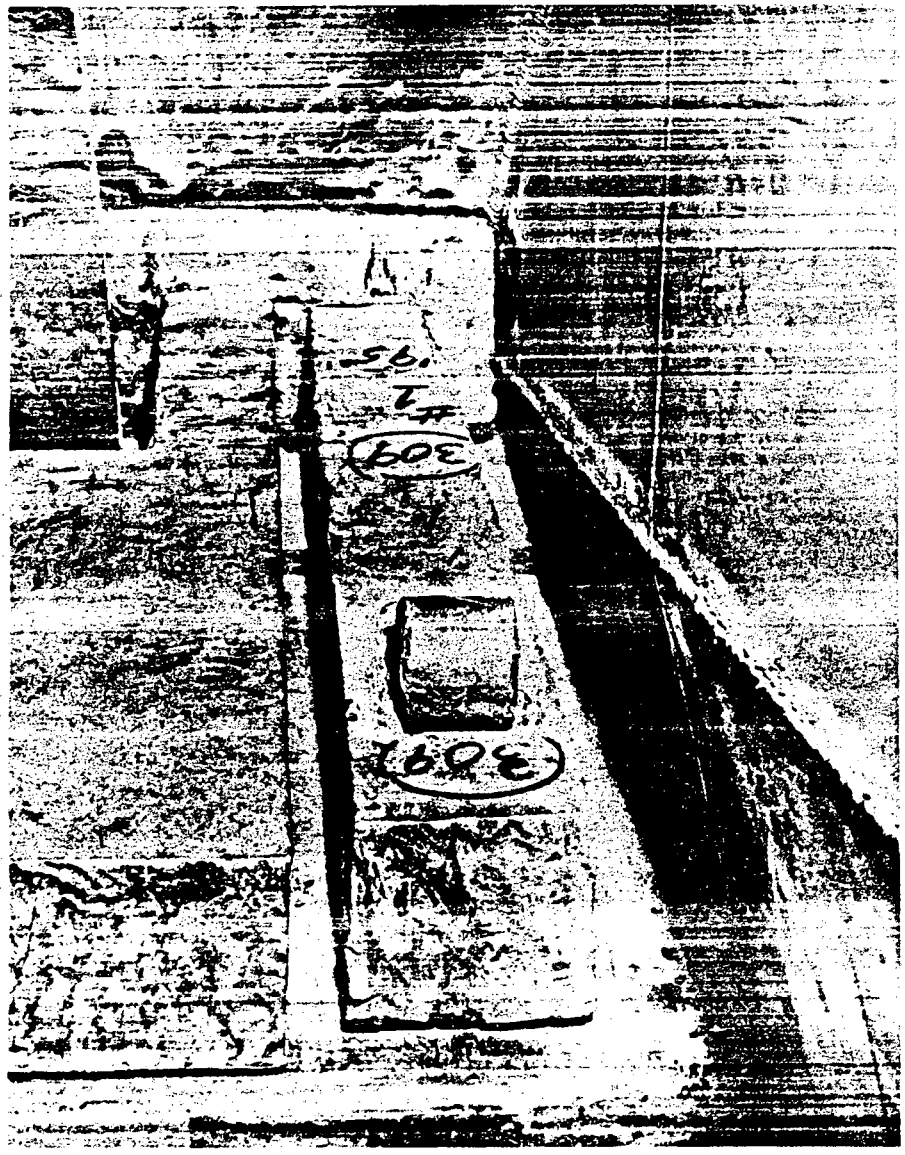


Fig. 6.19 — Positioning of lead slabs before bonding.

(f) Inspection of Seams After Lead Installation.[9] After installation, all seams are visually inspected to determine that the required bond has been obtained. In addition, radiographic inspections are conducted on those seams deemed acceptable by visual inspection for a minimum of 5 per cent of the total seam length. Seam inspection of the installed shield should be conducted over a good sampling of all seams. The selection of seam lengths should be concentrated on areas where difficulty of shield installation is apparent. If unsatisfactory seams are found, the test area should be enlarged in the vicinity of the defective section, and all defects should be repaired and reinspected to the satisfaction of the responsible inspector.

The equipment needed for this test is described below:

1. A Co^{60} source (100 mc strength or less will do in most cases); this can easily be handled on the end of a 5- to 6-ft pole (see Fig. 6.14 for dose rates).
2. Source holders, preferably magnetic.
3. Shielded container for source when it is not in use.

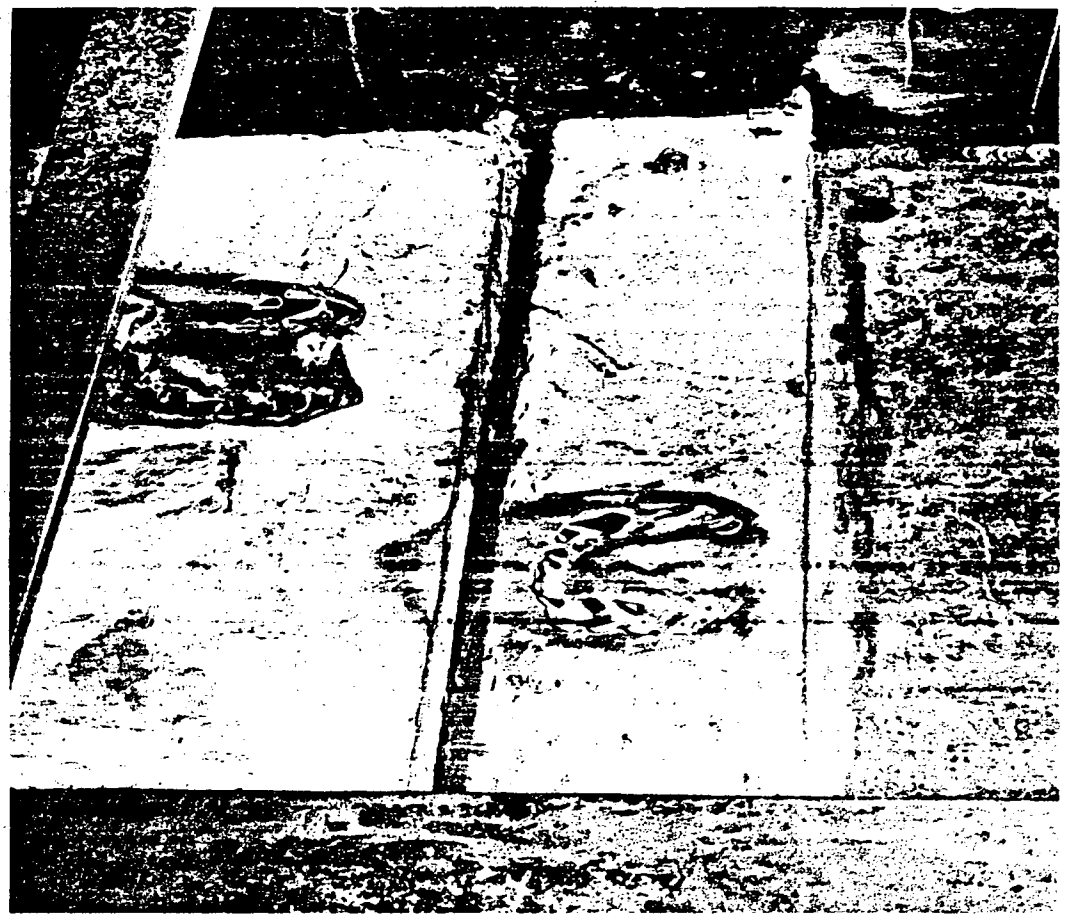


Fig. 6.20 —Bonding of lead slabs to structure.

4. A typical detector (Fig. 6.22) consists of an aluminum probe assembly (scintillation counter) combined with a high-voltage supply and electrometer.

(a) The scintillation counter consists of an anthracene crystal, an RCA No. 5819 photomultiplier tube (or equivalent), a metal tube shield, a lucite pipe to conduct light from the crystal to the tube, and all necessary wiring.

(b) The anthracene crystal is the sensitive element of the detector, and its dimensions should be approximately that of a 1- by 1-in. cylinder.

(c) The low-drift a-c electrometer should be built according to an Oak Ridge National Laboratory design or equivalent (see the wiring diagram of Fig. 5 of Report ORNL-CF-51-10-212).

(d) The high-voltage supply may consist of either three 300-volt batteries or a negative power supply equivalent to Atomic Instrument Co. model 316.

Procedure. The work generally must be performed during off-shift hours owing to the potential radiation hazard involved. Three people are required to carry out this test efficiently.

1. First, a seam suitable for testing must be selected. Such a seam must (a) allow positioning of a radioactive source on one side of it without excess difficulties and exposure of personnel and (b) offer a clear and accessible area on the opposite side so that measurements can be made by a man holding the detector.



Fig. 6.21—Deposited filler metal during an intermediate stage.

2. The source must be located as close to the center line of the seam as possible, preferably by a predetermined measurement. At a vertical shield section the source may simply be suspended, whereas on horizontal sections magnetic source holders should be employed.

3. Preliminary traverses (see Fig. 6.23) should then be taken with the detector on the opposite side of the shield in order to locate, from the detector side of the shield, the source position and any possible air gaps that might exist. This is done by finding the peak reading on the electrometer along traverses in both directions parallel to the shield.

4. The detector is then held at the point of the maximum reading, and the source is moved in small increments in an effort to improve alignment of the source with any possible gap. This determines immediately the existence or nonexistence of an air gap along the seam since the existence of an air gap will produce a sharp increase in the electrometer reading as soon as proper alignment is achieved.

5. With the source stationary in its optimum position, traverses are taken with the detector across and along the seam. This is done by recording the electrometer readings at 1-in. intervals or less. Failure of the gamma level to fall off appreciably as the detector moves along the seam away from the peak point is also indicative of an existent air gap. The traverses taken across the seam can be used to determine the results with those obtained in a laboratory mock-up [see (6) below].

6. Simple mock-ups of sample sections of the seams should be constructed in a laboratory experiment, using various widths of existing air gaps. Traverses should be taken with the same instruments as used in the field inspection. Results can be used to predict accurately the size of any existing gaps. A sample lead-iron seam mock-up test is described in the following paragraphs.

7. Calculations must be made to determine the maximum permissible size of gaps so that the inspectors will reject only those seams which fall outside this limit (see Chap. 8, Sec. 3.6d).

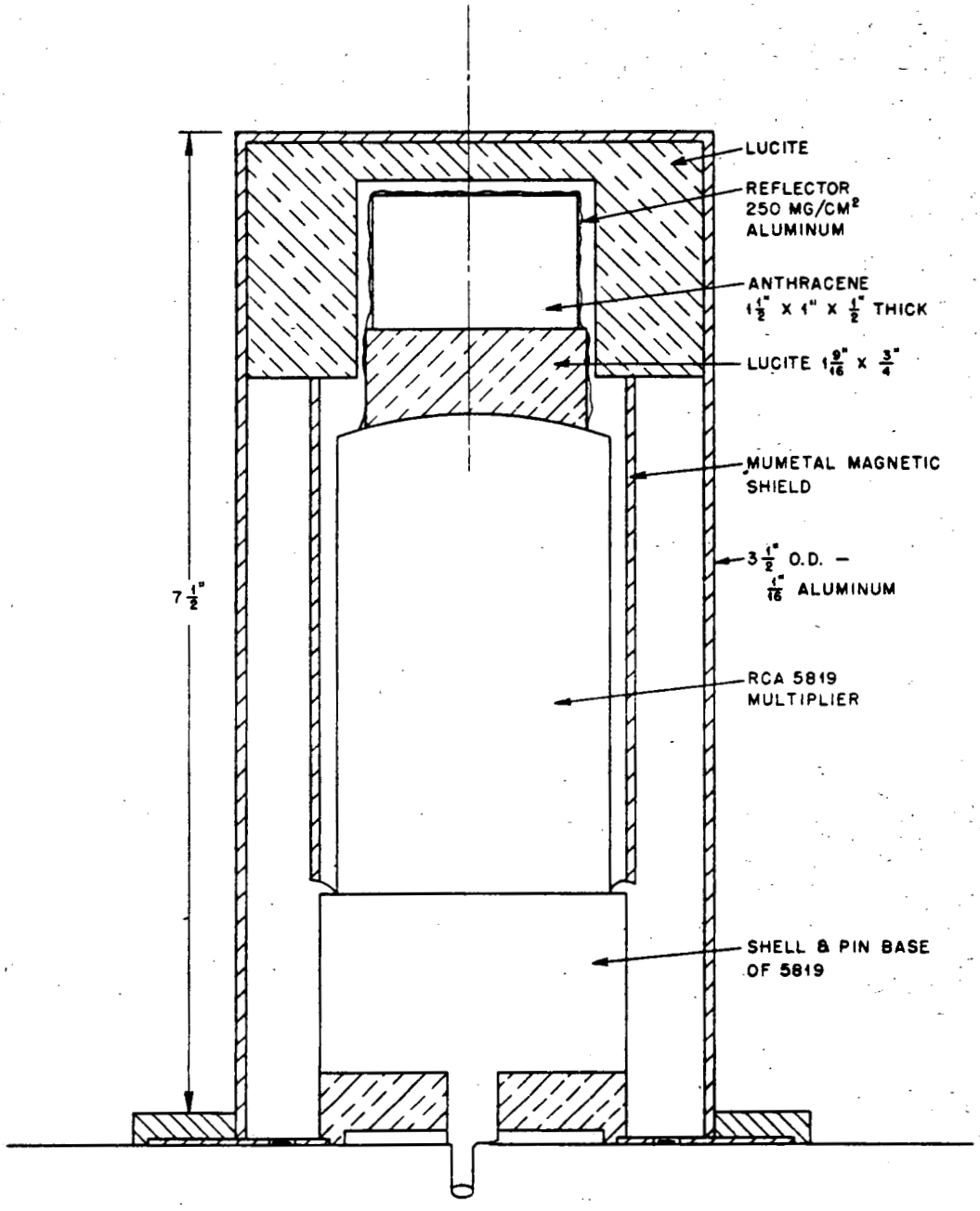


Figure 6.22

Sample Lead-Iron Mock-up Test of Seams. A mock-up of a typical shield seam condition is represented by two iron plates welded into a T shape to represent the shield surface and a structural support member. Inverting the T and placing closely machined lead bricks on the cross piece of the T results in a lead-to-iron seam condition on either side of the vertical member (see Fig. 6.24). The lead bricks can be increased in number to give several different shield thicknesses, and gaps of measured width can be opened along one of the seams.

The Co^{60} source is positioned above the lead on the vertical piece, directly over the seam in which the gap is opened. The distance from the source to the iron surface of the shield must remain the same throughout the mock-up and actual test (~15 in.).



Fig. 6.23 — Detector survey.

Scintillation counter readings taken across the seam on the surface of the bottom iron plate show a well-defined peak beneath the gap. A series of curves can be obtained showing the peak meter reading obtained across any size gap for different lead thicknesses (Fig. 6.24).

The procedure followed in making the actual seam test differs slightly from the mock-up test. With the source positioned along a seam, a grid pattern is laid out on the shield surface, with the center of coordinates opposite the source and one axis lying adjacent and parallel to the seam. Meter readings across and along the seam establish the exact position of the source and the width of any gap occurring at that point. Readings taken along the seam line for 1 ft to either side of the source give an indication of the condition of about 2 ft of seam length. Any deviation from a smooth-curve fall-off as the meter moves away from the source indicates an irregularity. Replacing the source opposite the point of the irregularity will give a measure of its magnitude. All readings are taken with the detector stationary against the shield. The counter should be calibrated before the mock-up test, and this calibration should be repeated before and after each test.

Innovations can be made to adjust this test to any particular type of shield construction. A modification has also been used to check lead-lead seams. Results have been obtained which indicate that this test will measure the width of gaps to within a few thousandths of an inch.

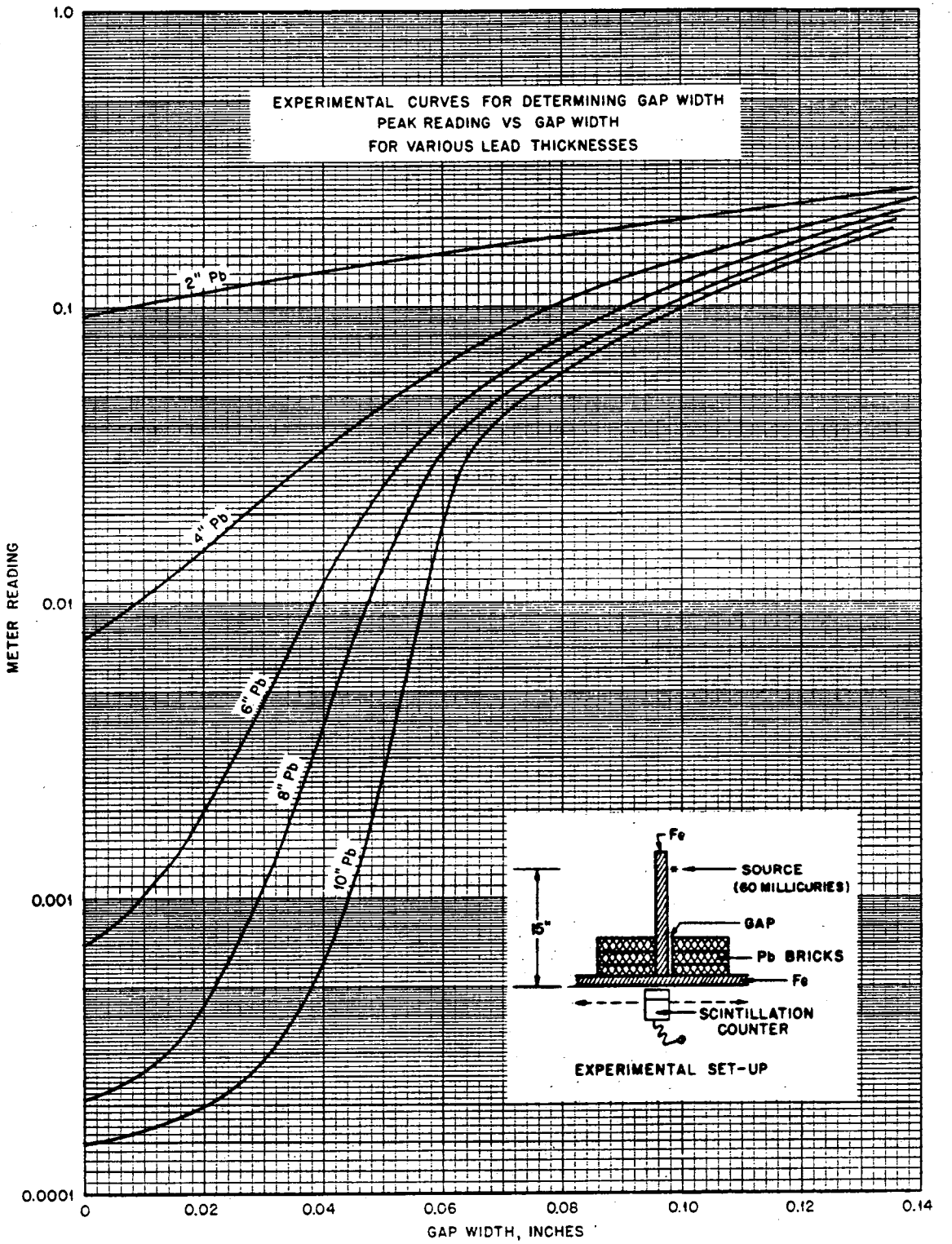

EXPERIMENTAL CURVES FOR DETERMINING GAP WIDTH
PEAK READING VS GAP WIDTH
FOR VARIOUS LEAD THICKNESSES
METER READING
1.0
0.1
0.01
0.001
0.0001
2" Pb
4" Pb
6" Pb
8" Pb
10" Pb
0
0.02
0.04
0.06
0.08
0.10
0.12
0.14
GAP WIDTH, INCHES
Fe
SOURCE
(60 MILLICURIES)
15"
GAP
Pb BRICKS
Fe
SCINTILLATION
COUNTER
EXPERIMENTAL SET-UP

Figure 6.24

4 OPERATIONAL TESTING

4.1 Objectives

The first objective of an operational shield test is to determine whether regions exist outside the shield where radiation levels exceed the design specifications and to give data for correcting any unsatisfactory conditions. In general, this objective can be attained by making appropriate radiation measurements under actual operating conditions in regions to which personnel will have access.

The shield test may also have, as a second objective, the procurement of as much data as possible on the radiation fields within the shield materials and within inaccessible regions of the nuclear power plant. Such data will enable the shield designer to test the accuracy of his calculations and will provide much valuable data for the design of future shields. For instance, a knowledge of the neutron fluxes permits prediction of the build-up of induced activities in the materials of the shield and in any impurities that exist in these materials. This information is especially important in predicting permissible personnel accessibility to components of the nuclear power plant, even long after reactor shutdown. Neutron and gamma measurements also help predict the amount of radiation damage, corrosion, and gas evolution that will occur in shield materials.

Section 4.2 gives a survey of instruments suitable for use in a shield test. Section 4.3 discusses calibration of the instruments, and Sec. 4.4 discusses the planning and procedure of a typical test.

4.2 Radiation Measuring Instruments

(a) Instruments for Measuring Dose Rates. In order to evaluate the biological effectiveness of a shield, it is necessary to use instruments that can be calibrated to give the radiation dose which would be imparted to human tissue. The radiation dose is obtained separately for gamma rays, fast neutrons, and thermal neutrons. The biological dose from gamma rays and fast neutrons is proportional to the energy lost by the radiation in passing through tissue. Accordingly, the gamma-ray and fast-neutron detectors should have absorption characteristics similar to human tissue. The biological dose from thermal neutrons, however, is proportional to the number of thermal neutrons absorbed in the body; therefore the thermal-neutron detector must measure the thermal-neutron *flux*.

Instruments used in surveying a biological shield should have the following features:

1. They must be rugged and must retain their calibration and response characteristics under strenuous usage.
2. The detector portion should be small and easy to position at the desired measurement points.
3. They must be capable of calibration to give accurate dose-rate readings in the energy range of reactor gammas and fast neutrons.
4. They should be simple to operate and should give quick readings.

If accurate data are required, the use of portable detectors with remote reading instruments will generally give more consistent and better correlated data than the self-contained type. Self-contained battery-powered instruments are convenient and may be satisfactory. They are usually less reliable, but some models are now quite good.

(b) Instruments for Obtaining Design Data. The choice of these instruments will depend on the nature of the data desired. The following paragraphs recommend types of instruments for measuring biological dose and for obtaining design and operational data. Table 6.12 lists commercial instruments which have been used in shield tests.

Gamma-radiation Instruments. (1) Scintillation Counter: This detector consists of an anthracene crystal and a photomultiplier tube. The dose-measuring process consists in measuring the current output of the photomultiplier tube produced by light formed in the anthracene crystal. The light intensity is proportional to the amount of ionization formed in

the crystal. The anthracene crystal is similar in composition to human tissue; therefore the ionization formed in the crystal is a reasonable measure of the energy that the gamma rays would lose in human tissue. The current output of the tube, therefore, is proportional to the biological dose. The complete setup consists of the detector, an electrometer to measure the current, and a high-voltage supply for the photomultiplier tube. This method is more completely described in reference 1.

(2) Ionization Chamber: This detector consists of a gas-filled or air-filled chamber through which a positive potential wire passes. The current in the wire is a measure of the energy lost by the gamma rays in the detector. The complete setup consists of the chamber, a current measuring device, and a voltage supply for the chamber.

Table 6.12—COMMERCIAL INSTRUMENTS USED IN SHIELD TESTS

Radiation detected	Type of detection	Manufacturer	Model
Gamma radiation	Ionization chamber	Victoreen Instrument Company	247
Gamma radiation	Ionization chamber	Jordan Electronic Mfg. Co.	
Gamma radiation	Geiger counter	Tracerlab, Inc.	Su5-A
Gamma radiation	Geiger counter	Nuclear Instrument & Chemical Corp.	2610-A
Thermal neutrons	BF_3	Nuclear Instrument & Chemical Corp.	2111 Pee Wee
Fast neutrons	Hurst	Radioactive Products, Inc.	Rudolph
Fast neutrons	Scintillation	Lermac, Inc.	Egghead

Thermal Neutrons. (1) BF_3 Counter: This detector consists of an ionization chamber filled with BF_3 gas, often enriched with B^{10} isotope. The thermal neutrons are detected by counting the pulses of ionization caused by the $B^{10}(n,\alpha)Li^7$ reaction. Smaller pulses caused by ionization due to gamma radiation can be easily discriminated against unless there are so many gamma rays that pile-up of the small pulses occurs. The complete setup consists of the detector, a preamplifier (if necessary) to drive the pulse through a long cable, an amplifier, a scaler, and a high-voltage supply for the detector.

A variation of this counter is the enriched-boron-lined ionization chamber.

(2) U^{235} Fission Counter: This detector is an ionization chamber lined with, or containing plates covered with, U^{235}. The thermal neutrons are detected by causing fission, and the large amounts of ionization caused by the resulting fission fragments are detected. This detector is not so sensitive as the BF_3 counter but has better gamma discrimination because of the large pulses. The instrumentation setup is identical to the BF_3 setup.

(3) Foils: Thermal neutrons can be counted by exposing various foil materials to the thermal-neutron flux and then measuring the induced activity. Foils have the advantage of unlimited gamma discrimination and minimum physical size. Some commonly used foil materials are indium (54-min half life) and gold (2.7-day half life).

Fast Neutrons. (1) Proton Recoil Counter: This detector is an ionization chamber lined with polyethylene and usually filled with ethylene gas. Fast neutrons collide with the atoms in the walls and gas of the chamber but lose appreciable energy only to the protons. The pulses produced by the ionization caused by the recoil protons are counted. Smaller gamma-ray pulses are discriminated against. To get counts proportional to the fast-neutron dose, or the energy loss of the fast neutrons, a rather elaborate pulse-integration system may be used. This system weights each proton recoil pulse by its size and gives a proportionate number of counts for each pulse. The complete setup consists of the detector, a preamplifier (if neces-

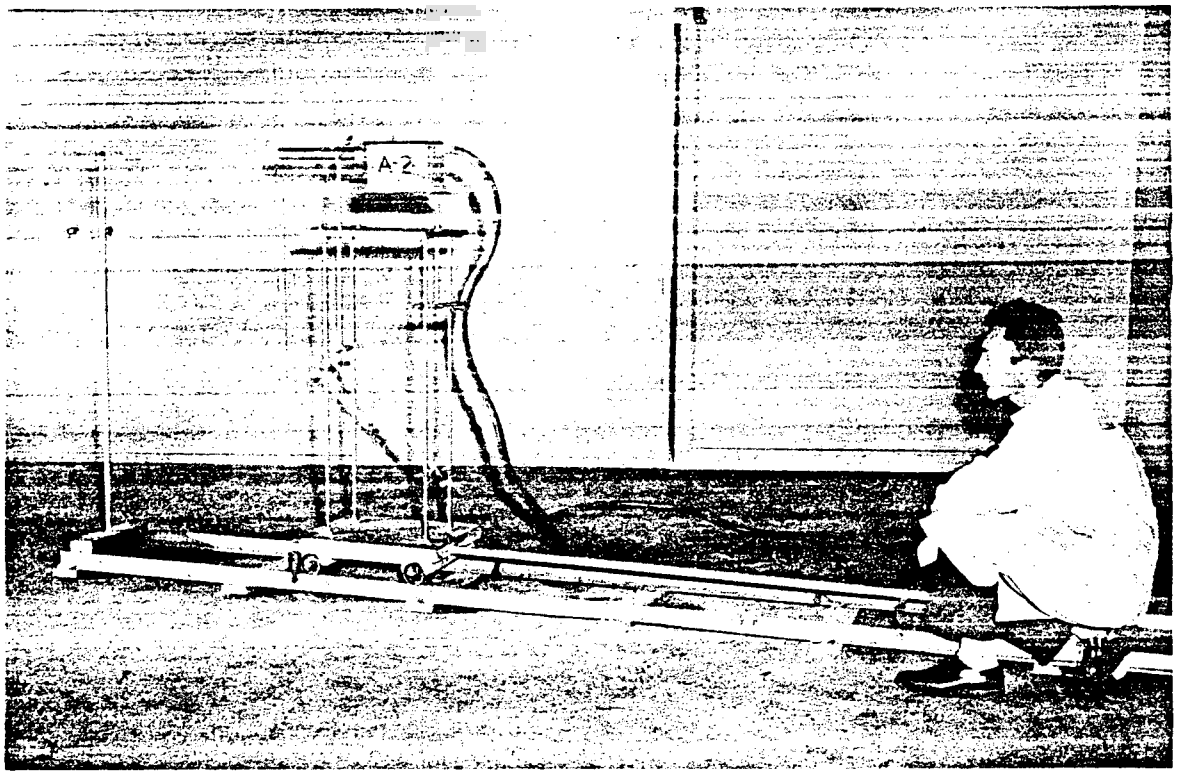


Fig. 6.25 — Close-up of the calibration device for a fast-neutron detector, showing neutron source on top of the rod at the left and detector on the carriage at the right. Box to the right of the detector encloses the preamplifier. Cables to counting instruments are enclosed in Tygon tubing. At the lower edge of the calibration device runs the metric scale. The detector may be positioned by means of a long rod connected to the carriage, enabling the operator to remain a safe distance from the source.

sary), an amplifier, a pulse-sorter, three scalers, and a high-voltage supply.[2,3] If desired, the pulse-height data may be integrated by hand, and no integrating equipment will be needed.

(2) Threshold Foils: Many nuclear reactions involving neutrons, such as (n,p), (n,2n), and (n,α) reactions, take place above certain energy thresholds. It is possible to get an indication of the fast-neutron flux and perhaps even the fast-neutron spectrum by activating suitable materials in a field of fast neutrons. This method has the advantage of unlimited gamma discrimination but can detect only a rather high fast-neutron flux. Usually the thermal-neutron activation must be suppressed by covering the foils with cadmium or boron (see reference 4).

4.3 Calibration of Instruments

(a) Gamma-radiation Detectors. These are most easily calibrated by exposing the detector to a known gamma-radiation flux. The most common method is to place the center of detection of the detector at a given distance from a Co^{60} source of known strength, for which the biological dose is easily calculated. It is best to use a rack such that the counter and source are supported in air at least 5 ft from the floor and walls to reduce scattering effects.

(b) Fast-neutron Detectors. These can be calibrated in air in a manner similar to the gamma instruments, except that a fast-neutron source is used. A polonium-beryllium source is most commonly used (see Fig. 6.25).

(c) Thermal-neutron Detectors. These must be calibrated in a known thermal-neutron field. One method is to use a fast-neutron source, polonium-beryllium preferably, inside a

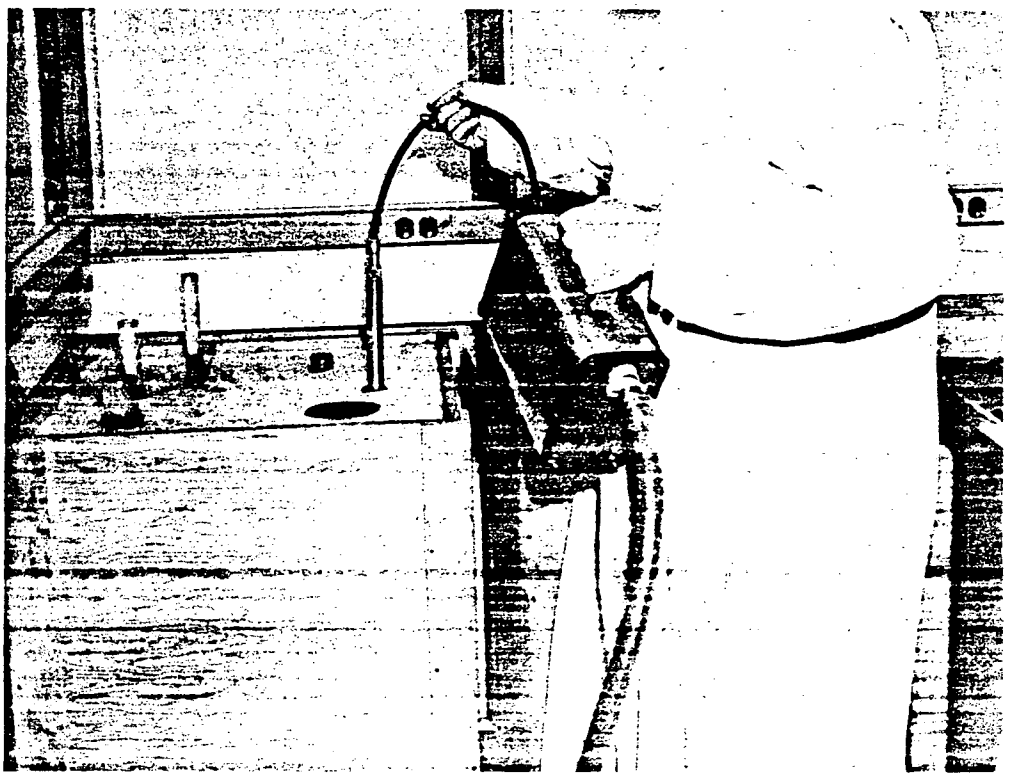


Fig. 6.26 — Close-up of the calibration device (paraffin-filled box) for a thermal-neutron detector. A BF_3 counter is being inserted into one of the holes. Other holes, when not in use, are filled with plastic rods. The neutron source is in the hole from which the longest rod protrudes.

container filled with water or paraffin to thermalize the neutrons (see Fig. 6.26). The thermal-neutron flux at a given counter location can be measured by means of foils which, in turn, have been calibrated in some known thermal-neutron flux such as in the BNL or ORNL reactors.

4.4 Planning and Performing the Shield Test

The test should be planned to perform measurements in all areas to which personnel will have access during operation of the reactor and also in the following regions, where possible, to obtain design data.

1. Outside the secondary shield, in normally uninhabited regions.
2. Inside the shielded compartment (i.e., the region that is shielded by the secondary shield. This region contains the reactor and its primary shield plus the surrounding pipes, heat exchangers, coolant pumps, coolant expansion tanks, etc.). The test should also include provision for monitoring equipment in the reactor compartment for several days after shutdown to determine the decay of activity of the various components.
3. Inside the reactor shield. Other measurements are also often useful in supplementing the measurements of radiation penetrating the reactor shield. These include chemical and radioactivity analyses on samples of the primary coolant or of the primary shield liquid to obtain information on the specific activities of these liquids and their impurities.

(a) Low- and High-power Tests. The shield tests are usually divided into low and high reactor power tests. Low-power tests are performed first at a few kilowatts; then the high-power tests are performed at 25 to 100 per cent full power. Low-power tests allow access to regions inaccessible at high power and must be done before prolonged high-power operation makes these regions permanently inaccessible.

(b) Determination of Biological Adequacy of the Shield. The determination of the biological adequacy of the shield must be a well organized and planned operation. Points at which measurements are to be taken should be premarked, using some sort of permanent grid pattern reference so that there can be exact correlation between a particular reading and the point at which the reading was taken. In regions where the shield is uniform and where no sharp variation in dose rates can occur, measurement points may be spaced as much as several feet apart. In regions where the shield is complicated by odd geometry, penetrations, and void spaces, or if the radiation dose rate is near the design level, measurement points should be closely spaced with possible overlapping of successive detector positions.

A *continuous* record should be kept of reactor power and coolant flow rates during the shield test. A record of primary coolant activity should also be kept when its activity takes more than a few minutes to reach saturation after a change in reactor power. This occurs, for example, when sodium is used as a coolant.

Measurements made on the surface of the shield and at several distances away from the shield give a complete picture of the radiation level in the area. Since most neutron instruments have to be corrected for gamma background, both types of readings are taken at each point.

Raw data taken at each point should include the actual meter or counter reading, meter scale setting (if any), the grid point and distance from the shield at which the reading was taken, and the time at which the reading was made. Also included in the data should be the type and serial number of the instrument used and the general area in which the survey was being made (see Fig. 6.27, a typical shield-test data sheet). Scale-up of raw data should not be attempted without having first made allowance for background, discrimination against gamma field for neutron readings, and having calibration data on each scale of the instrument being used. However, it has been found useful to calculate and plot in advance what the instrument readings should be so that actual readings can be plotted onto predicted curves and gross errors or significant trends can be quickly discovered and explored.

A well-designed shield will result in dose rates close to the design level. Areas in which the radiation level is found to be seriously over tolerance must be repaired by the addition of more shielding material.

(c) Obtaining Design and Operational Data. The experimental arrangement used in making a survey of the Submarine Thermal Reactor (STR) Mark I reactor shield tank is shown in Fig. 6.28 (reference 5). The thermal-neutron flux distribution and the gamma dose-rate distribution were obtained under low-power operation (i.e., 1 to 100 kw). The thermal-neutron flux distribution was measured by means of indium and gold foils, whereas the gamma dose-rate distribution was measured by means of pocket ionization chambers. The foils and dosimeters were placed on specially constructed racks designed to obtain the radial and vertical flux distribution in the primary shield tank. Agreement as to shape and order of magnitude between theoretical and experimental results was found to be close.

Figure 6.29 shows the apparatus for surveying the radiation in the water tank outside the reactor plant container ("the hull").

The initial test is a gamma-beam search conducted at ~10 per cent power and designed to cover the entire surface of the shield. Its purpose is the location of possible hot spots produced by voids. The gamma detector is scanned over the area associated with each grid point with a steady continuous motion, at the rate of about 3 in./sec. As the detector is moved over the surface, the reading should be observed for sudden changes in the radiation level over the typical shield area. A factor of 3 or greater is regarded as significant in indicating a shield defect. Relative readings are of greatest importance in this phase of the test. If no voids are indicated, the reactor level can be raised. A detailed survey is then made of gamma radiation, fast neutrons, and thermal neutrons. Since shields are designed to give specified dose rates at 100 per cent reactor power, data should be taken at as great a reactor power level as possible to minimize the error in extrapolation to 100 per cent.

When all data have been taken, the dose rate from each type of radiation is calculated in mrem/hr and extrapolated to the dose rate expected at 100 per cent full power, and the resultant

RECORD SHEET A-1 FOR TEST FORM NO. 786-4, Series R and S
RADIATION LEVEL SURVEY

Date_____ Applicable Test Form Series_____

Ref. Grid Sketch_____ Radiation Level Survey of_____

Test Point	*	Time	Power Level %	Gamma Instr. #___ Calib.Sht.No.____		Fast Neut.Instr. #____ Calib.Sht.No._____			Therm Neut.Instr. No._____ Calib. Sht. #_____	
				Meter Reading	Scale	Counts	Time	Count Rate	Meter Reading	Scale

Date Taken by:_____ Sheet No.____

* Height from walkway or distance from bulkhead.

Figure 6.27

values are tabulated and added together. A tabulation of the dose rates at all points is a ready reference, but the most concise representation of shield test data is a plan view of the area with radiation levels indicated. They may be shown either by isodose lines or by numerical values at each point.

4.5 Shield Test Experience

(a) Summary of STR Mark I Shield Test.[5,7] In the STR shield test, measurements were taken of gamma-ray dose-rate distributions, thermal-neutron flux distributions, and fast-neu-

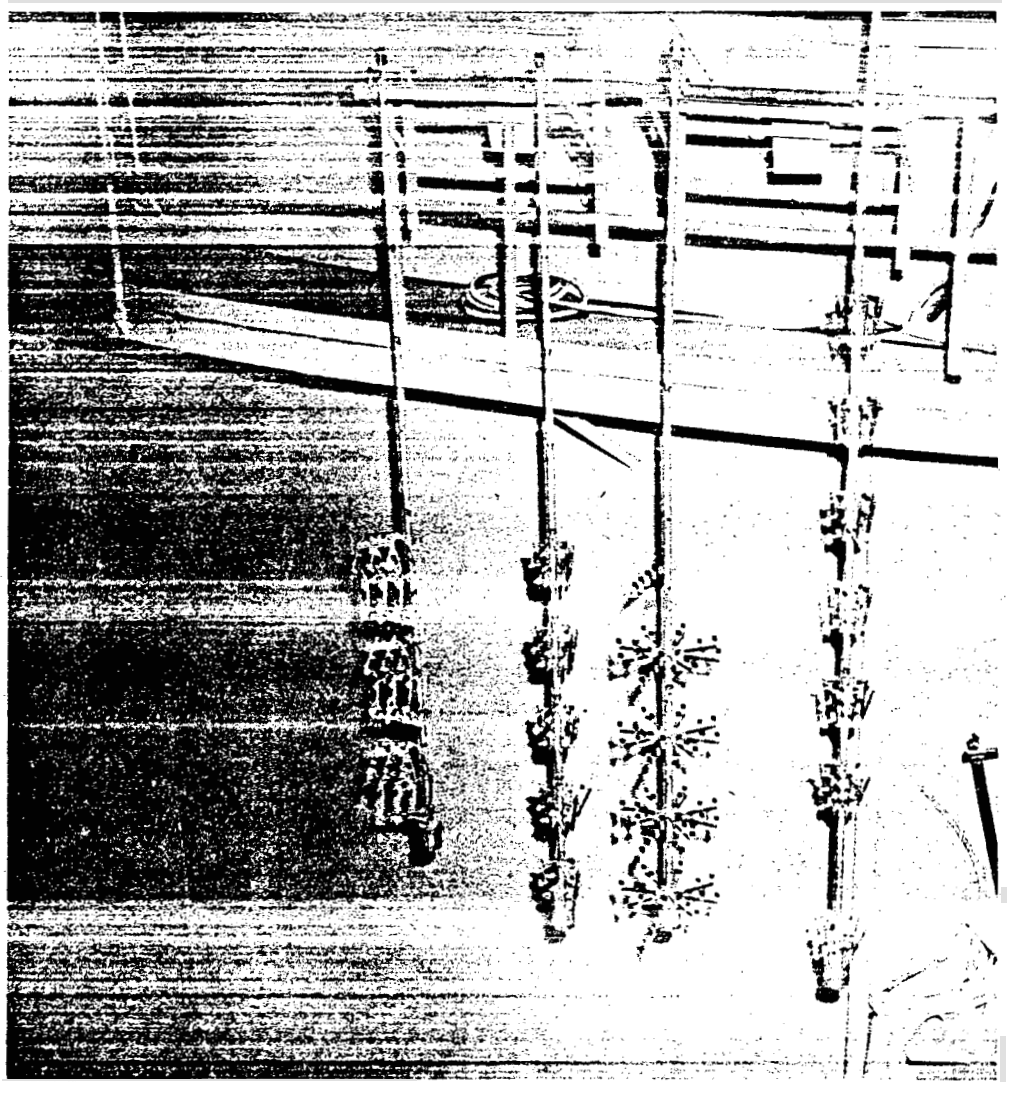


Fig. 6.28—STR Mark I shield test holder.

tron dose-rate distributions over much of the shielded surface, outside the hull with and without water in the sea tank, in the shielded reactor compartment, and in the reactor shield tank.

For gamma detection pocket ionization chambers were used in places where it was impossible to move a direct reading instrument (in the reactor shield tank and in various odd locations in the shielded reactor compartment). Anthracene scintillation detectors were used in conjunction with low-drift a-c electrometers to measure dose rate elsewhere.

Thermal neutrons were detected in inaccessible areas using indium and gold foils. Enriched BF_3 counters were used in most accessible locations in conjunction with preamplifiers, amplifiers, and scalers for thermal-neutron detection.

Fast neutrons were detected using "long counters" which measure fast-neutron flux. Fast-neutron dose rate was measured using an ethylene flow proton recoil counter and a pulse integrating system.

In general, the gamma and neutron levels that were measured were about as predicted in the reactor shield tank and in regions outside the secondary shield nearest the reactor. Outside the shield, near the reactor cooling system, the gamma levels were considerably lower than expected, probably because the shielding effectiveness of various components in the reactor compartment was only conservatively taken into account in determining the secondary-shield

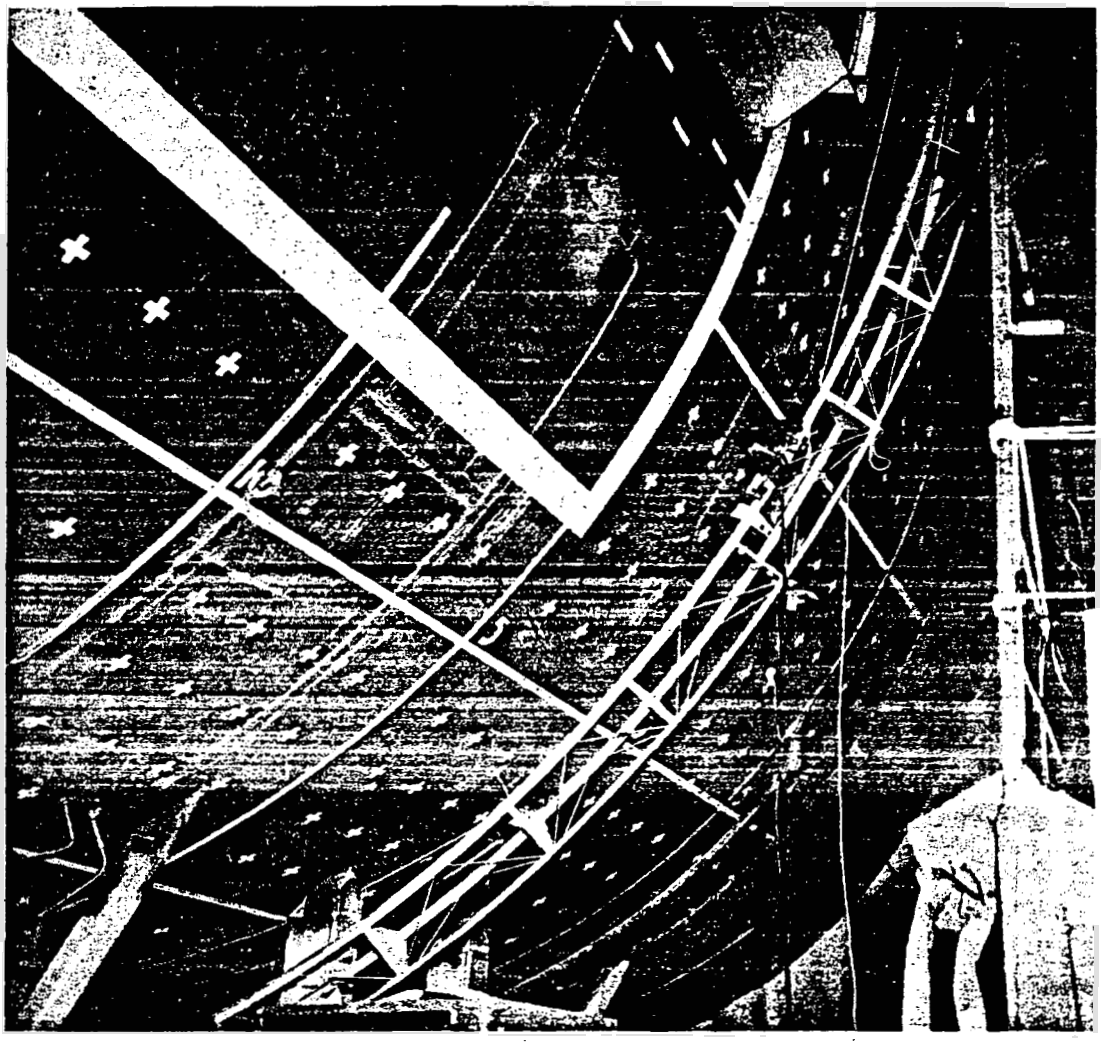


Fig. 6.29—STR Mark I hull grid and rack.

thickness. The neutron levels in these sections were also lower than expected, probably for the same reason as for the gamma levels and also because the $O^{17}(n,p)N^{17}$ activation cross section used in the calculations was later found to be too large.

The tests have proved very valuable as a source of information, both for the design of subsequent shields and for operations with SIR Mark A. In addition, they have much academic value of interest only to shielding people. The tests brought out, and it cannot be overstressed, that the persons performing the tests should be thoroughly familiar with the shield design and with general shielding theory. Otherwise, important discrepancies in the shield design or construction are apt to go unnoticed.

(b) General Conclusions from SIR Mark A Shield Tests. It certainly can be concluded from the SIR Mark A shield tests that the basic theory used in designing the shield was correct. No sizable discrepancy between theory and experiment was found in regions where the shield configurations were fairly simple. There were several exceptions to this last statement, but these were due to shield installation difficulties, not faulty shield design.

In regions where the shield configurations were complex, some unexpectedly high or unexpectedly low results were found. For the most part the complex shield configurations tended to be slightly overdesigned. In the SIR the major complex shield region is the area directly

above the reactor. The gamma radiation there was entirely secondary gamma radiation and was much lower than expected. On the other hand, there was found a circular region around the top of the reactor in which the secondary gamma radiation was unduly high, requiring additional shielding. Neutron measurements in this circular region were also higher than expected but were still within design limits. This region is directly above a cylindrical slot surrounding the reactor. Evidently the effect of this slot on neutron streaming had been underestimated.

During these tests thermal neutrons, fast neutrons, and intermediate-energy neutrons were measured. The intermediate-energy neutrons were measured with a paraffin-surrounded BF_3 counter. The number of these neutrons was unexpectedly high and constituted a substantial part of the neutron dose. It appears that a relatively large flux of intermediate-energy neutrons can be expected outside a shield which ends with several inches of steel.

The specific activation of the primary coolant agreed closely with the calculated activity. This is of prime importance since all the secondary-shield calculations were based on this activation. In addition, the build-up and decay of this activity during reactor operation and reactor shutdown have been as expected and thus far have revealed no unexpectedly large activation in the primary coolant system due to sodium impurities, mass transfer, or other causes.

The performance of instrumentation and auxiliary equipment (see Fig. 6.30) used during the SIR Mark A shield tests can be described briefly as follows:

1. Fast-neutron measurements:
   a. Proton recoil proportional counters used with pulse integrating systems. *Remarks:* Sealed type counters were used exclusively and on the whole these proved reliable. The ability of some of the detectors to discriminate against gamma radiation decreased with age.
   b. Threshold foils (phosphorus, iron, and silver). *Remarks:* Although all these foils were covered with cadmium, their activation due to (n,γ) reactions (caused by epithermal neutrons) was higher than expected. In a few cases this completely obscured the desired activity. In other cases it complicated the readings and increased their uncertainty.
2. Intermediate-neutron measurements:
   Long counter consisting of BF_3 detector in paraffin shield. *Remarks:* This counter proved to be very reliable and essential; no trouble was experienced.
3. Thermal-neutron measurements:
   a. BF_3 counters. *Remarks:* These counters were very reliable and no trouble was experienced.
   b. U^{235} fission counter. *Remarks:* This counter, intended primarily for use in high gamma fields, was used less than expected. This was because its gamma discrimination was not as good as had been hoped for.
   c. Foils (gold and indium). *Remarks:* In general, the gold foils were easier to use and gave more accurate results than the indium, although each had their uses.
4. Gamma-ray measurements:
   a. Scintillation counters using anthracene crystals and low-drift electrometers. *Remarks:* Some trouble was experienced with electrometer drift. More maintenance was required for these counters than the neutron counters. On the other hand, one of these has been operating continuously in the water outside the hull for six months. These are more accurate and more reliable than portable hand counters, but the fact that they read remotely is a definite disadvantage at times.
   b. Ionization chamber. *Remarks:* Proved reliable as a monitor, and no trouble was experienced.
   c. Portable counters (wide range, using Neher-White principle, made by Jordan Electronic Mfg. Co.). *Remarks:* Hand counters proved especially useful; easier to use at times than the scintillation counters.
   d. Remote reading counters (100 mr/hr to 10^5 r/hr). *Remarks:* These counters served well in some instances. However, they are not very rugged nor durable and require much maintenance. They should not be used as continuous monitors in a high radiation field

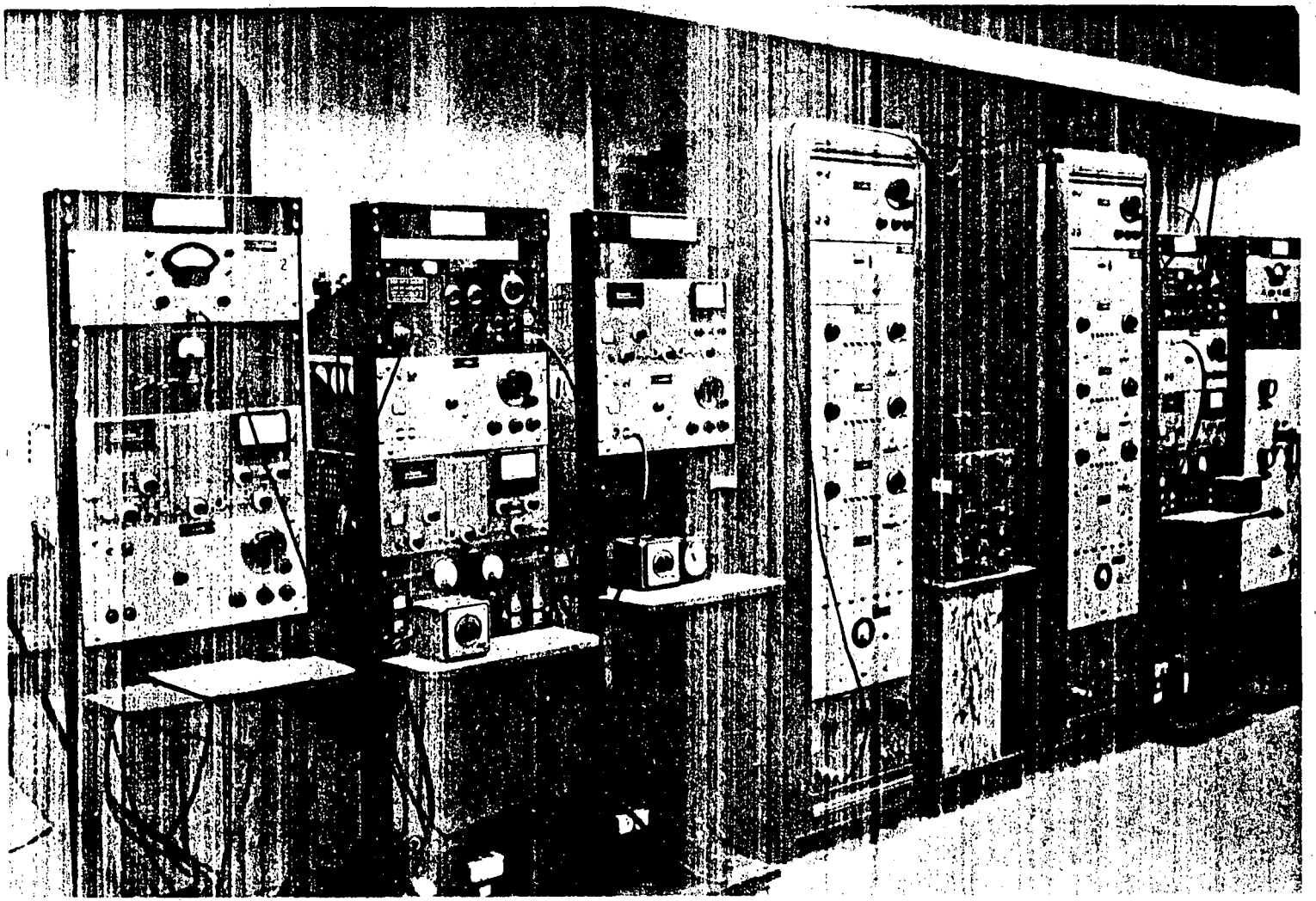


Fig. 6.30 — Photograph taken inside the instrument room, showing some of the instrumentation used during the SIR Mark A shield tests at West Milton. The two tall racks at the center are the pulse integrating systems for the fast-neutron dosimeters.

because they suffer radiation damage relatively fast. There is definite need for a reliable instrument capable of detecting large gamma dose rates.

e. Pencil dosimeters (200 mr to 50 r). *Remarks:* These proved useful in many instances. A higher range dosimeter could have been used at times. There are higher range dosimeters now being manufactured by several companies.

5. Foil-counting equipment:
   a. Geiger-Mueller counters (in shielded counting arrangements). *Remarks:* These counters were very useful and reliable for counting rates up to several thousand per minute; above this their dead-time losses become too large.
   b. Scintillation counters. *Remarks:* These counters were especially useful for counting rates greater than several thousand per minute. They count mainly gamma radiation, and this is inherently more accurate than beta counting. However, their sensitivity is not as constant as a Geiger-Mueller counter since they have no voltage plateau and very high counting rates temporarily reduce their efficiency.
6. Auxiliary equipment:
   a. Neutron source. *Remarks:* One polonium-beryllium neutron source was used during the tests, and it was sufficient. Its strength was originally about 3 curies, and it decayed to less than 1 curie.
   b. Gamma-ray sources. *Remarks:* Two Co^{60} gamma-ray sources of 1-mc and 78-mc strength were used. The 78-mc source was not often used, although there were occasions, such as when calibrating the higher range of the remote reading gamma counters, when a larger source could have been used.
   c. Calibration devices. *Remarks:* Two calibration devices were used. One was for calibrating fast-neutron and gamma detectors in air, and the other was for calibrating thermal-neutron counters inside a moderator. No trouble was experienced with these.
   d. Shield measuring device (for positioning detectors outside hull). *Remarks:* This device was never used since it could never be made to operate after it was submerged in water. Evidently its means of propulsion was not powerful enough to overcome the large frictional and binding forces that were present after being submerged. It was possible to obtain many and very reliable measurements simply by lowering detectors into the water. The detectors were positioned on the end of an L-shaped rod to reach the hull below the center of the ship. With the rod used at West Milton it was not possible to reach the very bottom of the hull this way. It is now generally agreed that the expense of a more powerful shield measuring device similar to that installed at West Milton would not be worth while in future tests. It is possible to get every measurement desired outside the hull by simpler means, or by designing a better and simpler device (e.g., permanently held L-shaped rods which could be moved vertically and whose horizontal leg could be varied in length.

REFERENCES

1. F. McGowan and C. Clifford, Application of a Scintillation Detector to Gamma-ray Dosimetry, Report ORNL-CF-51-01-212, Oct. 16, 1951.
2. G. S. Hurst, Fast-neutron Count-rate Dosimetry, Report ORNL-589, Feb. 17, 1950.
3. G. S. Hurst, R. H. Ritchie, and H. N. Wilson, A Count-rate Method of Measuring Fast-neutron Tissue Dose, Rev. Sci. Instr., 22: 12 (December 1951).
4. J. B. Trice et al., Report ORNL-CF-53-5-139, Oct. 29, 1953 (Classified).
5. Preliminary Report on Mark I STR Shield Test, Report W-STR-TS-20, August 1953 (Classified).
6. Robert Sevy, Final Reports on Mark I Shield Test, Reports WAPD-STR(ph)-40; WAPD-STR(ph)-45; and WAPD-STR(ph)-46, June 1955 (Classified).
7. P. A. Roys, Report W-STR-TS-62, March 1954 (Classified).

8. J. J. Taylor and K. Shure, Report WAPD-P-158, February 1952 (Classified).
9. P. E. F. Thurlow and J. J. Taylor, Report WAPD-P-171, March 1952 (Classified); H. E. Stone and L. H. Weinberg, Report KAPL-HES-15, 1954 (Classified); and B. A. Gottschalk and L. H. Weinberg, Report KAPL-SL-3, 1954 (Classified).

BIBLIOGRAPHY FOR NEUTRON SHIELDING MATERIALS

1. "Modern Plastics Encyclopedia and Charts," Plastics Catalogue Corp., New York, 1950 and 1951.
2. "Rubber in Engineering," Chemical Publishing Co., Inc., 1946.
3. C. C. Davis and J. T. Blake, "Chemistry and Technology of Rubber," Reinhold Publishing Corp., New York, 1937.
4. Simonds and Ellis, "Handbook of Plastics," D. Van Nostrand Co., Inc., New York, 1943.
5. Wakeman, "Chemistry of Commercial Plastics," Reinhold Publishing Corp., New York, 1947.
6. Synthetic Rubber, History and Importance Today, Technical Bulletin, United States Rubber Co.
7. Vistanex, Technical Bulletin, Enjay Company, Inc., New York 19, N. Y.
8. Butyl Rubber, Technical Bulletin, Enjay Company, Inc., New York 19, N. Y.
9. Sasso, "Plastics Handbook for Product Engineers," McGraw-Hill Book Company, Inc., New York, 1946.
10. Schock, "A Manual of Plastics and Resins," Chemical Publishing Co., Inc., Brooklyn, N. Y., 1950.
11. Brady, "Materials Handbook," 6th ed., McGraw-Hill Book Company, Inc., New York, 1947.
12. Chem. Eng. News, 27(20): 1463 (1949).
13. "Handbook of Plastics," 2d ed., D. Van Nostrand Co., Inc., New York, 1949.
14. Polythene, Du Pont Company, April 1946.
15. "Handbook of Molded and Extruded Rubber," Goodyear Tire & Rubber Co., 1949.

Chapter 7

RADIOACTIVITY OF SHUTDOWN SYSTEM (THE ACCESSIBILITY PROBLEM)

INTRODUCTION 229

1 GENERAL DISCUSSION OF SIGNIFICANT RADIATION SOURCES 229
- 1.1 Induced Activity of the Reactor Coolant Itself 230
- 1.2 Induced Activity of Structural Material 230
  - (a) External to Reactor Shield . . 230
  - (b) Within Reactor Pressure Vessel and Reactor Shield . . . 230
- 1.3 Photoneutron Production . . . 232
  - (a) In the Reactor Core . . . 232
  - (b) Secondary Gammas Produced by Photoneutrons 232
- 1.4 Fission Products in the Reactor Core 232
- 1.5 Delayed Neutrons in the Reactor Core 232
- 1.6 Activation of Impurities and Corrosion Products in the Coolant . . 232
- 1.7 Fission Products in the Coolant System from Corrosion or Failure of Fuel Elements 232

2 ASPECTS OF WATER TECHNOLOGY . . 233
- 2.1 Water Supply 233
- 2.2 Corrosion of Plant Materials . . 233
- 2.3 Purification Systems 234

3 ACTIVATION OF IMPURITIES IN THE COOLANT 235
- 3.1 Hypotheses 237
- 3.2 Formulation of the Problem . . 237
- 3.3 Solutions 239
  - (a) Equilibrium Solutions . . . 239
  - (b) Time-dependent Solutions . . 242
- 3.4 Determining Demineralizer Flow Rate 242
- 3.5 Concentration of Radioactivity by Ion Exchangers and Filters . . . 248
- 3.6 Time-dependent Neutron Flux . . 249

4 FISSION PRODUCTS IN THE COOLANT SYSTEM 249
- 4.1 Distribution of Fission-product Gases in Water-cooled Reactor Systems 250
- 4.2 Continuous Release of Fission-product Gases 250
  - (a) The Core 250
  - (b) The Primary Coolant . . . 251
  - (c) The Reactor Plant Container . 252
- 4.3 Noncontinuous Release of Fission Products 253
- 4.4 Alternate Approach to Case of Continuous Release of Fission-product Gases 255

Chapter 7

RADIOACTIVITY OF SHUTDOWN SYSTEM (THE ACCESSIBILITY PROBLEM)

INTRODUCTION

An important consideration in the design of power reactors is providing access to the reactor cooling system for the purpose of maintenance and repair. Three major sources of radiation which tend to prohibit such access are discussed below.

Induced Activity of the Reactor Coolant: When the reactor-coolant activity is short lived, e.g., the N^{16} and N^{17} activities in water, all that is necessary to gain access to the reactor cooling system is to shut down the reactor. When the reactor-coolant activity is comparatively long lived, it is necessary to shut down the reactor to drain the coolant from the reactor system, perhaps to flush out the reactor system, and to shut down the reactor and wait for the induced coolant activity to decay.

Activated Impurities in the Reactor Coolant: Impurities in the reactor coolant may be present in high enough concentrations so that their activation restricts accessibility for maintenance, even after the reactor is shut down. This is particularly true in the case of water, not only because of its highly corrosive nature and resultant high impurity production, but also because the activity of the water itself is very short lived, thus leaving the induced activity of impurities in the water as the major source of activity in the system after reactor shutdown. With water being used as a coolant, it may be necessary to remove some of the impurities by a continuous purification process to prevent a build-up of long-lived induced activity in the system from restricting access to the plant.

Radiation Originating in the Reactor Core Both During Reactor Operation and After Shutdown.

The shield designer is frequently called upon to analyze the accessibility problem. It is the purpose of this chapter to give him a general idea of the various phases of the problem and to discuss in detail those aspects of the problem which are not, strictly speaking, radiation *shielding*. In particular, this chapter treats the problems of determining equilibrium concentrations of impurities, evaluating the degree of deposition of impurities on system walls, calculating the required size of side-stream purification systems, and determining the effect of release of fission products from the reactor core.

1 GENERAL DISCUSSION OF SIGNIFICANT RADIATION SOURCES

In order to ensure that no major source of radiation is overlooked, an evaluation of the limits of accessibility after reactor shutdown should include an investigation of all potentially

significant sources of radiation which exist at that time. For the case of a compartment shield design (one in which a shield surrounds the reactor and its pressure vessel with a separate additional shield surrounding the primary-coolant loop), the sources of radiation which will be present are listed and discussed in the following sections.

1.1 Induced Activity of the Reactor Coolant Itself

The activity of the reactor coolant will persist after reactor shutdown for a period that depends on the half life of the induced activity of the coolant. This source of radiation is not important in the case of water-cooled reactors since the half lives of the activated nuclides is so short. However, when the half life of the induced activity of the reactor coolant is considerably longer than a few seconds, this source becomes quite important as, for example, in the case of sodium-cooled reactors. The half life of Na^{24} is about 15 hr. Thus, in a sodium-cooled reactor, two days after reactor shutdown the specific activity of the coolant will have decayed only by a factor of 10. In this case the coolant piping and heat-transfer equipment located outside the reactor shield remain strong sources of radiation for a considerable period after reactor shutdown. (See Fig. 7.1.)

To evaluate the effect of sources such as this on accessibility, the following procedure is recommended:

1. Select two examples of reactor operating history—a worst case and a typical case. Calculate the specific activity of the coolant at the moment of reactor shutdown, using the techniques of Chap. 4, Sec. 2.
2. Using the half life of the induced activity, draw decay curves for the two specific activities calculated in step 1.
3. Using the methods of Chap. 4, determine the general radiation level adjacent to the coolant system for a case corresponding to unit specific activity.
4. Using the results of step 3 and the curves of step 2, determine the waiting time required to attain the general radiation level that will permit access for maintenance without exceeding maximum permissible radiation exposures for personnel.

The specific activity of the coolant within the reactor pressure vessel will be the same as the activity in the external system. However, the coolant which is inside the reactor pressure vessel will be shielded somewhat by the material in the reactor shield. As long as coolant is in the reactor cooling system outside the reactor shield, the contribution to the radiation dose at a point outside the reactor shield from coolant within the reactor container will be a negligible fraction of the external sources.

In some cases operational considerations may require that access to the plant be obtained before the coolant activity has decayed to an acceptable level. It then becomes necessary to remove the activity by draining the radioactive coolant from the system into shielded tanks. In this case the activity from the coolant inside the reactor container must be considered.

1.2 Induced Activity of Structural Material

(a) External to Reactor Shield. Neutron capture in structural materials of the reactor cooling system generally results in the formation of radionuclides with fairly long half lives. In the case of iron the half life is 45 days. A large amount of such activation, if allowed to occur in a system, would severely limit access for maintenance and repair. Good design practice, therefore, limits the thermal-neutron flux emerging from the reactor (primary) shield to a level low enough to ensure that induced radioactivity in the pipe walls, etc., will be an insignificant source. In general, other criteria in the design of the reactor shield will accomplish this objective without special effort on the part of the shield designer.

(b) Within Reactor Pressure Vessel and Reactor Shield. The steel and other structural materials of the reactor core, reactor reflector, thermal blanket, reactor pressure vessel, and reactor shield are exposed to significant thermal-neutron fluxes during reactor operation. The induced activity of these materials is proportional to the neutron flux to which they are exposed and to the degree of saturation (length of exposure time). There is, however,

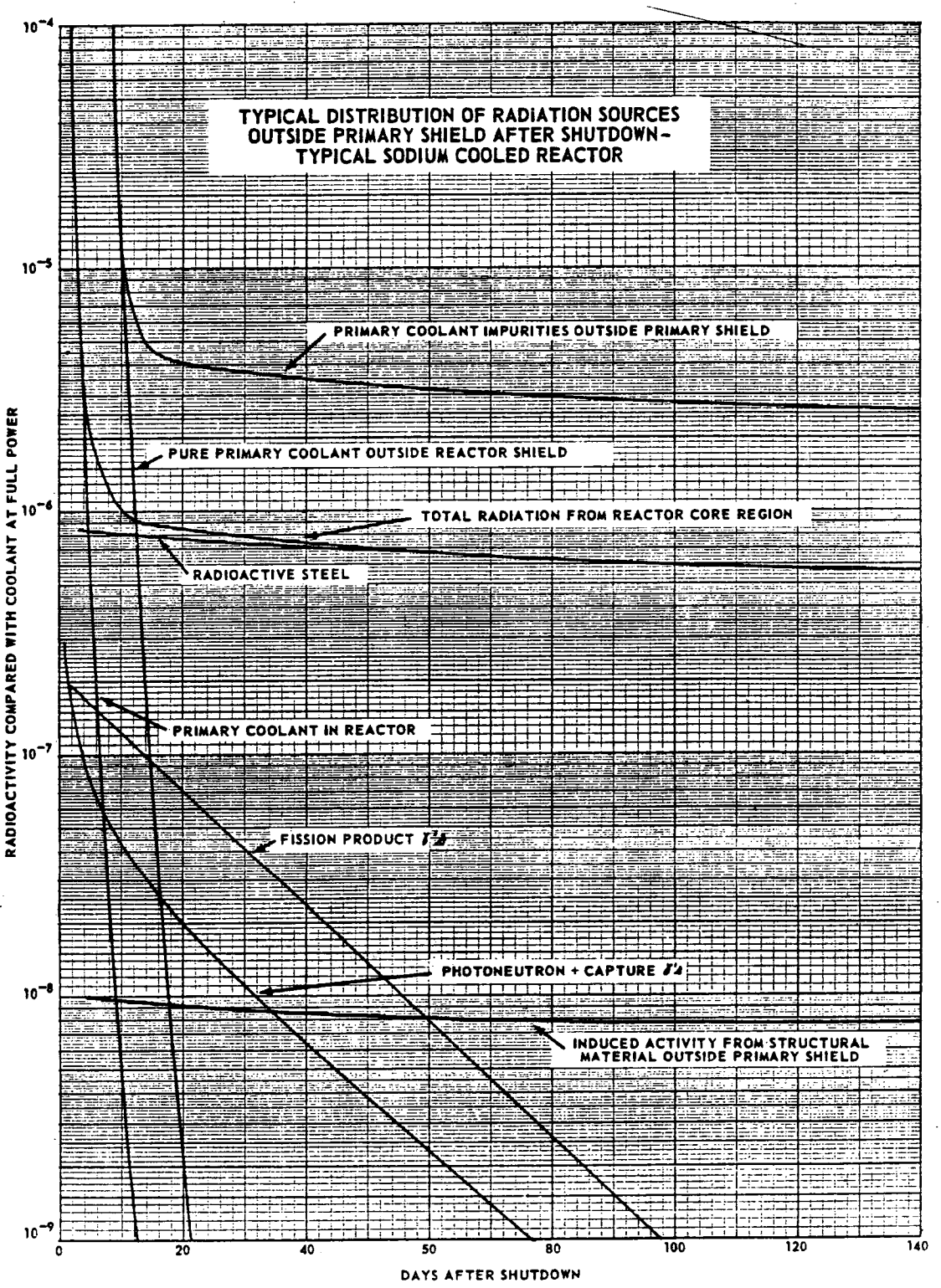

TYPICAL DISTRIBUTION OF RADIATION SOURCES
OUTSIDE PRIMARY SHIELD AFTER SHUTDOWN-
TYPICAL SODIUM COOLED REACTOR
PRIMARY COOLANT IMPURITIES OUTSIDE PRIMARY SHIELD
PURE PRIMARY COOLANT OUTSIDE REACTOR SHIELD
TOTAL RADIATION FROM REACTOR CORE REGION
RADIOACTIVE STEEL
PRIMARY COOLANT IN REACTOR
FISSION PRODUCT
PHOTONEUTRON + CAPTURE
INDUCED ACTIVITY FROM STRUCTURAL MATERIAL OUTSIDE PRIMARY SHIELD
RADIOACTIVITY COMPARED WITH COOLANT AT FULL POWER
10^{-4}
10^{-5}
10^{-6}
10^{-7}
10^{-8}
10^{-9}
0
20
40
50
80
100
120
140
DAYS AFTER SHUTDOWN

Figure 7.1

considerable self-shielding of the decay gammas coming from the activated material. Usually the worst source of this type is that due to the structural material (steel) at a water-structure interface, where the thermal-neutron flux tends to peak. Also, the water adjacent to the interface acts as a poor gamma shield. An example of this is the induced activity arising from structural material adjacent to the water in the reactor shield, which may be one of the important gamma sources during reactor shutdown.

1.3 Photoneutron Production

(a) In the Reactor Core. Photoneutrons are produced by (γ,n) reactions with certain light elements such as beryllium or deuterium. However, gamma rays of sufficient energy must be available to produce this reaction, and usually in a reactor the probability for a (γ,n) reaction is small. For beryllium the threshold energy for photoneutron production is 1.6 Mev; for deuterium it is 2.2 Mev. Some fission products emit gammas with higher energies than these thresholds, and some coolants, such as sodium, emit gammas which could also cause a photoneutron reaction, provided beryllium or deuterium is present in the reactor. These photoneutrons constitute a source of neutrons which is very small in comparison with the prompt-neutron source under normal power operating conditions but which should, however, be considered after shutdown. The neutron shielding characteristics built into the primary shield will generally attenuate the photoneutrons sufficiently. This neutron-source term will decrease with time by the same ratio as the gammas, which cause photoneutron production, decrease. The energy of photoneutrons is different from that of a fission spectrum and depends usually on the differences between the gamma energy available and the threshold energy for the photoneutron reaction. In general, photoneutrons will have a slightly lower energy than the average fission energy. The attenuation produced by the reactor shield of these neutrons will be different, therefore, from the attenuation by the reactor shield of the fission neutrons.

(b) Secondary Gammas Produced by Photoneutrons. If neutrons become inelastically scattered or are captured in a shield, prompt gamma rays are produced, ranging in energy up to 10 Mev, depending on the process and the shield material. The photoneutrons discussed in the preceding section should also be considered as sources for inelastic scattering and capture gammas; but, in general, these are a small fraction of all the sources present because of the low cross section for photoneutron production.

1.4 Fission Products in the Reactor Core

Many fission products emit gamma rays, ranging in energy up to $2\frac{1}{2}$ Mev. The amount of activity present due to fission products in the reactor core depends, of course, on the operating history of the core. The relative importance of fission products to other gamma sources depends on the particular reactor design. Hence attenuation of fission-product gammas must be considered when designing the reactor shield. For specific energy values see Chap. 3, Sec. 2.

1.5 Delayed Neutrons in the Reactor Core

About 1 per cent of the fission neutrons are delayed and are emitted after the fission process. In reactor designs where accessibility to the coolant loop is desired within a few minutes after reactor shutdown, these delayed neutrons should be considered as an activity source. For most practical cases, however, the time involved in attaining physical access to the plant is such that the delayed neutrons may be safely neglected.

1.6 Activation of Impurities and Corrosion Products in the Coolant

This topic is discussed in detail in Sec. 3.

1.7 Fission Products in the Coolant System from Corrosion or Failure of Fuel Elements

This topic is discussed in detail in Sec. 4.

2 ASPECTS OF WATER TECHNOLOGY

The following discussion covers aspects of the chemistry of water-cooled reactor plants which are of interest to the shield designer. It includes an explanation of the engineering aspects of purification systems as used in nuclear power plants.

As stated previously, the accessibility problem in a water-cooled reactor plant centers around the induced activity of the corrosion products and other impurities present in the cooling water.

The actual amount of corrosion products and other impurities which can be tolerated in the reactor coolant is very low. In current plant designs the allowable equilibrium concentration of combined impurities in the reactor coolant water is about 1.0 part per million by weight. (By contrast, drinking water contains impurities up to 200 ppm, and water in boiler systems contains impurities ranging between 50 and 500 ppm.)

The problem of maintaining a low concentration of corrosion products and other impurities in reactor coolant water is attacked in three ways: (1) by supplying very pure water to the plant in the original filling and in makeup, (2) by reducing the corrosion of plant materials to the lowest possible rate, and (3) by using a bypass purification system in the plant to purify the coolant continuously.

2.1 Water Supply

Natural water contains small quantities of dissolved and solid materials. These must be removed from water being supplied to the reactor system in order to eliminate them as a source of induced activity.

In a typical case this purification is accomplished by straining or filtering to remove the solid material and distilling to remove the dissolved material. The water is then sent through an ion exchanger for final cleanup before being charged into the reactor system. This ion exchanger removes the remaining few dissolved impurities which were passed from the previous purification or which were picked up from the metal piping and storage tank. As a result of this purification process, water entering the reactor plant contains less than 0.5 ppm total impurities and is at the practical engineering limit of purity for plant usage. Table 7.1 shows a typical analysis of water used in a reactor.

2.2 Corrosion of Plant Materials

The corrosion of plant materials is caused by the chemical reaction between metal and water to form corrosion products. Some of the corrosion products remain in solution and some become insoluble, forming a black granular material called "crud." In the case of steel, the primary element, i.e., iron, and also alloying elements, such as chromium and nickel (used in stainless steel), form insoluble corrosion products. On the other hand, impurities present in the steel, such as sodium and manganese, remain in solution as soluble corrosion products.

The rate of the corrosion reaction is dependent upon the temperature, the material involved, and the "newness" of the material. The initial rate of corrosion in a new plant may be 10 to 20 times higher than the eventually reached equilibrium corrosion rate. With stainless steel the equilibrium corrosion rate is reached after only a few hundred hours at plant operating conditions. With carbon steel about 1000 to 1500 hr at plant operating conditions is necessary to reach an equilibrium rate. Subsequently, the corrosion rate remains relatively constant throughout the life of the plant. The equilibrium corrosion rate of materials in a reactor plant is held to a low value by use of corrosion inhibitors in the system. For nuclear plants the inhibitors used may be (1) the maintenance of an excess of hydrogen gas dissolved in the water or (2) the control of pH conditions of the water. The actual equilibrium corrosion rate in a nuclear plant is about 0.1 mil/year (14 mg/dm^2/month or 5.4×10^{-11} g/cm^2/sec). This is considerably lower than corrosion encountered in boiler systems and chemical plants, where corrosion rates of 1.0 to 5.0 mils/year are considered normal.

2.3 Purification Systems

Calculations on the size of the purification system in a nuclear power plant are generally based on the equilibrium corrosion rate of plant materials. The removal of corrosion products from the plant before equilibrium is reached is handled by auxiliary purification units or by accepting a shorter lifetime for the purification units.

Table 7.1—TYPICAL IMPURITIES IN COMMERCIAL SODIUM AND WATER FOR REACTOR USE

Commercial Sodium			
Element	Ppm	Element	Ppm
Al	1	Li	67
B	2	Mn	1
Ba	2	Ni	1
Cd	1	P	11
Cl	4	Pb	1
Co	1	S	35
Cr	1.4	Sb	0.5*
Cs	2	Sc	0.5*
Cu	1	Si	21
Fe	10	C	60
Hg	2	Ca	350
K	150		

Water for Reactor Use	
Electrical conductivity, μmhos/cm^3	0.50
pH at 25°C	7.5
Iron, ppm	< 0.1
Sodium, ppm	< 0.3
Silica, ppm	< 0.1
Total impurities, ppm	< 0.5

*Estimated.

A purification system performs two functions: (1) removal of soluble materials and (2) removal of insoluble materials.

The soluble corrosion products are removed from the coolant by an ion-exchange process in which water ions are substituted for ions of soluble corrosion product. The component which performs this function is called a "demineralizer," "deionizer," or "ion exchanger." The insoluble corrosion product is physically separated from the coolant by a strainer or filter. Frequently separation of both soluble and insoluble material from the coolant can be accomplished by the same component. For example, in one demineralizer design the bed of ion-exchange material also acts as a filter for the removal of insoluble material. This is accomplished with no impairment of the efficiency of the unit as a remover of solubles.

Since components in the purification system accumulate activity, they become strong sources in themselves and thus affect accessibility for maintenance and repair. Frequently, therefore, these components require special shielding.

The flow of coolant to the purification system must be at least sufficient to maintain the equilibrium concentration in the coolant within the limits set by accessibility considerations. Although the requirements for purity of the water used in reactor plants are quite stringent, in practice the actual flow to the purification system is only about 0.1 per cent of the main stream flow.

For practical design purposes the accessibility problem divides itself into two parts: (1) effects due to short-lived activities and (2) effects due to long-lived activities. High specific short-lived activities interfere with immediate access to the plant after shutdown. High specific long-lived activities interfere with continuous access to the plant when it is shut down for long working periods. (See Fig. 7.2.)

For plants built of steel (either stainless or carbon), almost all the short-lived activity in the coolant is caused by activation of the soluble corrosion products in the water. Conversely, almost all the long-lived activity is associated with the insoluble corrosion products.

The major contributor to the total activity in a steel system is the short-lived (2.6 hr) Mn^{56} activity. This results from the activation of manganese in the system, a constituent of the steel, which appears as a soluble corrosion product in the coolant. Since manganese is the predominant short-lived activity in the coolant, it is the controlling activity when considering the problem of immediate access to the plant after shutdown, and thus it forms the basis for selection of the coolant flow rate to the ion exchanger in the purification system. This flow rate must be sufficient to maintain the equilibrium concentration of manganese in the coolant below the point where the manganese activity interferes with access to the plant within the time limits set for accessibility to the plant. With this as a basis for the purification flow rate, effects due to other short-lived activities in the coolant of lesser magnitude than Mn^{56} can be safely ignored.

The problem with the long-lived activity is one of gradual build-up of background radiation in the plant over long periods of operation to the point where access to the plant for long continuous periods during shutdown is limited by high radiation levels. The build-up may either be gradually accumulated over the entire interior plant surface or concentrated in specific components which become "hot spots." The long-lived activity is predominantly Fe^{59} (45-day half life) and Co^{60} (5.3-year half life). This results from the activation of iron and cobalt in the steel that has corroded and entered the coolant as insoluble corrosion product.

The gradual build-up of activity on the interior surface of the plant is caused by the substitution (or "transfer") of activated corrosion product with nonactivated product. The corrosion product is activated by originating in the vicinity of the reactor core (e.g., core structural members), where it has been exposed to considerable radiation and has become saturated, or as a result of circulating around the reactor cooling system and through the core. This activity is then dissipated through the system by an exchange or transfer process in which the active corrosion product in the coolant is deposited on the system interior and is replaced in the coolant by nonactive material.

Hot spots in the plant would most likely be caused by selective deposition of insoluble corrosion products on specific plant components as a result of pressure differentials or changes in flow patterns within the components. Deposition could occur, for example, in valves or flow-metering devices. This problem is most readily surmounted by maintaining flow to the purification system in such a manner that the equilibrium concentration of insoluble corrosion products in the coolant is below the concentration necessary to cause deposition. However, in most plant designs this problem is not acute since the requirements for removal of soluble corrosion products dictate a larger flow than that required for removal of insolubles. In other words, the concentration of insolubles is maintained well below the point where deposition would occur.

3 ACTIVATION OF IMPURITIES IN THE COOLANT

The impurities present in a reactor coolant are important when accessibility problems are evaluated. Impurity activation depends on the amount of impurities present, their mode and time of circulation, the amount of deposition, and the specific isotopes involved. The methods outlined below, although written for a typical water-cooled reactor, apply equally well to other reactor coolants.

The purpose of this section is to provide nuclear engineers with methods of computing the expected activity levels of impurities. The activity of the pure coolant is covered in Chap. 4.

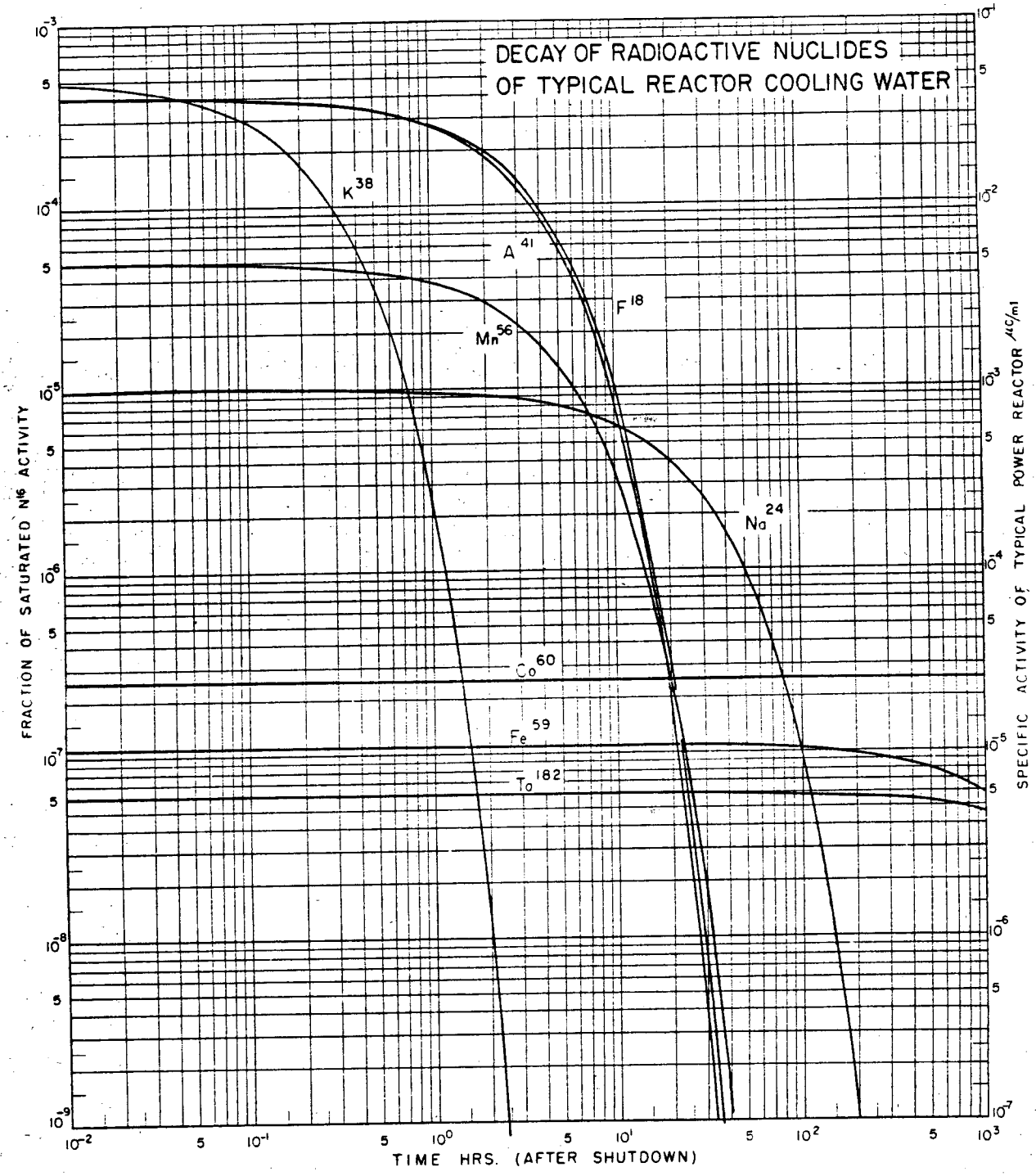

DECAY OF RADIOACTIVE NUCLIDES
OF TYPICAL REACTOR COOLING WATER
K38
A41
F18
Mn56
Na24
Co60
Fe59
Ta182
FRACTION OF SATURATED N16 ACTIVITY
SPECIFIC ACTIVITY OF TYPICAL POWER REACTOR μC/ml
TIME HRS. (AFTER SHUTDOWN)

Figure 7.2

3.1 Hypotheses

A system of six coupled first-order linear differential equations has been derived, which seems to describe adequately the normal time behavior of activity build-up due to corrosion-product activation. The arrangement of system components and the factors considered in setting up the equations are shown in Fig. 7.3.

Note: It should be noted that any change in activity due to impurities in feedwater has not been considered in setting up these equations.

It has been assumed that the material of the system corrodes uniformly and homogeneously and, furthermore, that the chemical species in a sample of corrosion products leaving the corroding surface are in the same ratio as those within the material in its solid form. A discussion of the typical behavior of a reactor cooling system made of steel is given in Sec. 2. The equations given in this section are applicable regardless of the pattern that corrosion follows. However, the most practical case is that where the system corrosion rate is constant, and that case is discussed in detail.

In formulating these equations, in order to account for activity that is deposited on surfaces exposed to coolant water, it has been postulated that the quantity of active material deposited per unit time per unit area of surface is proportional to the concentration of the material in the water. It has been further postulated that some of the material present on a given surface as scale is reintroduced into the coolant at a rate proportional to the surface density of the material. The ion exchanger and filter are assumed to remove impurities from the coolant at rates proportional to their concentration in the coolant. No return of material from the ion exchanger and filter to the cooling water is assumed. (This assumption is true for all normal operation.)

3.2 Formulation of the Problem

The following system of rate equations has been formulated using the above hypotheses. The *rate of change of the concentration (n_w) of active material in the primary water* is

$$\frac{dn_w}{dt} = \sigma\phi_\epsilon N_w - \left(\sum_j \frac{\epsilon_j Q_j}{V_w} + \sum_k \frac{l_k}{V_w} + \lambda\right) n_w + \frac{K_p}{V_w} n_p + \frac{K_c}{V_w} n_c \qquad (1)$$

where σ = thermal cross section for the production of the active isotope from the target nuclide (cm^2)

ϕ_ϵ = effective flux for $(\Delta\tau/\tau)\phi_0$ [ϕ_0 being the thermal-neutron flux averaged over the geometry of the core, τ being the period of time required for a test particle to traverse the length of the primary loop once, and $\Delta\tau$ being the interval of time during which the test particle resides in the thermal flux during its course around the loop (neutrons/cm^2-sec)]

N_w = concentration of target nuclide in the water (atoms/cm^3)

$\sum_j \epsilon_j Q_j = \epsilon_I Q_I + \epsilon_p Q_p + \epsilon_c Q_c + \epsilon_f Q_f$

V_w = volume of the coolant water (cm^3)

l_k = rate at which the loop loses water through the k*th* leak (cm^3/sec)

λ = decay constant of active nuclide (sec^{-1})

K_p = rate at which material is removed from scale on the piping (cm^3/sec)

n_p = concentration of active nuclide on the piping (atoms/cm^3 of scale)

K_c = rate at which material is removed from scale on the core (cm^3/sec)

n_c = concentration of active nuclide on the core (atoms/cm^3 of scale)

The quantities $\epsilon_I Q_I$, $\epsilon_p Q_p$, $\epsilon_f Q_f$, and $\epsilon_c Q_c$ are the removal rates from the ion exchanger, piping, filter, and core, respectively, in cubic centimeters per second.

The first term represents the production of active nuclide by the transmutation of the stable target nuclide in the thermal flux. The second term is the rate at which the active nuclide is lost as a result of purification by the ion exchanger, purification by the filter, deposition on the piping surfaces, deposition on the core, leakage, and decay. The third and

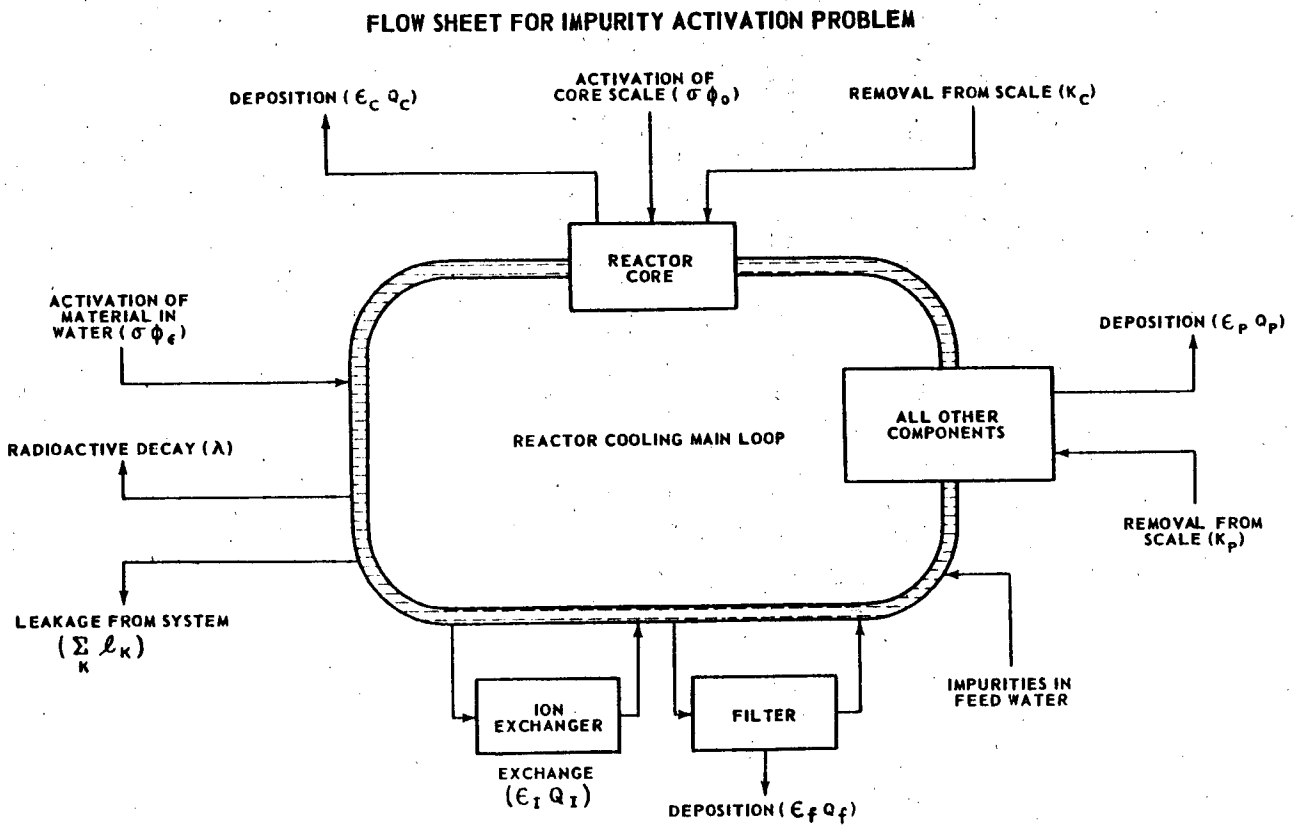

FLOW SHEET FOR IMPURITY ACTIVATION PROBLEM
DEPOSITION (ϵ_c Q_c)
ACTIVATION OF CORE SCALE ($\sigma \phi_o$)
REMOVAL FROM SCALE (K_c)
REACTOR CORE
ACTIVATION OF MATERIAL IN WATER ($\sigma \phi_\epsilon$)
DEPOSITION (ϵ_p Q_p)
ALL OTHER COMPONENTS
REACTOR COOLING MAIN LOOP
RADIOACTIVE DECAY (λ)
REMOVAL FROM SCALE (K_p)
LEAKAGE FROM SYSTEM
$(\sum_K \ell_K)$
ION EXCHANGER
FILTER
IMPURITIES IN FEED WATER
EXCHANGE
$(\epsilon_I Q_I)$
DEPOSITION (ϵ_f Q_f)

Figure 7.3

fourth terms are the rates at which activity is reintroduced into the coolant water as a result of erosion of scale or re-solution of deposited activity from the piping and from the core.

The *rate at which the concentration of the target nuclide builds up* is given by

$$\frac{dN_w}{dt} = -\left(\sum_j \frac{\epsilon_j Q_j}{V_w} + \sum_k \frac{l_k}{V_w} + \sigma\phi_\epsilon\right) N_w + \frac{K_p}{V_w} N_p + \frac{K_c}{V_w} N_c + \frac{C_0 S}{V_w}\frac{N_0}{A} f_n f_s \tag{2}$$

where N_p = concentration of target nuclide on the piping (atoms/cm^3 of scale)
N_c = concentration of target nuclide on the core (atoms/cm^3 of scale)
C_0 = the effective corrosion rate of system (g/cm^2-sec)
S = area of system material exposed to coolant (cm^2)
$N_0 = 6.023 \times 10^{23}$ (atoms/gram-mole), Avogadro's number
A = gram-isotopic weight of the target nuclide
f_n = natural abundance of the target nuclide
f_s = abundance of chemical element in system material (wt. %)

The first term is the rate of loss of target material due to purification by the ion exchanger and filters, to deposition and leakage, and to burn-up in the thermal-neutron flux. The second and third terms are the rates at which material is reintroduced from scale on the piping and core, respectively. The last term represents the rate at which target material is introduced into the loop as a result of the corrosion of system material.

The next equation describes the *rate at which activity builds up on the surface of the core*

$$\frac{dn_c}{dt} = \sigma\phi_0 N_c + \frac{\epsilon_c Q_c}{V_c} n_w - \left(\frac{K_c}{V_c} + \lambda\right) n_c \tag{3}$$

where V_c = volume of scale on the core (cm^3)
ϕ_0 = thermal-neutron flux averaged over the geometry of the core (neutrons/cm^2-sec)

The *rate of build up of the target nuclide on the core* is

$$\frac{dN_c}{dt} = \frac{\epsilon_c Q_c}{V_c} N_w - \left(\frac{K_c}{V_c} + \sigma\phi_0\right) N_c \tag{4}$$

The *rate at which active atoms are deposited on the piping* is given by

$$\frac{dn_p}{dt} = \frac{\epsilon_p Q_p}{V_p} n_w - \left(\frac{K_p}{V_p} + \lambda\right) n_p \tag{5}$$

where $V_p \equiv$ volume of scale on the piping (cm^3).

The *rate at which target material builds up on the pipe walls* is

$$\frac{dN_p}{dt} = \frac{\epsilon_p Q_p}{V_p} N_w - \frac{K_p}{V_p} N_p \tag{6}$$

3.3 Solutions

(a) Equilibrium Solutions. Assume that

$$\frac{C_0 S}{V_w}\frac{N_0}{A} f_n f_s \equiv S_w = \text{a constant}$$

i.e., the corrosion rate of the system material is constant.

When a state of equilibrium has been attained, the rates of change of the n's and N's become simultaneously identically zero. Hence, to obtain expressions for the equilibrium values of the n's and N's, the following matrix equation must be solved:

Eq. No.	N_w	N_p	N_c	n_w	n_p	n_c			
2	α_{11}	α_{12}	α_{13}	0	0	0	$N_w(\infty)$		S_w
6	α_{21}	α_{22}	0	0	0	0	$N_p(\infty)$		0
4	α_{31}	0	α_{33}	0	0	0	$N_c(\infty)$	=	0
1	α_{41}	0	0	α_{44}	α_{45}	α_{46}	$n_w(\infty)$		0
5	0	0	0	α_{54}	α_{55}	0	$n_p(\infty)$		0
3	0	0	α_{63}	α_{64}	0	α_{66}	$n_c(\infty)$		0

where $\alpha_{11} \equiv -\left(\sum_j \frac{\epsilon_j Q_j}{V_w} + \sum_k \frac{l_k}{V_w} + \sigma\phi_\epsilon\right)$

$\alpha_{12} \equiv \frac{K_p}{V_w}$

$\alpha_{13} \equiv \frac{K_c}{V_w}$

$S_w \equiv \frac{C_0 S}{V_w}\frac{N_0}{A} f_n f_s$

$\alpha_{21} \equiv \frac{\epsilon_p Q_p}{V_p}$

$\alpha_{22} \equiv -\frac{K_p}{V_p}$

$\alpha_{31} \equiv \frac{\epsilon_c Q_c}{V_c}$

$\alpha_{33} \equiv -\left(\frac{K_c}{V_c} + \sigma\phi_0\right)$

$\alpha_{41} = \sigma\phi_\epsilon$

$\alpha_{44} = -\left(\sum_j \frac{\epsilon_j Q_j}{V_w} + \sum_k \frac{l_k}{V_w} + \lambda\right)$

$\alpha_{45} = \frac{K_p}{V_w}$

$\alpha_{46} = \frac{K_c}{V_w}$

$\alpha_{54} = \frac{\epsilon_p Q_p}{V_p}$

$\alpha_{55} = -\left(\frac{K_p}{V_p} + \lambda\right)$

$\alpha_{63} = \sigma\phi_0$

$\alpha_{64} = \frac{\epsilon_c Q_c}{V_c}$

$\alpha_{66} = -\left(\frac{K_c}{V_c} + \lambda\right)$

Note that the variables $N_w(\infty)$, $N_p(\infty)$, and $N_c(\infty)$ are in no way coupled to any of the n's. Hence they may be obtained by solving the system

$$\begin{Vmatrix} \alpha_{11} & \alpha_{12} & \alpha_{13} \\ \alpha_{21} & \alpha_{22} & 0 \\ \alpha_{31} & 0 & \alpha_{33} \end{Vmatrix} \begin{Vmatrix} N_w(\infty) \\ N_p(\infty) \\ N_c(\infty) \end{Vmatrix} = \begin{Vmatrix} S_w \\ 0 \\ 0 \end{Vmatrix}$$

Let the determinant of coefficients be Δ_1. Then

$$\Delta_1 = \begin{vmatrix} \alpha_{11} & \alpha_{12} & \alpha_{13} \\ \alpha_{21} & \alpha_{22} & 0 \\ \alpha_{31} & 0 & \alpha_{33} \end{vmatrix} = \alpha_{11}\alpha_{22}\alpha_{33} - \alpha_{13}\alpha_{22}\alpha_{31} - \alpha_{12}\alpha_{21}\alpha_{33}$$

$N_w(\infty)$ is then given by

$$N_w(\infty) = \begin{vmatrix} S_w & \alpha_{12} & \alpha_{13} \\ 0 & \alpha_{22} & 0 \\ 0 & 0 & \alpha_{33} \end{vmatrix} \Delta_1^{-1} = \alpha_{22}\alpha_{33} S_w \Delta_1^{-1}$$

and

$$N_p(\infty) = -\frac{\alpha_{21}}{\alpha_{22}} N_w(\infty) = -\alpha_{21}\alpha_{33}S_w\Delta_1^{-1}$$

and

$$N_c(\infty) = -\frac{\alpha_{31}}{\alpha_{33}} N_w(\infty) = -\alpha_{31}\alpha_{22}S_w\Delta_1^{-1}$$

$n_w(\infty)$, $n_p(\infty)$, and $n_c(\infty)$ are obtained by solving the system

$$\begin{Vmatrix} \alpha_{44} & \alpha_{45} & \alpha_{46} \\ \alpha_{54} & \alpha_{55} & 0 \\ \alpha_{64} & 0 & \alpha_{66} \end{Vmatrix} \begin{Vmatrix} n_w \\ n_p \\ n_c \end{Vmatrix} = \begin{Vmatrix} s_w \\ 0 \\ s_c \end{Vmatrix}$$

where $s_w = -\alpha_{41} N_w(\infty)$ and $s_c = -\alpha_{63} N_c(\infty)$.

Let the determinant of coefficients be denoted by Δ_2. Then

$$\Delta_2 \equiv \begin{vmatrix} \alpha_{44} & \alpha_{45} & \alpha_{46} \\ \alpha_{54} & \alpha_{55} & 0 \\ \alpha_{64} & 0 & \alpha_{66} \end{vmatrix} = \alpha_{44}\alpha_{55}\alpha_{66} - \alpha_{46}\alpha_{55}\alpha_{64} - \alpha_{45}\alpha_{54}\alpha_{66}$$

$n_w(\infty)$ is given by

$$n_w(\infty) = \begin{vmatrix} s_w & \alpha_{45} & \alpha_{46} \\ 0 & \alpha_{55} & 0 \\ s_c & 0 & \alpha_{66} \end{vmatrix} \Delta_2^{-1} = \alpha_{55}\left(\alpha_{66}s_w - \alpha_{46}s_c\right)\Delta_2^{-1}$$

$$= -\alpha_{55}\left(\alpha_{41}\alpha_{66} + \frac{\alpha_{46}\alpha_{63}\alpha_{31}}{\alpha_{33}}\right) N_w(\infty)\,\Delta_2^{-1}$$

$$n_p(\infty) = -\frac{\alpha_{54}}{\alpha_{55}} n_w(\infty) = \alpha_{54}\left(\alpha_{41}\alpha_{66} + \frac{\alpha_{31}\alpha_{46}\alpha_{63}}{\alpha_{33}}\right) N_w(\infty)\,\Delta_2^{-1}$$

$$n_c(\infty) = -\frac{\alpha_{64}}{\alpha_{66}} n_w(\infty) - \frac{\alpha_{63}}{\alpha_{66}} N_c(\infty)$$

$$= \alpha_{55}\alpha_{64}\left(\alpha_{41} + \frac{\alpha_{31}\alpha_{46}\alpha_{63}}{\alpha_{33}\alpha_{66}}\right) N_w(\infty)\,\Delta_2^{-1} + \frac{\alpha_{31}\alpha_{63}}{\alpha_{33}\alpha_{66}} N_w(\infty)$$

Summarizing, the steady-state solutions to the above system of rate equations are as follows:

$$N_w(\infty) = \alpha_{22}\alpha_{33}S_w\,\Delta_1^{-1}$$

$$N_p(\infty) = -\alpha_{21}\alpha_{33}S_w\,\Delta_1^{-1}$$

$$N_c(\infty) = -\alpha_{31}\alpha_{22}S_w\,\Delta_1^{-1}$$

$$n_w(\infty) = -\alpha_{55}\left(\alpha_{41}\alpha_{66} + \frac{\alpha_{31}\alpha_{46}\alpha_{63}}{\alpha_{33}}\right) N_w(\infty)\,\Delta_2^{-1}$$

$$n_p(\infty) = \alpha_{54}\left(\alpha_{41}\alpha_{66} + \frac{\alpha_{31}\alpha_{46}\alpha_{63}}{\alpha_{33}}\right) N_w(\infty)\ \Delta_2^{-1}$$

$$n_c(\infty) = \alpha_{55}\alpha_{64}\left(\alpha_{41} + \frac{\alpha_{31}\alpha_{46}\alpha_{63}}{\alpha_{33}\alpha_{66}}\right) N_w(\infty)\ \Delta_2^{-1} + \frac{\alpha_{31}\alpha_{63}}{\alpha_{33}\alpha_{66}} N_w(\infty)$$

In practical cases equilibrium is reached very rapidly, and the corrosion rate is constant; therefore the above solutions are normally applicable. The quantities $\epsilon_j Q_j/V_q$ and K_j/V_q may be described by the generic term "fractional exchange rate." Thus, $(\epsilon_j Q_j/V_q)N_j$ is the fraction per second of the quantity N_j which is exchanged from a region or component characterized by the index j to the region or component characterized by the index q. Similarly, $(K_j/V_q)N_q$ represents the fraction per second of the quantity N_q which is exchanged from region indexed by q to that indexed by j.

The quantities $\epsilon_I Q_I/V_w$ and $\epsilon_I Q_I/V_I$ can be determined directly from a knowledge of the efficiency ϵ_I with which the ion-exchange region of the demineralizer removes the nuclide in question, of the demineralizer flow rate Q_I, and of the volumes of the demineralizer resin bed and the primary system given, respectively, by V_I and V_w. The quantities $\epsilon_p Q_p/V_w$, $\epsilon_p Q_p/V_p$, K_p/V_w, K_p/V_p, $\epsilon_c Q_c/V_w$, $\epsilon_c Q_c/V_c$, K_c/V_w, and K_c/V_c cannot be directly related to the geometry of the system but must be inferred from activity measurements taken in an actual reactor system or in an experiment simulating a reactor loop. They are the observable macroscopic results of microscopic adsorption and scale-forming reactions which cannot be analyzed by existing methods. Values of these parameters have been inferred from activity measurements taken at the Naval Reactor Testing Facility, Arco, Idaho. These values are tabulated in Table 7.2.

Table 7.2—"FRACTIONAL EXCHANGE RATES" MEASURED AT NRTF

Deposition on the core	$\frac{\epsilon_c Q_c}{V_w} = 5.835 \times 10^{-6}\ \text{sec}^{-1}$	$\frac{\epsilon_c Q_c}{V_c} = 8.811 \times 10^{-6}\ \text{sec}^{-1}$
Deposition on the piping	$\frac{\epsilon_p Q_p}{V_w} = 1.00 \times 10^{-6}\ \text{sec}^{-1}$	$\frac{\epsilon_p Q_p}{V_p} = 1.00 \times 10^{-5}\ \text{sec}^{-1}$
Ion-exchanger removal	$\frac{\epsilon_I Q_I}{V_w} = 5.7 \times 10^{-5}\ \text{sec}^{-1}$	
Re-solution ratio for core and piping	$\frac{K_c}{V_w} = 2.918 \times 10^{-6}\ \text{sec}^{-1}$	$\frac{K_c}{V_c} = 4.406 \times 10^{-6}\ \text{sec}^{-1}$
	$\frac{K_p}{V_w} = 5.0 \times 10^{-7}\ \text{sec}^{-1}$	$\frac{K_p}{V_p} = 5.0 \times 10^{-6}\ \text{sec}^{-1}$
Primary water volume	$V_w = 1.37 \times 10^7\ \text{cm}^3$	

(b) Time-dependent Solutions. Time-dependent solutions to Eqs. 1 to 6 have been obtained and appear in graphical form in Figs. 7.4 to 7.8. (These solutions were obtained with the aid of an Electronic Associates, Inc., general purpose analogue computer.)

3.4 Determining Demineralizer Flow Rate

For purposes of estimating the value of the purification removal rate $\epsilon_I Q_I/V_w$, it is convenient to regard deposition, re-solution, and leakage as second-order effects, being negligible in comparison with removal of activity from the coolant by the demineralizer. Under this assumption, Eqs. 1 and 2 can be written

$$\frac{dn_w}{dt} = \sigma\phi_\epsilon N_w - \left(\frac{\epsilon_I Q_I}{V_w} + \lambda\right) n_w$$

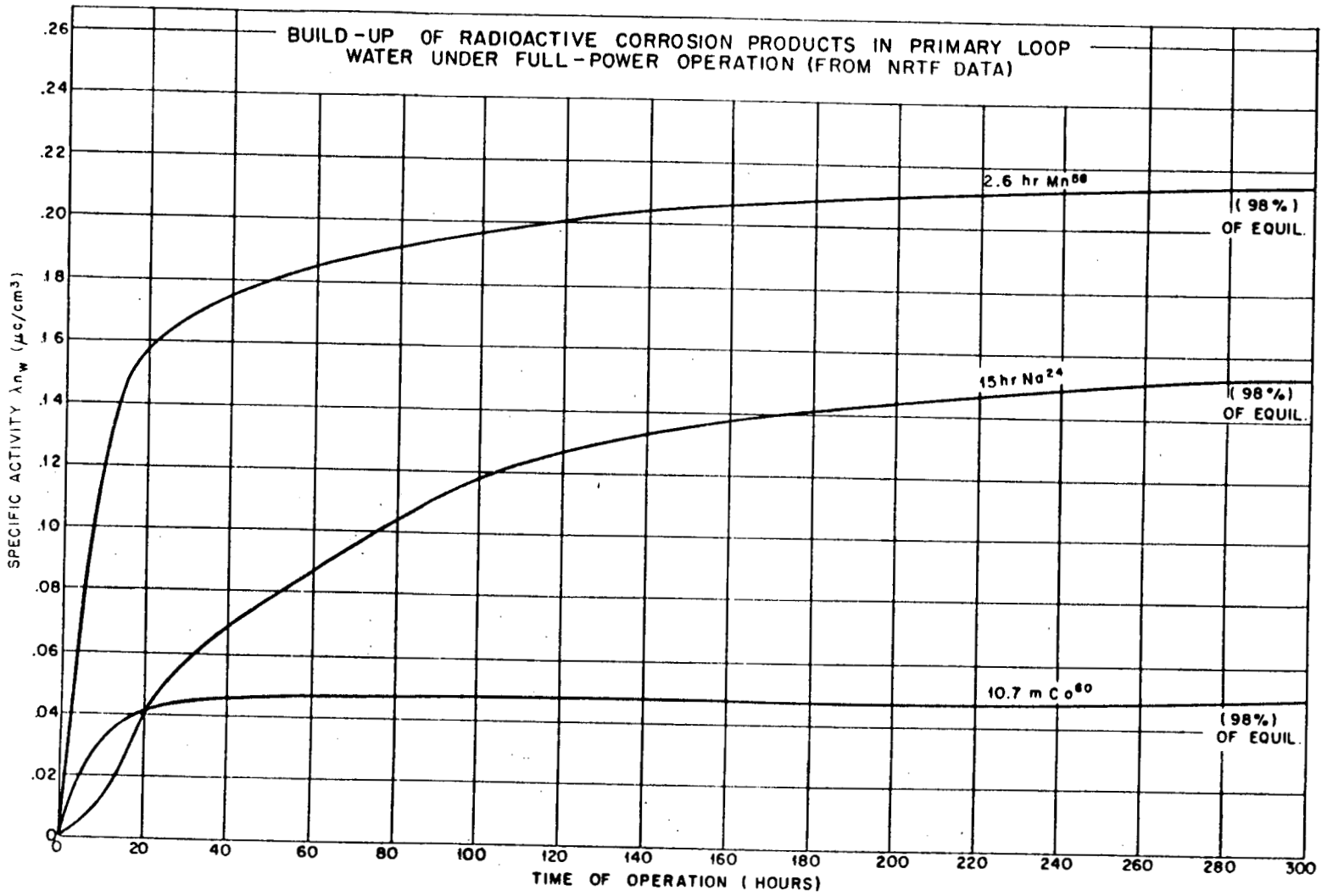

BUILD-UP OF RADIOACTIVE CORROSION PRODUCTS IN PRIMARY LOOP WATER UNDER FULL-POWER OPERATION (FROM NRTF DATA)
SPECIFIC ACTIVITY λn_w ($\mu c/cm^3$)
TIME OF OPERATION (HOURS)
2.6 hr Mn^{56}
(98 %) OF EQUIL.
15 hr Na^{24}
(98 %) OF EQUIL.
10.7 m Co^{60}
(98 %) OF EQUIL.
0
.02
.04
.06
.08
.10
.12
.14
.16
.18
.20
.22
.24
.26
0
20
40
60
80
100
120
140
160
180
200
220
240
260
280
300

Figure 7.4

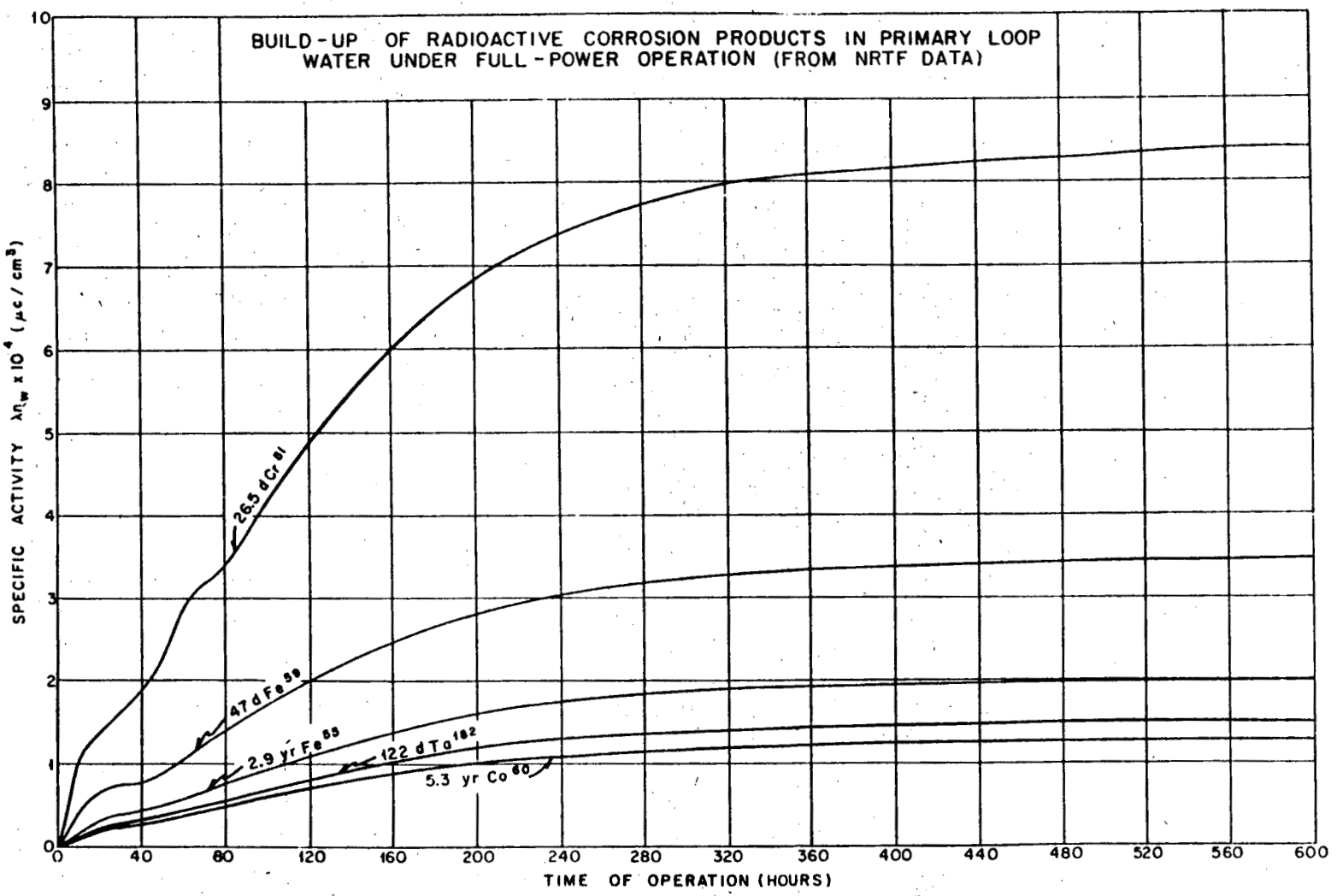

BUILD-UP OF RADIOACTIVE CORROSION PRODUCTS IN PRIMARY LOOP WATER UNDER FULL-POWER OPERATION (FROM NRTF DATA)
SPECIFIC ACTIVITY $\lambda n_w \times 10^4$ ($\mu c / cm^3$)
TIME OF OPERATION (HOURS)
26.5 d Cr^{51}
47 d Fe^{59}
2.9 yr Fe^{55}
122 d Ta^{182}
5.3 yr Co^{60}
0
1
2
3
4
5
6
7
8
9
10
0
40
80
120
160
200
240
280
320
360
400
440
480
520
560
600

Figure 7.5

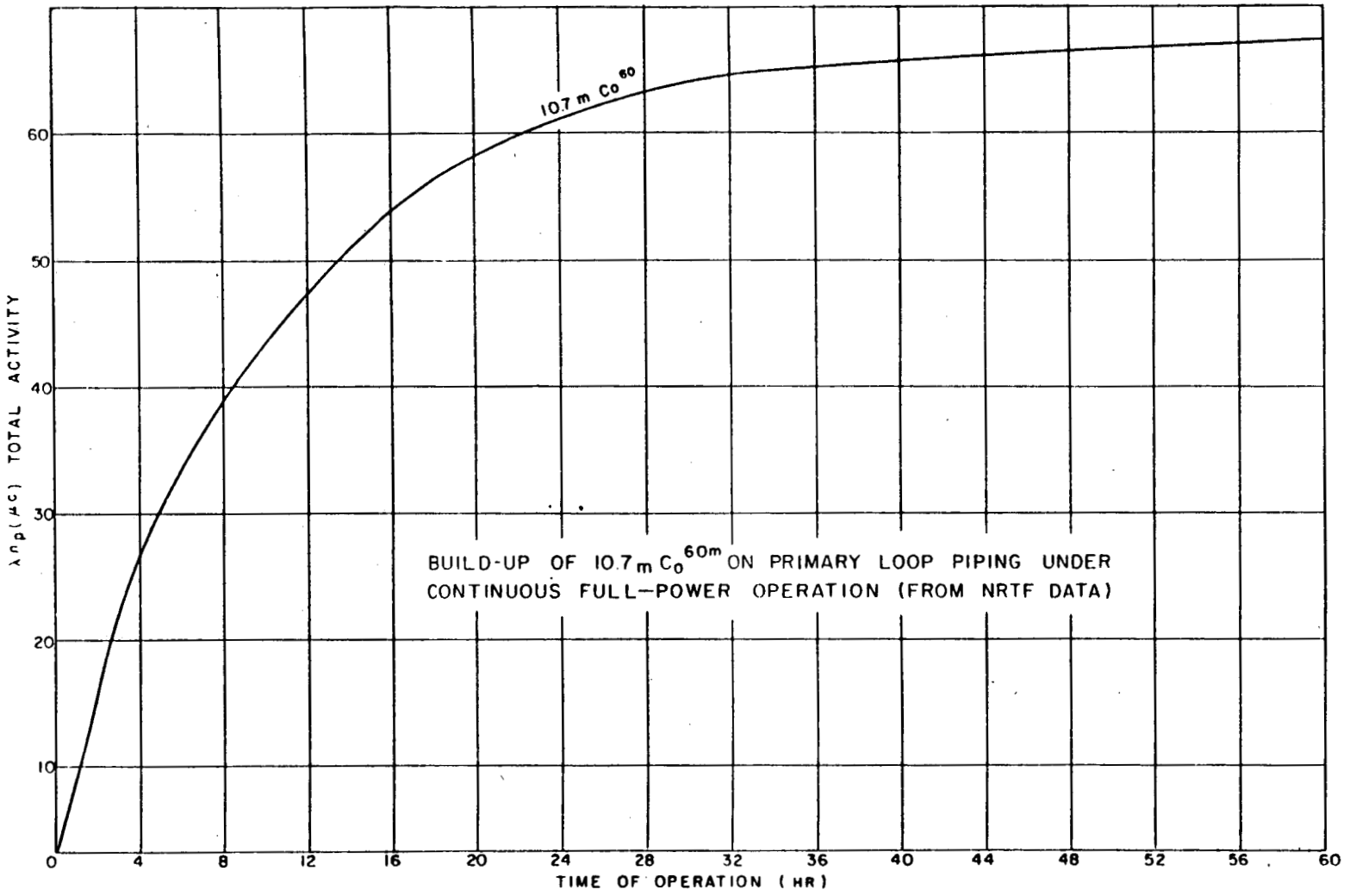

10.7 m Co 60
BUILD-UP OF 10.7 m Co 60m ON PRIMARY LOOP PIPING UNDER
CONTINUOUS FULL-POWER OPERATION (FROM NRTF DATA)
λnp(μc) TOTAL ACTIVITY
TIME OF OPERATION (HR)
0
4
8
12
16
20
24
28
32
36
40
44
48
52
56
60
10
20
30
40
50
60

Figure 7.6

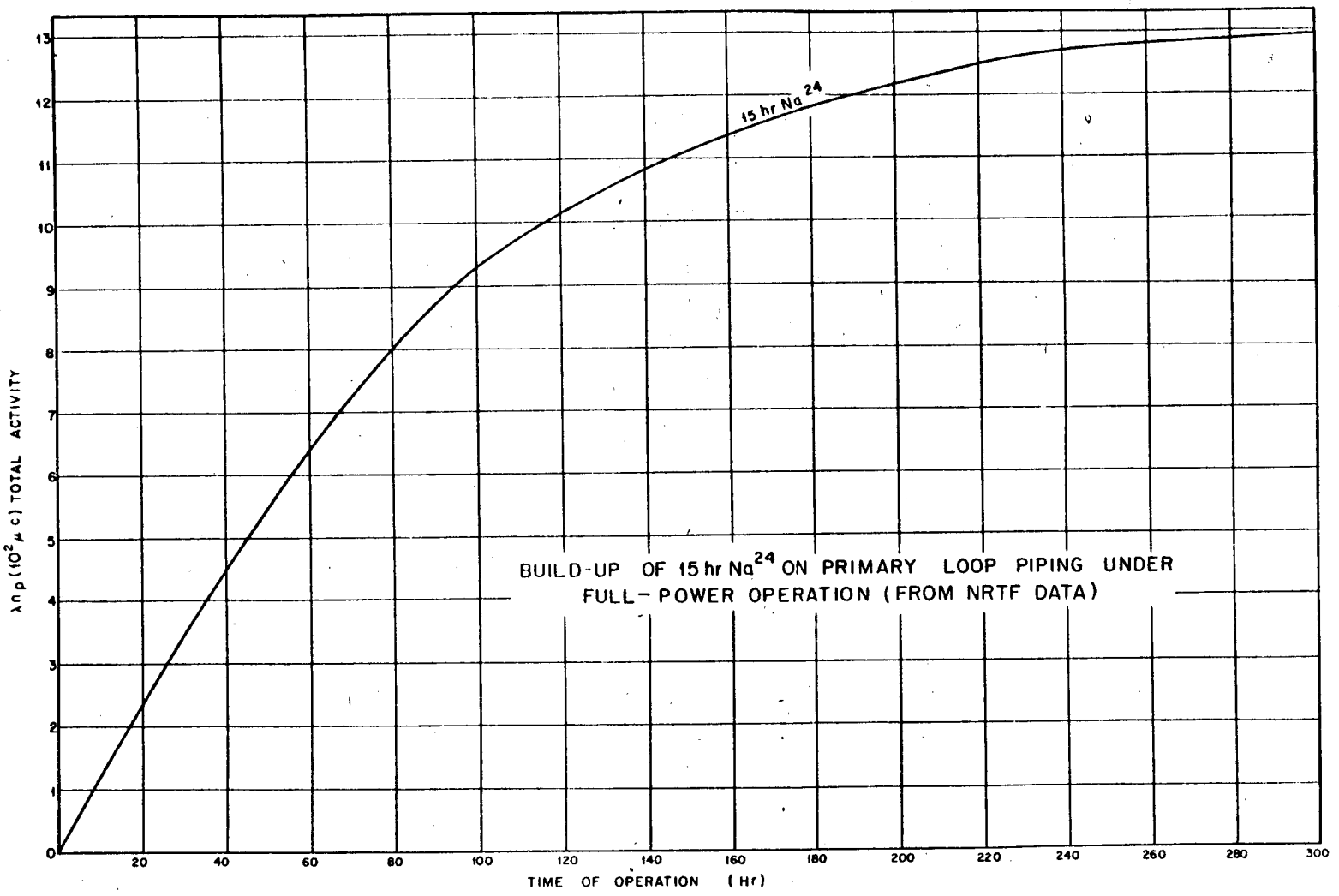

BUILD-UP OF 15 hr Na24 ON PRIMARY LOOP PIPING UNDER FULL-POWER OPERATION (FROM NRTF DATA)
15 hr Na 24
λnp (10² μc) TOTAL ACTIVITY
TIME OF OPERATION (Hr)
0
1
2
3
4
5
6
7
8
9
10
11
12
13
20
40
60
80
100
120
140
160
180
200
220
240
260
280
300

Figure 7.7

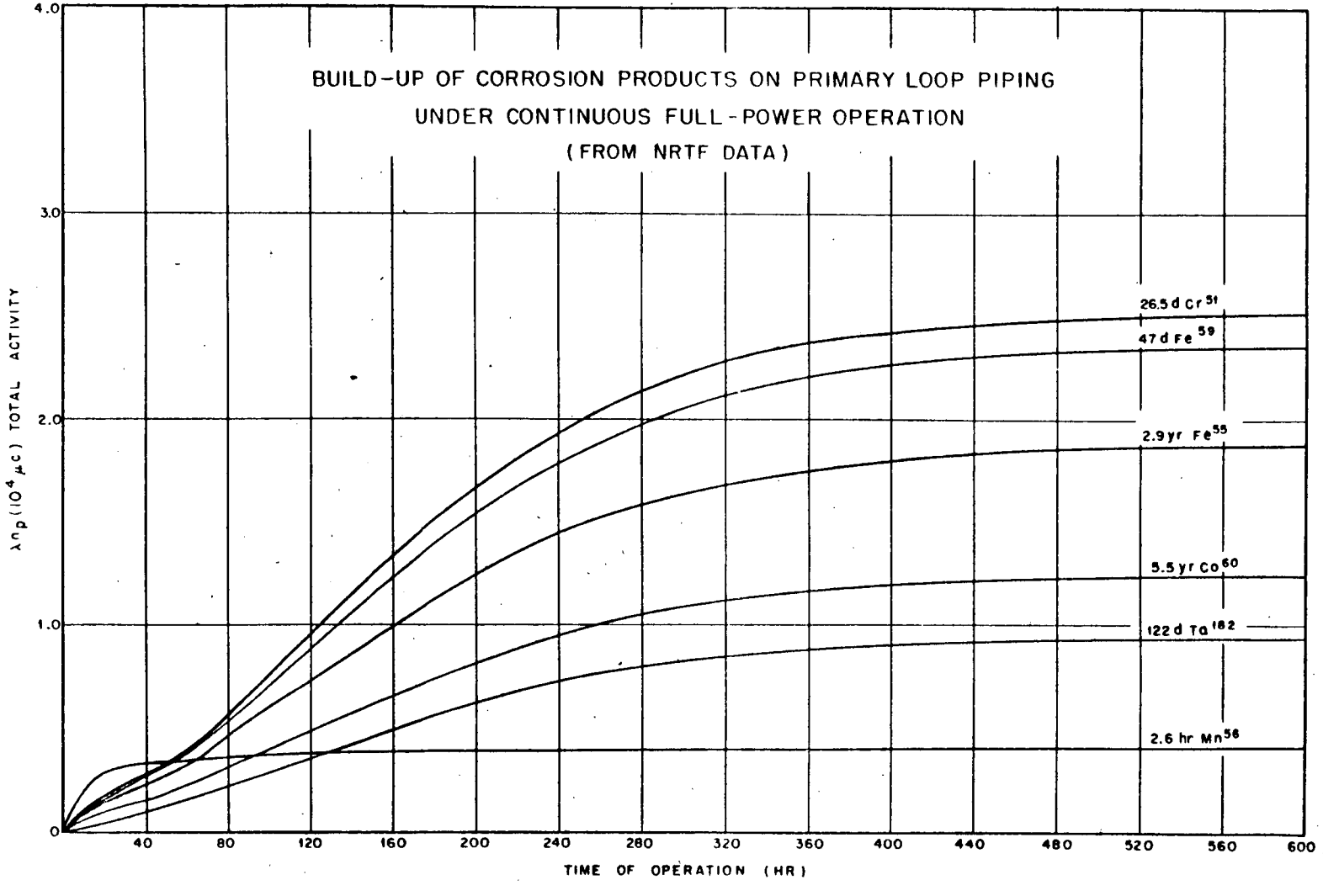

BUILD-UP OF CORROSION PRODUCTS ON PRIMARY LOOP PIPING
UNDER CONTINUOUS FULL-POWER OPERATION
(FROM NRTF DATA)
λn_p (10^4 μc) TOTAL ACTIVITY
TIME OF OPERATION (HR)
26.5 d Cr^{51}
47 d Fe^{59}
2.9 yr Fe^{55}
5.5 yr Co^{60}
122 d Ta^{182}
2.6 hr Mn^{56}
0
1.0
2.0
3.0
4.0
40
80
120
160
200
240
280
320
360
400
440
480
520
560
600

Figure 7.8

$$\frac{dN_w}{dt} = -\left(\frac{\epsilon_I Q_I}{V_w} + \sigma\phi_\epsilon\right) N_w + \frac{C_0 S}{V_w}\frac{N_0}{A} f_n f_s$$

If it is given that the equilibrium activity level of a dominant activity (for example, 2.5-hr Mn^{56}) must not exceed a prescribed value Γ (disintegrations per unit volume per unit time), then solution of Eqs. 1 and 2 for $\epsilon_I Q_I / V_w$ when $dn_w/dt = dN_w/dt = 0$, such that $\lambda N_w(\infty) = \Gamma$ yields

$$\frac{\epsilon_I Q_I}{V_w} = -\frac{\sigma\phi_\epsilon + \lambda}{2} + \left[\frac{(\sigma\phi_\epsilon)^2 + \lambda^2}{2} + \frac{\lambda\sigma\phi_\epsilon}{\Gamma}\frac{C_0 S}{V_w}\frac{N_0}{A} f_n f_s\right]^{1/2}$$

The conditions under which deposition, re-solution, and leakage are truly second-order effects is given by

$$\frac{\epsilon_p Q_p}{V_w} + \frac{\epsilon_c Q_c}{V_w} + \sum_k \frac{l_k}{V_w} \ll \frac{\epsilon_I Q_I}{V_w}$$

These conditions are satisfied for stainless-steel systems. In general the above assumptions will result in a slight overestimate of the required demineralization flow rate Q_I. Since the deposition constants for carbon steel are comparable in value with the demineralizer flow rate, the above methods do not apply to carbon-steel systems.

3.5 Concentration of Radioactivity by Ion Exchangers and Filters

The *rate of activity build-up in an ion exchanger* can be expressed by the following equation

$$\frac{dn_I}{dt} = \frac{\epsilon_I Q_I}{V_I} n_w - \lambda n_I$$

where n_I is the concentration of active nuclide in the ion exchanger (atoms/cm^3) and V_I is the volume of ion-exchange resin.

The *rate of activity build-up in the filter* is

$$\frac{dn_f}{dt} = \frac{\epsilon_f Q_f}{V_f} n_w - \lambda n_f$$

where n_f is the concentration of active nuclide in filter deposit (atoms/cm^3 of deposit) and V_f is the volume of deposit in filter.

The rate of return of active material to the cooling system from the filter and ion exchanger has been assumed to be negligible. For the equilibrium solution to these equations, when the corrosion rate of the system material is constant S_w, the equilibrium solutions discussed in Sec. 3.3a can be used. The following results are obtained

$$n_I(\infty) = -(\alpha_{22}\alpha_{33}\alpha_{41}\alpha_{55}\alpha_{66} + \alpha_{22}\alpha_{31}\alpha_{46}\alpha_{55}\alpha_{63})\frac{\epsilon_I Q_I}{V_I \lambda} S_w \Delta_1^{-1}\Delta_2^{-1}$$

$$n_f(\infty) = -(\alpha_{22}\alpha_{33}\alpha_{41}\alpha_{55}\alpha_{66} + \alpha_{22}\alpha_{31}\alpha_{46}\alpha_{55}\alpha_{63})\frac{\epsilon_f Q_f}{V_f \lambda} S_w \Delta_1^{-1}\Delta_2^{-1}$$

In practical cases, V_f cannot be determined accurately because reactor plant operation will produce unpredictable changes in the thickness of filter deposit. Fortunately, the degree of accuracy required in practical problems is not great; V_f can be estimated and the shielding required by the filter can be calculated on the basis of this estimate.

3.6 Time-dependent Neutron Flux

In the preceding paragraphs it has been assumed that the thermal-neutron flux remained constant over the entire reactor life. It should be noted, however, that, if a reactor is to be operated continuously throughout its life span at a constant power level, then its thermal-neutron flux must increase with time in such a way as to maintain the specific fission rate at a constant level; this variation will depend on the reactor design.

For a typical case

$$\phi(t) = \frac{\phi_0}{(1 - \sigma_a \phi_0 t)}$$

where σ_a is the total thermal cross section of U^{235} (cm^2) and ϕ_0 is the initial value of thermal-neutron flux (neutrons/cm^2-sec).

The fraction f of the initial quantity of U^{235} which has been burned out of the core as a consequence of fissioning is simply

$$f = \sigma_a \phi_0 t$$

The value which f can attain before a core reaches the end of its life span is in the neighborhood of 0.25 to 0.40. The thermal flux of a reactor is bounded according to the inequality

$$\phi_0 < \phi(t) < \frac{\phi_0}{1 - \sigma_a \phi_0 T_R}$$

where T_R is the estimated life of the reactor core.

Since the coolant activity resulting from the transmutation of corrosion products is proportional to ϕ, the lower and upper bounds for the activity levels with respect to the thermal flux are obtained by assuming $\phi = \phi_0$ and $\phi = \phi_0/(1 - \sigma_a \phi T_R)$, respectively. Since the coolant activity is directly proportional to flux, it follows that the equilibrium coolant activity level at times approaching the end of reactor life will be, at most, a factor of $(1 - \sigma_a \phi_0 T_R)^{-1}$ times higher than that which occurs during the first part of the life of the reactor. (See Table 7.3.)

4 FISSION PRODUCTS IN THE COOLANT SYSTEM

The previous section dealt with a situation wherein the corrosion integrity of the reactor core itself was high. In the event that the corrosion integrity of the core is low, it is also necessary to calculate the effect on system activities of corrosion of the fuel-bearing material and the consequent release of fission products into the reactor cooling system. These fission products are released as gases, insolubles, and solubles.

At present little is known regarding the manner in which fuel-bearing material of a given composition corrodes. Lack of knowledge regarding the chemical behavior of many of the fission products further limits such a determination. The *mathematical* formulation of this problem would, of course, be similar to, but more complex than, that developed to describe the corrosion of the system material.

A technique has been developed for determining the distribution of fission-product gases in water-cooled reactor systems, and it is described below. As an approximation it is possible to treat nongaseous fission products in a similar manner by making simplifying assumptions with respect to deposition and also removal of the solids from the surfaces of the coolant loop. The generalized problem for all fission products is presently being coded for a digital computer.

Table 7.3—RADIOACTIVITY OF TYPICAL REACTOR COOLING WATER*

Nuclide	Half life	Specific activity†	Source
N^{16}	7.3 sec	100 μc/ml	O^{16} in H_2O
N^{17}	4.1 sec	800 neutrons/cm^3-sec	O^{17} in H_2O
K^{38}	7.7 min	5×10^{-2} μc/ml	?
A^{41}	1.8 hr	4×10^{-2} μc/ml‡	Air in H_2O
F^{18}	1.9 hr	4×10^{-2} μc/ml	?
Mn^{56}	2.6 hr	0.5×10^{-2} μc/ml	Steel
Na^{24}	15 hr	10^{-3} μc/ml‡	Na in H_2O
Co^{60}	5.3 yr	2.5×10^{-5} μc/ml	Steel
Fe^{59}	45 days	1.1×10^{-5} μc/ml	Steel
Ta^{182}	111 days	0.6×10^{-5} μc/ml	Steel
Total activity of crud: 10 to 100 μc/mg			

*Data from Pressurized Water Reactor Chemistry, by T. Rockwell and P. Cohen, presented for the International Conference on Peaceful Uses of Atomic Energy, 1955.

†Saturation activity of primary coolant water at full power, full flow.

‡Varies with rate and composition of charging water.

NOTES: (a) Fifteen minutes after shutdown the loop activity is 0.05 to 0.1 μc/cm^3, giving a field of 2 to 200 mr/hr. At 100 hr it is down to 5 to 50 mr/hr.

(b) Maximum surface contamination from spillage of primary-loop water has been 50,000 counts/min from a smear taken over 12 sq in. Normal surface activity is negligible.

(c) Maximum air contamination during serious leakage of primary coolant into the shielding compartment has been 10^{-7} μc/cm^3. Normal air activity under the shield is less than 10^{-10} μc/cm^3.

4.1 Distribution of Fission-product Gases in Water-cooled Reactor Systems

There are two modes by which fission-product gases may be released into the water: (1) the fission products may be released continuously through a defect in the cladding of a fuel element or (2) the fuel element may fail completely and release some fraction of its contents instantaneously. Both modes of release are discussed.

4.2 Continuous Release of Fission-product Gases

The most probable fuel-element failure is one which is brought about by a small defect of the fuel-element cladding. This allows the fission-product gases to be released into the water and from there into the air. The gases are assumed to escape continuously from the fracture at some constant fraction of their direct production rate by fission.

The fission products may, for calculational purposes, be divided into two groups: (1) those isotopes which are formed only directly in fission (denoted by the subscript x) and (2) those isotopes which result from the decay of parent isotopes (denoted by the subscript y); these may also be formed directly in fission.

(a) The Core. The behavior of these isotopes in the core or individual fuel element may be described by the following two differential equations:

$$\frac{dn_{x_1}}{dt} = Y_x K - \lambda_x n_{x_1} - \alpha Y_x K \quad \text{(atoms/sec)} \tag{7}$$

and

$$\frac{dn_{y_1}}{dt} = Y_y K + \lambda_x n_{x_1} - \lambda_y n_{y_1} - \alpha Y_y K \quad \text{(atoms/sec)} \tag{8}$$

where n_{x_1} ≡ the number of active atoms of isotope x in the core (atoms)
n_{y_1} ≡ the number of active atoms of isotope y in the core (atoms)
Y_x ≡ fission yield of isotope x
Y_y ≡ fission yield of isotope y
K ≡ the fissioning rate (fissions/sec)
λ_x ≡ the decay constant of parent isotope x (sec^{-1})
λ_y ≡ the decay constant of isotope y (sec^{-1})
α ≡ fraction of the number of atoms formed which is released into the primary coolant

The solution of Eq. 7 is given by

$$\lambda_x n_{x_1} = (1-\alpha) Y_x K (1 - e^{-\lambda_x}) \quad \text{(dis/sec)} \tag{9}$$

where t is the operation time in seconds.

The solution of Eq. 8 is given by

$$\lambda_y n_{y_1} = (1-\alpha)(Y_y + Y_x)\, K(1 - e^{-\lambda_y t}) + \frac{(1-\alpha) Y_x K \lambda_y [1 - e^{-(\lambda_x - \lambda_y)t}] e^{-\lambda_x t}}{\lambda_x - \lambda_y} \quad \text{(dis/sec)} \tag{10}$$

For very short lived precursors the second term on the right of Eq. 10 is negligible compared to the first.

(b) The Primary Coolant. When the gases escape from the fuel element at the rate $\alpha Y_x K$ atoms per second, then the build-up of active atoms in the coolant is given by Eqs. 11 and 12

$$\frac{dn_{x_2}}{dt} = \alpha Y_x K - \lambda_x n_{x_2} - \beta n_{x_2} - \frac{l}{V_w} n_{x_2} \quad \text{(atoms/sec)} \tag{11}$$

and

$$\frac{dn_{y_2}}{dt} = \alpha Y_y K + \lambda_x n_{x_2} - \lambda_y n_{y_2} - \beta n_{y_2} - \frac{l}{V_w} n_{y_2} \quad \text{(atoms/sec)} \tag{12}$$

where β ≡ the fractional removal rate of the ion exchanger or degassifier (sec^{-1})
l ≡ the leak rate from the cooling system into reactor-compartment air (cm^3/sec)
V_w ≡ volume of primary coolant (cm^3)
and the subscript 2 denotes the primary coolant.

The last term of Eqs. 11 and 12 may be neglected in most cases since the fraction of water leaking out of the primary system is very small. The time-dependent solutions of these equations are as follows:

$$\lambda_x n_{x_2} = \frac{\lambda_x \alpha Y_x K}{\lambda_x + \beta} [1 - e^{-(\lambda_x + \beta)t}] \quad \text{(dis/sec)} \tag{13}$$

and

$$\lambda_y n_{y_2} = \frac{\alpha \lambda_y}{\lambda_y + \beta} \left(Y_y K + \frac{\lambda_x Y_x K}{\lambda_x + \beta} \right) [1 - e^{-(\lambda_y + \beta)t}] + \frac{\lambda_x \lambda_y \alpha Y_x K}{(\lambda_x + \beta)(\lambda_x - \lambda_y)} [1 - e^{-(\lambda_y - \lambda_x)t}]\, e^{-(\lambda_x + \beta)t} \quad \text{(dis/sec)} \tag{14}$$

The second term on the right of Eq. 14 may be negligible if the operation time, t sec, is large compared to $(\lambda_x + \beta)^{-1}$.

The steady-state solutions of Eqs. 11 and 12 are:

$$\lambda_x \, n_{x_2}(\infty) = \frac{\lambda_x \alpha \, Y_x K}{\lambda_x + \beta} \quad \text{(dis/sec)}$$

and

$$\lambda_y \, n_{y_2}(\infty) = \frac{\alpha \, \lambda_y}{\lambda_y + \beta}\left(Y_y K + \frac{\lambda_x Y_x K}{\lambda_x + \beta}\right) \quad \text{(dis/sec)}$$

These equations give the total activity of the primary-coolant system due to the particular isotope, x or y; the specific activity may be obtained by dividing the equations by the primary-coolant water volume.

(c) The Reactor Plant Container. In cases where the reactor plant is contained in an airtight space, leakage of fission-product gases from the coolant system introduces a potential health hazard. Most of the hazard associated with these gases is one of breathing and ingestion and not direct radiation exposure. In such cases the concentration of fission-product gases in the air must be determined. The rate of change of the number of active atoms in the reactor plant container is given by Eqs. 15 and 16 for isotopes of type x and y, respectively.

For isotope x

$$\frac{dn_{x_3}}{dt} = \frac{l}{V_c} n_{x_2} - \lambda_x n_{x_3} - \frac{L}{V_c} n_{x_3} \tag{15}$$

and for isotope y

$$\frac{dn_{y_3}}{dt} = \frac{l}{V_c} n_{y_2} + \lambda_x n_{x_3} - \lambda_y n_{y_3} - \frac{L}{V_c} n_{y_3} \tag{16}$$

where $L \equiv$ the rate of air evacuation (cm^3/sec), if any

$V_c \equiv$ the reactor plant container volume (cm^3)

and the subscript 3 denotes the reactor plant container.

The time-dependent solutions of Eqs. 15 and 16 are:

$$\lambda_x \, n_{x_3}(t) = \frac{\lambda_x (l/V_c)\alpha}{\lambda_x + \beta} \, Y_x K \left\{ \frac{1 - e^{-[\lambda_x + (L/V_c)]t}}{\lambda_x + L/V_c} + \frac{1 - e^{-[\beta - (L/V_c)]t}}{\beta - (L/V_c)} \, e^{-[\lambda_x + (L/V_c)]t} \right\} \quad \text{(dis/sec)} \tag{17}$$

and

$$\lambda_y \, n_{y_3}(t) = \frac{\lambda_y (l/V_c)\alpha}{\lambda_y + \beta}\left(Y_y K + \frac{\lambda_x Y_x K}{\lambda_x + \beta}\right)\left\{ \frac{1 - e^{-[\lambda_y + (L/V_c)]t}}{\lambda_y + L/V_c} + \frac{[1 - e^{-(L/V_c - \beta)t}]e^{-(\lambda_y + \beta)t}}{\beta - L/V_c} \right\} + \frac{\lambda_y \lambda_x (l/V_c)\alpha Y_x K}{(\lambda_x + \beta)(\lambda_x - \lambda_y)}\left(\frac{[1 - e^{-(L/V_c - \beta)t}]e^{-(\lambda_y + \beta)t}}{\beta - L/V_c} + \frac{\{1 - e^{-[\lambda_x - \lambda_y + \beta - (L/V_c)]t}\}e^{-[\lambda_y + (L/V_c)]t}}{\lambda_x - \lambda_y + \beta - L/V_c} \right)$$

$$+ \lambda_y \lambda_x \frac{l/V_c}{\lambda_x + \beta} \alpha Y_x K \left(\frac{1 - e^{-[\lambda_y t (L/V_c)]t}}{[\lambda_x + (L/V_c)][\lambda_y + (L/V_c)]} \right.$$

$$+\frac{\{1-e^{-[\lambda_x-\lambda_y+\beta-(L/V_c)]t}\}e^{-[\lambda_y t(L/V_c)]t}}{[\lambda_x-\lambda_y+\beta-(L/V_c)][\beta-(L/V_c)]}$$

$$+\left[\frac{1}{\lambda_x+(L/V_c)}+\frac{1}{\beta-(L/V_c)}\right]\left\{\frac{[1-e^{-(\lambda_y-\lambda_x)t}]e^{-[\lambda_y+(L/V_c)]t}}{\lambda_x-\lambda_y}\right\}\Bigg) \quad \text{(dis/sec)} \quad (18)$$

The steady-state solutions of Eqs. 15 and 16 in the reactor plant container are as follows: For isotope x

$$\lambda_x n_{x_3}(\infty)=\frac{\lambda_x(l/V_c)\alpha Y_x K}{(\lambda_x+\beta)[\lambda_x+(L/V_c)]} \quad \text{(dis/sec)}$$

For isotope y

$$\lambda_y n_{y_3}(\infty)=\frac{\lambda_y(l/V_c)}{\left(\lambda_y+\frac{L}{V_c}\right)\left\{\frac{Y_y K}{\lambda_y+\beta}+\left[\frac{1}{\lambda_y+\beta}+\frac{1}{\lambda_x+(L/V_c)}\right]\left(\frac{\lambda_x Y_x K}{\lambda_x+\beta}\right)\right\}}$$

4.3 Noncontinuous Release of Fission Products

A second type of fuel-element failure is one which releases fission products into the primary coolant instantaneously. A failure of this type is usually less likely to occur than the pin-hole failure described in the previous section. Assuming such an event to occur, the following is a mathematical description of the behavior of the fission products in the coolant and reactor plant container.

The build-up of radioactive atoms in the core is given by Eqs. 7 and 8. In order to describe the release of the fission products in a general manner, assume that the reactor has been operating and that, at some time $t = T_b$, a burst or instantaneous release occurs. At this point another time coordinate t', whose origin corresponds to $t = T_b$, must be introduced. Another parameter to be considered is the time at which a primary-coolant leak occurs. This time T_l is measured from the time $t = T_b$ in the t' frame of reference.

The rate of change of active atoms in the primary coolant is given by

$$\frac{dn_{x_2}}{dt'}=-(\lambda_x+\beta)n_{x_2} \qquad n_{x_2}\Big|_{t'=0}=\theta\, n_{x_1}\Big|_{t=T_b} \quad (19)$$

$$\frac{dn_{y_2}}{dt'}=\lambda_x n_{x_2}-(\lambda_y+\beta)n_{y_2} \qquad n_{y_2}\Big|_{t'=0}=\theta\, n_{y_1}\Big|_{t=T_b} \quad (20)$$

where n_{x_2} and n_{y_2} are as previously defined. The net rate of change in the number of atoms of isotope x in the coolant is dn_{x_2}/dt'. The term $-(\lambda_x+\beta)n_{x_2}$ is the rate of decrease in n_{x_2} due to the combined effects of radioactive decay and coolant purification. At the instant $t' = 0$ ($t = T_b$), a quantity $\theta\, n_{x_1}(T_b)$ atoms of isotope x is released into the coolant by the instantaneous disintegration of θ (the number of) fuel elements. This value determines the initial level of x activity in the coolant. The net rate of change in the number of atoms of isotope y in the coolant is dn_{y_2}/dt'. The rate at which the parent isotope x present in the coolant is decaying to form its daughter isotope y is represented by $\lambda_x n_{x_2}$. The rate at which n_{y_2} decreases due to the combined effects of radioactive decay and coolant purification is $(\lambda_y+\beta)n_{y_2}$. At the instant $t' = 0$ ($t = T_b$), a quantity $\theta\, n_{y_1}(T_b)$ atoms of isotope y is released into the coolant by the instantaneous disintegration of θ fuel elements. This value determines the initial level of y activity in the coolant.

The rate of build-up in the vapor-container air due to a leak of l cubic centimeters of water per second is given by

$$\frac{dn_{x_3}}{dt'} = \frac{l}{V_c} n_{x_2} u(t' - T_l) - \left(\lambda_x + \frac{L}{V_c}\right) n_{x_3} \qquad n_{x_3}\Big|_{t'=0} = 0 \tag{21}$$

$$\frac{dn_{y_3}}{dt'} = \frac{l}{V_c} n_{y_2} u(t' - T_l) + \lambda_x n_{x_3} - \left(\lambda_y + \frac{L}{V_c}\right) n_{y_3} \qquad n_{y_3}\Big|_{t'=0} = 0 \tag{22}$$

where $u(t' - T_l) = 0$ when $t' < T_l$
$= 1$ when $t' \geq T_l$

The rate of change of the number of atoms of isotope x in the reactor plant container is dn_{x_3}/dt', and $[(l/V_c)n_{x_2}u(t' - T_l)]$ is the number of atoms per second introduced into the reactor plant container, assuming the reactor is housed in a reasonably airtight structure, as a result of a leak of l cubic centimeters per second of coolant occurring at, and continuing subsequent to, $t' = T_l$. The rate of decrease of n_{x_3} due to the combined effects of radioactive decay and air purification is $-(\lambda_x + L/V_c)n_{x_3}$. The rate of change of the number of atoms of isotope y in the reactor plant container is dn_{y_3}/dt', and $[(l/V_c)n_{y_2}u(t' - T_l)]$ is the number of atoms per second introduced into the reactor plant container as a result of a leak of l cubic centimeters per second of coolant occurring at, and continuing subsequent to, $t' = T_l$. The rate of production of n_{y_3} as a result of the decay of its parent n_{x_3} is $\lambda_x n_{x_3}$. The rate of decrease of n_{y_2} due to the combined effects of radioactive decay and air purification is represented by $-(\lambda_y + L/V_c)n_{y_3}$.

The solutions to the above equations are as follows:

In the primary coolant

$$\begin{aligned} \lambda_x n_{x_2} &= \theta\lambda_x n_{x_1}(T_b)\, e^{-(\lambda_x+\beta)(t-T_b)} && t > T_b \\ &= 0 && t < T_b \end{aligned} \tag{23}$$

$$\begin{aligned} \lambda_y n_{y_2} &= \theta\lambda_y n_{y_1}(T_b)\, e^{-(\lambda_y+\beta)(t-T_b)} \\ &\quad + \frac{\lambda_x\theta\, n_{x_1}(T_b)}{\lambda_y - \lambda_x}\left[e^{-(\lambda_x+\beta)(t-T_b)} - e^{-(\lambda_y+\beta)(t-T_b)}\right] && t > T_b \\ &= 0 && t < T_b \end{aligned} \tag{24}$$

In the reactor plant container (assumed reasonably airtight)

$$\begin{aligned} \lambda_x n_{x_3}(t') &= \lambda_y \frac{l}{V_c} \frac{\theta\, n_{x_1}(T_b)}{(L/V_c) - \beta} e^{-[\lambda_x+(L/V_c)](t'-T_l)} && t' > T_l \\ &= 0 && t' < T_l \end{aligned} \Bigg\} \frac{L}{V_c} \neq \beta$$

$$\begin{aligned} \lambda_x n_{x_3}(t') &= \lambda_x \frac{l}{V_c} \theta\, n_{x_1}(T_b)\,(t' - T_l) e^{-[\lambda_x+(L/V_c)](t'-T_l)} && t' > T_l \\ &= 0 && t' < T_l \end{aligned} \Bigg\} \frac{L}{V_c} = \beta \tag{25}$$

$$\lambda_y n_{y_3}(t') = \lambda_y \frac{l}{V_c} \frac{\theta\, n_{y_1}(T_b)}{\frac{L}{V_c} - \beta} \left\{e^{-(\lambda_y+\beta)(t'-T_l)} - e^{-[\lambda_y+(L/V_c)](t'-T_l)}\right\}$$

$$+ \lambda_y \frac{l}{V_c} \lambda_x n_{x_1}(T_b) \left\{\left(\frac{1}{\frac{L}{V_c} - \beta} - \frac{1}{\lambda_y - \lambda_x}\right) \frac{e^{-(\lambda_x+\beta)(t'-T_l)} - e^{-[\lambda_y+(L/V_c)](t'-T_l)}}{\beta - \frac{L}{V_c} - \lambda_y - \lambda_x}\right.$$

$$+\frac{e^{-[\lambda_x+(L/V_c)](t'-T_l)} - e^{-(\lambda_y+\beta)(t'-T_l)}}{\left(\beta-\frac{L}{V_c}\right)(\lambda_y-\lambda_x)}\Bigg\}. \qquad t' > T_l \Bigg\} \frac{L}{V_c} \neq \beta \tag{26}$$

$$= 0 \qquad t' < T_l \Bigg\}$$

$$\lambda_y\, n_{y_3}(t') = \lambda_y\lambda_x \frac{l}{V_c} \frac{\theta\, n_{x_1}(T_b)}{(\lambda_y-\lambda_x)^2}\left[(\lambda_y-\lambda_x)(t'-T_l)-2\right]\left[e^{-(\lambda_y+\beta)(t'-T_l)} - e^{-(\lambda_y+\beta)(t'-T_l)}\right]$$

$$+\lambda_y \frac{l}{V_c}\theta\, n_{y_1}(T_b)\,(t'-T_l)\, e^{-(\lambda_y+\beta)(t'-T_l)} \qquad t' > T_l \Bigg\} \frac{L}{V_c} = \beta$$

$$= 0 \qquad t' < T_l \Bigg\}$$

Note: The above development is applicable to nonvolatile fission products as well as volatile fission products.

4.4 Alternate Approach to Case of Continuous Release of Fission-product Gases

In Sec. 4.2 the case of continuous release of the fission-product gases was considered. The release rate was assumed to be a constant fraction of the fission rate. This assumption is particularly applicable to fuel materials which are porous to fission gases.

If the fuel material is not porous, another assumption may be more applicable. The quantity of the isotope released may be proportional to the total quantity in the fuel element. Specifically

$$\frac{dn_{x_1}}{dt} = Y_x K - \lambda_x n_{x_1} - \alpha' n_{x_1} \tag{27}$$

and

$$\frac{dn_{x_2}}{dt} = \alpha' n_{x_1} - (\lambda_x + \beta) n_{x_2} \tag{28}$$

where α' is now a rate and has the units sec^{-1}; all other terms have been defined in Sec. 4.2a.

The solutions of Eqs. 27 and 28 are

$$\lambda_x\, n_{x_1}(t) = \frac{\lambda_x Y_x K}{\lambda_x + \alpha'}\left[1 - e^{-(\lambda_x+\alpha')t}\right] \tag{29}$$

and

$$\lambda_x\, n_{x_2}(t) = \frac{\alpha'\lambda_x Y_x K}{\lambda_x + \alpha'}\left[\frac{1-e^{-(\lambda_x+\beta)t}}{\lambda_x+\beta} - \frac{1-e^{-(\beta-\alpha')t}}{\beta-\alpha'}\, e^{-(\lambda_x+\beta)t}\right] \tag{30}$$

These equations should be compared with Eqs. 9 and 13. From the above equations it can be seen that the build-up to equilibrium is dependent on α'; thus at the beginning the rate of introduction is small and builds up to a maximum.

If the equilibrium level predicted, using one of the above formulations, is to be equal to that predicted by the other, then it is necessary that $\alpha = \alpha'/(\lambda_x + \alpha')$. For $\lambda_x \ll \alpha'$, the activity in the coolant is independent of the release rate; this is equivalent to saying that α is unity in Sec. 4.2a or that the rate of release is equal to the fission rate. If $\lambda_x \geq \alpha'$, then $\alpha < 1$. Therefore, the smaller the half life the less the probability of escape. The escape probability for this description depends strongly on the half life of the isotope.

If the equations of both descriptions are written, the functional dependence of α and α' may be made clear.

For the total activity

$$\lambda_X n_{X_T} = Y_X K \qquad \alpha = \text{const.} \qquad\qquad \lambda_X n_{X_T} = Y_X K \qquad \alpha' = \text{rate } (\text{sec}^{-1}) \tag{31}$$

For activity in the fuel element

$$\frac{dn_{X_1}}{dt} = (1-\alpha) Y_X K - \lambda_X n_{X_1} \qquad \alpha = \text{const.} \qquad\qquad \frac{dn_{X_1}}{dt} = Y_X K - (\lambda_X + \alpha') n_{X_1}$$

$$\alpha' = \text{rate } (\text{sec}^{-1}) \tag{32}$$

$$\lambda_X\, n_{X_1}(\infty) = (1-\alpha) Y_X K \qquad \alpha = \text{const.} \qquad\qquad \lambda_X\, n_{X_1}(\infty) = \frac{\lambda_X Y_X K}{\lambda_X + \alpha'}$$

$$\alpha' = \text{rate } (\text{sec}^{-1}) \tag{33}$$

For activity in the coolant

$$\frac{dn_{X_2}}{dt} = \alpha Y_X K - (\lambda_X + \beta) n_{X_2} \qquad \alpha = \text{const.} \qquad\qquad \frac{dn_{X_2}}{dt} = \alpha' n_{X_1} - (\lambda_X + \beta) n_{X_2}$$

$$\alpha' = \text{rate } (\text{sec}^{-1}) \tag{34}$$

$$\lambda_X\, n_{X_2}(\infty) = \frac{\alpha \lambda_X Y_X K}{\lambda_X + \beta} \qquad \alpha = \text{const.} \qquad\qquad \lambda_X\, n_{X_2}(\infty) = \frac{\alpha' \lambda_X Y_X K}{(\lambda_X + \alpha')(\lambda_X + \beta)}$$

$$\alpha' = \text{rate } (\text{sec}^{-1}) \tag{35}$$

For activity in the ion exchanger

$$\frac{dn_{X_i}}{dt} = \beta n_{X_2} - \lambda_X n_{X_i} \qquad \alpha = \text{const.} \qquad\qquad \frac{dn_{X_i}}{dt} = \beta n_{X_2} - \lambda_X n_{X_i}$$

$$\alpha' = \text{rate } (\text{sec}^{-1}) \tag{36}$$

$$\lambda_X\, n_{X_i}(\infty) = \frac{\beta \alpha Y_X K}{\lambda_X + \beta} \qquad \alpha = \text{const.} \qquad\qquad \lambda_X\, n_{X_i}(\infty) = \frac{\beta \alpha' Y_X K}{(\lambda_X + \beta)(\lambda_X + \alpha')}$$

$$\alpha' = \text{rate } (\text{sec}^{-1}) \tag{37}$$

Taking the ratio of Eq. 37 to Eq. 31

$$\frac{\lambda_X\, n_{X_i}(\infty)}{\lambda_X\, n_{X_T}(\infty)} = \frac{\alpha \beta}{\lambda_X + \beta} \qquad \alpha = \text{const.} \qquad\qquad \frac{\lambda_X\, n_{X_i}(\infty)}{\lambda_X\, n_{X_T}(\infty)} = \frac{\alpha' \beta}{(\lambda_X + \beta)(\lambda_X + \alpha')}$$

$$\alpha' = \text{rate } (\text{sec}^{-1})$$

For $\lambda_X \gg \beta$

$$\alpha = \frac{\lambda_X\, n_{X_i}(\infty)}{\lambda_X\, n_{X_T}(\infty)} \frac{\lambda_X}{\beta} \qquad \alpha = \text{const.} \qquad\qquad \alpha' = \frac{\lambda_X\, n_{X_i}(\infty)}{\lambda_X\, n_{X_T}(\infty)} \frac{\lambda_X}{\beta} (\lambda_X + \alpha')$$

$$\alpha' = \text{rate } (\text{sec}^{-1})$$

For $\lambda_X \ll \beta$

$$\alpha = \frac{\lambda_X\, n_{X_i}(\infty)}{\lambda_X\, n_{X_T}(\infty)} \qquad \alpha = \text{const.} \qquad\qquad \alpha' = \frac{\lambda_X \dfrac{\lambda_X\, n_{X_i}(\infty)}{\lambda_X\, n_{X_T}(\infty)}}{1 - \dfrac{\lambda_X\, n_{X_i}(\infty)}{\lambda_X\, n_{X_T}(\infty)}} \qquad \alpha' = \text{rate } (\text{sec}^{-1})$$

The quantity $\lambda_X n_{X_I}(\infty)/\lambda_X n_{X_T}(\infty)$ is observable and may be measured in a suitable experiment. It is seen in the first description that α may be equated to this quantity for $\lambda_X \ll \beta$ and is a constant; however, α' is always dependent on the half life of the isotope in question.

Table 7.4 gives a list of important fission-product gases along with representative values of α and β.

Table 7.4—FISSION-PRODUCT GASES AND ASSOCIATED DECAY PRODUCTS

Isotope*	Decay constant of parent (λ_X), sec^{-1}	Decay constant of daughter (λ_Y), sec^{-1}	Fission-chain yields, %	Fraction of fission rate released to coolant (α) Max.	Min.	Purification removal rates (β), sec^{-1}
4.36-hr Kr^{85}	4.42×10^{-5}		1.3	1.0	0.1	0
9.4-yr Kr^{85}	2.34×10^{-9}		1.3	1.0	0.1	0
75-min Kr^{87}	1.54×10^{-4}		2.8	0.1	0.01	0
3-hr Kr^{88}	6.42×10^{-5}		3.47	1.0	0.1	0
8-day I^{131}(D)	6.4×10^{-6}	1.0×10^{-6}	3.3	1.0	0.1	1.0×10^{-4}
2.4-hr I^{132}(D)	2.5×10^{-6}	8.02×10^{-5}	3.76	1.0	0.1	1.0×10^{-4}
22-hr I^{133}(D)	1.93×10^{-4}	8.75×10^{-6}	4.9	1.0	0.1	1.0×10^{-4}
6.7-hr I^{135}	2.87×10^{-5}		5.9	1.0	0.1	1.0×10^{-4}
5.3-day Xe^{133}(D)	8.75×10^{-6}	1.6×10^{-6}	4.9	1.0	0.1	0
9.2-hr Xe^{135}(D)	2.88×10^{-5}	2.09×10^{-5}	5.9	1.0	0.1	0
15-min Xe^{135}(D)	2.88×10^{-5}	7.55×10^{-4}	0.59	0.1	0.01	0
20-yr Sr^{90}	1.1×10^{-9}		5.1	0.1	0.01	1.0×10^{-4}
37-yr Cs^{137}	5.94×10^{-10}		6.2	0.1	0.01	1.0×10^{-4}

*D denotes daughter.

Chapter 8

EFFECT OF IRREGULARITIES IN SHIELD

1 INTRODUCTION 261
1.1 General 261
1.2 Résumé of Formulas 261
(a) Fast Neutrons 262
(b) Gammas 263

2 NEUTRONS 264
2.1 Transmission Through Rectangular Slots 264
(a) Effect of Slot Thickness . . 264
(b) Effect of Slot Length . . . 267
(c) Effect of Offsets in Slot . . 267
(d) Effect of Wall Material . . 273
(e) Effect of Source-to-slot Size Ratio 273
(f) Sample Calculation . . . 273
2.2 Transmission Through Cylindrical Ducts 274
(a) Simon-Clifford Equation . . 274
(b) Experiments and Correction Factors 276
(c) Sample Calculations . . . 278
(d) Experiments with the MIT Cyclotron 279
2.3 Transmission Through Annuli . . 280
2.4 Effect of Small Voids in Shield . . 281
2.5 Streaming Along Steel Paths . . 281
(a) Statement of the Problem . . 281
(b) Experimental Results . . . 283
(c) Calculational Methods . . . 284
(d) Sample Calculation . . . 287

3 GAMMAS 288
3.1 Source Geometries 288
3.2 Rectangular Slots 289
3.3 Cylindrical Ducts 290
3.4 Annular Ducts 292
3.5 Verification with Experimental Results 294
3.6 Effect of Voids in Shield . . . 295
(a) Analysis 304
(b) An Exact Calculation of the Tonks Approximation . . . 307
(c) Reduced Thickness Approximation 310
(d) Streaming Effect in Shield Containing Many Voids . . 311
(e) Sample Calculation . . . 313
3.7 Gamma Streaming Along Steel Paths 313
(a) The Problem 313
(b) Analysis 314
(c) Experimental Data . . . 314

4 RADIATION SCATTERING AROUND SHIELD EDGE 316
4.1 Introduction 316
4.2 Gamma Scattering 316
(a) Basic Compton Scattering Effect 316
(b) Single Scattering 317
(c) Double Scattering 318
(d) Single Vs. Double Scattering . 319
(e) Simplified Double-scattering Integration 322
(f) Scattering from Surfaces . . 328
(g) Experiments with Collimated Gamma Rays in Water . . 336
4.3 Neutron Scattering 342

REFERENCES 342

Chapter 8

EFFECT OF IRREGULARITIES IN SHIELD

1 INTRODUCTION

1.1 General

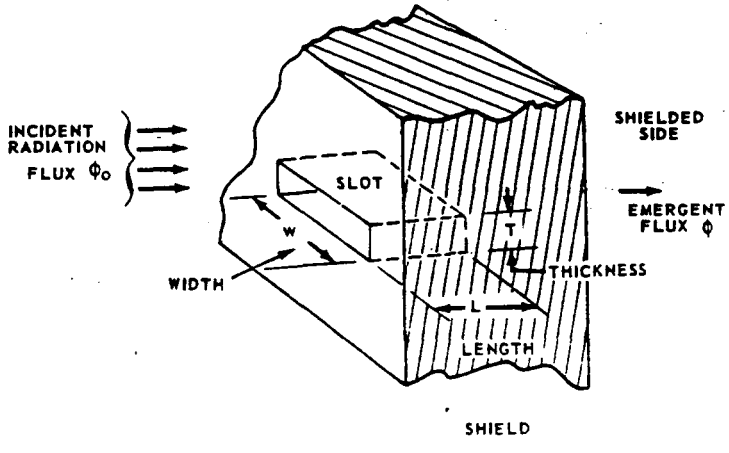
The most troublesome aspects of shield design—the ones least susceptible to clean and simple analysis—are those dealing with geometric irregularities in the shield. Slots, gaps, voids, and streaming paths are often introduced into a shield long after conceptual design is complete. Steel structural pieces through a water tank, through a concrete wall, or through a lead slab can provide streaming paths for radiation very much out of proportion to their size. A duct penetrating a shield may be carefully compensated for, and then thermal insulation or clearance gaps around it can completely undo the job.

This chapter discusses the problems of geometric irregularities in the shield. It does not cover geometric variations in the radiation source; these are discussed in Chap. 9.

The reader may discover some inconsistencies and discrepancies in the formulas and data given in this chapter. The editors have assembled the best experiments and analyses available to them on this subject, they have made some comparisons, and they have noted some discrepancies. It is hoped that further use and consideration of this material will greatly improve this situation before the next edition of this manual is issued.

1.2 Résumé of Formulas

Warning: These formulas are based on meager data over a narrow range of conditions. They are approximations and do not in all cases merge smoothly from one geometry to another. They should not be used without an understanding of their origin and limitations as described in this chapter, in particular, the angular distribution of the source.



(a) Fast Neutrons.

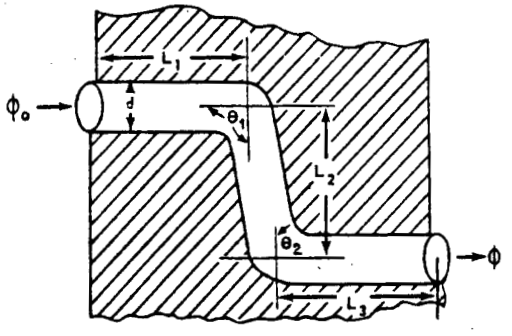
1. Rectangular slot through shield (W > 10T and L > 10T):

$$\frac{\phi}{\phi_0} = \frac{\text{fast-neutron flux leaving slot}}{\text{fast-neutron flux entering slot}} = 20\left(\frac{\text{thickness of slot, T}}{\text{length of slot, L}}\right)^2$$

2. Effect of offsets in slot (see Figs. 8.5 to 8.8):
   (a) Effect is maximum when offset is halfway along slot.
   (b) Effect increases rapidly as amount of offset increases, up to twice the slot thickness.
   (c) Can increase slot attenuation as much as 300-fold, for offset equal to two slot widths.
   (d) Multiple offsets are not much more effective than a single one at optimum location.
3. Effect of wall material:
   (a) No significant effect on fast neutrons.
   (b) Can decrease thermal neutrons severalfold by adding absorber to walls.
4. Cylindrical duct:

$$\frac{\phi}{\phi_0} = 10\left[\frac{1}{8}\left(\frac{d}{L_i}\right)^2 \frac{\alpha}{\sin\theta_i}\right]^n \qquad \text{(for each section)}$$

where d = duct diameter
L_i = length of each straight section
θ_i = angle between each section and previous one
n = number of sections
α = reflection coefficient of elbows = 1.0 for water



If duct is filled with poor shielding material (rather than being empty), the above answers must be multiplied by $e^{-\Sigma L}$ to account for attenuation of this material, where Σ is the effective removal cross section and L is the total duct length, both in the same length units.

5. Annular slot:

$$\frac{\phi}{\phi_0} = 10\left[(2R^2 - r^2)\cos^{-1}\frac{r}{R} - r\sqrt{R^2 - r^2}\right]^n \left(\frac{1}{L_1^2} + \frac{1}{L_2^2} + \cdots \frac{1}{L_n^2}\right)$$

where R = outer radius of annulus, r = inner radius of annulus, and the other terms are as defined above.

6. Streaming, down iron slabs:

$$\frac{\phi_s}{\phi_w} = \frac{1}{8}T^{2.3}e^{0.080L}\,(1 - e^{0.0077W}) \qquad \text{(for plate, where W > 10T)}$$

$$= 3.2 \times 10^{-4} D^{3.42} e^{0.080L} \qquad \text{(for cylinder)}$$

where ϕ_s = streaming flux (neutrons in excess of those in unperturbed hydrogenous shield)
ϕ_w = thermal-neutron flux in hydrogenous shield, 2 in. beyond end of slab
T = thickness of slab (in.)
W = width of slab (in.)
L = length of slab or cylinder (in.)
D = diameter of cylinder (in.)

7. Voids in shield: Line-of-sight results are tabulated to give tolerable void areas for various void thicknesses in order to ensure no more than a few per cent increase in dose due to voids in the shield material.

(b) Gammas.

1. Three source geometries are considered:
(a) Spherical isotropic emission (negligible self-absorption).

$$\phi = \frac{\phi_0}{2\pi} \text{ gammas/cm}^2\text{-sec per unit solid angle}$$

(b) Cosine emission (self-absorbing homogeneous source).

$$\phi = \frac{2\phi_0 \cos\theta}{2\pi}$$

(c) Fermi distribution (self-absorbing, activity proportional to distance from surface).

$$\phi = \frac{0.928\phi_0(\cos\theta + \sqrt{3}\cos^2\theta)}{2\pi}$$

In the forward direction these are in the ratio of 1 : 2 : 2.54.

2. Leakage from slot:

		Nondirectional detector	Directional detector
(a) Spherical emitter	$\frac{\phi}{\phi_0} =$	$\frac{1}{2}\left(\frac{T}{L}\right)$	$\frac{1}{\pi}\left(\frac{T}{L}\right)$
(b) Cosine emitter	$\frac{\phi}{\phi_0} =$	$\frac{2}{\pi}\left(\frac{T}{L}\right)$	$\frac{1}{2}\left(\frac{T}{L}\right)$
(c) Fermi emitter	$\frac{\phi}{\phi_0} =$	$\frac{1}{1.4}\left(\frac{T}{L}\right)$	$\frac{1}{1.7}\left(\frac{T}{L}\right)$

where T is the slot thickness and L is the slot length.

3. Cylindrical ducts:
(a) Spherical $\frac{\phi}{\phi_0} = \frac{1}{8}\left(\frac{d}{L}\right)^2$
(b) Cosine $\frac{\phi}{\phi_0} = \frac{1}{4}\left(\frac{d}{L}\right)^2$ (where d = diameter of duct and L = length of duct)
(c) Fermi $\frac{\phi}{\phi_0} = \frac{1}{3}\left(\frac{d}{L}\right)^2$

(d) Where only oblique or scattered gammas are being shielded, the shield may need only be corrected for the reduction in density caused by the penetrations.

4. Annular ducts:

(a) Spherical $\frac{\phi}{\phi_0} = \frac{1}{2\pi L^2}\left[\left(\cos^{-1}\frac{r}{R}\right)(2R^2 - r^2) - r\sqrt{R^2 - r^2}\right]$

(b) Cosine $\frac{\phi}{\phi_0} = \frac{1}{\pi L^2}\left[\quad \text{same as above} \quad\right]$ for $R^2 - r^2 \ll L^2$

(c) Fermi $\frac{\phi}{\phi_0} = \frac{1.27}{\pi L^2}\left[\quad \text{same as above} \quad\right]$

5. Voids in shield: A method is given for calculating the effect of voids in a shield composed of several materials. Compensation for the density reduction caused by the voids is generally adequate.

$$L_{eff} = L_0(1 - v)f$$

where L_{eff} = effective shield thickness
L_0 = actual bulk shield thickness
v = volume-fraction voids
f = streaming factor = $1 - (dv^2/2)$
d = average distance between voids in relaxation lengths

2 NEUTRONS

2.1 Transmission Through Rectangular Slots

In order to predict the neutron dose leaving air slots, ducts, voids, or annuli between concentric shells, one is faced with many variables, some of which are difficult to separate. For example, since the neutron dose depends greatly on the energy of the neutrons, something should be known about the spectrum, i.e., the energy distribution of the emerging neutron flux.

Experimental investigations of ducts are still scarce at this time. Some attempts have been made to predict analytically neutron leakage through ducts; these are listed at the end of the chapter. No satisfactory theory has been developed, and the designer must lean heavily on the scarce amount of experimental data.

An attempt has been made by R. Schamberger, F. Shore, and H. P. Sleeper, Brookhaven National Laboratory (BNL), to measure neutron leakage from air slots as a function of slot length and thickness. The slots were very wide (34 in.) compared to the thickness; width was not a variable. The type of experiments performed also produced results that can be used to study the "attenuation characteristics" in water following the air duct, which gives an indication of the effective energy and direction of the neutrons that emerge from the duct.

(a) Effect of Slot Thickness. Thermal-neutron flux measurements have been made in water behind the air slot. As the amount of water between the counter and the slot increases, the thermal detector records neutrons due to fast neutrons closer to the source, i.e., a number which is proportional to fast-neutron dose.

If one chooses the thermal-neutron flux at 1.5 in. beyond the end of the slot as a parameter to characterize the behavior of the neutrons, the family of curves shown in Fig. 8.1 is obtained. Ordinates are thermal-neutron flux (in logarithmic units) in excess of the background in the water, and abscissas are logarithms of the dimension of the slot, which is varied. The slot lengths ranged from 1 to 6 ft (penetrating into the shield from the source side), with the thickness varying from 0.125 to 3 in. Owing to the difficulty of stacking the experimental mock-ups, the 0.125-in. points contain considerable uncertainty. It must be noted that the curves for constant lengths are parallel straight lines with a slope of 2, indicating that the transmitted integrated flux (neutrons/cm-sec) varies as the square of the slot thickness (cf. Sec. 3.2). This is the behavior predicted by a line-of-sight two-dimensional calculation assuming that the water surrounding the slots is opaque to the neutrons and that the emergent flux is essentially integrated by the detector. In Fig. 8.2 the thermal-neutron flux at 7.5 in. beyond the end of the slot was chosen as a parameter. The slopes of the resulting family of curves agree with the 1.5-in. set.

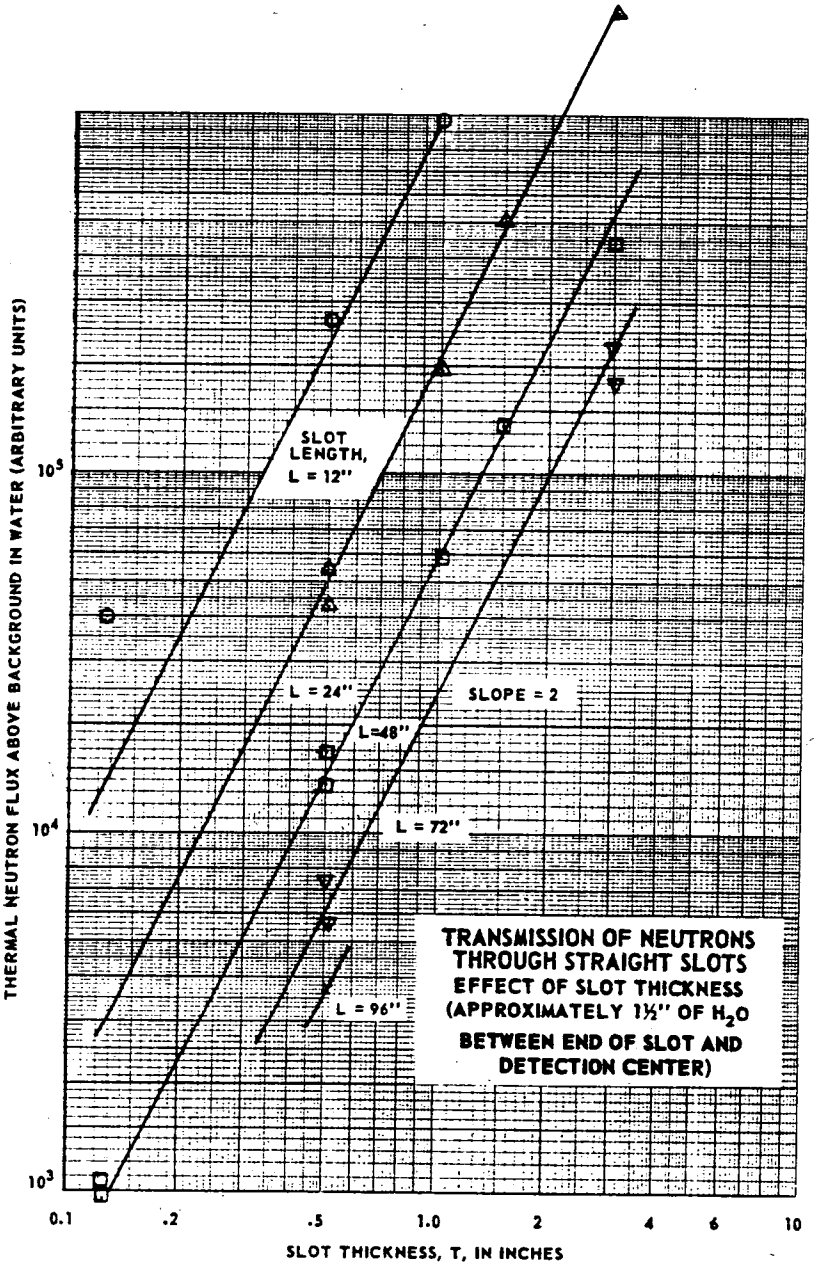

THERMAL NEUTRON FLUX ABOVE BACKGROUND IN WATER (ARBITRARY UNITS)
10^5
10^4
10^3
SLOT LENGTH, L = 12"
L = 24"
L=48"
L = 72"
L = 96"
SLOPE = 2
TRANSMISSION OF NEUTRONS THROUGH STRAIGHT SLOTS
EFFECT OF SLOT THICKNESS
(APPROXIMATELY 1½" OF H_2O
BETWEEN END OF SLOT AND DETECTION CENTER)
0.1
.2
.5
1.0
2
4
6
10
SLOT THICKNESS, T, IN INCHES

Figure 8.1

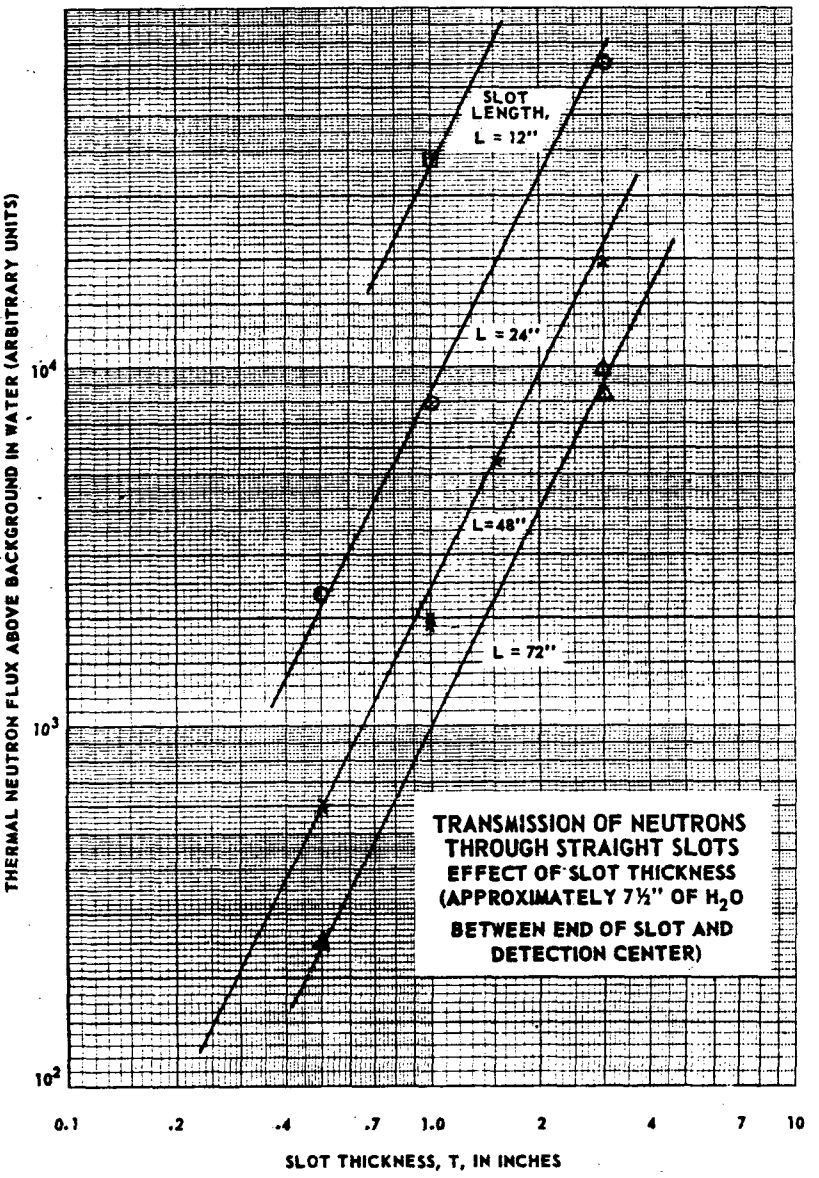

SLOT LENGTH, L = 12"
L = 24"
L=48"
L = 72"
TRANSMISSION OF NEUTRONS THROUGH STRAIGHT SLOTS
EFFECT OF SLOT THICKNESS
(APPROXIMATELY 7½" OF H_2O BETWEEN END OF SLOT AND DETECTION CENTER)
THERMAL NEUTRON FLUX ABOVE BACKGROUND IN WATER (ARBITRARY UNITS)
10^4
10^3
10^2
0.1
.2
.4
.7
1.0
2
4
7
10
SLOT THICKNESS, T, IN INCHES

Figure 8.2

(b) Effect of Slot Length. The length dependence observed for a constant slot thickness is indicated in Figs. 8.3 and 8.4. The curves have been drawn with slope of −2 to fit the data. The length dependence is found to approximate an inverse-square law.

The "relaxation length" (thickness of shielding required to reduce flux by a factor of e, or 2.72) may be used as some measure of the predominant neutron energy. Thus a long relaxation length (7 to 9 cm) indicates high-energy neutrons (several Mev).

Note: The relaxation length in centimeters = 1.1 × tenth-thickness in inches; e.g., if *11 cm* of water reduces a given neutron flux by a factor of 2.72, then *10 in.* of water will reduce it *10-fold.*

Close to the slot exits, the thermal flux falls off very rapidly. For a 48-in. slot the relaxation length for thermal neutrons 7.5 in. beyond the slot is 5.1 cm, whereas one measured in the same position with a fast-neutron dosimeter is 5.7 cm. Checks made with the fast-neutron dosimeter are consistent with the square law dependence obtained from thermal-neutron data. BNL concludes that the thermal-neutron detector close to the slot yields a parameter that is also valid for fast-neutron dose.

From thermal-flux measurements taken across the slot and away from the slot, an estimate of the fast-neutron flux leaving the slot can be made. The reason for the interest in the fast-neutron flux stems from its importance when neutron dose is desired. For example, approximately 8.7 fast neutrons/cm^2-sec result in 1 mrem/hr, and 480 thermal neutrons/cm^2-sec also produce 1 mrem/hr. The designer of a shield usually knows the order of magnitude of the fast-neutron flux at the entrance of an air slot or annulus, and it would be most desirable to be able to estimate the fast-neutron flux leaving such voids. Within the range of the available data (see Figs. 8.1 through 8.3), the following estimate can be made

$$\text{Attenuation} = \frac{\text{fast-neutron flux leaving slot}}{\text{fast-neutron flux entering slot}} = 20\left(\frac{\text{thickness of slot}}{\text{length of slot}}\right)^2 \qquad (1)$$

(c) Effect of Offsets in Slot. The thickness and length dependence for straight air slots having been established, an attempt is made to investigate the effect of offsets. The thermal-neutron flux leaving the slots was recorded when each of the following variations was made:

1. Single offset — position of offset along slot path varied; slot, 48 in. long and 0.5 in. thick; X = 1.8 in. (X = distance between center of slot and center of offset).
2. Single offset — varied X using two 0.5-in. slots, 24 in. long.
3. Single offset — same as (2) except slots were 1.5 in. thick.
4. Double offset — varying X using three 0.5-in. slots, 12, 24, and 12 in. long.
5. Triple offset — single point using four 0.5-in. slots, 12 in. long, with 1.8-in. offsets.

Figure 8.5 indicates the result of varying the position of an offset along the length direction of 0.5-in.-thick slots having an over-all length of 48 in. It can be seen that the position of maximum effect for a step is halfway along the slot (attenuation ~ 300). Curve A was plotted 1.5 in. behind the slot (1.5 in. of water between detector and end of slot); curve A′, 7.5 in. behind the slot.

Figure 8.6 shows the effect of varying the magnitude of the offset from zero to infinity. The two curves are again for the detector at 1.5 and 7.5 in. behind the slot (measuring slow and something proportional to fast leakage flux, respectively). There is a sharp effect due to the offset as X approaches the slot thickness until X is about twice the slot thickness, after which the effect of further increasing X becomes small, as the flux approaches that in water.

Figure 8.7 shows the summary of available information on multiple offsets. Double offsets consisting of 0.5-in.-thick air slots, 12, 24, and 12 in. long, show the same qualitative behavior as single offsets except, of course, the attenuation is larger (about another factor of 10).

It appears that after two offsets additional steps do not materially decrease the transmission of the lower component (compare Figs. 8.6 and 8.7). One good offset at the center seems almost as effective as two or more disposed throughout the over-all length for fast-neutron leakage. The offsets, however, are large compared to the slot thickness.

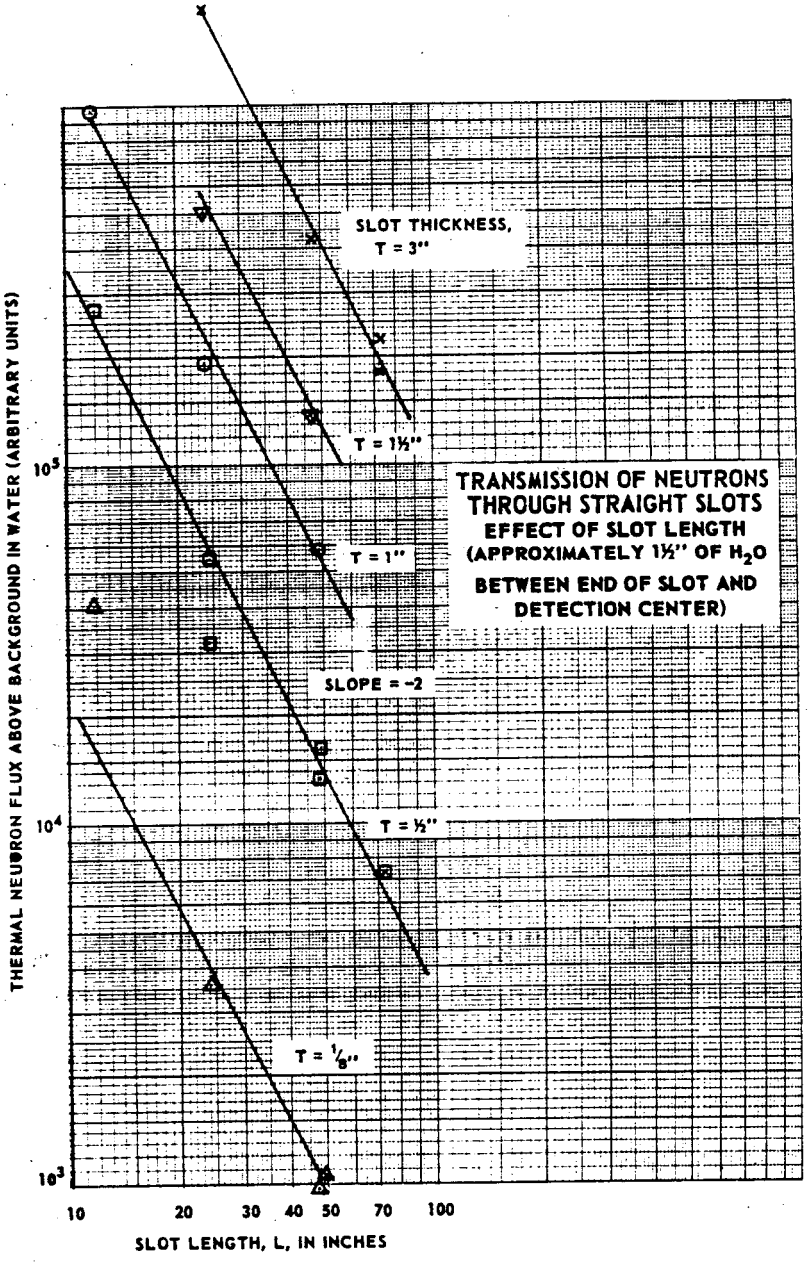

TRANSMISSION OF NEUTRONS
THROUGH STRAIGHT SLOTS
EFFECT OF SLOT LENGTH
(APPROXIMATELY 1½" OF H_2O
BETWEEN END OF SLOT AND
DETECTION CENTER)
SLOT THICKNESS,
T = 3"
T = 1½"
T = 1"
SLOPE = -2
T = ½"
T = ⅛"
THERMAL NEUTRON FLUX ABOVE BACKGROUND IN WATER (ARBITRARY UNITS)
10^5
10^4
10^3
10
20
30
40
50
70
100
SLOT LENGTH, L, IN INCHES

Figure 8.3

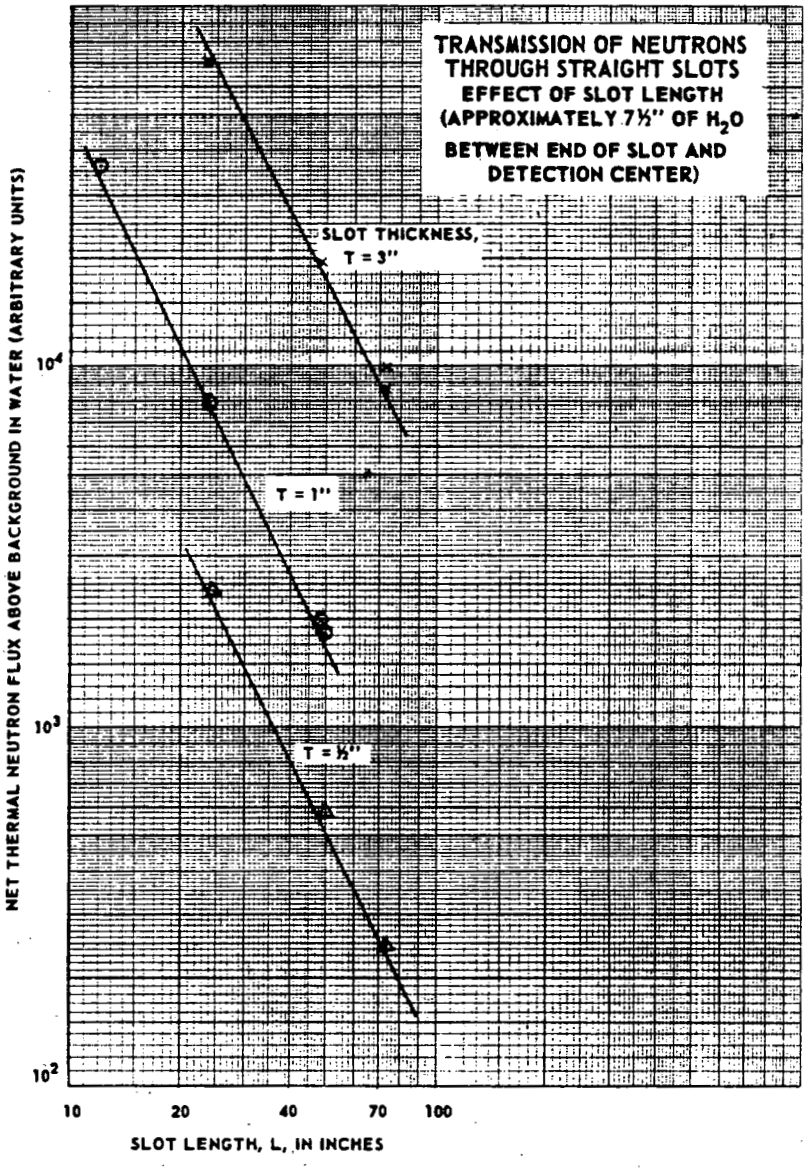

TRANSMISSION OF NEUTRONS
THROUGH STRAIGHT SLOTS
EFFECT OF SLOT LENGTH
(APPROXIMATELY 7½" OF H_2O
BETWEEN END OF SLOT AND
DETECTION CENTER)
SLOT THICKNESS,
T = 3"
T = 1"
T = ½"
NET THERMAL NEUTRON FLUX ABOVE BACKGROUND IN WATER (ARBITRARY UNITS)
10^4
10^3
10^2
10
20
40
70
100
SLOT LENGTH, L, IN INCHES

Figure 8.4

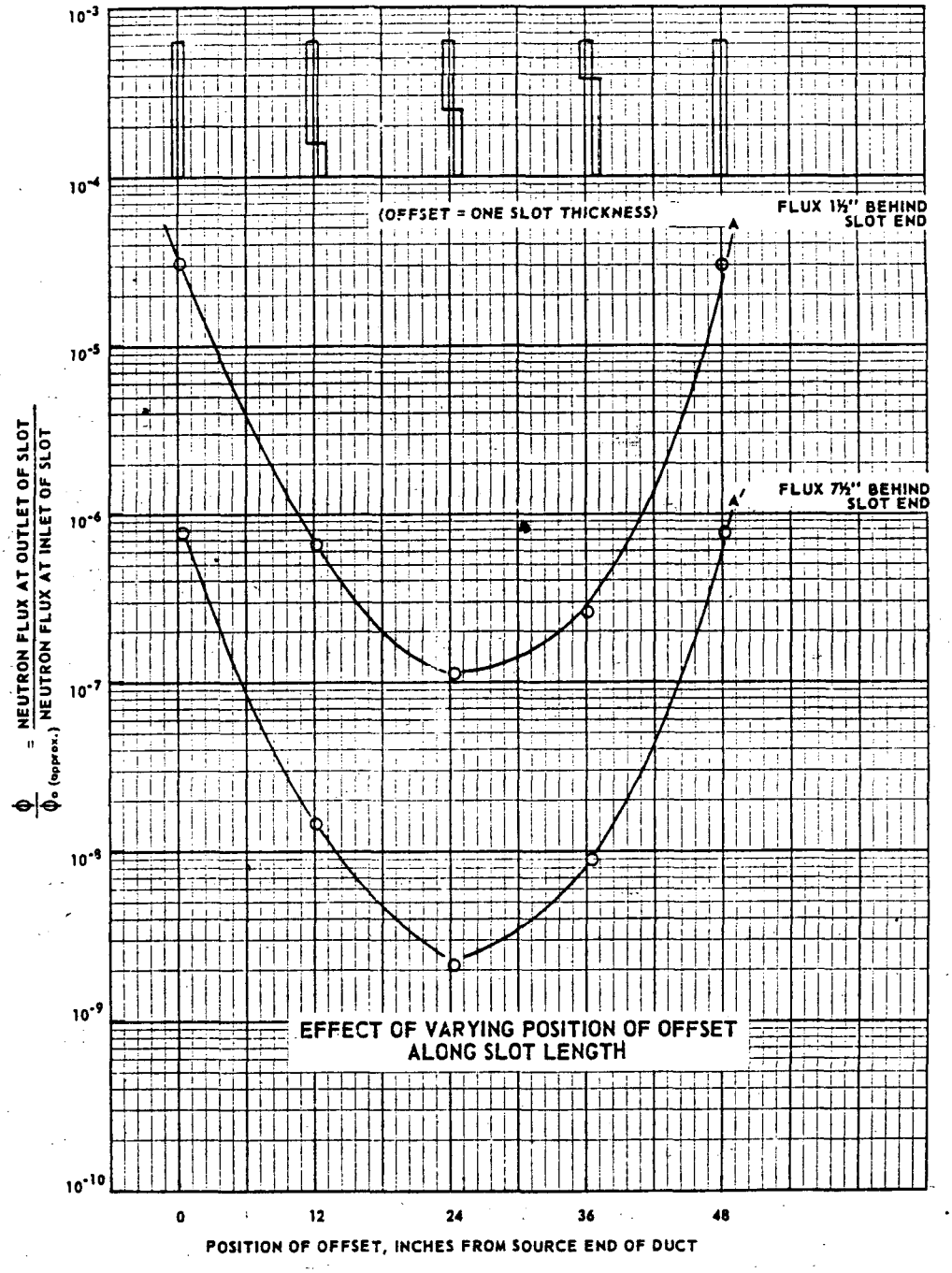

10^{-3}
10^{-4}
10^{-5}
10^{-6}
10^{-7}
10^{-8}
10^{-9}
10^{-10}
(OFFSET = ONE SLOT THICKNESS)
FLUX 1½" BEHIND SLOT END
FLUX 7½" BEHIND SLOT END
A
A'
EFFECT OF VARYING POSITION OF OFFSET ALONG SLOT LENGTH
$\frac{\phi}{\phi_{o\ (approx.)}}$ = NEUTRON FLUX AT OUTLET OF SLOT / NEUTRON FLUX AT INLET OF SLOT
0
12
24
36
48
POSITION OF OFFSET, INCHES FROM SOURCE END OF DUCT

Figure 8.5

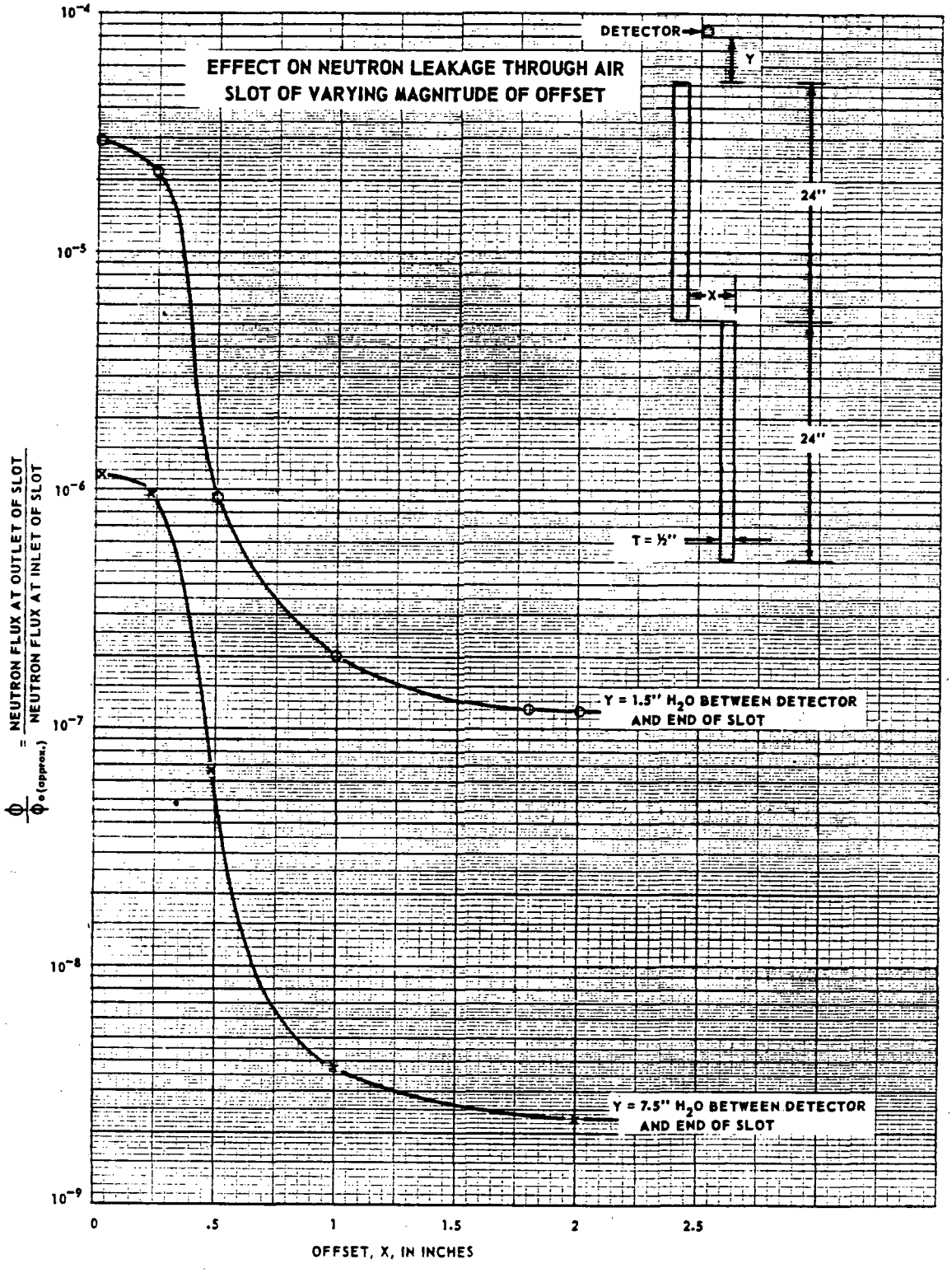

EFFECT ON NEUTRON LEAKAGE THROUGH AIR SLOT OF VARYING MAGNITUDE OF OFFSET
DETECTOR
Y
24"
X
24"
T = ½"
Y = 1.5" H2O BETWEEN DETECTOR AND END OF SLOT
Y = 7.5" H2O BETWEEN DETECTOR AND END OF SLOT
10⁻⁴
10⁻⁵
10⁻⁶
10⁻⁷
10⁻⁸
10⁻⁹
0
.5
1
1.5
2
2.5
OFFSET, X, IN INCHES
ϕ/ϕ₀ (approx.) = NEUTRON FLUX AT OUTLET OF SLOT / NEUTRON FLUX AT INLET OF SLOT

Figure 8.6

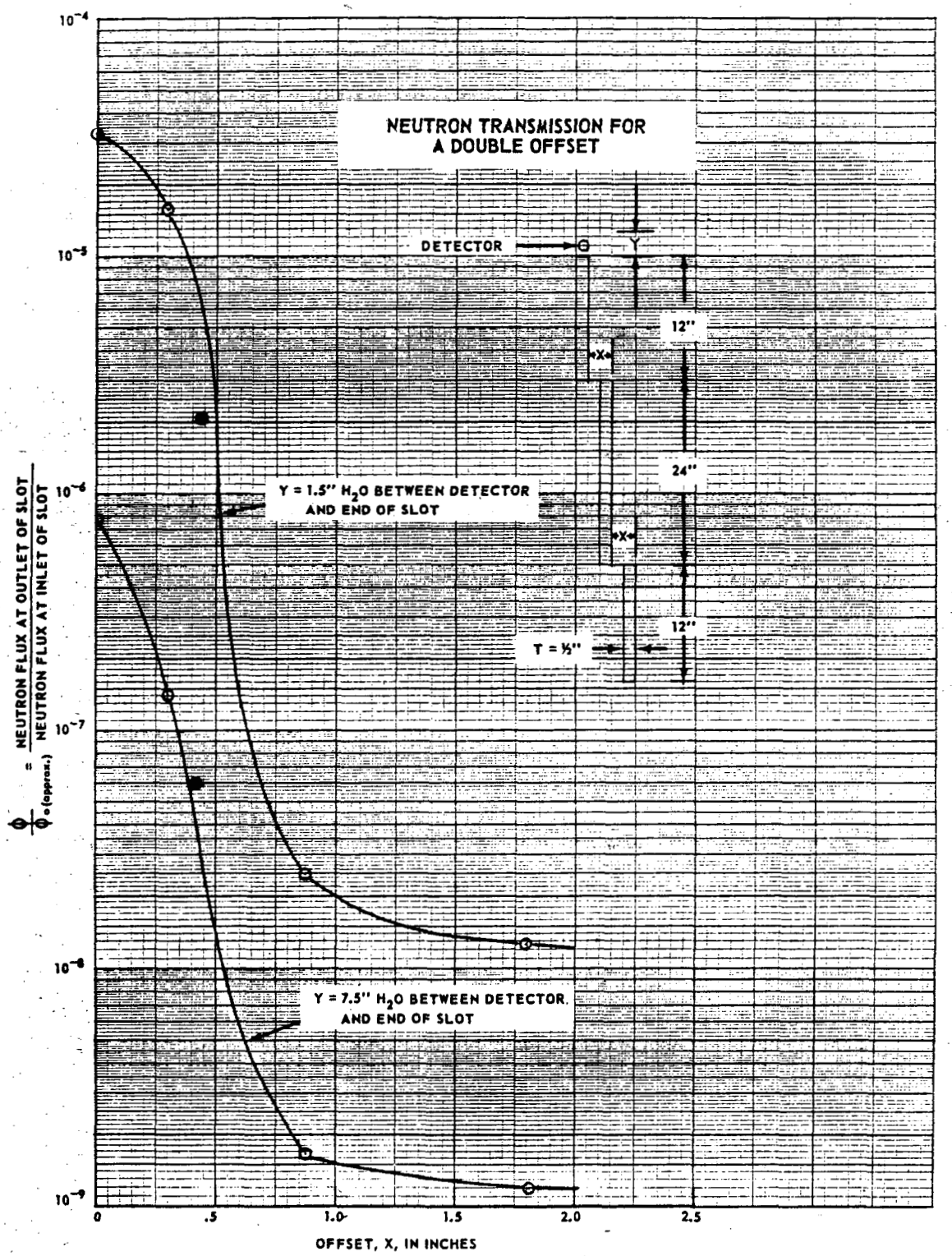

NEUTRON TRANSMISSION FOR
A DOUBLE OFFSET
DETECTOR
Y
12"
X
24"
X
12"
T = ½"
Y = 1.5" H2O BETWEEN DETECTOR
AND END OF SLOT
Y = 7.5" H2O BETWEEN DETECTOR
AND END OF SLOT
10⁻⁴
10⁻⁵
10⁻⁶
10⁻⁷
10⁻⁸
10⁻⁹
0
.5
1.0
1.5
2.0
2.5
OFFSET, X, IN INCHES
NEUTRON FLUX AT OUTLET OF SLOT / NEUTRON FLUX AT INLET OF SLOT

Figure 8.7

(d) Effect of Wall Material. The importance of streaming along, or capture in, the walls of a slot must also be investigated. If the air slots are large, it can be expected that these effects may be negligible. A 48-in.-long, 34-in.-wide, and 0.5-in.-thick air slot was investigated with lucite walls (to simulate the effect of water walls) and with 0.5-in.-thick carbon steel walls. The thermal-flux data with the steel wall showed a 40 per cent reduction in neutron leakage over the lucite wall data. There was no significant effect on the fast-neutron flux.

Figure 8.8 shows data obtained with a typical stepped slot, 24 in. long, with a 1.8-in. offset (X = 1.8 in.). Neutron data compare the transmission of a 0.5-in. lucite-walled stepped slot with slots of the same size in which the following changes were made in the wall materials: (1) 0.5 in.-steel walls everywhere, (2) a 2- by 3- by 36-in. bar of steel was substituted for lucite at the step, and (3) a thin piece of cadmium was added as shown.

The fast flux (shown at large distances in water) was only reduced 30 per cent; however, the effect on the thermal flux (shown at the first few inches behind the slot) is significant (factor of 5). A decrease in the transmission of thermal neutrons through carbon steel walled ducts (straight or stepped) is evident, provided the "air streaming" through the slots is predominant. The steel effect on fast neutrons is relatively small.

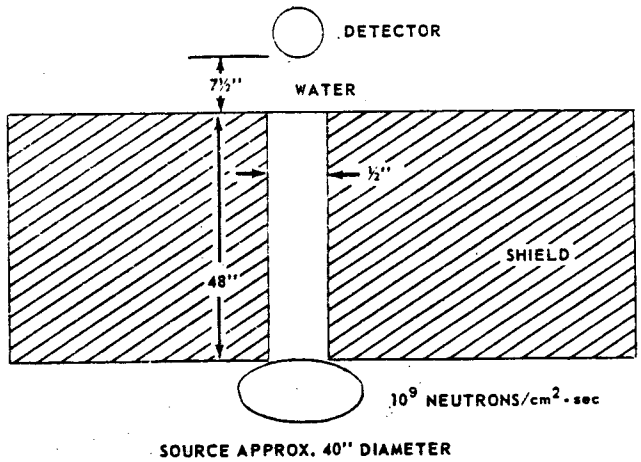
(e) Effect of Source-to-slot Size Ratio. It is believed that there is some streaming dependence on the size ratio of slot to source. In geometries as discussed above, the important streaming contributor is that part of the source which "sees" the air slot directly. The source-size effect seems to be small with air slots, although it may be appreciable with cylindrical air voids (ducts) where the source size exceeds the area of the duct entrance.

For fast-neutron leakage through straight ducts, Eq. 1, $\phi/\phi_0 = 20(T/L)^2$, can be used, provided the fast-neutron flux entering the slot is known. The dose can be calculated from the fast-neutron flux leaving the slot. To this must be added the dose contribution from the thermal-neutron flux. In most shield designs there is some shielding material between the end of the slot and the receptor. If water or plastic is used, the relaxation length for fast neutrons is long (8 to 10 cm), and the attenuation in this shielding material can be estimated. Thermal neutrons, however, fall off more rapidly. Fortunately neutron fluxes were measured at BNL as a function of water behind the end of the slot. Most curves in this chapter show the loci of points taken with $1\frac{1}{2}$ and $7\frac{1}{2}$ in. of water behind the slot. In the following example $7\frac{1}{2}$ in. was used, but a thorough analysis of the available experimental data will allow the use of any amount of shielding. In order to estimate the effect of steps on fast-neutron attenuation, it is suggested that the same method be used as is shown in the following example, employing data with as much water as possible behind the slot. The reason for this is that after sufficient moderator material the slow and fast neutrons are again in equilibrium, and the slow neutrons measured indicate fast neutrons leaving the slot. Owing to the many uncertainties in this type of analysis, a moderate safety factor should be employed, i.e., multiply the calculated results (flux leaving the slot) by a factor of 2 or 3.

(f) Sample Calculation. Consider a source emitting 10^9 neutrons/cm^2-sec covered by a slab shield. Directly over the source there is a slot in a good shield 34 in. wide and $\frac{1}{2}$ in. thick. The length of the slot from the source to the outside of the shield is 48 in. (see sketch). The problem is to determine the thermal-neutron flux leaving the slot. Consider the detector placed at 7.5 in. in water beyond the end of the slot. Using the curve on Fig. 8.4 for a $\frac{1}{2}$-in.-thick slot, we can find the attenuation through 48 in. of length. This is equivalent to the attenuation between 10 and 58 in. The net thermal flux for 10 in. is 1.3×10^4, and for 58 in. it is 3.9×10^2; therefore, the neutron flux leaving the slot is

$$\frac{(10^9)\ (3.9 \times 10^2)}{1.3 \times 10^4} = 3 \times 10^7 \text{ nv} = \text{N} \qquad (2)$$

Offsets along the length of the slot could further reduce the neutron flux leaving the slot. Figure 8.5 shows that the best attenuation is achieved by an offset at the mid-length position. The attenuation achieved by an offset is shown in Fig. 8.6 for varying magnitudes of the offset. Using a 1-in. offset for a $\frac{1}{2}$-in.-thick slot, we obtain the following values for the case of 7.5 in.



between the detector and the end of the slot. For 0 in. (no offset), the value of ϕ/ϕ_0 is 1.1×10^{-6} and for 1 in., 3.7×10^{-9}. Applying this proportion to the value of N obtained in Eq. 2, we get

$$(3.0 \times 10^{7}) \left(\frac{3.7 \times 10^{-9}}{1.1 \times 10^{-6}}\right) = 1.01 \times 10^{5} \text{ nv} = N' \tag{3}$$

N′ is the thermal-neutron flux leaving a ½-in. slot, 48 in. long, with a 1-in. offset at the mid-length position (24 in.).

If the offset were not at the mid-position, it would be necessary to increase the flux by the ratio shown in Fig. 8.5. For example, if the offset were at the 12-in. position, the value of N′ would be multiplied by $(1.1 \times 10^{-8}/2.2 \times 10^{-9})$:

$$(1.01 \times 10^{5}) \left(\frac{1.1 \times 10^{-8}}{2.2 \times 10^{-9}}\right) = 5.05 \times 10^{5} \text{ nv} = N'' \tag{4}$$

N″ is the thermal-neutron flux leaving a ½-in. slot, 48 in. long, with a 1-in. offset at the 12-in. position along the length with 7½ in. of water after the slot. The fast flux may be estimated from the thermal flux by the method given in Chap. 4, Sec. 4.1, assuming no wall effects.

As stated above, N, N′, or N″ should be multiplied with a moderate safety factor of 2 or 3 to be conservative.

2.2 Transmission Through Cylindrical Ducts

(a) Simon-Clifford Equation. At the present time the simplest and best verified method for calculating neutron leakage through cylindrical ducts is the Simon-Clifford equation.[1] This equation is for calculating neutron leakage through long, thin, empty cylindrical ducts that penetrate a reactor shield. It is an inverse-square theory in which empirical coefficients describe the reflection properties of the duct elbows. Earlier approaches[2–6] were either too cumbersome to apply or over-simplified special cases of little practical usefulness.

Simon and Clifford develop their equation in the following manner: The uncollided flux straight through the duct is

$$\phi = \phi_0 \frac{d^2}{8L^2} \tag{5}$$

where ϕ_0 is the flux at the entrance to the duct and L is the length of the duct. In addition to this flux there will be contributions due to neutrons that have collided with the walls of the duct. Considering isotropic reradiation and cosine reradiation from the walls, the equation for flux at the end of the duct becomes

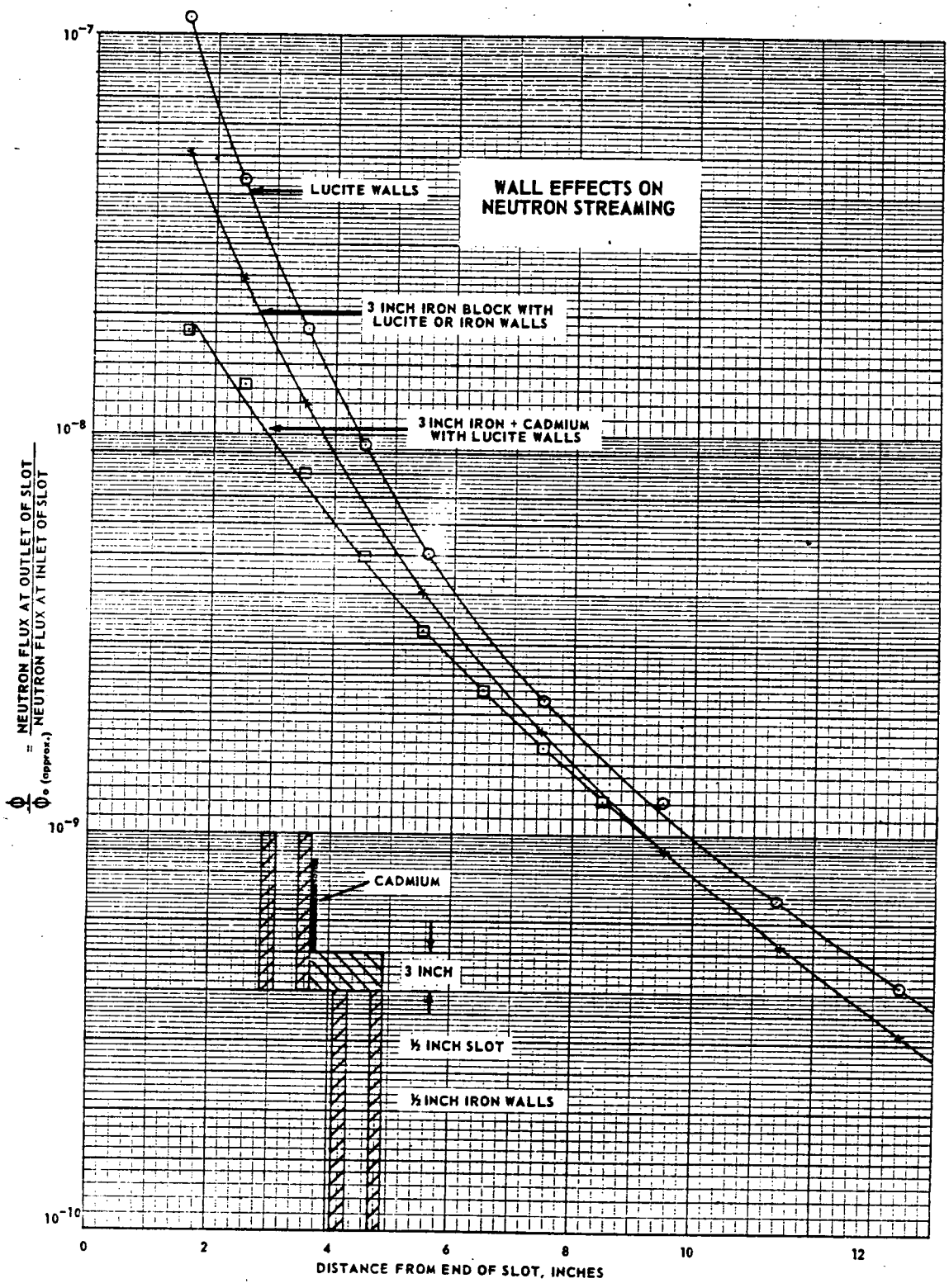

WALL EFFECTS ON NEUTRON STREAMING
LUCITE WALLS
3 INCH IRON BLOCK WITH LUCITE OR IRON WALLS
3 INCH IRON + CADMIUM WITH LUCITE WALLS
CADMIUM
3 INCH
½ INCH SLOT
½ INCH IRON WALLS
10^{-7}
10^{-8}
10^{-9}
10^{-10}
$\frac{\phi}{\phi_0} = \frac{\text{NEUTRON FLUX AT OUTLET OF SLOT}}{\text{NEUTRON FLUX AT INLET OF SLOT (approx.)}}$
0
2
4
6
8
10
12
DISTANCE FROM END OF SLOT, INCHES

Figure 8.8

$$\phi = \phi_0 \frac{d^2}{8L^2}\left(1 + A\alpha' + 2B\alpha' \frac{d}{L}\right) \tag{6}$$

where A = the fraction of wall scattering which is isotropic
B = the fraction of wall scattering which is cosine distributed
α' = a reflection coefficient for duct walls (the "albedo" of the wall)
d = the diameter of the duct

Equation 6 is still incomplete because it takes into account only single scattering. Now, taking into consideration the effect of multiple scattering, the equation becomes

$$\phi = \phi_0 \frac{d^2}{8L^2}\left[1 + A\frac{\alpha'}{(1-\alpha')} + 2B\frac{d}{L}\frac{\alpha'}{(1-\alpha')}\right] \tag{7}$$

ϕ and ϕ_0 can be expressed either as flux or as total neutrons per second as long as they both are given in the same units.

If we assume A + B = 1, and α' is of the order of 0.1 by experiment, the second and third terms of Eq. 7 may be neglected. The first term gives a reasonable approximation of the flux. Hence, the flux at the end of a long thin duct ($d \ll L$) is due to just the uncollided flux.

Simon and Clifford then extended their theory to ducts with many long straight sections of equal lengths with the angle θ between them (see Fig. 8.9a). They evolved the following equation giving the number of neutrons leaving the end of such a duct.

$$\frac{\phi}{\phi_0} = \frac{1}{8}\left(\frac{d}{L}\right)^2 \left(\frac{d^2}{8L^2}\frac{\alpha}{\sin\theta}\right)^n (A + 2B\sin\theta)^n \tag{8}$$

In Eq. 8 $\alpha = \alpha'/K$, where K is an undetermined constant and α is the albedo (or reflection coefficient) at duct elbows. Now, since we have assumed A + B = 1, Eq. 8 becomes

$$\frac{\phi}{\phi_0} = \frac{1}{8}\frac{d^2}{L^2}\left(\frac{d^2}{8L^2}\frac{\alpha}{\sin\theta}\right)^n [1 - B(1 - 2\sin\theta)]^n \tag{9}$$

If B is assumed zero, we have

$$\boxed{\frac{\phi}{\phi_0} = \frac{1}{8}\frac{d^2}{L^2}\left(\frac{d^2}{8L^2}\frac{\alpha}{\sin\theta}\right)^n} \tag{10}$$

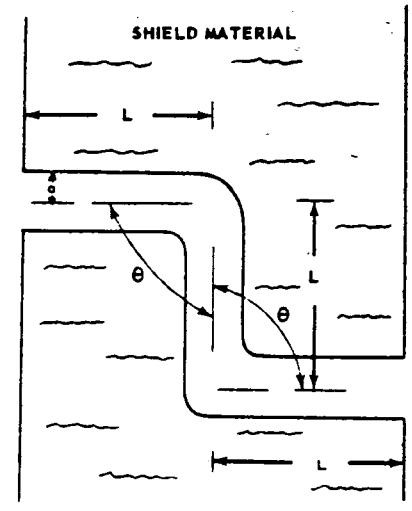
The equation gives best results for angles near 90°. Checked with experimental results, it predicts neutron leakage for empty ducts within a factor of 2. Equation 10 can further be extended to ducts with long straight sections of different lengths (see Fig. 8.9b). Thus

$$\boxed{\frac{\phi}{\phi_0} = \frac{1}{8}\left(\frac{d}{L_1}\right)^2 \left(\frac{d^2}{8L_2^2}\frac{\alpha}{\sin\theta_1}\right)\left(\frac{d^2}{8L_3^2}\frac{\alpha}{\sin\theta_2}\right)\cdots\left(\frac{d^2}{8L_{m+1}}\frac{\alpha}{\sin\theta_m}\right)} \tag{11}$$

where θ_m is the angle between the m*th* and (m + 1)*th* straight section and L_m is the length of the m*th* section. These equations do not hold for small angles.

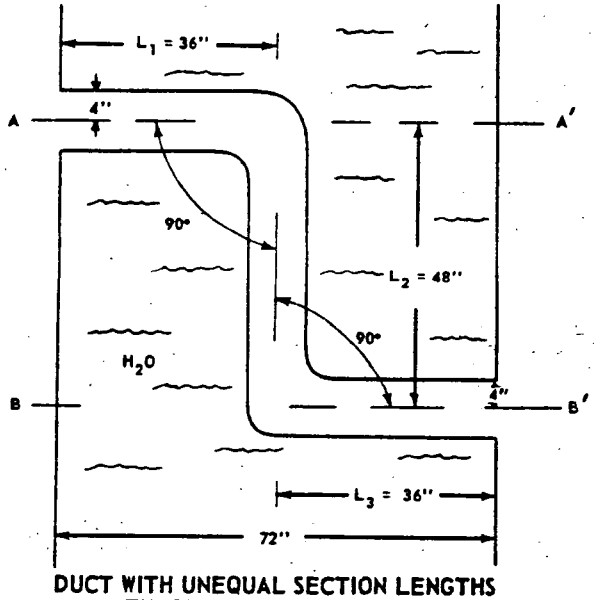
(b) Experiments and Correction Factors. The validity of the Simon-Clifford equation was checked with experiments run at Oak Ridge National Laboratory[7] (ORNL), and Eq. 11 was corrected to be applicable to filled cylindrical ducts adjacent to a large neutron source. (The original treatment was for a duct-end size source.)

Two corrections were necessary to apply to the equation. The presence of material in the duct, for example, sodium, is compensated for by a simple exponential involving an average removal cross section for the duct materials and the over-all duct length. After checking theoretical calculations with experimental results, it was found that an arbitrary factor of 5 is



DUCT WITH EQUAL SECTION LENGTHS
m = 3

(a)



DUCT WITH UNEQUAL SECTION LENGTHS
THROUGH A WATER SHIELD

(b)

Figure 8.9

necessary to correct the equation for a large neutron source. It was further found that by placing the empirical constant α equal to unity the equation checked with the experimental results within the approved range of a factor of 2. It must also be remembered that the Simon-Clifford equation (Eq. 11) gives best results with angles of $\theta = 90°$ or ducts with right-angle bends. With this information the following equation is applicable for engineering problems of calculating neutron leakage through long filled cylindrical ducts penetrating a reactor shield

$$\boxed{\frac{\phi}{\phi_0} = 10\, e^{-\bar{\Sigma}L}\, \frac{1}{8}\left(\frac{d}{L_1}\right)^2 \frac{1}{8}\left(\frac{d}{L_2}\right)^2 \cdots \frac{1}{8}\left(\frac{d}{L_i}\right)^2}$$

where ϕ = flux of fast neutrons leaving duct end
ϕ_0 = flux of fast neutrons emitted at duct-end sized source
$\bar{\Sigma}$ = average removal cross section (cm^{-1}) for material in duct ($\cong 0$ for air)
L = over-all duct length (cm)
d = duct diameter (cm)
L_i = length of *ith* section (cm)
10 = product of source-size correction 5 and factor of 2 needed to guarantee conservative results

The validity of the Simon-Clifford equation was checked with foil measurements taken in the ORNL Lid Tank on the wall of a long straight duct in the Knolls Atomic Power Laboratory (KAPL) duct test. After corrections for geometry it was shown that the foil activity follows the inverse-square curve of the duct beyond 20 cm along the duct. The assumption of setting the empirical constant α equal to unity was verified with the experimental data.

(c) Sample Calculations. Consider a 6-in. schedule 40 pipe that is filled with sodium inside an 8-in. duct penetrating a water shield 72 in. thick. The duct has three sections, 36, 48, and 36 in. long, respectively, with two bends of 90° each (see Fig. 8.9b). To find the attenuation through the duct, we have

$$\frac{\phi}{\phi_0} = 10\, e^{-\bar{\Sigma}L}\, \frac{1}{8}\left(\frac{d}{L_1}\right)^2 \frac{1}{8}\left(\frac{d}{L_2}\right)^2 \frac{1}{8}\left(\frac{d}{L_3}\right)^2$$

where

$$\bar{\Sigma} \cong \frac{\Sigma_{Na}A_{Na} + \Sigma_{Fe}A_{Fe} + \Sigma_{air}A_{air}}{A_{total}} \quad \text{and} \quad A = \text{area of material in the duct}$$

Using experimental removal cross sections, we obtain

$$\Sigma_{Na} = \frac{(0.98\ g/cm^3)\ (0.6 \times 10^{24}\ \text{nuclei/mole})\ (1.31 \times 10^{-24}\ cm^2/\text{nuclei})}{23\ g/\text{mole}}$$

$$= 0.0335\ cm^{-1}$$

$$\Sigma_{Fe} = \frac{(7.85\ g/cm^3)\ (0.6 \times 10^{24}\ \text{nuclei/mole})\ (1.95 \times 10^{-24}\ cm^2/\text{nuclei})}{55.85\ g/\text{mole}}$$

$$= 0.164\ cm^{-1}$$

$$\Sigma_{air} = 0$$

$$\bar{\Sigma} = \frac{(0.0335\ cm^{-1})\ (47.74\ \pi\ cm^2) + (0.164\ cm^{-1})\ (10.32\ \pi\ cm^2)}{103.22\ \pi\ cm^2}$$

$$= 0.0319\ cm^{-1}$$

$$L_{total} = 120 \text{ in.} = 304.8 \text{ cm}$$

$$\frac{\phi}{\phi_0} = 10\, e^{-9.723} \frac{1}{8}\left(\frac{8}{36}\right)^2 \frac{1}{8}\left(\frac{8}{48}\right)^2 \frac{1}{8}\left(\frac{8}{36}\right)^2$$

$$= 8.06 \times 10^{-11}$$

The relaxation length for fast neutrons in water is approximately 8 cm; hence, straight attenuation through 72 in. of water shield yields

$$\frac{\phi}{\phi_0} = e^{-22.9} = 1.13 \times 10^{-10}$$

Since this value is less than the attenuation of the duct, the duct design is adequate. Note, however, that the shield is still weak along lines A – A′ and B – B′ (Fig. 8.9b). One can calculate the attenuation through the first section and then find the attenuation in the water following same by comparison with experimental data. For line B – B′, first, calculate the attenuation in water; then compute the attenuation in the straight duct section by the equations given above. The attenuation through the first section of the duct along line A – A′ is

$$\frac{\phi}{\phi_0} = 10\, e^{-2.82} \frac{1}{8}\left(\frac{8}{36}\right)^2$$

$$= 3.33 \times 10^{-3}$$

Through the remaining 36 in. of water, the attenuation is $A = e^{-11.43} = 1.09 \times 10^{-5}$; hence the total attenuation is 3.63×10^{-8}. Comparing this value with the attenuation through 72 in. of pure water, it is found that the shield is weak at point A′ by a factor of 0.003. This can be compensated for by placing a blister with a water thickness of 18.3 in. at point A′ and also at B′ since the attenuation is the same.

(d) Experiments with the MIT Cyclotron. Description. Two series of experiments were performed at Massachusetts Institute of Technology (MIT) on the attenuation of neutrons and gamma rays in cylindrical-duct penetrations through shields. The radiation source for these experiments was the scattered neutron and gamma radiation from the MIT cyclotron (produced by deuteron bombardment of various targets). No effort was made to determine the spectrums of the incident radiations.

The first series of experiments[8] was made using a concrete shield. This shield, with the duct to be tested, was positioned in the doorway of the cyclotron room. Experiments determined that the radiation incident upon the face of the shield was approximately uniform. Three 6-in.-diameter duct configurations were used: (1) straight through, (2) single offset (two right-angle bends), and (3) helical.

The second series of experiments[9] was made using a water shield. The same experimental setup was used for these experiments as was used on the concrete shield. The duct diameters used for these tests were 4, 6, and 8 in. Two duct configurations were used for each duct size: (1) straight through and (2) single offset (two right-angle bends).

In both sets of experiments partial voids were introduced at various depths in the shields. A horizontal T-shaped duct through the water shield was also investigated to determine the effect on the neutron distribution of scattering at a bend.

The radiation attenuation through the ducts along the face of the shield and through the shield was measured as follows:

1. Thermal and epithermal neutrons: The cadmium-indium difference technique was used. Normalization techniques were used to account for irregularities of the source strength from one experiment to the next.

2. Fast neutrons: Aluminum and phosphorus foils were used as threshold detectors in the series of experiments performed on the concrete shields. A fast-neutron survey meter was used for the water shield. In the latter case no normalization was used.

3. Gamma ray: The gamma-ray distribution was measured with an ionization chamber.

Results. Analysis of the results obtained from these experiments indicated the following trends:

1. The neutron flux decreases less rapidly in the first 10 in. of the duct. This is predicted by diffusion theory for the neutron distribution within the shield, and diffusion from the shield to the duct presumably causes the observed change in attenuation.

2. The thermal-neutron flux falls off rapidly near the exit of the duct. This drop can be explained by the increased diffusion of the neutrons out of the duct into the surrounding area.

3. The effect of the duct can be explained by a superposition of the following effects: (1) direct radiation streaming through the duct, (2) scattering of the radiation along the duct, and (3) scattering and diffusion of radiation from the shield into the duct. Attenuation factors (distance required to reduce radiation 10-fold) were determined for the thermal and indium resonance neutrons through the shield and straight ducts. These are listed here.

Attenuation Factors (Centimeters for Factor of 10)

Medium	Thermal neutrons	Indium resonance neutrons
Concrete (without holes)	20.4	19
Water (without holes)	23.4	19
6-in. duct in concrete	50.7	44.5
4-in. duct in water	45.7	48.3
6-in. duct in water	66	68.6
8-in. duct in water	67.3	71.1

Detailed curves showing the effects of the straight, curved, helical, and partial ducts may be found in references 8 and 9.

4. It was found that, for straight ducts in the water shield, the ratio of neutron flux in the duct to the neutron flux in the adjacent shield could be represented to a good approximation by the following equation:

$$\frac{\phi_D}{\phi_S} = KL^y$$

where K is a constant depending on the particular experiment, L is the distance along the duct axis, and y varied with duct diameter as shown in the following table.

Experimental Values of y

Duct diameter, in.	Thermal neutrons	Indium resonance neutrons
4	2.61	2.44
6	3.80	2.83
8	3.94	3.13

5. Insufficient gamma and fast-neutron data were taken to allow a reasonable correlation to be made.

2.3 Transmission Through Annuli

The problem of calculating fast-neutron transmission through annuli may be treated by combining the methods given in Secs. 2.2 and 3.4. Section 2.2 considered the neutron attenuation of a cylindrical duct to be essentially the product of the attenuations of each section multiplied by a factor of 10 (to account for the source size and the uncertainty). Section 3.4 will develop the annular leakage of gamma rays by means of a "line-of-sight" path.

Combining these methods, we can relate the fast flux leaving an annulus to that entering (see Fig. 8.10).

$$\frac{\phi}{\phi_0} = 10\left[(2R^2 - r^2)\cos^{-1}\frac{r}{R} - r\sqrt{R^2 - r^2}\right]^n \Big/ \left(\frac{1}{L_1^2} + \frac{1}{L_2^2} + \frac{1}{L_3^2} + \cdots \frac{1}{L_n^2}\right)$$

where ϕ_0 = fast flux entering (neutrons/cm^2-sec)
r = inner radius of annulus
L_i = length of i*th* section of annular path
n = number of "legs" of annular path (see Fig. 8.10)

This formula does agree reasonably well with test data presented in reference 7 if one uses experiments G and R as annulus tests, with H and S as background (the letters referring to run numbers as used in reference 7).

2.4 Effect of Small Voids in Shield

The presence of voids in the neutron shield causes an increase in the neutron dose outside the shield. A method similar to that employed for the calculation of gamma rays through internal voids may be used as an approximation. For neutrons, however, the value of the gamma absorption coefficient, μ, should be replaced by the appropriate cross-section value, Σ, for neutrons. Where 0.9-Mev neutrons (i.e., from N^{17}) are predominant, this cross section can be obtained from Chap. 4; for fission neutrons a value of 0.1 cm^{-1} should be satisfactory for water-like shields. For small penetrations a build-up factor of 1 may be used.

In purchasing polyethylene for naval reactor shields, fairly good production standards were maintained, and void volume in commercial-grade polyethylene was held at very low values. Listed here is a set of typical permissible voids specified. These were derived from a line-of-sight calculation for a point source and should result in no more than a 5 per cent local increase in neutron flux.

Depth of flaw measured normal to plane of slab, in.	Maximum permissible area of flaw, sq in.
1/32 to 1/16	1.60
1/16 to 1/8	0.50
1/8 to 1/4	0.25
1/4 to 1/2	0.10

2.5 Streaming Along Steel Paths

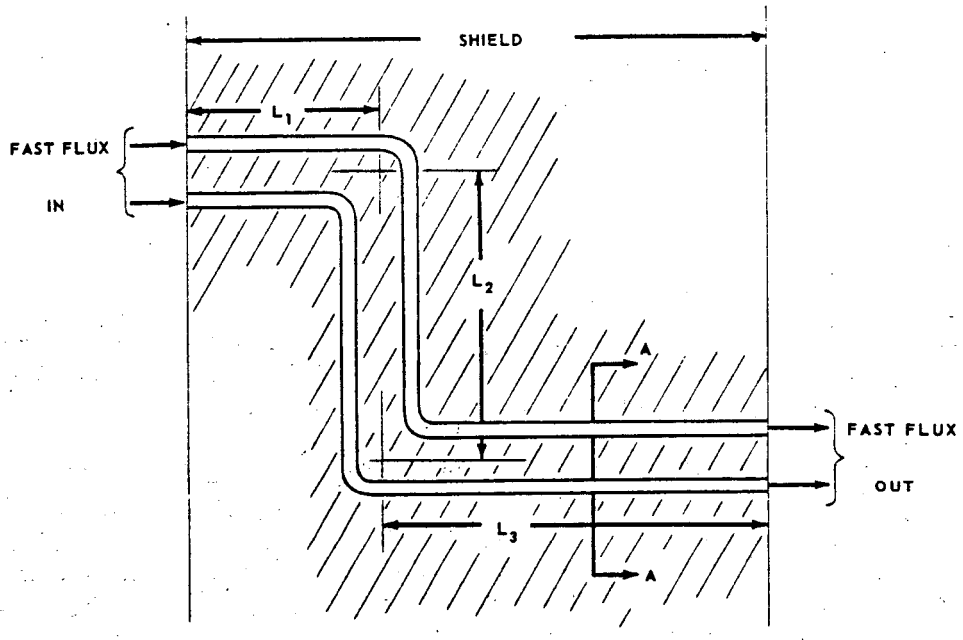
(a) Statement of the Problem. Neutron streaming may be defined as the selective transmission of specific energy bands of neutrons through a shield material as a result of "valleys" in the cross section. Streaming is particularly important because the structural materials (e.g., carbon steel) which penetrate an otherwise adequate shield often exhibit this behavior.

As an illustration of shielding weakness induced by a cross-section valley, consider the example suggested by Blizard.[10]

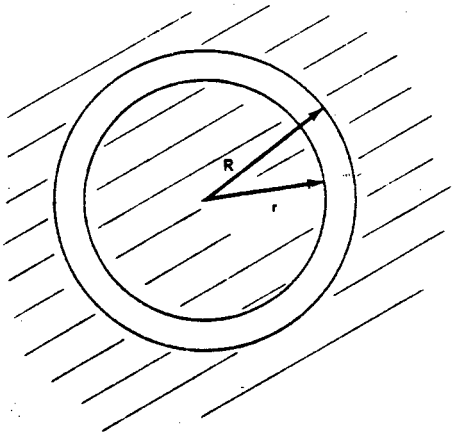
A shield 120 cm thick has a flat neutron spectrum of the following description incident upon it

$\phi_0(E) = 1 \qquad 0 < E < 10$ ev

$\phi_0(E) = 0 \qquad E > 10$ ev



SKETCH OF ANNULUS PENETRATING NEUTRON SHIELD



SECTION AA

Figure 8.10

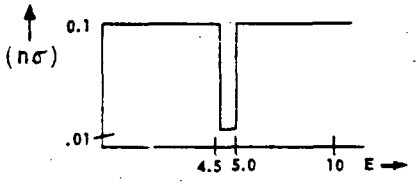
The shield material has n atoms/cm^3 and a microscopic cross section $\sigma(E)$ such that

$$n\,\sigma(E) = \Sigma(E) = 0.1\ \text{cm}^{-1} \qquad 0 < E < 4.5\ \text{ev}$$

$$n\,\sigma(E) = \Sigma(E) = 0.01\ \text{cm}^{-1} \qquad 4.5 < E < 5\ \text{ev}$$

$$n\,\sigma(E) = \Sigma(E) = 0.1\ \text{cm}^{-1} \qquad 5 < E < 10\ \text{ev}$$

A sketch of this cross section is shown below:



Then 95 per cent of the incident spectrum sees a macroscopic cross section of 0.1 cm^{-1}, and the 5 per cent between 4.5 and 5 sees 0.01 cm^{-1}. Assuming the cross section to be for a removal process, the shield attenuation can be written as the ratio of emergent to incident fluxes

$$\frac{\phi}{\phi_0} = 0.95 \exp[-(120)(0.1)] + 0.05 \exp[-(120)(0.01)]$$

$$= 6 \times 10^{-6} + 1.5 \times 10^{-2}$$

or

$$\frac{\phi}{\phi_0} = 1.5 \times 10^{-2}$$

Therefore the attenuation of the shield is described solely by the "hole" in the cross section, and virtually all emergent neutrons would have this streaming energy of 4.5 to 5.

A more realistic case has been calculated by Podgor.[11] Instead of a flat spectrum a fission spectrum was attenuated in the manner described above for an iron-water shield using energy-dependent cross sections for each material. The result was a peak in the emergent spectrum at 1 Mev. Since no energy degradation was considered and the assumed fission spectrum was valid only down to 0.1 Mev, the effect of holes at lower energies would be minimized in this calculation.

(b) Experimental Results. Langsdorf et al.[12] have observed such streaming effects experimentally. A long filter of a given material is followed by a thin shield of one of several other materials. The long filter acts as a monochromatizer. The thin shield of the same or different material then attenuates this flux so that a cross section can be assigned to the thin shield material for the monochromatic neutrons. It was noted that the thin shield of the same material as the thick filter generally exhibits a markedly lower cross section. Langsdorf's results are reproduced in the tabulation on the following page.

More recent measurements of this type are described by Shore.[13] Two successive thick filters of iron were used, and thin filters of various materials were inserted in a space between them. The effective cross sections found were compared with those of Langsdorf[12] and with those given in Report AECU-2040[14] at 25 kev. It was concluded that streaming occurs in pure iron at about 25 kev. The iron cross section given in reference 14 shows the expected dip there.

The fact that iron does allow neutron streaming then led to experiments designed to compare streaming in iron, stainless steel, and carbon steel. The latter two are of particular interest since they are commonly used in structure penetrating reactor shields.

CROSS SECTIONS FOR THIN SHIELDS FOR NEUTRONS PASSED THROUGH VARIOUS LONG FILTERS

Thin shields	Thin shield, gram-atom/cm^2	Long filter: 16-in. aluminum, barns	12-in. iron, barns	6-in. nickel, barns	6-in. copper, barns
Polystyrene (CH)	0.2	23	14	11	12
Graphite-C	0.164	4.6	4	4	4
H (by difference)		18	10	7	8
Aluminum	0.26	[1.2]	2.0	3.3	2.5
Iron	0.54	6	[0.8]	2.7	4.5
Nickel	0.12	19	8	[2.7]	8
Copper	0.18	8	7	5	[3]
Molybdenum	0.32	7	8.5	7.5	6

Schamberger and Shore[15] at BNL provide an excellent demonstration of the dependence of streaming in steels on the nickel content. A plate of either stainless steel, armor plate (carbon steel with a small percentage of additional elements), or carbon steel was placed above the BNL neutron source. The long dimension of the plate was perpendicular to the source. Measurements of thermal-neutron flux in water beyond the plates showed the carbon steel to stream far more than stainless steel and somewhat more than the armor plate. A laminated stack of carbon steel strips each parallel to the source was then made up to the same dimensions as the original carbon steel plate. The streaming was found to be the same. Then some of the carbon steel strips were replaced by nickel strips, thus maintaining the dimensions of the stack but varying the nickel content. It was found that the introduction of nickel percentages comparable to those of stainless steel reduced the streaming of the stack to that of the stainless-steel plate. As a final test the nickel content of the armor plate was estimated from the carbon steel–nickel stack data and found to be 1.5 ± 0.4 per cent. Chemical analysis shows the armor plate to contain 1.9 per cent nickel.

The stack was also tested with the nickel strips uniformly dispersed and with them lumped at the top, middle, and bottom of the stack. Minimum transmission in all cases was observed when the nickel strips were lumped at the center. This phenomenon is interestingly like the BNL results on the effectiveness of offsets in breaking up air-slot streaming paths (see Sec. 2.1c of this chapter).

Schamberger and Shore note the coincidence of a high nickel cross section at 25 kev, the suspected iron streaming energy.

Work on the comparison of iron and stainless-steel streaming was also performed at ORNL by Blizard, Chapman, and Flynn.[16] The results are in agreement with those of Schamberger and Shore. Two examples of cylinder streaming were tested, as well as plate streaming.

(c) Calculational Methods. Tests of arrangements of various streaming cases of interest to the shield designer have been conducted.[16–19]

Reference 19 is of particular interest since an empirical relation is given between a measure of streaming in carbon steel and the geometry of the plate or cylinder. This relation for a plate is (see Fig. 8.11)

$$\boxed{\left(\frac{\phi}{\phi_w} - 1\right)_{peak} = 0.004T^{2.3}W^{1.12}e^{0.080L}} \qquad \text{for plate}$$

where ϕ_w = thermal-neutron flux in pure water beyond source, measured at the point of maximum flux difference

ϕ = thermal-neutron flux beyond streaming path, measured at the point of maximum flux difference

T = plate thickness (in.)

W = plate width (in.)

L = plate length (in.)

W > 10T

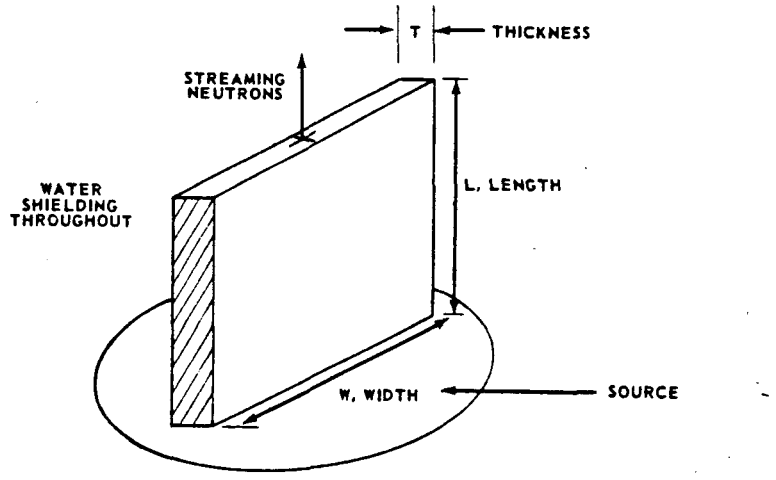


Figure 8.11

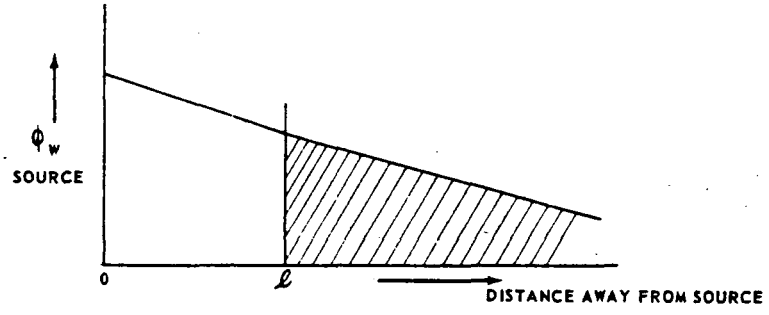


Figure 8.12

Similarly for a cylinder

$$\left(\frac{\phi}{\phi_w} - 1\right)_{peak} = 0.003D^{3.42}e^{6.080L} \qquad \text{for cylinder}$$

where D is the cylinder diameter (in.).

It should be noted that these formulas relate thermal-neutron fluxes; that is, the presence of streaming neutrons can only be inferred from the appearance of the thermals to which they give rise by water degradation.

It is desirable to relate these "streaming" thermals to their parent group, the true streaming neutrons. One approach is as follows: Assume an infinite-plane fission source followed by a water shield. Figure 8.12 shows a plot of thermal-neutron flux for this case. Assume further that only a thickness l of water is required to reduce the neutron dose to tolerance. Note that the dose outside such a shield would be primarily due to fast neutrons since the iron of a tank wall, etc., would quickly remove the dose due to thermals. The fast flux leaking beyond l can be inferred, however, by noting that the thermals which are measured in a shield result from recently degraded fast neutrons and that at equilibrium the rate of creation of thermals (or degradation of fast) must equal the rate of removal (absorption) of thermals. It follows then that

$$\phi_f(l) = \int_l^\infty \varphi_w \Sigma_a \, dz$$

where Σ is the macroscopic absorption cross section of water and $\phi_f(l)$ is the fast flux passing position l.

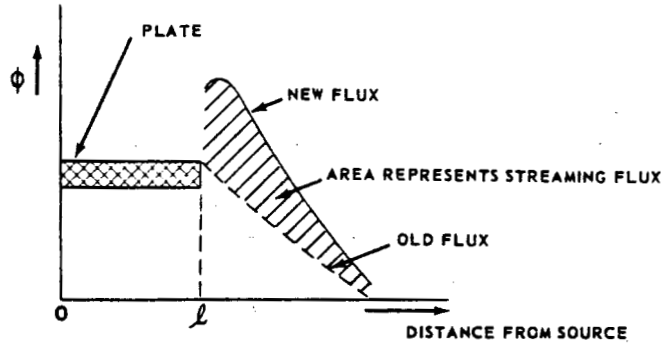


Figure 8.13

Now suppose a carbon steel plate is introduced to provide a streaming path. A new thermal flux is now detected beyond l, as in Fig. 8.13. Thus the leaking fast flux can (to an approximation) be written as

$$\phi_f^1(l) = \int_l^\infty \phi \Sigma_a \, dz$$

The fast or streaming flux added by the introduction of the plate is then

$$\phi_f^1(l) - \phi_f(l) = \int_l^\infty \phi \Sigma_a \, dz - \int_l^\infty \phi_w \Sigma_a \, dz$$

or

$$\varphi_{\text{streaming}} \cong \phi_s = \Sigma_a \int_l^\infty (\varphi - \varphi_w) \, dz$$

The quantity $(\varphi - \phi_w)$ in the integral is of course the excess thermal flux which can be calculated.

Now a general description of the excess thermal flux beyond a plate is given in Report BNL-265.[19] Using this and performing the integration yields, in general,

$$\phi_s \cong \frac{1}{8} (\varphi - \phi_w)_{\text{peak}}$$

$$\frac{\phi_s}{\varphi_w} \cong \frac{1}{8} K T^{2.3} W^{1.12} e^{0.080L}$$

where the peak occurs at about 2 in. beyond the end of the plate.

In practice the width W of a streaming plate is greater than the range of widths covered in Report BNL-265. For the case of a large width, an alternative form for R might be chosen such as

$$R = \left(\frac{\varphi}{\phi_w} - 1\right)_{\text{peak}} = K' \, T^{2.3} \, e^{0.080L} \, (1 - e^{-0.0077W})$$

Empirically K′ is found to vary between 0.5 and 1.0.

Note that for small widths

$$K'(1 - e^{-0.0077W}) \cong K'[1 - (1 - 0.0077W + \ldots)]$$
$$\cong 7.7 \times 10^{-3}\, WK'$$
$$\cong 3.8 \times 10^{-3}\, W \quad \text{for } K' \cong 0.5$$

The form suggested in Report BNL-265 was

$$KW^{1.12} = 3.8 \times 10^{-3}\, W^{1.12}$$

The forms are then essentially equivalent for small widths.

The final form for the streaming flux from a plate is then

$$\boxed{\frac{\phi_s}{\phi_w} \cong \frac{1}{8} T^{2.3} e^{0.080L} (1 - e^{-0.0077W})}$$ for K′ assumed to be 1

For the case of a *cylinder*

$$\boxed{\frac{\phi_s}{\phi_w} \cong 3.2 \times 10^{-4} D^{3.42} e^{0.080L}}$$

where ϕ_w is measured about 2 in. of water beyond the end of the plate. All dimensions are given in inches.

(d) Sample Calculation. A typical thermal-flux distribution in a water and lead secondary shield is shown in Fig. 8.14. One would like to calculate the streaming dose leaving a steel web which is part of the water tank structure. (See Fig. 8.15.) Then

$T = 1.2$ in. Peak $\phi_w = \phi_w$ at 38 in. = 20 neutrons/cm²-sec
$L = 36$ in. $W \to \infty$ for a large tank

$$(\phi - \phi_w)_{peak} \cong 1.2^{2.3} \times e^{(0.08)(36)} \times (1 - e^{-\infty})\ (20)$$
$$\cong 540 \text{ neutrons/cm}^2\text{-sec}$$

and

$$\phi_s \cong \frac{1}{8}(\phi - \phi_w)$$
$$\cong 68 \text{ neutrons/cm}^2\text{-sec}$$

that are present due to streaming through the plate. It is somewhat indeterminate as to what dose conversion to use. If it is assumed that these neutrons are roughly equivalent to thermals,

$$D_s \cong \frac{68}{480} \text{ mrem/hr}$$
$$\cong 0.14 \text{ mrem/hr}$$

The streaming dose is then negligible.

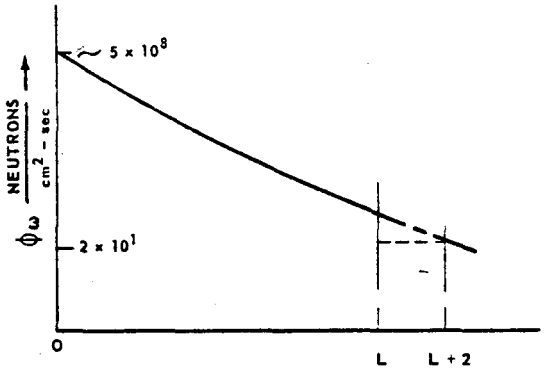


Figure 8.14

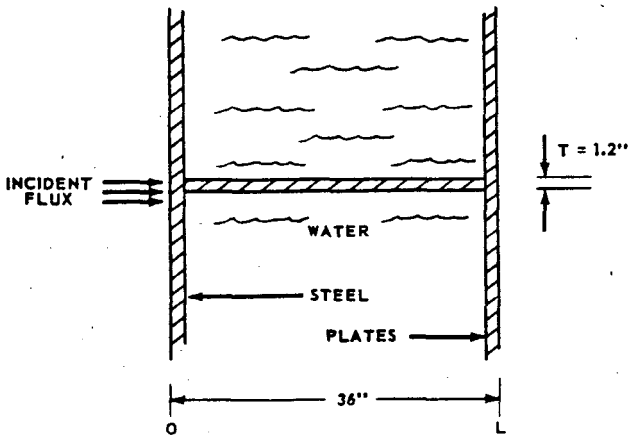


Figure 8.15

3 GAMMAS

3.1 Source Geometries

The gamma flux escaping from an air void in a shield depends on the geometry of the void and the angular distribution of the radiation emerging from the source. Three methods of treating the angular distribution of the radiation will be illustrated here.

(a) Spherical Distribution: In cases where self-absorption in the source is unimportant, the gamma flux may be considered uniformly distributed in all directions. Then the flux emitted through a unit solid angle is $\phi_0/2\pi$ (gammas/cm^2-sec).

(b) Cosine Distribution: A self-absorbing homogeneous source emits more strongly in the forward direction. The flux emitted into a unit solid angle at the angle θ is then $(2\phi_0 \cos\theta)/2\pi$ (gammas/cm^2-sec).

(c) Fermi Distribution: In a self-absorbing inhomogeneous source in which the gamma activity per unit volume increases with increasing distance below the surface, the emission is even more strongly forward. Therefore, the flux into the unit solid angle at the angle θ is $[0.928\phi_0(\cos\theta + \sqrt{3}\cos^2\theta)]/2\pi$.

In the forward direction the three distributions stand in the ratio, spherical : cosine : Fermi = 1 : 2 : 2.54.

3.2 Rectangular Slots

Consider a long, narrow slot of thickness T and length L cut in a slab shield (Fig. 8.16). The number of gamma photons escaping per unit width of the slot is found as the integral of the

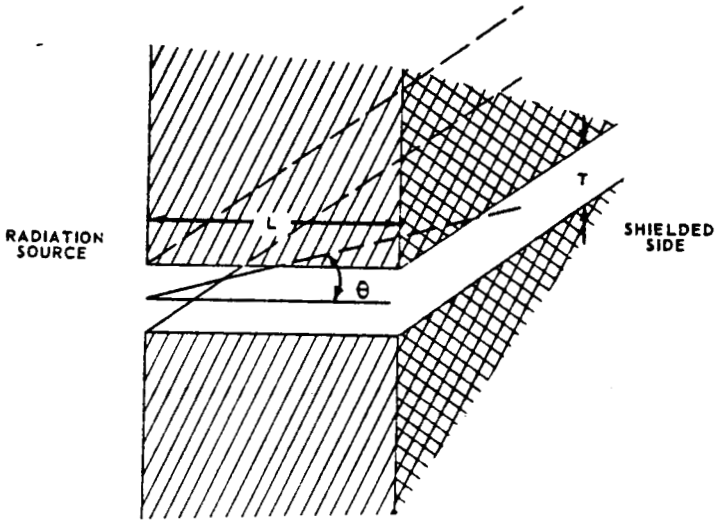


Figure 8.16

following factors: the probability of emission into the unit solid angle at the angle $\phi(1/2\pi)$ times the projected area of the receptor in the direction θ divided by the square of the distance from the emitting element d(L tan θ) to the receptor [this factor, (T cos θ/L^2 $\sec^2\theta$), defines the solid angle subtended by the detector] times the source strength [ϕ_0Td (L tan θ)]. The integration is performed over θ from $-\pi/2$ to $\pi/2$ or twice the integral from 0 to $\pi/2$.

(a) Spherical Emitter: For a spherical emitter

$$\text{N particles/cm-sec} = 2\int_0^{\pi/2} \frac{1}{2\pi}\,\frac{(T\cos\theta)}{L^2\sec^2\theta}\,\phi_0 Td\,(L\tan\theta)$$

Integrating,

$$\text{N gammas/cm-sec} = \frac{\phi_0 T^2}{\pi L}$$

N is in terms of gammas per centimeter of width per second; the flux is obtained by dividing both sides of the equation by the thickness, T, of the slot,

$$\phi \text{ gammas/cm}^2\text{-sec} = \frac{\phi_0 T}{\pi L}$$

(b) Cosine Emitter: In the same way, for a cosine emitting source,

$$N = \frac{\phi_0 T^2}{2L}$$

and

$$\phi = \frac{\varphi_0 T}{2L}$$

(c) Fermi Emitter: If the source is a Fermi emitter, the results become

$$N = 0.573\,\frac{\varphi_0 T^2}{L}$$

and

$$\phi = 0.573\,\frac{\varphi_0 T}{L}$$

If a directional detector is not used, the equations for N gammas per centimeter-second will be as follows:

For a spherical emitter

$$N = \frac{\varphi_0 T^2}{2L} \qquad \frac{\phi}{\varphi_0} = \frac{1}{2}\left(\frac{T}{L}\right)$$

For a cosine emitter

$$N = \frac{2\varphi_0 T^2}{\pi L} \qquad \frac{\phi}{\varphi_0} = \frac{2}{\pi}\left(\frac{T}{L}\right)$$

For a Fermi emitter

$$N = \frac{0.698\ \varphi_0 T^2}{L} \qquad \frac{\phi}{\varphi_0} = \frac{1}{1.4}\left(\frac{T}{L}\right)$$

3.3 Cylindrical Ducts

Consider a long, thin, straight cylindrical duct, of radius r and length L, through a shield (see Fig. 8.17).

(a) Spherical Emitter: The duct abuts perpendicularly on a source that is characterized as a spherical emitter out of which the flux is ϕ_0 gamma photons/cm^2-sec. The total number of gammas entering the duct per second is $N_0 = \phi_0 \pi r^2$; the fraction of those which go into the unit solid angle toward the exit is $1/2\pi$; and the solid angle of an element of the duct through which the gammas must escape is $2\pi \sin\theta\, d\theta$. The integral of these factors from $\theta = 0$ to $\theta = \arcsin\sqrt{r^2/(r^2 + L^2)}$ gives the total number of gammas escaping from the duct. With long thin ducts the value of r^2 is negligible compared to L^2; hence, the integration can be performed from 0 to $\sin^{-1} r/L$.

$$N = \int_0^{\sin^{-1} r/L} (\phi_0 \pi r^2)\,\frac{1}{2\pi}\,\frac{2\pi \sin\theta\, d\theta\, L^2}{L^2}$$

$$N = \frac{\phi_0 \pi r^4}{2L^2} \text{ gammas/sec}$$

Dividing both sides of the equation by the cross-sectional area of the duct entrance, we obtain flux in gamma photons per square centimeter-second.

$$\frac{\phi}{\varphi_0} = \frac{r^2}{2L^2} \tag{12}$$

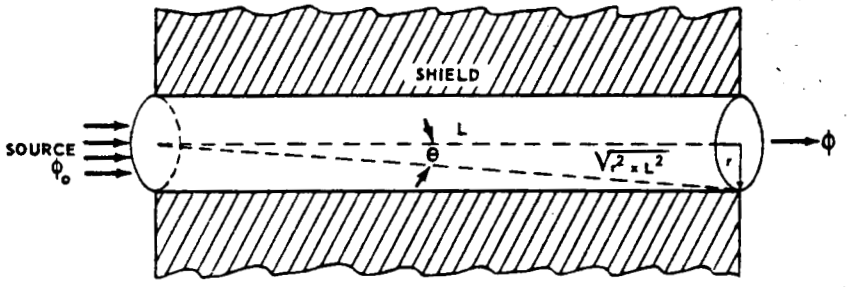


Figure 8.17

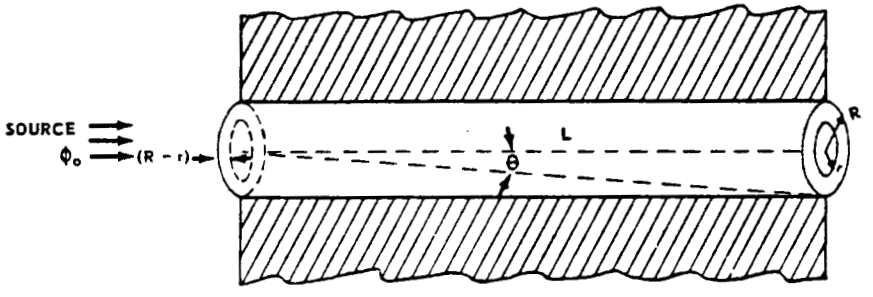


Figure 8.18

(b) Cosine Emitter: If the cylindrical duct abuts perpendicularly on a cosine emitter, the fraction of gammas which goes into the unit solid angle toward the exit is $(2 \cos \theta)/2\pi$. If the other factors remain the same as described in (a), the integration of these factors from $\theta = 0$ to $\theta = \arcsin r/L$ gives

$$N = \int_0^{\sin^{-1} r/L} (\phi_0 \pi r^2) \frac{(2 \cos \theta)}{2\pi} \frac{(2\pi L^2 \sin \theta \, d\theta)}{L^2}$$

which yields

$$N \text{ gammas/sec} = \frac{\phi_0 \pi r^4}{L^2}$$

or

$$\phi \text{ gammas/cm}^2\text{-sec} = \phi_0 \frac{r^2}{L^2}$$

(c) Fermi Emitter: If the angular distribution of the source entering the cylindrical duct is best described as a Fermi emitter, the fraction of gammas going into the unit solid angle is $0.928 (\cos \theta + \sqrt{3} \cos^2 \theta)/2\pi$. Using the same factors described in (a) and integrating from 0 to $\sin^{-1} r/L$,

$$N = \int_0^{\sin^{-1} r/L} \phi_0 \pi r^2 \left[\frac{0.928 (\cos \theta + \sqrt{3} \cos^2 \theta)}{2\pi} \right] 2\pi \sin \theta \, d\theta$$

The final result is N particles/sec $= 3.98 \, \phi r^4/L^2$, and ϕ/ϕ_0 gammas/cm^2-sec $= 1.266 \, r^2/L^2$.

3.4 Annular Ducts

Consider an annular opening of outer radius R and inner radius r through a slab shield of large thickness L (Fig. 8.18).

(a) Spherical Emitter: The annulus abuts perpendicularly on a source emitting φ_0 gammas/cm^2-sec. The number of gammas entering the annulus is $\phi_0\pi(R^2 - r^2)$. If the source is a spherical emitter, the fraction of particles which goes into the unit solid angle toward the exit

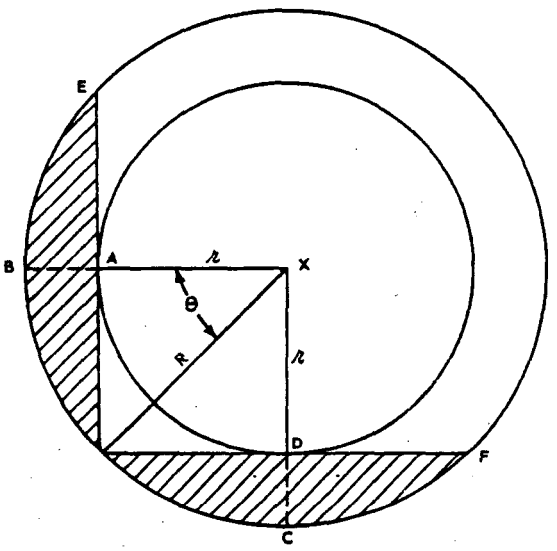


Figure 8.19

is $1/2\pi$. The solid angle through which the particles must escape is $2\pi \sin\theta\, d\theta$. Integrating these factors from $\theta = 0$ to $\theta = \arctan 2(\sqrt{R^2 - r^2}/L)$ gives the number of particles which could escape from the annulus.

$$N = \int_0^{\tan^{-1}2(\sqrt{R^2-r^2}/L)} \frac{\phi_0\pi(R^2 - r^2)}{2\pi} (2\pi \sin\theta\, d\theta)$$

$$= \frac{\varphi_0 2\pi(R^2 - r^2)^2}{L^2}$$

However, all the particles do not escape through the annulus exit. The ratio of the escape area of the annulus exit to the total escape area times the value of N gives the total number of particles per second escaping through the annulus.

The shaded area in Fig. 8.19 shows the maximum surface area of escape of a particle emitted from the source.

The formula for area is derived in the following manner:

Area of ABCD = area XBC − area XAD

$$= \frac{\pi R^2 2\theta}{2\pi} - \frac{\pi r^2 2\theta}{2\pi}$$

Area of ABCD = $\theta(R^2 - r^2)$

$$\theta = \cos^{-1}\frac{r}{R}$$

Area of ABCD = $\cos^{-1}\frac{r}{R}(R^2 - r^2)$

Area of (AEB + DFC) = area of segment of cord length $2\sqrt{R^2 - r^2}$

$$= \frac{\pi R^2 2\theta}{2\pi} - \frac{R^2 \sin 2\theta}{2}$$

$$= R^2 \cos^{-1}\frac{r}{R} - R^2 \sin\theta\cos\theta$$

$$= R^2 \cos^{-1}\frac{r}{R} - R^2\frac{\sqrt{R^2 - r^2}}{R}\frac{r}{R}$$

$$= R^2 \cos^{-1}\frac{r}{R} - r\sqrt{R^2 - r^2}$$

Maximum area of escape = $\cos^{-1}\frac{r}{R}(R^2 - r^2) + R^2\cos^{-1}\frac{r}{R} - r\sqrt{R^2 - r^2}$

Total area subtended by the escape angle = $\pi\,(2\sqrt{R^2 - r^2})^2$

The ratio of the maximum area of escape to the total area subtended by the escape angle is

$$\frac{2R^2\cos^{-1}(r/R) - r^2\cos^{-1}(r/R) - r\sqrt{R^2 - r^2}}{4\pi(R^2 - r^2)}$$

hence the number of gammas escaping per second is

$$N = \frac{\phi_0 2\pi(R^2 - r^2)^2}{4\pi L^2(R^2 - r^2)}\left[\left(\cos^{-1}\frac{r}{R}\right)(2R^2 - r^2) - r\sqrt{R^2 - r^2}\right]$$

$$N = \frac{\phi_0(R^2 - r^2)}{2L^2}\left[\left(\cos^{-1}\frac{r}{R}\right)(2R^2 - r^2) - r\sqrt{R^2 - r^2}\right] \qquad (13)$$

$$\boxed{\frac{\phi}{\phi_0} = \frac{1}{2\pi L^2}\left[\left(\cos^{-1}\frac{r}{R}\right)(2R^2 - r^2) - r\sqrt{R^2 - r^2}\right]} \qquad \text{for } R^2 - r^2 \ll L^2$$

As r approaches 0 the equation reduces to the equation for the escape from a cylindrical hole.

(b) Cosine Emitter: The number of gammas which could escape from an annulus is

$$N = \int_0^{\tan^{-1}2(\sqrt{R^2-r^2}/L)} \phi_0\frac{\cos\theta}{\pi}\,\pi(R^2 - r^2)\,2\pi\sin\theta\,d\theta$$

$$= \phi_0 2\pi(R^2 - r^2)\int_0^{\tan^{-1}2(\sqrt{R^2-r^2}/L)} \sin\theta\cos\theta\,d\theta$$

$$= \phi_0\pi(R^2 - r^2)\,(\sin^2\theta)_0^{\tan^{-1}2(\sqrt{R^2-r^2}/L)}$$

$$= \frac{\phi_0 4\pi(R^2 - r^2)(R^2 - r^2)}{L^2}$$

This value times the ratio of the areas is equal to the number of gammas per second which do escape from the annulus exit.

$$N = \frac{\phi_0 4\pi(R^2 - r^2)(R^2 - r^2)}{L^2 4\pi(R^2 - r^2)} \left[\cos^{-1}\frac{r}{R}(2R^2 - r^2) - r\sqrt{R^2 - r^2}\right]$$

$$= \frac{\phi_0(R^2 - r^2)}{L^2}\left[\left(\cos^{-1}\frac{r}{R}\right)(2R^2 - r^2) - r\sqrt{R^2 - r^2}\right] \tag{14}$$

$$\frac{\phi}{\phi_0} = \frac{1}{\pi L^2}\left[\left(\cos^{-1}\frac{r}{R}\right)(2R^2 - r^2) - r\sqrt{R^2 - r^2}\right]$$

(c) Fermi Emitter: The number of gammas which escape from the annulus of a Fermi emitter source is

$$N = \int_0^{\tan^{-1}2(\sqrt{R^2-r^2}/L)} \phi_0 \frac{0.9284\,(\cos\theta + \sqrt{3}\cos^2\theta)}{2\pi}\,\pi(R^2 - r^2)2\pi\sin\theta\,d\theta \text{ (ratio of areas)}$$

$$N = \frac{1.27\,\phi_0\,(R^2 - r^2)}{L^2}\left[\left(\cos^{-1}\frac{r}{R}\right)(2R^2 - r^2) - r\sqrt{R^2 - r^2}\right] \tag{15}$$

$$\frac{\phi}{\phi_0} = \frac{1.27}{\pi L^2}\left[\left(\cos^{-1}\frac{r}{R}\right)(2R^2 - r^2) - r\sqrt{R^2 - r^2}\right]$$

The equations for escape from an annulus presented in Report TNX-7[20] are as follows: For a spherical emitter:

$$N = \frac{2.8\phi_0 R^{3/2}(R - r)^{5/2}}{L^2} \qquad \frac{\phi}{\phi_0} = \frac{2.8R^{3/2}(R - r)^{3/2}}{\pi(R + r)L^2}$$

For a cosine emitter:

$$N = \frac{5.6\phi_0 R^{3/2}(R - r)^{5/2}}{L^2} \qquad \frac{\phi}{\phi_0} = \frac{5.6R^{3/2}(R - r)^{3/2}}{\pi(R + r)L^2}$$

For a Fermi emitter:

$$N = \frac{7.2\phi_0 R^{3/2}(R - r)^{5/2}}{L^2} \qquad \frac{\phi}{\phi_0} = \frac{7.2R^{3/2}(R - r)^{3/2}}{\pi(R + r)L^2}$$

These equations are based on an approximation that requires $(R - r)$ to be less than r; they will not converge to the cylindrical formula when $r = 0$.

3.5 Verification with Experimental Results

Some experiments were made at BNL on leakage of reactor gammas through air voids. For the experiments on cylindrical voids performed and reported by Kouts,[21] good agreement with the equations is obtained only for cylinders of small diameter and of length equal to the height of the water tank in which the measurements were made. This is to be expected since the shorter length cylinders have a large amount of water between the source and the cylinder entrance.

A few experiments (K. Shure, unpublished work) have been performed using the WAPD-10 water activation loop at the Materials Testing Reactor, which provide information about high-energy gamma-ray (i.e., the 6-Mev gammas from N^{16}) penetration through simple ducts in a

4-in. lead slab. This information is needed in the design of penetrations for electrical conduit and other small-diameter lines through secondary shields of water-cooled reactors.

A flat plastic disk having a 7.75-in. outside diameter through which freshly irradiated water flows serves as the source of radiation. The source intensity is fairly uniform, being only 17 per cent greater at the center than at the edge of the disk. A description of the ducts is given in the figures, which also show the results. The relation of the source and detector with respect to the ducts is seen in Fig. 8.20, this relation being the same for all the ducts. Plotted as a function of distance across the duct is the ratio of the gamma-ray dose rate above the duct to that measured through a 4-in. lead slab at that point, both measured in air.

Figure 8.20 shows the results for a straight-through 2-in.-diameter duct. The beam broadens as the detector is raised from the lead surface. There is a considerable contribution to the dose rate even at large horizontal distances from the duct. Figures 8.21 and 8.22 show the results for a straight-through 1-in.-diameter duct and $\frac{1}{4}$-in.-diameter duct, respectively.

The results, as seen in Fig. 8.23 for a $\frac{1}{4}$-in. bent duct with no line-of-sight between the source and detector, show no apparent increase in the dose rate above the duct as compared to a solid lead slab since the accuracy of the results is good to only about 10 per cent.

The transmission through a 1-in.-diameter "stovepipe" duct with a 2-in. and a 3-in. offset is seen in Figs. 8.24 and 8.25. Near the lead surface a peak appears for each portion of the duct perpendicular to the slab, that through the last leg of the duct being more prominent. At a distance of about 7 in. above the 3-in. offset duct, the dose rate is about 50 per cent greater than that through a solid lead slab. At the same distance above the 2-in. offset duct, the dose rate is about a factor of 2 greater than that through the solid lead slab.

It should be noted that all these ducts represent total voids in the lead. In many actual applications the void would be partially, if not completely, filled with electrical cable or water, which would tend to reduce the magnitudes of the values represented in the curves as well as to make the structure of the curves less definitive.

Only in the case of the straight ducts is it possible to make an attempt at an analytic calculation of the profile of the radiation pattern. This can be done under several simplifying assumptions. It is assumed that any radiation striking the lead is lost and cannot appear above the duct. It is further assumed that the source plane-detector distance is large compared with the duct diameter; thus essentially all points on the exposed surface of the source plane as seen by the detector through the duct are equidistant from the detector. The portion of the area of the source disk that can be seen by the detector "looking" through the duct can then be calculated. This profile would go to zero at well-defined geometric limits.

It is expected that this simple analysis would be inadequate but that it would be most valid for larger values of source-detector distance, where changes in the inverse-square effect would be smallest, and for larger values of duct diameter, where the ratio of the area of the duct to its perimeter is largest (smaller relative amounts of radiation coming through the edges of the duct).

A qualitative comparison between the simple analysis and the results of the measurements is seen in Fig. 8.26 for a 2-in.-diameter duct with a large source-detector distance and in Fig. 8.27 for a $\frac{1}{4}$-in.-diameter duct with a small source-detector distance. It is seen that the simple analysis describes the profile of the beam rather well for the large-diameter duct out to 3 in. from the center of the duct, whereas it does not adequately describe the profile of the $\frac{1}{4}$-in. duct at all.

3.6 Effect of Voids in Shield

The presence of voids in the fabricated lead of a bulk shield causes an increase in the dose rate outside the shield directly above the void. The following analysis presents an equation for calculating the fractional increase in dose due to a void in the shield. A specific case is calculated as an example, and the results of the calculation are presented in Fig. 8.31.

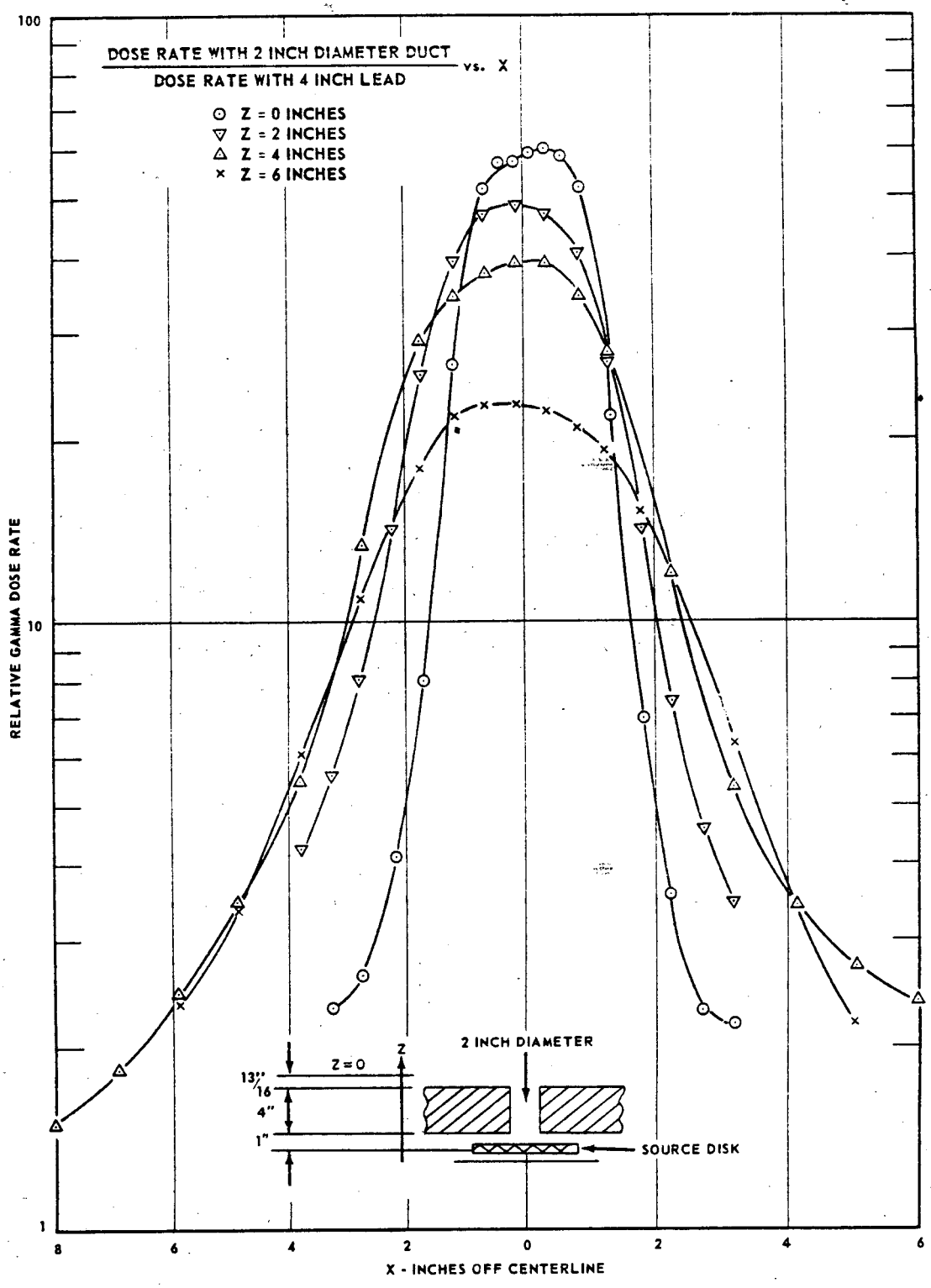

DOSE RATE WITH 2 INCH DIAMETER DUCT
DOSE RATE WITH 4 INCH LEAD
vs. X
Z = 0 INCHES
Z = 2 INCHES
Z = 4 INCHES
Z = 6 INCHES
RELATIVE GAMMA DOSE RATE
100
10
1
8
6
4
2
0
2
4
6
X - INCHES OFF CENTERLINE
2 INCH DIAMETER
Z=0
Z
13/16"
4"
1"
SOURCE DISK

Figure 8.20

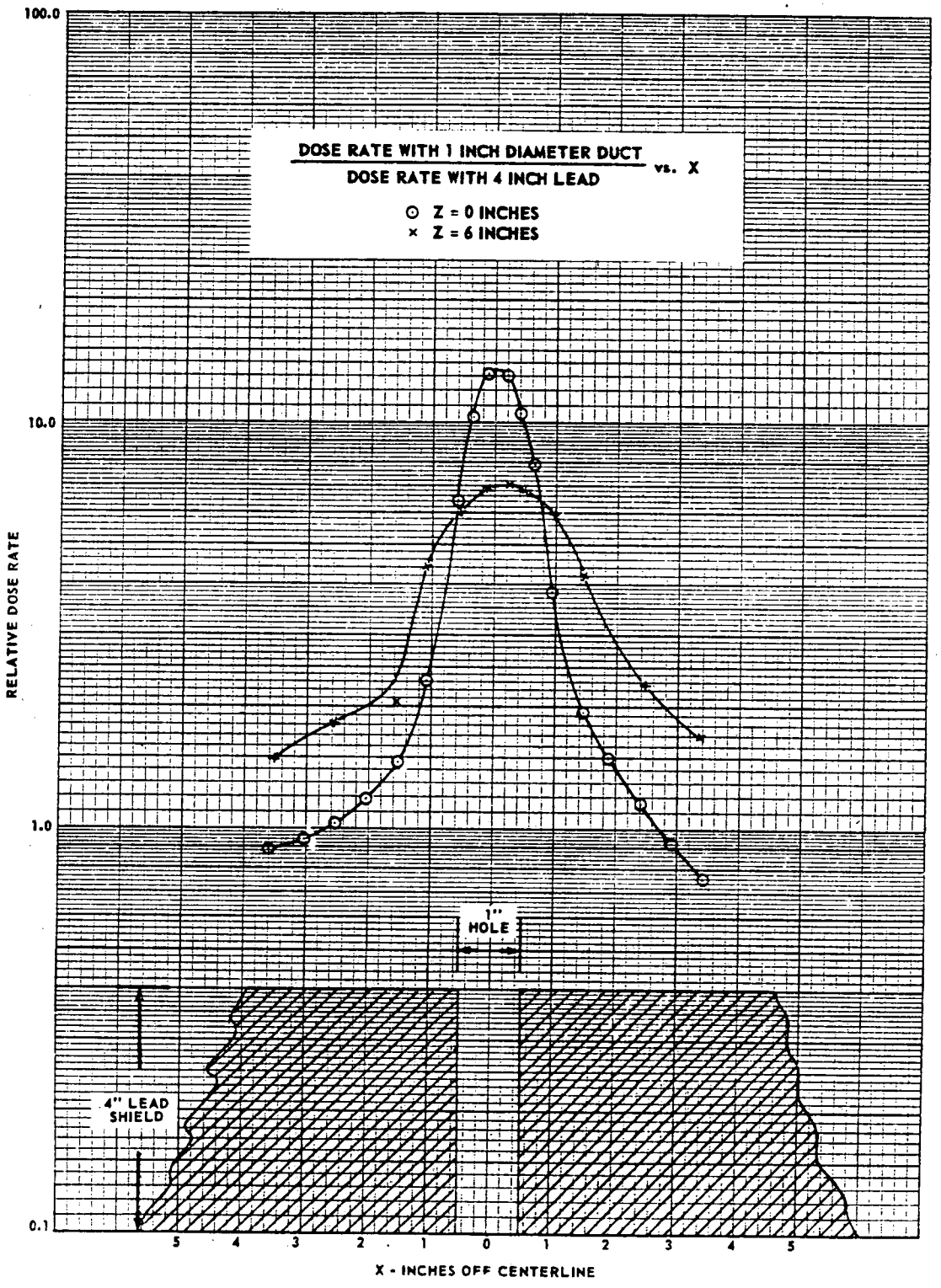

DOSE RATE WITH 1 INCH DIAMETER DUCT
DOSE RATE WITH 4 INCH LEAD
vs. X
⊙ Z = 0 INCHES
× Z = 6 INCHES
100.0
10.0
1.0
0.1
RELATIVE DOSE RATE
1" HOLE
4" LEAD SHIELD
5 4 3 2 1 0 1 2 3 4 5
X - INCHES OFF CENTERLINE

Figure 8.21

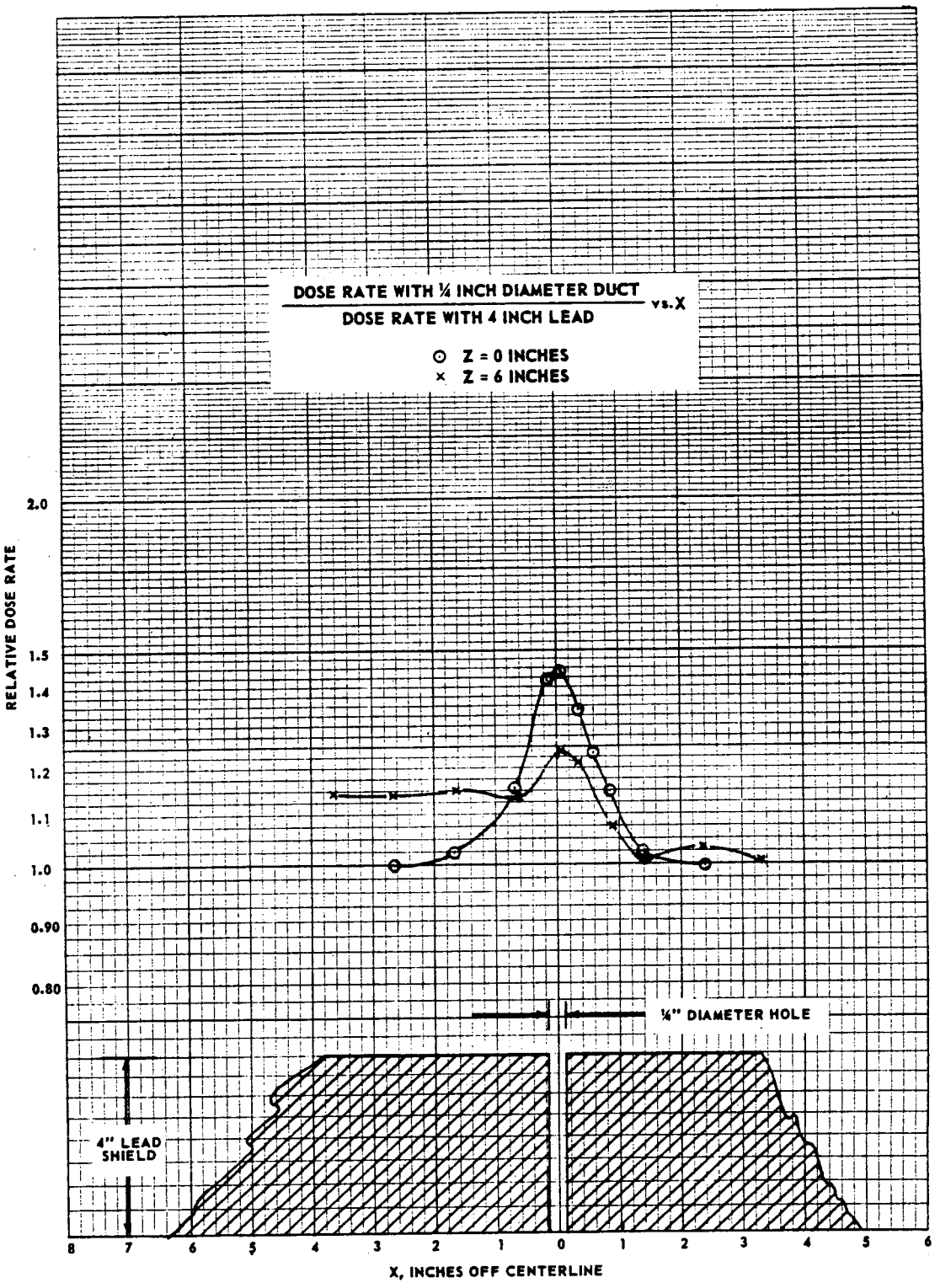

DOSE RATE WITH ¼ INCH DIAMETER DUCT
DOSE RATE WITH 4 INCH LEAD
vs. X
⊙ Z = 0 INCHES
× Z = 6 INCHES
RELATIVE DOSE RATE
2.0
1.5
1.4
1.3
1.2
1.1
1.0
0.90
0.80
¼" DIAMETER HOLE
4" LEAD SHIELD
8 7 6 5 4 3 2 1 0 1 2 3 4 5 6
X, INCHES OFF CENTERLINE

Figure 8.22

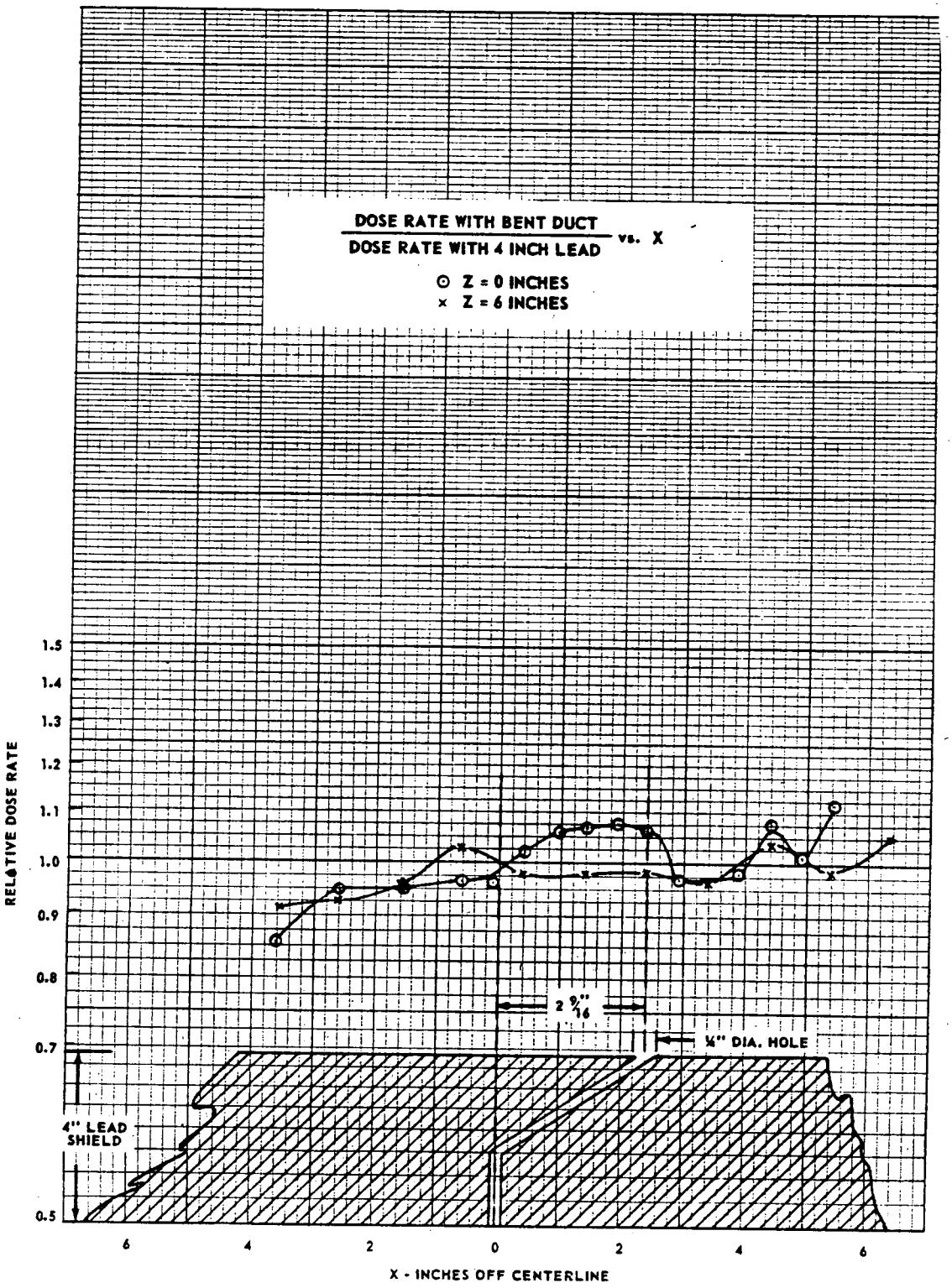

DOSE RATE WITH BENT DUCT / DOSE RATE WITH 4 INCH LEAD vs. X
⊙ Z = 0 INCHES
× Z = 6 INCHES
RELATIVE DOSE RATE
1.5
1.4
1.3
1.2
1.1
1.0
0.9
0.8
0.7
0.5
2 9/16"
¼" DIA. HOLE
4" LEAD SHIELD
6
4
2
0
2
4
6
X - INCHES OFF CENTERLINE

Figure 8.23

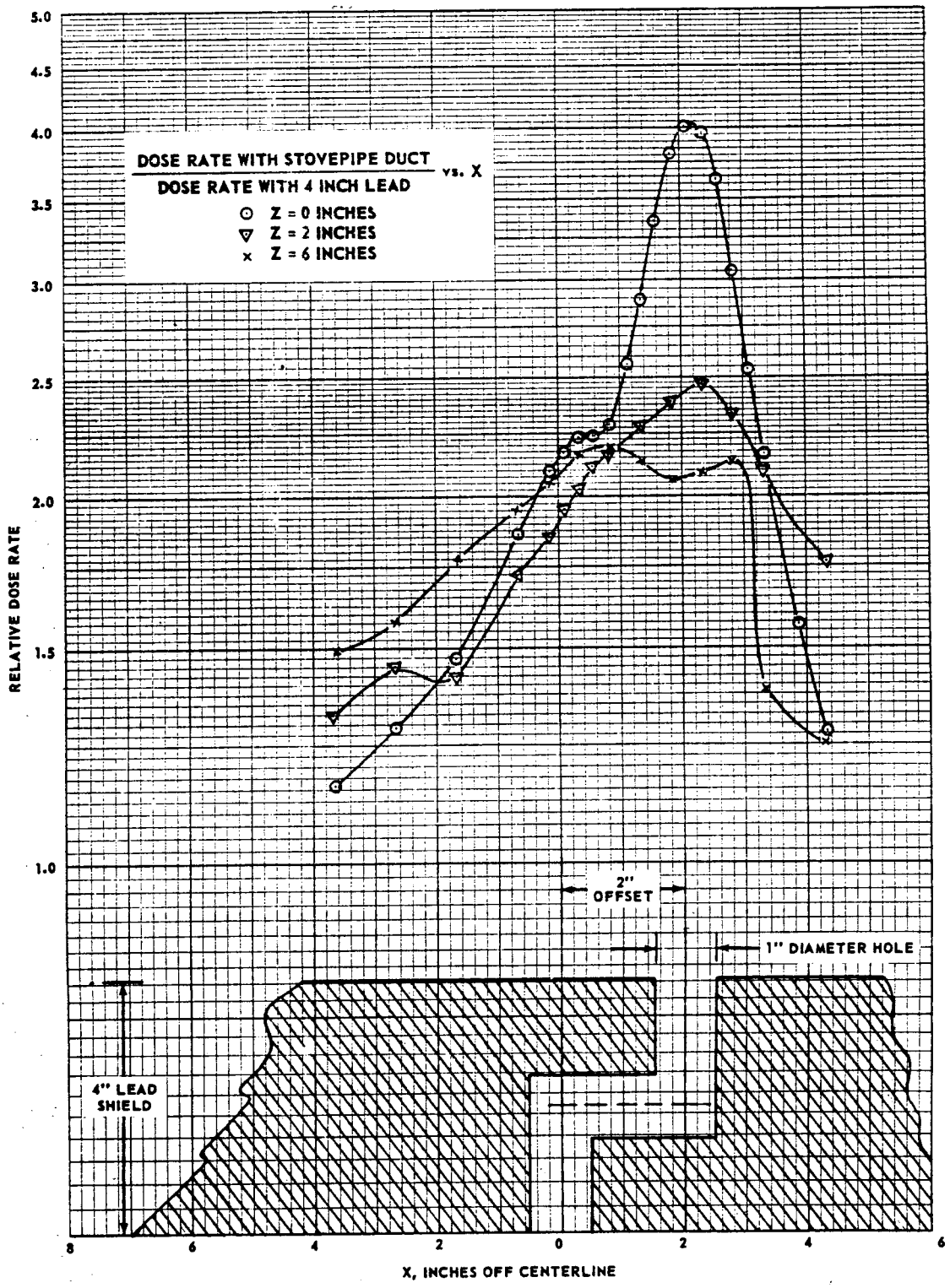

DOSE RATE WITH STOVEPIPE DUCT / DOSE RATE WITH 4 INCH LEAD vs. X
⊙ Z = 0 INCHES
▽ Z = 2 INCHES
× Z = 6 INCHES
RELATIVE DOSE RATE
5.0
4.5
4.0
3.5
3.0
2.5
2.0
1.5
1.0
2" OFFSET
1" DIAMETER HOLE
4" LEAD SHIELD
8
6
4
2
0
2
4
6
X, INCHES OFF CENTERLINE

Figure 8.24

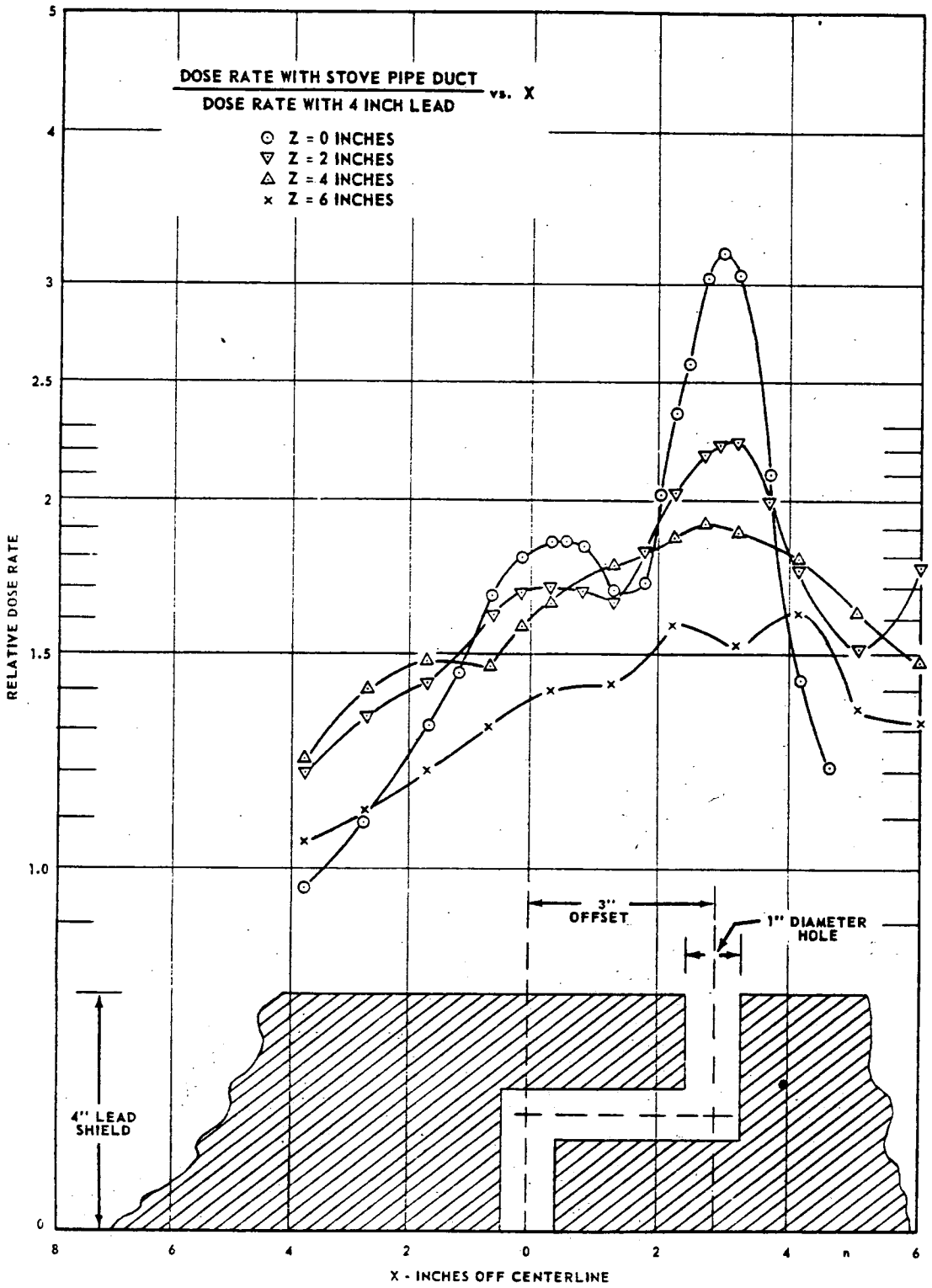

DOSE RATE WITH STOVE PIPE DUCT / DOSE RATE WITH 4 INCH LEAD vs. X
Z = 0 INCHES
Z = 2 INCHES
Z = 4 INCHES
Z = 6 INCHES
RELATIVE DOSE RATE
5
4
3
2.5
2
1.5
1.0
0
3" OFFSET
1" DIAMETER HOLE
4" LEAD SHIELD
8
6
4
2
0
2
4
6
X - INCHES OFF CENTERLINE

Figure 8.25

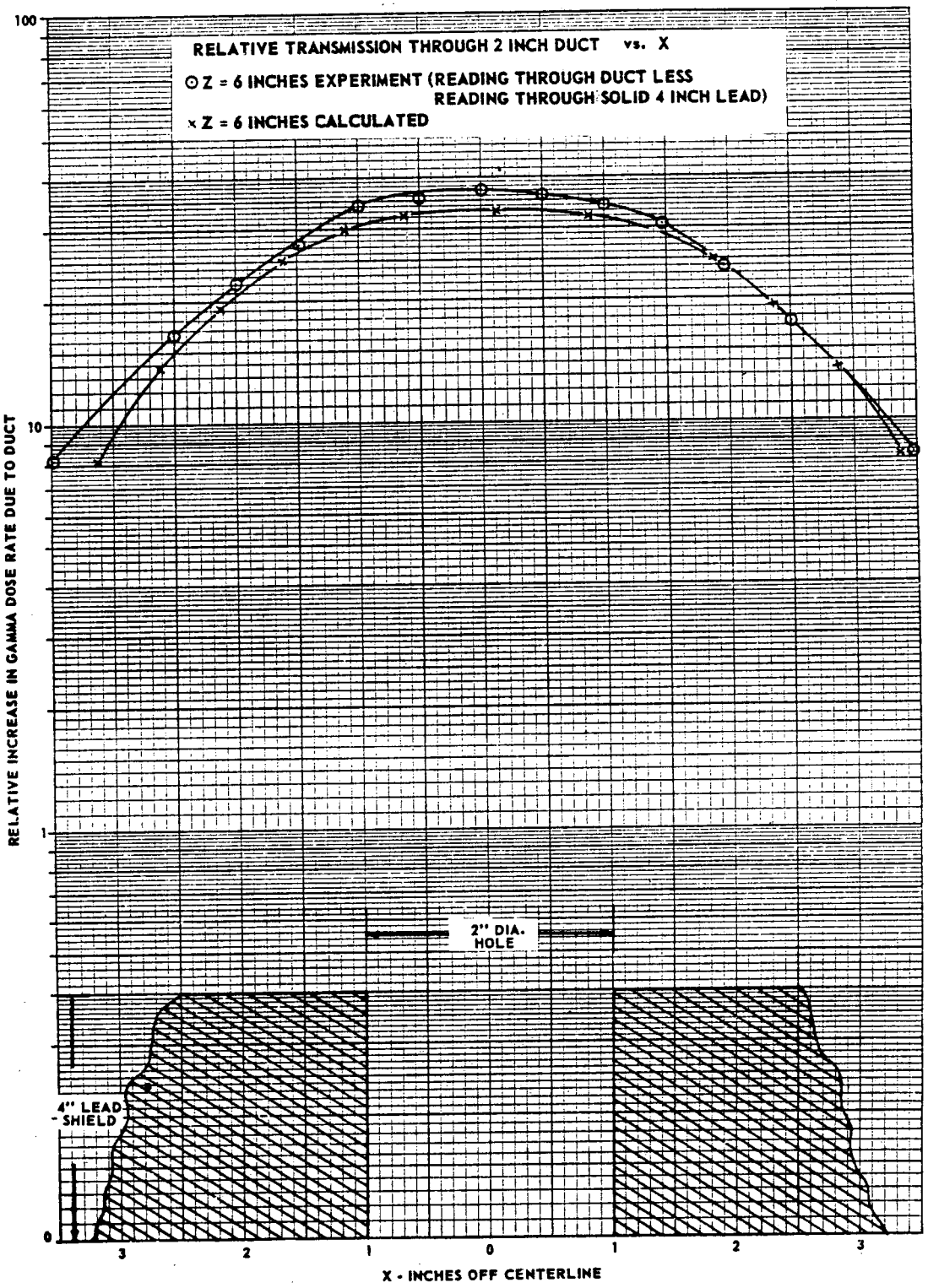

RELATIVE TRANSMISSION THROUGH 2 INCH DUCT vs. X
⊙ Z = 6 INCHES EXPERIMENT (READING THROUGH DUCT LESS READING THROUGH SOLID 4 INCH LEAD)
× Z = 6 INCHES CALCULATED
RELATIVE INCREASE IN GAMMA DOSE RATE DUE TO DUCT
100
10
1
0
2" DIA. HOLE
4" LEAD SHIELD
3
2
1
0
1
2
3
X - INCHES OFF CENTERLINE

Figure 8.26

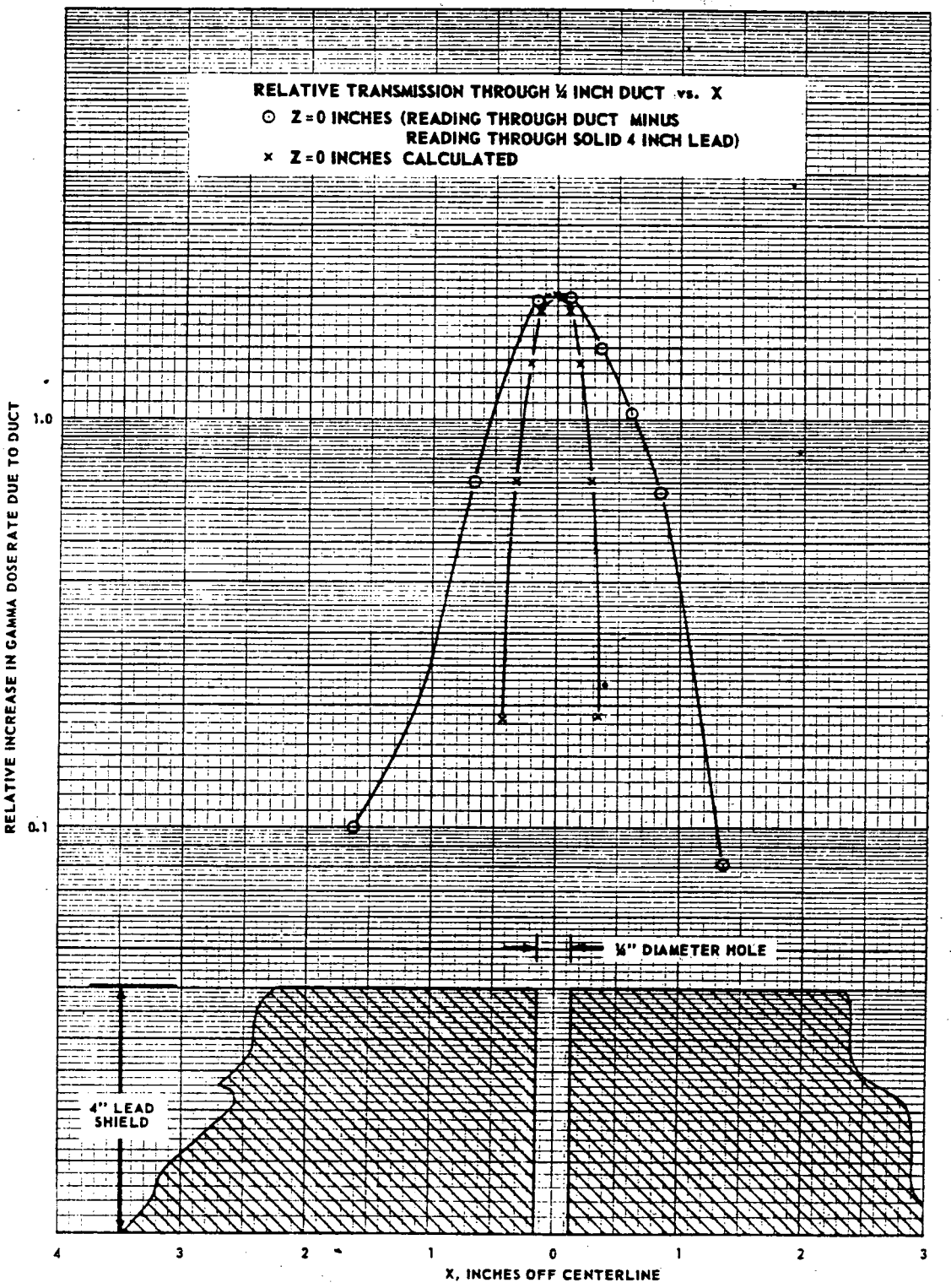

RELATIVE TRANSMISSION THROUGH ¼ INCH DUCT vs. X
⊙ Z = 0 INCHES (READING THROUGH DUCT MINUS READING THROUGH SOLID 4 INCH LEAD)
× Z = 0 INCHES CALCULATED
RELATIVE INCREASE IN GAMMA DOSE RATE DUE TO DUCT
1.0
0.1
¼" DIAMETER HOLE
4" LEAD SHIELD
4
3
2
1
0
1
2
3
X, INCHES OFF CENTERLINE

Figure 8.27

Figure 8.28 shows a particular shield geometry with a void in the lead slab. A hypothetical disk-shaped void at the top of the lead serves to simulate the actual void. The source of gamma radiation is considered as an infinite-plane source.

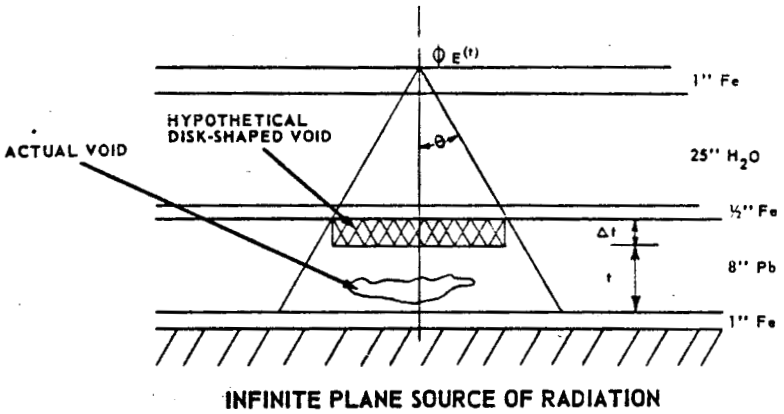


Figure 8.28

(a) Analysis. Let $\phi_E(t + \Delta t)$ be the dose with no void; then $\phi_E(t)$ is the dose with the void since in Fig. 8.28 $(t + \Delta t)$ equals inches of lead in the shield.

By Sievert's equation for an infinite-plane source (see Chap. 9)

$$\phi_E(t + \Delta t) = S_A \frac{B_1}{2} E_1(b_1) \tag{16}$$

where S_A = source strength of plane source ($cm^{-2} - sec^{-1}$)

$b_1 = \mu_1 x_1 + \mu_2 x_2 + \mu_{Pb}(t + \Delta t)$

B_1 = build-up factor through b_1

$$E_1(b_1) = \int_b^\infty \frac{e^{-t}}{t} dt \text{ (see Chap. 9)}$$

and

$$\phi_E(t) = \phi_A \frac{B_1}{2} E_1(b_1) - \phi_A \frac{B_1}{2} [E_1(b_1) - E_1(b_1 \sec \theta)] + \phi_A \frac{B_2}{2} [E_1(b_2) - E_1(b_2 \sec \theta)]$$

or

$$\phi_E(t) = \frac{\phi_A}{2} \left\{ B_1 E_1(b_1 \sec \theta) + B_2 [E_1(b_2) - E_1(b_2 \sec \theta)] \right\} \tag{17}$$

where $b_2 = \mu_1 x_1 + \mu_2 x_2 + \mu_{Pb}(t)$

B_2 = build-up factor through b_2

The fractional increase in dosage caused by a void of thickness Δt will be

$$\frac{\phi_E(t) - \phi_E(t + \Delta t)}{\phi_E(t + \Delta t)} = \frac{B_1 [E_1(b_1 \sec \theta) - E_1(b_1)] + B_2 [E_1(b_2) - E_1(b_2 \sec \theta)]}{B_1 E_1(b_1)} \tag{18}$$

If we let

$$\Delta b_1 = b_1 \sec \theta - b_1 = b_1 (\sec \theta - 1)$$

$$\Delta b_2 = b_2 \sec \theta - b_2 = b_2 (\sec \theta - 1)$$

then for small Δb_1; i.e., sec $\theta \approx 1$,

$$E_1(b_1 \sec\theta) = E_1(b_1 + \Delta b_1)$$

$$E_1(b_1 \sec\theta) - E_1(b_1) = E_1(b_1 + \Delta b_1) - E_1(b_1) = \frac{dE_1(b_1)}{db_1}\Delta b_1 = E_1'(b_1)\,\Delta b$$

Similarly,

$$E_1(b_2 \sec\theta) - E_1(b_2) = \frac{dE_1(b_2)}{db_2}\Delta b_2 = E_1'(b_2)\,\Delta b_2$$

Equation 18 now becomes

$$\frac{\phi_E(t) - \phi_E(t + \Delta t)}{\phi_E(t + \Delta t)} = \frac{E_1'(b_1)\,\Delta b_1}{E_1(b_1)} - \frac{B_2}{B_1}\frac{E_1'(b_2)\,\Delta b_2}{E_1(b_1)} \tag{19}$$

To solve Eq. 19 numerically, $E_1'(b)$ is determined as follows:

$$\int_b^\infty \frac{e^{-t}}{t}\,dt = E_1(b)$$

asymptotically, for large b's,

$$E_1'(b) = -\frac{e^{-b}}{b} \cong -E_1(b)$$

Inserting this equation in Eq. 19, we obtain

$$\frac{\phi_E(t) - \phi_E(t + \Delta t)}{\phi_E(t + \Delta t)} = -\Delta b_1 + \frac{B_2}{B_1}\frac{E_1(b_2)}{E_1(b_1)}\Delta b_2$$

$$= \frac{B_2}{B_1}\frac{E_1(b_2)}{E_1(b_1)}\Delta b_2 - \Delta b_1 \tag{20}$$

Since $\Delta b_1 = b_1$ (sec $\theta - 1$) and $\Delta b_2 = b_2$ (sec $\theta - 1$), Eq. 20 can be written in terms of b_1, b_2, and sec θ

$$\frac{\phi_E(t) - \phi_E(t + \Delta t)}{\phi_E(t + \Delta t)} = (\sec\theta - 1)\left[\frac{B_2}{B_1}\frac{E_1(b_2)}{E_1(b_1)}b_2 - b_1\right] \tag{21}$$

In order to calculate Eq. 21 numerically, it is best to put $E_1(b)$ in exponential form. Since the function $E_1(b)$ is essentially exponential, it can be very accurately represented over any small range of b by an equation of the form

$$E_1(b) = A\,e^{-Rb} \tag{22}$$

where A and R are constants to be determined. The range chosen will depend on the relaxation length of the shield. Combining Eqs. 21 and 22, we have

$$\boxed{\frac{\phi_E(t) - \phi_E(t + \Delta t)}{\phi_E(t + \Delta t)} = (\sec\theta - 1)\left[\frac{B_2}{B_1}e^{R(b_1 - b_2)}b_2 - b_1\right]} \tag{23}$$

The angle θ is determined by the cross-sectional area of the void and the perpendicular distance from the void through the shield.

$$\phi = \tan^{-1} \frac{r_0}{(x_1 + x_2 + \ldots)} \tag{24}$$

where r_0 is the radius of the void and $(x_1 + x_2 + \ldots)$ is the total distance through the remaining shield.

Build-up factors are dependent on the energy of the initial gamma radiation, the thickness of the shield, and the particular shielding material. Chapter 9 presents the gamma build-up factors in the form of the sum of two simple exponentials.

$$B(b_1 E_0) = A_1(E_0)\, e^{-\alpha_1(E_0)b} + A_2(E_0)\, e^{-\alpha_2(E_0)b} \tag{25}$$

where $A_1 + A_2 = 1$ and $b = \mu x$. The value of α_1, α_2, and A_1 for dose build-up and energy build-up factors are presented graphically in Chap. 9 for various materials as a function of energy. Whenever gamma radiation passes through a layer of heavy material and then a layer of water, the build-up factor* can be represented with sufficient accuracy by

$$B = B_{Pb} + B_{Fe} + B_{H_2O} - 1 \tag{26}$$

Once a specific shield design has been established, Eq. 23 can be used to determine the permissible size of voids in the heavy material (lead) of the shield. The fractional increase in dose due to the voids can be plotted as a function of area of the void with thickness of the void (Δt) as parameter. Sets of such curves can be plotted for varying initial thickness of lead. This method must be used for direct radiation, whereas the reduced density approximation only applies to areas that see low-energy scattered radiation.

Specific Example. Figure 8.28 shows a specific shield configuration with an initial lead thickness of 8 in. If $E_0 = 2.7$ Mev, the value of b_1 for these shield dimensions is computed as follows:

Material	μ/ρ, cm^2/g	ρ, g/cm^3	μ, cm^{-1}	Thickness (x), cm	b, μx
Water	0.042	1	0.042	63.5	2.67
Iron	0.036	7.8	0.281	6.35	1.78
Lead	0.041	11.3	0.464	(t+Δt)2.54	1.18(t+Δt)

$$b_1 = 4.45 + 1.18(t+\Delta t)$$

Hence, $b_2 = 4.45 + 1.18t$ and $b_1 - b_2 = 1.18\Delta t$ (t and Δt are in inches). Reducing Eq. 23 in terms of t_1, Δt, θ, and B_2/B_1,

$$\frac{\phi_E(t) - \phi_E(t + \Delta t)}{\phi_E(t + \Delta t)} = (\sec\theta - 1)\left[\frac{B_2}{B_1} e^{R(1.18\Delta t)}\ (4.45 + 1.18t) - 4.45 + 1.18(t + \Delta t)\right] \tag{27}$$

If $(t + \Delta t) = 8$ in. of lead, then Eq. 22, fitted to the curve between b = 12 and b = 15, becomes $E_1(b) = 0.274e^{-1.1b}$ and Eq. 27 is

$$\frac{\phi_E(t) - \phi_E(t + \Delta t)}{\phi_E(t + \Delta t)} = (\sec\theta - 1)\left[\frac{B_2}{B_1} e^{1.3\Delta t}\ (4.45 + 1.18t) - 13.9\right] \tag{28}$$

*This method of combining build-up factors is perhaps not justified. It is included here to show one method of determining tolerable void size in a composite shield. Other methods of combining build-up factors could be used if preferred.

If $(t + \Delta t) = 4$ in. of lead, Eq. 27 becomes

$$\frac{\phi_E(t) - \phi_E(t + \Delta t)}{\phi_E(t + \Delta t)} = (\sec \theta - 1)\left[\frac{B_2}{B_1} e^{1.3\Delta t}\ (4.45 + 1.18t) - 9.17\right] \tag{29}$$

Equation 25 must be solved for each material and then substituted in Eq. 26 to obtain the build-up factor, B. The coefficients of Eq. 25 (α_1, α_2, A_1, and A_2) are plotted on graphs in Chap. 9. The dose build-up factor curve was used for iron and lead, and the energy-absorption build-up factor curve was used for water, since dose build-up data were not available.

Equation 26 is now (for this particular problem)

$$B = 4.05 + 2.3\, e^{0.094t} - 1.3\, e^{-0.088t}$$

where t is in inches. This equation is plotted as a function of lead thickness (t) in Fig. 8.30.

The solutions of Eqs. 28 and 29 are plotted in Fig. 8.31 as a function of the area of the void with Δt as parameter. θ is found from Eq. 24, where $r_0 = \sqrt{A/\pi}$ and $(x_1 + x_2 + \ldots) = 26.5$ in., from Fig. 8.28. Once the percentage of dose increase is determined as the overdose that may be tolerated from flaws, Fig. 8.31 can be used to quickly determine the permissible size of flaws that can exist in the lead of the shield. Equation 23 can be calculated for many shield configurations in which the source of radiation can be approximated by an infinite plane.

For comparison purposes a more rigorous calculation is presented in the following section.

(b) An Exact Calculation of the Tonks[22] Approximation. Tonks's equation for leakage through a void in a shield is

$$F_v = \frac{1}{4\pi r_0^2} \int_{-\infty}^{\infty} \int_{-\infty}^{\infty} e^{-\mu r}\, r_0\, d\theta_x\, r_0\, d\theta_y \tag{30}$$

From Fig. 8.29, $x \simeq r_0\theta_x$ and $y \simeq r_0\theta_y$; therefore

$$r \simeq r_0 + \frac{r_0}{2}\theta_x^2 + \frac{r_0}{2}\frac{\theta_y^2}{2} \tag{31}$$

The geometry of the shield is the same as that shown in Fig. 8.28, except that the void is a cylinder having a cross section of 1 sq in. and a height of 1 in. in an 8-in. lead layer. The result of this integration can be compared with the value on Fig. 8.31 for $\Delta t = 1$ and $A = 1$ in an 8-in. lead shield.

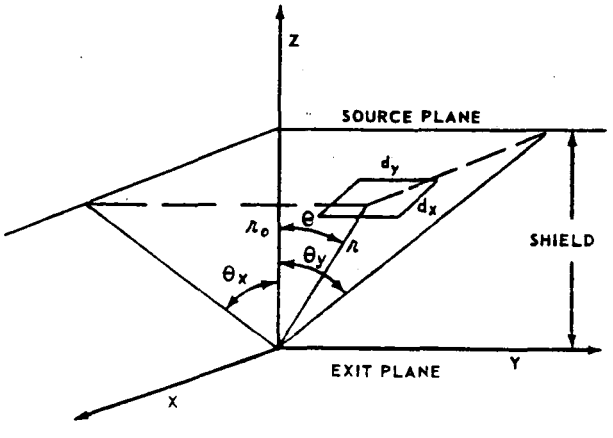


Figure 8.29

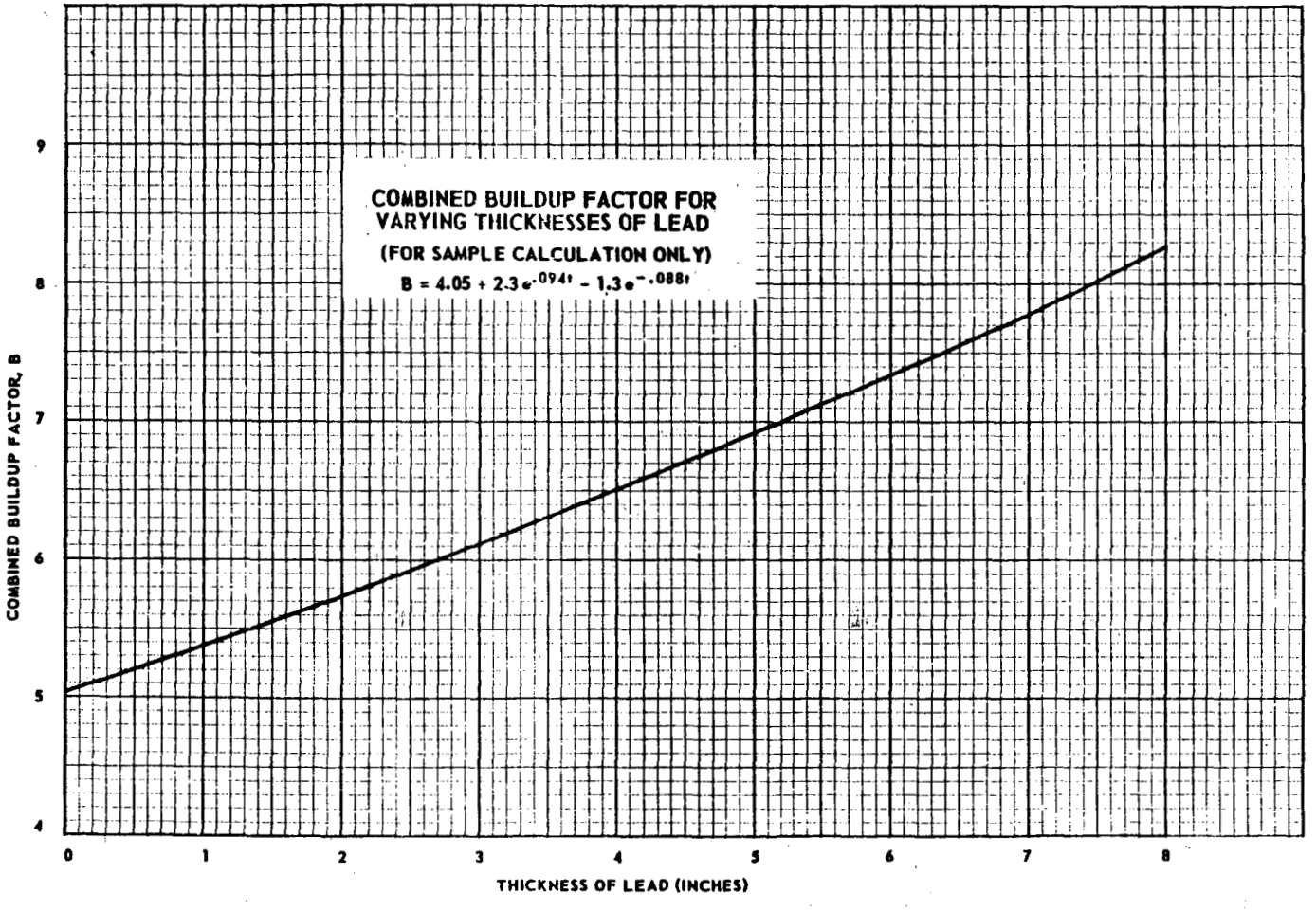

COMBINED BUILDUP FACTOR FOR
VARYING THICKNESSES OF LEAD
(FOR SAMPLE CALCULATION ONLY)
B = 4.05 + 2.3e^-.094t - 1.3e^-.088t
COMBINED BUILDUP FACTOR, B
4
5
6
7
8
9
0
1
2
3
4
5
6
7
8
THICKNESS OF LEAD (INCHES)

Figure 8.30

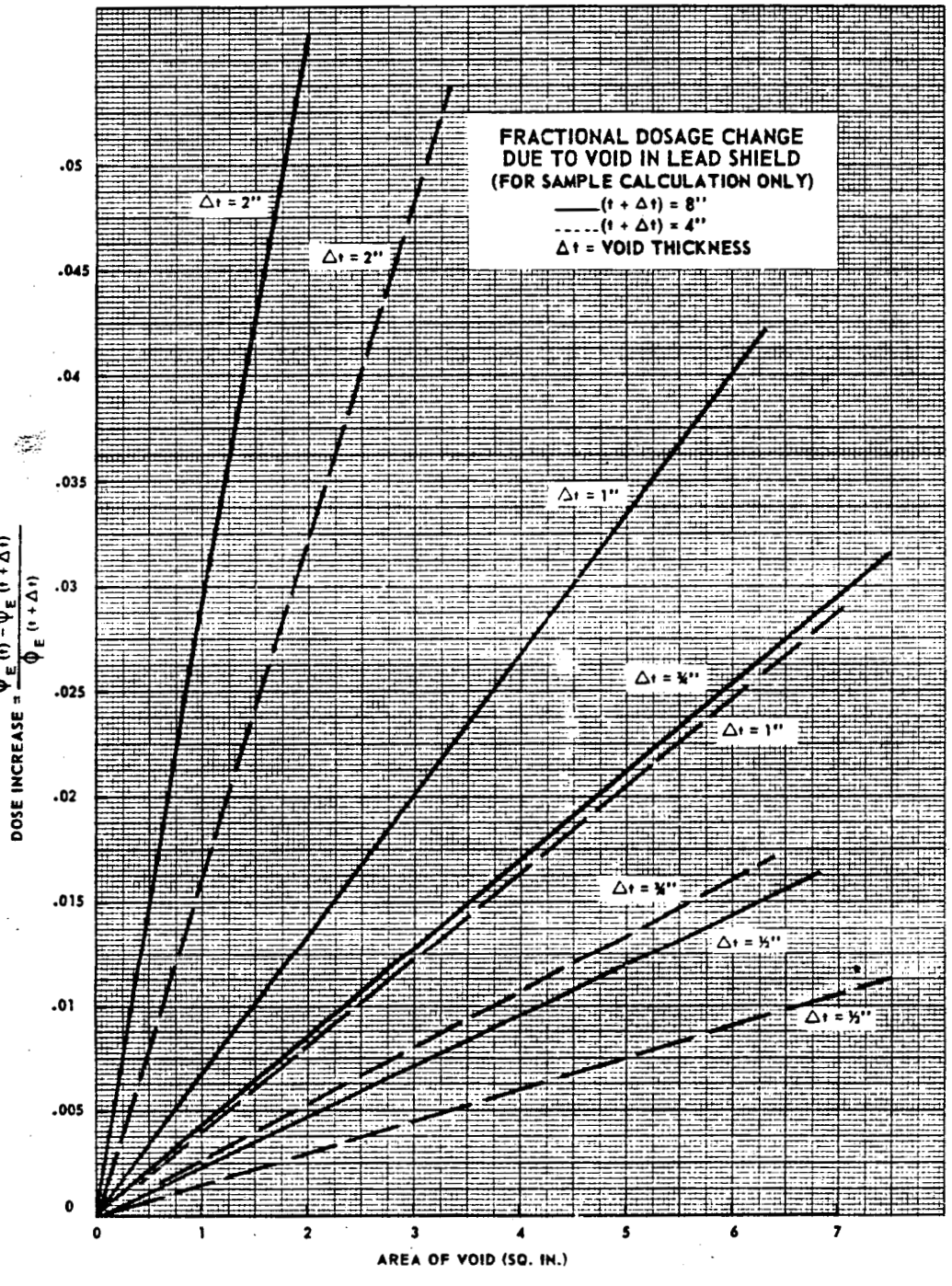

FRACTIONAL DOSAGE CHANGE
DUE TO VOID IN LEAD SHIELD
(FOR SAMPLE CALCULATION ONLY)
——(t + Δt) = 8"
- - - -(t + Δt) = 4"
Δt = VOID THICKNESS
Δt = 2"
Δt = 2"
Δt = 1"
Δt = ¾"
Δt = 1"
Δt = ¾"
Δt = ½"
Δt = ½"
DOSE INCREASE = $\frac{\phi_E(t) - \phi_E(t+\Delta t)}{\phi_E(t+\Delta t)}$
.05
.045
.04
.035
.03
.025
.02
.015
.01
.005
0
0
1
2
3
4
5
6
7
AREA OF VOID (SQ. IN.)

Figure 8.31

Restricting the integration to the first quadrant of the θ_x,θ_y plane, Eq. 30 becomes

$$F_v = \frac{1}{\pi}\int_0^\infty \int_0^\infty e^{-\mu r}\, d\theta_x\, d\theta_y \tag{32}$$

where $\mu r = \mu r_0[1 + (\theta_x^2/2) + (\theta_y^2/2)]$ when the ray does not pass through the void and $\mu r = (\mu r_0 - \mu_{Pb}\,\Delta t)\,[1 + (\theta_x^2/2) + (\theta_y^2/2)]$ when the ray passes through the void.

The void will have an angular radius of 0.0211 radian so that the rays will pass through the void when $\theta_x^2 + \theta_y^2 \le (0.0211)^2$. Hence we can write

$$\int_{\theta_x=0}^{\infty}\int_{\theta_y=0}^{\infty} = \int_{\theta_x=0}^{0.0211}\int_{\theta_y=0}^{\sqrt{(0.0211)^2-\theta_x^2}} + \int_{\theta_x=0}^{0.0211}\int_{\theta_y=\sqrt{(0.0211)^2-\theta_x^2}}^{\infty} + \int_{\theta_x=0.0211}^{\infty}\int_{\theta_y=0}^{\infty} \tag{33}$$

where the first integral will include all rays that pass through the void and the second integral will include all the remaining area in the first quadrant. For the first integral $\mu r = k'\,[1 + (\theta_x^2/2) + (\theta_y^2/2)]$, where $k' = (\mu r_0 - \mu_{Pb}\,\Delta t) = 12.71$. In the last two integrals $\mu r = k\,[1 + (\theta_x^2/2) + (\theta_y^2/2)]$, where $k = \mu r_0 = 13.89$.

Substituting these values in Eq. 32, we have

$$F_v = \frac{e^{-k'}}{\pi}\int_0^{0.0211} e^{-k'\theta_x^2/2}\left[\int_0^{\sqrt{(0.0211)^2-\theta_x^2}} e^{-k'\theta_y^2/2}\, d\theta_y\right] d\theta_x$$

$$+ \frac{e^{-k}}{\pi}\int_0^{0.0211} e^{-k\theta_x^2/2}\left[\int_{\sqrt{(0.0211)^2-\theta_y}}^{0} e^{-k\theta_y^2/2}\, d\theta_y\right] d\theta_x$$

$$+ \frac{e^{-k}}{\pi}\int_{0.0211}^{\infty} e^{-k\theta_x^2/2}\left[\int_0^{\infty} e^{-k\theta_y^2/2}\, d\theta_y\right] d\theta_x \tag{34}$$

The result of this integration is

$$F_v = (4.216 \times 10^{-10}) + (3.104 \times 10^{-8}) + (1.947 \times 10^{-9}) = 3.341 \times 10^{-8}$$

Without the void

$$F_0 = \frac{e^{-\mu r_0}}{2\mu r_0} = \frac{e^{-13.89}}{2(13.89)} = 3.312 \times 10^{-7}$$

therefore

$$\frac{F_v - F_0}{F_0} = \frac{3.341 - 3.312}{3.312} = 0.00875$$

This answer compares very well with the value of 0.0070 from Fig. 8.31. The slight difference might be in the fact that build-up factors were considered in the previous method, and no build-up was considered in this integration.

(c) Reduced Thickness Approximation. The preceding methods apply to the calculation of radiation flux through voids in the shield in the case where the void "looks" directly at a primary source of radiation. In regions of the secondary shield where the impinging radiation is scattered and not collimated, it is possible to employ a reduced-shield thickness technique to predict the required amount of shielding.

$$\text{Reduced thickness} = \frac{\text{actual weight}}{\text{density} \times \text{area}}$$

or

(Actual thickness) × (1 − volume-fraction voids)

This means that in the shield calculations a reduced thickness is used that is equivalent to the *actual thickness minus the total void thickness*. To illustrate this concept, an experiment performed at the Naval Reactor Testing Facility, Arco, Idaho, is described below.

To simplify secondary-shield construction, straight-through shield penetrations have been used in regions of the secondary shield where scattered radiation impinges on the shield or where direct radiation from the nearest source impinges obliquely on the penetration region. Experiments were performed on arrays of $1\frac{7}{16}$-in.- and also 3-in.-diameter penetrations to evaluate the increase of radiation level around the pipe arrays. The experiment was essentially a comparison test of the area-weighted dose between a reference (unpenetrated) shield and shields with arrays of penetrations. The reference shield consisted of 8 in. of polyethylene and 3 in. of lead covered at top and bottom by $\frac{1}{2}$-in. iron plates. The penetrated test section (22 in. in diameter) consisted of 25 penetrations of $1\frac{7}{16}$ in. diameter. The section with 3-in.-diameter penetrations consisted of five pipes. These test sections were similar in all respects to the reference shield with the exception of the penetrations. A plexiglas dosimeter rack was used containing 25 penetrations of $1\frac{7}{16}$ in. diameter and 54 individual spaces containing gamma-sensitive dosimeters. These dosimeters were exposed for 1 hr. The rack was then removed, and the dosimeters were read on charging meters. The testing was performed with the pipes empty and then with the pipes filled with water.

Subsequent tests were performed with a 1-in. lead cover installed over the penetrations and also with a 3-in. lead cover. This phase of the experiment was performed to determine the attenuation characteristics of the streaming radiation.

The results of the experiment were as are shown below.

	Area-averaged dose	
Test section condition	Array with $1\frac{7}{16}$-in.-diam. penetrations, mr/hr	Array with 3-in.-diam. penetrations, mr/hr
Empty, no lead cover	43.6	46.3
Empty plus 1-in. lead cover	17.3	19.9
Empty plus 3-in. lead cover	9.4	10.8
Water filled, no lead cover	42.6	

The dose measurement on the reference mock-up was 39.2 mr/hr. The results were also plotted; see Fig. 8.32. No dose measurements were taken inside the pipe because, in a practical application, the pipes themselves generally restrict persons from being directly over the pipe-penetration region. The additional lead shield required to reduce the dose measurement with penetrations down to the radiation level of the shield with no penetration was small. The additional lead-shield thickness can be approximated by using the reduced-density concept.

Warning: It would be very dangerous to apply these conclusions to a condition where the sources are directly below the penetrations rather than where the shield sees mostly scattered or obliquely incident radiation.

(d) Streaming Effect in Shield Containing Many Voids. In a section of shield containing many small voids, the concept of reduced density may be subject to error. If all the voids were small and were scattered homogeneously through the shield so that no "lining up" occurred, reduced density would adequately describe the shielding effect. That is,

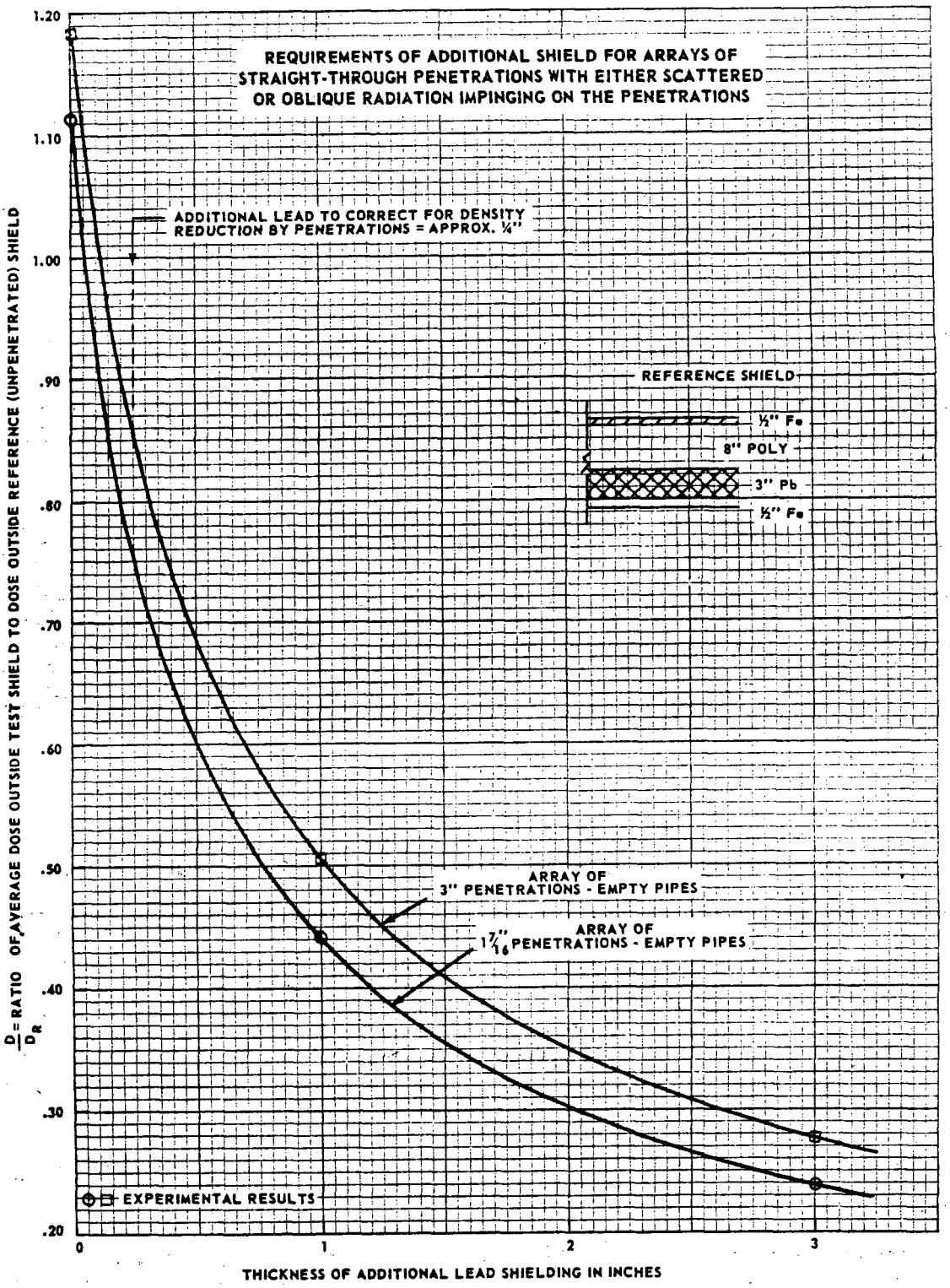

REQUIREMENTS OF ADDITIONAL SHIELD FOR ARRAYS OF STRAIGHT-THROUGH PENETRATIONS WITH EITHER SCATTERED OR OBLIQUE RADIATION IMPINGING ON THE PENETRATIONS
ADDITIONAL LEAD TO CORRECT FOR DENSITY REDUCTION BY PENETRATIONS = APPROX. ¼"
REFERENCE SHIELD
½" Fe
8" POLY
3" Pb
½" Fe
ARRAY OF 3" PENETRATIONS - EMPTY PIPES
ARRAY OF 1 7/16" PENETRATIONS - EMPTY PIPES
EXPERIMENTAL RESULTS
D/D_R = RATIO OF AVERAGE DOSE OUTSIDE TEST SHIELD TO DOSE OUTSIDE REFERENCE (UNPENETRATED) SHIELD
1.20
1.10
1.00
.90
.80
.70
.60
.50
.40
.30
.20
0
1
2
3
THICKNESS OF ADDITIONAL LEAD SHIELDING IN INCHES

Figure 8.32

Effective shield thickness $L_{eff} = L_{actual} \times \rho_r$

where ρ_r = reduced density = material density $\times (1 - v)$ and v = volume-fraction voids.

Since attenuation is exponential if some of the voids line up, a partial duct is formed and streaming occurs. Statistically, this is bound to happen to some extent. N. M. Smith studied this situation analytically (reported in Reports CF-48-10-44, p. 182, and CNL-21R), and the results were checked in the ORNL Lid Tank by comparing boxes of loose $^3/_4$-in. steel disks with equal weights of steel plate.

An additional factor to correct for this streaming was developed

$$\boxed{f = 1 - \frac{dv^2}{2}}$$

where f = streaming factor
d = average distance between voids, expressed in relaxation lengths of the shield material
v = volume-fraction voids

Then

$$\boxed{L_{eff} = L_{actual}\, \rho_r \times f}$$

(e) Sample Calculation. Consider a shield formed by filling an inaccessible region with $^3/_8$-in. lead chunks, packed to 65 per cent density (i.e., 65 per cent lead and 35 per cent voids). This region is 24 in. in the direction of attenuation. What is the effective lead thickness? (Three-eighths inch is about one-half relaxation length.)

$$L_{eff} = (24)(0.65)\left[1 - \frac{0.5(0.35)^2}{2}\right] = (24)(0.65)(0.97) = 15 \text{ in.}$$

3.7 Gamma Streaming Along Steel Paths

(a) The Problem. The structural support requirements for a shield bring forth a series of problems in shield design. The three basic questions which occur are: (1) What type of structure will least reduce the effectiveness of the shield? (2) What is the magnitude of the radiation streaming that results? (3) What is the most effective way of compensating for the excess radiation leakage? These problems were considered in Sec. 2.5 for neutrons; here the gamma problems will be considered.

The first question is important because the usual structural materials are rarely as effective attenuators as the shield materials they support or contain. Thus, a judicious choice of the manner in which the support is provided can realize large savings in weight. As a typical example, a secondary shield, composed largely of lead, must be supported by steel structure members. Two possible methods of providing this support are shown schematically in Fig. 8.33.

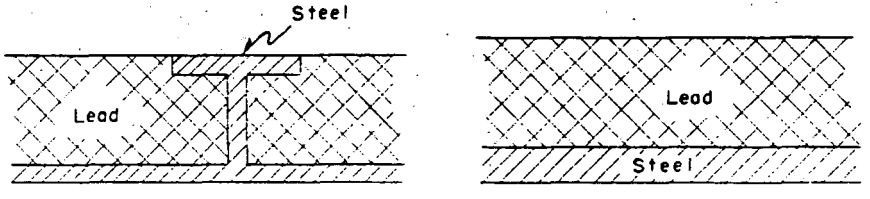


Figure 8.33

In method (a) conventional stiffeners project through the lead and are attached to a base plate on which the lead rests. In method (b) the entire structure consists of a base plate, which must be substantially thicker than in (a).

Calculations of the relative loss in shielding effectiveness entailed in these two methods reveal that method (a) is preferable. For method (a), with the thickness of the steel stiffener assumed to be $\frac{3}{4}$ in. and the lead thickness taken as 5 in., only a 1.4 per cent increase in lead weight is needed to make up for the loss in attenuation due to the stiffener. For method (b), even if the base plate were as thick as 1 in., a greater addition of lead would be needed than in method (a).

(b) Analysis. The calculation of the radiation streaming pattern in the cases cited above is quite conventional. A ray analysis, using the appropriate attenuation coefficients and build-up factors, is sufficient since the problem is basically one of straight-through penetration. A plot in cross section of the ratio of the gamma dose rate with the stiffener of method (a) to that for a solid shield is shown in Fig. 8.34. It is seen that the peak flux above the stiffener reaches 7.4 times the design value for the solid shield. The gamma-ray source chosen for the calculation was a simulation of the conditions in a water-cooled power reactor system: a plane isotropic source of N^{16} gammas, effectively infinite in extent located directly under the shield. The shield proper is lead, assumed to be 5 in. thick, and the stiffener is as described above.

It is seen from an examination of these results that, although the peak streaming value is many times the average leakage value through the shield, the peak is highly localized, having a half-width of less than 1 in. Thus, when the effect of such streaming is considered in terms of whole-body irradiation, it is seen that one of two conditions will ensue: (1) A person moving over the shield will receive an average whole-body dose that is not much greater than the average leakage through the solid shield. For example, if the stiffeners are positioned 18 in. apart, the average dose would be only approximately 10 per cent greater than that through a solid shield. (2) A person located directly over the streaming point and not moving would be subjected to the peak flux only over a small portion of his body. Since the permissible average radiation leakage through the shield is quite low, this peak dose rate can cause no local damage. Thus the person is, in effect, subjected to an average whole-body dose only 10 per cent above that for the solid shield. This problem should be considered in specifying the allowable radiation levels for a particular application (see Chap. 2). From these considerations it was decided in the case of this problem to permit the streaming to occur, increasing the over-all shield thickness so as to reduce the average leakage by 10 per cent. The alternative procedures of installing lead strips over the top of the stiffeners or attempting to fabricate stiffener shapes which would not penetrate straight through the shield were discarded.

(c) Experimental Data. During the period of installation of the shield at the Naval Reactor Testing Facility (NRTF) at Arco, Idaho, as part of the inspection procedure a series of measurements was made of the streaming of gamma radiation through such stiffeners. A Co^{60} source 1 cm in diameter and 1 cm in length was used. Three plots were made for each location, one for the source centered under the stiffener and one each for the sources located $\frac{1}{2}$ in. off center on either side of the stiffener. Although the results were not directly comparable with the calculated illustration cited above because of the difference in source energy and geometry, the experimental streaming effects were of the same order.

An additional effect that was observed during later operational tests of the NRTF shield is worth mentioning for its bearing on this problem. The lead shield in this case is covered by a polyethylene layer several inches thick. When measurements of the streaming pattern from the stiffener were taken at the surface of the shield through the polyethylene, the peak value was reduced by about a factor of 2 because of the scattering and diffusion produced by the polyethylene. In other parts of the shield, equipment located on the shield surface smeared out the peaks even more markedly. Thus, in the actual completed shield, there was a tendency to approach the average leakage value without consideration of the averaging effect of whole-body irradiation.

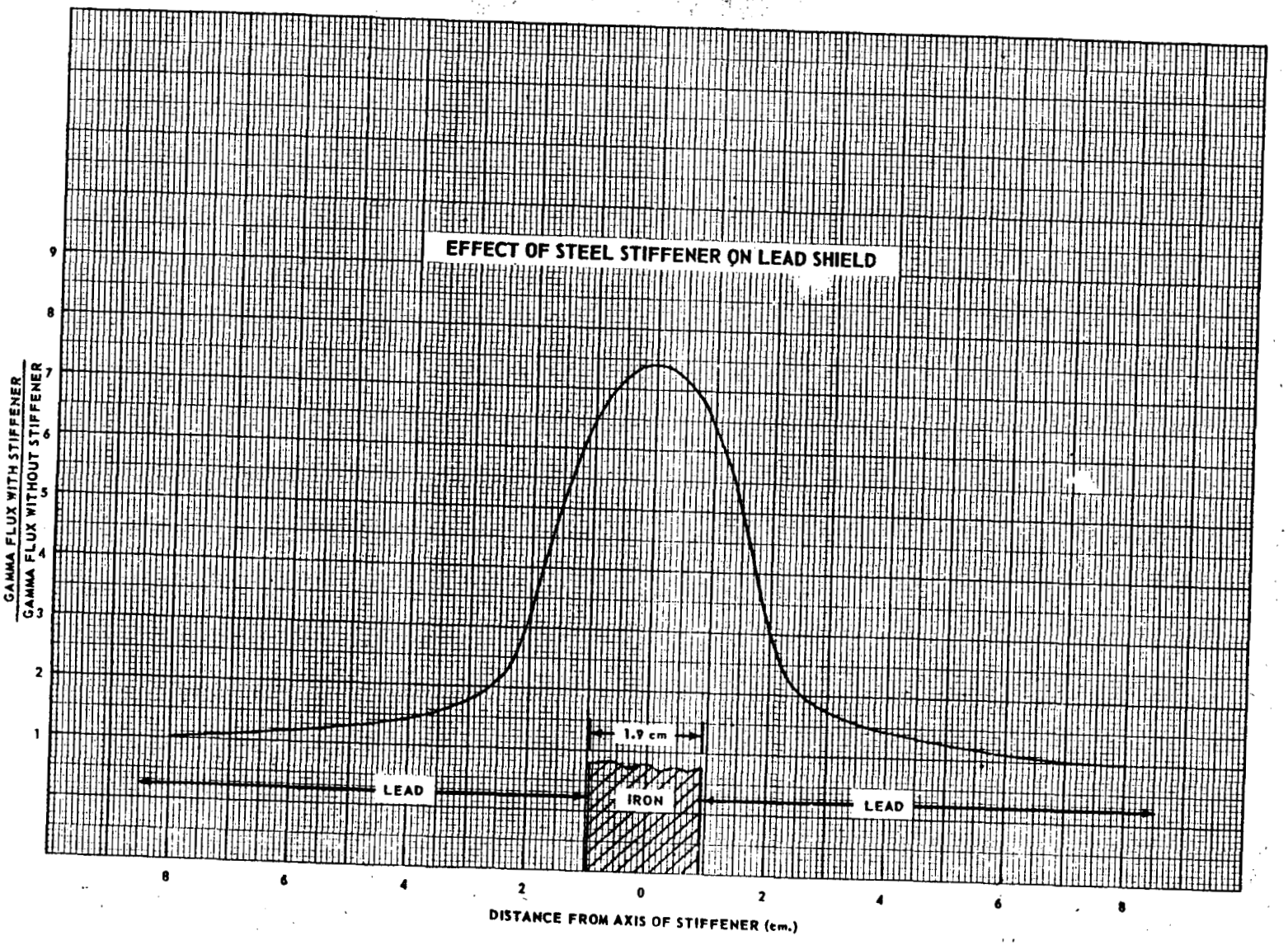

EFFECT OF STEEL STIFFENER ON LEAD SHIELD
GAMMA FLUX WITH STIFFENER / GAMMA FLUX WITHOUT STIFFENER
9
8
7
6
5
4
3
2
1
1.9 cm
LEAD
IRON
LEAD
8
6
4
2
0
2
4
6
8
DISTANCE FROM AXIS OF STIFFENER (cm.)

Figure 8.34

4 RADIATION SCATTERING AROUND SHIELD EDGES

4.1 Introduction

Up to now, scattering has been considered only as a part of the attenuation process. Neutrons are degraded in energy by scattering collisions and are quickly gobbled up as thermal neutrons. Gamma rays lose energy through Compton scattering, but they keep on going, leading to build-up factors. Now it is necessary to consider scattering in a new light. Real reactor shields are finite in extent; therefore radiation can sneak around the shield. Even though radiation travels a longer distance in taking this path, it may receive less attenuation due to the lower cross section of the material traversed. Calculations assuming that the gammas are scattered only once or twice are developed in this chapter, and they show that a more sophisticated treatment is often required. Some preliminary information is presented on a Monte Carlo technique being developed for this purpose.

Special applications, such as nuclear-powered aircraft, require an even more detailed knowledge of scattering. This is classified information and is not presented in this section.

4.2 Gamma Scattering

The definitions of the terms used in this section are as follows:

E_0	Initial energy (Mev)
E	Final energy (Mev)
$F_1(E_0,\theta)$	$I/I_0 = [(2.818 \times 10^{-13})^2/2](1/R^2)P^3[(1/P) + P - \sin^2\theta]$
I_0	Intensity of the initial beam
I	Intensity of the scattered beam
R	Distance from source to scatter point (cm) or from scatter point to detector
S	Source strength (photons/sec)
Δv	Volume element (cm^3)
η	Number of electrons per cubic centimeter of the medium
θ	Angle between the initial path direction and the final path direction of the photon
μ	Linear absorption coefficient of the medium (cm^{-1})
μr	Thickness of the medium in relaxation lengths

(a) Basic Compton Scattering Effect. In reference 23 and elsewhere the relation for the energy of a photon before and after collision with an electron is derived. The ratio of the energy of the photon after the interaction to its energy before striking the electron is given by

$$P = \frac{E}{E_0} = \frac{1}{1 + (E_0/m_0c^2)\,(1 - \cos\theta)} \tag{35}$$

where m_0c^2 is 0.51 Mev.

The expression for the intensity of the scattered beam of gamma-ray photons is derived in reference 24 in which the probability of interaction between a gamma-ray photon and an electron is given by the Klein-Nishina formula. The differential cross section per unit solid angle Ω, as derived by Klein and Nishina, is given by

$$\frac{d\sigma}{d\Omega} = \frac{r_0^2}{2}\,P^2\left(\frac{1}{P} + P - \sin^2\theta\right) \quad (cm^2/\text{electrons-steradian}) \tag{36}$$

where r_0 is the classical radius of the electron

$$r_0 = \frac{e^2}{mc^2} = 2.818 \times 10^{-13}\,cm$$

If photons in a beam of ϕ_0 photons/cm^2-sec of energy E_0 strike electrons in an element of volume, the element of volume will look like a point source of photons of source strength varying with the scattering angle θ. This source will have the strength

$$\phi_0 \frac{d\sigma}{d\Omega}$$

hence at a distance R from the scattering point, assuming attenuation in the medium to be negligible at this distance, the photon beam will consist of

$$\phi = \frac{\phi_0}{R^2} \frac{d\sigma}{d\Omega} \quad \text{(photons/cm}^2\text{-sec)}$$

The intensity of the initial beam consisting of photons of energy E_0 Mev/photon is $I_0 = E_0\phi_0$ Mev/cm^2-sec. The intensity of the scattered beam of photons of energy E Mev/photon (E and E_0 related through the scattering angle by Eq. 35) is $I = E\phi$. Making the proper substitutions, the intensity of a scattered beam of photons can be written as

$$I = \frac{I_0}{R^2} \frac{E}{E_0} \frac{d\sigma}{d\Omega} \tag{37}$$

and, inserting the Klein-Nishina cross section in Eq. 37, we have

$$\frac{I}{I_0} = \frac{(2.818 \times 10^{-13})^2}{2} \frac{1}{R^2} P^3\left(\frac{1}{P} + P - \sin^2\theta\right) \tag{37a}$$

Extensive tables of this relation normalized to $(7.94 \times 10^{-26})/R^2 = 1$ are found in reference 25.

(b) Single Scattering. In Fig. 8.35 consider a point source at 0 of gamma rays with a source strength S_0 (photons/sec) of energy E_0 (Mev/photon). It is desired to find the dose at

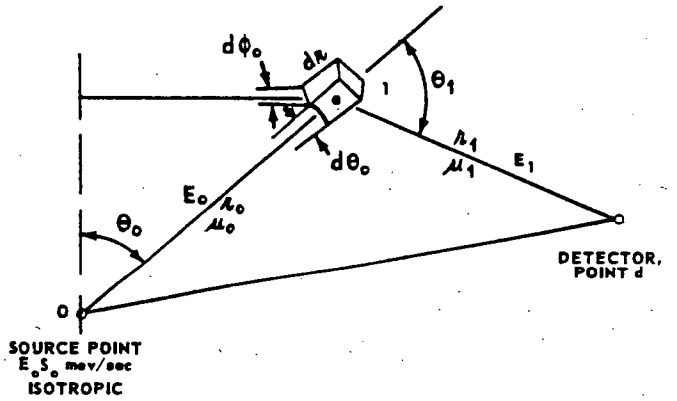


Figure 8.35

point d due to all photons that scatter once and only once in going from 0 to d. Assume that scattering takes place at a point 1 which is at a distance r_0 from the source point 0. The medium from 0 to 1 has an absorption coefficient μ_0 and an energy build-up factor of $B_0(E_0,\mu_0 r_0)$.

The energy crossing an element of area at point 1, distance r_0 and area $r_0\, d\theta\, r_0 \sin\theta_0\, d\phi_0$, is

$$I_0 = E_0 S_0 B_0 \frac{e^{-\mu_0 r_0}}{4\pi r_0^2} \quad \text{(Mev/cm}^2\text{-sec)} \tag{38}$$

Suppose scattering now occurs in the volume element $\Delta v = r_0^2 \sin\theta_0\, d\phi_0\, dr$. The intensity of radiation at 1 cm (R = 1) from the point of scattering going in a new direction at angle θ_1 from the original direction is given by

$$I = I_0 \times 7.94 \times 10^{-26}\ \eta\ F_1(E_0,\theta_1)\ \Delta v \quad (\text{Mev/cm}^2\text{-sec}) \tag{39}$$

where $F_1(E_0,\theta_1) = I/I_0$ and is given by Eq. 37a and where η is the number of electrons per cubic centimeter of the medium. Some magnitudes of η are:

For H_2O, $\eta = 3.37 \times 10^{23}$ electrons/cm^3
For air, $\eta = 3.895 \times 10^{20}$ electrons/cm^3 (S.T.P.)
For iron, $\eta = 2.19 \times 10^{24}$ electrons/cm^3
For lead, $\eta = 2.71 \times 10^{24}$ electrons/cm^3

At this point note that F_1 is indicated as a function of E_0 and θ_1. Actually, the radiation reaching the volume element is not all at energy E_0 but ranges in energy from E_0 down to 0. The actual spectrum is a function of the material and $\mu_0 r_0$. Calculated spectrums for different materials are given in reference 26. In calculating the energy reaching the scattering volume elements, the build-up factor, B_0, is used to allow for the photons of lower energy which reach this point. If the scattering process were treated rigorously, the probability of scattering each photon would be a function of its energy and the scattering angle; thus a different magnitude of F_1 would be required for each energy of incident photon. To simplify the calculations, it is assumed that the probability of scattering is the same for all photons and that the intensity of energy in the new direction is given by $F(E_0,\theta_1)$. It will be shown below that this assumption and others yet to be discussed lead to satisfactory results.

The intensity of the radiation reaching point d after passing through a medium of relaxation length $\mu_1 r_1$ is (combining Eqs. 38 and 39 and attenuating with the build-up factor from point 1 to d)

$$\boxed{I_{d_1} = E_0 S_0\ B_0(\mu_0 r_0, E_0)\ \frac{e^{-\mu_0 r_0}}{4\pi r_0^2}\ 7.94 \times 10^{-26}\ \eta\ F_1(E_0,\theta_1)\ \Delta v\ B_1\ \frac{e^{-\mu_1 r_1}}{r_1^2} \quad (\text{Mev/cm}^2\text{-sec})} \tag{40}$$

The energy at which μ_1 is calculated is that resulting in scattering from energy E_0 through an angle θ_1. Here again, since there is a spectrum of energy reaching the scattering volume, there is a spectrum of energy leaving the scattering volume in the new direction. In addition to this, each energy range of photons leaving the scattering volume at point 1 arrives at d as a spectrum of energy; therefore reaching d there is a spectrum which ranges from the energy E_1, resulting from the scattering of E_0 through the angle θ_1, to 0.

The relation between the intensity of radiation reaching d as calculated using Eq. 40 and that actually reaching point d can be qualitatively deduced in the following manner.

Equation 39 will apply to photons of all energies which arrive at point 1.

$$\Delta I(E') = \Delta I_0(E)\ F_1(E,\theta_1) \times 7.94 \times 10^{-26}\ \eta\ \Delta v$$

As E decreases from E_0, F_1 increases; thus

$$I = \int_E dI(E') = 7.94 \times 10^{-26}\ \eta\ \Delta v \int_E F(E,\theta_1)\ dI_0(E)$$

is larger than that computed by Eq. 39.

In Eq. 40 the energy reaching point d is attenuated in going from point 1 to point d by the factor $e^{-\mu_1 r_1}$. The value of μ_1 is obtained from the energy E_1 resulting from photons at E_0 scattering through θ_1. If the spectrum of energy is considered, the photons will have energies ranging from E_1 down to 0. As energy decreases μ increases; therefore the attenuation computed using μ_1 will be less than that actually existing due to the spectrum. This latter underestimate of the attenuation tends to compensate for the overestimate of the attenuation of the scattering process.

(c) Double Scattering. If double scattering occurs so that photons are scattered again at point 2 and are attenuated in going from point 2 to point d (see Fig. 8.36), Eq. 40 can be extended to read as follows

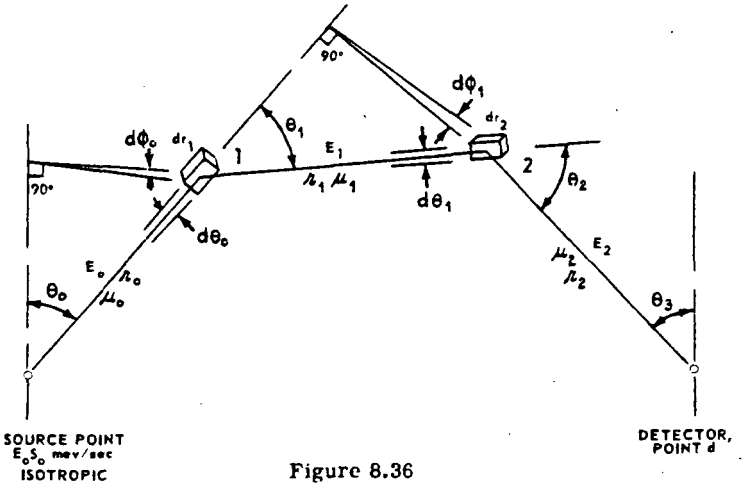


Figure 8.36

$$I_d = E_0 S_0 \, B_0(\mu_0 r_0, E_0) \frac{e^{-\mu_0 r_0}}{4\pi r_0^2} \, 7.94 \times 10^{-26} \, F_1(E_0, \theta_1) \, \eta_1 \, \Delta v_1 \, B_1(\mu_1 r_1, E_1) \frac{e^{-\mu_1 r_1}}{r_1^2} \, 7.94 \times 10^{-26} \times F_2(E_1, \theta_2) \, \eta_2 \, \Delta v_2 \, B_2(\mu_2 r_2, E_2) \frac{e^{-\mu_2 r_2}}{r_2^2} \quad (\text{Mev/cm}^2\text{-sec}) \tag{41}$$

The total radiation reaching the detector is the summation of the contribution of all volume elements Δv_1 and Δv_2 where scattering can occur.

(d) Single Vs. Double Scattering. Between two points scattering can occur as single scattering, double scattering, and multiple scattering (in addition to direct transfer). In general, the more times scattering takes place the greater the total attenuation. When source and detector are close together, the source–scatter point–detector path may be relatively short, and the angle for scatter may be small. As the distance between source and detector increases, the path length and scattering angle increase for the single-scattering process, and the contribution from double scattering becomes more important. Reference 27 gives the criteria for the importance of single vs. double scattering, and this will now be explained.

For single scattering the total amount of energy reaching the detector at d is obtained by integrating Eq. 40,

$$I_{d_1} = \frac{E_0 S_0}{4\pi} \, 7.94 \times 10^{-26} \, \eta \int_v B_0(\mu_0 r_0, E_0) \frac{e^{-\mu_0 r_0} e^{-\mu_1 r_1}}{r_0^2 r_1^2} \, B_1(\mu_1 r_1, E_1) \, F_1(E_0, \theta_1) \, dv \tag{42}$$

Since μ_1 is always greater than μ_0, the criterion is based on the magnitude of $e^{-\mu_1 r_1}$. If a value of r_1, say $r_1 = R$, exists such that $e^{-\mu_1 R} \geq 0.5$ and furthermore that all contributions to the integral of Eq. 42 from regions of $r_1 > R$ may be neglected (arbitrarily state F_1 to be less than 0.05), then only single scattering need be considered. To illustrate the use of these criteria, three examples are given.

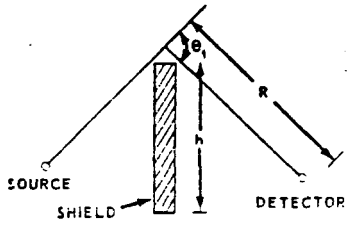


Figure 8.37

Example 1. As the first example (Fig. 8.37) consider the following assumptions: (1) The source and detector are on opposite sides of an impervious shield of negligible thickness in a

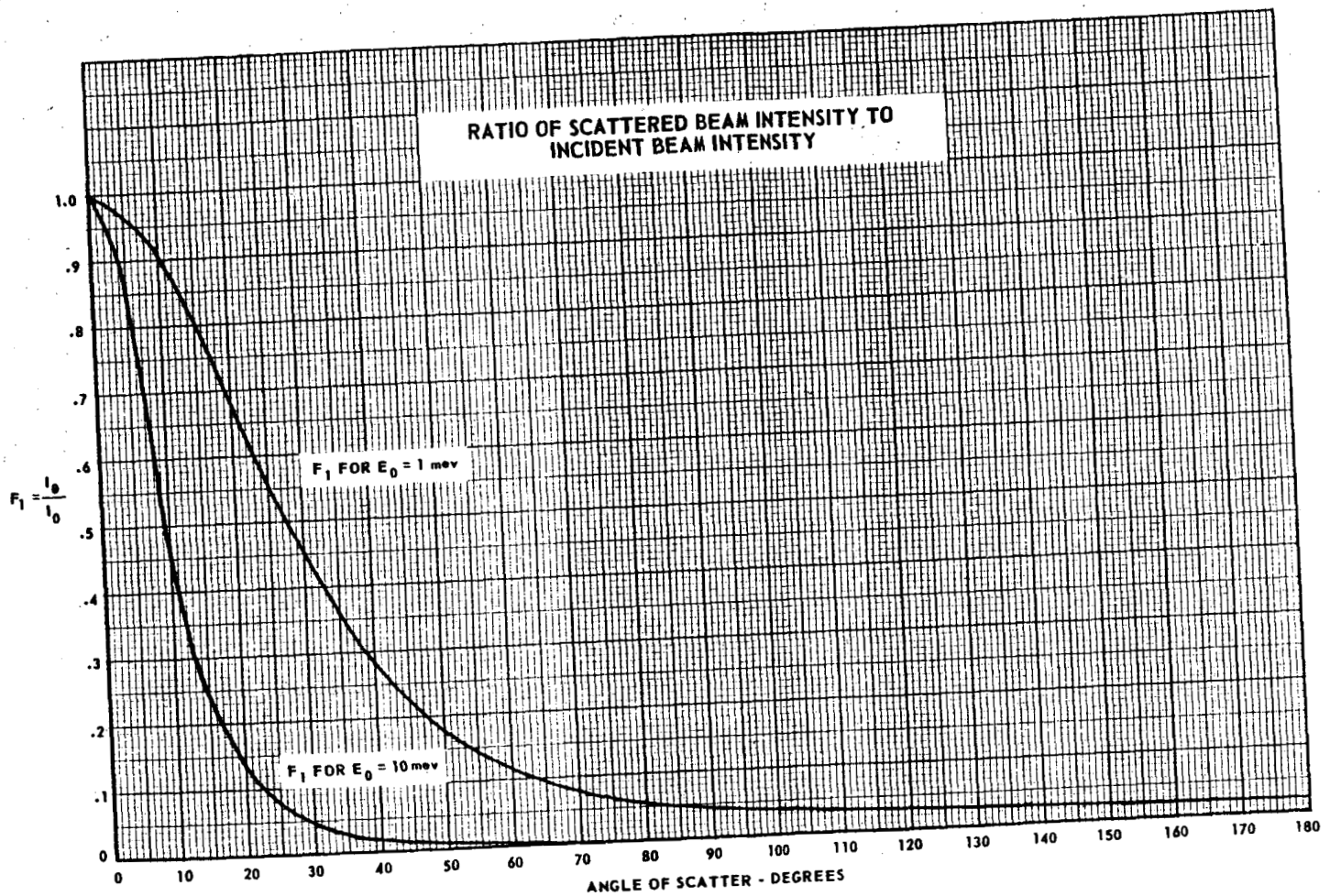

RATIO OF SCATTERED BEAM INTENSITY TO INCIDENT BEAM INTENSITY
$F_1 = \frac{I_\theta}{I_0}$
1.0
.9
.8
.7
.6
.5
.4
.3
.2
.1
0
F_1 FOR E_0 = 1 mev
F_1 FOR E_0 = 10 mev
0 10 20 30 40 50 60 70 80 90 100 110 120 130 140 150 160 170 180
ANGLE OF SCATTER - DEGREES

Figure 8.38

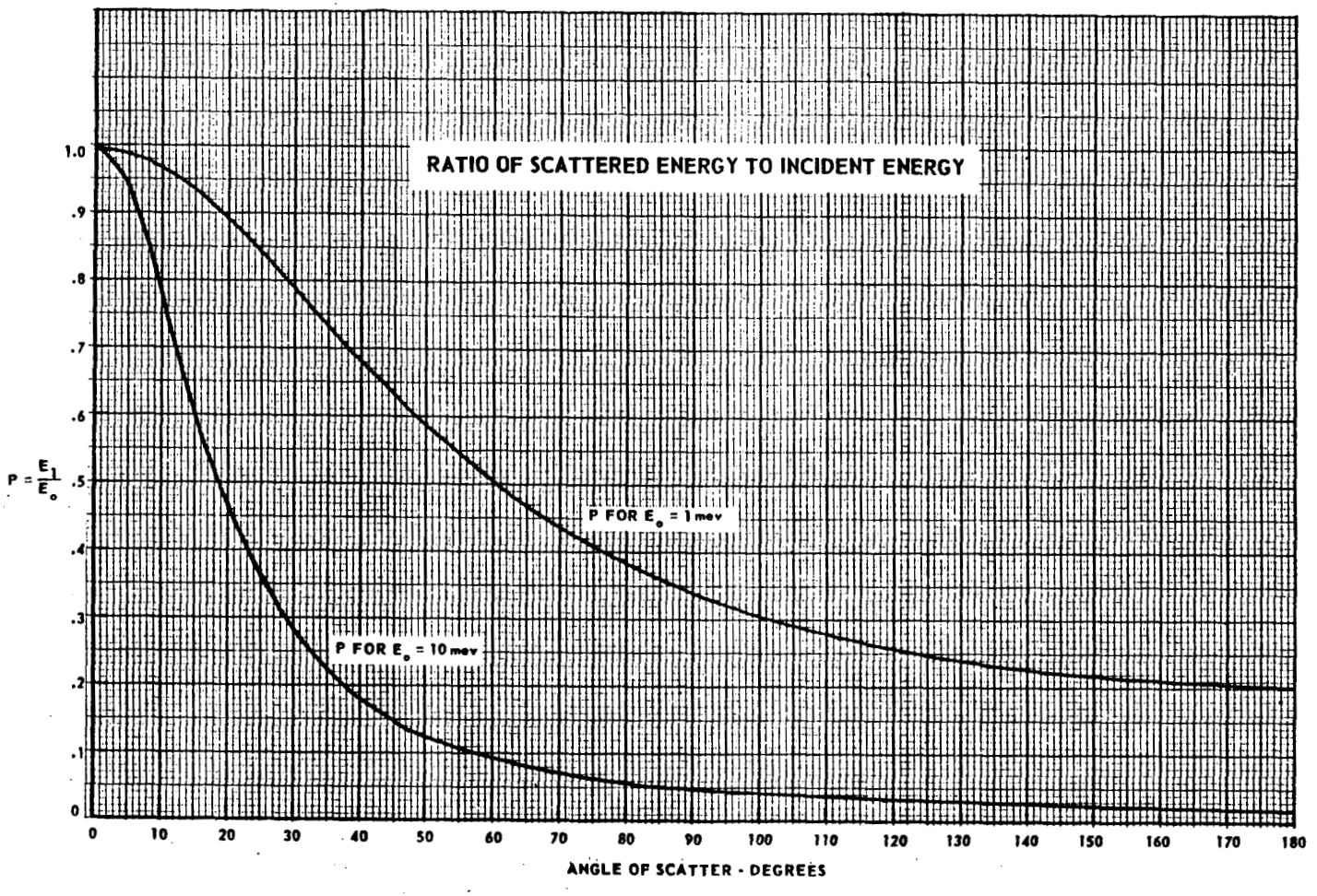

RATIO OF SCATTERED ENERGY TO INCIDENT ENERGY
P = E1/Eo
1.0
.9
.8
.7
.6
.5
.4
.3
.2
.1
0
P FOR Eo = 1 mev
P FOR Eo = 10 mev
0
10
20
30
40
50
60
70
80
90
100
110
120
130
140
150
160
170
180
ANGLE OF SCATTER - DEGREES

Figure 8.39

water medium and (2) the energy of source photons is 10 Mev. The minimum angle of scatter θ_1 is determined by the size of the shield (h). From Fig. 8.38 for these conditions the scattering angle for which F_1 would be less than 0.05 is 27°. With an initial photon energy of 10 Mev, a scattering angle of 27° results in the photons of the scattered beam having an energy of 3.2 Mev (Fig. 8.39). The μ_1 of water for 3.2 Mev is 0.0381 cm^{-1}; therefore, in order for $e^{-\mu_1 R}$ to be equal to, or greater than, 0.5, R must be equal to, or less than, 18.2 cm. These conditions determine the limiting case for which single-scattering effects predominate. Figure 8.37 shows the geometry for these conditions, and, if R equals 18.2 cm, h is equal to 8.2 cm. For a larger shield and greater distance between source and shield (> 35.4 cm), double- or multiple-scattering processes are more important contributors to the dose.

Example 2. Consider the same geometry given in Fig. 8.37 with a 1-Mev gamma-ray source and air as the medium. In this case the value of F_1 would be less than 0.05 for all angles greater than 82°. Then, from Fig. 8.39, for a 1-Mev photon source, a scattering angle of 82° gives a scattered-beam photon energy of 0.37 Mev. The μ_1 of air for this energy is 1.26×10^{-4} cm^{-1}; hence, for $e^{-\mu_1 R}$ to equal 0.5, R must equal 5500 cm, and h is equal to 7200 cm.

Comparing this result to that of example 1, it is easily seen that, in a medium such as air and with a low-energy photon source, single-scattering effects predominate; in heavier mediums and with high-energy sources, double- and multiple-scattering effects are more important.

Example 3. In a submarine there is a possibility that gamma rays will go out of the hull of the boat into the sea from the reactor compartment, will scatter in the water, and will enter some protected compartment (see Fig. 8.40). The geometry of source and receptor are such that the minimum angle of single scattering is 105° by measurement. For such an angle of scatter and with E_0 equal to 2.76 Mev, the scatter beam has an energy of 0.33 Mev, and its intensity is about 0.007 of that of the incident beam.[25] With a 3-ft shield, as shown in Fig. 8.40, R is equal to 74 cm. The value of $\mu_1 r_1$ equals the contribution of the water (0.115×72) plus the contribution of the iron ($0.104 \times 7.8 \times 2.54$); hence $e^{-\mu_1 r_1} = 3.3 \times 10^{-5}$. This low value clearly shows that double- and multiple-scattering effects must be considered rather than single-scattering effects.

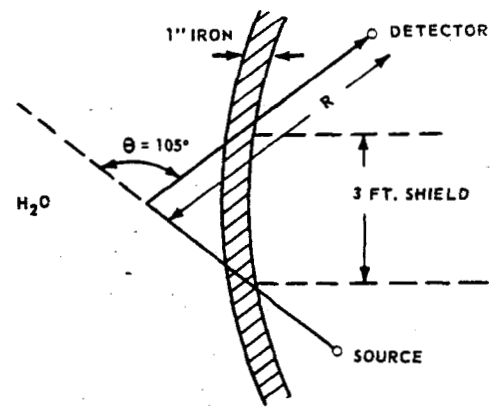


Figure 8.40

(e) Simplified Double-scattering Integration. Use of Lid-tank Scattering Experiment.[28] From the three previous examples, it is seen that, in general, problems of scattering of gamma rays in air may be analyzed by considering single scattering only. On the other hand multiple scattering becomes the primary mechanism of transmission of gamma rays around shields in water. Considerable analysis has been done on single scattering in air.[29,30] The fact that in air scattering only single scattering need be considered is further brought out in reference 31.

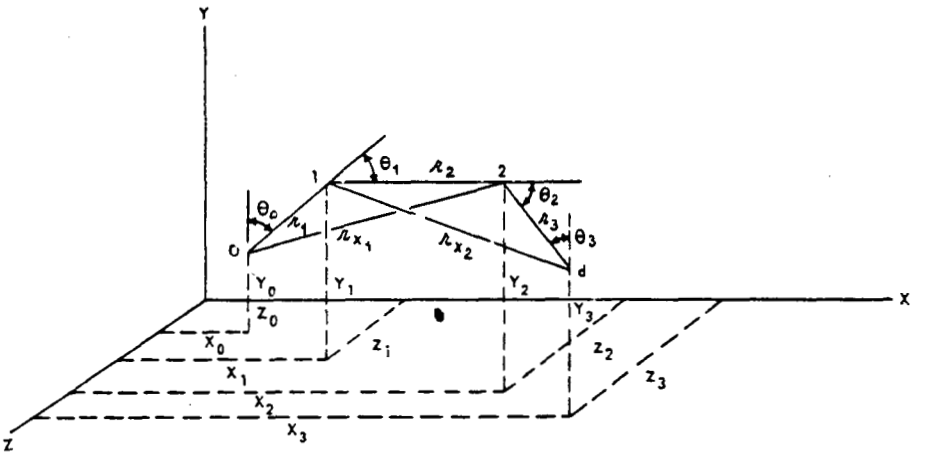


Figure 8.41

The evaluation of Eq. 41 for all elements of volume involves double integration over space. To simplify this, an approximation is made, and the calculations give results that agree within a factor of 2 with test results given in reference 28, which refers to a test made for KAPL in the ORNL Lid tank.

Refer to the coordinate system shown in Fig. 8.41. In general, with source at (x_0,y_0,z_0), detector at (x_d,y_d,z_d), and scatter points (x_1,y_1,z_1) and (x_2,y_2,z_2),

$$r_0^2 = (x_1 - x_0)^2 + (y_1 - y_0)^2 + (z_1 - z_0)^2$$

$$r_1^2 = (x_2 - x_1)^2 + (y_2 - y_1)^2 + (z_2 - z_1)^2$$

$$r_2^2 = (x_d - x_2)^2 + (y_d - y_2)^2 + (z_d - z_2)^2$$

$$r_{x_1} = (x_2 - x_0)^2 + (y_2 - y_0)^2 + (z_2 - z_0)^2$$

$$r_{x_2} = (x_d - x_1)^2 + (y_d - y_1)^2 + (z_d - z_1)^2$$

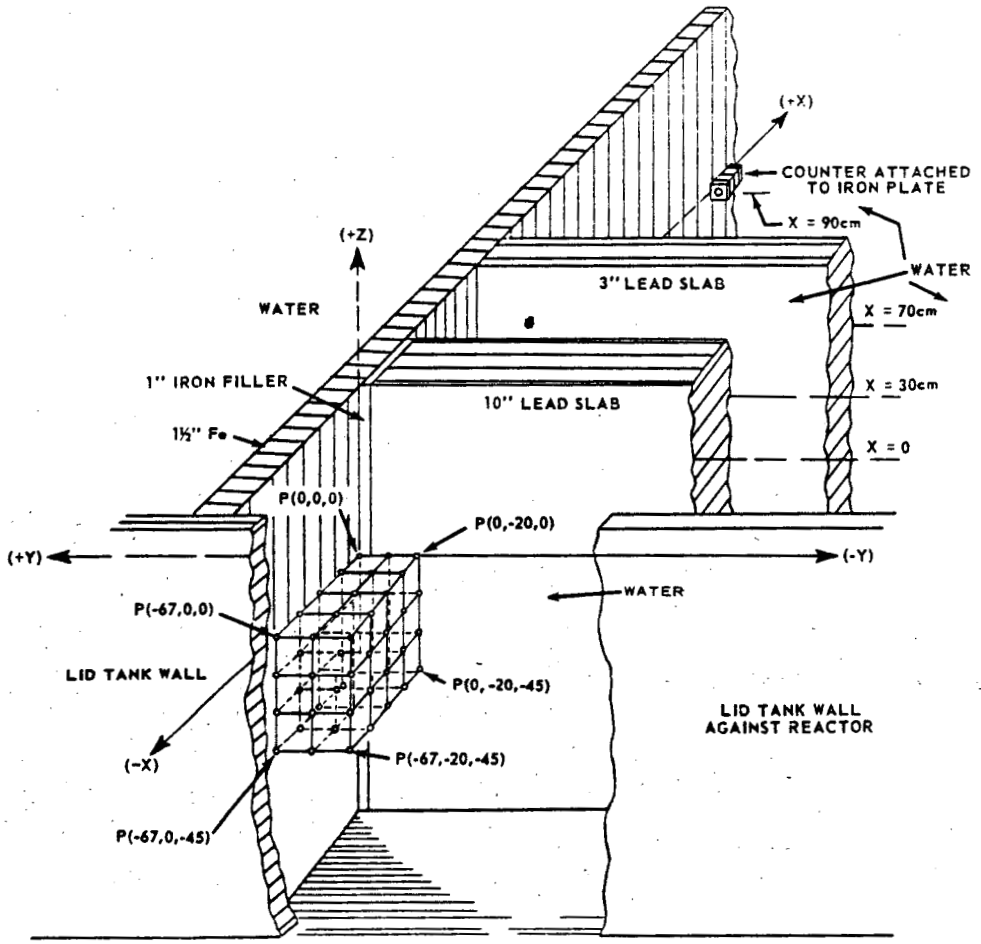
$$\text{Cos } \theta_0 = \frac{y_1 - y_0}{r_0}$$

$$\text{Cos } \theta_1 = \frac{r_{x_1}^2 - r_0^2 - r_1^2}{2r_0r_1}$$

$$\text{Cos } \theta_2 = \frac{r_{x_2}^2 - r_1^2 - r_2^2}{2r_1r_2}$$

Drawings 13017R1 and 13011R1 of reference 28 are reproduced here as Figs. 8.42 and 8.43. In Fig. 8.42 the coordinate system of reference 28 has been changed to agree with that established in Fig. 8.41. In Fig. 8.43 additional data are shown which were obtained by G. A. Allard of KAPL while he was following this test at ORNL.

The following calculations were made in an attempt to predict the experimental results: Initially a scattering volume of 1 cm^3 was assumed at points 1 and 2 as shown in Fig. 8.44. For a stationary point 2, point 1 was moved in the x-direction. The contribution to the dose at the detector was then calculated and is shown in Fig. 8.44 normalized to the maximum contribution. Point 1 was then held stationary at the point giving the maximum contribution, and



GAMMA SCATTERING EXPERIMENT

Figure 8.42

point 2 was varied in the x-direction to find where the maximum contribution to the dose at the detector occurred. These results are shown in Fig. 8.44. The maximum contribution occurs with point 1 at (9,5,0) and point 2 at (84,5,0) [source at (0,0,0) and detector at (90,0,0)]. For a Na_{24} source of 2.76-Mev gamma rays, these points give $E_0 = 2.76$ Mev, $E_1 = 1.63$ Mev, and $E_2 = 0.85$ Mev. The significance of this calculation is that the line of $y = 0$ in Fig. 8.43 has a slope of $\lambda = 19.1$ cm, which corresponds to gamma rays of 1.77 Mev in water. This is very close to the energy of 1.63 Mev calculated above, which indicates that the major contribution to the dose is that which just skirts around the shield. A similar calculation with the 1.38-Mev gamma rays from the sodium source indicated that the contribution to the dose from these would amount to no more than 6 per cent of the total.

For subsequent calculations the following arbitrary assumption as to the volume of the scattering element was made.

At scatter point 1, which is at distance r_0 from the source point and where r_0 makes an angle θ_0 with the y-axis (see Fig. 8.41), the volume element Δv_1 is given by

$$\Delta v_1 = \frac{1}{3} r_0^3 \sin \theta_0 \, \Delta\theta_0 \, \Delta\phi_0 \left[\left(\frac{r_0 + l}{r_0} \right)^3 - 1 \right]$$

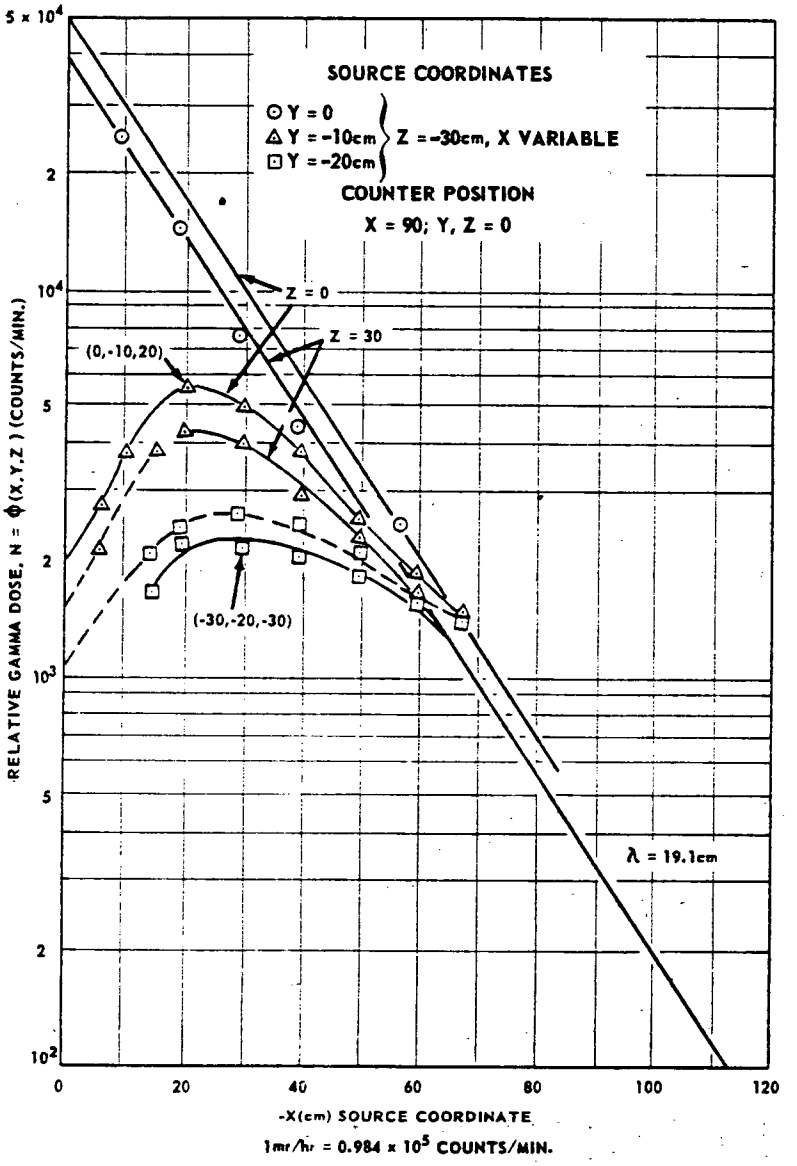


Figure 8.43

All scattering in this volume is assumed to occur at point 1. For point 1 the distance l was assumed equal to $3\lambda_0/4$, where λ_0 is the relaxation length of gamma rays of energy E_0 in the scattering medium (water in this case).

At scatter point 2, which is at distance r_2 from the detector, the volume Δv_2 is assumed to be given by

$$\Delta v_2 = \frac{1}{3} r_2^3 \sin\theta_3 \, \Delta\theta_3 \, \Delta\phi_3 \left[\left(\frac{r_2 + l'}{r_2} \right)^3 - 1 \right]$$

In this case l' is equal to $^3/_4 \lambda_2$, where λ_2 is an approximate relaxation. Twelve elements of volume were considered for scatter point 1, and five elements of volume were considered for scatter point 2. These along with the angles $\Delta\phi_0$ and $\Delta\phi_3$ are described in Fig. 8.45 and Table 8.1.

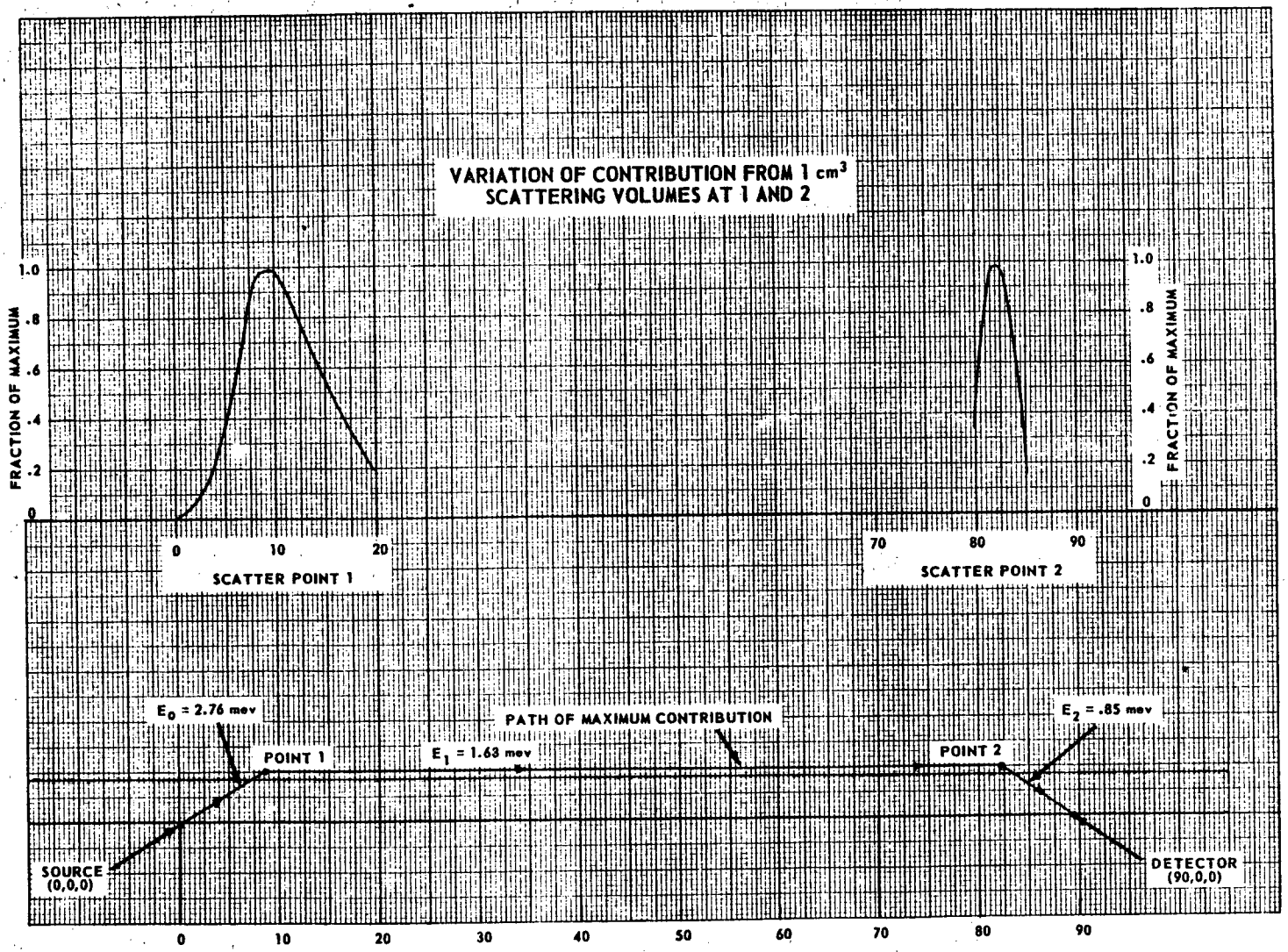

VARIATION OF CONTRIBUTION FROM 1 cm³
SCATTERING VOLUMES AT 1 AND 2
FRACTION OF MAXIMUM
1.0
.8
.6
.4
.2
0
0
10
20
SCATTER POINT 1
70
80
90
SCATTER POINT 2
E₀ = 2.76 mev
POINT 1
E₁ = 1.63 mev
PATH OF MAXIMUM CONTRIBUTION
POINT 2
E₂ = .85 mev
SOURCE
(0,0,0)
DETECTOR
(90,0,0)
0
10
20
30
40
50
60
70
80
90

Figure 8.44

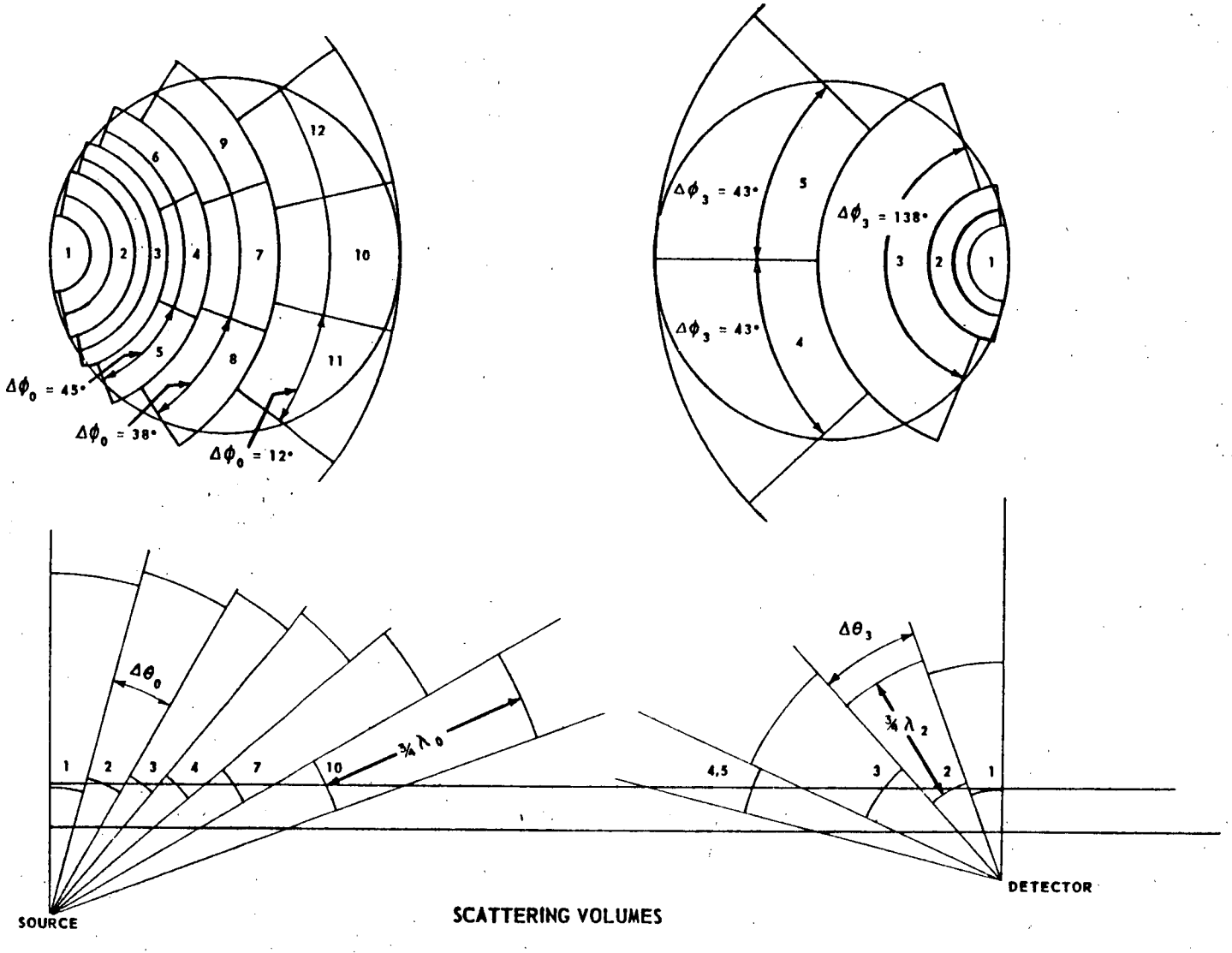

1
2
3
4
5
6
7
8
9
10
11
12
$\Delta\phi_0$ = 45°
$\Delta\phi_0$ = 38°
$\Delta\phi_0$ = 12°
$\Delta\phi_3$ = 43°
$\Delta\phi_3$ = 43°
$\Delta\phi_3$ = 138°
$\Delta\theta_0$
$\Delta\theta_3$
¾ λ_0
¾ λ_2
4,5
SOURCE
DETECTOR
SCATTERING VOLUMES

Figure 8.45

Table 8.1 — VOLUME ELEMENT ANGLES

Scatter point 1				Scatter point 2			
Δv	θ_0, deg	$\Delta\theta_0$, deg	$\Delta\phi_0$, deg	Δv	θ_3, deg	$\Delta\theta_3$, deg	$\Delta\phi_3$, deg
1	7.5	15	180	1	10	20	180
2	22.5	15	160	2	31	22	180
3	35	10	148	3	54	24	138
4	45	10	45	4	71	10	43
5	45	10	45	5	71	10	43
6	45	10	45				
7	55	10	38				
8	55	10	38				
9	55	10	38				
10	65	10	12				
11	65	10	12				
12	65	10	12				

$$r_0 = (5 - y) \sec \theta_0$$

$l = 18$ ($\frac{3}{4}\lambda$ for water and 2.76-Mev gamma rays)

Coordinates of scatter points are given by

$$(x - x_S) = (5 - y) \tan \theta_0 \cos \alpha$$

$$z = (5 - y) \tan \theta_0 \sin \alpha$$

where the angle α is either 0 or $\Delta\phi$

$$r_3 = (5 - y) \sec \theta_3$$

$$(x - x_S) = (5 - y) \tan \theta_3 \cos \alpha$$

$$z = (5 - y) \tan \theta_3 \sin \alpha$$

Using the above elements and keeping the detector at (90,0,0), the results given in Table 8.2 were obtained from calculations using Eq. 41. Scattering occurs from each point 1 to each point 2.

The dose is computed using an average energy of the gamma rays reaching the detector point. The agreement obtained between calculation and experiment above is sufficiently good so that this method of integrating Eq. 41 is considered adequate for the design of the scatter shielding encountered in the naval reactor projects to date.

(f) Scattering from Surfaces. Results of NRL Monte Carlo Calculations of 6.13-Mev Gamma Rays. The radiation scattered from thick surfaces, such as structural steel, consists largely of multiply scattered radiation. For this reason, single-scattering theory is inadequate in surface-scattering problems, and albedo theory must be employed. (An *albedo* is a reflection coefficient, giving the ratio of emergent to incident radiation.) This technique is still in a preliminary stage of development, but it appears to offer a great deal of promise.

Table 8.3 gives results of some detailed albedo calculations for iron run at the Naval Research Laboratory (NRL).[32] The albedos were obtained for several incident angles. A Monte Carlo technique was employed, using the NAREC high-speed computer at NRL. (In a *Monte Carlo* calculation, the individual photons are followed through the shield as their histories are determined by a random selection of the possible scattering or absorption proc-

esses. The probability of any given process is determined by its nuclear cross section as fed to the computer. From the histories of the cases studied, statistical predictions are made for the history of actual gammas going through the shield.) About 15,000 case histories were followed in this calculation for each incident angle at the rate of about 1 sec per history.

The albedos were calculated for photons with an incident energy of 6.13 Mev. These photons are produced by decay of N^{16} formed by the $O^{16}(n,p)N^{16}$ reaction and are responsible for most of the radioactivity of the water in water-cooled reactors during operation.

Table 8.2

Source point	Calculated dose, mr/hr	Experimental dose, mr/hr	Calculated / Experimental
(−20,−10,0)	0.094	0.059	1.65
(−20,−20,0)	0.0228	0.0222	1.025
(−30,−20,0)	0.0358	0.0258	1.39
(−30,0,0)	0.0726	0.0976	0.743

The photons emerging from the slab were grouped according to their angles of emergence as follows: The point of emergence was covered by a hemisphere. This hemisphere was divided into 28 sectors, each subtending the same solid angle at the source. All photons going through the same sector were grouped together. Photons going through the same sector were further subdivided according to their energies.

The sectors were defined by an angle ϕ, measured in the shield plane, and the angle θ_e, measured with respect to the normal to the shield plane. The angle ϕ was measured between the projection of the emergent ray on the shield plane and an axis that was chosen to be the projection of the incident ray on the shield plane.

The layout of the sectors is shown in Fig. 8.46. It is seen that the albedos should be symmetric with respect to ϕ.

The energies of the scattered photons were grouped into the following intervals:

Interval	Range, Mev
E_1	0 to 0.25
E_2	0.25 to 0.50
E_3	0.50 to 0.75
E_4	0.75 to 1.00
E_5	1.00 to 1.25
E_6	1.25 to 1.50
E_7	1.50 to 6.13

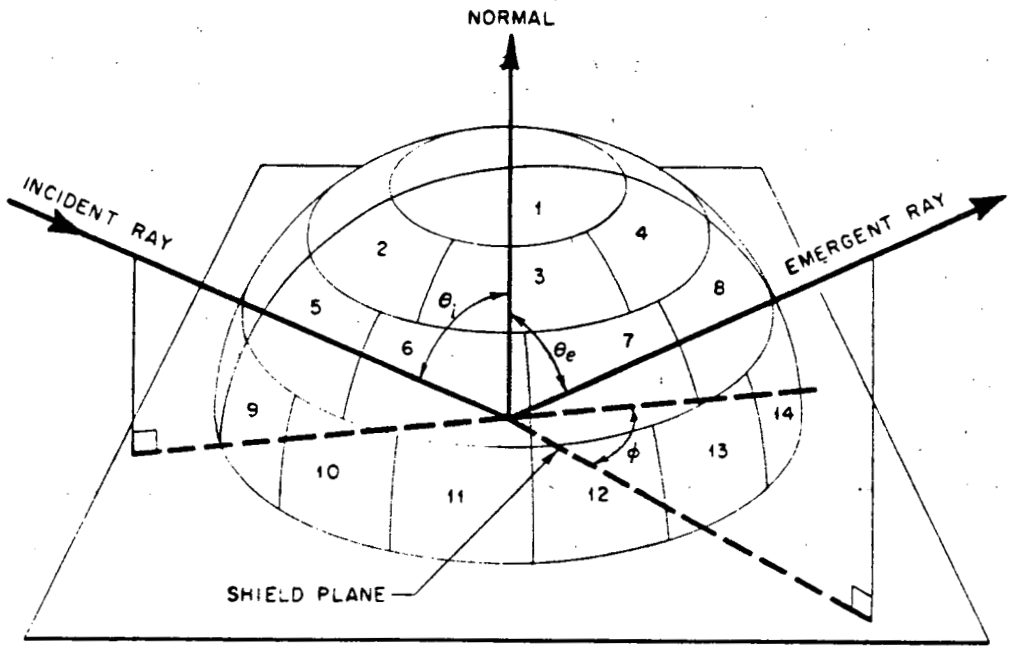
In Table 8.3 the results are expressed in terms of the percentage of the incident energy emerging per unit solid angle within the specified sector. Because the albedos were obtained by a statistical process, they differ from the true mean albedo applicable to an infinite number of incident particles. An idea of the scatter of the albedo data about the mean may be obtained from an examination of the data for normal incidece. The albedos for sectors 2 to 4, 5 to 8, and 9 to 14 should be equal, but they differ because of statistical variation in the calculated results.

The use of the energy albedos may be illustrated by the following example. A point source emits 10^6 photons/sec; radiation from the source travels a distance of 100 cm to a scattering surface whose area (arbitrarily) is 10^4 cm^2 and back to a dose point assumed to be 300 cm from the scatterer. The incident angle measured with respect to the normal at the center of the scattering area is 44°, and the sector of emergence of the scattered ray is No. 8.

Table 8.3—PERCENTAGE OF INCIDENT ENERGY SCATTERED PER UNIT SOLID ANGLE INTO VARIOUS SECTORS OF HEMISPHERE SURROUNDING THE SCATTER POINT FOR AN INCIDENT BEAM OF 6.13-MEV PHOTONS*

Incident angle with normal	Energy range, Mev	Sector number													
		1	2	3	4	5	6	7	8	9	10	11	12	13	14
0°	0–0.25	0.0790	0.0470	0.0540	0.0555	0.0358	0.0264	0.0332	0.0340	0.0075	0.0085	0.0146	0.0121	0.0143	0.0113
	0.25–0.50	0.126	0.132	0.129	0.120	0.114	0.109	0.115	0.0875	0.0483	0.0296	0.0492	0.0510	0.0464	0.0500
	0.50–0.75	0.109	0.099	0.134	0.116	0.102	0.084	0.0965	0.100	0.0347	0.0585	0.0396	0.0459	0.0413	0.0384
22°	0–0.25	0.0700	0.0715	0.0430	0.0510	0.0350	0.0497	0.0361	0.0276	0.0133	0.0187	0.0099	0.0133	0.0172	0.0094
	0.25–0.50	0.118	0.130	0.129	0.125	0.0970	0.121	0.134	0.116	0.0422	0.0276	0.0510	0.0540	0.0535	0.0515
	0.50–0.75	0.121	0.114	0.175	0.108	0.0940	0.0990	0.0965	0.0915	0.0493	0.0347	0.0333	0.0399	0.0520	0.0550
	0.75–1.00														0.0019
44°	0–0.25	0.0765	0.0730	0.0660	0.0495	0.0515	0.0499	0.0420	0.0231	0.0116	0.0174	0.0140	0.0125	0.0104	0.0116
	0.25–0.50	0.166	0.152	0.165	0.216	0.106	0.119	0.144	0.0935	0.0590	0.0312	0.0660	0.0685	0.0408	0.0448
	0.50–0.75	0.163	0.123	0.168	0.165	0.121	0.140	0.123	0.117	0.0520	0.0371	0.0334	0.0655	0.0965	0.121
	0.75–1.00							0.0042	0.0139					0.0200	0.0605
66°	0–0.25	0.102	0.0725	0.0815	0.0705	0.0850	0.0555	0.0499	0.0550	0.0239	0.0154	0.0200	0.0167	0.0184	0.0140
	0.25–0.50	0.262	0.220	0.248	0.251	0.181	0.203	0.198	0.133	0.0725	0.0605	0.0765	0.0705	0.0815	0.0625
	0.50–0.75	0.257	0.245	0.257	0.310	0.158	0.187	0.314	0.355	0.0840	0.0690	0.0660	0.147	0.116	0.0815
	0.75–1.00		0.0019	0.0265				0.0254	0.164				0.0122	0.109	0.0331
	1.00–1.25			0.0025				0.0025	0.101					0.0940	0.104
	1.25–1.50								0.0293					0.0505	0.176
	1.50–6.13								0.0038					0.0095	0.420
88°	0–0.25	0.105	0.101	0.0865	0.0750	0.0810	0.0670	0.0600	0.0590	0.0530	0.0332	0.0215	0.0292	0.0319	0.0292
	0.25–0.50	0.218	0.215	0.275	0.123	0.203	0.289	0.189	0.148	0.106	0.146	0.180	0.149	0.111	0.120
	0.50–0.75	0.525	0.540	0.493	0.650	0.424	0.468	0.660	0.459	0.270	0.325	0.347	0.475	0.334	0.351
	0.75–1.00	0.0020		0.0057	0.282			0.203	0.127				0.0745	0.174	0.0152
	1.00–1.25			0.0026	0.161			0.0463	0.355				0.0160	0.256	0.0248
	1.25–1.50				0.0101			0.0098	0.524				0.0128	0.337	0.0429
	1.50–6.13							0.0043	1.56					0.745	13.75

* Calculated for thick iron scatterer.



θ_i = angle of incident ray with normal
θ_e = angle of emergent ray with normal
ϕ = angle between projections on shield plane of incident and emergent rays

Sector No.	θ_e	ϕ
1	0–22	0–180
2	22–44.4	120–180
3	22–44.4	60–120
4	22–44.4	0–60
5	44.4–64.8	135–180
6	44.4–64.8	90–135
7	44.4–64.8	45–90
8	44.4–64.8	0–45
9	64.8–90	150–180
10	64.8–90	120–150
11	64.8–90	90–120
12	64.8–90	60–90
13	64.8–90	30–60
14	64.8–90	0–30

Fig. 8.46—Segmentation of hemisphere for defining direction of scattering.

Then the energy going through 1 cm^2/sec at the dose point is $[(6.13)(10^6)/(4\pi\ 10^4)] \times 10^4 \cos 44° \times 0.00247 \times (1/9 \times 10^{-4})$. Of this energy 9.4 per cent is in the range 0 to 26 Mev, 38 per cent cent is in the range of 0.25 to 0.5 Mev, 47 per cent is in the range 0.5 to 0.75 Mev, and 5.6 per cent is in the range 0.75 to 1.00 Mev.

In practice it is desired to calculate the dosage scattered to a particular point. To make the dosage calculation, it is necessary to know the absorption coefficients of the scattered radiation in air. Table 8.4 gives the dose rate in milliroentgens per hour at 1 cm from the scatterer in the direction within a specified sector for 10^6 photons/sec incident at a given angle.

Table 8.4—ANGULAR DISTRIBUTION OF DOSE RATE IN MR/HR AT 1 CM FROM IRON SCATTERER FOR 10^6 INCIDENT PHOTONS/SEC

Sector of emergent ray	Incident angle with normal				
	0°	22°	44°	66°	88°
1	39	38	50	76	104
2	34	39	43	66	105
3	39	42	49	72	106
4	36	35	53	81	157
5	31	28	34	52	87
6	27	33	37	55	101
7	30	33	38	73	143
8	27	29	29	101	333
9	11	13	15	22	53
10	12	10	11	18	62
11	13	12	14	20	68
12	14	13	18	31	93
13	13	15	21	57	211
14	12	14	29	84	1296

Values used for energy absorption coefficient for gamma rays in air

$\mu(E_1)$	$3.64 \times 10^5\ cm^{-1}$	$\mu(E_5)$	$3.48 \times 10^5\ cm^{-1}$
$\mu(E_2)$	$3.76 \times 10^5\ cm^{-1}$	$\mu(E_6)$	$3.34 \times 10^5\ cm^{-1}$
$\mu(E_3)$	$3.78 \times 10^5\ cm^{-1}$	$\mu(E_7)$	$2.72 \times 10^5\ cm^{-1}$
$\mu(E_4)$	$3.67 \times 10^5\ cm^{-1}$		

Table 8.5 gives the results of interpolation of the NRL data. The interpolation was made to simplify application of the data to practical shield problems. The results are given in the form of dose albedos. They were calculated before all the histories used for Tables 8.3 and 8.4 had been obtained and, accordingly, are based on slightly different average albedos. They were also calculated on the basis of a constant absorption coefficient of the scattered radiation in air, i.e., $3.7 \times 10^{-5}\ cm^{-1}$. The use of these dose albedos is shown in the following section.

Calculation of Scattering Within a Cylindrical Container. Many practical shielding problems involve scattering within a cylindrical container. The geometrical part of the calculations for these problems can best be handled in cylindrical coordinates. An example of a scattering situation is shown in Fig. 8.47.

Procedure for Calculation of Scattering:

1. *Define scattering surface.* This is bounded on one side by the intersection of lines drawn from the dose point through the edge of the shield to the scatter surface and on the other

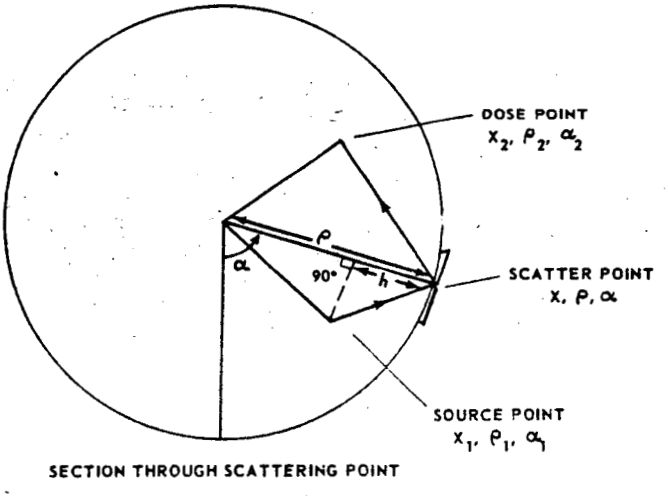
Table 8.5—DOSE ALBEDOS × 10^2 FOR 6.13-MEV PHOTONS BY INTERPOLATION OF NRL DATA*

		θ_e									
θ_i	ϕ	0	10	20	30	40	50	60	70	80	86 to 90
0–10	0–180	0.49	0.49	0.49	0.49	0.48	0.44	0.35	0.26	0.15	0.04
20	0	0.54	0.54	0.54	0.54	0.53	0.46	0.38	0.29	0.19	0.08
	10	0.54	0.54	0.54	0.54	0.53	0.46	0.38	0.28	0.18	0.06
	180	0.54	0.54	0.54	0.54	0.53	0.46	0.37	0.26	0.15	0.04
30	0	0.62	0.62	0.62	0.61	0.57	0.47	0.39	0.33	0.29	0.24
	10	0.62	0.62	0.62	0.61	0.57	0.47	0.39	0.31	0.25	0.19
	20	0.62	0.62	0.62	0.61	0.57	9.47	0.39	0.30	0.22	0.15
	30	0.62	0.62	0.62	0.61	0.57	0.47	0.39	0.29	0.21	0.11
	40	0.62	0.62	0.62	0.61	0.57	0.47	0.39	0.28	0.19	0.08
	180	0.62	0.62	0.62	0.61	0.57	0.47	0.39	0.26	0.15	0.03
40	0	0.72	0.72	0.70	0.67	0.60	0.50	0.43	0.45	0.49	0.47
	10	0.72	0.72	0.70	0.67	0.60	0.50	0.43	0.40	0.38	0.37
	20	0.72	0.72	0.70	0.67	0.60	0.50	0.42	0.37	0.33	0.29
	30	0.72	0.72	0.70	0.67	0.60	0.50	0.41	0.35	0.29	0.23
	40	0.72	0.72	0.70	0.67	0.60	0.50	0.41	0.33	0.24	0.14
	60	0.72	0.72	0.70	0.67	0.60	0.50	0.41	0.31	0.20	0.09
	180	0.72	0.72	0.70	0.67	0.60	0.50	0.40	0.29	0.18	0.05
50	0	0.82	0.82	0.81	0.79	0.74	0.67	0.69	0.78	0.80	0.75
	10	0.82	0.82	0.81	0.79	0.74	0.67	0.66	0.66	0.65	0.64
	20	0.82	0.82	0.81	0.79	0.74	0.66	0.63	0.58	0.54	0.47
	30	0.82	0.82	0.81	0.79	0.74	0.66	0.60	0.53	0.44	0.35
	40	0.82	0.82	0.81	0.79	0.74	0.65	0.58	0.47	0.37	0.26
	50	0.82	0.82	0.81	0.79	0.74	0.64	0.54	0.43	0.31	0.21
	60	0.82	0.82	0.81	0.79	0.74	0.63	0.51	0.40	0.28	0.15
	80	0.82	0.82	0.81	0.79	0.74	0.63	0.50	0.37	0.21	0.06
	180	0.82	0.82	0.81	0.79	0.74	0.63	0.49	0.33	0.16	0
60	0	0.92	0.92	0.92	0.92	0.96	1.03	1.21	1.36	1.44	1.40
	10	0.92	0.92	0.92	0.92	0.95	0.98	1.04	1.12	1.19	1.13
	20	0.92	0.92	0.92	0.92	0.94	0.96	1.00	1.01	0.98	0.91
	30	0.92	0.92	0.92	0.92	0.93	0.94	0.96	0.91	0.78	0.62
	40	0.92	0.92	0.92	0.92	0.92	0.92	0.92	0.79	0.64	0.44
	60	0.92	0.92	0.92	0.92	0.91	0.88	0.77	0.62	0.45	0.26
	80	0.92	0.92	0.92	0.92	0.91	0.83	0.66	0.46	0.28	0.07
	180	0.92	0.92	0.92	0.92	0.90	0.79	0.62	0.42	0.22	0
70	0	1.22	1.22	1.22	1.22	1.34	1.70	2.42	3.22	3.42	3.35
	10	1.18	1.18	1.18	1.18	1.30	1.56	2.06	2.64	2.76	2.64
	20	1.15	1.15	1.15	1.15	1.26	1.44	1.77	2.02	2.10	1.94
	30	1.14	1.14	1.14	1.14	1.23	1.40	1.61	1.65	1.55	1.29
	40	1.13	1.13	1.13	1.13	1.19	1.36	1.48	1.36	1.11	0.80
	50	1.12	1.12	1.12	1.12	1.16	1.32	1.30	1.13	0.87	0.60
	60	1.11	1.11	1.11	1.11	1.13	1.24	1.15	0.93	0.67	0.36
	80	1.09	1.09	1.09	1.09	1.06	1.01	0.86	0.62	0.51	0.12
	180	1.07	1.07	1.07	1.07	0.99	0.91	0.76	0.54	0.31	0
80	0	1.75	1.75	1.75	1.96	2.47	3.40	5.25	8.55	10.2	10.3
	10	1.65	1.65	1.65	1.75	2.06	2.88	4.32	6.69	8.24	8.10
	20	1.60	1.60	1.60	1.70	2.01	2.68	3.70	4.84	5.35	5.15
	30	1.55	1.55	1.55	1.65	1.96	2.47	3.20	3.40	3.50	3.19
	40	1.50	1.50	1.50	1.60	1.85	2.27	2.58	2.37	2.06	1.45
	50	1.45	1.45	1.45	1.55	1.75	2.06	2.06	1.85	1.55	1.03
	60	1.40	1.40	1.40	1.44	1.65	1.75	1.65	1.44	1.13	0.82
	80	1.34	1.34	1.34	1.34	1.34	1.24	1.24	1.03	0.72	0.41
	180	1.24	1.24	1.24	1.24	1.24	1.13	0.93	0.72	0.52	0.20

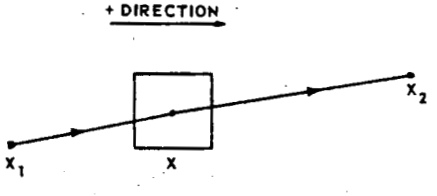
Table 8.5 — (Continued)

θ_i	ϕ	θ_e 0	10	20	30	40	50	60	70	80	86 to 90
88	0	2.47	2.47	2.47	2.47	3.71	6.18	13.9	40.6	44.8	44.8
	10	2.16	2.16	2.16	2.16	3.30	5.15	10.3	26.3	28.8	27.8
	20	1.90	1.90	1.90	1.90	2.88	4.32	8.24	11.8	12.6	10.3
	30	1.83	1.83	1.83	1.83	2.47	3.71	5.97	7.7	8.03	5.65
	40	1.76	1.76	1.76	1.76	2.16	3.09	4.53	4.63	3.91	1.43
	50	1.70	1.70	1.70	1.70	1.85	2.58	3.50	3.20	2.46	0.41
	60	1.65	1.65	1.65	1.65	1.65	2.06	2.57	2.37	1.65	0.31
	180	1.24	1.24	1.24	1.24	1.24	1.24	1.03	0.82	0.62	0.20

*Dose at distance r from scatterer of area A = incident dose times cos θ_i A$(1/r^2)$ times albedo. A and r^2 are in the same units.



SECTION THROUGH SCATTERING POINT



SIDE VIEW

GEOMETRY FOR CALCULATING SCATTERING ANGLES

Figure 8.47

side by the intersection of lines drawn from the source point through the edge of the shield to the scatter surface (see Fig. 8.48).

2. *Divide scattering surface into small areas.* (In submarine work it has proved convenient to divide the hull into scattering sectors having lengths equal to the length of a frame and having

METHOD FOR DETERMINING SCATTER SURFACE

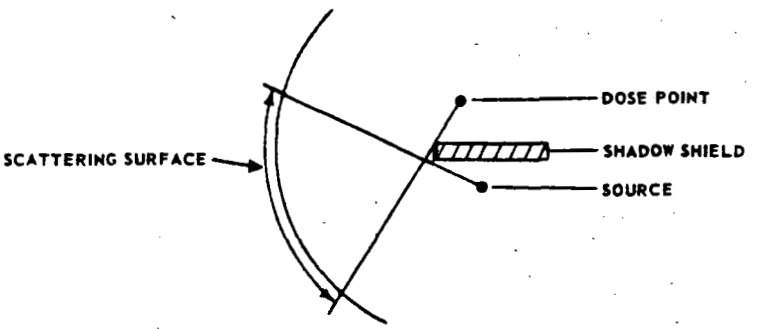


Figure 8.48

widths that subtend an angle of 10° from the center line of the ship. These scatter sections have areas of about 5 sq ft.) For the calculation each area will be considered to be a plane area located tangent to the center of the cylindrical area and, consequently, with the same normal as the center of the cylindrical area. The scattering will be calculated as though it all occurred at the center of the area.

3. *Refer to Fig. 8.47.* To get θ_i (angle between incident ray and normal), let

$\beta_1 = \alpha - \alpha_1$

$d = \sqrt{(\rho_1 \sin \beta_1)^2 + (x - x_1)^2}$ = perpendicular distance between source point and normal to scatter point

$h = \rho - \rho_1 \cos \beta_1$

$\theta_i = \tan^{-1} d/h$, where θ lies between 0 and 90°

α = angular cylindrical coordinate

ρ = radius

x = longitudinal coordinate

To get ϕ, consider the plane tangent to the scatter point. ϕ is the angle between the incident and emergent rays projected on the shield plane.

$$\phi_1 = \tan^{-1} \frac{\rho_1 \sin (\alpha - \alpha_1)}{x - x_1}$$

$\phi = |\phi_1 - \phi_2|$ where

$$\phi_2 = \tan^{-1} \frac{\rho_2 \sin (\alpha_2 - \alpha)}{x_2 - x}$$

If $x - x_1$ or $x_2 - x$ is positive, ϕ is between 0 to $\pi/2$ or 0 to $-\pi/2$, depending on the sign of $\tan \phi$. If $x - x_1$ or $x_2 - x$ is negative, ϕ is between $\pi/2$ to π or $-\pi/2$ to $-\pi$, depending on the sign of $\tan \phi$.

4. If $|\phi|$ is calculated to be greater than 180°, subtract it from 360°. Knowing θ_i, θ_e, and ϕ, obtain albedo from data presented in Tables 3 to 5.

5. For a given source strength S, expressed in roentgens per hour at 1 ft, the dose scattered to the dose point is given by

$$D = \frac{S(\cos \theta_i)(A)(R)}{r_1^2 r_2^2}$$

where A = the area of scattering sector
R = the albedo
r_1 = the distance from source to scatterer
r_2 = the distance from scatterer to dose point

A sample calculation sheet for a routine calculation of scattering in a cylindrical geometry is shown in Fig. 8.49.

(g) Experiments with Collimated Gamma Rays in Water. Several experiments and calculations have been performed to determine the flux distribution of gamma radiation scattered and absorbed in a water medium. The source geometries thus far investigated have included homogeneously distributed,[33] plane monodirectional,[34] and point isotropic sources.[34,35] Any attempt to depart from such relatively simple geometries leads to serious problems of computation since the expressions for the intensity pattern become mathematically complicated. One geometry that is difficult to compute because of its spatially unsymmetrical nature is the case of a point monodirectional source or beam. This geometry was chosen for experiments at Bettis to furnish data on the characteristics of multiple gamma scattering in water. Results obtained for water should be approximately correct for other light-scattering mediums.

The point monodirectional source is of particular interest since it is the basic source geometry in the study of multiple gamma scattering. Solutions for source geometries of arbitrary spectral and angular distributions can be constructed from point monodirectional source data by superposition. In addition, if full knowledge is gained of the spectral and angular distributions of the gammas scattered from this basic beam source, an understanding of the characteristics of multiple scattering in inhomogeneous scattering mediums would be possible through similar superposition techniques.

The experiment reported here* is a first step in the study of the scattering characteristics of a point monodirectional source. Dosage measurements were made of the scattered gamma field; its spectral and angular distributions were not investigated.

In order to obtain a narrow gamma beam, a 12-curie Co^{60} source was housed in a lead sphere 14 in. in diameter which had a 3-in.-diameter hole penetrating to the center line of the sphere. It was desired to direct the beam into a large enough water medium to be effectively infinite. For this purpose, a steel water tank 12 ft in diameter and 11 ft high was provided.

The beam orientation was determined by making traverses with the detector in the vertical plane in the region in which the beam was known to travel. These beam-profile measurements were made at increasing radial distances to calibrate the position indicators and to make certain that the detector and source centers remained in the same horizontal plane.

In meeting the need to measure gamma dose rate with good spatial discrimination, a scintillation type instrument seemed the most suitable. Such an instrument has a small detecting volume, large intensity range, good stability when properly pretreated, and an energy response approximately that of air, when a light organic scintillator is used.

Curves of gamma-ray dosage as a function of beam-detector angle are shown in Fig. 8.50. From these data a plot of dosage vs. radial distance is derived with the beam angle as a parameter (see Fig. 8.51). Included with these curves is a plot of dosage attenuation in the beam calculated from the expression

$$\frac{e^{-\mu_w r}}{16\,\mu_{Co}}\left\{\frac{1}{y^2}\left[1-\frac{2}{\mu_{Co}y}+\frac{6}{(\mu_{Co}y)^2}\right]-\frac{e^{-\mu_{Co}}}{(y+1)^2}\left[1-\frac{2}{\mu_{Co}(y+1)}+\frac{6}{\mu_{Co}^2(y+1)^2}\right]\right\}$$

where r is the distance in water in centimeters; $\mu_w = 0.064\ cm^{-1}$, the total macroscopic absorption coefficient for water at a gamma energy of 1.2 Mev; and y is the source-detector distance in centimeters. Although small, the correction for self-absorption by the source (1-cm long) was made, choosing $0.472\ cm^{-1}$ for the absorption coefficient for Co^{60} (μ_{Co}).

The close agreement in the shapes of the calculated and experimental curves shows the validity of uncollided beam relation in that region. The effects of multiple scattering back into

* F. W. Marasco and P. E. F. Thurlow, Report WAPD-RM-219.

CALCULATION OF SCATTERED RADIATION

Source point	Dose point			
x_1	x_2			
ρ_1	ρ_2			
α_1	α_2			
Sector symbol				
x				
ρ				
α				
$\beta_1 = \alpha - \alpha_1$				
Cos β_1				
Sin β_1				
$\rho_1 \cos \beta_1$				
$\rho_1 \sin \beta_1$				
$x - x_1$				
$d_1 = [(\rho_1 \sin \beta_1)^2 + (x - x_1)^2]^{1/2}$				
$h_1 = \rho - \rho_1 \cos \beta_1$				
d_1/h_1				
$\theta_i = \tan^{-1} d_1/h_1$				
$\tan \phi_1 = \rho_1 \sin \beta_1/(x - x_1)$				
ϕ_1				
$\beta_2 = \alpha_2 - \alpha$				
Cos β_2				
Sin β_2				
$\rho_2 \cos \beta_2$				
$\rho_2 \sin \beta_2$				
$x_2 - x$				
$d_2 = [(\rho_2 \sin \beta_2)^2 + (x_2 - x)^2]^{1/2}$				
$h_2 = \rho - \rho_2 \cos \beta_2$				
d_2/h_2				
$\theta_e = \tan^{-1} d_2/h_2$				
$\tan \phi_2 = \rho_2 \sin \beta_2/(x_2 - x)$				
ϕ_2				
$\varphi = \lvert\phi_1 - \phi_2\rvert$				
(1) $r_1^2 = \rho_1^2 + \rho^2 - 2\rho\rho_1 \cos \beta_1 + (x - x_1)^2$				
(2) $r_2^2 = \rho_2^2 + \rho^2 - 2\rho\rho_2 \cos \beta_2 + (x - x_2)^2$				
(3) Cos θ_i				
(4) Area of sector				
(5) Albedo for θ_i, θ_e, ϕ				
Dose factor = $\frac{(3) \times (4) \times (5)}{(1) \times (2)}$				

NOTE: If $\left.\begin{matrix} x - x_1 \\ x_2 - x \end{matrix}\right\}$ is positive, ϕ_i lies between $\begin{cases} 0 \text{ to } \pi/2 \\ 0 \text{ to } -\pi/2 \end{cases}$

If $\left.\begin{matrix} x - x_1 \\ x_2 - x \end{matrix}\right\}$ is negative, ϕ_i lies between $\begin{cases} \pi/2 \text{ to } \pi \\ -\pi/2 \text{ to } -\pi \end{cases}$

If $|\phi_1 - \phi_2|$ is >180°, subtract from 360°

Fig. 8.49—Sample calculation sheet.

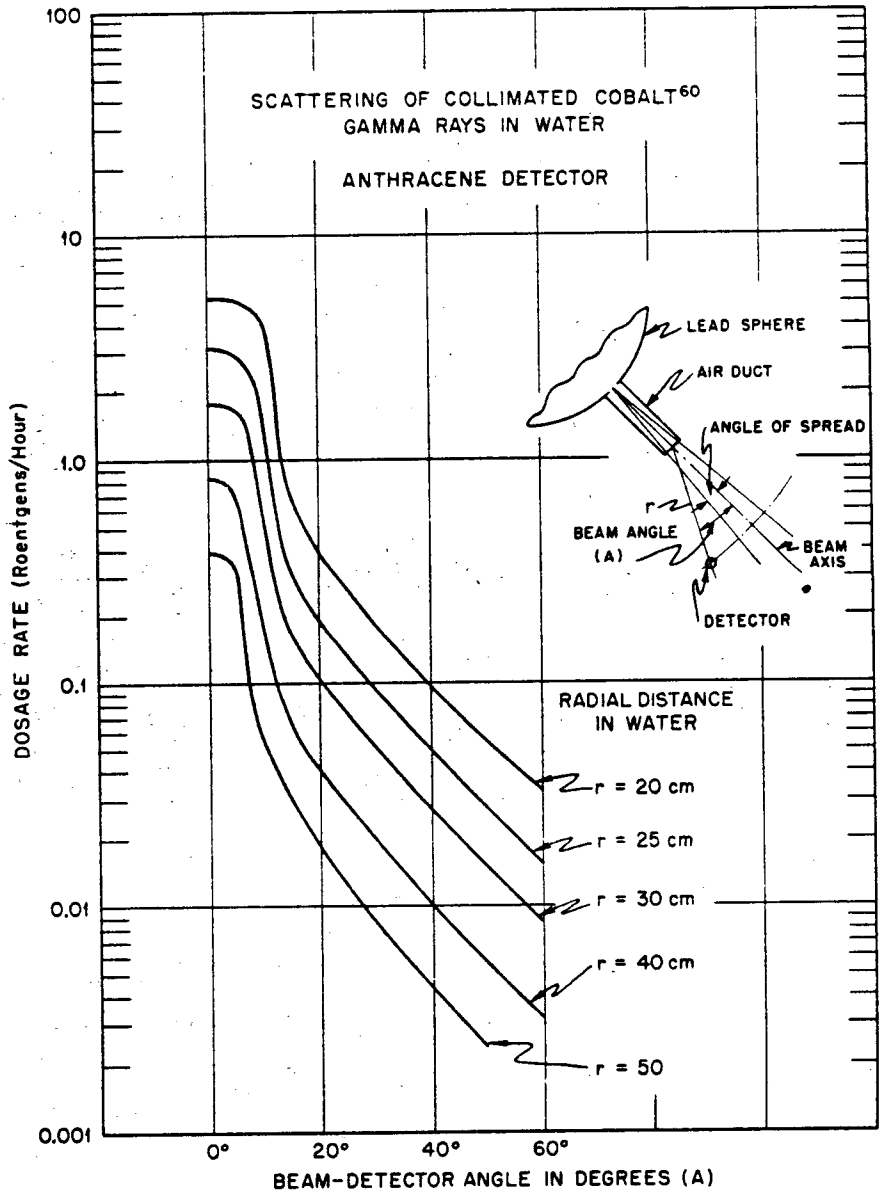


Figure 8.50

the beam from the water, as well as from the sphere, collimator, or detector supporting structure, are shown to be negligible.

Closer agreement in absolute dosage values in the beam would have been possible had a calibrated source strength been used. A nominal value of 10 curies was used in making the calculations for the theoretical curve shown.

It is seen in Fig. 8.50 that the curve plotted at 20 cm exhibits a broader, more flattened peak than the curve at 50 cm. This apparent narrowing of the beam is the result of the co-

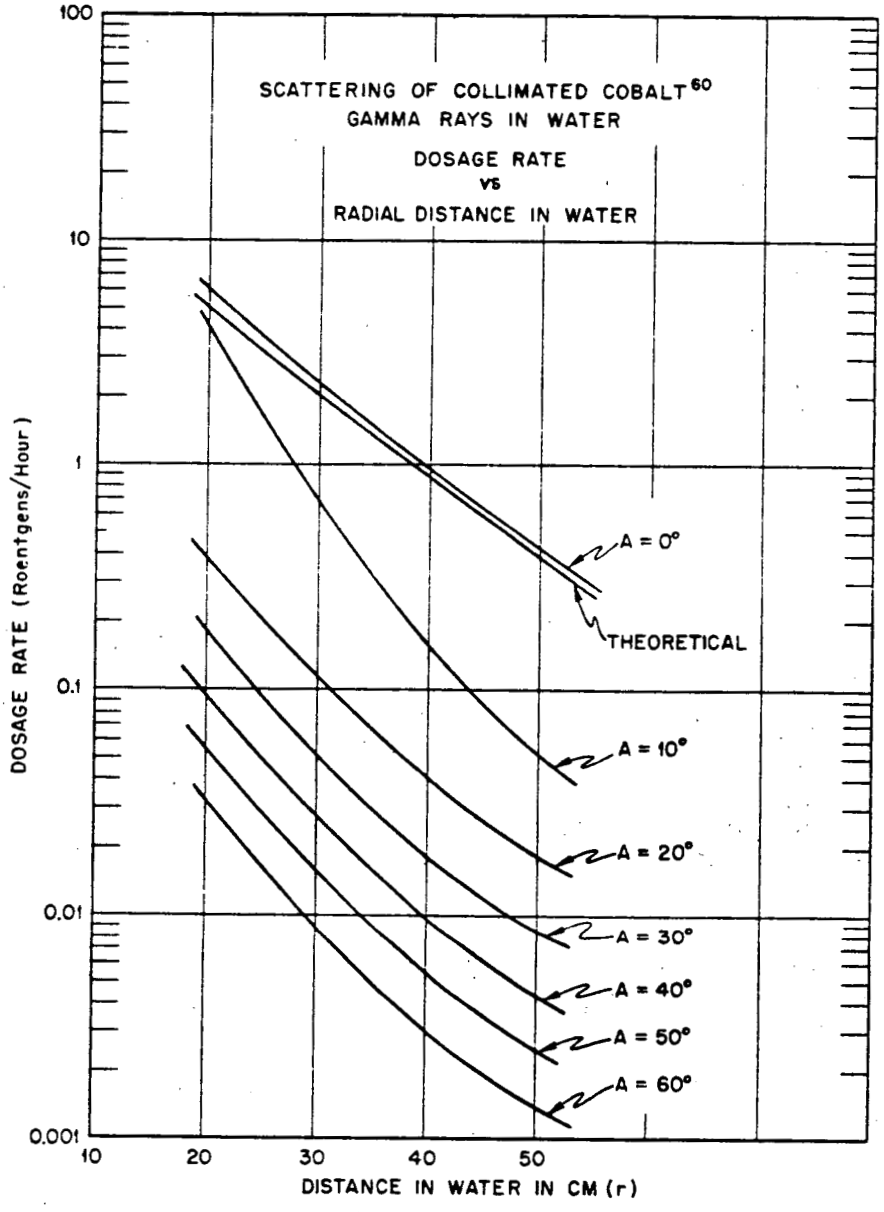

SCATTERING OF COLLIMATED COBALT 60
GAMMA RAYS IN WATER
DOSAGE RATE
VS
RADIAL DISTANCE IN WATER
DOSAGE RATE (Roentgens/Hour)
100
10
1
0.1
0.01
0.001
A = 0°
THEORETICAL
A = 10°
A = 20°
A = 30°
A = 40°
A = 50°
A = 60°
10
20
30
40
50
DISTANCE IN WATER IN CM (r)

Figure 8.51

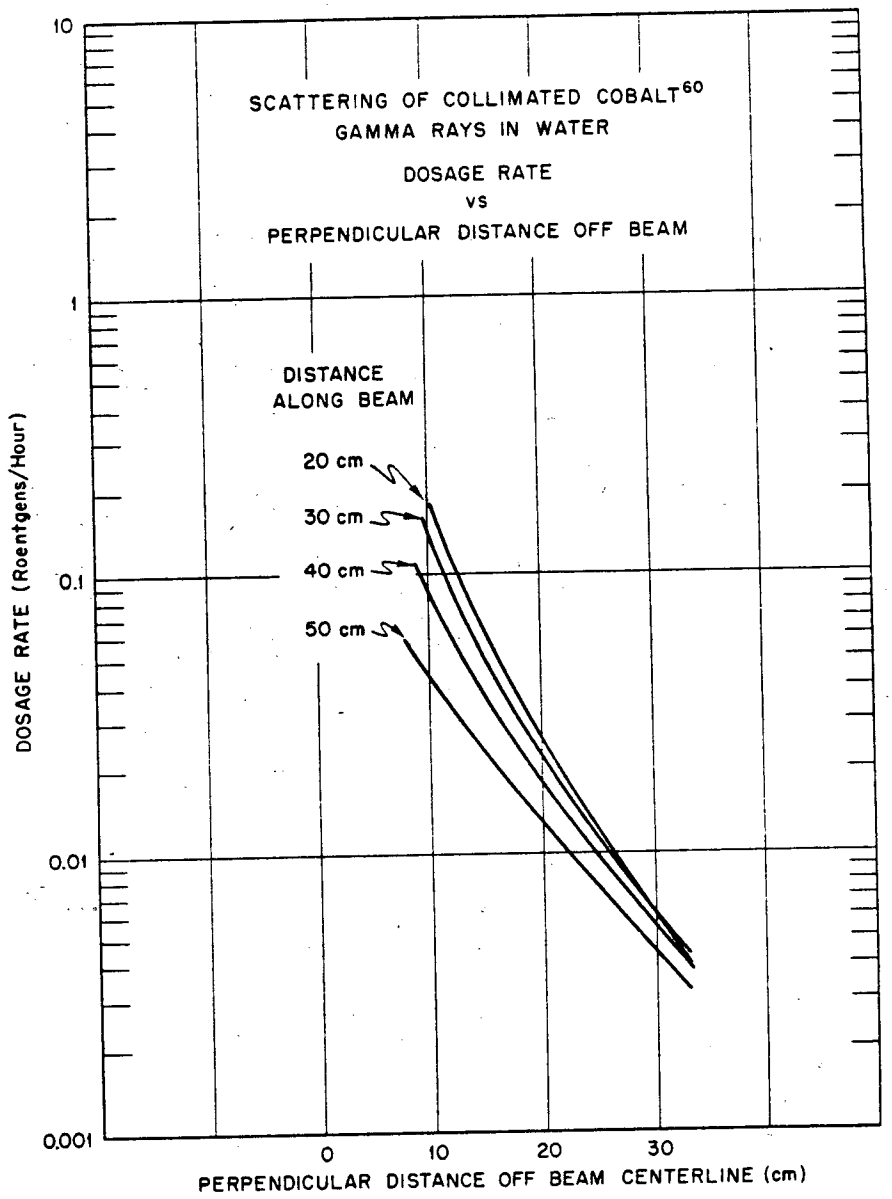

SCATTERING OF COLLIMATED COBALT60
GAMMA RAYS IN WATER
DOSAGE RATE
vs
PERPENDICULAR DISTANCE OFF BEAM
DISTANCE
ALONG BEAM
20 cm
30 cm
40 cm
50 cm
DOSAGE RATE (Roentgens/Hour)
10
1
0.1
0.01
0.001
0
10
20
30
PERPENDICULAR DISTANCE OFF BEAM CENTERLINE (cm)

Figure 8.52

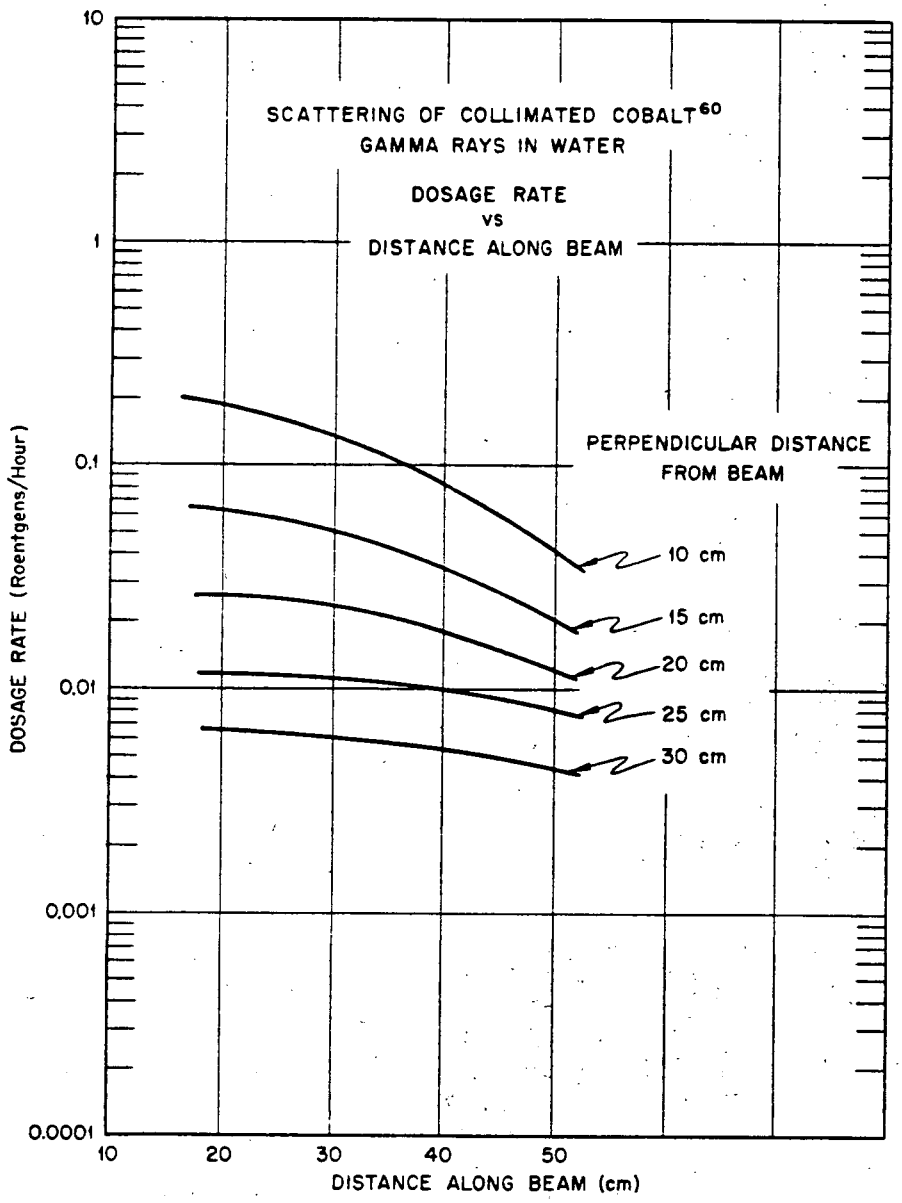

SCATTERING OF COLLIMATED COBALT 60
GAMMA RAYS IN WATER
DOSAGE RATE
VS
DISTANCE ALONG BEAM
PERPENDICULAR DISTANCE
FROM BEAM
10 cm
15 cm
20 cm
25 cm
30 cm
DOSAGE RATE (Roentgens/Hour)
10
1
0.1
0.01
0.001
0.0001
10
20
30
40
50
DISTANCE ALONG BEAM (cm)

Figure 8.53

ordinate system in which the data are plotted. Since it is a spherical coordinate system with the origin at the point of emergence of the beam, the perpendicular distance from the beam, measured by a constant polar angle (beam angle), increases in proportion to the distance from the origin.

From Fig. 8.50 a quantitative calculation was made to determine the spread of the uncollided beam. The polar angle of spread is defined as the solid angle subtending the half-width of the beam a half-maximum. The angle of spread computed in this way for the distances shown was found to be 3°. The merging of the dosage values at large distances from the beam, as evidenced in Fig. 8.52, is felt to be due to this spreading of the beam.

A plot of the gamma dosage as a function of the perpendicular distance from the beam axis is plotted in Fig. 8.52 for various distances along the beam. A cross plot of these curves is presented in Fig. 8.53. The plots in Figs. 8.52 and 8.53 show that the spatial distributions are primarily exponential in character. Investigation of the average relaxation lengths of the distribution perpendicular to the beam shows a length of 5.2 cm for the curve at 20 cm to a length of 8 cm for the one at 50 cm. The average relaxation length of the distribution parallel to the beam (Fig. 8.53) was found to vary from 23.2 cm for a distance of 10 cm to about 49 cm for a distance of 30 cm, as compared to the in-beam relaxation length of 10 cm.

In summary, this experiment showed

1. Uncollided beam concept is valid for these conditions.
2. Multiple scattering back into beam is negligible.
3. Polar angle of spread is 3° for this experiment.
4. Spatial distribution of radiation is primarily exponential.
5. Relaxation length *along beam* is 10 cm on beam center line, increasing rapidly to 49 cm at 30 cm off center line.
6. Relaxation length *perpendicular to beam* increases from 5 to 8 cm as distance from source increases from 20 to 50 cm.

4.3 Neutron Scattering

No completely satisfactory method has been devised for calculating the scattering of neutrons around shielding. This has not proved to be a serious problem, however, in designs of stationary or naval shielding. If partial shielding and large distances are being relied on, this could be a problem.

REFERENCES

1. A. Simon and C. E. Clifford, The Attenuation of Neutrons by Air Ducts in Shields, Report ORNL-1217(Rev.), Mar. 8, 1954.
2. W. G. Bourieius, Report NEPA-1536, Aug. 24, 1950 (Classified).
3. D. W. Whitcombe, Solution of the Diffusion Equation with Streaming for Three Basic Two-medium Geometries, Report ORNL-403, Oct. 7, 1949.
4. D. W. Whitcombe, A Diffusion Solution for the Cylindrical Ducting Problem of Infinite Geometry, Report ORNL-668, Apr. 19, 1950.
5. D. W. Whitcombe, A Diffusion Solution for a Black Thermal-neutron Pipe Duct Containing a Pure Scattering Material, Report ORNL-751, June 5, 1950.
6. G. M. Roe, The Penetration of Neutrons Through an Empty Cylindrical Duct in a Shield, Report KAPL-712, Mar. 29, 1952.
7. M. K. Hullings, Report ORNL CF-53-11-53, November 1953 (Classified).
8. J. W. Crawford, Jr., E. E. Kintner, and Clark Goodman, The Effects of Ducts on the Attenuation of Neutrons and Gamma Rays in the MIT Cyclotron Shield, Nuclear Shielding Studies, Part VII, Laboratory for Nuclear Science and Engineering, Technical Report 38, September 1950.
9. R. S. Brodsky, The Effect of Ducts on the Attenuation of Neutrons and Gamma Rays in a Water Shield, undergraduate thesis, Massachusetts Institute of Technology, May 1952.
10. E. P. Blizard, Repor. ORNL CF-50-8-17, Aug. 8, 1950 (Classified).

11. S. Podgor, Report ORNL CF-50-3-108 (Classified).
12. D. J. Hughes and F. C. Hoyt, Report ANL-4129, p. 7, Apr. 9, 1948 (Classified).
13. F. Shore, Report BNL-267, p. 37, November 1953 (Classified).
14. Neutron Cross Sections, Report AECU-2040.
15. R. D. Schamberger and F. J. Shore, Report BNL-1444, May 25, 1953 (Classified).
16. E. P. Blizard, G. T. Chapman, and J. D. Flynn, Report ORNL CF-53-6-186, June 30, 1953 (Classified).
17. H. J. Kouts et al., Report BNL-1443, May 25, 1953 (Classified).
18. C. E. Clifford, Report ORNL CF-52-5-1, Part 11, Oct. 4, 1952 (Classified).
19. F. J. Shore, R. D. Schamberger, and H. P. Sleeper, Report BNL-265, Dec. 1, 1953 (Classified).
20. C. W. J. Wende, Report TNX-7 (E. I. du Pont de Nemours & Co.), Jan 11, 1944 (Classified).
21. H. J. Kouts and W. W. Pratt, Report BNL-1328, Aug. 25, 1952 (Classified).
22. Lewi Tonks, Report KAPL-107, Jan. 17, 1949 (Classified).
23. D. Halliday, "Introductory Nuclear Physics," John Wiley & Sons, Inc., New York, 1950.
24. W. Heitler, "The Quantum Theory of Radiation," Oxford University Press, London, 1950.
25. G. Allen, Tables for Determining Reduction of Energy and Intensity of X Rays and Gamma Rays at Various Scattering Angles in Small Thicknesses of Matter, Report NACA-TN-2026.
26. H. Goldstein and J. E. Wilkins, Jr., Calculations of the Penetration of Gamma Rays, Report NYO-3075, June 30, 1954.
27. M. S. Plesset, Scattering of Gamma Rays and Neutrons, Report RAD-196.
28. Report ORNL-1216, Dec. 20, 1951 (Classified).
29. E. P. Blizard and H. Goldstein, Report ORNL-1575, July 12, 1954 (Classified).
30. J. B. Trice, Report NEPA-1296, Feb. 20, 1950 (Classified).
31. J. B. Trice, Report NEPA-1297, Feb. 27, 1950 (Classified).
32. R. B. Theus and L. A. Beach, Gamma Ray Albedo, NRL Quarterly on Nuclear Science and Technology, July–September 1955.
33. W. R. Faust and M. H. Johnson, Phys. Rev., 75: 467 (1949).
34. W. R. Faust, Phys. Rev., 77: 227 (1950).
35. G. R. White, Phys. Rev., 80: 154 (1950).

BIBLIOGRAPHY

Blizard, E. P., G. T. Chapman, and J. D. Flynn, Report ORNL CF-53-6-186, June 30, 1953 (Classified).
Blizard, E. P., Report ORNL CF-50-8-17, Aug. 8, 1950 (Classified).
Bourieius, W. G., Report NEPA-1536, Aug. 24, 1950 (Classified).
Clifford, C. E., Report ORNL CF-52-5-1, Part II, Oct. 4, 1952 (Classified).
Clifford, C. E., and C. L. Storrs, Report ORNL CF-52-6-158, June 26, 1952 (Classified).
Clifford, C. E., and A. Simon, Report ORNL CF-52-6-165, June 25, 1952 (Classified).
Ergen, W. K., Report ORNL CF-50-80-1, Aug. 1, 1950 (Classified).
Hughes, D. J., and F. C. Hoyt, Report ANL-4129, p. 7, Apr. 9, 1948 (Classified).
Hullings, M. K., Report ORNL CF-53-11-53, November 1953 (Classified).
Kouts, H. J., and W. W. Pratt, Report BNL-1328, Aug. 25, 1952 (Classified).
Kouts, H. J., et al., Report BNL-1443, May 25, 1953 (Classified).
Kouts, H. J., Report BNL-1357, Sept. 15, 1952 (Classified).
Neutron Cross Sections, Report AECU-2040.
Podgor, S., Report ORNL CF-50-3-108 (Classified).
Roe, G. M., The Penetration of Neutrons Through an Empty Cylindrical Duct in a Shield, Report KAPL-712, Mar. 29, 1952.
Schamberger, R. D., and F. J. Shore, Report BNL-1444, May 25, 1953 (Classified).
Schamberger, R. D., F. J. Shore, and H. P. Sleeper, Reports BNL-2019, -2021, and -2027, Sept. 1, 1954 (Classified).
Shore, F. J., Report BNL-267, p. 37, November 1953 (Classified).

Shore, F. J., R. D. Schamberger, and H. P. Sleeper, Report BNL-265, Dec. 1, 1953 (Classified).

Simon, A., and C. E. Clifford, The Attenuation of Neutrons by Air Ducts in Shields, Report ORNL-1217(Rev.), Mar. 8, 1954.

Simon, A., Reactor Handbook, Volume 1, Physics, Chapter 2.6, June 1953 (Classified).

Storrs, C. L., and J. D. Flynn, Report ORNL CF-52-12-188, Dec. 15, 1953 (Classified).

Tonks, L., Report KAPL-107, Jan. 17, 1949 (Classified).

Tonks, L., Report KAPL-224, Oct. 6, 1949 (Classified).

Wende, C. W. J., Report TNX-7, E. I. du Pont de Nemours & Co., Jan 11, 1944 (Classified).

Whitcombe, D. W., A Diffusion Solution for a Black Thermal-neutron Pipe Duct Containing a Pure Scattering Material, Report ORNL-751, June 5, 1950.

Whitcombe, D. W., A Diffusion Solution for the Cylindrical Ducting Problem of Infinite Geometry, Report ORNL-668, Apr. 19, 1950.

Whitcombe, D. W., Report ORNL-899, Mar. 15, 1951 (Classified).

Whitcombe, D. W., Solution of the Diffusion Equation with Streaming for Three Basic Two-medium Geometries, Report ORNL-403, Oct. 7, 1949.

Chapter 9

EFFECT OF GEOMETRY OF RADIATION SOURCE

NOMENCLATURE 346

INTRODUCTION 347

PART I EQUATIONS FOR THE FLUX . . 347

I-1 Point Source 347
I-2 Line Source 348
I-3 Disk Source 348
I-4 Infinite-slab Source 353
I-4.1 Exterior 353
I-4.2 Interior 353
I-5 Truncated Right-circular Cone Source 359
I-6 Cylindrical Source 360
I-6.1 Exterior on Side . . . 360
I-6.2 Exterior on End ($h < 3/\mu_s$) . . 364
I-6.3 Exterior on End ($h \geq 3/\mu_s$) . . 364
I-6.4 Interior 365
I-7 Spherical Source 368
I-7.1 Exterior 368
I-7.2 Interior 371
I-8 e^{-b}, $E_1(b)$, and $E_2(b)$ 372
I-9 The Function $F(\theta,b)$ 385

PART II DERIVATIONS 391

II-1 Point Source 391
II-2 Line Source 392
II-3 Disk Source 393
II-4 Infinite-slab Source 395
II-4.1 Exterior 395
II-4.2 Interior 397
II-5 Truncated Right-circular Cone Source 398
II-6 Cylindrical Source 400
II-6.1 Exterior on Side . . . 400
II-6.2 Exterior on End . . . 401
II-6.3 Interior 402
II-7 Spherical Source 404
II-7.1 Exterior 404
II-7.2 Interior 405
II-8 The Functions $E_n(b)$, $F_n(t,a)$, $F(\theta,b)$, and $G(\mu_s h,b)$ 407
II-8.1 The Functions $E_n(b)$ . . . 407
II-8.2 The Functions $F_n(t,a)$ . . 408
II-8.3 The Function $F(\theta,b)$ . . . 408
II-8.4 The Function $G(\mu_s h,b)$ . . 409

PART III ASYMPTOTIC APPROXIMATIONS 409

III-1 Line Source 409
III-2 Disk Source 410
III-3 Truncated Right-circular Cone Source 411

PART IV EFFECT OF SCATTERED RADIATION 412

IV-1 Build-up in an Infinite Medium . . 412
IV-2 Build-up Within a Source . . . 413
IV-3 Build-up Through Laminations . . 414

PART V BUILD-UP FACTORS FOR IRON, WATER, LEAD, AND CONCRETE . 415

PART VI TRANSFORMATION FROM ONE GEOMETRY TO ANOTHER . . 424

VI-1 Disk-source to Point-source Transformation 424
VI-2 Plane to Sphere Transformation . . 424
VI-3 Plane to Cylinder Transformation . 424
VI-4 Disk to Infinite-plane Transformation 424

REFERENCES 425

Nomenclature

ϕ	Scalar flux ($cm^{-2}sec^{-1}$)
S_0	Source strength of point source (sec^{-1})
S_L	Source strength of line source ($cm^{-1}sec^{-1}$)
S_A	Source strength of plane source ($cm^{-2}sec^{-1}$)
S_V	Source strength of volume source ($cm^{-3}sec^{-1}$)
μ_s	Macroscopic cross section of source material (cm^{-1})
$\mu_1, \mu_2, \ldots \mu_n$	Macroscopic cross sections of shields 1, 2, ... n (cm^{-1})
t_i	Thickness of i*th* shield (cm)
b_1	$\sum_1^n \mu_i t_i$
b_2	$b_1 + \mu_s Z$
b_3	$b_1 + \mu_s h$
Z	Effective self-attenuation distance (cm)
R_0	Radius of disk, cylinder, or sphere (cm)
B	Symbolic build-up factor
$E_n(b)$	$b^{n-1} \int_b^\infty \frac{e^{-t}}{t^n}\, dt \quad n \geq 0 \quad E_0(b) = \frac{e^{-b}}{b}$
$F(\theta,b)$	$\int_0^\theta e^{-b \sec \theta'}\, d\theta'$
$G(a,b)$	$\int_0^b F\left(\tan^{-1}\frac{a}{b'}, b'\right) db'$ where F is the function defined above
$F_n(t,a)$	$\int_0^t e^{ab} E_n(b)\, db$

Chapter 9

EFFECT OF GEOMETRY OF RADIATION SOURCE

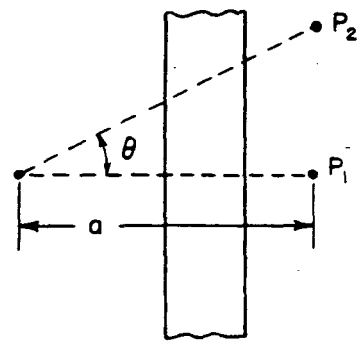
INTRODUCTION

Among the most useful items on the bookshelf of the shield designer is a compilation of formulas for the fluxes from regular geometric sources. One of the earliest such compilations is that of Sievert[1] which appeared in *Acta Radiologica* in 1921. An extension of Sievert's work to include an approximation for the fluxes from cylindrical sources was made in the *Project Handbook*[2] in 1945. These equations have been widely reproduced in the literature on reactor shielding. In recent years exact numerical calculations have been carried out which indicate that some of these equations may, in certain cases, yield answers that are in error by greater than a factor of 10. This chapter consists of a corrected set of equations together with the curves and data necessary for hand computation. Because of the usefulness of these curves in saving time and labor in shielding computations, Parts I to IV were issued as soon as completed as Report WAPD-TN-508.

The quantity B, which appears in each equation, is symbolic for "build-up factor"; a discussion of this factor may be found in Chap. 1. If B is set equal to 1, the equations yield the uncollided flux from the various sources. The attenuating mediums external to the sources are assumed to be in the form of slabs.

Part I Equations for the Flux

I-1 POINT SOURCE



At P_1

$$\phi = B \frac{S_0}{4\pi a^2} e^{-b_1}$$

At P_2

$$\phi = B \frac{S_0}{4\pi (a \sec \theta)^2} e^{-b_1 \sec\theta}$$

I-2 LINE SOURCE

At P_1

$$\phi = B\frac{S_L}{4\pi a}\left[F(\theta_2,b_1) - F(\theta_1,b_1)\right]$$

At P_2

$$\phi = B\frac{S_L}{4\pi a}\left[F(\theta_2,b_1) + F(\theta_1,b_1)\right]$$

At P_2, when $\theta_1 = \theta_2$,

$$\phi = B\frac{S_L}{2\pi a}F(\theta_1,b_1)$$

At P_2, when $l = \infty$ and $\theta_1 = \theta_2 = \pi/2$,

$$\phi = B\frac{S_L}{2\pi a}F\left(\frac{\pi}{2},b_1\right)$$

At P_3, when $\theta_2 = 0$,

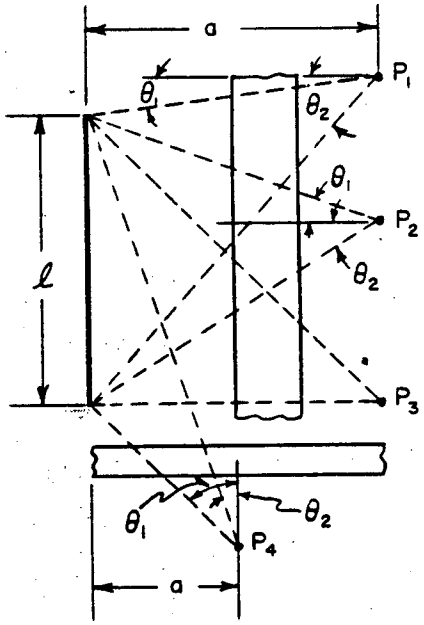
$$\phi = B\frac{S_L}{4\pi a}F(\theta_1,b_1)$$

At P_3, when $\theta_2 = \upsilon$ and $l = \infty$,

$$\phi = B\frac{S_L}{4\pi a}F\left(\frac{\pi}{2},b_1\right)$$

At P_4

$$\phi = B\frac{S_L}{4\pi a}\left[F(\theta_1,b_1) - F(\theta_2,b_1)\right]$$



I-3 DISK SOURCE (K CURVES)

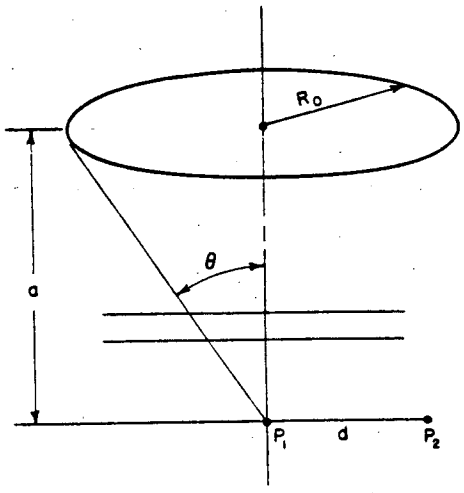
At P_1

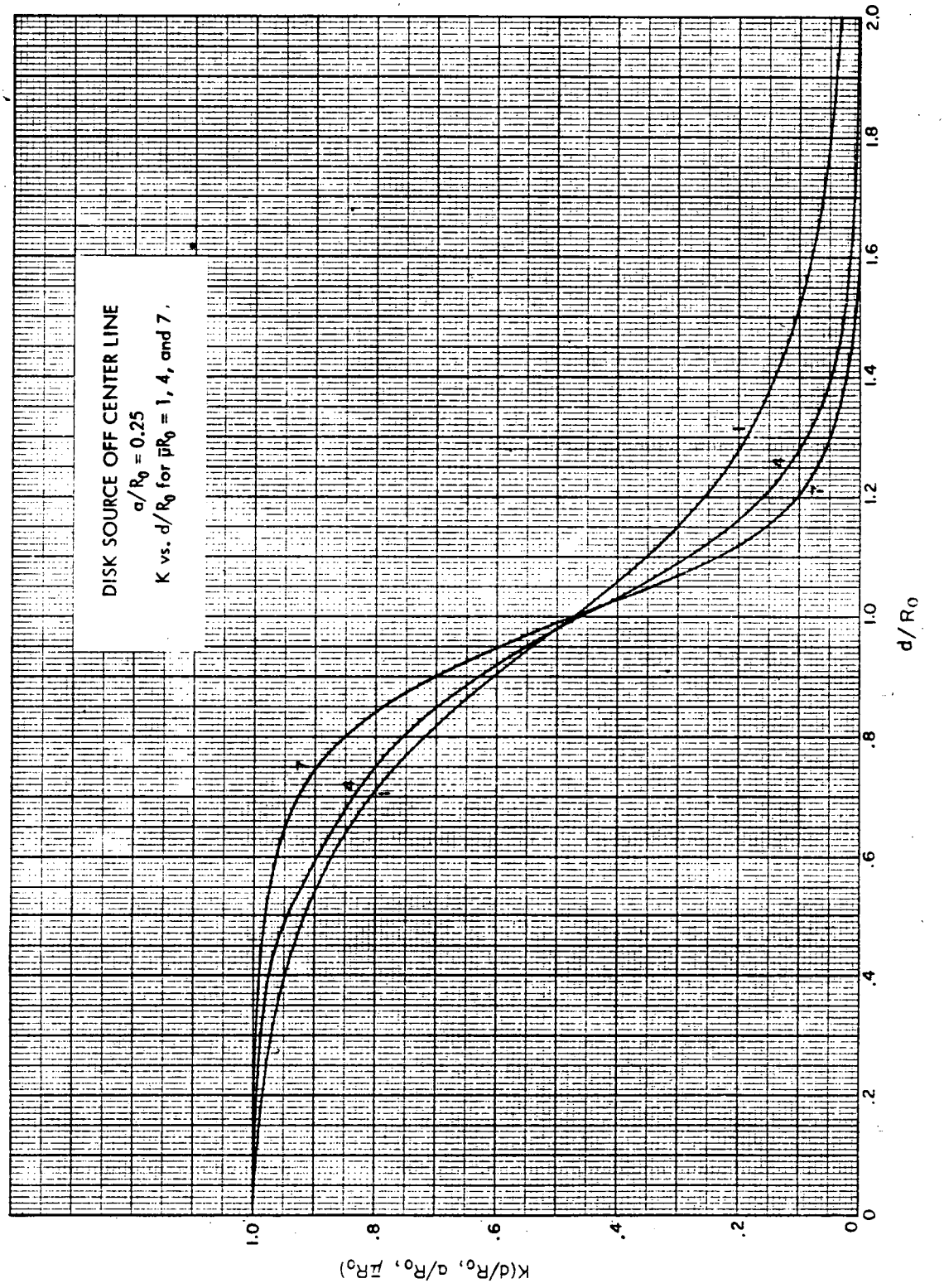
$$\phi = \frac{BSA}{2}\left[E_1(b_1) - E_1(b_1 \sec\theta)\right]$$

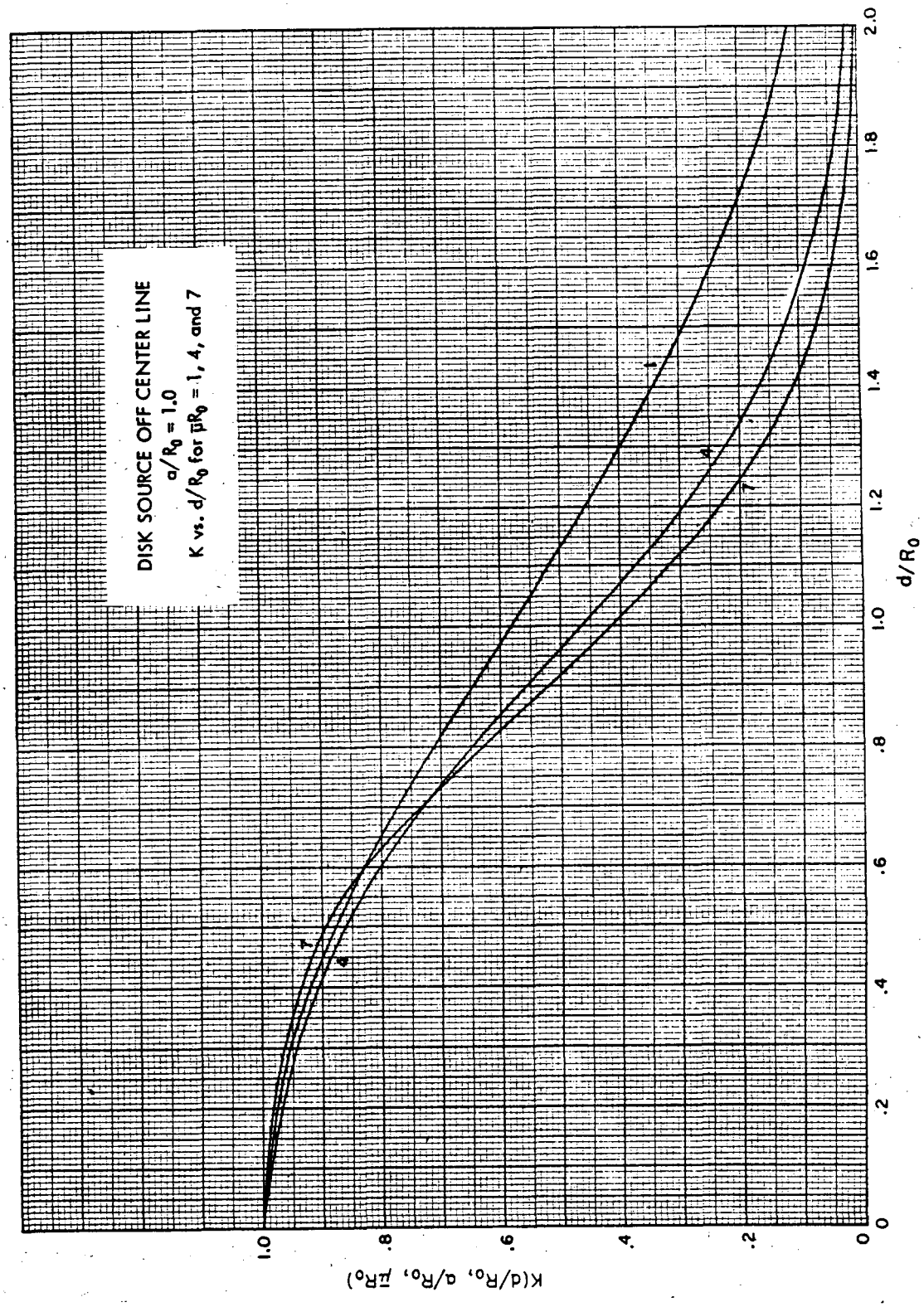
At P_2

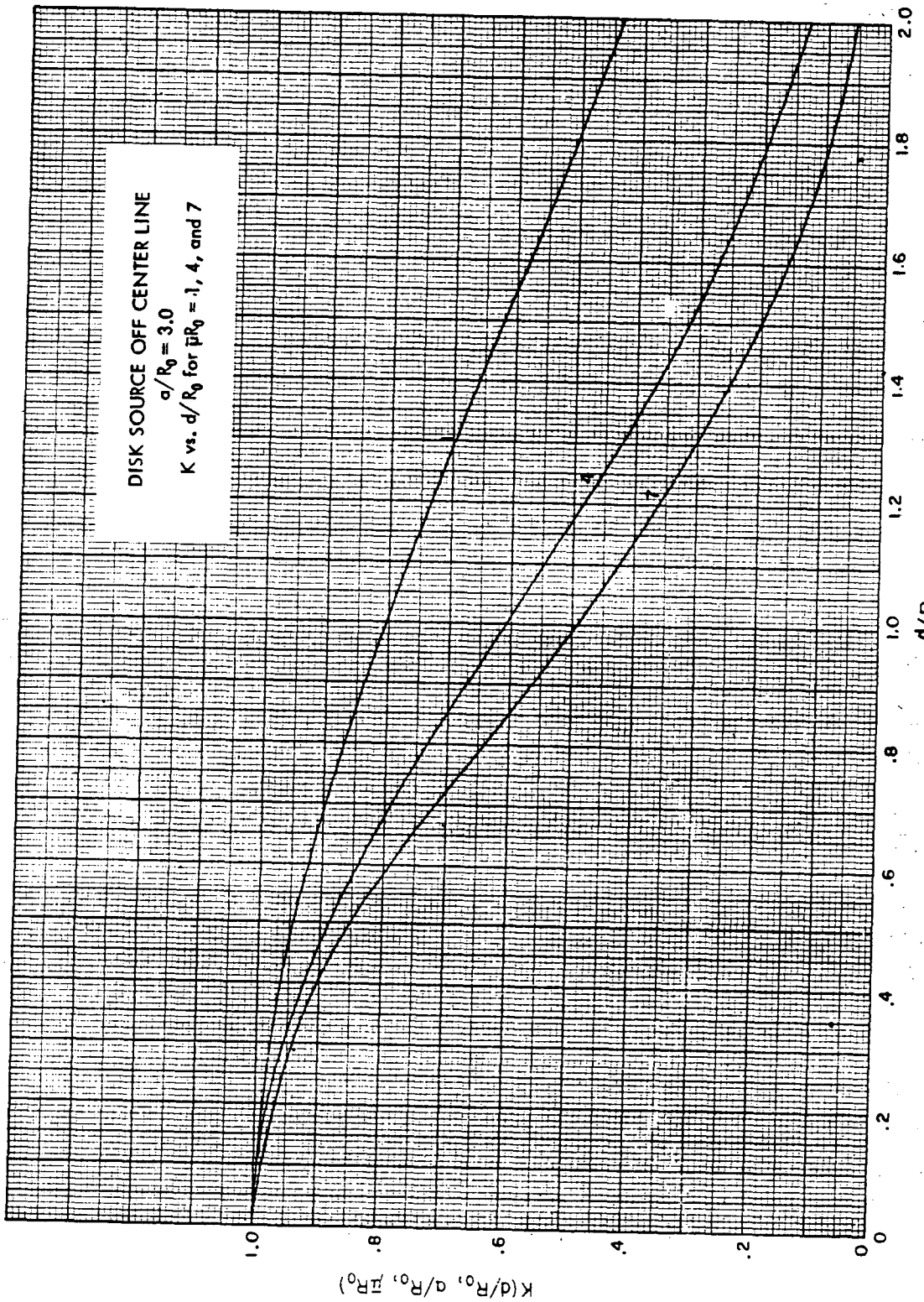
$$\phi = \frac{BSA}{2}\left[E_1(b_1) - E_1(b_1 \sec\theta)\right] \times K\left(\frac{d}{R_0},\frac{a}{R_0},\bar{\mu}R_0\right)$$

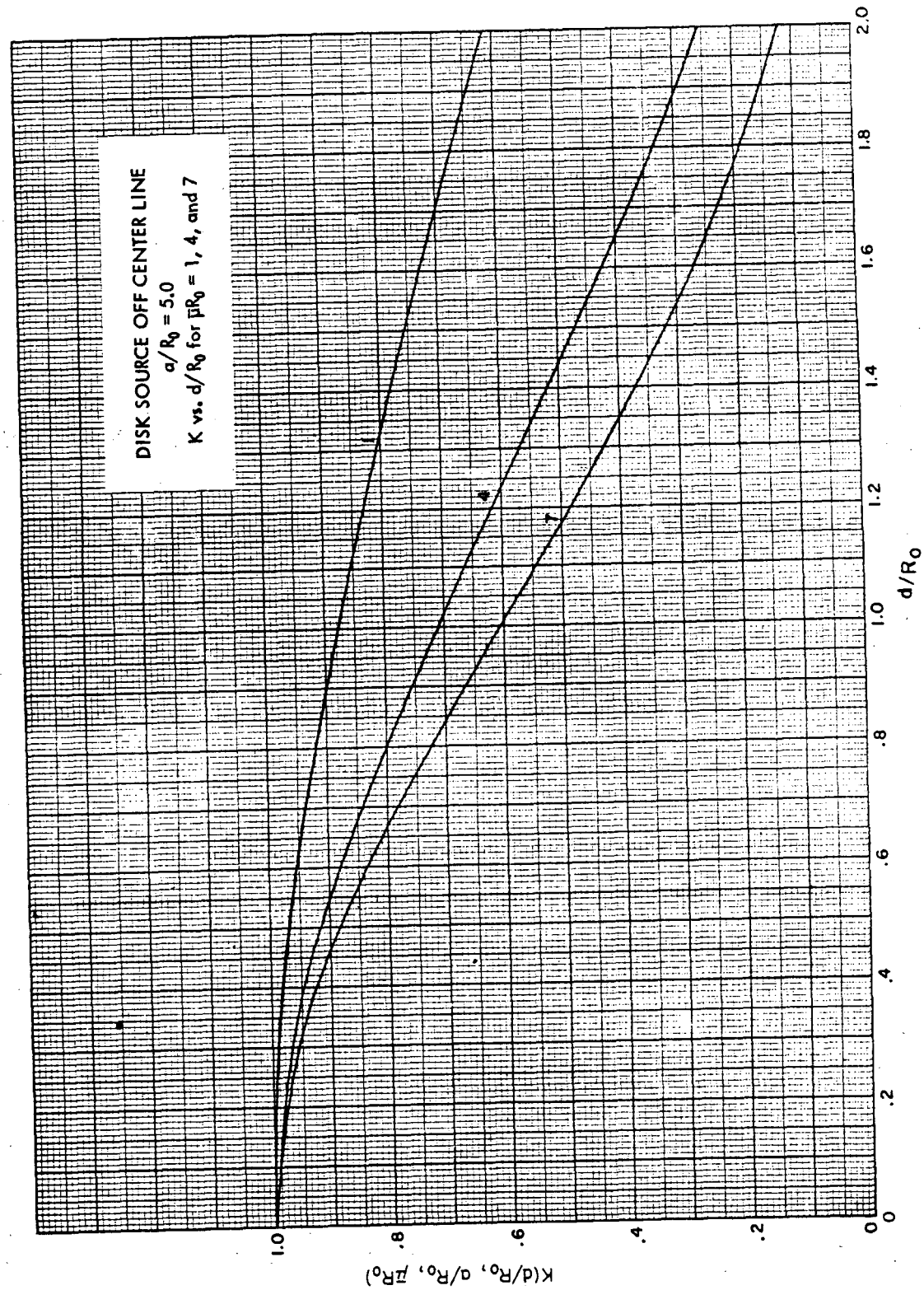
where $\bar{\mu} \equiv \dfrac{\sum_i \mu_i t_i}{\sum_i t_i}$




DISK SOURCE OFF CENTER LINE
a/R0 = 0.25
K vs. d/R0 for ρR0 = 1, 4, and 7.
K(d/R0, a/R0, ρR0)
d/R0
0
.2
.4
.6
.8
1.0
1.2
1.4
1.6
1.8
2.0
1
4
7


DISK SOURCE OFF CENTER LINE
a/R0 = 1.0
K vs. d/R0 for μR0 = 1, 4, and 7
1
4
7
K(d/R0, a/R0, μR0)
1.0
.8
.6
.4
.2
0
0
.2
.4
.6
.8
1.0
1.2
1.4
1.6
1.8
2.0
d/R0

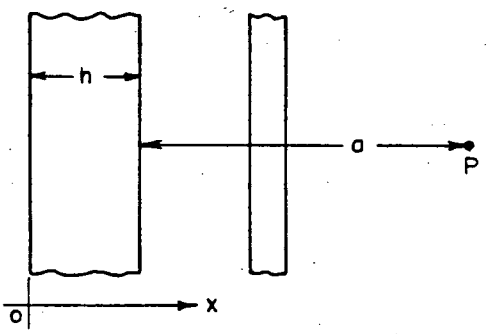

DISK SOURCE OFF CENTER LINE
σ/R0 = 3.0
K vs. d/R0 for μ̄R0 = 1, 4, and 7
1
4
7
K(d/R0, σ/R0, μ̄R0)
d/R0
0
.2
.4
.6
.8
1.0
1.2
1.4
1.6
1.8
2.0


DISK SOURCE OFF CENTER LINE
a/R0 = 5.0
K vs. d/R0 for μR0 = 1, 4, and 7
1
4
7
K(d/R0, a/R0, μR0)
d/R0
0
.2
.4
.6
.8
1.0
1.2
1.4
1.6
1.8
2.0

I-4 INFINITE-SLAB SOURCE

I-4.1 Exterior

At P, a distance a from the slab, if $S_V(x)$ = constant,



$$\phi = \frac{BS_V}{2\mu_s}\left[E_2(b_1) - E_2(b_3)\right]$$

If $S_V(x) = \sum_i S_i e^{k_i x}$,

$$\phi = \frac{B}{2\mu_s}\sum_i S_i e^{k_i b_3/\mu_s}\left[F_1\left(b_3, \frac{-k_i}{\mu_s}\right) - F_1\left(b_1, \frac{-k_i}{\mu_s}\right)\right]$$

If $S_V(x) = \sum_{n=0}^{N} S_n (x+c)^n$,

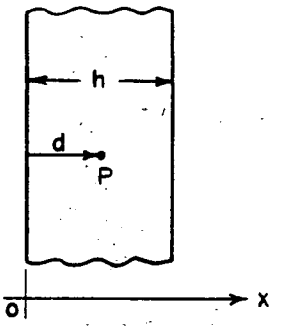
$$\phi = \frac{B}{2\mu_s}\sum_{n=0}^{N} S_n \sum_{i=0}^{n} \frac{(-1)^i n!}{(\mu_s)^i (n-i)!}\left[(h+c)^{n-i}\, E_{2+i}(b_1) - c^{n-i}\, E_{2+i}(b_3)\right]$$

If h = 0, the infinite-plane source obtains, in which case

$$\phi = \frac{BS_A}{2} E_1(b_1)$$

I-4.2 Interior (F_1 Curves)

At P, a distance d from the origin plane, if $S_V(x)$ = constant,



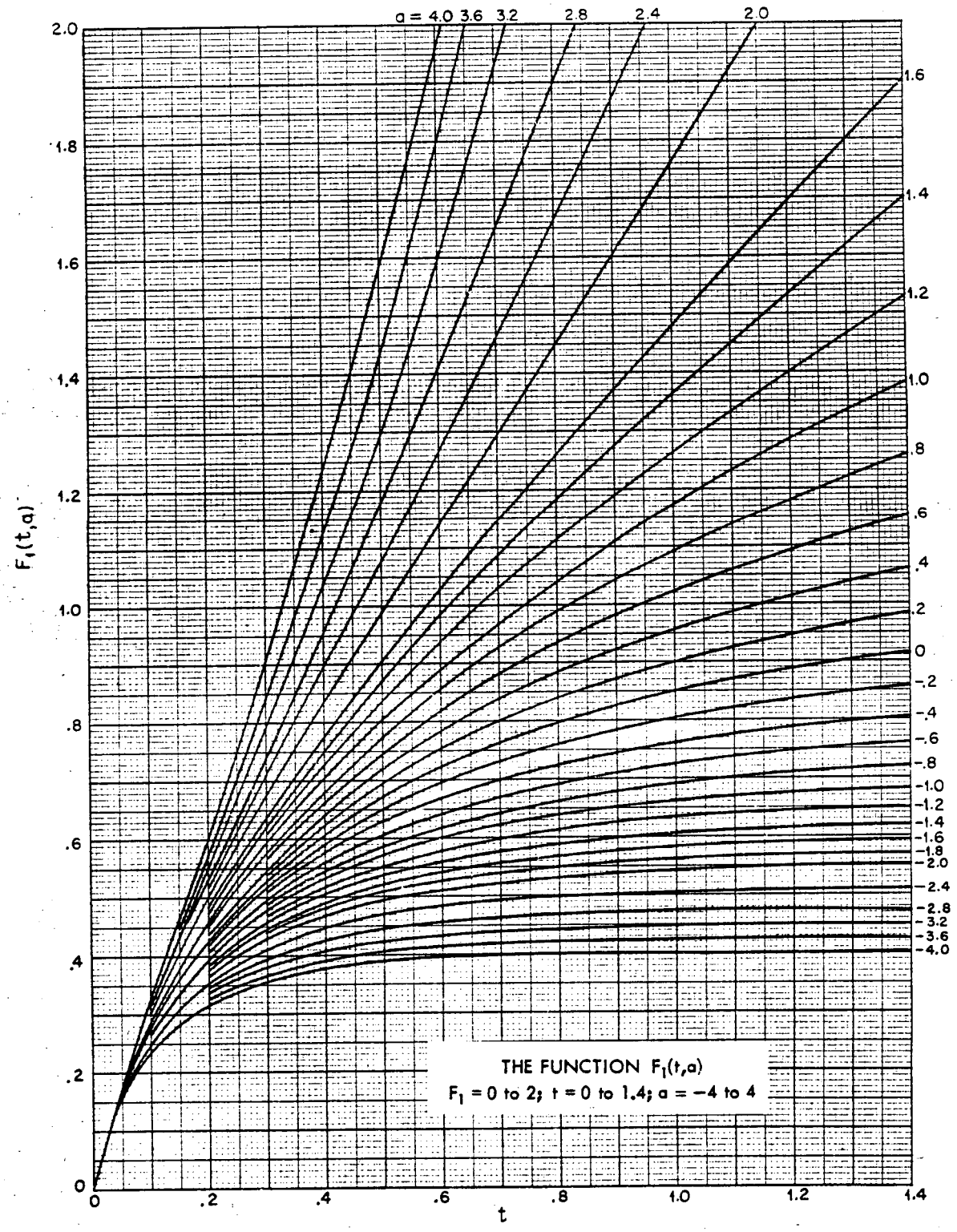
$$\phi = \frac{BS_V}{2\mu_s}\left\{2 - E_2(\mu_s d) - E_2[\mu_s(h-d)]\right\}$$

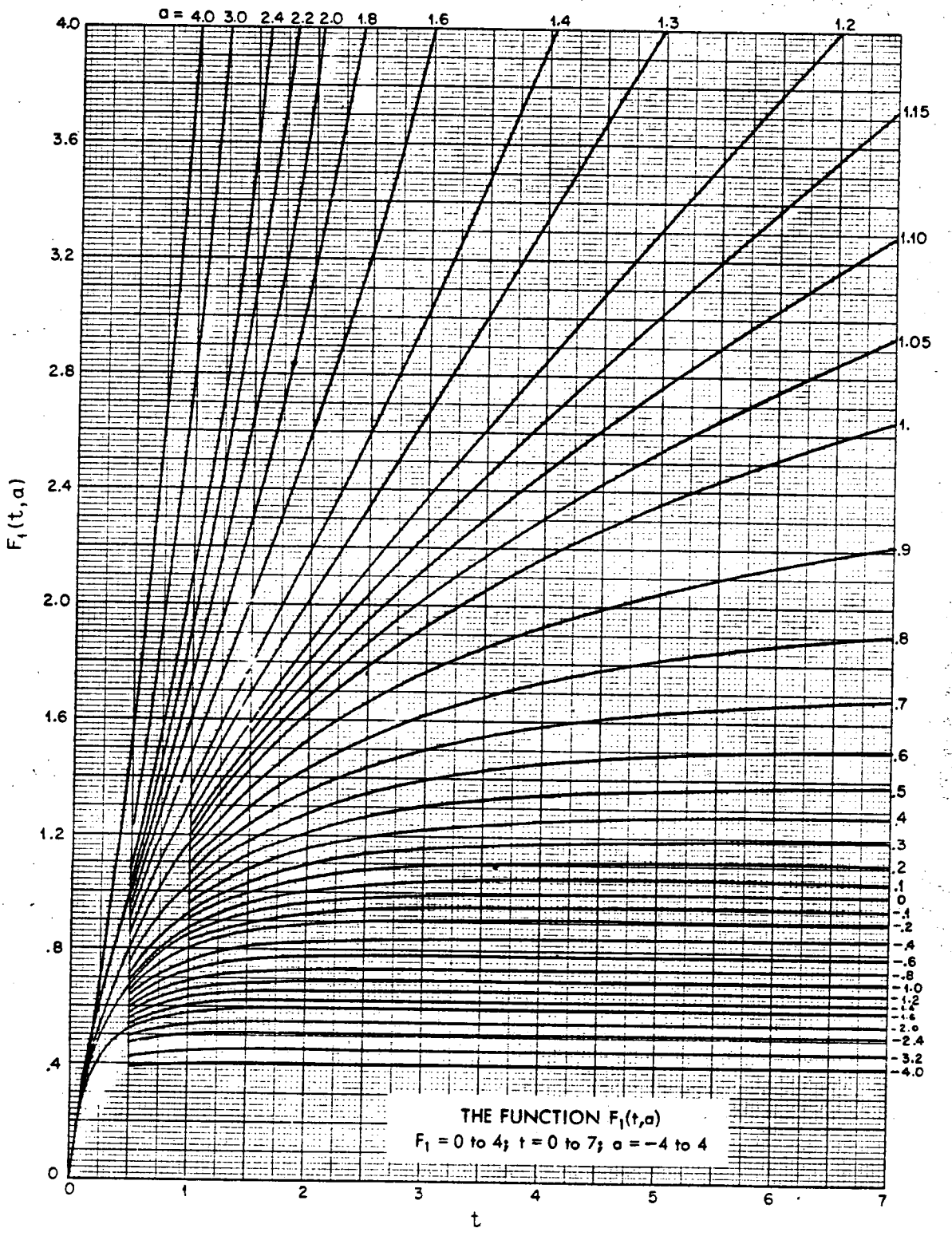
If $S_V(x) = \sum_i S_i e^{k_i x}$,

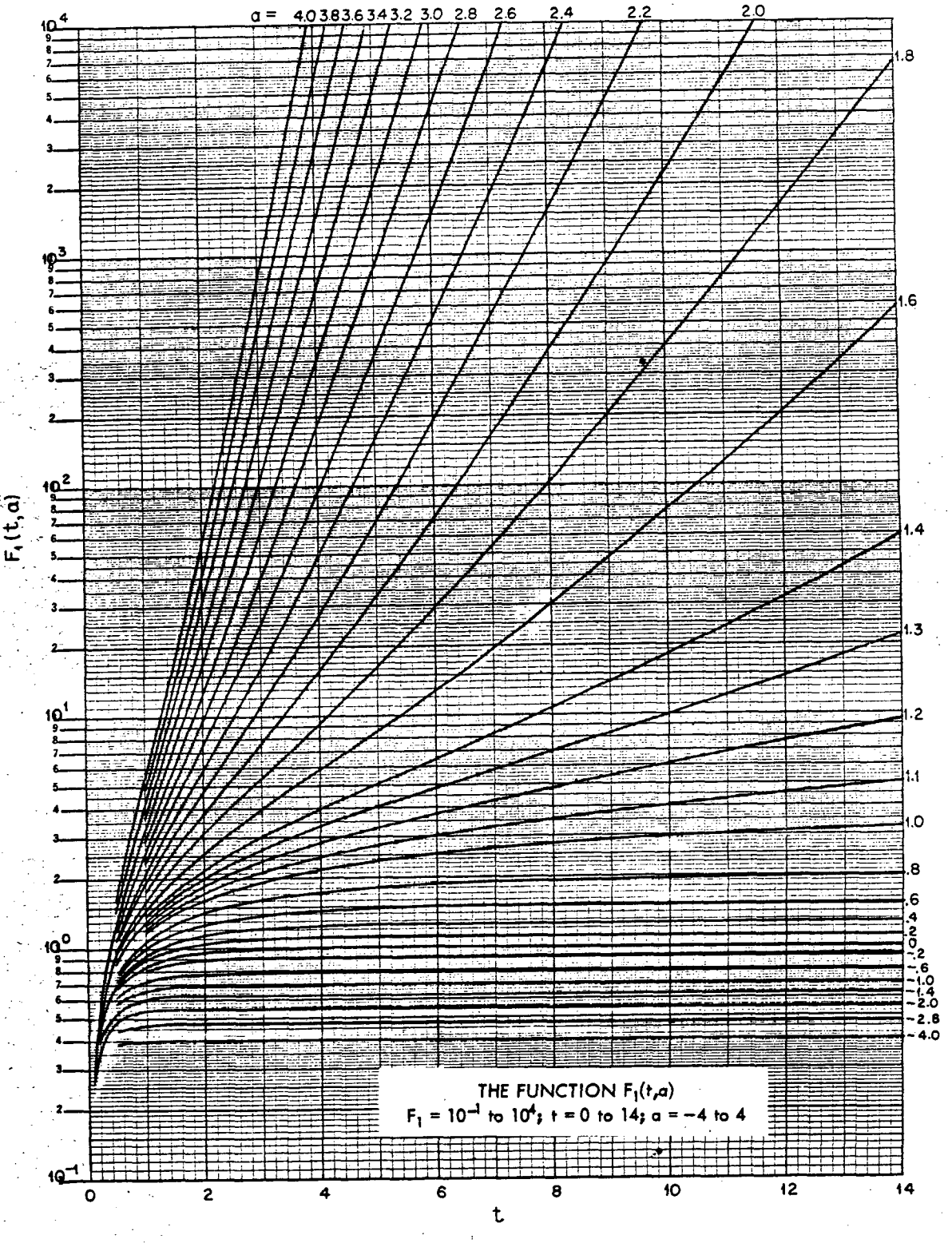
$$\phi = \frac{B}{2\mu_s}\sum_i S_i e^{k_i d}\left\{F_1\left(\mu_s d, \frac{-k_i}{\mu_s}\right) + F_1\left[\mu_s(h-d), \frac{k_i}{\mu_s}\right]\right\}$$

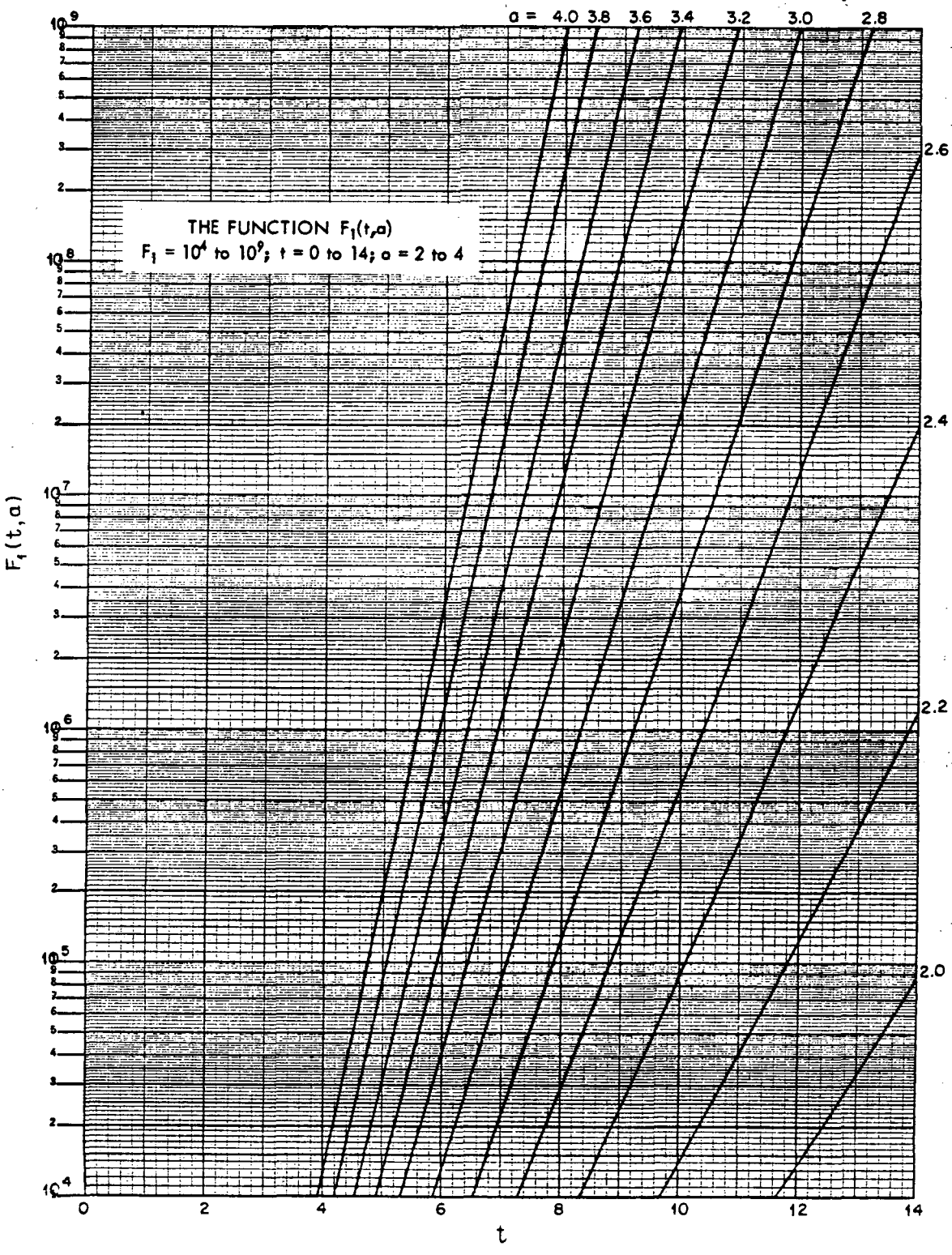
If $S_V(x) = \sum_{n=0}^{N} S_n (x+c)^n$,

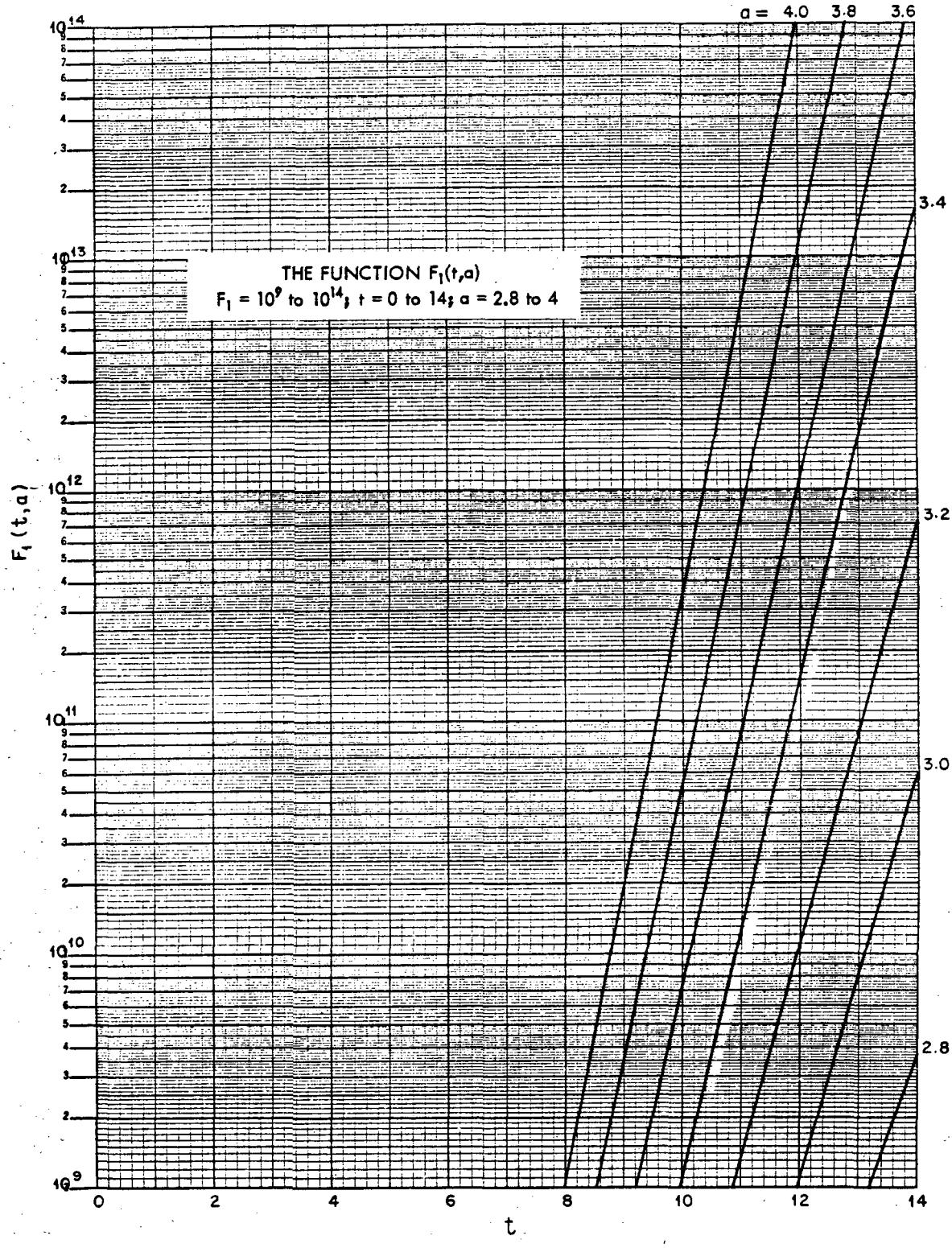
$$\phi = \frac{B}{2\mu_s}\sum_{n=0}^{N}\frac{S_n}{\mu_s^n}\sum_{p=0}^{n}\frac{n!}{(n-p)!}\left\{[1+(-1)^p]\,\frac{[\mu_s(d+c)]^{n-p}}{1+p} - [\mu_s(h+c)]^{n-p}\, E_{2+p}[\mu_s(h-d)] - (-1)^p(\mu_s c)^{n-p}\, E_{2+p}(\mu_s d)\right\}$$


a = 4.0 3.6 3.2 2.8 2.4 2.0
1.6
1.4
1.2
1.0
.8
.6
.4
.2
0
-.2
-.4
-.6
-.8
-1.0
-1.2
-1.4
-1.6
-1.8
-2.0
-2.4
-2.8
-3.2
-3.6
-4.0
$F_1(t,a)$
t
0
.2
.4
.6
.8
1.0
1.2
1.4
1.6
1.8
2.0
THE FUNCTION $F_1(t,a)$
F_1 = 0 to 2; t = 0 to 1.4; a = −4 to 4


a = 4.0 3.0 2.4 2.2 2.0 1.8 1.6 1.4 1.3 1.2
1.15
1.10
1.05
1.
.9
.8
.7
.6
.5
.4
.3
.2
.1
0
-.1
-.2
-.4
-.6
-.8
-1.0
-1.2
-1.4
-1.6
-2.0
-2.4
-3.2
-4.0
4.0
3.6
3.2
2.8
2.4
2.0
1.6
1.2
.8
.4
0
$F_1(t,a)$
0 1 2 3 4 5 6 7
t
THE FUNCTION $F_1(t,a)$
F_1 = 0 to 4; t = 0 to 7; a = −4 to 4


a = 4.0 3.8 3.6 3.4 3.2 3.0 2.8 2.6 2.4 2.2 2.0
1.8
1.6
1.4
1.3
1.2
1.1
1.0
.8
.6
.4
.2
0
-.2
-.6
-1.0
-1.4
-2.0
-2.8
-4.0
$F_1(t,a)$
10^4
10^3
10^2
10^1
10^0
10^{-1}
0 2 4 6 8 10 12 14
t
THE FUNCTION $F_1(t,a)$
$F_1 = 10^{-1}$ to 10^4; t = 0 to 14; a = −4 to 4

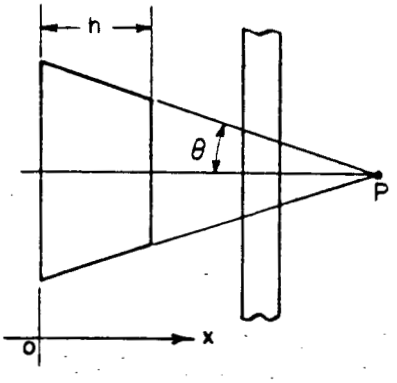

THE FUNCTION $F_1(t,a)$
$F_1 = 10^4$ to 10^9; t = 0 to 14; a = 2 to 4
a = 4.0 3.8 3.6 3.4 3.2 3.0 2.8
2.6
2.4
2.2
2.0
$F_1(t,a)$
t
0 2 4 6 8 10 12 14
10^9 10^8 10^7 10^6 10^5 10^4


a = 4.0 3.8 3.6
3.4
3.2
3.0
2.8
THE FUNCTION $F_1(t,a)$
$F_1 = 10^9$ to 10^{14}; t = 0 to 14; a = 2.8 to 4
$F_1(t,a)$
10^{14}
10^{13}
10^{12}
10^{11}
10^{10}
10^9
0 2 4 6 8 10 12 14
t

I-5 TRUNCATED RIGHT-CIRCULAR CONE SOURCE

At P, the apex of the cone, if $S_V(x) =$ constant,

$$\phi = \frac{BS_V}{2\mu_s}\left[E_2(b_1) - E_2(b_3) + \frac{E_2(b_3 \sec\theta)}{\sec\theta} - \frac{E_2(b_1 \sec\theta)}{\sec\theta}\right]$$



If $S_V(x) = \sum_i S_i e^{k_i x}$, $k_i \neq 0$,

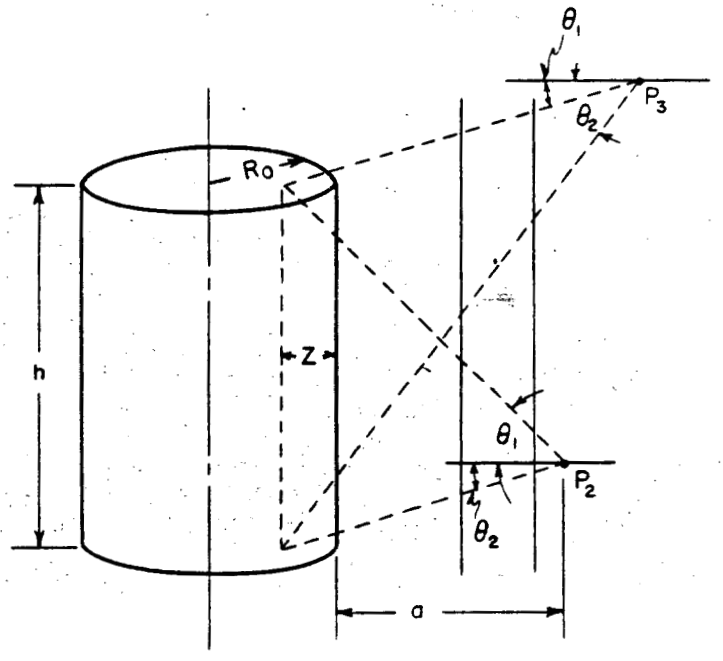
$$\phi = B\sum_i \frac{S_i}{k_i}\left\{e^{k_i h}\left[E_1(b_1) - E_1(b_1 \sec\theta)\right] - e^{k_i b_3/\mu_s} \times \left[E_1\left(b_1\frac{\mu_s + k_i}{\mu_s}\right) - E_1\left(b_3\frac{\mu_s + k_i}{\mu_s}\right)\right] - \left[E_1(b_3) - E_1(b_3\sec\theta)\right] + e^{k_i b_3/\mu_s}\left[E_1\left(b_1\frac{\mu_s \sec\theta + k_i}{\mu_s}\right) - E_1\left(b_3\frac{\mu_s \sec\theta + k_i}{\mu_s}\right)\right]\right\}$$

If $S_V(x) = \sum_{n=0}^{N} S_n (x + c)^n$,

$$\phi = \frac{B}{2\mu_s}\sum_{n=0}^{N} S_n \sum_{i=0}^{n} \frac{(-1)^i\, n!}{(\mu_s)^i\,(n-i)!}\left\{(h+c)^{n-i}\left[E_{2+i}(b_1) - \frac{E_{2+i}(b_1\sec\theta)}{(\sec\theta)^{i+1}}\right] - c^{n-i}\left[E_{2+i}(b_3) - \frac{E_{2+i}(b_3\sec\theta)}{(\sec\theta)^{i+1}}\right]\right\}$$

I-6 CYLINDRICAL SOURCE

I-6.1 Exterior on Side ($\mu_s Z$ Curves)



At P_2

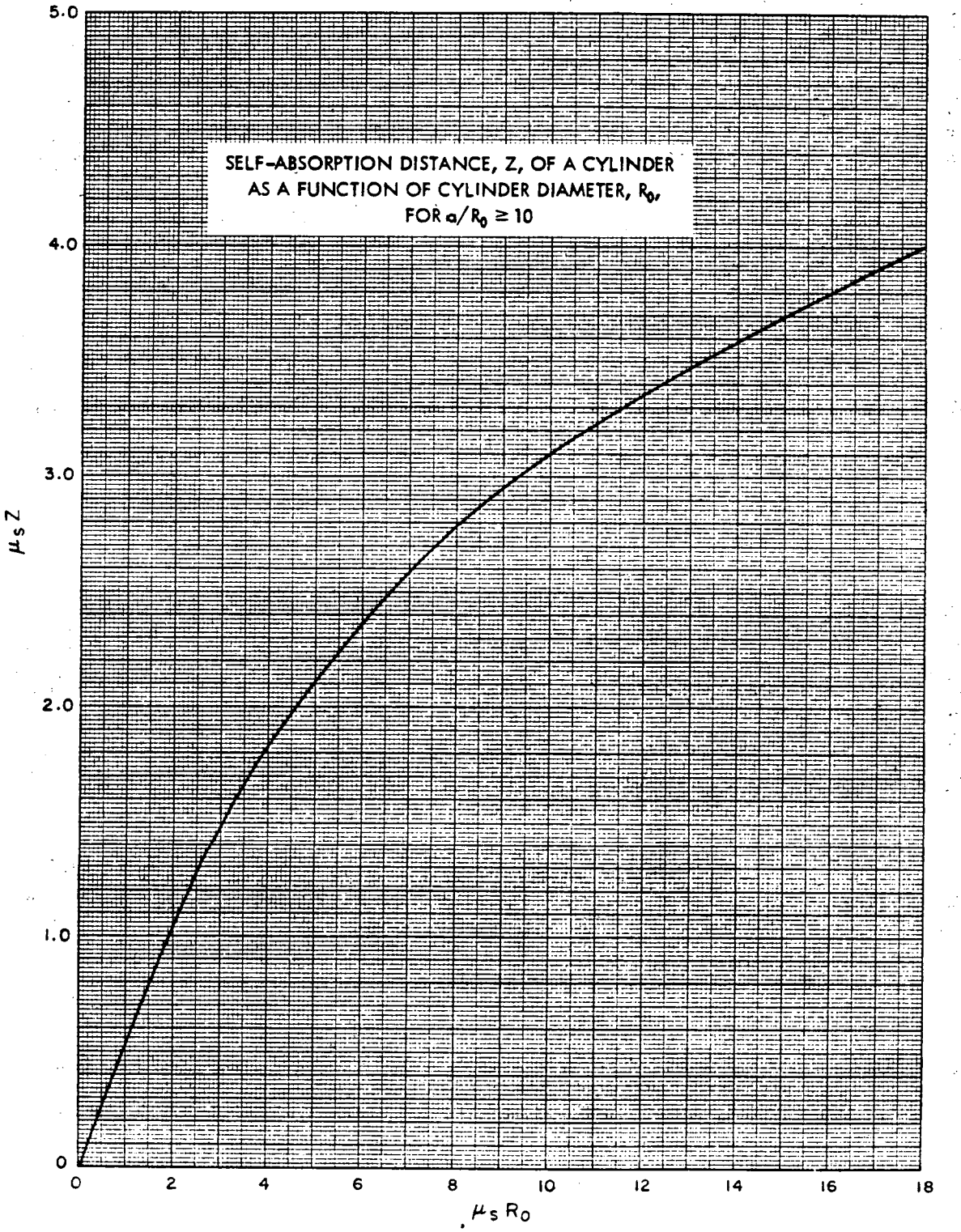
$$\phi = \frac{BS_V R_0^2}{4(a+z)} \left[F(\theta_1, b_2) + F(\theta_2, b_2)\right] \qquad \theta_1 \neq \theta_2$$

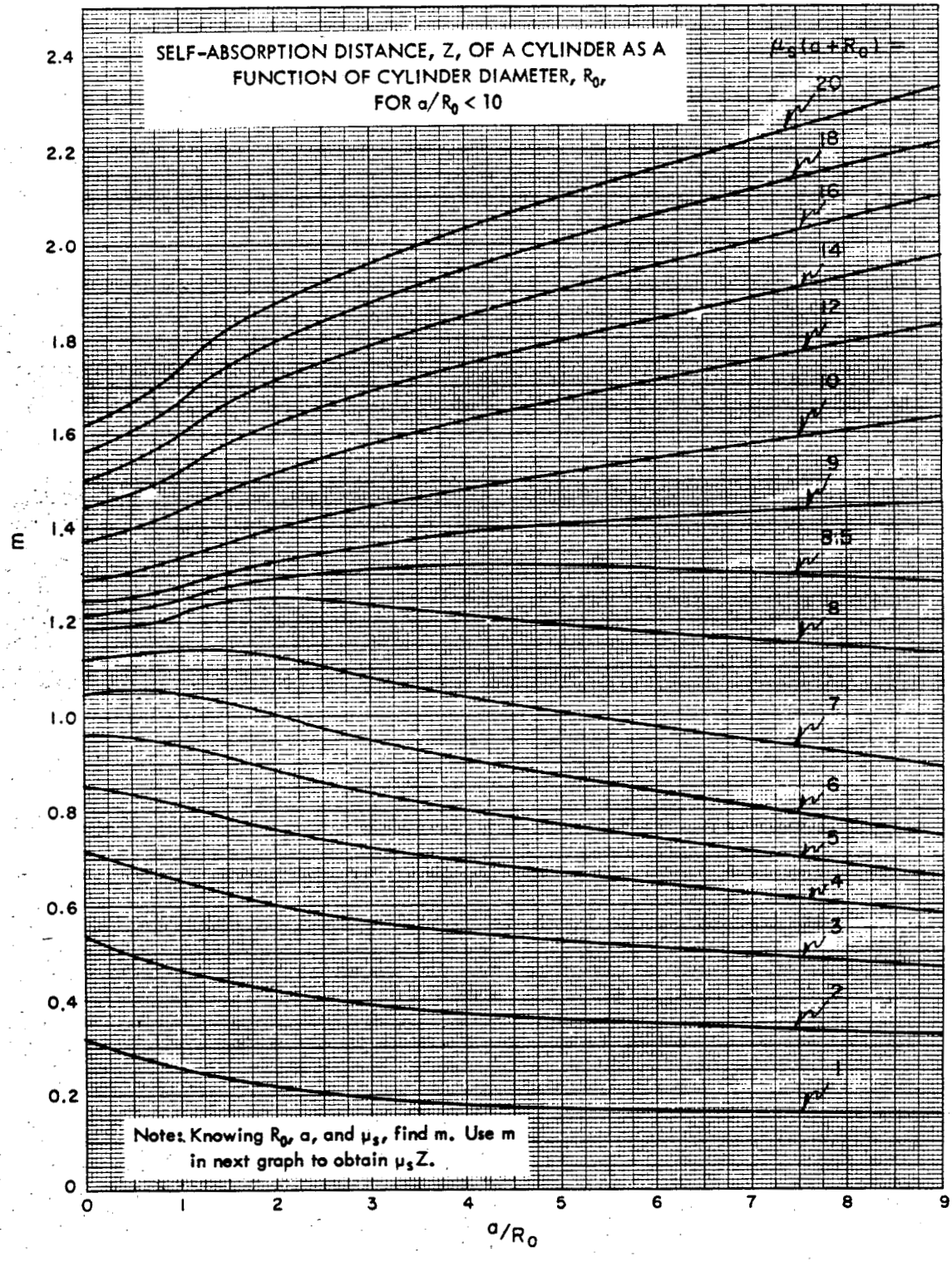
At P_2

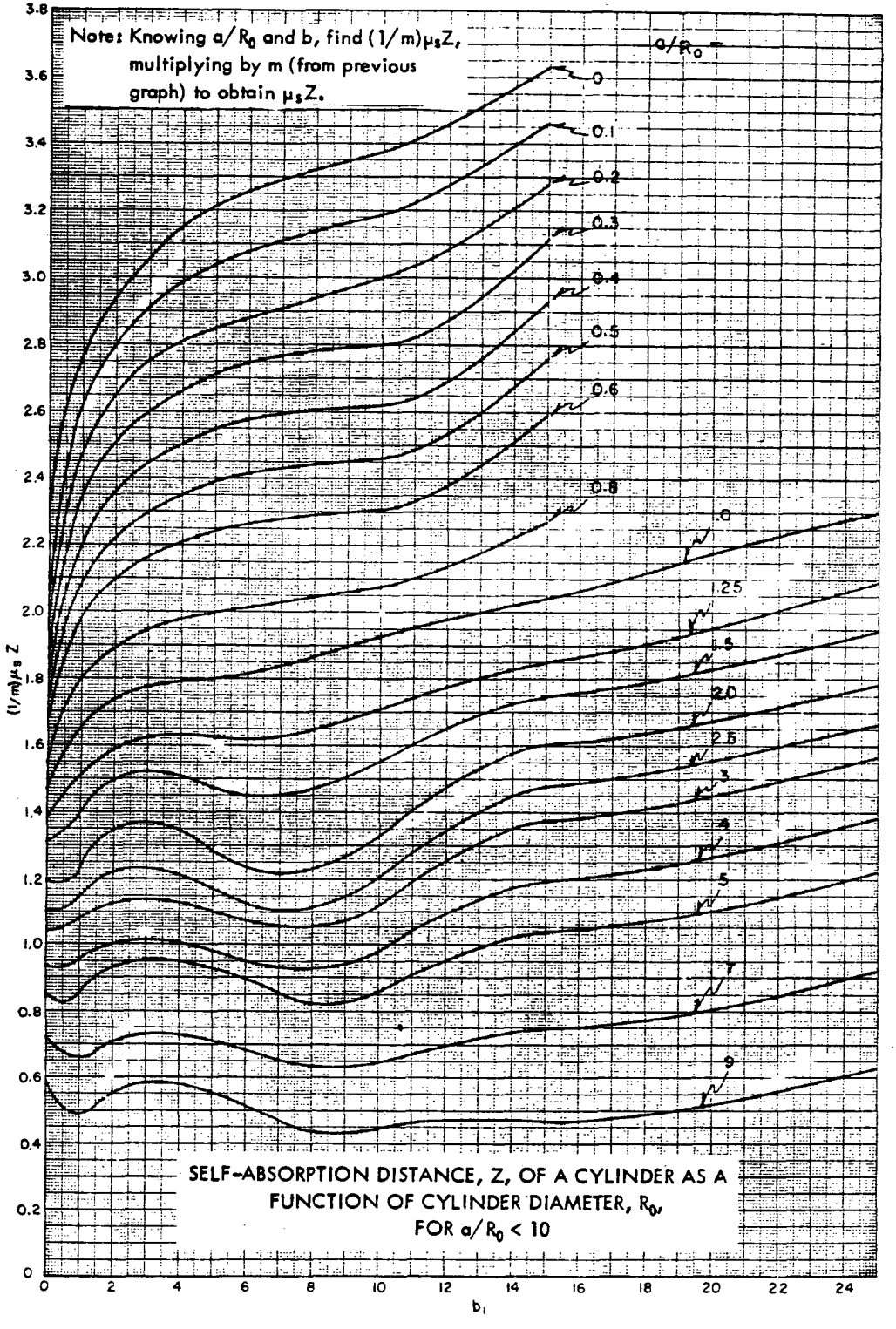
$$\phi = \frac{BS_V R_0^2}{2(a+z)} F(\theta, b_2) \qquad \theta_1 = \theta_2 = \theta \qquad \text{if } h = \infty,\ \theta = \pi/2$$

At P_3

$$\phi = \frac{BS_V R_0^2}{4(a+z)} \left[F(\theta_2, b_2) - F(\theta_1, b_2)\right]$$


SELF-ABSORPTION DISTANCE, Z, OF A CYLINDER AS A FUNCTION OF CYLINDER DIAMETER, R_0, FOR $a/R_0 \geq 10$
5.0
4.0
3.0
2.0
1.0
0
$\mu_s Z$
0
2
4
6
8
10
12
14
16
18
$\mu_s R_0$


SELF-ABSORPTION DISTANCE, Z, OF A CYLINDER AS A FUNCTION OF CYLINDER DIAMETER, R_0, FOR $a/R_0 < 10$
$\mu_s(a+R_0) =$
20
18
16
14
12
10
9
8.5
8
7
6
5
4
3
2
1
E
a/R_0
0
0.2
0.4
0.6
0.8
1.0
1.2
1.4
1.6
1.8
2.0
2.2
2.4
0
1
2
3
4
5
6
7
8
9
Notes: Knowing R_0, a, and μ_s, find m. Use m in next graph to obtain $\mu_s Z$.


Note: Knowing a/R_0 and b, find $(1/m)\mu_s Z$, multiplying by m (from previous graph) to obtain $\mu_s Z$.
a/R_0 =
0
0.1
0.2
0.3
0.4
0.5
0.6
0.8
1.0
1.25
1.5
2.0
2.5
3
4
5
7
9
$(1/m)\mu_s Z$
b_1
SELF-ABSORPTION DISTANCE, Z, OF A CYLINDER AS A FUNCTION OF CYLINDER DIAMETER, R_0, FOR $a/R_0 < 10$

I-6.2 Exterior on End ($h < 3/\mu_s$)

1. Upper limit

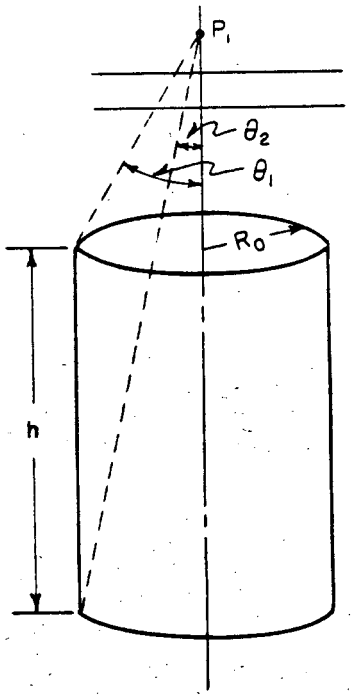
At P_1

$$\phi = \frac{BSV}{2\mu_s}\left[E_2(b_1) - E_2(b_3) + \frac{E_2(b_3 \sec\theta_1)}{\sec\theta_1} - \frac{E_2(b_1 \sec\theta_1)}{\sec\theta_1}\right]$$

2. Lower limit

At P_1

$$\phi = \frac{BSV}{2\mu_s}\left[E_2(b_1) - E_2(b_3) + \frac{E_2(b_3 \sec\theta_2)}{\sec\theta_2} - \frac{E_2(b_1 \sec\theta_2)}{\sec\theta_2}\right]$$



I-6.3 Exterior on End ($h \geq 3/\mu_s$)

1. Upper limit

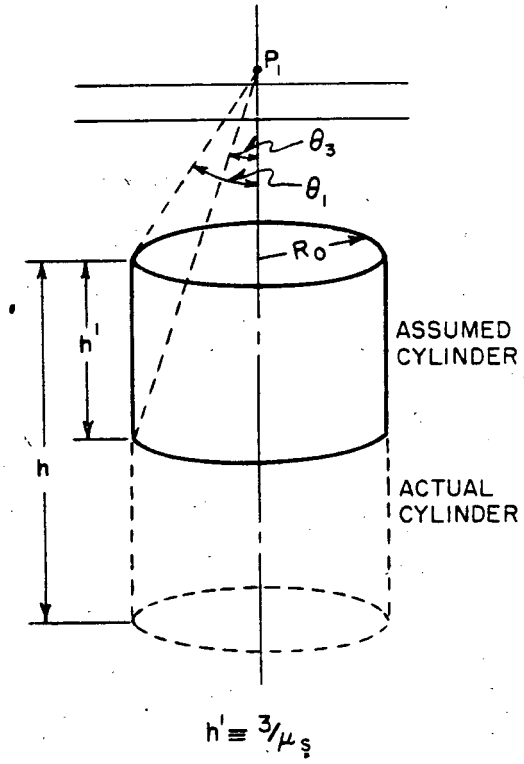
At P_1

$$\phi = \frac{BSV}{2\mu_s}\left[E_2(b_1) - \frac{E_2(b_1 \sec\theta_1)}{\sec\theta_1}\right]$$

2. Lower limit

At P_1

$$\phi = \frac{BSV}{2\mu_s}\left[E_2(b_1) - \frac{E_2(b_1 \sec\theta_3)}{\sec\theta_3}\right]$$



I-6.4 Interior (G Curves)

P_1 and P_2 are on axial center line

At P_1

$$\phi = \frac{BS_V}{2\mu_s} [G(\mu_s h_1, b) + G(\mu_s h_2, b)]$$

where $b \equiv \mu_s R_0$.

At P_2

$$\phi = \frac{BS_V}{2\mu_s} G(\mu_s h, b)$$

where $b \equiv \mu_s R_0$.

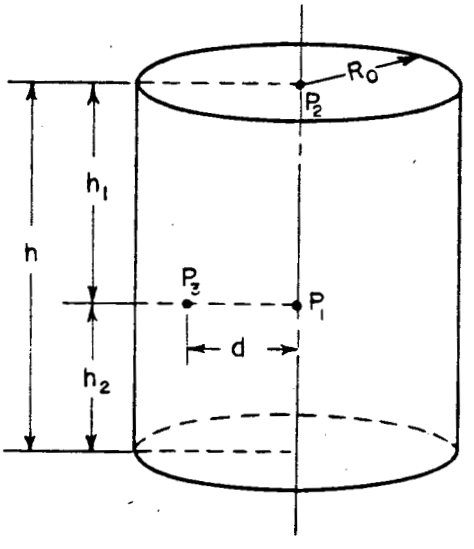
At P_3, upper limit,

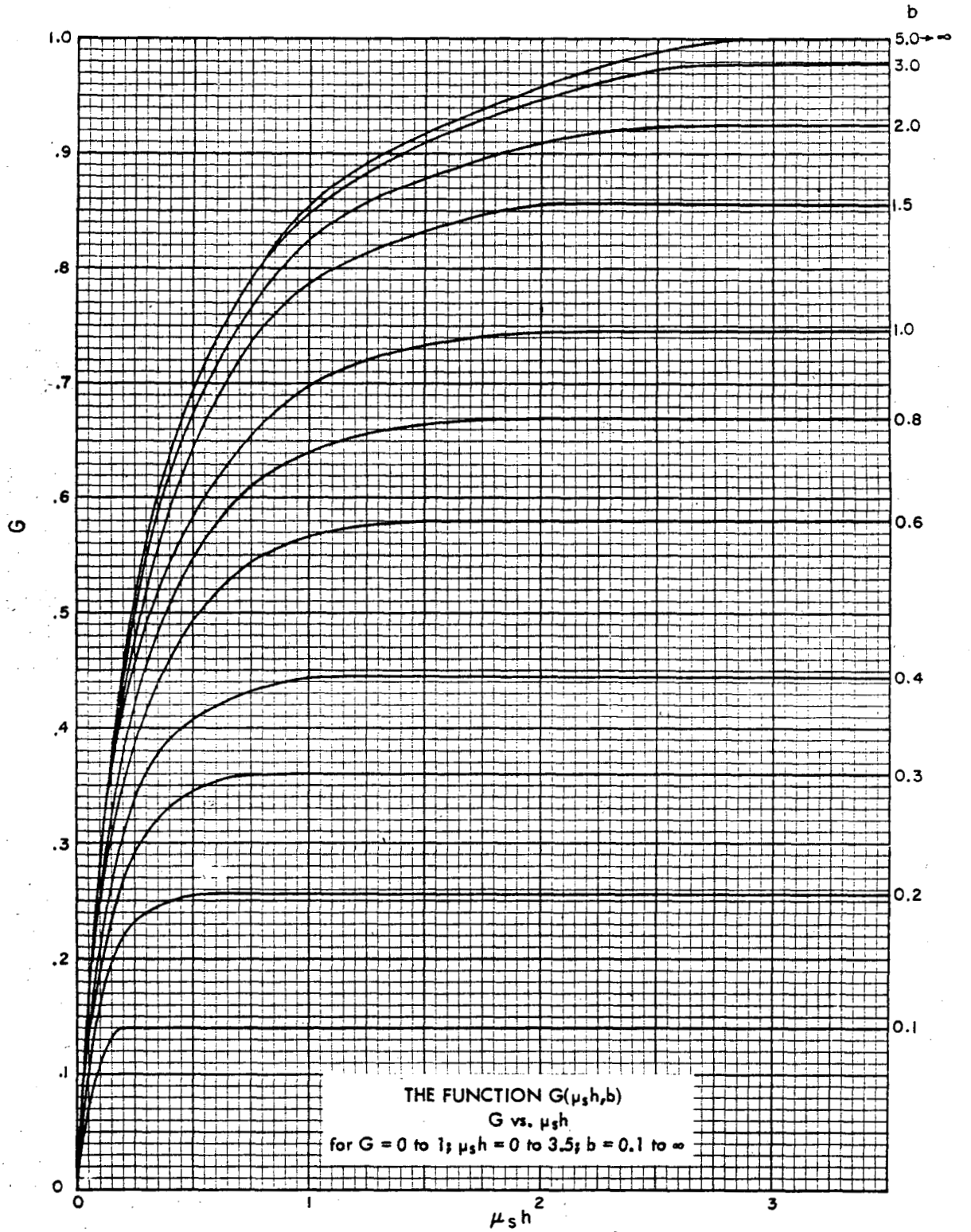
$$\phi = \frac{BS_V}{4\mu_s} [G(\mu_s h_1, b_5) + G(\mu_s h_2, b_5) + G(\mu_s h_1, b_6) + G(\mu_s h_2, b_6)]$$

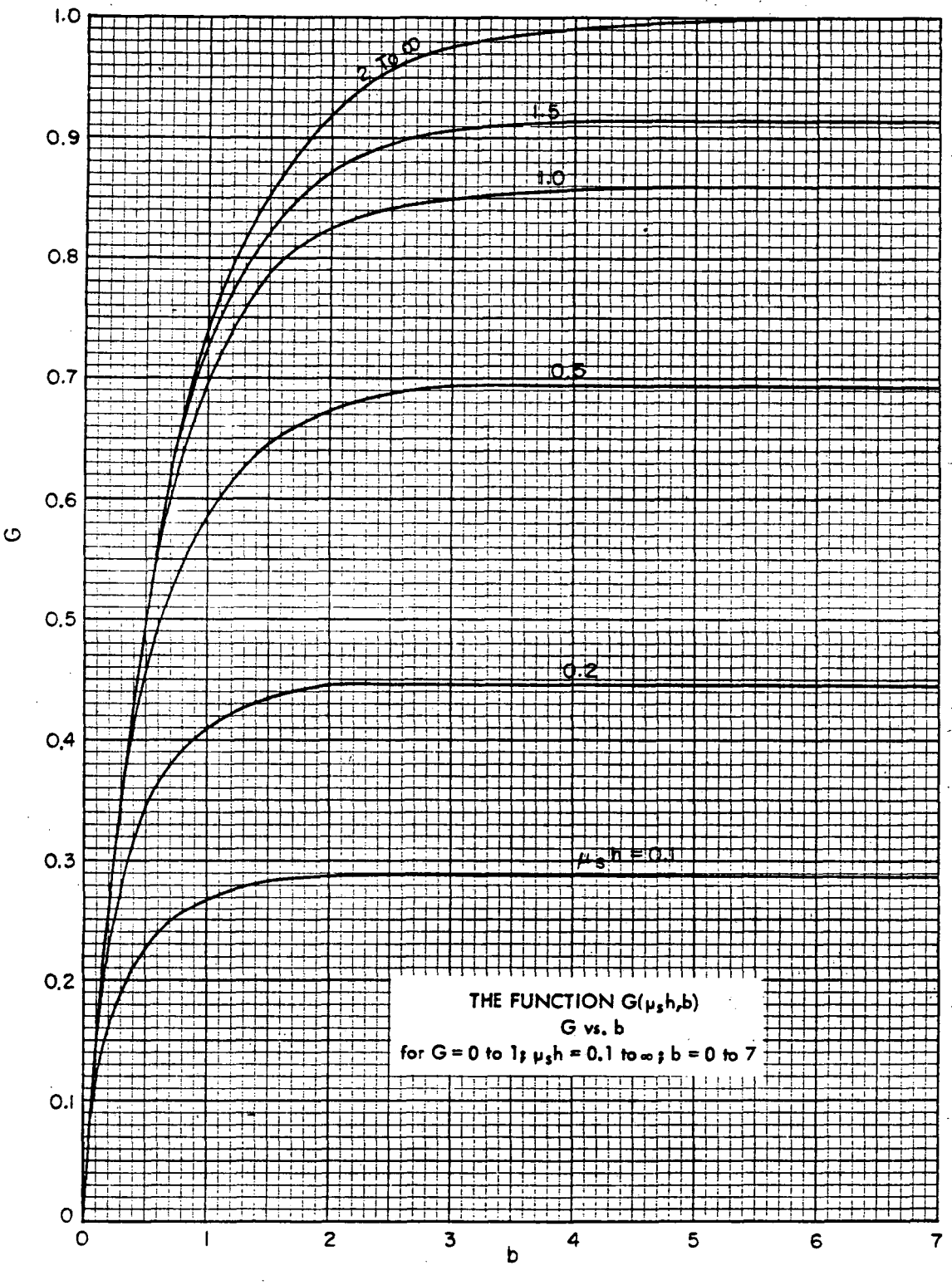
At P_3, lower limit,

$$\phi = \frac{BS_V}{4\mu_s} [G(\mu_s h_1, b_6) + G(\mu_s h_2, b_6) + G(\mu_s h_1, b_4) + G(\mu_s h_2, b_4)]$$

where $b_4 \equiv \mu_s(R_0 - d)$, $b_5 \equiv \mu_s(R_0 + d)$, and $b_6 \equiv \mu_s\sqrt{R_0^2 - d^2}$

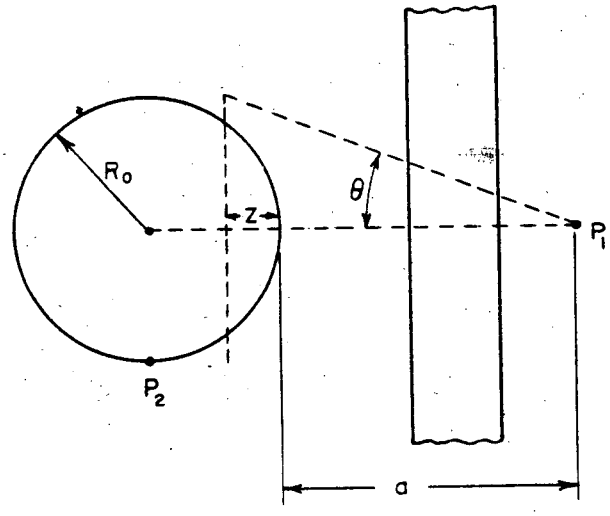



b
5.0→∞
3.0
2.0
1.5
1.0
0.8
0.6
0.4
0.3
0.2
0.1
G
1.0
.9
.8
.7
.6
.5
.4
.3
.2
.1
0
0
1
2
3
$\mu_s h$
THE FUNCTION G(μ_sh,b)
G vs. μ_sh
for G = 0 to 1; μ_sh = 0 to 3.5; b = 0.1 to ∞


1.0
0.9
0.8
0.7
0.6
0.5
0.4
0.3
0.2
0.1
0
G
0
1
2
3
4
5
6
7
b
2 TO ∞
1.5
1.0
0.5
0.2
μsh = 0.1
THE FUNCTION G(μsh,b)
G vs. b
for G = 0 to 1; μsh = 0.1 to ∞; b = 0 to 7

I-7 SPHERICAL SOURCE

I-7.1 Exterior (Z Curves)

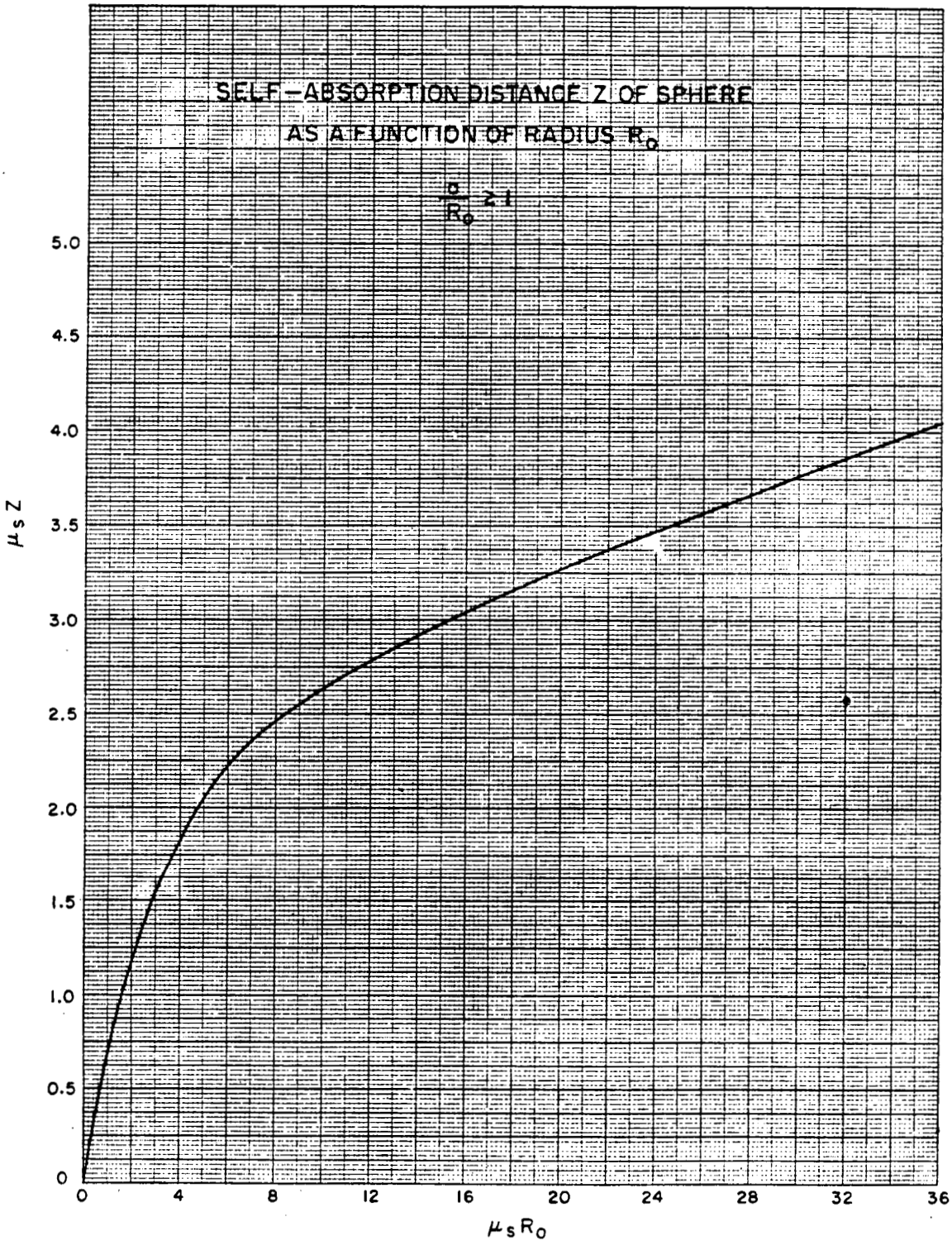


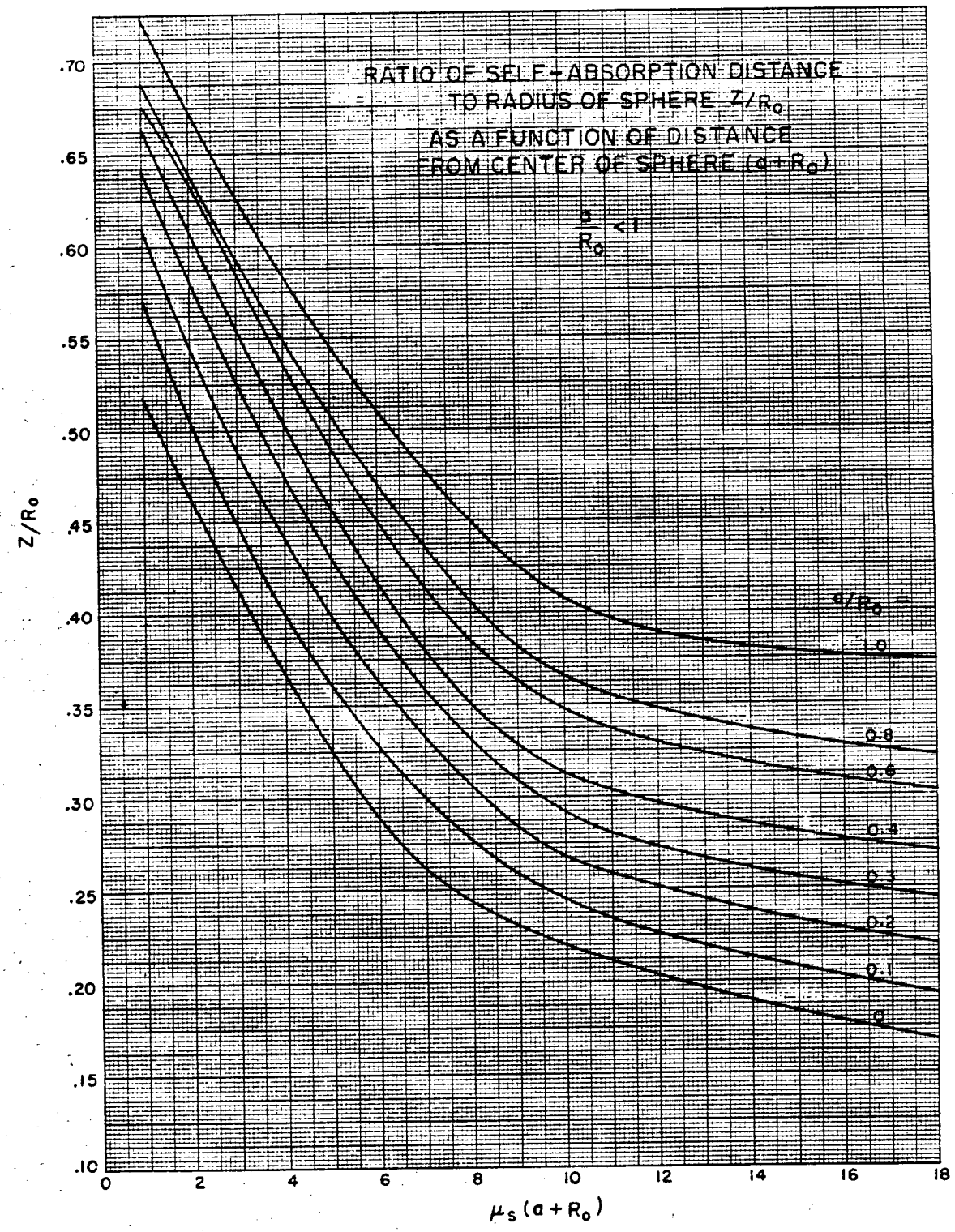
At P_1

$$\phi = \tfrac{2}{3}BS_V R_0[E_1(b_2) - E_1(b_2 \sec \theta)]$$

At P_2, if $b_1 = 0$,

$$\phi = \frac{BS_V}{2\mu_s}\left(1 - \frac{1}{2\mu_s R_0} + \frac{e^{-2\mu_s R_0}}{2\mu_s R_0}\right)$$

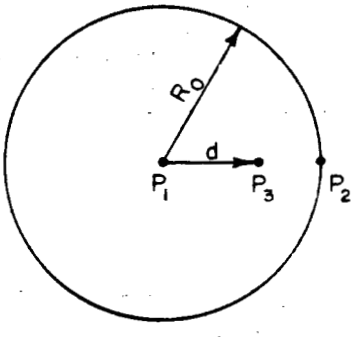

SELF-ABSORPTION DISTANCE Z OF SPHERE
AS A FUNCTION OF RADIUS R_0
$\frac{a}{R_0} \geq 1$
$\mu_s Z$
$\mu_s R_0$
0
0.5
1.0
1.5
2.0
2.5
3.0
3.5
4.0
4.5
5.0
0
4
8
12
16
20
24
28
32
36


RATIO OF SELF-ABSORPTION DISTANCE TO RADIUS OF SPHERE Z/R_0 AS A FUNCTION OF DISTANCE FROM CENTER OF SPHERE $(a+R_0)$
$\frac{a}{R_0} < 1$
Z/R_0
.70
.65
.60
.55
.50
.45
.40
.35
.30
.25
.20
.15
.10
0
2
4
6
8
10
12
14
16
18
$\mu_s (a+R_0)$
$a/R_0 =$
1.0
0.8
0.6
0.4
0.2
0.1
0

I-7.2 Interior

At P_1

$$\phi = \frac{BS_V}{\mu_s}\ (1 - e^{-\mu_s R_0})$$



At P_2

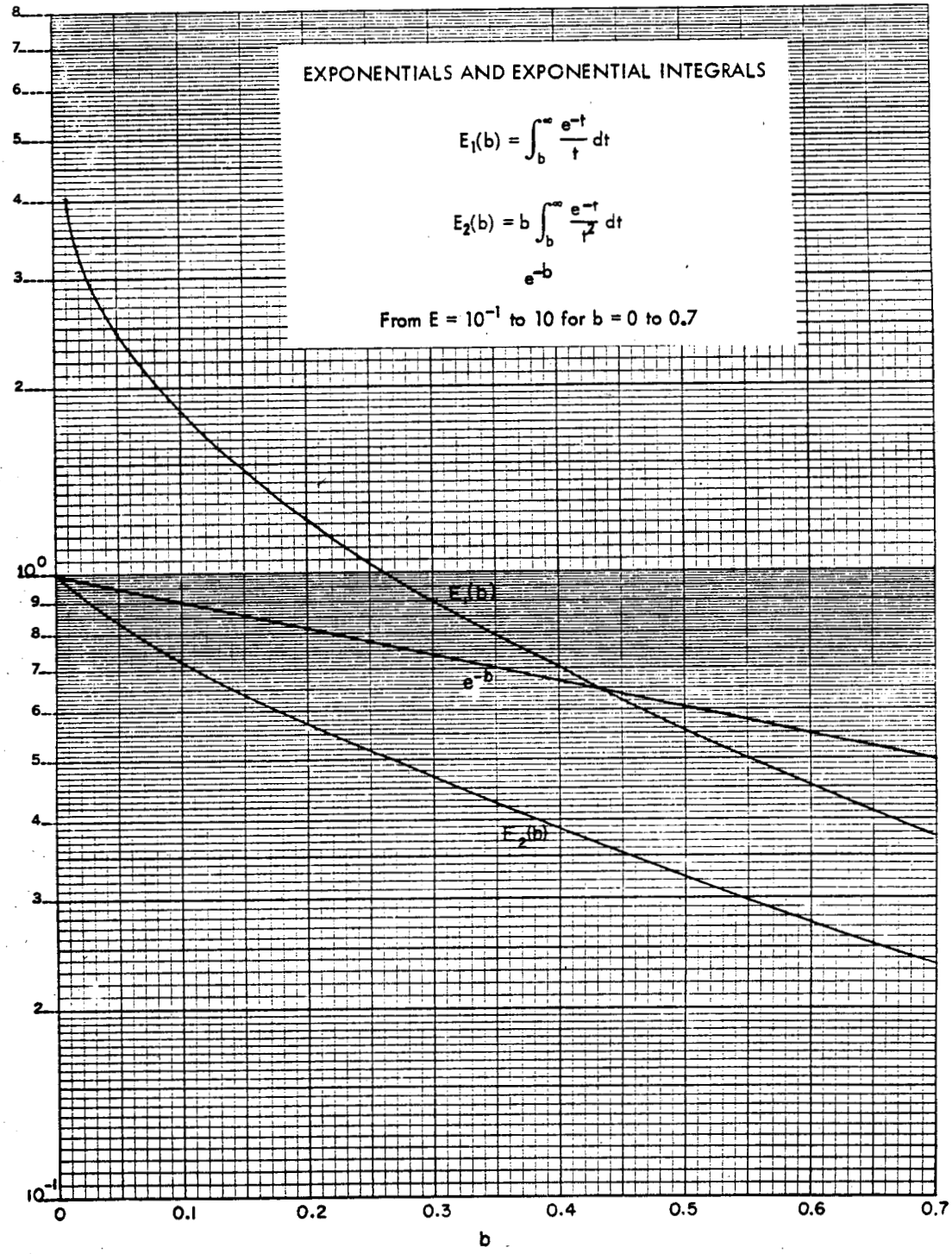
$$\phi = \frac{BS_V}{2\mu_s}\left(1 - \frac{1}{2\mu_s R_0} + \frac{e^{-2\mu_s R_0}}{2\mu_s R_0}\right)$$

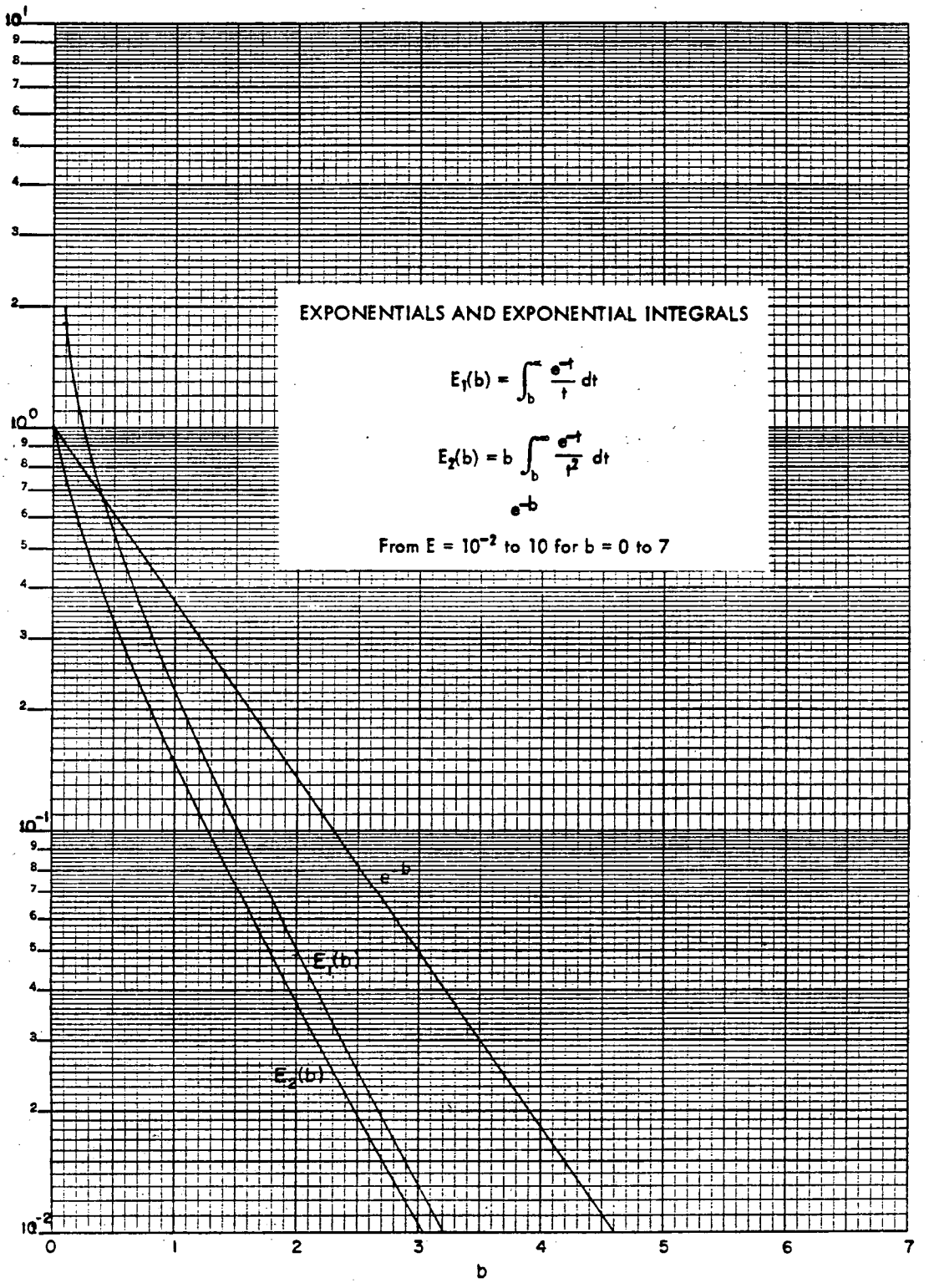
At P_3

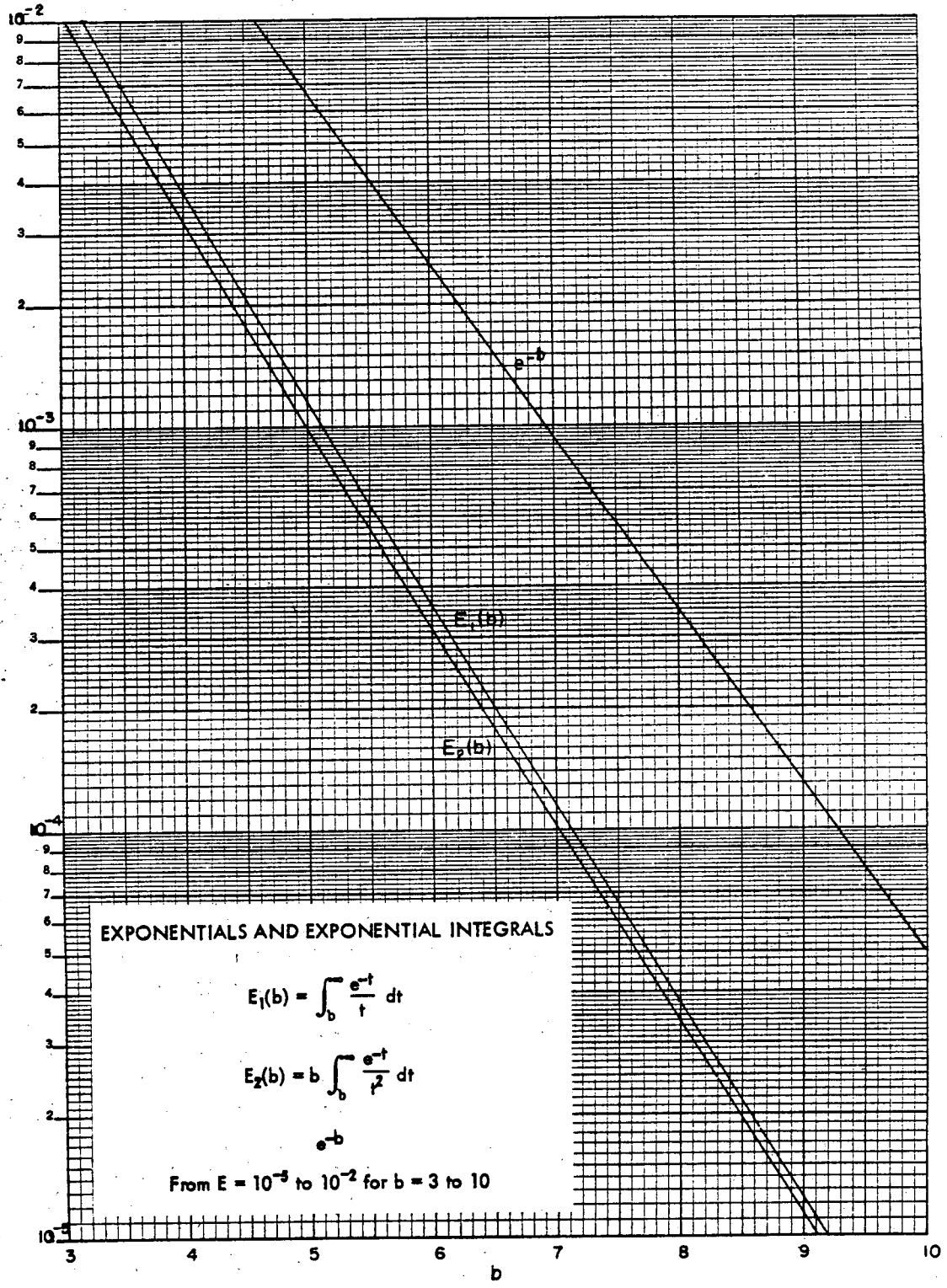
$$\phi = \frac{BS_V}{\mu_s}\left\{1 - \frac{e^{-b_4}}{2} - \frac{e^{-b_5}}{2} - \frac{1}{4\mu_s d}\left[e^{-b_4}(1 + b_4) - e^{-b_5}(1 + b_5)\right] + \frac{b_4 b_5}{4\mu_s d}\left[E_1(b_4) - E_1(b_5)\right]\right\}$$

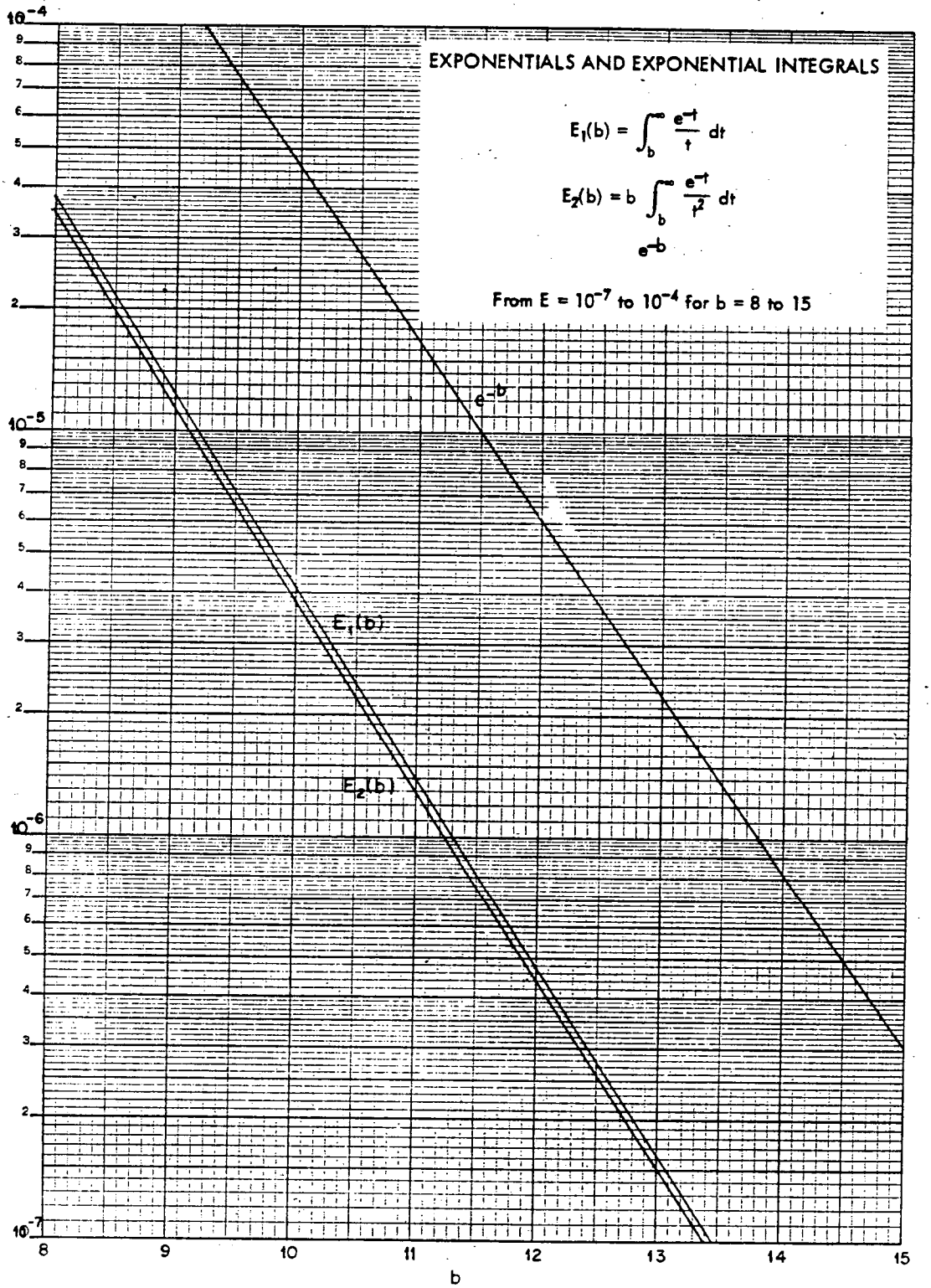
where $b_4 \equiv \mu_s(R_0 - d)$ and $b_5 \equiv \mu_s(R_0 + d)$.

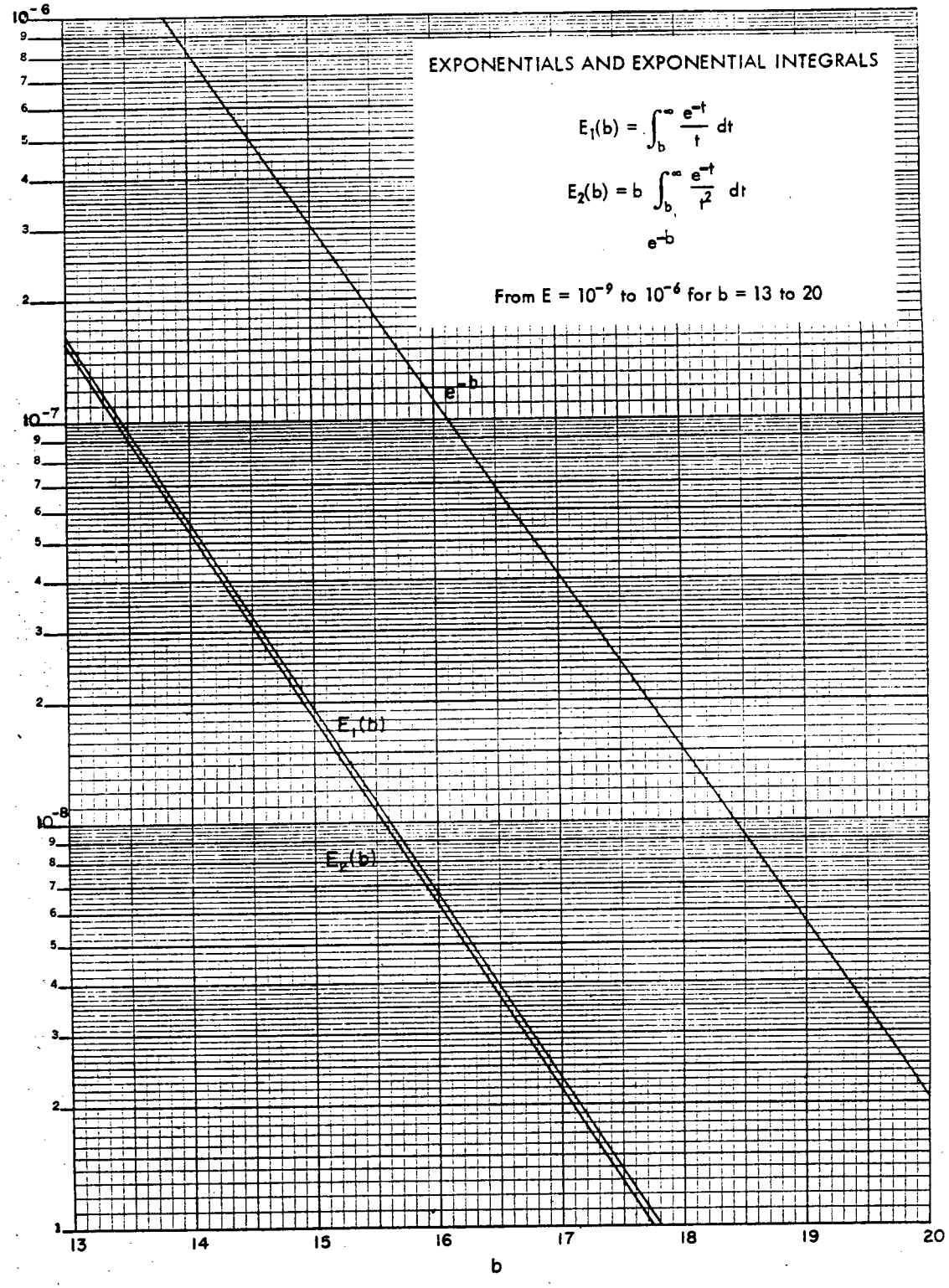
I-8 e^{-b}, $E_1(b)$, AND $E_2(b)$

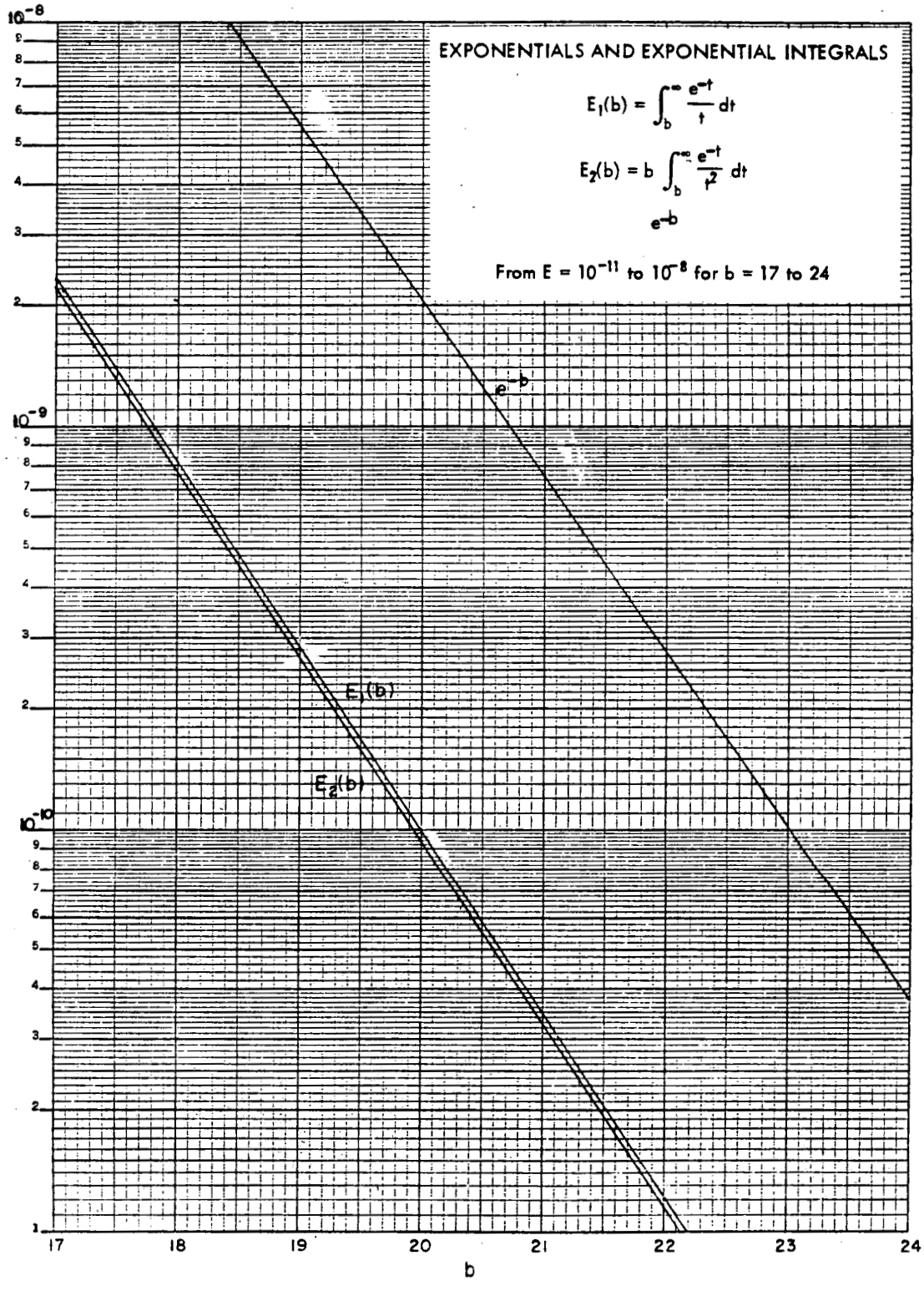


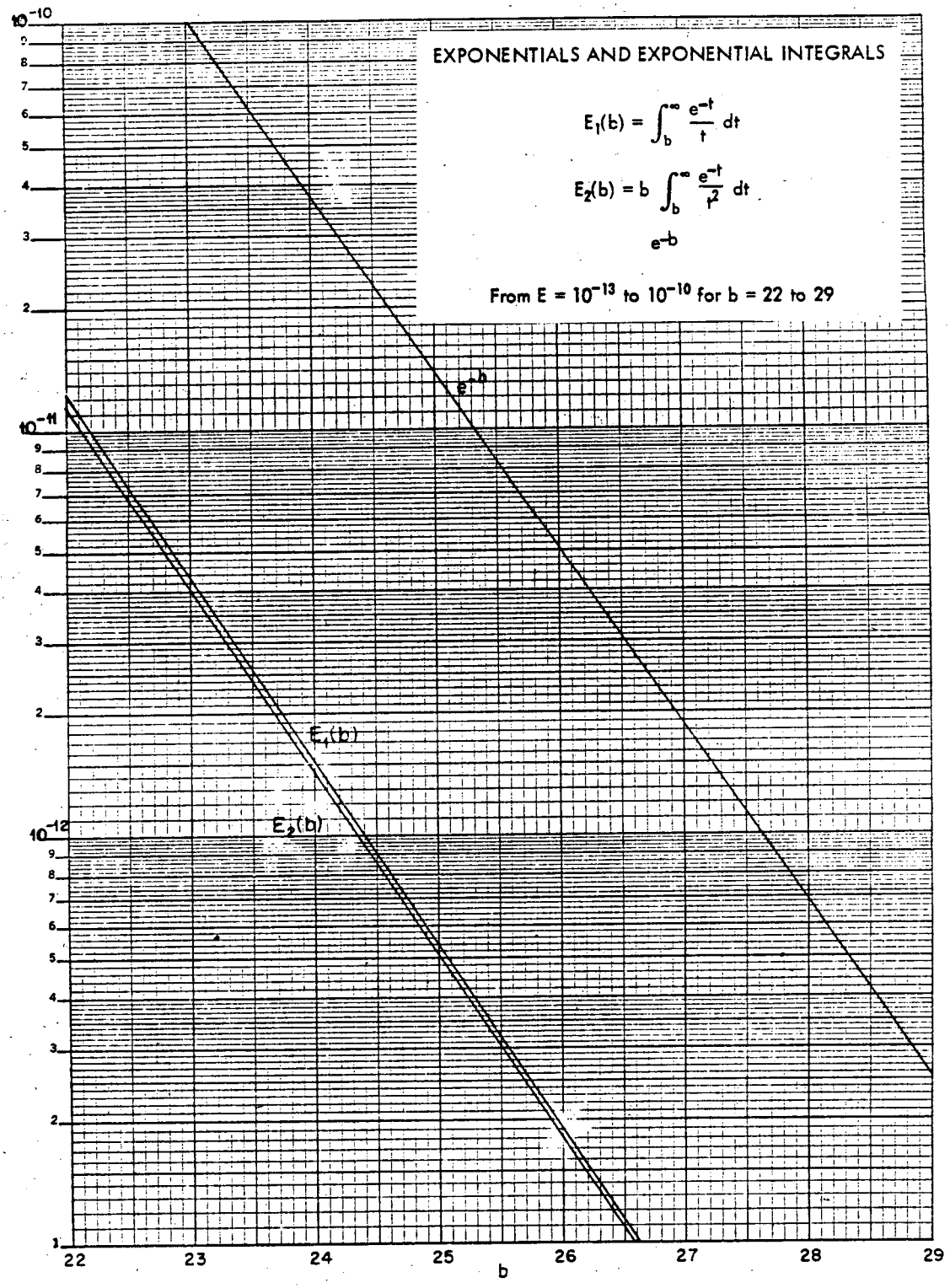

EXPONENTIALS AND EXPONENTIAL INTEGRALS
$E_1(b) = \int_b^\infty \frac{e^{-t}}{t}\,dt$
$E_2(b) = b\int_b^\infty \frac{e^{-t}}{t^2}\,dt$
e^{-b}
From E = 10^{-2} to 10 for b = 0 to 7
10^1
10^0
10^{-1}
10^{-2}
e^{-b}
$E_1(b)$
$E_2(b)$
0
1
2
3
4
5
6
7
b

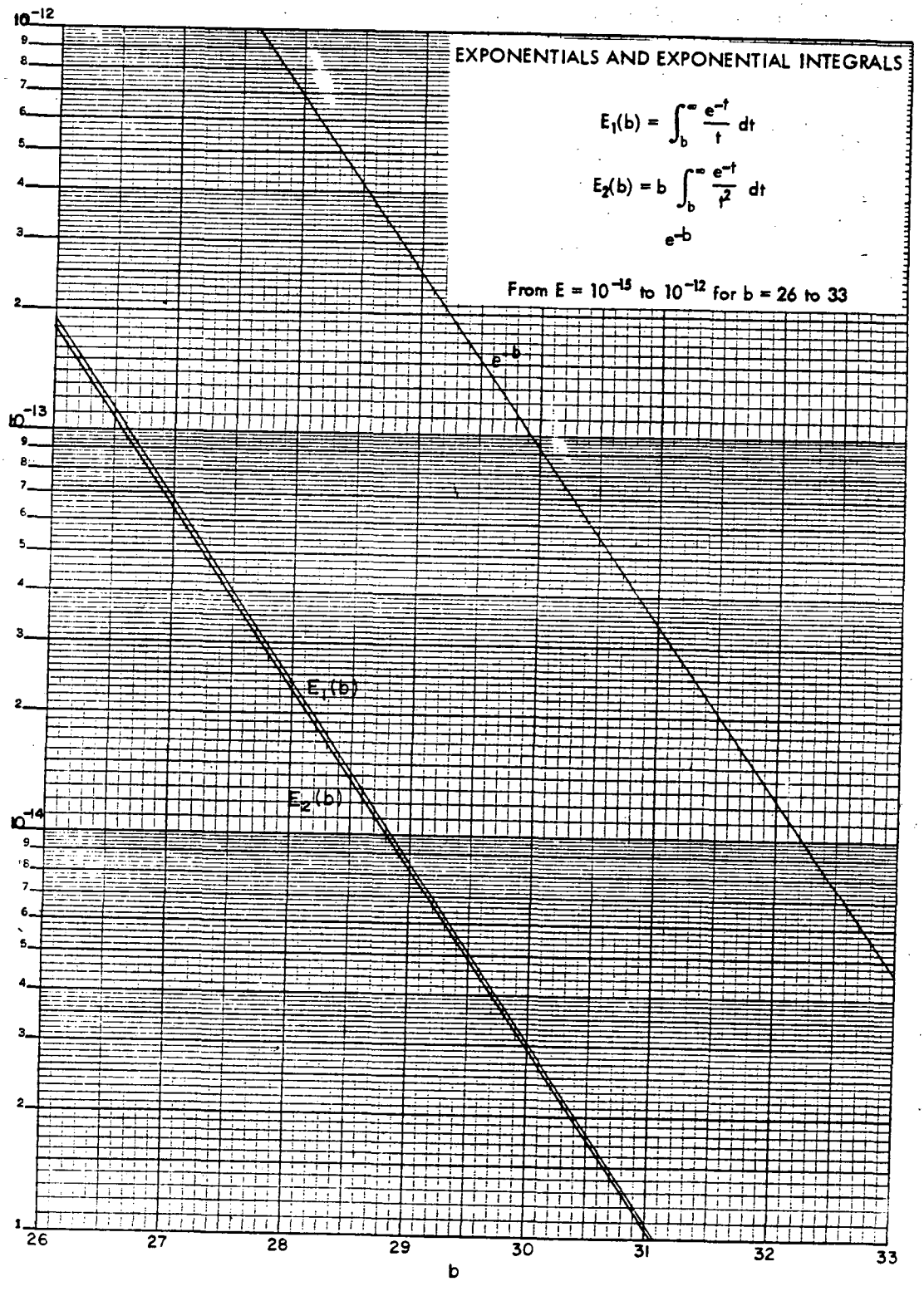

10^{-2}
9
8
7
6
5
4
3
2
10^{-3}
9
8
7
6
5
4
3
2
10^{-4}
9
8
7
6
5
4
3
2
10^{-5}
e^{-b}
$E_1(b)$
$E_2(b)$
EXPONENTIALS AND EXPONENTIAL INTEGRALS
$E_1(b) = \int_b^\infty \frac{e^{-t}}{t}\,dt$
$E_2(b) = b\int_b^\infty \frac{e^{-t}}{t^2}\,dt$
e^{-b}
From $E = 10^{-5}$ to 10^{-2} for $b = 3$ to 10
3
4
5
6
7
8
9
10
b

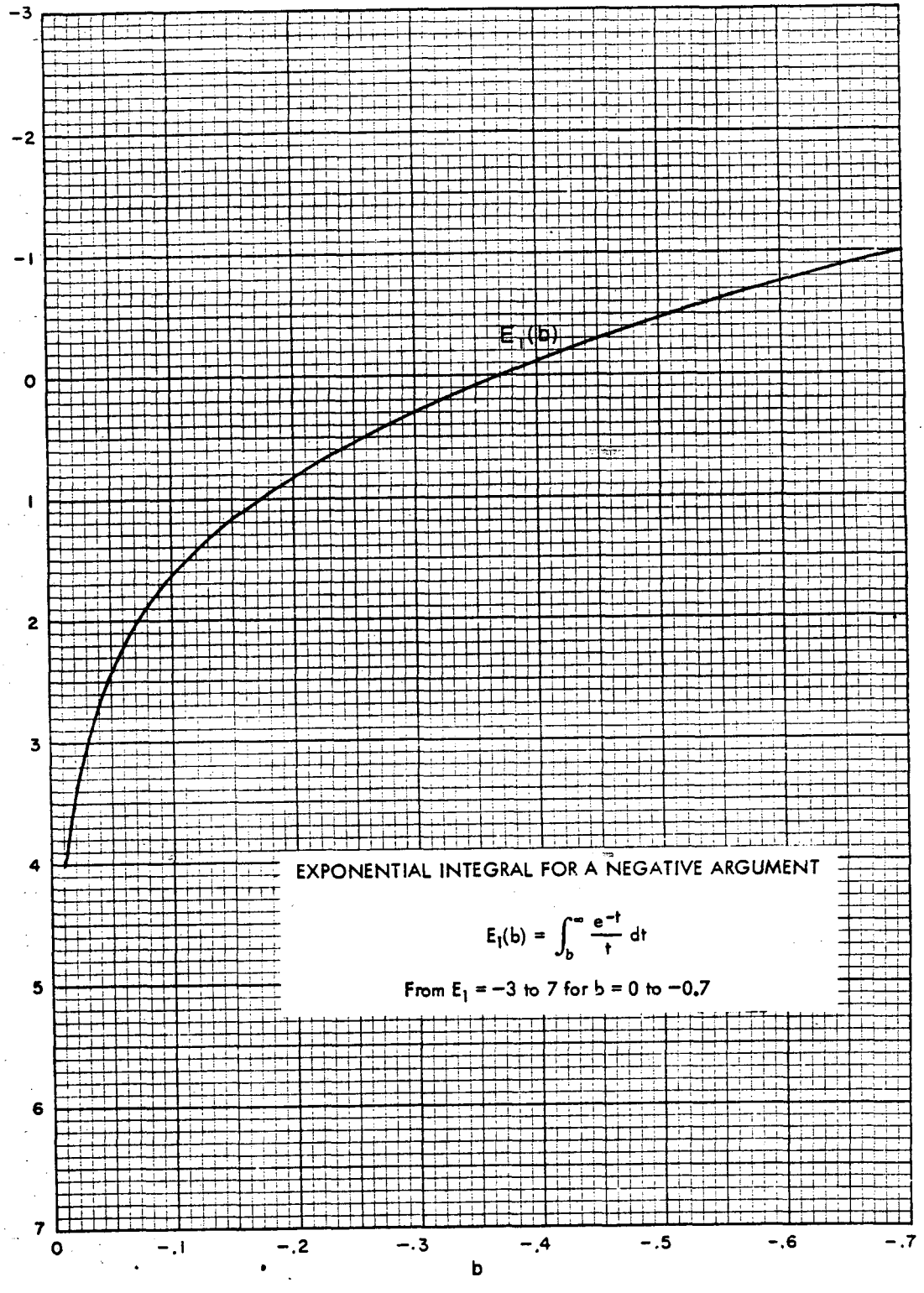

EXPONENTIALS AND EXPONENTIAL INTEGRALS
$E_1(b) = \int_b^\infty \frac{e^{-t}}{t}\,dt$
$E_2(b) = b\int_b^\infty \frac{e^{-t}}{t^2}\,dt$
e^{-b}
From E = 10^{-7} to 10^{-4} for b = 8 to 15
e^{-b}
$E_1(b)$
$E_2(b)$
10^{-4}
10^{-5}
10^{-6}
10^{-7}
8
9
10
11
12
13
14
15
b

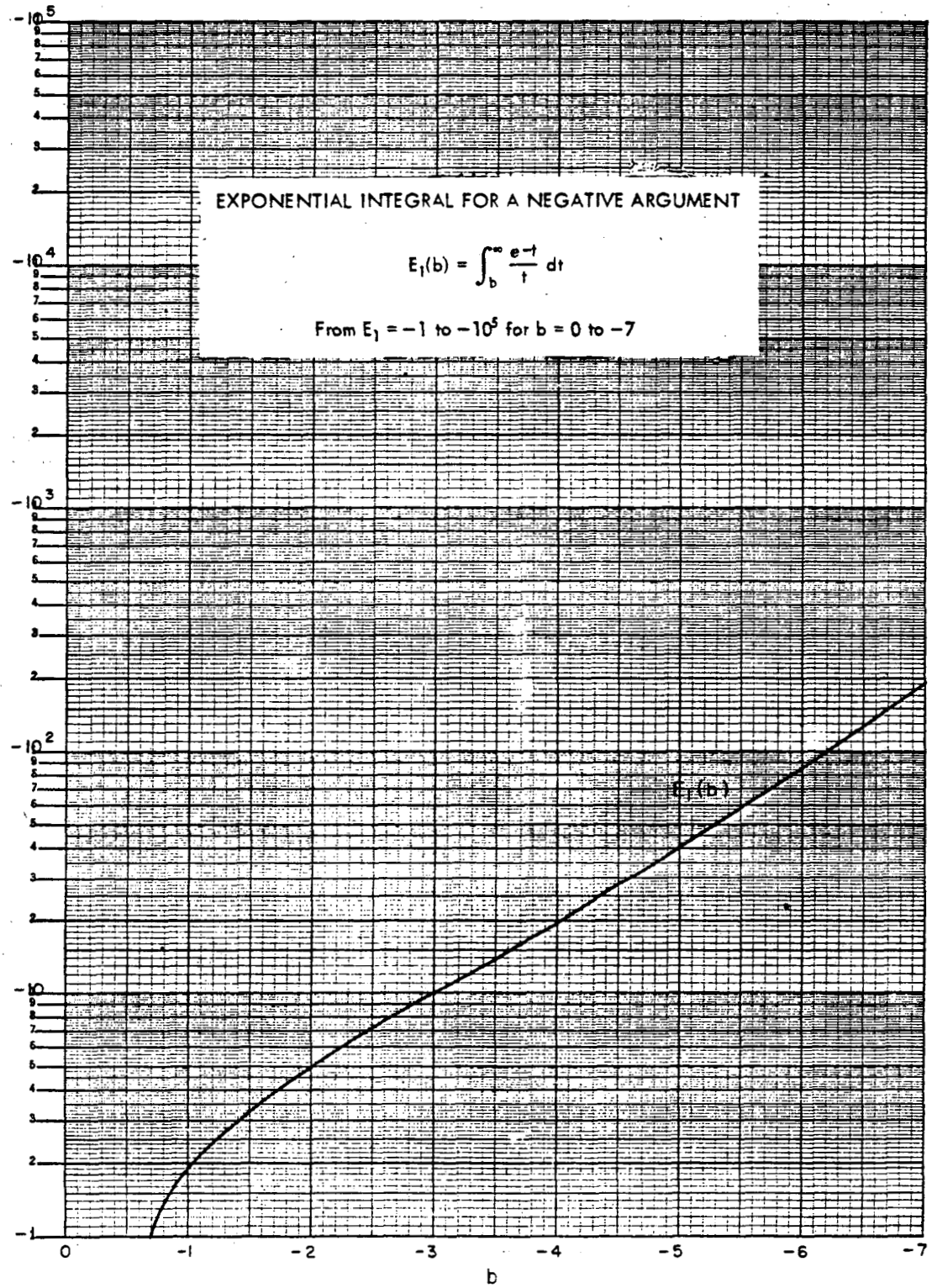

EXPONENTIALS AND EXPONENTIAL INTEGRALS
$E_1(b) = \int_b^\infty \frac{e^{-t}}{t}\,dt$
$E_2(b) = b\int_b^\infty \frac{e^{-t}}{t^2}\,dt$
e^{-b}
From E = 10^{-9} to 10^{-6} for b = 13 to 20
10^{-6}
10^{-7}
10^{-8}
e^{-b}
$E_1(b)$
$E_2(b)$
13
14
15
16
17
18
19
20
b

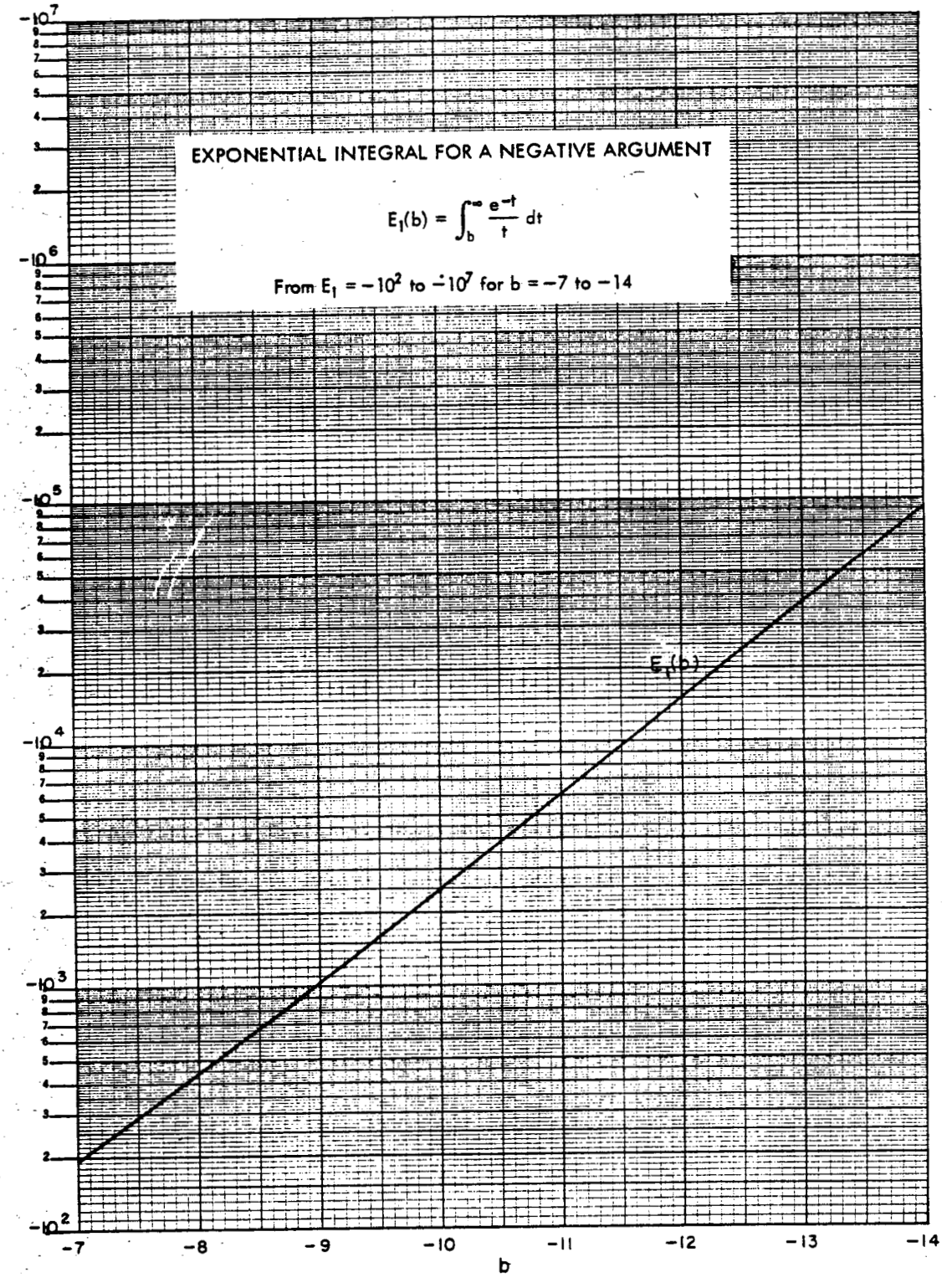

EXPONENTIALS AND EXPONENTIAL INTEGRALS
$E_1(b) = \int_b^\infty \frac{e^{-t}}{t}\,dt$
$E_2(b) = b\int_b^\infty \frac{e^{-t}}{t^2}\,dt$
e^{-b}
From E = 10^{-11} to 10^{-8} for b = 17 to 24
e^{-b}
$E_1(b)$
$E_2(b)$
10^{-8}
10^{-9}
10^{-10}
17
18
19
20
21
22
23
24
b

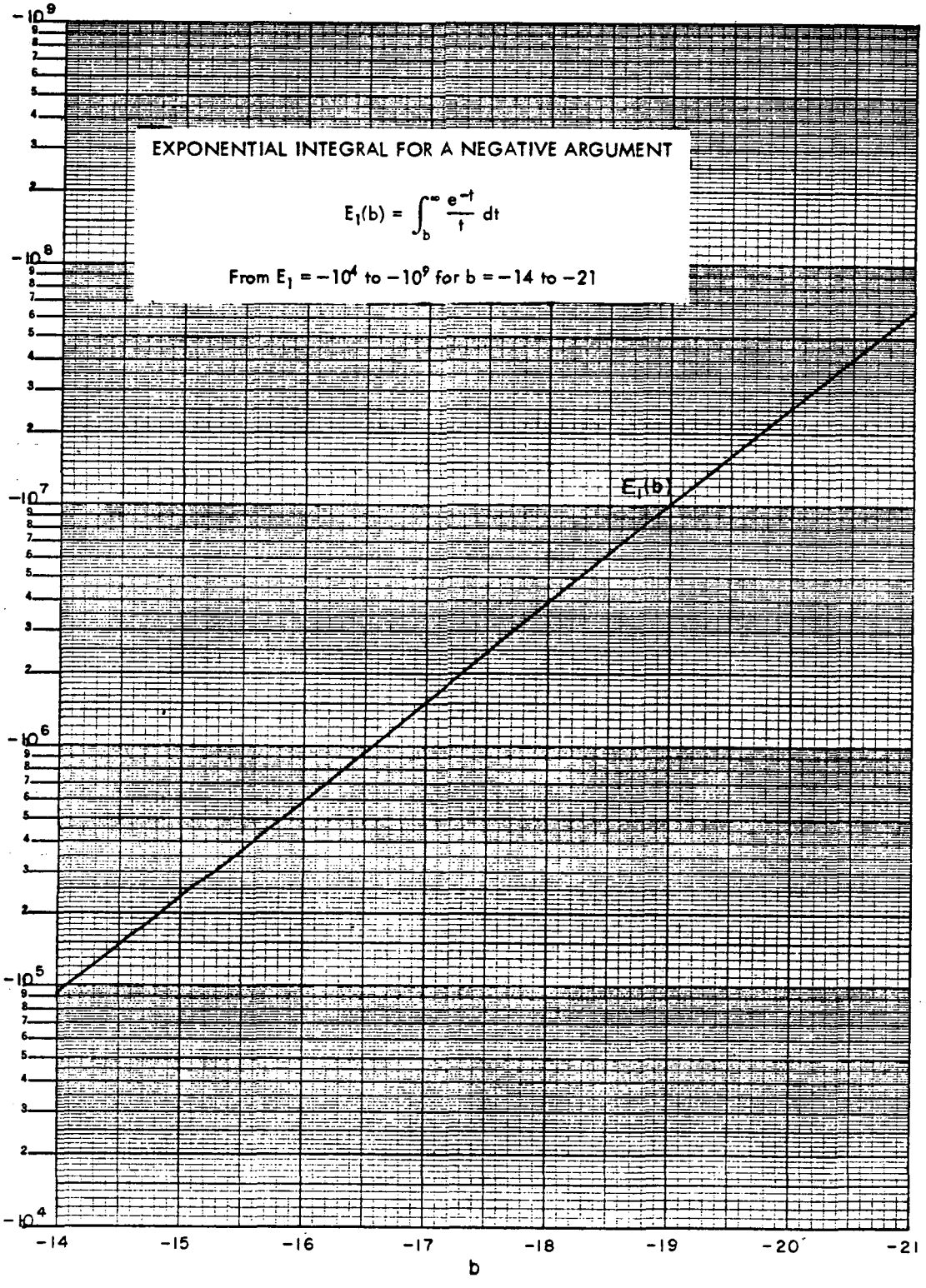

EXPONENTIALS AND EXPONENTIAL INTEGRALS
$E_1(b) = \int_b^\infty \frac{e^{-t}}{t}\,dt$
$E_2(b) = b\int_b^\infty \frac{e^{-t}}{t^2}\,dt$
e^{-b}
From $E = 10^{-13}$ to 10^{-10} for b = 22 to 29
10^{-10}
10^{-11}
10^{-12}
e^{-b}
$E_1(b)$
$E_2(b)$
22
23
24
25
26
27
28
29
b

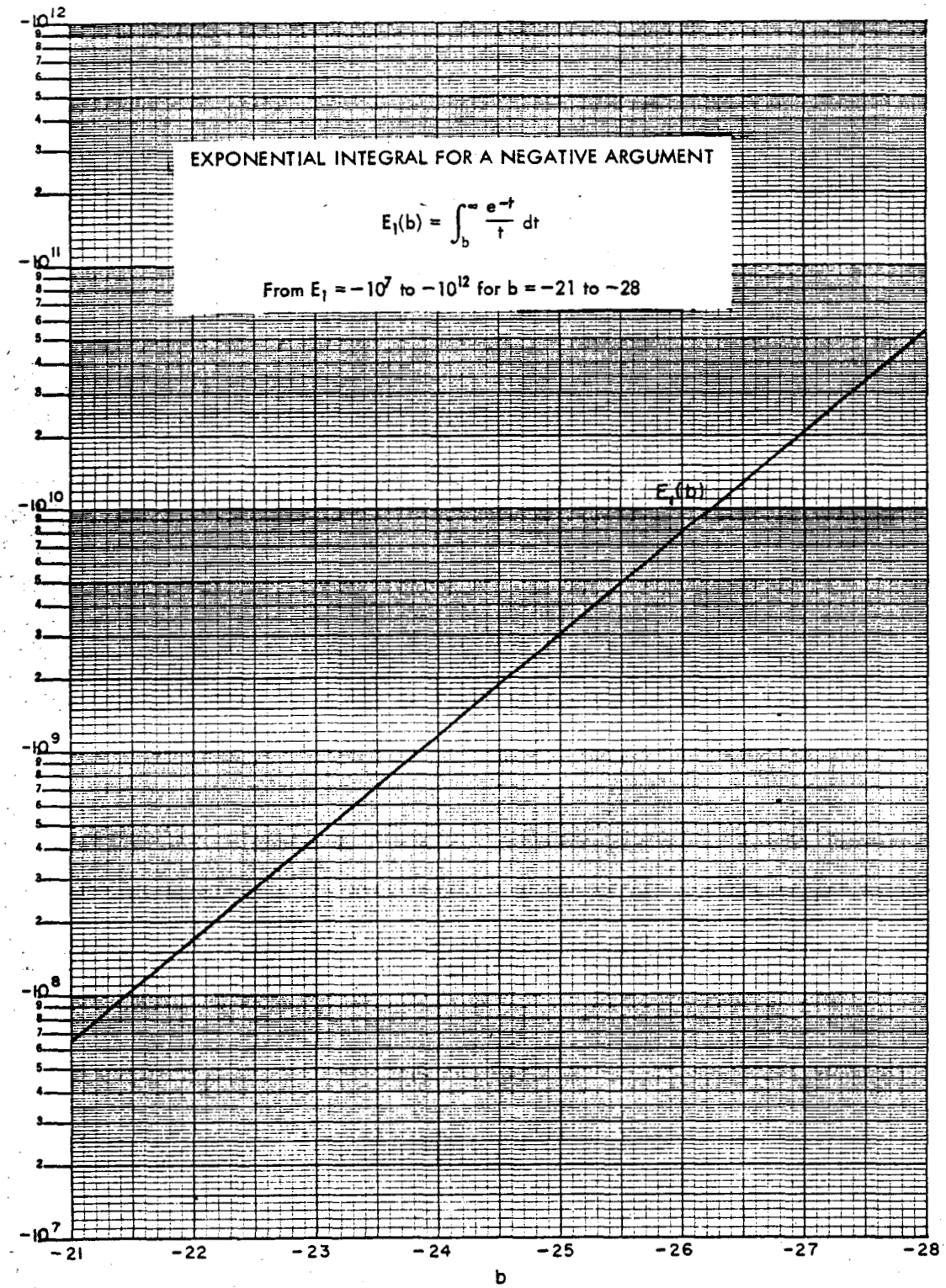

EXPONENTIALS AND EXPONENTIAL INTEGRALS
$E_1(b) = \int_b^\infty \frac{e^{-t}}{t}\,dt$
$E_2(b) = b\int_b^\infty \frac{e^{-t}}{t^2}\,dt$
e^{-b}
From $E = 10^{-15}$ to 10^{-12} for b = 26 to 33
e^{-b}
$E_1(b)$
$E_2(b)$
10^{-12}
10^{-13}
10^{-14}
26
27
28
29
30
31
32
33
b


−3
−2
−1
0
1
2
3
4
5
6
7
$E_1(b)$
EXPONENTIAL INTEGRAL FOR A NEGATIVE ARGUMENT
$E_1(b) = \int_b^\infty \frac{e^{-t}}{t}\,dt$
From $E_1 = -3$ to 7 for $b = 0$ to -0.7
0
−.1
−.2
−.3
−.4
−.5
−.6
−.7
b

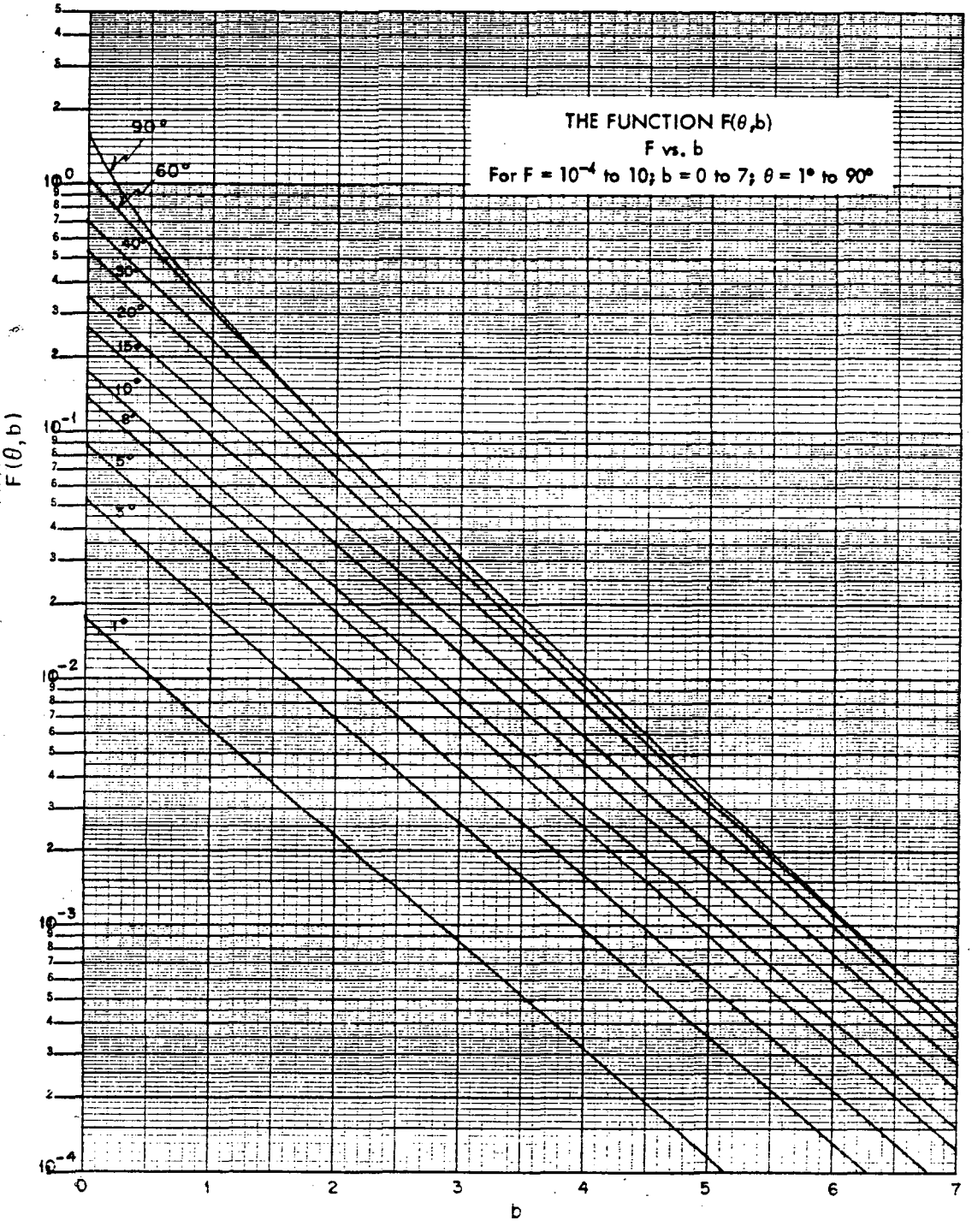

EXPONENTIAL INTEGRAL FOR A NEGATIVE ARGUMENT
$E_1(b) = \int_b^\infty \frac{e^{-t}}{t}\,dt$
From $E_1 = -1$ to -10^5 for b = 0 to −7
-10^5
-10^4
-10^3
-10^2
-10
-1
$E_1(b)$
0
-1
-2
-3
-4
-5
-6
-7
b

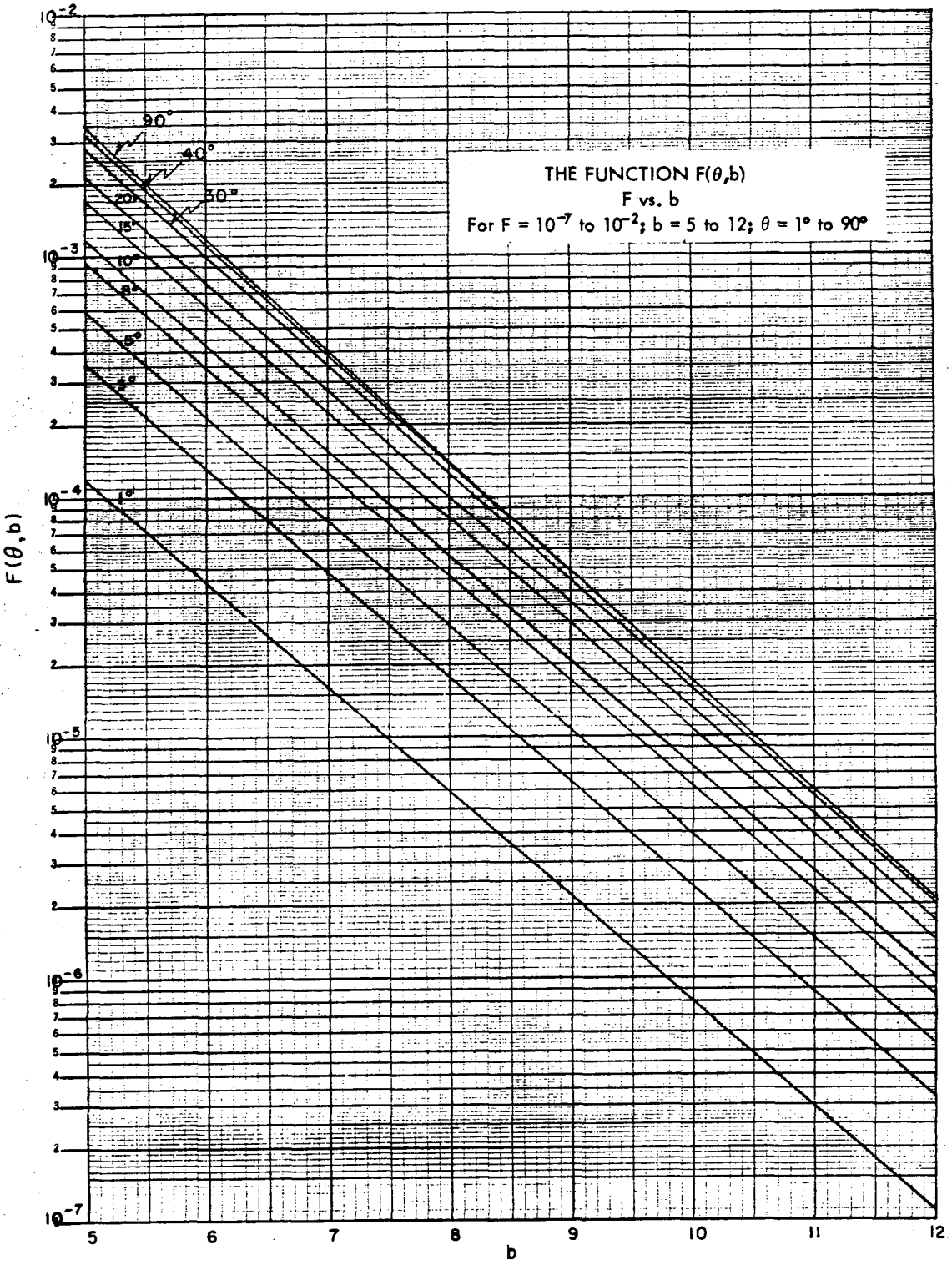

EXPONENTIAL INTEGRAL FOR A NEGATIVE ARGUMENT
$E_1(b) = \int_b^\infty \frac{e^{-t}}{t}\,dt$
From $E_1 = -10^2$ to -10^7 for b = −7 to −14
$E_1(b)$
b
−7
−8
−9
−10
−11
−12
−13
−14

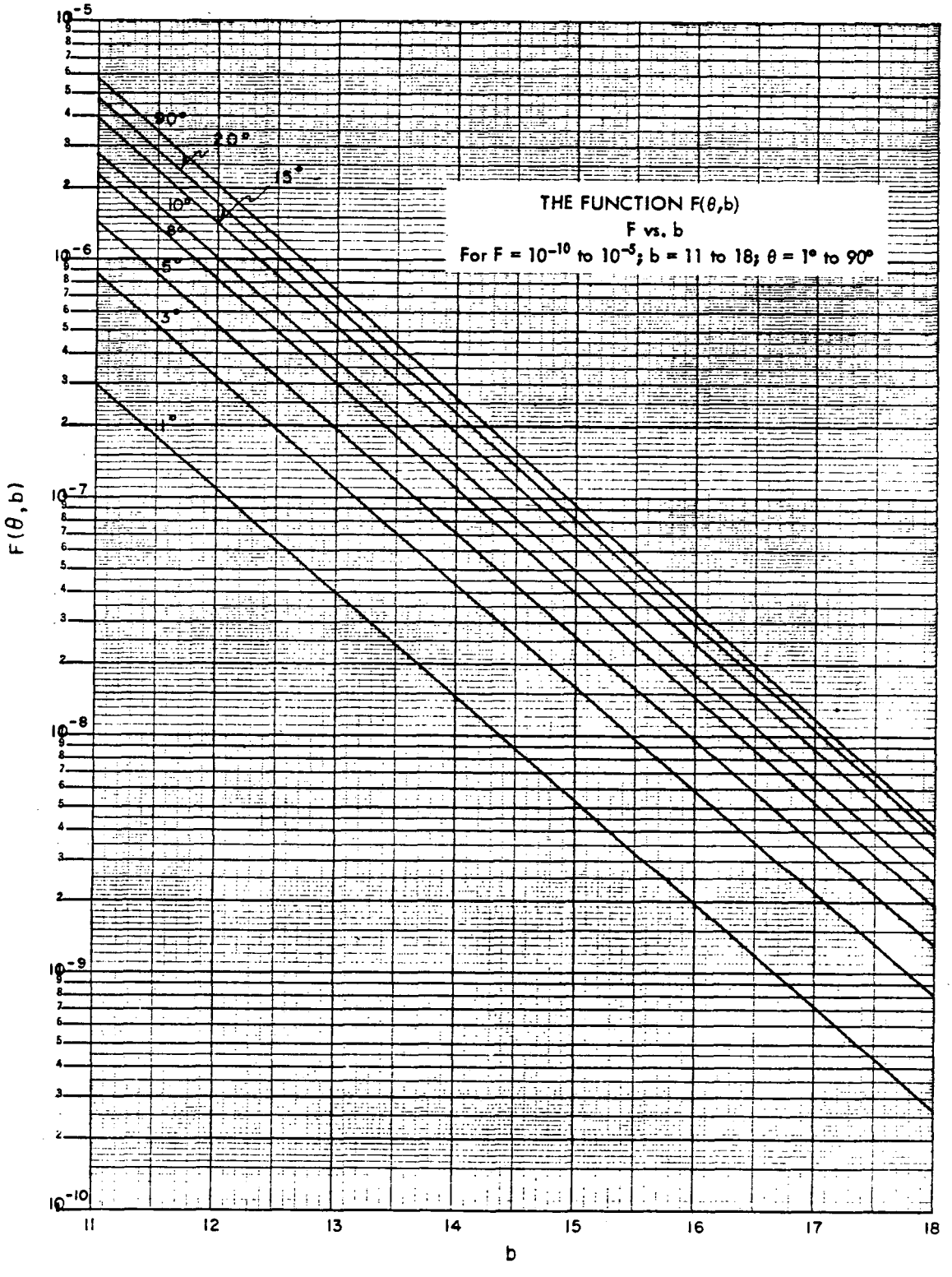

EXPONENTIAL INTEGRAL FOR A NEGATIVE ARGUMENT
$E_1(b) = \int_b^\infty \frac{e^{-t}}{t}\,dt$
From $E_1 = -10^4$ to -10^9 for b = −14 to −21
$E_1(b)$
-10^9
-10^8
-10^7
-10^6
-10^5
-10^4
−14
−15
−16
−17
−18
−19
−20
−21
b

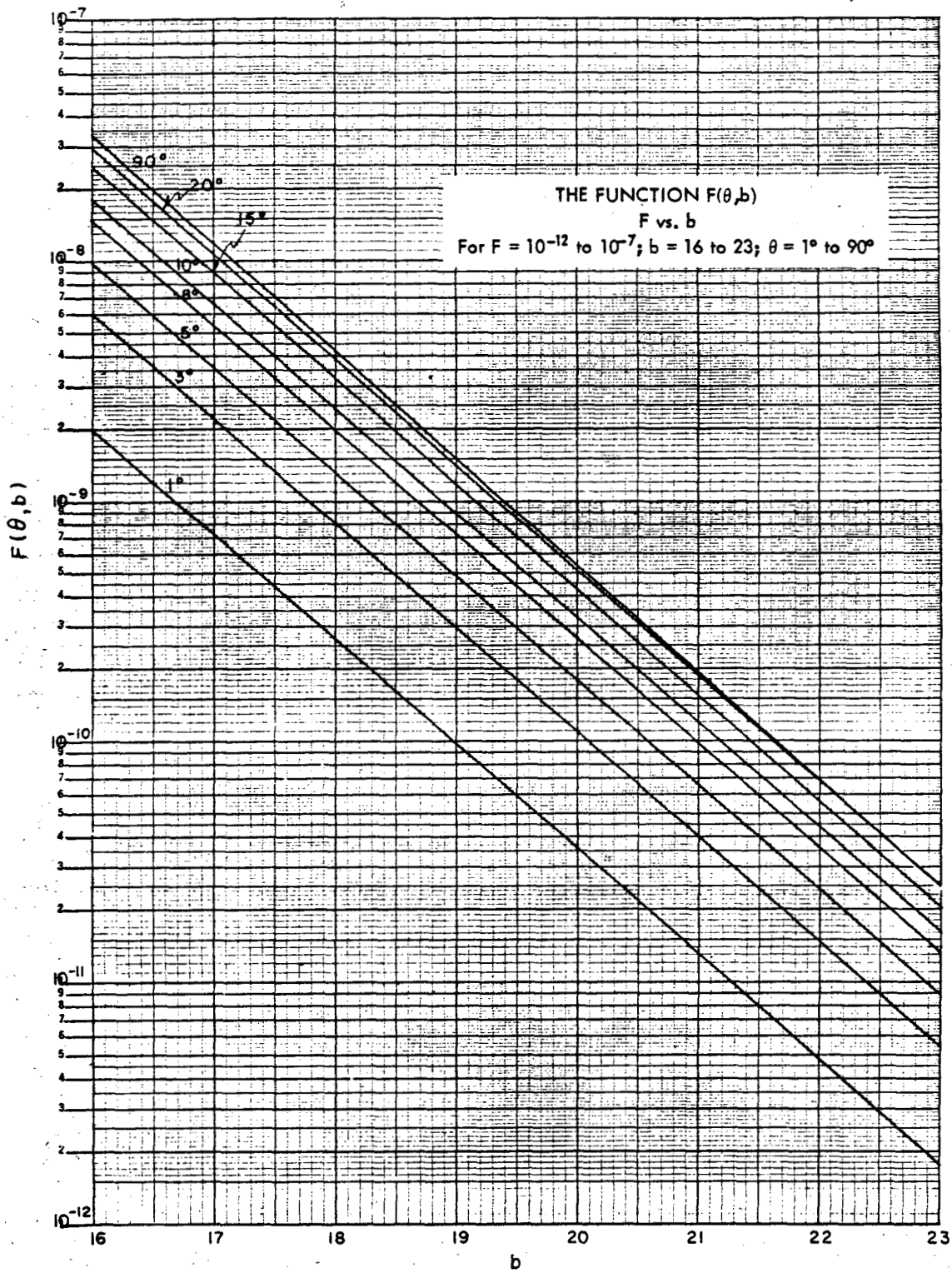

EXPONENTIAL INTEGRAL FOR A NEGATIVE ARGUMENT
$E_1(b) = \int_b^\infty \frac{e^{-t}}{t}\,dt$
From $E_1 = -10^7$ to -10^{12} for b = −21 to −28
$E_1(b)$
-10^{12}
-10^{11}
-10^{10}
-10^{9}
-10^{8}
-10^{7}
−21
−22
−23
−24
−25
−26
−27
−28
b

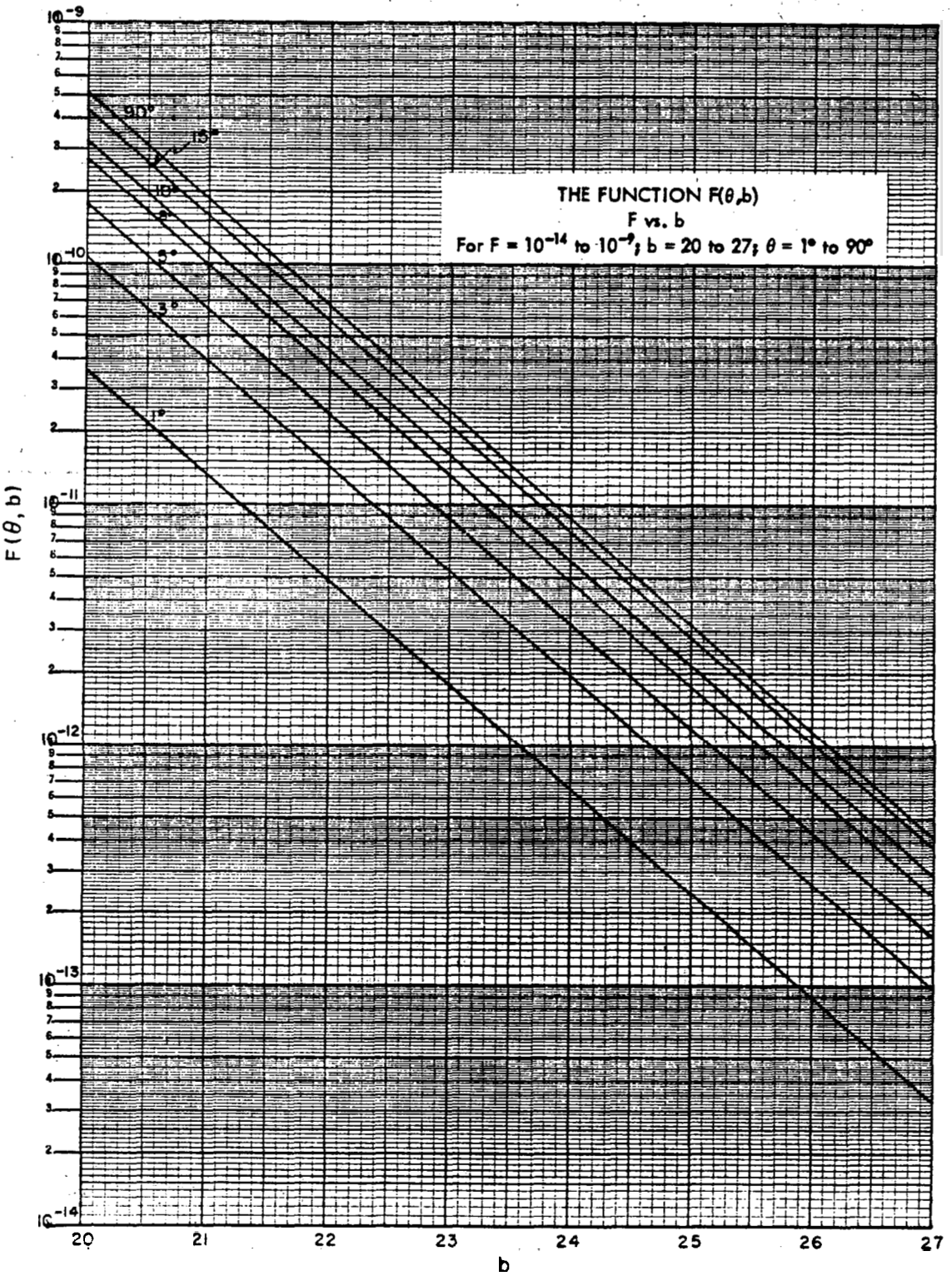
I-9 THE FUNCTION F(θ,b)

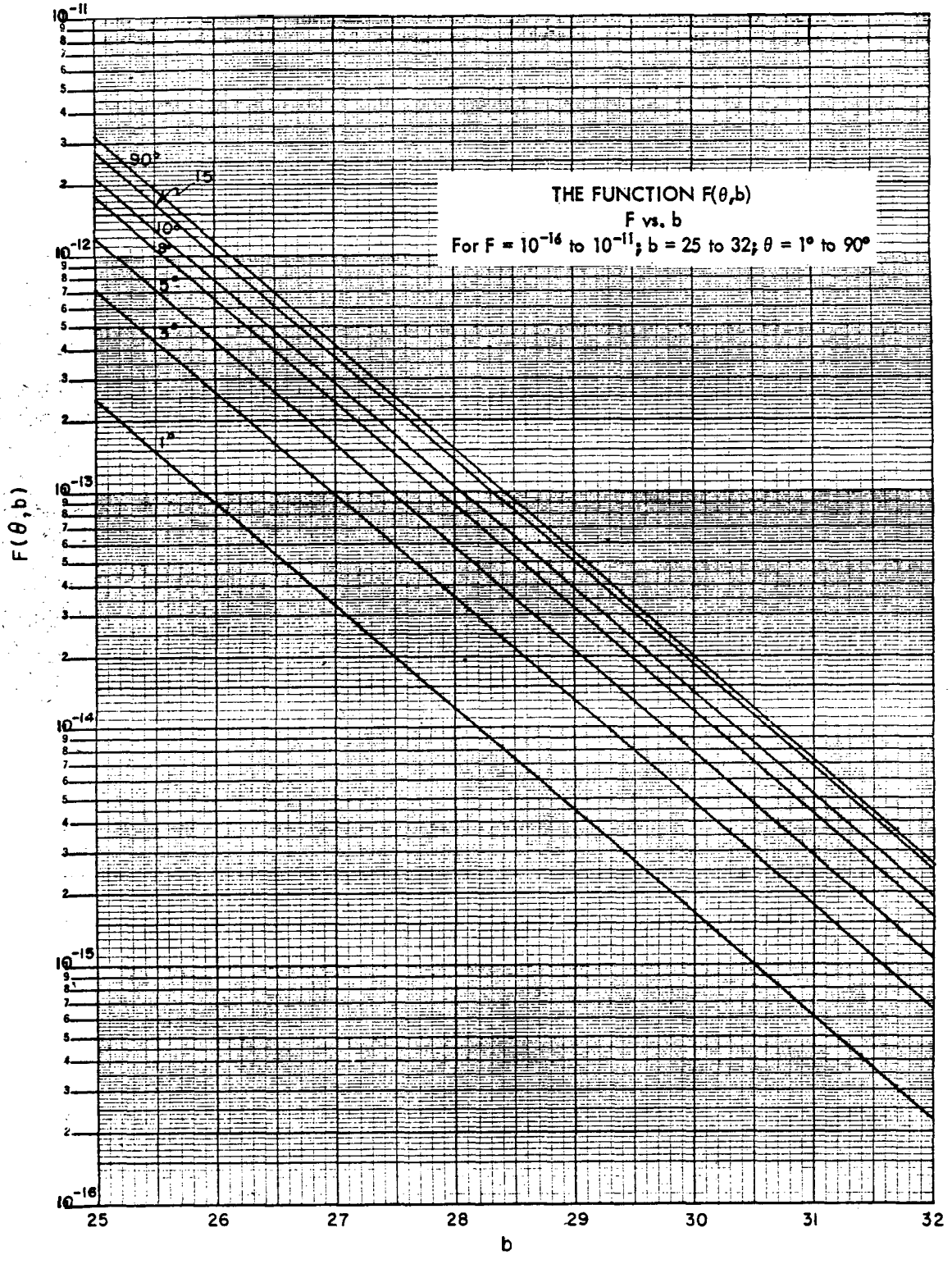



THE FUNCTION F(θ,b)
F vs. b
For F = 10⁻⁷ to 10⁻²; b = 5 to 12; θ = 1° to 90°
90°
40°
30°
20°
15°
10°
8°
6°
4°
1°
F(θ,b)
b
10⁻²
10⁻³
10⁻⁴
10⁻⁵
10⁻⁶
10⁻⁷
5
6
7
8
9
10
11
12


THE FUNCTION F(θ,b)
F vs. b
For F = 10⁻¹⁰ to 10⁻⁵; b = 11 to 18; θ = 1° to 90°
90°
20°
15°
10°
8°
5°
3°
1°
F(θ,b)
b
11
12
13
14
15
16
17
18


THE FUNCTION F(θ,b)
F vs. b
For F = 10⁻¹² to 10⁻⁷; b = 16 to 23; θ = 1° to 90°
90°
20°
15°
10°
8°
6°
5°
1°
F(θ,b)
b
16
17
18
19
20
21
22
23


THE FUNCTION F(θ,b)
F vs. b
For F = 10⁻¹⁴ to 10⁻⁹; b = 20 to 27; θ = 1° to 90°
90°
15°
10°
5°
3°
1°
F(θ, b)
b
20
21
22
23
24
25
26
27

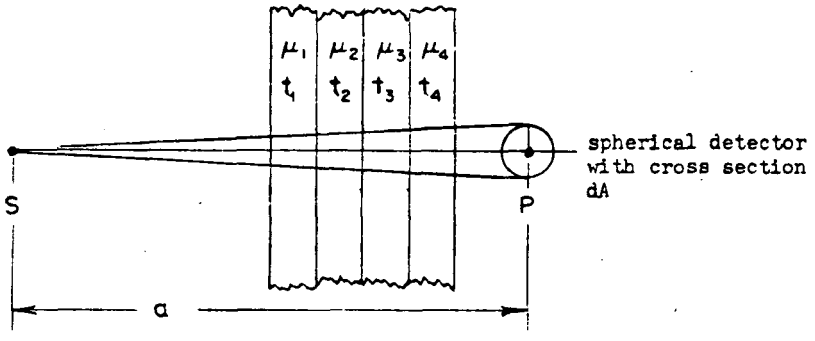

THE FUNCTION F(θ,b)
F vs. b
For F = 10^-16 to 10^-11; b = 25 to 32; θ = 1° to 90°
90°
15°
10°
8°
5°
3°
1°
F(θ,b)
b
10^-11
10^-12
10^-13
10^-14
10^-15
10^-16
25
26
27
28
29
30
31
32

Part II Derivations

There are two basic assumptions made in deriving the equations in this report: (1) that the emission of the quanta is isotropic and (2) that the attenuation of the quanta is exponential.

Almost all the sources encountered in nuclear shielding studies obey the first criterion, and the most penetrating quanta with which the shield designer must contend, gamma rays and high-energy neutrons, obey the second.

II-1 POINT SOURCE



The probability that a quantum leaves the source within a differential cone of directions such that it can intercept the detector is (the solid angle subtended at S by the detector) divided by (the total number of steradians in a sphere).

$$\frac{dA/a^2}{4\pi} \tag{1}$$

The probability that a quantum in the cone will reach the detector without collision is

$$\exp\left[-(\mu_1 t_1 + \mu_1 t_2 + \ldots + \mu_n t_n)\right] \tag{2}$$

or, by definition of b_1,

$$e^{-b_1} \tag{3}$$

Since Eqs. 1 and 3 represent independent probabilities, the probability that a quantum emitted at S will be detected at P is simply the product

$$\frac{dA}{4\pi a^2} e^{-b_1} \tag{4}$$

If the source is emitting S_0 quanta/sec, then

$$S_0 \frac{dA}{4\pi a^2} e^{-b_1} \quad \text{quanta/sec} \tag{5}$$

will be detected at P. Since the uncollided scalar flux at P is defined as the uncollided quanta crossing unit area per unit time

$$\phi_u = \frac{S_0}{4\pi a^2} e^{-b_1} \quad \text{quanta/cm}^2\text{-sec} \tag{6}$$

This equation is true in general, regardless of the number or shape of attenuating mediums, provided that the exponent is the total number of mean free paths along the line between the source point and the detector and that a is the total distance between the source and the detector.

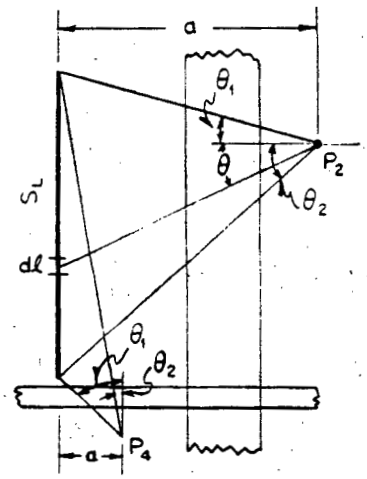
The quantity on the right side of Eq. 6 will subsequently be referred to as the "point kernel."

II-2 LINE SOURCE

The uncollided flux at P_2 from the line source can be derived by integration over the point kernel.

The contribution from line segment dl is simply

$$d\phi_u \equiv \frac{S_L\, dl\, e^{-b_1 \sec\theta}}{4\pi(a \sec\theta)^2} \tag{7}$$



since

$$dl = a \sec^2\theta\, d\theta \tag{8}$$

Therefore

$$d\phi_u = S_L \frac{e^{-b_1 \sec\theta}}{4\pi a} d\theta \tag{9}$$

and

$$\phi_u = \frac{S_L}{4\pi a}\left(\int_0^{\theta_1} e^{-b_1 \sec\theta}\, d\theta + \int_0^{\theta_2} e^{-b_1 \sec\theta}\, d\theta\right) \tag{10}$$

and, by definition of the $F(\theta,b)$ functions,

$$\phi_u = \frac{S_L}{4\pi a}[F(\theta_1,b_1) + F(\theta_2,b_1)] \tag{11}$$

At P_4 the proof is much the same

$$d\phi_u = \frac{S_L\, dl\, e^{-b_1 \sec\theta}}{4\pi(a \csc\theta)^2} \tag{12}$$

and

$$dl = a \csc^2\theta\, d\theta \tag{13}$$

Therefore

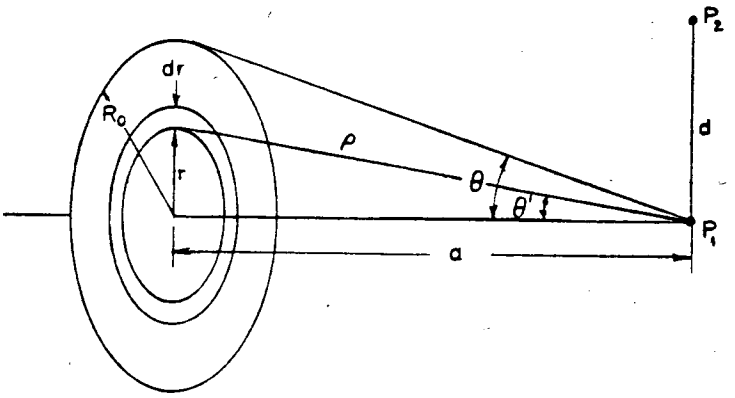
$$\phi_u = \frac{S_L}{4\pi a}\left(\int_0^{\theta_1} e^{-b_1 \sec\theta}\, d\theta - \int_0^{\theta_2} e^{-b_1 \sec\theta}\, d\theta\right) \tag{14}$$

or

$$\phi_u = \frac{S_L}{4\pi a}\left[F(\theta_1,b_1) - F(\theta_2,b_1)\right] \tag{15}$$

The fluxes at all other points of interest can be derived similarly.

II-3 DISK SOURCE



At P_1 on the center line of the disk, which is emitting S_A quanta per unit area per unit time, the uncollided flux from the differential ring between r and r + dr is

$$d\phi_u = \frac{S_A\,(2\pi r\,dr)}{4\pi\rho^2}\,e^{-b_1\sec\theta'} \tag{16}$$

But

$$\rho^2 = r^2 + a^2 \tag{17}$$

therefore

$$\rho\,d\rho = r\,dr \tag{18}$$

Also

$$\sec\theta' = \frac{\rho}{a} \tag{19}$$

therefore

$$d\phi_u = \frac{S_A}{2}\,\frac{d\rho}{\rho}\,e^{-b_1\rho/a} \tag{20}$$

Substituting $b_1\rho/a \equiv t$ and integrating over the disk

$$\phi_u = \frac{S_A}{2} \int_{b_1}^{b_1 \sec\theta} \frac{e^{-t}}{t}\, dt \tag{21}$$

Since, by definition,

$$E_1(x) \equiv \int_x^\infty \frac{e^{-t}}{t}\, dt \tag{22}$$

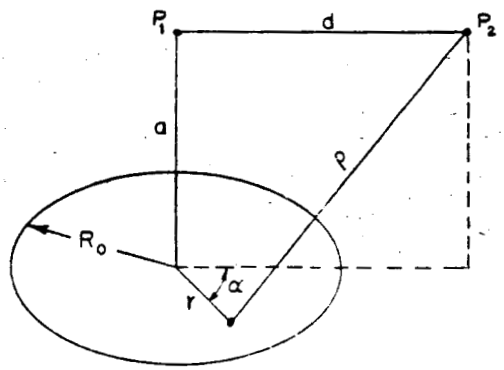
finally

$$\phi_u = \frac{S_A}{2} [E_1(b_1) - E_1(b_1 \sec\theta)] \tag{23}$$

At P_2, a point that is a distance d off the center line of the disk, the flux is given by the flux at P_1 times a correction factor which is a function of d/R_0, a/R_0, and $\bar{\mu}R_0$. The complete derivation of this factor may be found in references 3 and 4 from which the curves of K were drawn. Only a brief sketch of the problem will be given here.

At P_2

$$\phi_u = S_A \int_0^{R_0} \int_0^{2\pi} \frac{e^{-\bar{\mu}\rho}}{4\pi\rho^2}\, r\, dr\, d\alpha \tag{24}$$



where

$$\bar{\mu} = \frac{\sum_i \mu_i t_i}{\sum_i t_i}$$

the sum being over all the slabs between the disk and the detector, including vacuum if any. But

$$\rho = (a^2 + r^2 + d^2 - 2rd\cos\alpha)^{1/2} \tag{25}$$

Therefore

$$\phi_u = \frac{S_A}{4\pi} \int_0^{R_0} \int_0^{2\pi} \frac{\exp[-\bar{\mu}(a^2 + r^2 + d^2 - 2rd\cos\alpha)^{1/2}]}{(a^2 + r^2 + d^2 - 2rd\cos\alpha)}\, r\, dr\, d\alpha \tag{26}$$

Equation 26 can be reduced to one integration by expanding the inner integral in a power series in $\cos\alpha$ and then integrating term by term over α. Alternately, for $d^2 < a^2 + R_0^2$ the double integral is expanded about d = 0, and, again, the integral over α is performed termwise. In this case the final answer is a double summation. In the region where $R_0^2 < a^2 + d^2$, the integral is expanded in a power series in r, and the integration over α, then over r, is performed, yielding a double sum. The results are as follows.

When $d^2 < a^2 + R_0^2$

$$\phi_u = \frac{S_A}{2} \int_a^{\sqrt{a^2+R_0^2}} \frac{e^{-\bar{\mu}r}}{r^2}\, r\, dr + \frac{S_A}{2} \sum_{n=1}^{\infty} \frac{d^{2n}}{2^n(n)} \sum_{j=1}^{n} \frac{jR_0^{2j}}{2^j(n-j)\,!\,(j!)^2} D^{n+j-1} \left(\frac{e^{-\bar{\mu}r}}{r^2}\right)_{\sqrt{a^2+R_0^2}} \tag{27}$$

When $d^2 > R_0^2 - a^2$

$$\phi_u = \frac{S_A R_0^2}{4} \sum_{n=0}^{\infty} \frac{R_0^{2n}}{2^n (n+1)} \sum_{j=0}^{n} \frac{d^{2j}}{2^j (n-j)!\ (j!)^2} D^{n+j} \left(\frac{e^{-\bar{\mu} r}}{r^2} \right)_{\sqrt{a^2+d^2}} \tag{28}$$

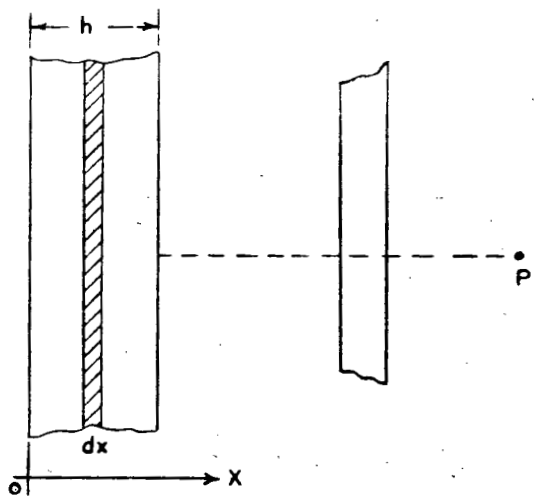
where

$$D^M \left(\frac{e^{-\bar{\mu} r}}{r^2} \right) = \frac{(-1)^M e^{-\bar{\mu} r}}{r^{2M+2}} \sum_{k=0}^{M} (\bar{\mu} r)^k \sum_{i=0}^{k} \frac{(-1)^i}{i!\ (k-i)!} (2-i)\ (2-i+2) \ldots (2-i+2M-2) \tag{29}$$

The correction function $K(d/R_0, a/R_0, \bar{\mu}R_0)$ is defined as the ratio $[\phi_u(a,R_0,d)]/[\phi_u(a,R_0,0)]$. The numerator is computed by Eq. 27 or 28, coupled with Eq. 29, and the denominator is given by Eq. 23.

II-4 INFINITE-SLAB SOURCE

II-4.1 Exterior



The uncollided flux reaching P from the differential element between x and x + dx is given by the infinite-plane-source kernel with $S_A = S_V(x)\,dx$. [The infinite-plane-source kernel may be obtained by setting $\theta = 90°$ in the disk-source case previously derived and noting that $E_1(\infty) = 0$.]

$$d\phi_u = \frac{S_V(x)\,dx}{2} E_1 [b_1 + \mu_s (h - x)] \tag{30}$$

If $S_V(x) = S_i e^{k_i x}$, then

$$\phi_u = \frac{S_i}{2} \int_0^h e^{k_i x} E_1 [b_1 + \mu_s (h - x)]\,dx \tag{31}$$

Following the transformation $y \equiv b_1 + \mu_s(h - x)$

$$\phi_u = \frac{S_i e^{k_i b_3/\mu_s}}{2\mu_s} \int_{b_1}^{b_3} e^{-k_i y/\mu_s} \; E_1(y)\, dy$$

$$= \frac{S_i e^{k_i b_3/\mu_s}}{2\mu_s} \left[\int_0^{b_3} e^{-k_i y/\mu_s} \; E_1(y)\, dy - \int_0^{b_1} e^{-k_i y/\mu_s} \; E_1(y)\, dy \right] \tag{32}$$

where $b_3 \equiv b_1 + \mu_s h$.

From the definition of the F_1 function,

$$\phi_u = \frac{S_i e^{k_i b_3/\mu_s}}{2\mu_s} \left[F_1\left(b_3, \frac{-k_i}{\mu_s}\right) - F_1\left(b_1, \frac{-k_i}{\mu_s}\right) \right] \tag{33}$$

If the source is a linear sum of exponentials, then ϕ_u is given by a linear sum of terms like the one above.

If the source is constant through the slab, $S_V(x) = S_V$ = constant, then from Eq. 33 and the fact that $F_1(t,0) = 1 - E_2(t)$,

$$\phi_u = \frac{S_V}{2\mu_s} [E_2(b_1) - E_2(b_3)] \tag{34}$$

If $S_V(x) = S_n(x + c)^n$ with $n \geq 0$, then Eq. 31 is replaced by

$$\phi_u = \frac{S_n}{2} \int_0^h (x + c)^n \; E_1 [b_1 + \mu_s(h - x)]\, dx \tag{35}$$

Following the transformation $y \equiv x + c$

$$\phi_u = \frac{S_n}{2} \int_c^{h+c} y^n \; E_1[b_1 + \mu_s(h + c - y)]\, dy \tag{36}$$

Using the integration formula[5]

$$\int x^m \; E_n(ax + b)\, dx = -\sum_{i=0}^{m} \frac{m!}{(m - i)!} \frac{x^{m-i}}{a^{i+1}} E_{n+i+1}\,(ax + b) \tag{37}$$

For $m \geq 0$

$$\phi_u = -\frac{S_n}{2} \sum_{i=0}^{n} \frac{n!}{(n - i)!} \frac{y^{n-i}}{(-\mu_s)^{i+1}} \; E_{2+1}[b_1 + \mu_s(h + c - y)] \Bigg|_c^{h+c} \tag{38}$$

$$\phi_u = \frac{S_n}{2\mu_s} \sum_{i=0}^{n} \frac{(-1)^i\, n!}{(\mu_s)^i\, (n - i)!} [(h + c)^{n-i} \; E_{2+1}(b_1) - c^{n-i} \; E_{2+1}(b_3)] \tag{39}$$

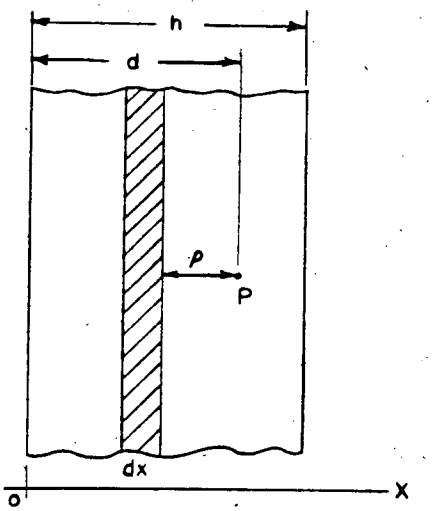
If the source variation is given in the form of a power series,

$$S_V(x) = \sum_{n=0}^{N} S_n(x + c)^n$$

then the uncollided flux is simply a linear sum over terms like the one above.

II-4.2 Interior

The uncollided flux is given by an integral over the infinite-plane-source kernel.



$$\phi_u = \tfrac{1}{2} \int_0^d S_V(x)\, E_1(\mu_s \rho)\, d\rho + \tfrac{1}{2} \int_0^{h-d} S_V(x)\, E_1(\mu_s \rho)\, d\rho \qquad (40)$$

If $S_V(x) = S_i e^{k_i x}$, then

$$\phi_u = \tfrac{1}{2} S_i \int_0^d e^{k_i x}\, E_1(\mu_s \rho)\, d\rho + \tfrac{1}{2} S_i \int_0^{h-d} e^{k_i x}\, E_1(\mu_s \rho)\, d\rho \qquad (41)$$

Following the transformations $x = d - \rho$ in the first integral and $x = d + \rho$ in the second

$$\phi_u = \frac{1}{2} S_i \frac{e^{k_i d}}{\mu_s} \left[\int_0^{\mu_s d} e^{-k_i \mu_s \rho/\mu_s}\, E_1(\mu_s \rho)\, \mu_s\, d\rho + \int_0^{\mu_s (h-d)} e^{k_i \mu_s \rho/\mu_s}\, E_1(\mu_s \rho)\, \mu_s\, d\rho \right] \qquad (42)$$

and by definition of the F_1 function

$$\phi_u = \frac{1}{2\mu_s} S_i e^{k_i d} \left\{ F_1\left(\mu_s d, \frac{-k_i}{\mu_s}\right) + F_1\left[\mu_s (h-d), \frac{k_i}{\mu_s}\right] \right\} \qquad (43)$$

If the source is a linear sum of exponentials, then the flux is given by a sum over i of terms like the one above.

If the source is constant through the slab, $S_V(x) = S_V$ = constant, then from the Eq. 43, plus the fact that $F_1(t,0) = 1 - E_2(t)$,

$$\phi_u = \frac{S_V}{2\mu_s} \left\{ 2 - E_2(\mu_s d) - E_2[\mu_s (h-d)] \right\} \qquad (44)$$

If $S_V(x) = S_n (x + c)^n$, then

$$\phi_u = \frac{S_n}{2} \int_0^d (x + c)^n\, E_1(\mu_s \rho)\, d\rho + \frac{S_n}{2} \int_0^{h-d} (x + c)^n\, E_1(\mu_s \rho)\, d\rho \qquad (45)$$

Making the substitutions $x = d - \rho$ and $x = d + \rho$ in the first and second integrals, respectively, results in

$$\phi_u = \frac{S_n}{2} \int_0^d (d - \rho + c)^n\, E_1(\mu_s \rho)\, d\rho + \frac{S_n}{2} \int_0^{h-d} (d + \rho + c)^n\, E_1(\mu_s \rho)\, d\rho \qquad (46)$$

Substituting $y = d - \rho + c$ and $y = d + \rho + c$ in the first and second integrals, respectively, results in

$$\phi_u = -\frac{S_n}{2} \int_{d+c}^{c} y^n\, E_1[-\mu_s y + \mu_s (d + c)]\, dy + \frac{S_n}{2} \int_{d+c}^{h+c} y^n\, E_1[\mu_s y - \mu_s (d + c)]\, dy \qquad (47)$$

since

$$\int y^n E_1(ay + b)\, dy = -\sum_{p=0}^{n} \frac{n!}{(n-p)!} \frac{y^{n-p}}{a^{p+1}} E_{2+p}(ay + b)$$

Therefore

$$\phi_u = \frac{S_n}{2}\left[\sum_{p=0}^{n} \frac{n!}{(n-p)!} \frac{y^{n-p}}{(-\mu_s)^{p+1}} E_{2+p}[-\mu_s y + \mu_s(d+c)]\right]_{d+c}^{c}$$

$$- \frac{S_n}{2}\left[\sum_{p=0}^{n} \frac{n!}{(n-p)!} \frac{y^{n-p}}{(\mu_s)^{p+1}} E_{2+p}[\mu_s y - \mu_s(d+c)]\right]_{d+c}^{h+c} \qquad (48)$$

After multiplying and dividing each term by μ_s^n,

$$\phi_u = -\frac{S_n}{2\mu_s}\frac{1}{\mu_s^n}\left[\sum_{p=0}^{n} \frac{n!}{(n-p)!} (-1)^p (\mu_s y)^{n-p} E_{2+p}[-\mu_s y + \mu_s(d+c)]\right]_{d+c}^{c}$$

$$- \frac{S_n}{2\mu_s}\frac{1}{\mu_s^n}\left[\sum_{p=0}^{n} \frac{n!}{(n-p)!} (\mu_s y)^{n-p} E_{2+p}[\mu_s y - \mu_s(d+c)]\right]_{d+c}^{h+c} \qquad (49)$$

After substituting the limits and rearranging terms,

$$\phi_u = \frac{S_n}{2\mu_s}\frac{1}{\mu_s^n}\sum_{p=0}^{n} \frac{n!}{(n-p)!}\left\{[1 + (-1)^p]\frac{[\mu_s(d+c)]^{n-p}}{1+p}\right.$$

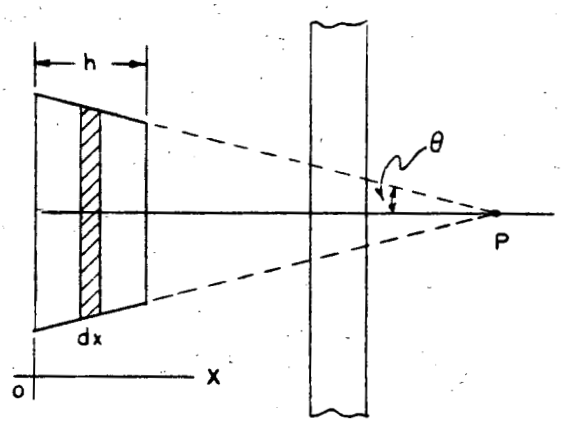
$$\left. - [\mu_s(h+c)]^{n-p} E_{2+p}[\mu_s(h-d)] - (-1)^p (\mu_s c)^{n-p} E_{2+p}(\mu_s d)\right\} \qquad (50)$$

If the source has the form of a polynomial

$$S_V(x) = \sum_n S_n(x+c)^n$$

then the answer is a sum over n terms like Eq. 50.

II-5 TRUNCATED RIGHT-CIRCULAR CONE SOURCE



The uncollided flux reaching P from the differential volume element between x and x + dx is given by the disk kernel previously derived with

$$S_A = S_V\, dx$$

$$d\phi_u = \frac{S_V(x)\, dx}{2}\left\{E_1[b_1 + \mu_s(h - x)] - E_1[(b_1 + \mu_s h - \mu_s x)\sec\theta]\right\} \tag{51}$$

The flux ϕ_u is the integral from 0 to h of this kernel. If $S_V(x) = S_i e^{k_i x}$ with $k_i \neq 0$, then

$$\phi_u = \frac{S_i}{2}\int_0^h e^{k_i x}\left\{E_1[b_1 + \mu_s h - \mu_s x] - E_1[(b_1 + \mu_s h)\sec\theta - \mu_s x \sec\theta_x]\right\} dx \tag{52}$$

Using the integration formula[5]

$$\int e^{kx}\, E_1(b + ax)\, dx = \frac{1}{k}\left\{e^{kx}\, E_1(\beta + ax) - e^{kb/a}\, E_1\left[(b + ax)\left(1 - \frac{k}{a}\right)\right]\right\} \tag{53}$$

$$\phi_u = \frac{S_i}{2k_i}\left\{e^{k_i x}\, E_1(b_1 + \mu_s h - \mu_s x) - e^{k_i b_3/\mu_s}\, E_1\left[(b_1 + \mu_s h - \mu_s x)\left(1 + \frac{k_i}{\mu_s}\right)\right]\right\}$$

$$- e^{k_i x}\, E_1[(b_1 + \mu_s h)\sec\theta - \mu_s x \sec\theta]$$

$$+ e^{k_i b_3/\mu_s}\, E_1\left[(b_1 + \mu_s h - \mu_s x)\sec\theta\left(1 + \frac{k_i}{\mu_s \sec\theta}\right)\right]\Bigg|_0^h \tag{54}$$

where $b_3 \equiv b_1 + \mu_s h$. After substituting the limits and rearranging

$$\phi_u = \frac{S_i}{2k_i}\left(\left\{e^{k_i h}\,[E_1(b_1) - E_1(b_1\sec\theta)] - e^{k_i b_3/\mu_s}\left[E_1\left(b_1\frac{\mu_s + k_i}{\mu_s}\right) - E_1\left(b_3\frac{\mu_s + k_i}{\mu_s}\right)\right]\right\}\right.$$

$$\left. - [E_1(b_3) - E_1(b_3\sec\theta)] + e^{k_i b_3/\mu_s}\left[E_1\left(b_1\frac{\mu_s\sec + k_i}{\mu_s}\right) - E_1\left(b_3\frac{\mu_s\sec + k_i}{\mu_s}\right)\right]\right) \tag{55}$$

If the source is a linear sum of exponentials, then ϕ_u is given by a linear sum of terms like that above.

If $S_V(x) = S_n(x + c)^n$ with $n \geq 0$, then Eq. 52 is replaced by

$$\phi_u = \frac{S_n}{2}\int_0^h (x + c)^n\left\{E_1(b_1 + \mu_s h - \mu_s x) - E_1[(b_1 + \mu_s h)\sec\theta - \mu_s x \sec\theta]\right\} dx \tag{56}$$

After substitution, $y \equiv x + c$

$$\phi_u = \frac{S_n}{2}\int_c^{h+c} y^n\left\{E_1(b_1 + \mu_s h + \mu_s c - \mu_s y) - E_1[(b_1 + \mu_s h + \mu_s c)\sec\theta - \mu_s y \sec\theta]\right\} dy \tag{57}$$

$$\phi_u = -\frac{S_n}{2}\sum_{i=0}^{n}\frac{n!}{(n-i)!}\frac{y^{n-i}}{(-\mu_s)^{i+1}}\left\{E_{2+1}(b_1 + \mu_s h + \mu_s c - \mu_s y)\right.$$

$$\left. - E_{2+1}[(b_1 + \mu_s h + \mu_s c)\sec\theta - \mu_s y \sec\theta]\right\}\Bigg|_c^{h+c} \tag{58}$$

or

$$\phi_u = \frac{S_n}{2\mu_s} \sum_{i=0}^{n} \frac{(-1)^i\, n!}{(\mu_s)^i\,(n-i)!} \left\{ (h+c)^{n-i} \left[E_{2+i}(b_1) - \frac{E_{2+i}(b_1 \sec\theta)}{(\sec\theta)^{i+1}} \right] - c^{n-i} \left[E_{2+i}(b_3) - \frac{E_{2+i}(b_3 \sec\theta)}{(\sec\theta)^{i+1}} \right] \right\} \quad (59)$$

If the source strength per unit volume is given by a power series

$$S_V(x) = \sum_{n=0}^{N} S_n (x+c)^n$$

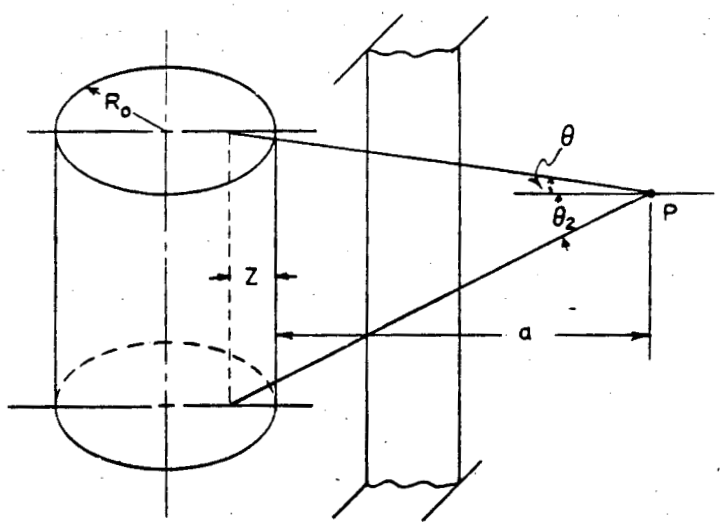
then the flux is a linear sum of terms like that above.

If, as a special case of the above, $S_V(x) = S_V$ = constant, then it follows directly from Eq. 59 that

$$\phi_u = \frac{S_V}{2\mu_s} \left[E_2(b_1) - E_2(b_3) + \frac{E_2(b_3 \sec\theta)}{\sec\theta} - \frac{E_2(b_1 \sec\theta)}{\sec\theta} \right] \quad (60)$$

II-6 CYLINDRICAL SOURCE

II-6.1 Exterior on Side



A right-circular cylindrical source with constant source strength S_V per unit volume can be approximated by a line source having source strength per unit length

$$S_L = (\pi R_0^2) S_V \quad (61)$$

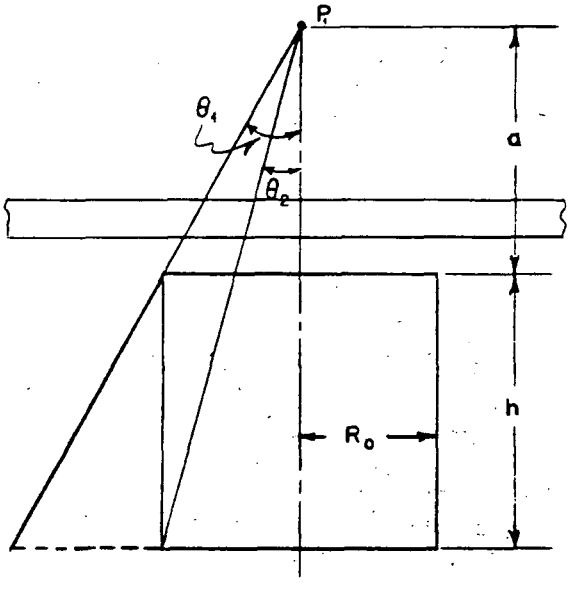
provided the line source is placed within the cylinder to correctly account for the self-absorption of the cylinder. There is no simple relation of the form $Z = Z(R_0, a, b_1)$ governing the

placement of the equivalent line source. However, by empirically fitting the approximate method to the exact calculations of Report WAPD-RM-213,[6] it has been found possible to reduce the many pages of curves in that report to three curves for Z plus the $F(\theta,b)$ curves.

For values of $a/R_0 \geq 10$ the curve of $\mu_s Z$ vs. $\mu_s R_0$ (which originally appeared in the Project Handbook[2]) has been found to yield an error in the flux of less than 10 per cent. For certain values of $a/R_0 < 10$, this curve will yield fluxes which are off by more than a factor of 10.

For values of $a/R_0 < 10$ the other two graphs should be used in conjunction with each other to obtain $\mu_s Z$. Knowing R_0, a, and μ_s, find m from the first graph; knowing a/R_0 and b_1, find $\mu_s Z/m$ from the second graph; then multiply these together to obtain $\mu_s Z$. In all cases the error in the flux will be equal to, or less than, +40 per cent and −5 per cent. The maximum positive errors tend to appear with large values of b_1 and small values of a/R_0; the maximum negative errors appear with large values of a/R_0.

II-6.2 Exterior on End



P_1 is a point on the axis of a right-circular cylinder of radius R_0 and height h.

An upper limit to the uncollided flux that reaches P_1 can be obtained by replacing the cylinder with a truncated cone, the apex of which is at P_1. The radius of that face of the truncated cone nearest the point P_1 is taken to be R_0. Defining

$$\theta_1 \equiv \tan^{-1}\left(\frac{R_0}{a}\right) \tag{62}$$

then, from the equations for the truncated cone source (Eqs. 51 to 60)

$$\phi_u = \frac{S_V}{2\mu_s}\left[E_2(b_1) - E_2(b_3) + \frac{E_2(b_3 \sec\theta_1)}{\sec\theta_1} - \frac{E_2(b_1 \sec\theta_1)}{\sec\theta_1}\right] \tag{63}$$

A lower limit can be obtained by replacing the cylinder with a truncated cone having apex angle

$$\theta_2 \equiv \tan^{-1}\left(\frac{R_0}{a+h}\right) \tag{64}$$

in which case

$$\phi_u = \frac{S_V}{2\mu_s}\left[E_2(b_1) - E_2(b_3) + \frac{E_2(b_3 \sec\theta_2)}{\sec\theta_2} - \frac{E_2(b_1 \sec\theta_2)}{\sec\theta_2}\right] \tag{65}$$

It is obvious that Eq. 63 overestimates and that Eq. 65 underestimates the flux. The degree of over- and underestimation can be somewhat reduced in those cases where $\mu_s h > 3$ by assuming that only the first three mean free paths of cylinder material will contribute appreciably to the flux. Furthermore, since $E_2(b_1 + 3) \ll E_2(b_1)$, all terms involving b_3 can be dropped.

The upper limit is given by

$$\phi_u = \frac{S_V}{2\mu_s}\left[E_2(b_1) - \frac{E_2(b_1 \sec\theta_1)}{\sec\theta_1}\right] \tag{66}$$

where $\theta_1 \equiv \tan^{-1}\left(\frac{R_0}{a}\right)$

The lower limit is given by

$$\phi_u = \frac{S_V}{2\mu_s}\left[E_2(b_1) - \frac{E_2(b_1 \sec\theta_3)}{\sec\theta_3}\right] \tag{67}$$

where $\theta_3 \equiv \tan^{-1}\left(\frac{R_0}{a + h'}\right)$ and $h' \equiv \frac{3}{\mu_s}$

II-6.3 Interior

The point P_1 is on the principal axis of a right-circular cylinder of radius R_0 and height h. It is a distance h_1 from one end and h_2 from the other. Consider first only contributions to the uncollided flux from above the point P_1.

The "line source" located between r and r + dr and α and $\alpha + d\alpha$ subtends an angle $\tan^{-1}(h_1/r)$ at P_1 and has a source strength $S_L = S_V r\, d\alpha\, dr$ per unit length. It is shielded from P_1 by a slab of thickness $b' \equiv \mu_s r$.

It therefore contributes

$$\frac{S_L}{4\pi r} F(\theta, b') = \frac{S_V\, d\alpha\, dr}{4\pi} F\left(\tan^{-1}\frac{h_1}{r}, \mu_s r\right) \tag{68}$$

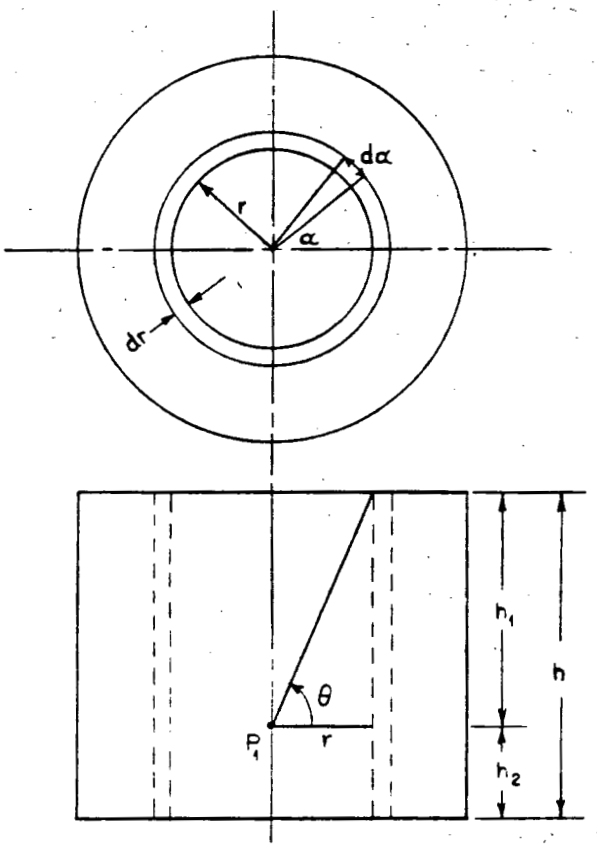
to the uncollided flux at P_1. Integrating over α yields the contribution from the annulus between r and r + dr

$$\frac{S_V}{2}\, dr\, F\left(\tan^{-1}\frac{h_1}{r}, \mu_s r\right) \tag{69}$$

and integrating over r yields the contribution from the entire cylinder above P_1

$$\frac{S_V}{2}\int_0^{R_0} dr\, F\left(\tan^{-1}\frac{h_1}{r}, \mu_s r\right) \tag{70}$$

By definition, $b' \equiv \mu_s r$ and $b \equiv \mu_s R_0$; therefore



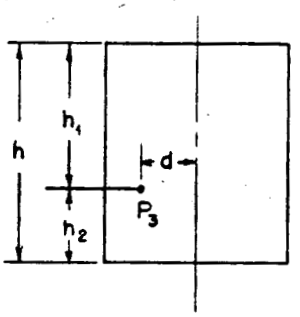
$$\frac{S_V}{2\mu_s}\int_0^b F\left(\tan^{-1}\frac{\mu_s h_1}{b'}, b'\right) db' \tag{71}$$

The part of the cylinder below P_1 yields a similar term; thus

$$\phi_u = \frac{S_V}{2\mu_s}\int_0^b db'\left[F\left(\tan^{-1}\frac{\mu_s h_1}{b'}, b'\right) + F\left(\tan^{-1}\frac{\mu h_2}{b'}, b'\right)\right] \tag{72}$$

or

$$\phi_u = \frac{S_V}{2\mu_s}\left[G(\mu_s h_1, b) + G(\mu_s h_2, b)\right] \tag{73}$$

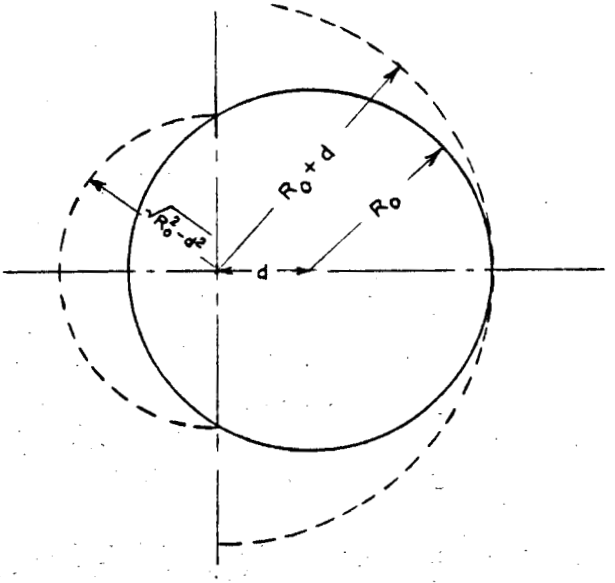


where the function $G(\mu_s h, b)$ is defined as

$$G(\mu_s h, b) \equiv \int_0^b db' F\left(\tan^{-1}\frac{\mu_s h}{b'}, b'\right) \tag{74}$$

and is included in graphical form in this report.

An upper limit to the uncollided flux at a point P_3 which is a distance d from the center line of the cylinder may be obtained by adding the contributions from the two regions enclosed by the dashed lines in the figure below.



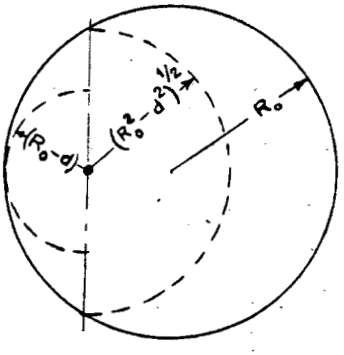
By applying Eq. 73 to the case of the two half-cylinders shown above, there results

$$\varphi_u = \frac{S_V}{4\mu_S} [G(\mu_S h_1, b_5) + G(\mu_S h_2, b_5) + G(\mu_S h_1, b_6) + G(\mu_S h_2, b_6)] \tag{75}$$

where $b_5 \equiv \mu_S (R_0 + d)$ and $b_6 \equiv \mu_S \sqrt{R_0^2 - d^2}$.

The lower limit may be obtained similarly.

The uncollided flux at P_3 from the region enclosed by the dashed lines in the accompanying figure is



$$\phi_u = \frac{S_V}{4\mu_S} [G(\mu_S h_1, b_6) + G(\mu_S h_2, b_6) + G(\mu_S h_1, b_4) + G(\mu_S h_2, b_4)] \tag{76}$$

where $b_4 \equiv \mu_S (R_0 - d)$ and $b_6 \equiv \mu_S \sqrt{R_0^2 - d^2}$.

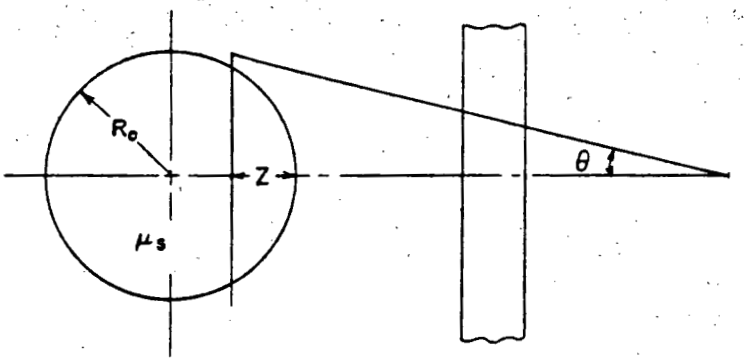
II-7 SPHERICAL SOURCE

II-7.1 Exterior

A spherical source with constant source strength S_V per unit volume can be approximated by a disk source of the same radius as the sphere having a source strength per unit area

$$S_A = (4/3\ R_0)\ S_V \tag{77}$$

provided the self-absorption distance Z is correctly chosen.



The self-absorption distance was found by empirically fitting this approximation to the exact calculations.[7]

If the point where the flux is to be calculated is at a distance from the surface of the sphere equal to, or greater than, the radius of the sphere, the first graph ($\mu_s Z$ vs. $\mu_s R_0$) (p. 369) should be used. The maximum errors will not exceed −5 per cent and +15 per cent.

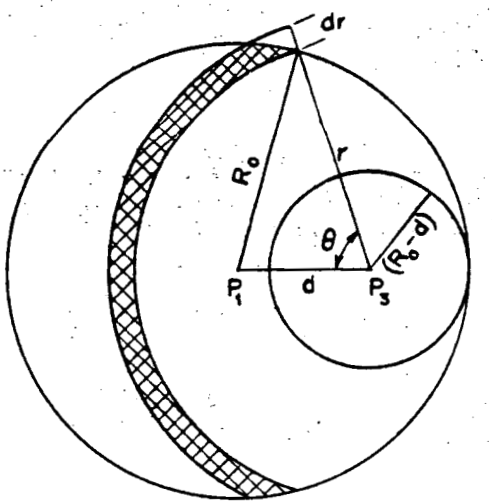
When the flux is to be calculated at a distance less than the radius away from the surface of the sphere, the second graph [Z/R_0 vs. $\mu_s(a + R_0)$] (p. 370) should be used. The maximum errors in this region are −20 to +50 per cent; the largest negative errors appearing for small shield absorption distances b_1 and points close to the sphere. The largest positive error appears with large b_1's and points close to the sphere. At the surface of the sphere, with b_1 equal to 0, the exact solution should be used.

II-7.2 Interior

The uncollided flux reaching P_3 will be the sum of the flux from the sphere of radius ($R_0 - d$) centered at P_3 plus the flux from the region outside this small sphere but inside the large sphere centered at P_1. The integral over the small sphere yields

$$\phi_1 = S_V \int_0^{R_0-d} 4\pi r^2 \, dr \, \frac{e^{-\mu_s r}}{4\pi r^2}$$

$$= \frac{S_V}{\mu_s}\left[1 - e^{-\mu_s(R_0-d)}\right] \qquad (78)$$



The volume element used in the integration over the rest of the source is a segment of a spherical shell as shown in the accompanying diagram. Its volume is

$$dV = 2\pi r^2(1 - \cos\theta)\, dr \qquad (79)$$

Thus

$$\phi_2 = S_V \int_{R_0-d}^{R_0+d} \frac{e^{-\mu_s r}}{4\pi r^2} \, 2\pi r^2(1 - \cos\theta)\, dr \qquad (80)$$

Replacing cos θ by its expression in terms of the sides of the triangle

$$\cos\theta = \frac{1}{2}\left[\frac{r}{d} + \frac{1}{r}\left(\frac{d^2 - R_0^2}{d}\right)\right] \tag{81}$$

yields

$$\phi_2 = \phi_{21} + \phi_{22} + \phi_{23} \tag{82}$$

where

$$\phi_{21} = \frac{S_V}{2}\int_{R_0-d}^{R_0+d} e^{-\mu_s r}\, dr$$

$$= \frac{S_V}{2\mu_S}\left[e^{-\mu_s(R_0-d)} - e^{-\mu_s(R_0+d)}\right] \tag{83}$$

$$\phi_{22} = -\frac{S_V}{4}\int_{R_0-d}^{R_0+d} e^{-\mu_s r}\,\frac{r}{d}\, dr$$

$$= -\frac{S_V}{4\mu_S^2 d}\left\{e^{-\mu_s(R_0-d)}\left[\mu_S(R_0 - d) + 1\right] - e^{-\mu_s(R_0+d)}\left[\mu_S(R_0 + d) + 1\right]\right\} \tag{84}$$

$$\phi_{23} = -\frac{S_V}{4}\int_{R_0-d}^{R_0+d} \frac{e^{-\mu_s r}}{r}\left(\frac{d^2 - R_0^2}{d}\right) dr$$

$$= -\frac{S_V}{4}\left(\frac{d^2 - R_0^2}{d}\right)\left\{E_1[\mu_S(R_0 - d)] - E_1[\mu_S(R_0 + d)]\right\} \tag{85}$$

After defining $b_4 \equiv \mu_S(R_0 - d)$, $b_5 \equiv \mu_S(R_0 + d)$, adding $\phi_1 + \phi_{21} + \phi_{22} + \phi_{23} = \phi_u$, and rearranging terms

$$\phi_u = \frac{S_V}{\mu_S}\left\{1 - \frac{e^{-b_4}}{2} - \frac{e^{-b_5}}{2} - \frac{1}{4\mu_S d}\left[e^{-b_4}(1 + b_4) - e^{-b_5}(1 + b_5)\right] + \frac{b_4 b_5}{4\mu_S d}\left[E_1(b_4) - E_1(b_5)\right]\right\} \tag{86}$$

In the special case of a point on the surface of a spherical source, $d = R_0$; $b_4 = 0$; $b_5 = 2\mu_S R_0$; and the term involving $(R_0^2 - d^2)/4d$ does not appear in the expression for ϕ_u. In this case Eq. 86 reduces to

$$\phi_u = \frac{S_V}{2\mu_S}\left(1 - \frac{1}{2\mu_S R_0} + \frac{e^{-2\mu_s R_0}}{2\mu_S R_0}\right) \tag{87}$$

The uncollided flux in the special case of a point at the center of a spherical source is given by Eq. 77 with $d = 0$.

$$\phi_u = \frac{S_V}{\mu_S}\left(1 - e^{-\mu_s R_0}\right) \tag{88}$$

II-8 THE FUNCTIONS $E_n(b)$, $F_n(t,a)$, $F(\theta,b)$, AND $G(\mu_s h,b)$

II-8.1 The Functions $E_n(b)$

The exponential functions $E_n(b)$ are defined by the integrals

$$E_n(b) \equiv b^{n-1} \int_b^\infty \frac{e^{-t}}{t^n}\, dt \qquad \begin{matrix} n \text{ is an integer} \geq 0 \\ b \geq 0 \end{matrix} \tag{89}$$

The graphs of $E_1(b)$ and $E_2(b)$, included in Sec. I-9, were drawn from the tables compiled by G. Placzek.[8] Interpolation in these tables, which include values of n from 0 to 20 and b from 0 to 10, is simplified by the relation

$$\frac{dE_n(b)}{db} = -E_{n-1}(b) \tag{90}$$

Thus

$$E_n(b+\delta) = E_n(b) - \delta\, E_{n-1}(b) + \frac{\delta^2}{2!} E_{n-2}(b) - \frac{\delta^3}{3!} E_{b-3}(b) + \cdots \tag{91}$$

For values of b larger than 10, an asymptotic expansion may be used

$$E_n(b) = \frac{e^{-b}}{b}\left[1 - \frac{n}{b} + \frac{n(n+1)}{b^2} - \frac{n(n+1)(n+2)}{b^3} + \cdots\right] \tag{92}$$

An approximate value for $E_n(b)$ can be obtained from the inequality

$$\frac{e^{-b}}{b+n-1} > E_n(b) > \frac{e^{-b}}{b+n} \qquad n \geq 1 \tag{93}$$

The following expansion of $E_1(b)$ is useful for small values of b.

$$E_1(b) = \sum_{n=1}^{\infty} (-1)^{n-1} \frac{b^n}{n \cdot n!} - r - \ln|b| \tag{94}$$

where $r = 0.577216\ldots$ is the Euler-Mascheroni constant.

Any other $E_n(b)$ can be reduced to $E_1(b)$ by repeated use of the recurrence relation

$$E_n(b) = \frac{1}{n-1}\left[e^{-b} - b\, E_{n-1}(b)\right] \qquad n > 1 \tag{95}$$

$E_1(b)$ is defined for negative values of the argument by

$$E_1(b) = -\mathrm{Ei}(-b) \qquad b < 0 \tag{96}$$

The function Ei(b) is defined by the integral

$$\mathrm{Ei}(b) \equiv \int_{-\infty}^{b} \frac{e^t}{t}\, dt \qquad (-\infty < b < \infty) \tag{97}$$

This function has been tabulated over the range from 0 to 10 in intervals of 0.001 in the W. P. A. tables.[9] Beyond b = 10 an asymptotic expansion may be used

$$\mathrm{Ei}(b) = \frac{e^b}{b}\left(1 + \frac{1}{b} + \frac{2!}{b^2} + \frac{3!}{b^3} + \cdots\right) \tag{98}$$

II-8.2 The Functions $F_n(t,a)$

The functions $F_n(t,a)$ arise frequently in problems of radiative transfer. The functions are defined as

$$F_n(t,a) \equiv \int_0^t e^{ax} E_n(x)\, dx \tag{99}$$

The function of particular interest in shielding applications is $F_1(t,a)$. This function has the following forms in various regions of a. For $a > 1$

$$F_1(t,a) = \frac{1}{a}\left\{e^{at} E_1(t) - E_1[t(1-a)] - \ln(a-1)\right\}$$

For $a = 1$

$$F_1(t,1) = e^t E_1(t) + \ln(t) + r$$

where $r = 0.5772156\ldots$. For $a < 1$ but $\neq 0$

$$F_1(t,a) = \frac{1}{a}\left\{e^{at} E_1(t) - E_1[t(1-a)] - \ln(1-a)\right\}$$

For $a = 0$

$$F_1(t,0) = 1 - E_2(t)$$

Tables of $F_n(t,a)$ may be found in references 10 and 11. Graphs of $F_1(t,a)$ are included here in Sec. I-4.2.

II-8.3 The Function $F(\theta,b)$

The function $F(\theta,b)$ is defined by the integral

$$F(\theta,b) \equiv \int_0^\theta e^{-b\sec\theta}\, d\theta \qquad \begin{matrix} b \geq 0 \\ \frac{\pi}{2} \geq \theta \geq 0 \end{matrix} \tag{100}$$

Graphs of this function computed by M. J. Burns and L. Ondis on the Circle Digital Computer at the Westinghouse Atomic Power Division are given in Sec. I-9. The included ranges are $32 \geq b \geq 0$ and $90° \geq \theta \geq 1°$. For values of θ less than 5° a good approximation is

$$F(\theta,b) \doteq \theta\, e^{-b} \qquad \theta < 5° \tag{101}$$

A useful interpolation formula is

$$F(\theta + \delta, b) \doteq F(\theta, b) + \delta\, e^{-b\sec\theta} \qquad (\delta \text{ in radians}) \qquad (102)$$

II-8.4 The Function $G(\mu_s h, b)$

The function $G(\mu_s h, b)$ is defined by the integral

$$G(\mu_s h, b) \equiv \int_0^b F\left(\tan^{-1}\frac{\mu_s h}{b'}, b'\right) db' \qquad (103)$$

where F is the function $F(\theta, b)$ previously defined, i.e.,

$$F\left(\tan^{-1}\frac{\mu_s h}{b'}, b'\right) = \int_0^{\tan^{-1}(\mu_s h/b')} e^{-b'\sec\theta}\, d\theta \qquad (104)$$

The curves $G(\mu_s h, b)$ included in Sec. I-7.4 were computed by numerical integration of the F function.

Part III Asymptotic Approximations

At sufficiently large distances from any finite source, the spatial variation of the flux will closely approximate that of a point source; i.e., it will fall off as the inverse square of the distance from the source. The regions of validity of the point-source approximations are derived below for several common finite sources.

III-1 LINE SOURCE

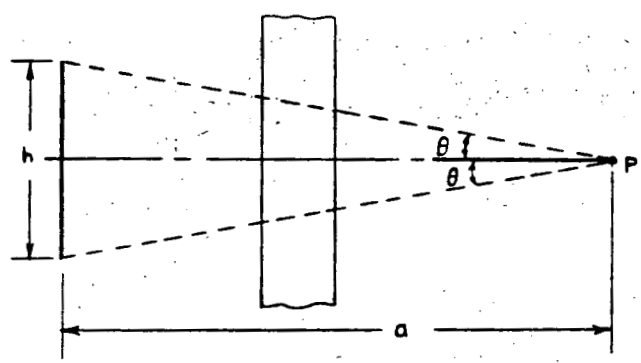
The uncollided flux at P from the line source is

$$\phi = \frac{S_L}{2\pi a} F(\theta, b_1) \qquad (105)$$

$$\phi \doteq \frac{S_L}{2\pi a}\, \theta\, e^{-b_1\sec\theta} \qquad (106)$$

$$\phi \doteq \frac{S_L}{2\pi a}\, \theta\, e^{-b_1} \qquad (107)$$

$$\phi \doteq \frac{S_L}{2\pi a}\, \frac{h/2}{a}\, e^{-b_1} \qquad (108)$$



or

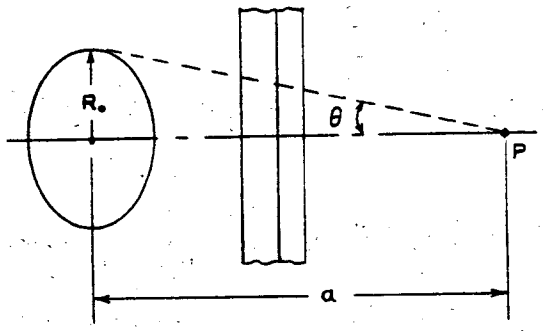
$$\phi \doteq (S_L h)\, \frac{e^{-b_1}}{4\pi a^2} \qquad (109)$$

Thus for small θ the line may be replaced by a point source at the center of the line having a source strength $S_0' = S_L h$. The errors involved in this approximation are indicated in the following table.

ϕ_{approx} (Eq. 109)/ϕ_{exact} (Eq. 105)

θ	$b_1 = 0$	$b_1 = 1$	$b_1 = 5$	$b_1 = 11$	$b_1 = 25$
1°	1.001	1.001	1.001	1.001	1.002
5°	1.003	1.004	1.009	1.016	1.036
10°	1.010	1.016	1.036	1.067	1.142
30°	1.103	1.157	1.376	1.698	2.372

III-2 DISK SOURCE



The uncollided flux at P from the disk source is

$$\phi = \frac{S_A}{2}\left[E_1(b_1) - E_1(b_1 \sec\theta)\right] \tag{110}$$

$$\phi \doteq \frac{S_A}{2}\left[E_1(b_1) - E_1\left(b_1 + \frac{b_1\theta^2}{2}\right)\right] \tag{111}$$

[$\sec\theta = 1 + (\theta^2/2)$ with less than 1 per cent error for $\theta \leq 25°$]

$$\phi \doteq \frac{S_A}{2}\left[E_1(b_1) - E_1(b_1) + \frac{b_1\theta^2}{2}\frac{e^{-b_1}}{b_1}\right] \tag{112}$$

[$E_1(b+\delta) = E_1(b) - \delta\, E_0(b)$ for $\delta \ll b$ where $E_0(b) = e^{-b}/b$]

$$\phi \doteq \frac{S_A}{4}\theta^2 e^{-b_1} \tag{113}$$

$$\phi \doteq \frac{S_A}{4}\frac{R_0^2}{a^2}e^{-b_1} \tag{114}$$

($\theta = \tan\theta$ with less than 1 per cent error for $\theta < 10°$).

Finally

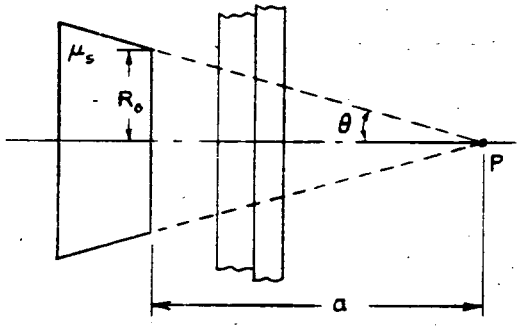
$$\phi \doteq (S_A \pi R_0^2)\frac{e^{-b_1}}{4\pi a^2} \tag{115}$$

Thus the disk source may be replaced asymptotically by a point source at its center having a source strength $S_0' = S_A \pi R_0^2$. The errors involved in this approximation are indicated in the following table.

ϕ_{approx} (Eq. 115)/ϕ_{exact} (Eq. 110)

θ	$b_1 = 0$	$b_1 = 1$	$b_1 = 5$	$b_1 = 11$	$b_1 = 25$
1°	1.00	1.00	1.00	1.00	1.00
5°	1.01	1.01	1.01	1.04	1.06
10°	1.02	1.02	1.05	1.12	1.20
30°	1.22	1.30	1.65	2.34	4.36

III-3 TRUNCATED RIGHT-CIRCULAR CONE SOURCE



The uncollided flux at P from the truncated right-circular cone source is

$$\phi = \frac{S_V}{2\mu_s}\left[E_2(b_1) - \frac{E_2(b_1 \sec\theta)}{\sec\theta}\right] \tag{116}$$

$$\phi \doteq \frac{S_V}{2\mu_s}\left[E_2(b_1) - \frac{E_2(b_1)}{1+\frac{\theta^2}{2}} + \frac{b_1\theta^2}{2}\frac{E_1(b_1)}{1+\frac{\theta^2}{2}}\right] \tag{117}$$

$$\phi \doteq \frac{S_V}{2\mu_s}\left[\frac{\theta^2}{2}E_2(b_1) + \frac{b_1\theta^2}{2}E_1(b_1)\right] \tag{118}$$

$$\phi \doteq \frac{S_V}{4\mu_s}\theta^2\left[E_2(b_1) + b_1 E_1(b_1)\right] \tag{119}$$

$$\phi \doteq \frac{S_V \pi R_0^2}{\mu_s 4\pi a^2}\left[E_2(b_1) + b_1 E_1(b_1)\right] \tag{120}$$

but $E_2(b_1) \doteq E_1(b_1)$ for $b_1 > 1$

$$\phi \doteq \frac{S_V(\pi R_0^2)}{\mu_s}\frac{1}{4\pi a^2}(b_1+1)E_1(b_1) \tag{121}$$

but $e^{-b_1}/b_1 > E_1(b_1) > e^{-b_1}/(b_1 + 1)$

$$\phi \doteq \frac{S_V \pi R_0^2}{\mu_S} \frac{e^{-b_1}}{4\pi a^2} \tag{122}$$

The truncated cone source may be replaced by a point source having a source strength $S_0' = S_V \pi R_0^2/\mu_S$ with errors as indicated in the table below.

ϕ_{approx} (Eq. 122)/ϕ_{exact} (Eq. 116)

θ	$b_1 = 0$	$b_1 = 1$	$b_1 = 5$	$b_1 = 11$	$b_1 = 25$
1°	1.02	1.02	1.02	1.02	1.02
5°	1.02	1.02	1.02	1.03	1.06
10°	1.02	1.03	1.08	1.12	1.23
30°	1.08	1.34	1.75	2.49	4.56

Part IV Effect of Scattered Radiation

The equations in Part I were derived for the uncollided flux from certain regular geometrical sources. A capital letter B (for "build-up factor") was prefixed on all equations to indicate that the answers were incomplete since they did not include quanta that were scattered one or more times before reaching the detector.

With the one exception of the point source, including B as a multiplicative factor is a purely symbolic device. Actually the build-up of radiation is usually accounted for by suitable modifications of the macroscopic cross sections. The NDA-NBS build-up factors[12] for point isotropic gamma sources in infinite mediums are functions of the initial energy of the gamma and the number of mean free paths from the source. They may be fit by a sum of exponentials[13]

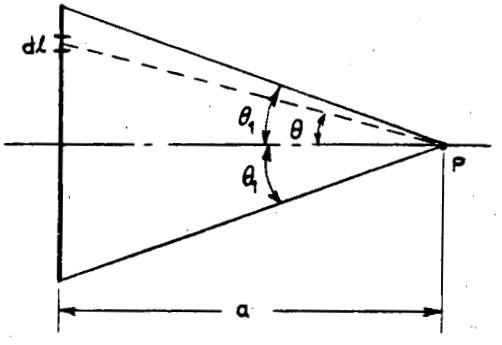
$$B(E_0,\mu\rho) = \sum_n^N A_n e^{-\alpha_n \mu\rho}$$

where A_n and α_n are functions of E_0 for a particular attenuating medium. In practice, it has been found that only two terms are required in the sum to fit the build-up factors to within 5 per cent.

IV-1 BUILD-UP IN AN INFINITE MEDIUM

Build-up can be accounted for exactly only in those cases in which the source is a group of point isotropic emitters in an infinite homogeneous medium. As an example, the flux at a distance a along the transverse center line of a line source embedded in an infinite homogeneous medium will be derived. The total macroscopic cross section of the medium is μ; the build-up factor is

$$B = \sum_{n=1}^{N} A_n e^{-\alpha_n \mu\rho}$$



The flux at P can be derived as before by integrating over the point kernel. The contribution to the uncollided flux from line segment dl is

$$d\phi_u = \frac{S_L\, dl\, e^{-\mu a \sec\theta}}{4\pi(a \sec\theta)^2} \tag{123}$$

The contribution from dl including build-up is

$$d\phi = \left(\sum_{n=1}^{N} A_n e^{-\alpha_n \mu a \sec\theta}\right) \frac{S_L\, dl\, e^{-\mu a \sec\theta}}{4\pi(a \sec\theta)^2} \tag{124}$$

or

$$d\phi = \frac{S_L\, dl}{4\pi(a \sec\theta)^2} \sum_{n=1}^{N} A_n \exp\left[-\mu(1 + \alpha_n)a \sec\theta\right] \tag{125}$$

The reason for fitting the build-up factor by a sum of exponentials is now clear. It merely replaces the old uncollided point kernel by a sum of N weighted point kernels in which the macroscopic cross sections have been modified. The integral over dl is carried out exactly as in the case of the uncollided flux. The result is

$$\phi = \frac{S_L}{2\pi a} \sum_{n=1}^{N} A_n\, F(\theta_1, b_{1n}) \tag{126}$$

where $b_{1n} = \mu(1 + \alpha_n)a$.

This equation should be compared with the one for the uncollided flux

$$\phi_u = \rho \frac{S_L}{2\pi a} F(\theta, b_1) \qquad b_1 = \mu a \tag{127}$$

The rule for including build-up which is demonstrated here is quite general for infinite homogeneous mediums.

Replace the equation for the uncollided flux by a sum of N terms (where N is the number of exponentials required to fit the point isotropic build-up factor) identical in form to the original equation but having ficticious macroscopic cross sections given by $\mu(1 + \alpha_n)$ and weights given by A_n.

IV-2 BUILD-UP WITHIN A SOURCE

If the point of interest is sufficiently deep within a source of photons that boundary effects on the flux are negligible, then the rule for the infinite medium case will apply. "Sufficiently deep" is probably of the order of one mean free path at the initial energy. As an example of this, consider the flux within a cylindrical source on the axial center line. The uncollided flux is given by

$$\phi_u = \frac{S_V}{2\mu_s} \left[G(\mu_s h_1, \mu_s R_0) + G(\mu_s h_2, \mu_s R_0)\right] \tag{128}$$

The flux including build-up is simply

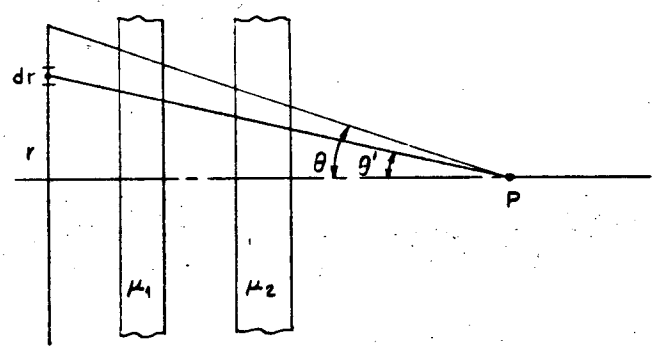
$$\phi = \frac{S_V}{2} \sum_{n=1}^{N} \frac{A_n}{\mu_{sn}} \left[G(\mu_{sn} h_1, \mu_{sn} R_0) + G(\mu_{sn} h_2, \mu_{sn} R_0)\right] \tag{129}$$

where $\mu_{sn} = \mu_s(1 + \alpha_n)$.

IV-3 BUILD-UP THROUGH LAMINATIONS

If the source is shielded by slabs of several different materials, the problem is complicated physically by the unanswered question of the correct way to combine build-up factors in multiple mediums. This physical problem will not be considered. The mathematical problem is again a simple one.

As an example, assume that the source is a disk shielded by two slabs of material with macroscopic cross sections μ_1 and μ_2.



Assume further that it has been determined (by experiment, computation, reasoning, or intuition) that the build-up factor for the flux traveling along any ray from the source to the detector is given by the product of the point isotropic build-up factors for the segments of the paths in the various mediums.

If the build-up factor in the first medium is written

$$B_1(\mu_1\rho_1) = \sum_{n=1}^{2} A_{1n} e^{-\alpha_{1n}\mu_1\rho_1}$$

and that in the second medium is written

$$B_2(\mu_2\rho_2) = \sum_{m=1}^{2} A_{2m} e^{-\alpha_{2m}\mu_2\rho_2}$$

then the flux from the differential ring between r and r + dr including build-up is

$$d\phi = \left(\sum_{n=1}^{2} A_{1n} e^{-\alpha_{1n}\mu_1\rho_1}\right)\left(\sum_{m=1}^{2} A_{2m}\, e^{-\alpha_{2m}\mu_2\rho_2}\right) \frac{S_A 2\pi r\, dr}{4\pi\rho^2} \exp\left[-(\mu_1 t_1 + \mu_2 t_2)\sec\theta'\right] \qquad (130)$$

After rearranging terms

$$d\phi = \sum_{n,m=1}^{2} A_{1n}A_{2m} \exp\left[-(\mu_{1n} t_1 + \mu_{2m} t_2)\sec\theta'\right] \frac{S_A 2\pi r\, dr}{4\pi\rho^2} \qquad (131)$$

where $\mu_{ab} \equiv (1 + \alpha_{ab})\mu_a$.

Defining:

$$b_{nm} \equiv \mu_{1n} t_1 + \mu_{2m} t_2 \qquad (132)$$

If Eq. 132 is substituted into Eq. 131, then Eq. 131 has exactly the form of the flux in the uncollided case previouslv derived. The answer is therefore

$$\phi = \frac{S_A}{2} \sum_{n,m=1}^{2} A_{1n} A_{2m} \left[E_1(b_{nm}) - E_1(b_{nm} \sec \theta) \right] \tag{133}$$

Similarly, if there were three slab shields, the answer would be

$$\phi = \frac{S_A}{2} \sum_{n,m,p=1}^{2} A_{1n} A_{2m} A_{3p} \left[E_1(b_{nmp}) - E_1(b_{nmp} \sec \theta) \right] \tag{134}$$

where $b_{nmp} \equiv \mu_{1n} t_1 + \mu_{2m} t_2 + \mu_{3p} t_3$.

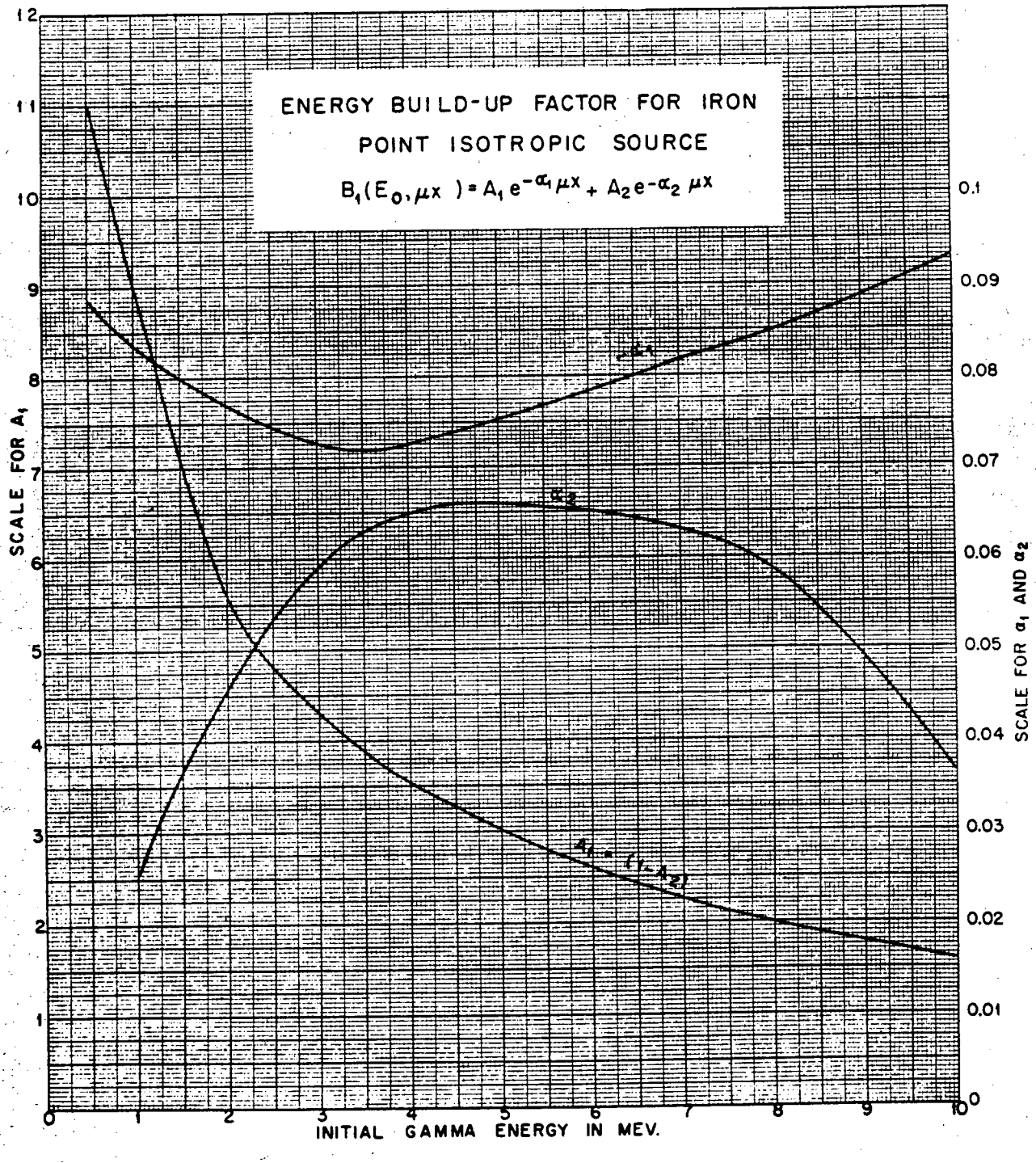
It can be seen that there are a total of 2^s terms to be evaluated, where s is the number of slabs. Each term has the same form as the uncollided flux.

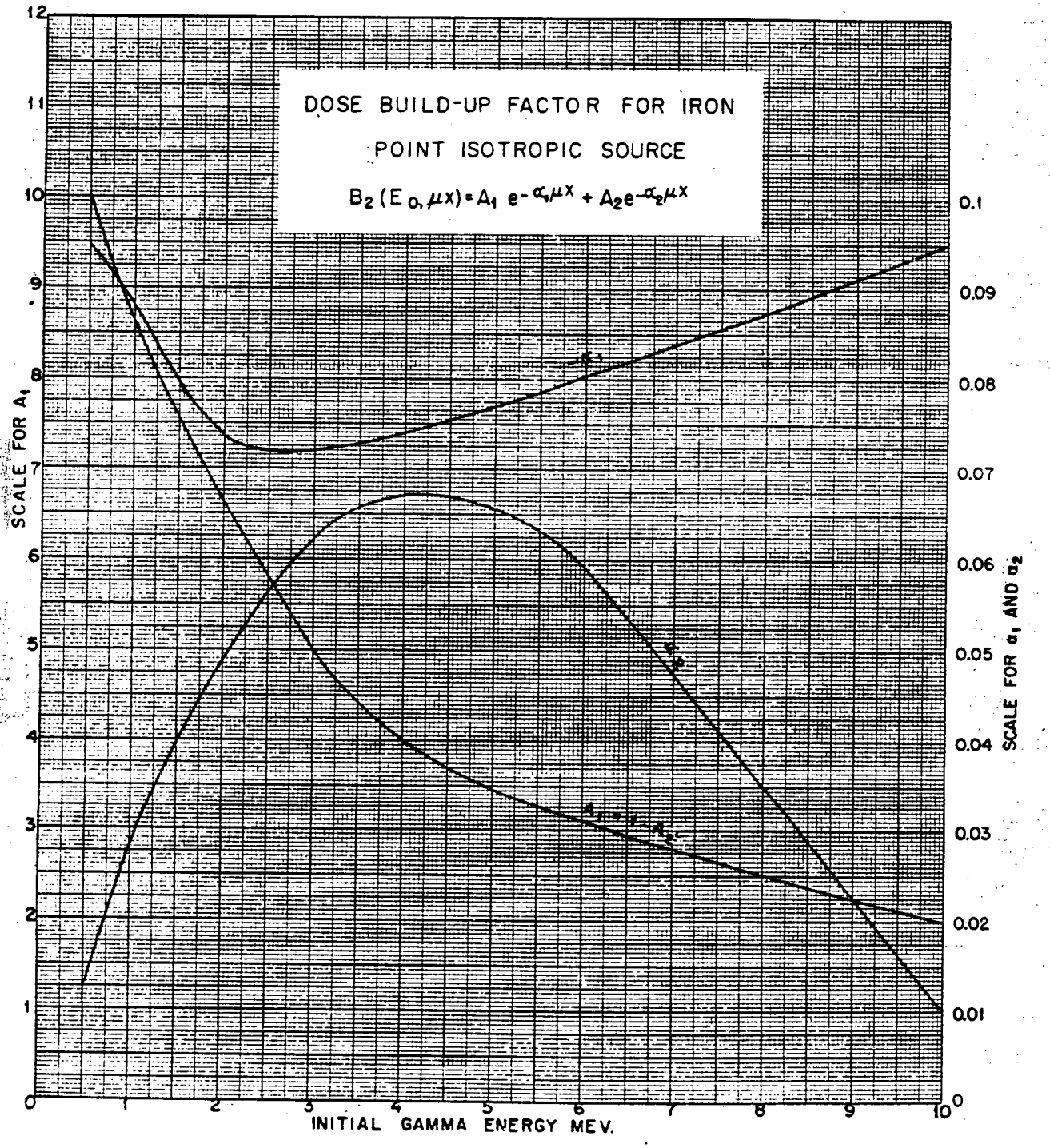
Part V Build-up Factors for Iron, Water, Lead, and Concrete

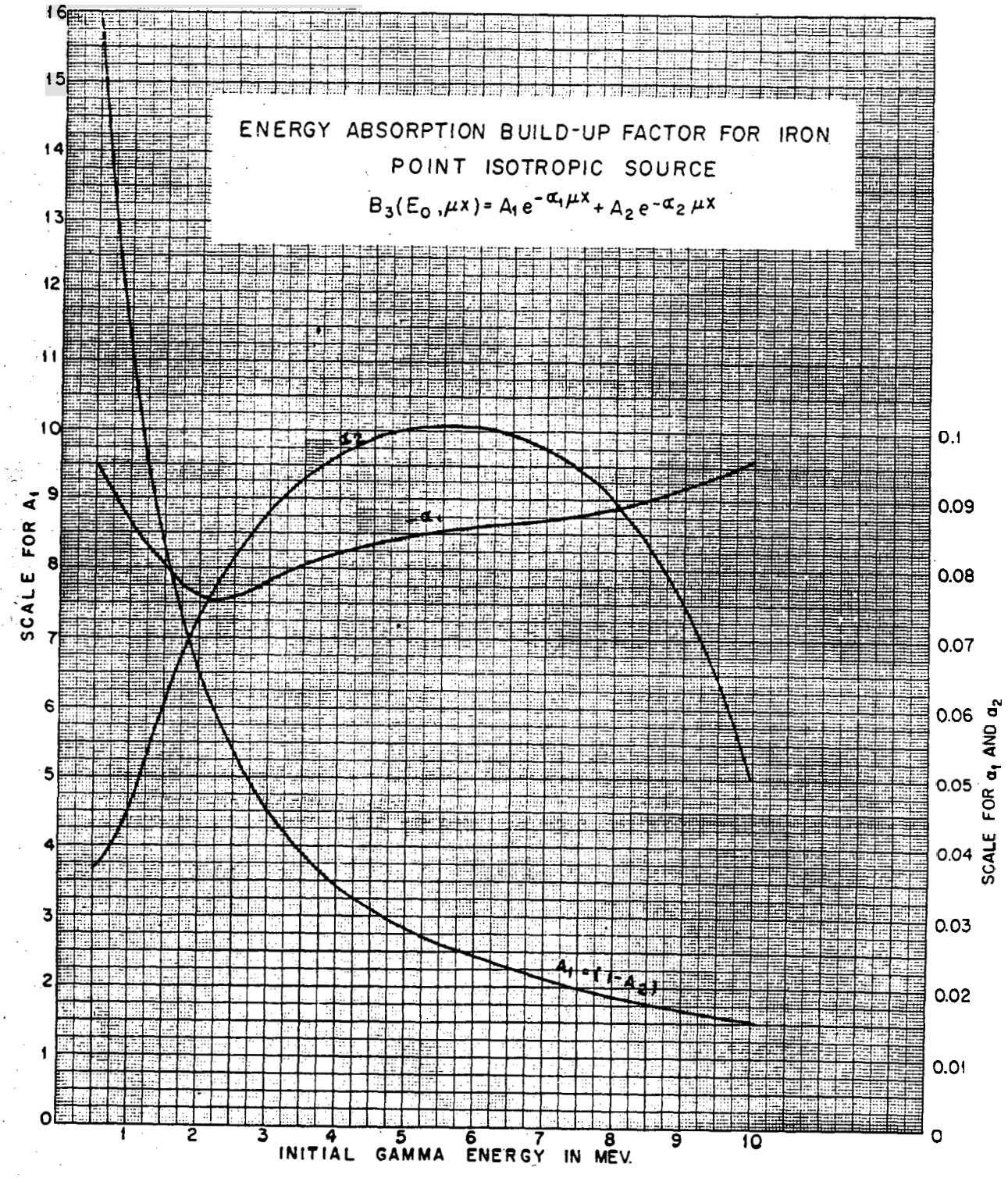
In this section are plotted parameters from which build-up factors can be calculated for iron, water, lead, and concrete. These were obtained by fitting a sum of two exponentials to the build-up factors plotted in Chap. 10, a device which simplifies many shielding calculations. The build-up factors can then be calculated from the curves by the relation

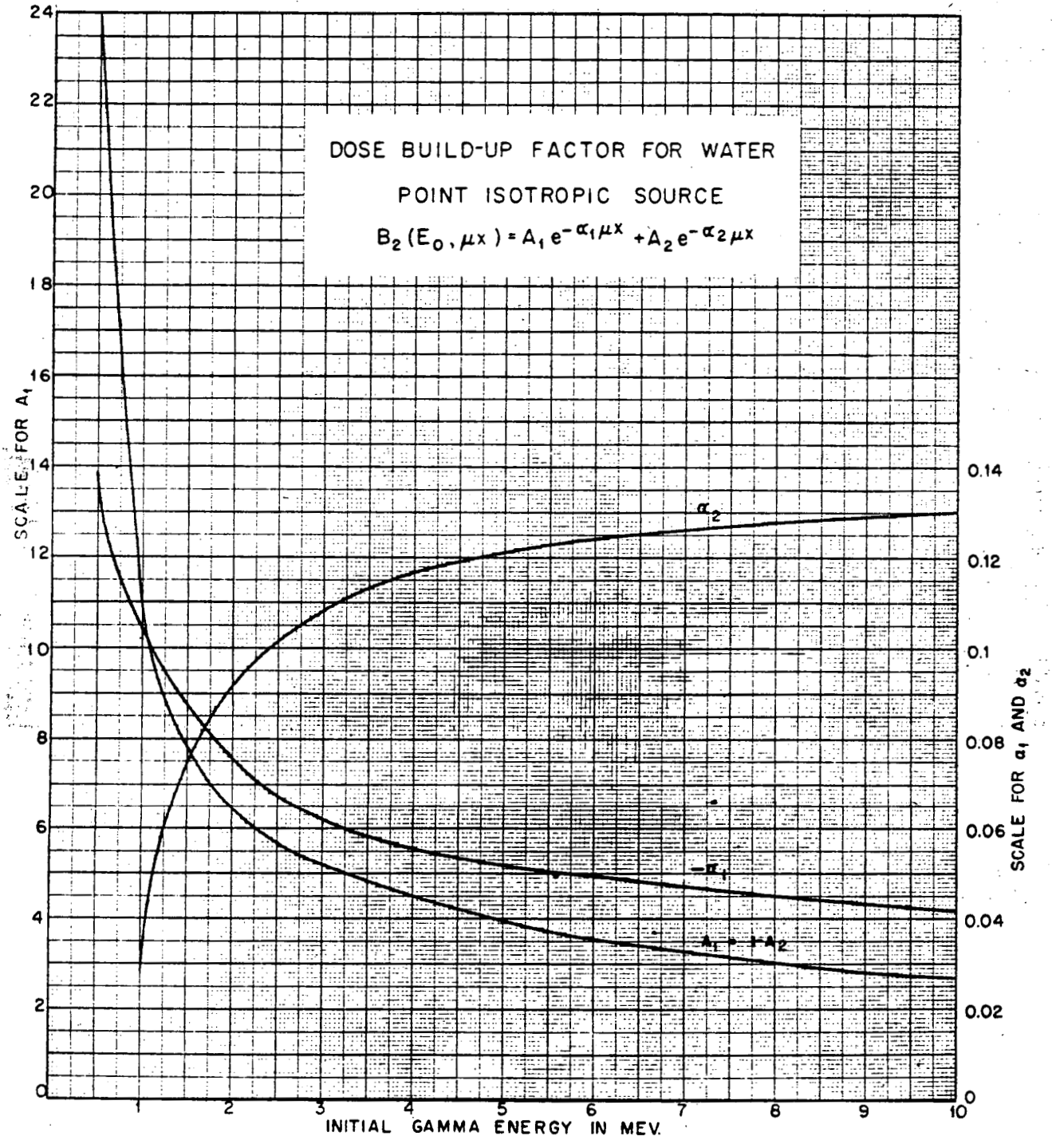
$$B(E_0, \mu x) = A_1 e^{-\alpha_1 \mu x} + A_2 e^{-\alpha_2 \mu x}$$

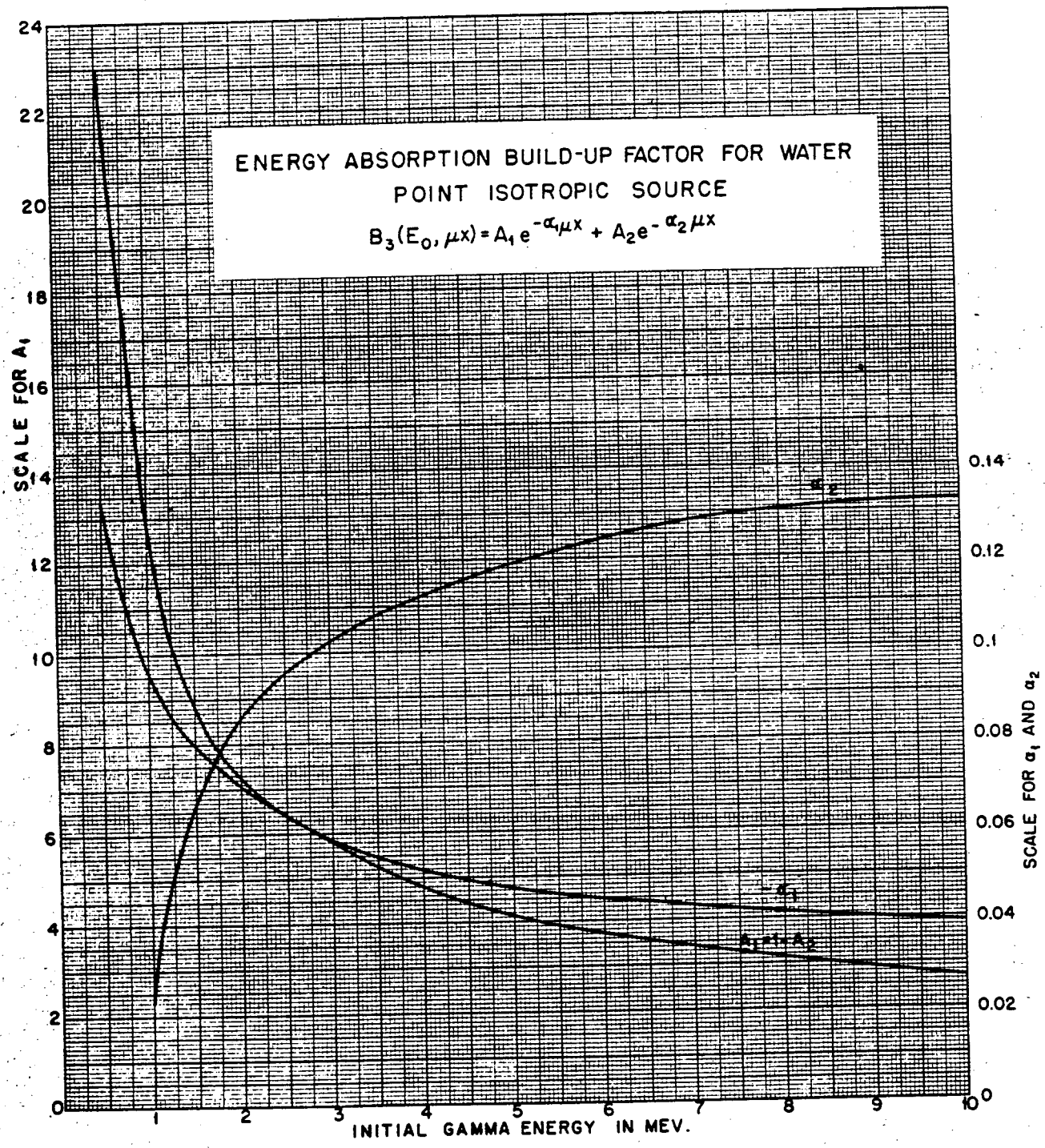
where A_1, α_1, and α_2 are plotted against E_0 (in million electron volts) and $A_2 = 1 - A_1$.

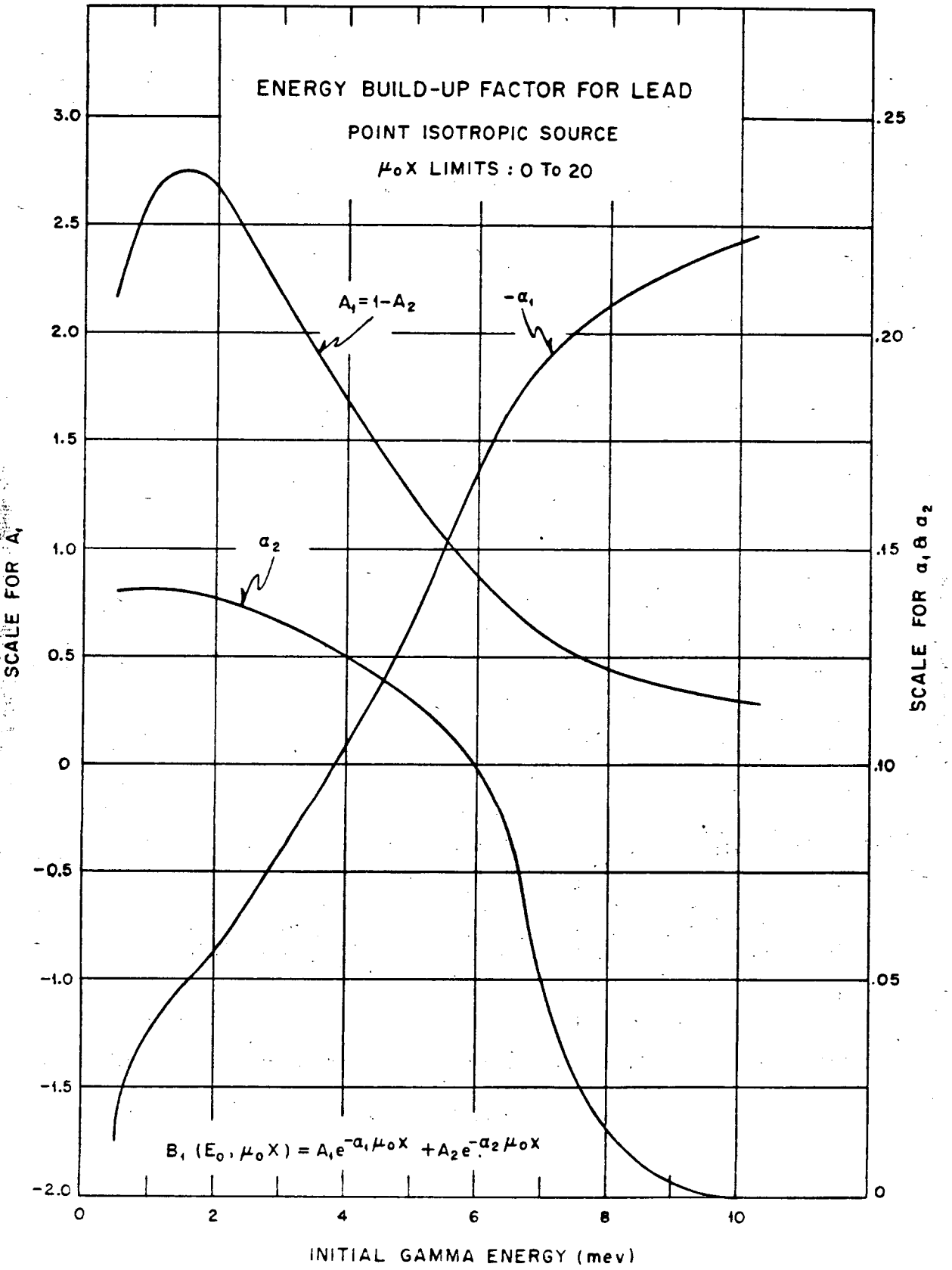

ENERGY BUILD-UP FACTOR FOR IRON
POINT ISOTROPIC SOURCE
$B_1(E_0, \mu x) = A_1 e^{-\alpha_1 \mu x} + A_2 e^{-\alpha_2 \mu x}$
SCALE FOR A_1
SCALE FOR α_1 AND α_2
INITIAL GAMMA ENERGY IN MEV.
α_1
α_2
$A_1 = (1 - A_2)$
0
1
2
3
4
5
6
7
8
9
10
11
12
0.01
0.02
0.03
0.04
0.05
0.06
0.07
0.08
0.09
0.1

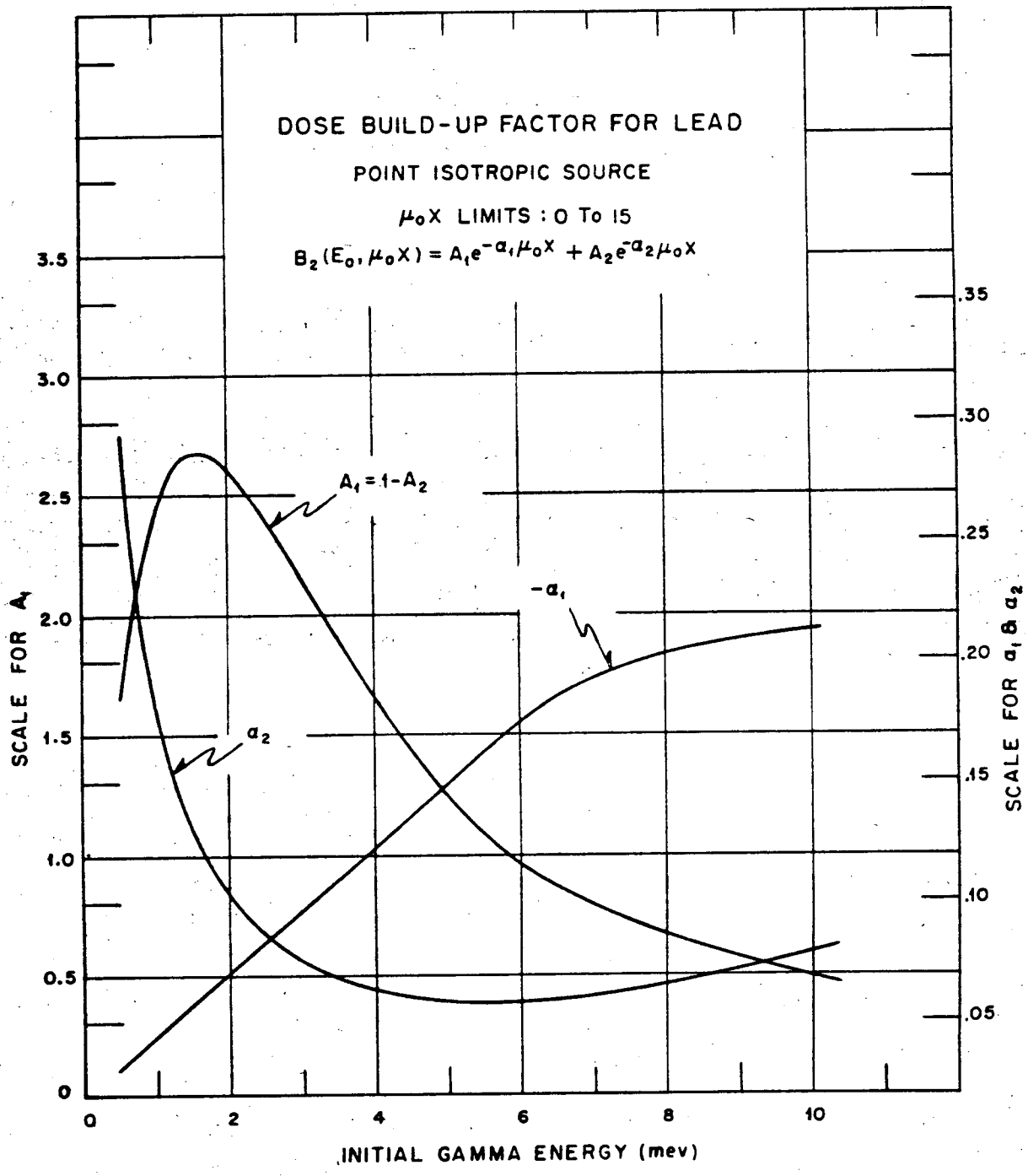

DOSE BUILD-UP FACTOR FOR IRON
POINT ISOTROPIC SOURCE
$B_2(E_0,\mu x) = A_1 e^{-\alpha_1 \mu x} + A_2 e^{-\alpha_2 \mu x}$
SCALE FOR A_1
SCALE FOR α_1 AND α_2
INITIAL GAMMA ENERGY MEV.
0
1
2
3
4
5
6
7
8
9
10
11
12
0.01
0.02
0.03
0.04
0.05
0.06
0.07
0.08
0.09
0.1

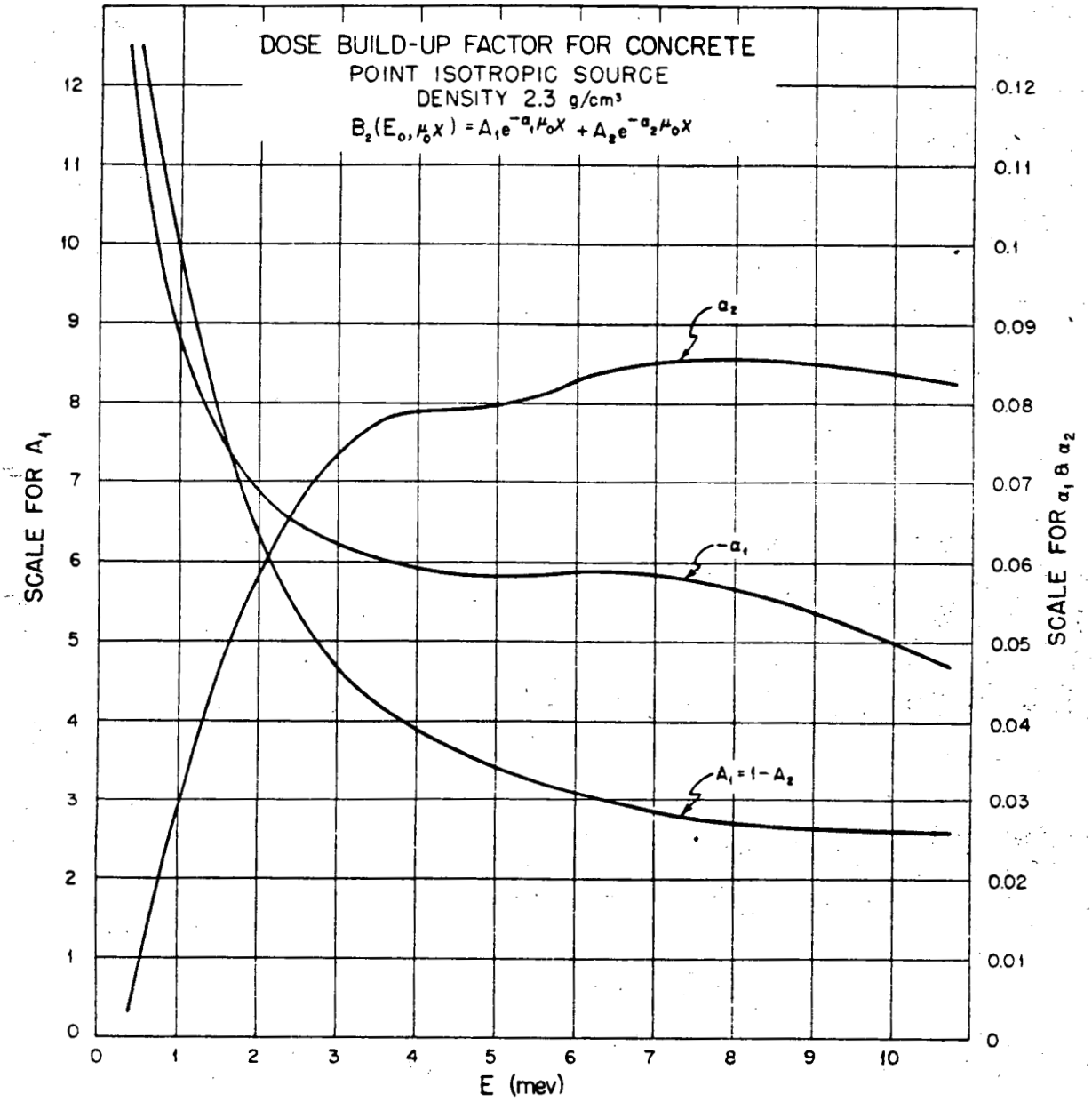

ENERGY ABSORPTION BUILD-UP FACTOR FOR IRON
POINT ISOTROPIC SOURCE
$B_3(E_0, \mu x) = A_1 e^{-\alpha_1 \mu x} + A_2 e^{-\alpha_2 \mu x}$
α_2
$-\alpha_1$
$A_1 = 1 - A_2$
SCALE FOR A_1
SCALE FOR α_1 AND α_2
INITIAL GAMMA ENERGY IN MEV.
0
1
2
3
4
5
6
7
8
9
10
11
12
13
14
15
16
0.01
0.02
0.03
0.04
0.05
0.06
0.07
0.08
0.09
0.1


DOSE BUILD-UP FACTOR FOR WATER
POINT ISOTROPIC SOURCE
$B_2(E_0, \mu x) = A_1 e^{-\alpha_1 \mu x} + A_2 e^{-\alpha_2 \mu x}$
SCALE FOR A_1
SCALE FOR α_1 AND α_2
α_2
$-\alpha_1$
$A_1 + A_2$
INITIAL GAMMA ENERGY IN MEV.
0
2
4
6
8
10
12
14
16
18
20
22
24
0.02
0.04
0.06
0.08
0.1
0.12
0.14
1
2
3
4
5
6
7
8
9
10


ENERGY ABSORPTION BUILD-UP FACTOR FOR WATER
POINT ISOTROPIC SOURCE
$B_3(E_0, \mu x) = A_1 e^{-\alpha_1 \mu x} + A_2 e^{-\alpha_2 \mu x}$
SCALE FOR A_1
SCALE FOR α_1 AND α_2
INITIAL GAMMA ENERGY IN MEV.
α_2
α_1
A_1+A_2
0
2
4
6
8
10
12
14
16
18
20
22
24
0.02
0.04
0.06
0.08
0.1
0.12
0.14
1
2
3
4
5
6
7
8
9
10


ENERGY BUILD-UP FACTOR FOR LEAD
POINT ISOTROPIC SOURCE
$\mu_0 X$ LIMITS : 0 To 20
$A_1 = 1 - A_2$
$-\alpha_1$
α_2
$B_1(E_0, \mu_0 X) = A_1 e^{-\alpha_1 \mu_0 X} + A_2 e^{-\alpha_2 \mu_0 X}$
SCALE FOR A_1
SCALE FOR α_1 & α_2
INITIAL GAMMA ENERGY (mev)
3.0
2.5
2.0
1.5
1.0
0.5
0
-0.5
-1.0
-1.5
-2.0
.25
.20
.15
.10
.05
0
0
2
4
6
8
10


DOSE BUILD-UP FACTOR FOR LEAD
POINT ISOTROPIC SOURCE
$\mu_0 X$ LIMITS : 0 To 15
$B_2(E_0, \mu_0 X) = A_1 e^{-\alpha_1 \mu_0 X} + A_2 e^{-\alpha_2 \mu_0 X}$
$A_1 = 1 - A_2$
$-\alpha_1$
α_2
SCALE FOR A_1
SCALE FOR α_1 & α_2
INITIAL GAMMA ENERGY (mev)
0
0.5
1.0
1.5
2.0
2.5
3.0
3.5
.05
.10
.15
.20
.25
.30
.35
2
4
6
8
10


DOSE BUILD-UP FACTOR FOR CONCRETE
POINT ISOTROPIC SOURCE
DENSITY 2.3 g/cm³
$B_2(E_0, \mu_0 X) = A_1 e^{-\alpha_1 \mu_0 X} + A_2 e^{-\alpha_2 \mu_0 X}$
α_2
α_1
$A_1 = 1 - A_2$
SCALE FOR A_1
SCALE FOR α_1 & α_2
E (mev)
0
1
2
3
4
5
6
7
8
9
10
11
12
0.01
0.02
0.03
0.04
0.05
0.06
0.07
0.08
0.09
0.1
0.11
0.12

Part VI *Transformation from One Geometry to Another*

VI-1 DISK-SOURCE TO POINT-SOURCE TRANSFORMATION

For a disk of radius a and at a distance z from the detector

$$D_{pl}(z,a) = 2\pi \int_z^{\sqrt{z^2+a^2}} G(R)\, dR \tag{135}$$

Differentiating Eq. 135 and defining

$$B(z) = -\frac{D'_{pl}(z,a)}{2\pi z}$$

we obtain by the recursion formula

$$G(z) = B(z) + B(\sqrt{z^2 + a^2}) + B(\sqrt{z^2 + 2a^2}) + \ldots$$

$$G(z) = \sum_{v=0}^{\infty} B(\sqrt{z^2 + va^2}) \tag{135a}$$

VI-2 PLANE TO SPHERE TRANSFORMATION

$$D_s(r_0,r) = \frac{r}{r_0} D_{pl}(r_0 - r,\infty) - D_{pl}(r_0 + r,\infty) \tag{136}$$

where r = radius of the sphere
r_0 = the distance from the axis of the sphere to the detector
$D_{pl}(x,\infty)$ = the dose from an infinite plane at distance x from the detector
x = $(r_0 - r)$ and $(r_0 + r)$

VI-3 PLANE TO CYLINDER TRANSFORMATION

$$D_c(r_0,r) = \sqrt{\frac{r}{r_0}}\, D_{pl}(r_0 - r,\infty) \tag{137}$$

where r = the radius of the cylinder
r_0 = the distance from the axis of the cylinder to the measuring point
$D_{pl}(r_0 - r,\infty)$ = the dose to be expected at a distance $(r_0 - r)$ from an infinite-plane source

VI-4 DISK TO INFINITE-PLANE TRANSFORMATION[15]

A further simplification in a bulk shield calculation may be made by calculating an equivalent infinite-plane source. If the dose from a finite disk source is known as a function of distance along the axis, then the dose to be expected from an infinite source is also known.

$$D_{pl}(z,\infty) = \sum_{v=0}^{\infty} D_{pl}(\sqrt{z^2 + va^2},a) \tag{138}$$

The total dose calculated due to this equivalent infinite plane will result in a conservative estimate of the bulk shielding requirements. When the design is more advanced, a more detailed calculation of the bulk shield should follow. This is discussed in Chap. 4, Sec. 3.4.

References

1. R. M. Sievert, Acta. Radiol., 1: 89 (1921).
2. Project Handbook, Report CL-697, Vol. II, May 1945(Classified).
3. J. H. Smith and M. L. Storm, Report KAPL-918, 1953.
4. M. L. Storm and J. H. Smith, Report KAPL-966, 1953.
5. J. LeCaine, Natl. Research Council Can., MT-131, April 1948.
6. J. J. Taylor and F. E. Obenshain, Report WAPD-RM-213, 1953.
7. F. E. Obenshain, WAPD, unpublished work.
8. G. Placzek, Natl. Research Council Can., MT-1, 1946.
9. W. P. A. Tables of Sine, Cosine, and Exponential Integrals, Vols. I and II, 1939.
10. H. C. Van de Hulst, Astrophys. J., 107: 220 (1948).
11. S. Chandrasekhar, Astrophys. J., 108: 92 (1948).
12. H. Goldstein and J. E. Wilkins, Report NYO-3075, 1954.
13. J. J. Taylor, Report WAPD-RM-217, 1954.
14. A. Foderaro and F. E. Obenshain, Report WAPD-TN-509, 1955.
15. Samuel Glasstone, "Principles of Nuclear Reactor Engineering," Chap. 10, D. Van Nostrand Company, Inc., New York, 1955.
16. A. Foderaro and F. E. Obenshain, Report WAPD-TN-508, June 1955 (Classified).

Chapter 10

BASIC DATA

CURVES OF BUILD-UP AND DIFFERENTIAL ENERGY SPECTRUMS FOR LEAD, IRON, AND WATER 430

CURVES OF ENERGY ABSORPTION AND MASS ABSORPTION COEFFICIENTS VS. ENERGY 447

RADIATION DAMAGE SUMMARY TABLES FOR SHIELDING ENGINEERS 451

TABLES AND NOMOGRAMS FOR BUILD-UP AND DECAY 456

THERMAL-NEUTRON CROSS SECTIONS AND RELATED DATA 462

CHART OF THE NUCLIDES 467

Chapter 10

BASIC DATA

This chapter contains several bits of miscellaneous data and some calculation aids which have been found useful in shield design.

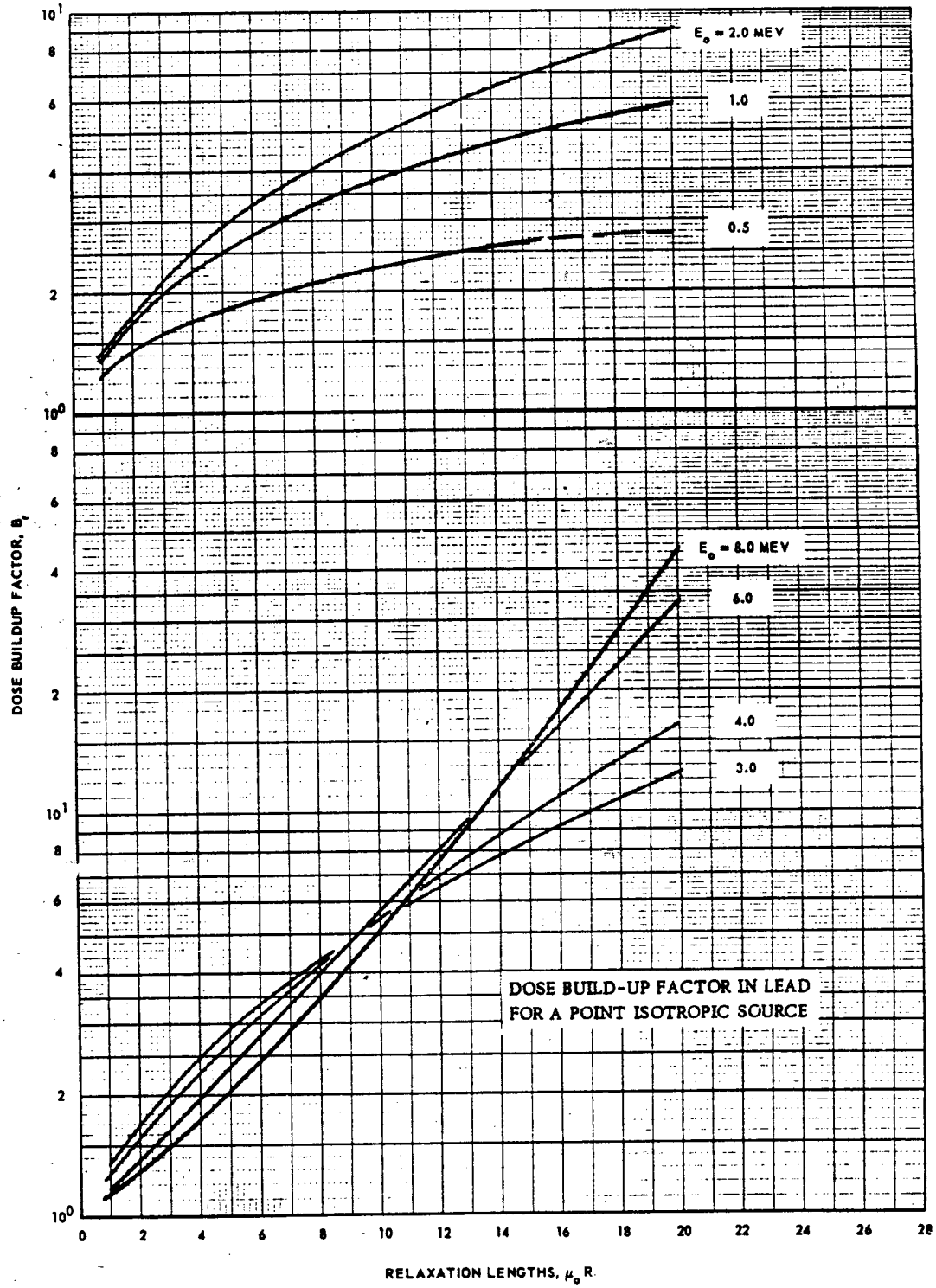
First are plotted dose build-up factors and energy absorption build-up factors for a point isotropic source for lead, iron, and water as a function of penetration into the shield expressed in relaxation lengths. Curves for several initial energies are given. These curves are taken from Report APEX-176, by John Moteff, based on data from Report NYO-3075, Calculations of the Penetration of Gamma Rays, by H. Goldstein and J. E. Wilkins, Jr. These data were calculated by the moments method developed by U. Fano and L. V. Spencer at the National Bureau of Standards.

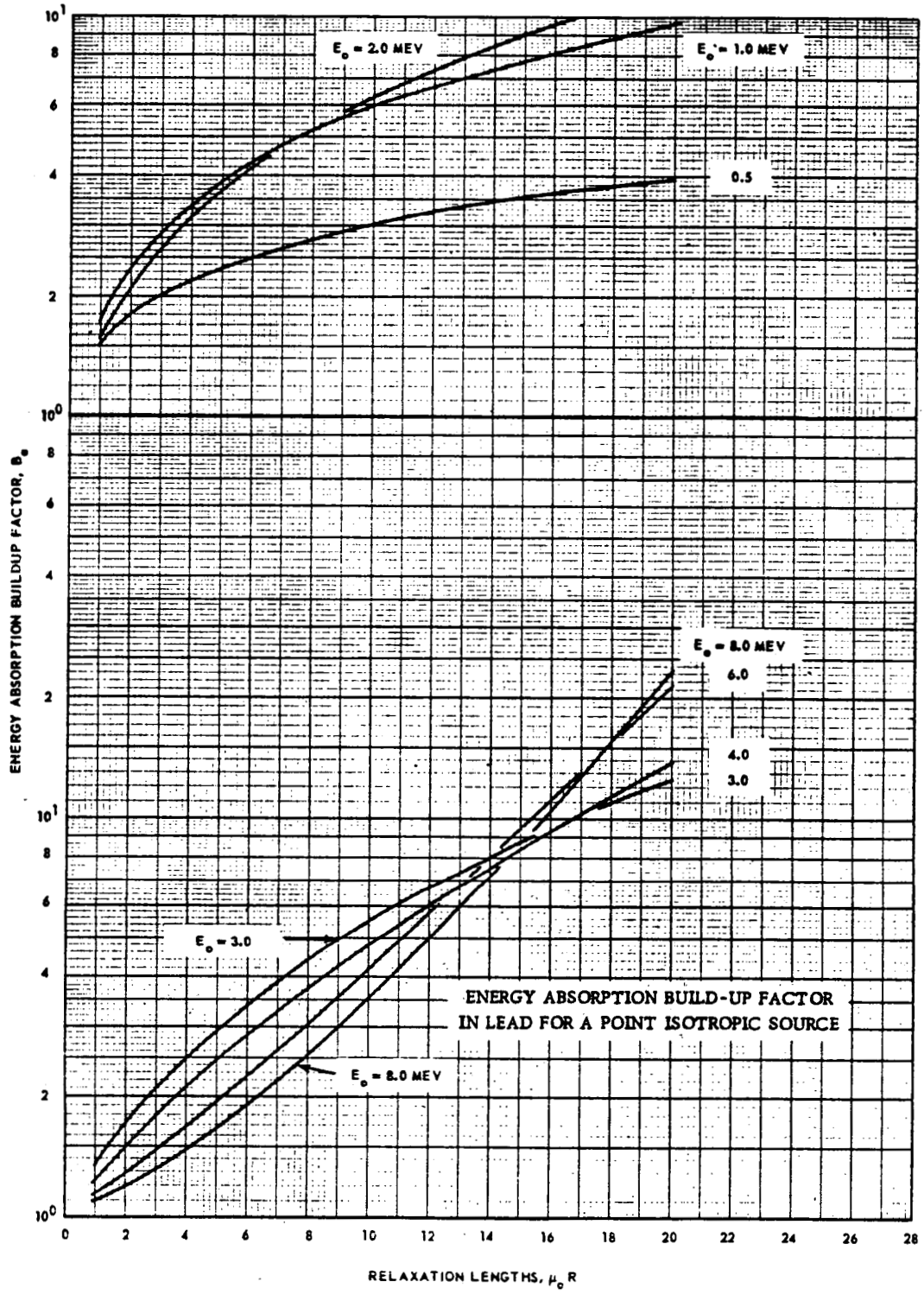
The energy absorption build-up factor B_a is defined by the following relation:

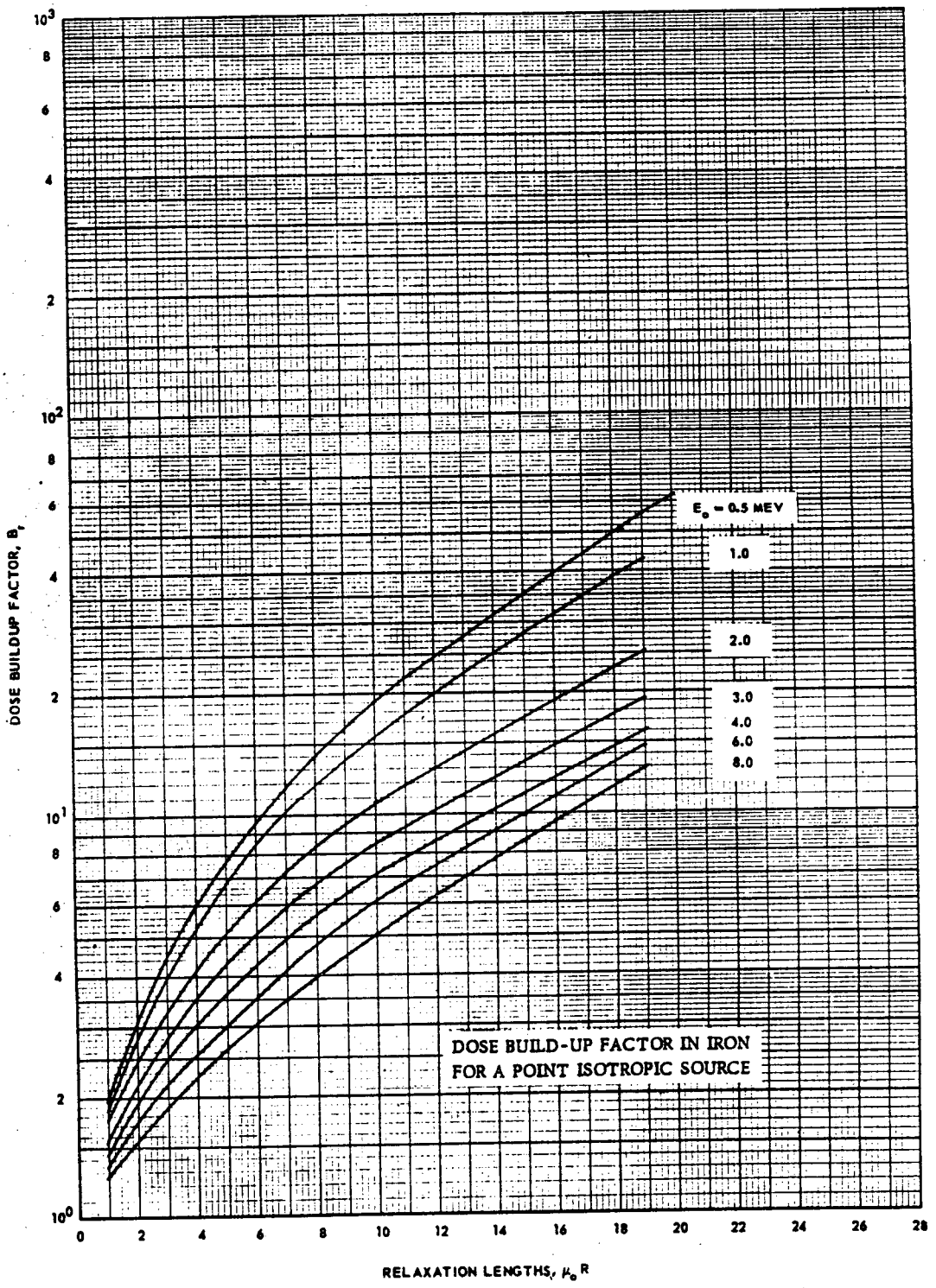
$$B_a = \frac{\int \mu_a(E)\, I_0(\vec{r},E)\, dE}{\int \mu_a(E)\, I_0^0(\vec{r},E)\, dE}$$

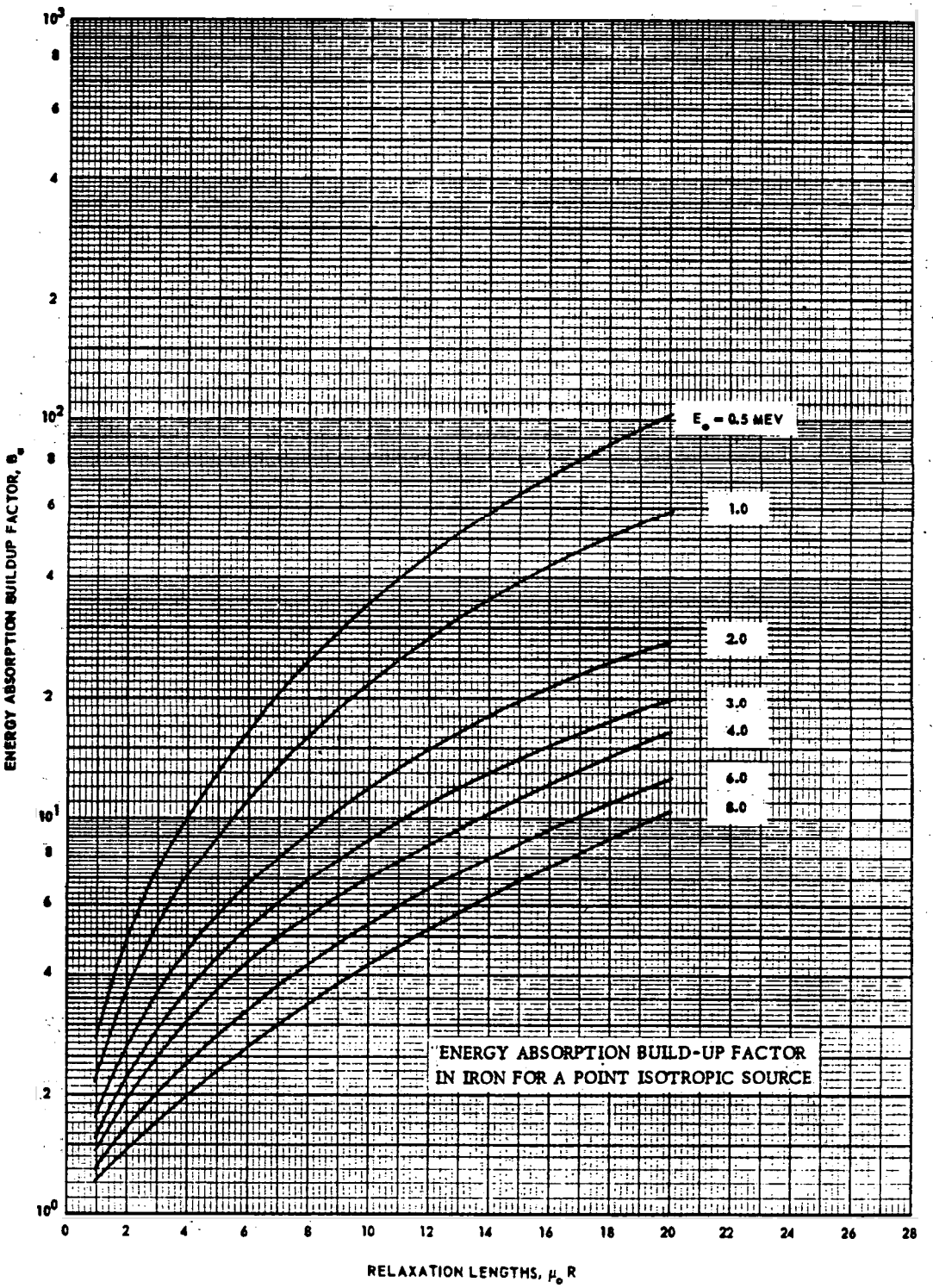
where $\mu_a(E)$ is the energy absorption coefficient of the medium itself and $I_0(\vec{r},E)$ is the total energy flux of energy E, incident on a unit differential volume at $\vec{r}$ and $I_0^0(\vec{r},E)$ is the unscattered portion of the flux at $\vec{r}$. The dose build-up factor B_r is defined by the same expression as the energy absorption build-up except that the absorption coefficient is that of air (detector assumed to be an ideal air-wall ionization chamber).

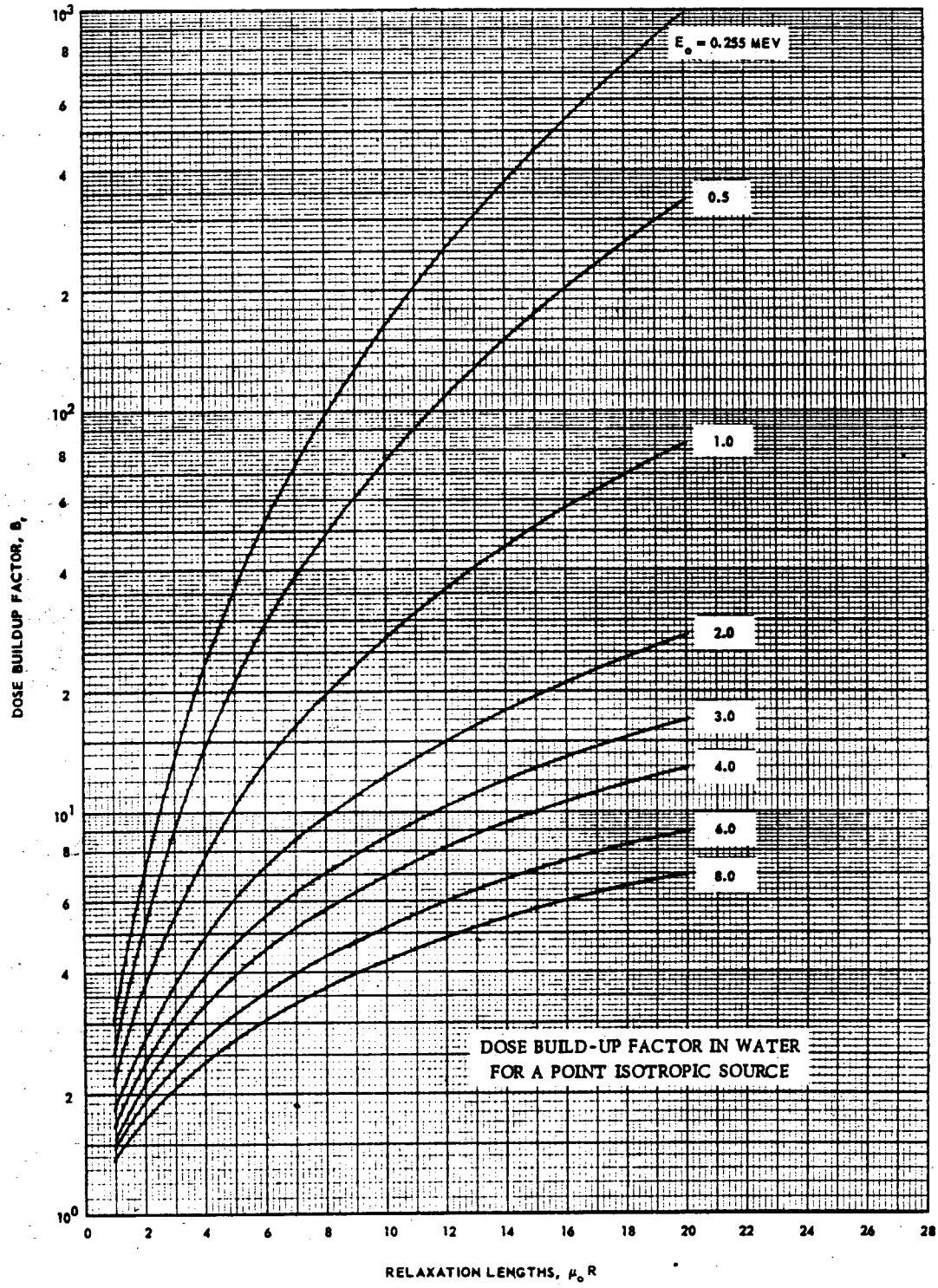
Also included from Report NYO-3075 are differential energy spectrums for lead, iron, and water.

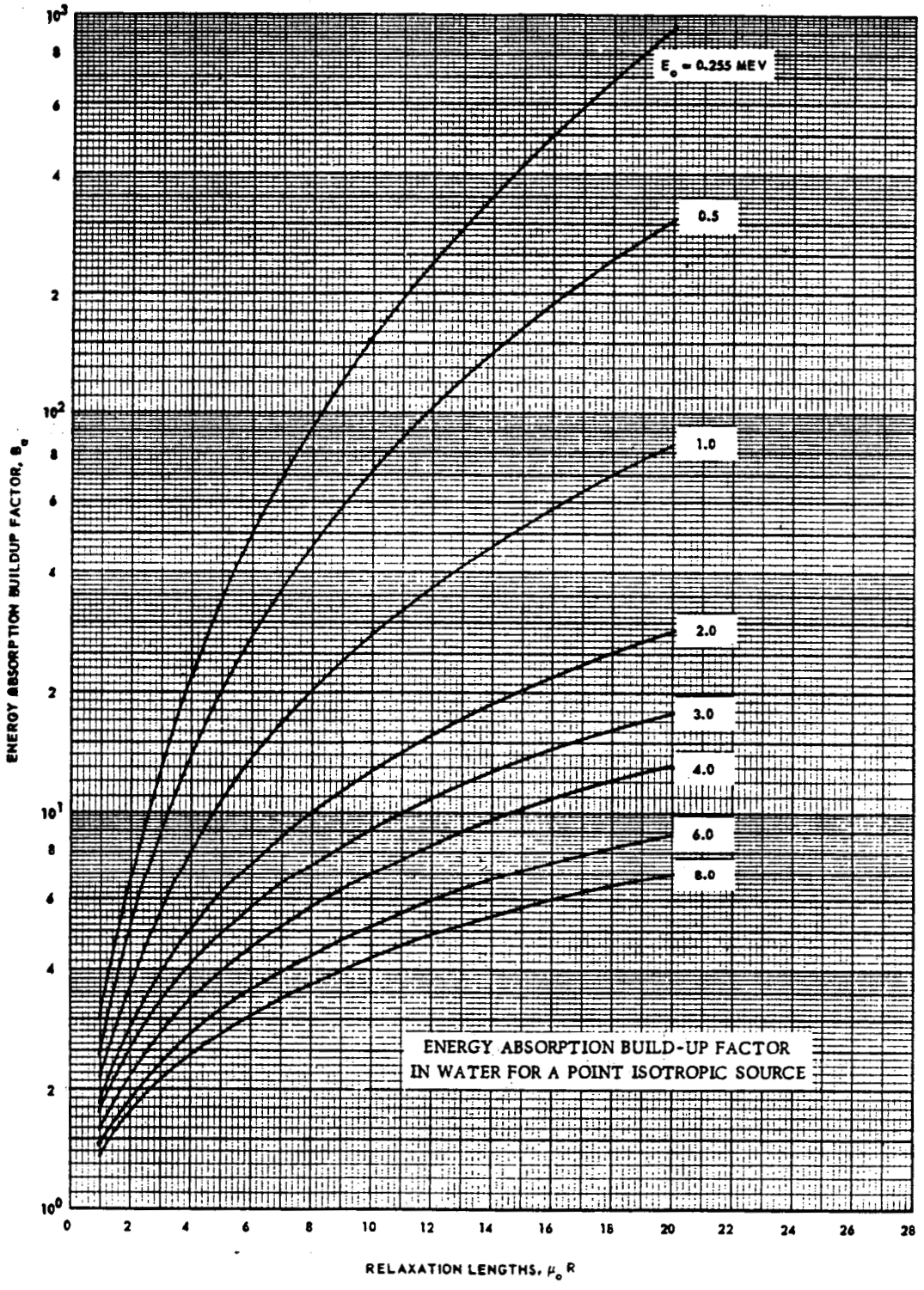

E_o = 2.0 MEV
1.0
0.5
E_o = 8.0 MEV
6.0
4.0
3.0
DOSE BUILD-UP FACTOR IN LEAD
FOR A POINT ISOTROPIC SOURCE
DOSE BUILDUP FACTOR, B_f
RELAXATION LENGTHS, $\mu_o R$
10^1
8
6
4
2
10^0
0
2
4
6
8
10
12
14
16
18
20
22
24
26
28

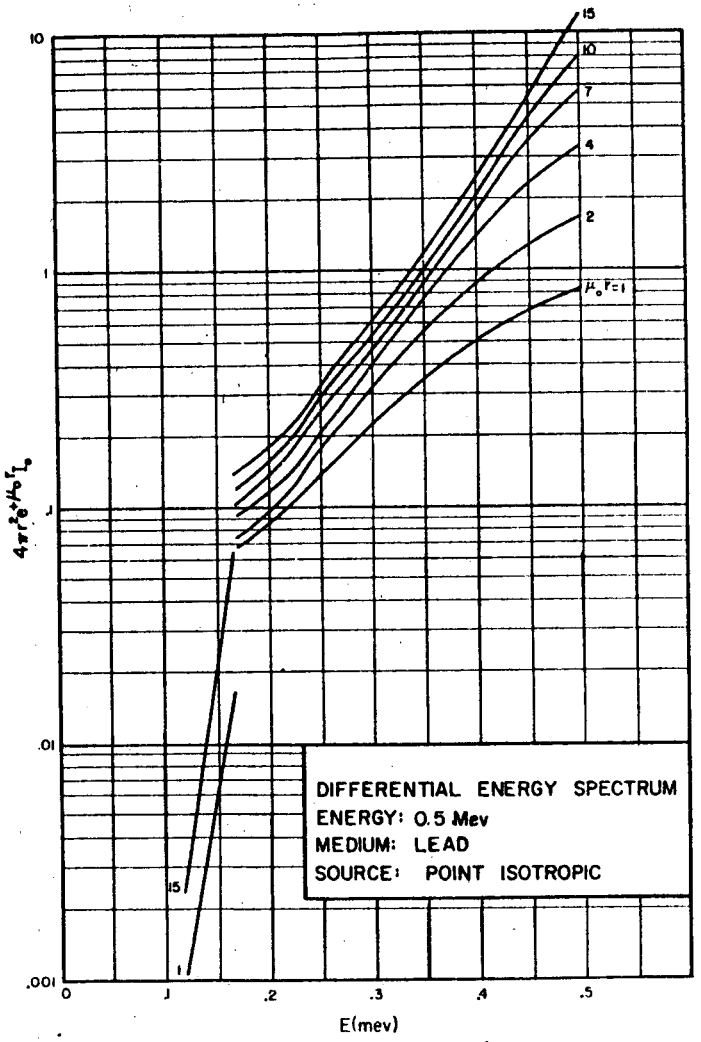

E_o = 2.0 MEV
E_o = 1.0 MEV
0.5
E_o = 8.0 MEV
6.0
4.0
3.0
E_o = 3.0
ENERGY ABSORPTION BUILD-UP FACTOR
IN LEAD FOR A POINT ISOTROPIC SOURCE
E_o = 8.0 MEV
ENERGY ABSORPTION BUILDUP FACTOR, B_e
RELAXATION LENGTHS, $\mu_o R$

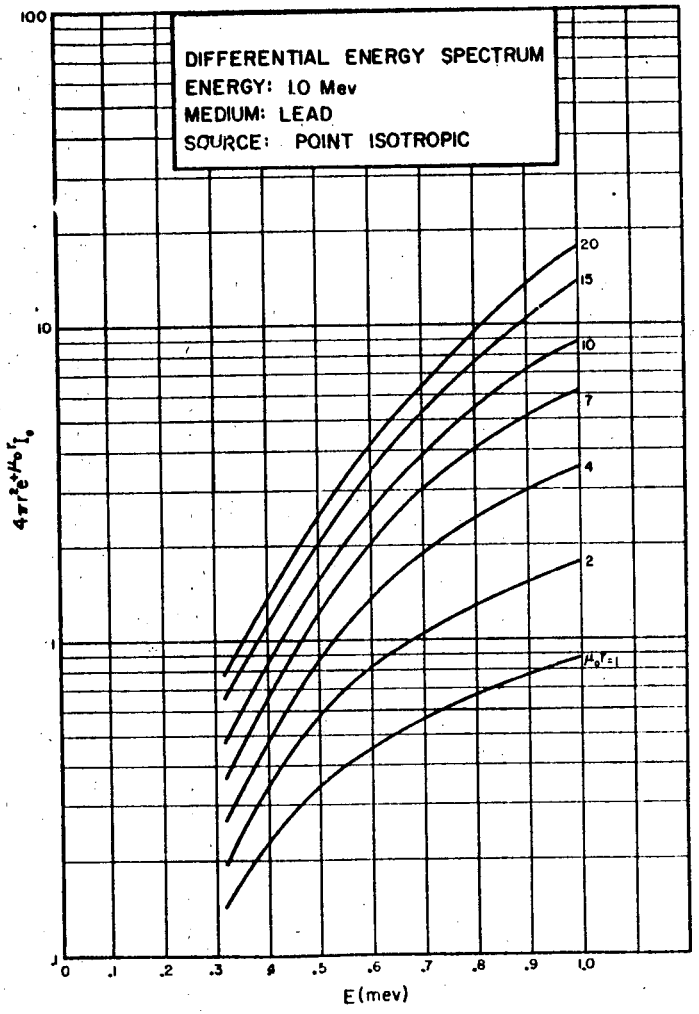

DOSE BUILDUP FACTOR, B_r
10^3
8
6
4
2
10^2
8
6
4
2
10^1
8
6
4
2
10^0
E_o = 0.5 MEV
1.0
2.0
3.0
4.0
6.0
8.0
DOSE BUILD-UP FACTOR IN IRON
FOR A POINT ISOTROPIC SOURCE
0 2 4 6 8 10 12 14 16 18 20 22 24 26 28
RELAXATION LENGTHS, $\mu_o R$

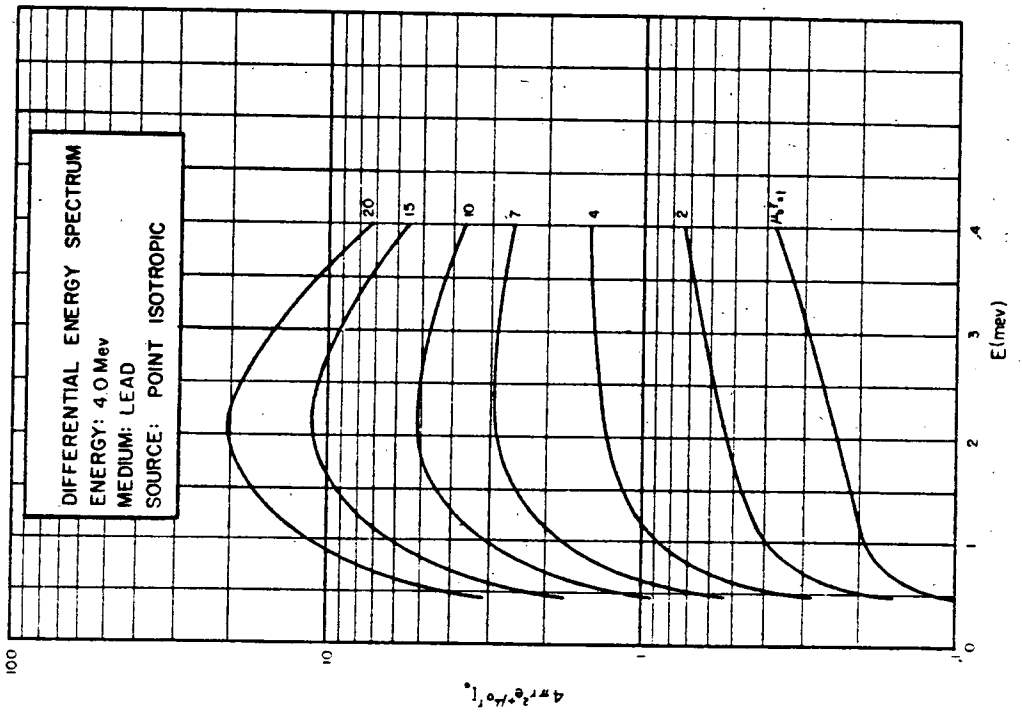

ENERGY ABSORPTION BUILDUP FACTOR, B_e
10^3
8
6
4
2
10^2
8
6
4
2
10^1
8
6
4
2
10^0
0
2
4
6
8
10
12
14
16
18
20
22
24
26
28
RELAXATION LENGTHS, $\mu_o R$
E_o = 0.5 MEV
1.0
2.0
3.0
4.0
6.0
8.0
ENERGY ABSORPTION BUILD-UP FACTOR
IN IRON FOR A POINT ISOTROPIC SOURCE

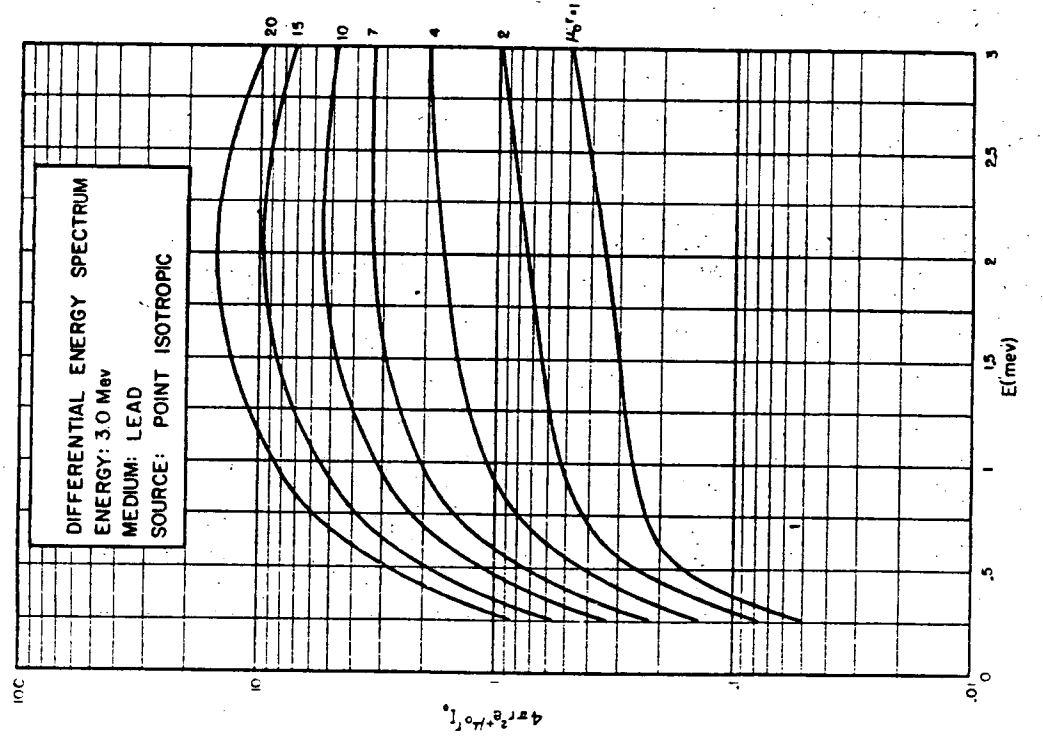

E_o = 0.255 MEV
0.5
1.0
2.0
3.0
4.0
6.0
8.0
DOSE BUILD-UP FACTOR IN WATER
FOR A POINT ISOTROPIC SOURCE
DOSE BUILDUP FACTOR, B_r
RELAXATION LENGTHS, $\mu_o R$
10^3
10^2
10^1
10^0
0
2
4
6
8
10
12
14
16
18
20
22
24
26
28

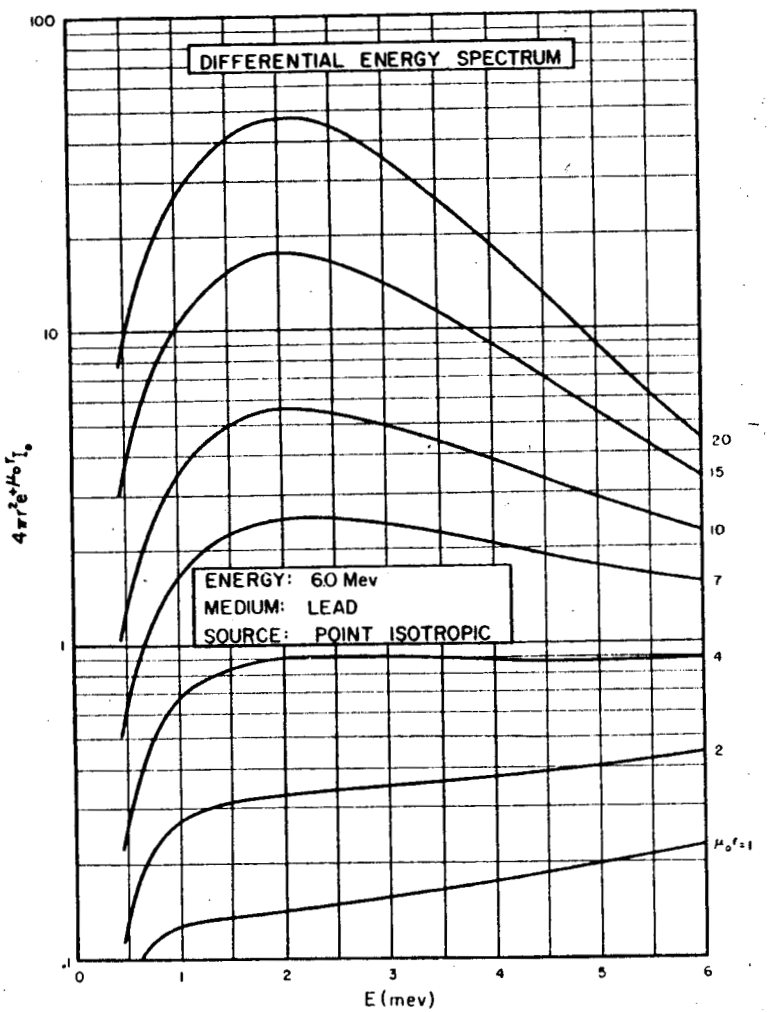

E_o = 0.255 MEV
0.5
1.0
2.0
3.0
4.0
6.0
8.0
ENERGY ABSORPTION BUILD-UP FACTOR IN WATER FOR A POINT ISOTROPIC SOURCE
ENERGY ABSORPTION BUILDUP FACTOR, B_e
RELAXATION LENGTHS, $\mu_o R$
10^3
10^2
10^1
10^0
0
2
4
6
8
10
12
14
16
18
20
22
24
26
28

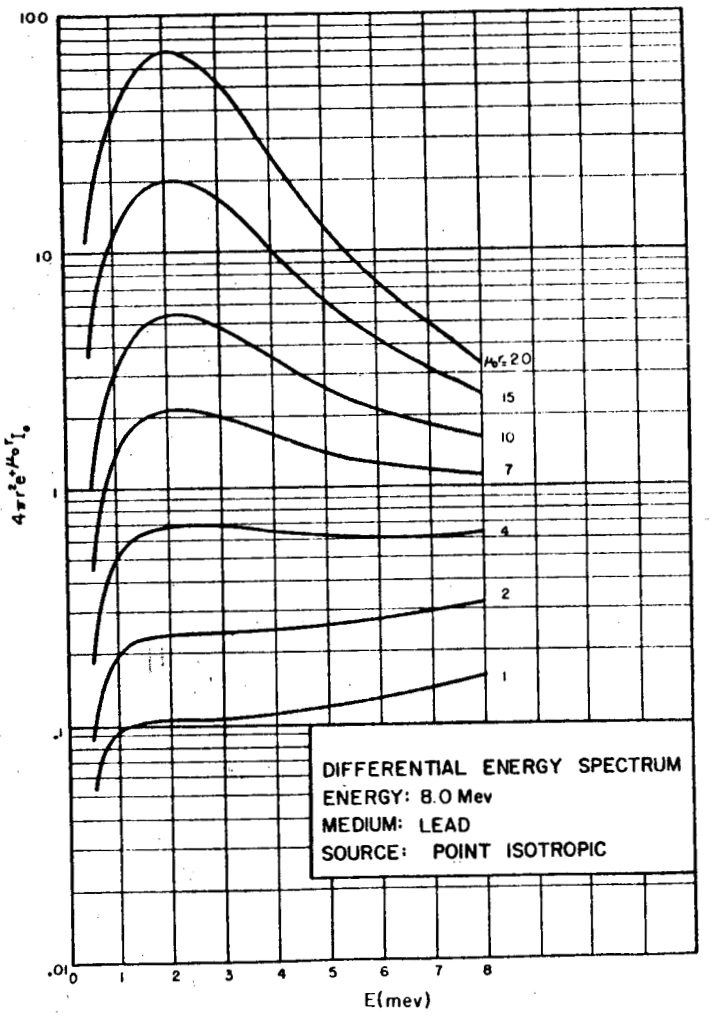

DIFFERENTIAL ENERGY SPECTRUM
ENERGY: 0.5 Mev
MEDIUM: LEAD
SOURCE: POINT ISOTROPIC
15
10
7
4
2
μ₀r=1
1
10
1
.01
.001
0
.1
.2
.3
.4
.5
E(mev)
4πr²e^{+μ₀r}/I₀

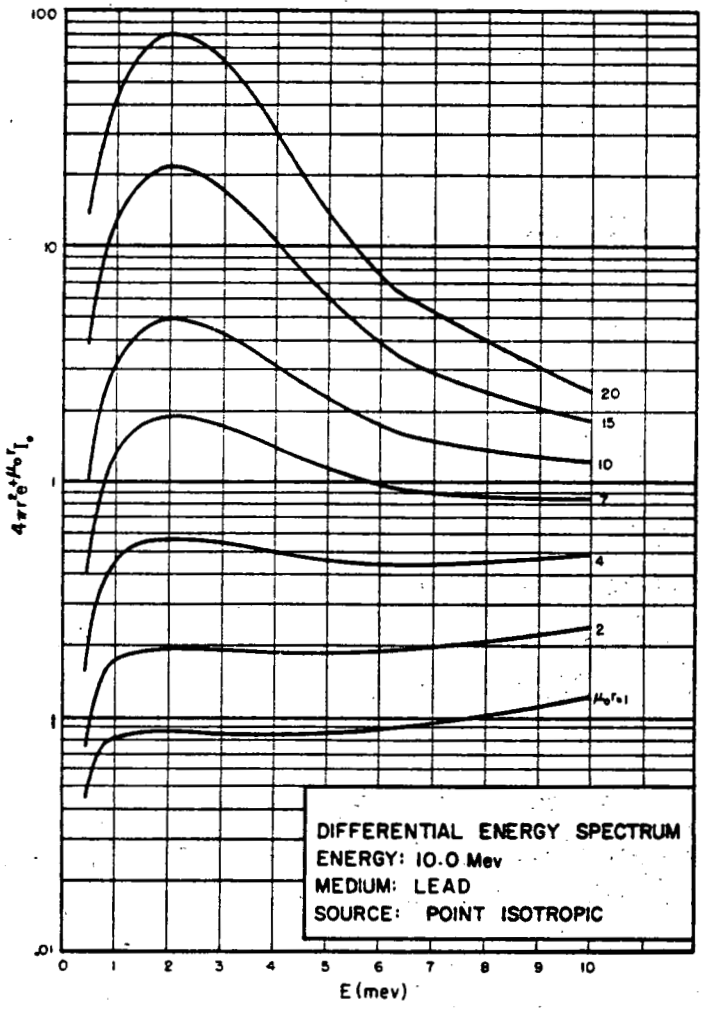

DIFFERENTIAL ENERGY SPECTRUM
ENERGY: 1.0 Mev
MEDIUM: LEAD
SOURCE: POINT ISOTROPIC
20
15
10
7
4
2
μ₀r=1
100
10
1
0
.1
.2
.3
.4
.5
.6
.7
.8
.9
1.0
E(mev)
4πr²e^{+μ₀r}/I₀

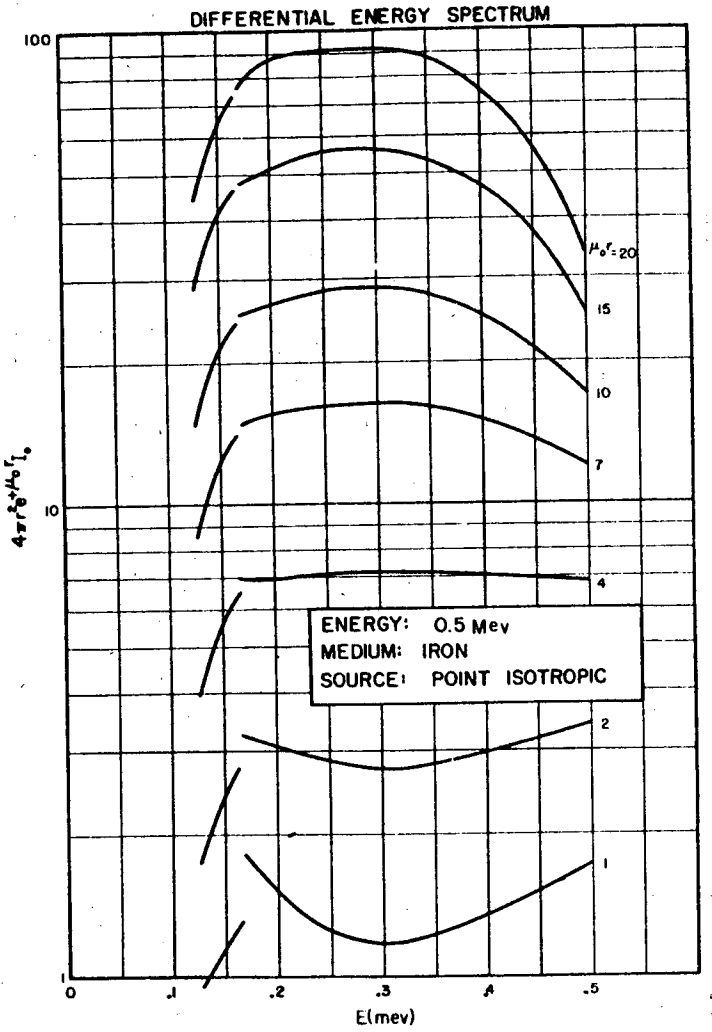

DIFFERENTIAL ENERGY SPECTRUM
ENERGY: 4.0 Mev
MEDIUM: LEAD
SOURCE: POINT ISOTROPIC
20
15
10
7
4
2
μ₀r=1
E(mev)
4πr²e^{+μ₀r}I₀

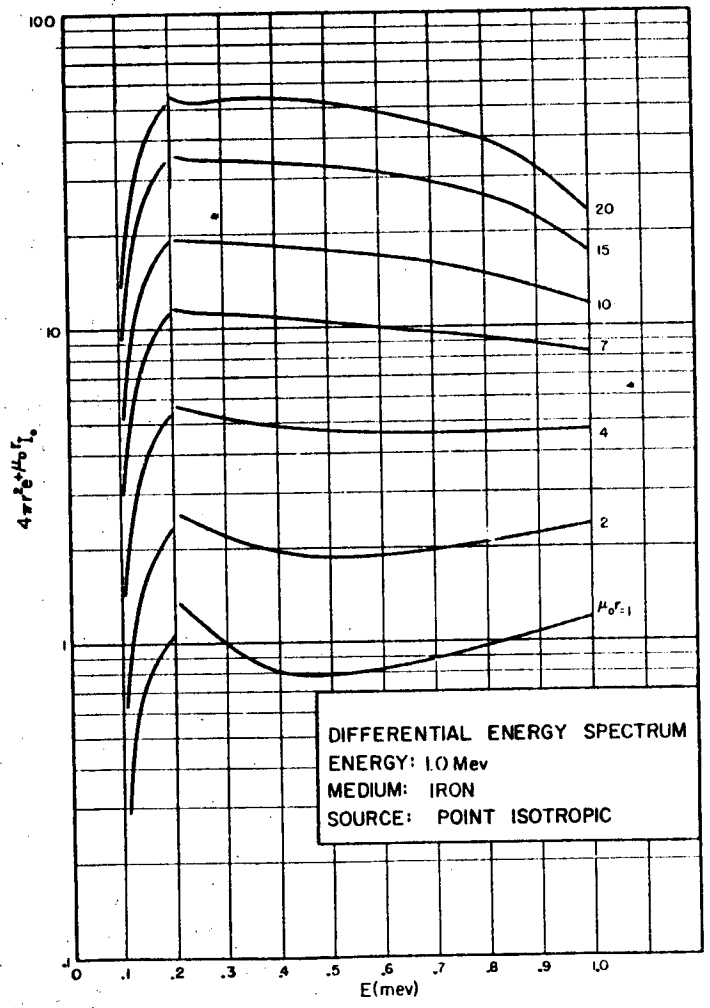

DIFFERENTIAL ENERGY SPECTRUM
ENERGY: 3.0 Mev
MEDIUM: LEAD
SOURCE: POINT ISOTROPIC
20
15
10
7
4
2
μ₀r=1
E(mev)
4πr²e^{+μ₀r}I₀

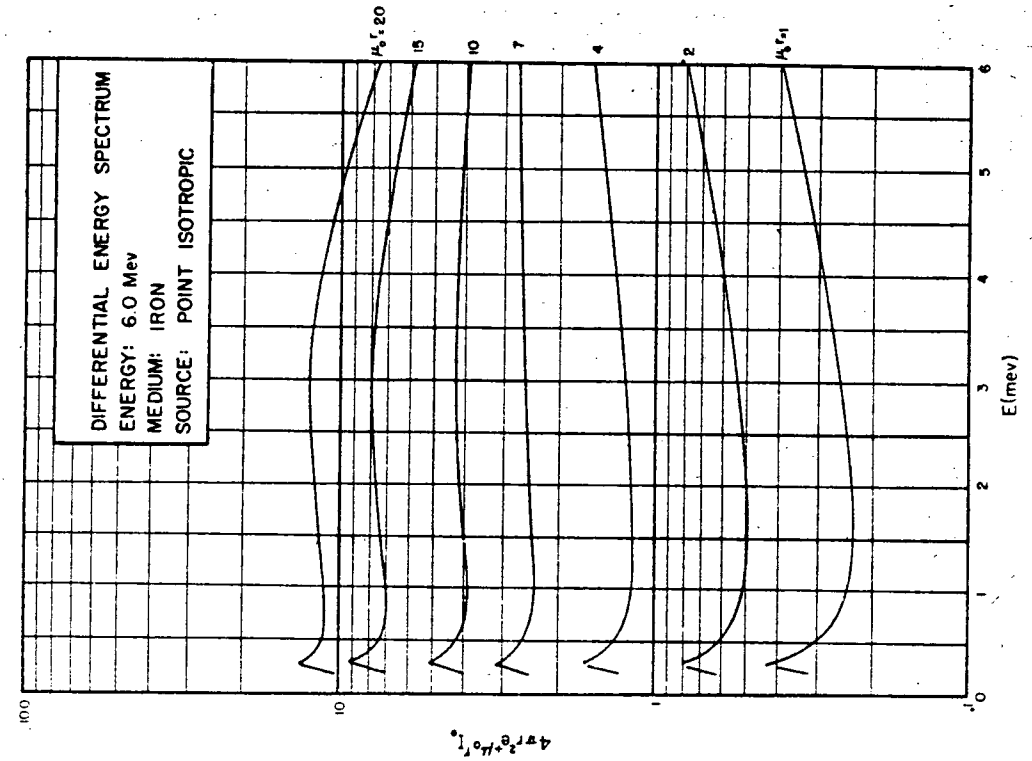

DIFFERENTIAL ENERGY SPECTRUM
ENERGY: 6.0 Mev
MEDIUM: LEAD
SOURCE: POINT ISOTROPIC
100
10
1
.1
0
1
2
3
4
5
6
E (mev)
20
15
10
7
4
2
μ₀r=1

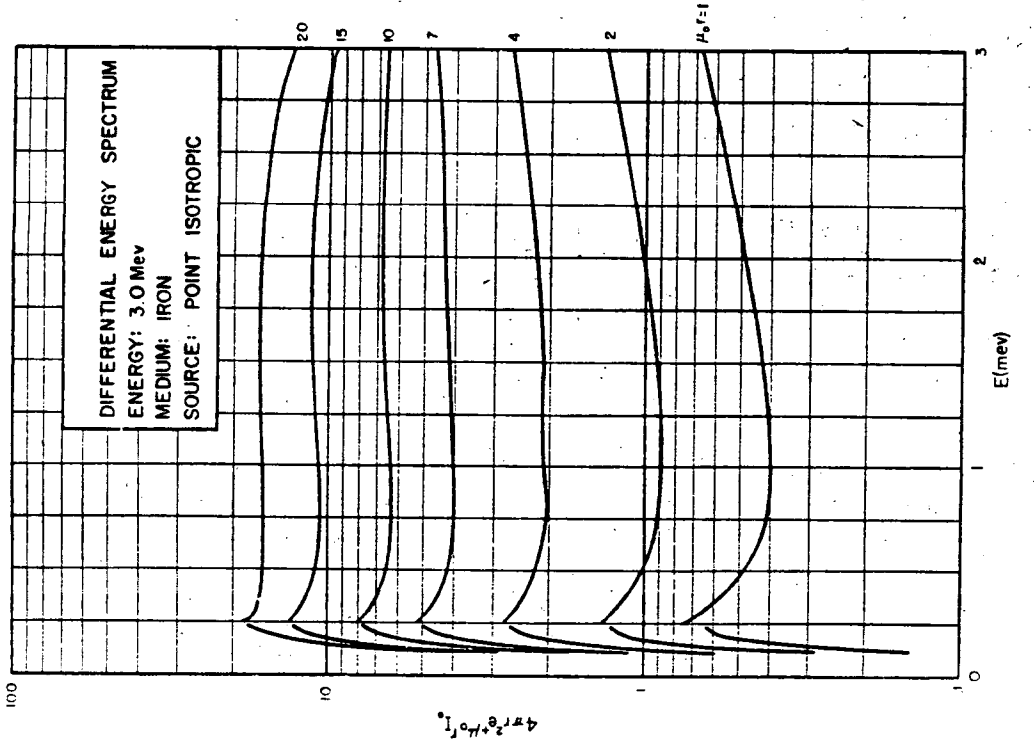

DIFFERENTIAL ENERGY SPECTRUM
ENERGY: 8.0 Mev
MEDIUM: LEAD
SOURCE: POINT ISOTROPIC
100
10
1
.1
.01
0
1
2
3
4
5
6
7
8
E(mev)
μ₀r=20
15
10
7
4
2
1

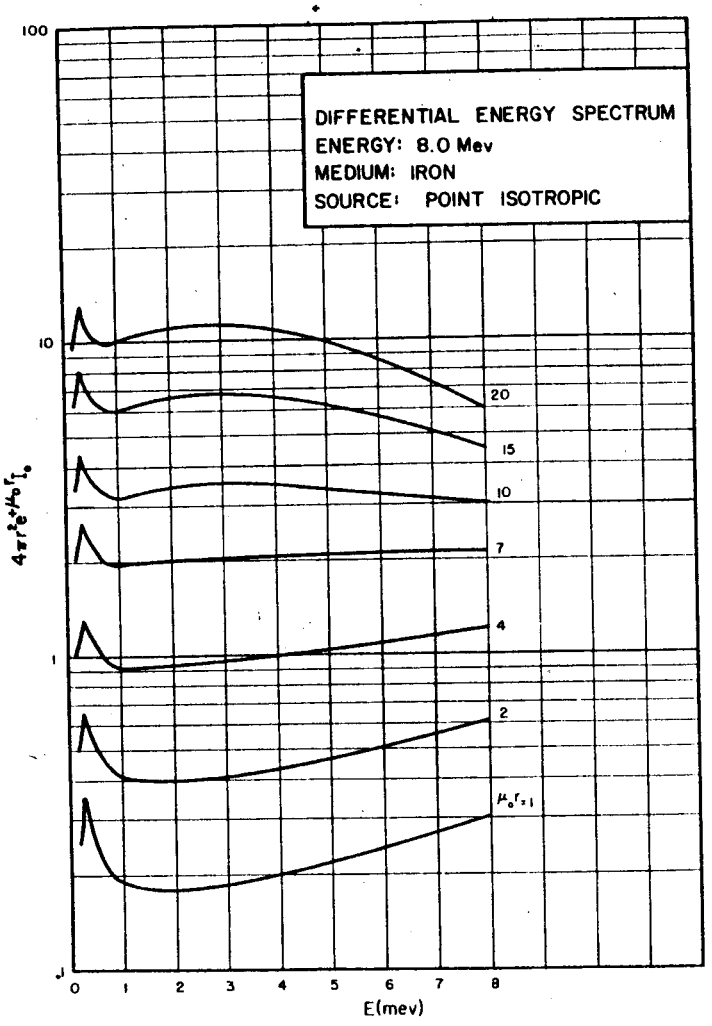

100
10
1
.1
$4\pi r^2 e^{+\mu_0 r} I_0$
20
15
10
7
4
2
$\mu_0 r = 1$
DIFFERENTIAL ENERGY SPECTRUM
ENERGY: 10.0 Mev
MEDIUM: LEAD
SOURCE: POINT ISOTROPIC
0 1 2 3 4 5 6 7 8 9 10
E (mev)

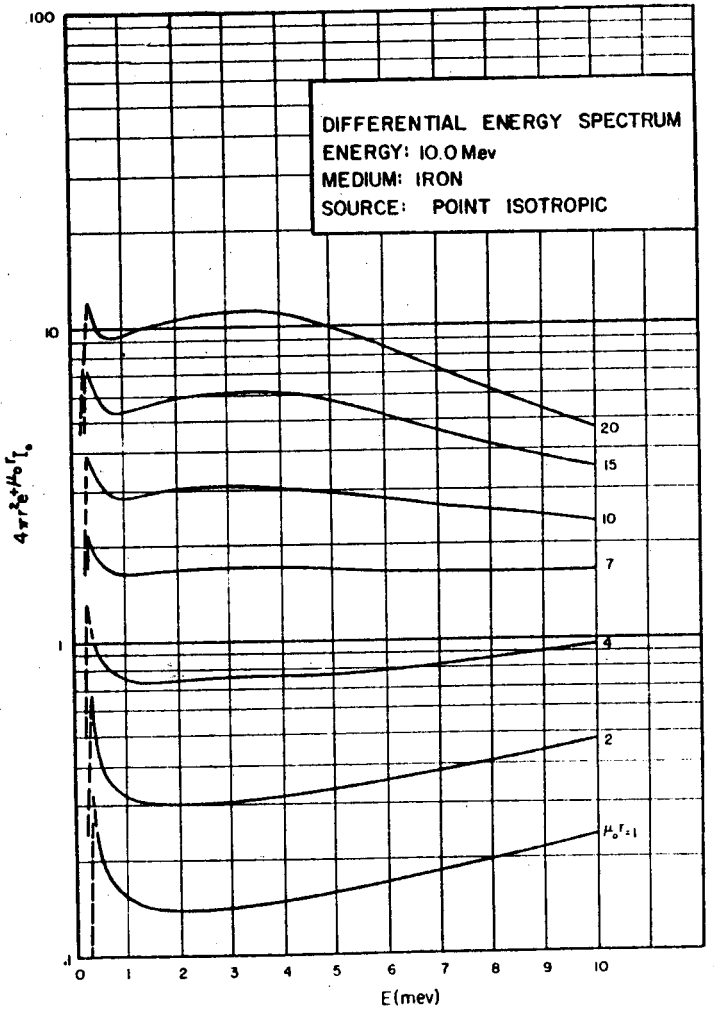

DIFFERENTIAL ENERGY SPECTRUM
100
10
1
$4\pi r^2 e^{+\mu_0 r} I_0$
$\mu_0 r = 20$
15
10
7
4
2
1
ENERGY: 0.5 Mev
MEDIUM: IRON
SOURCE: POINT ISOTROPIC
0
.1
.2
.3
.4
.5
E(mev)

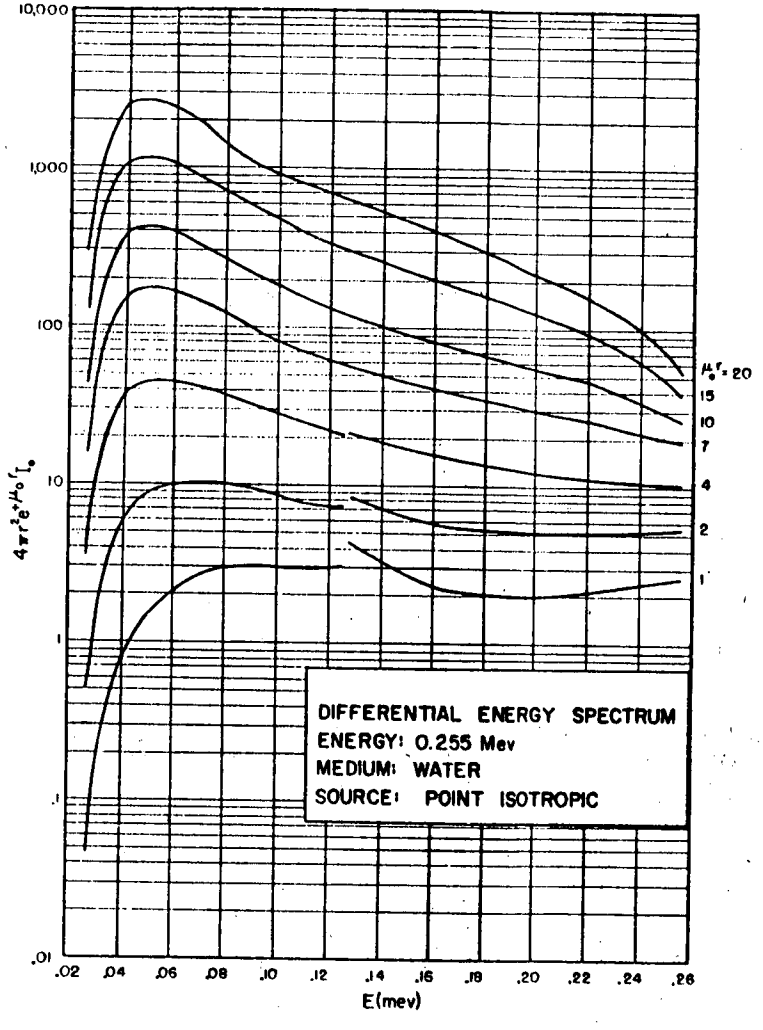

100
10
1
$4\pi r^2 e^{+\mu_0 r} I_0$
20
15
10
7
4
2
$\mu_0 r = 1$
DIFFERENTIAL ENERGY SPECTRUM
ENERGY: 1.0 Mev
MEDIUM: IRON
SOURCE: POINT ISOTROPIC
0
.1
.2
.3
.4
.5
.6
.7
.8
.9
1.0
E(mev)

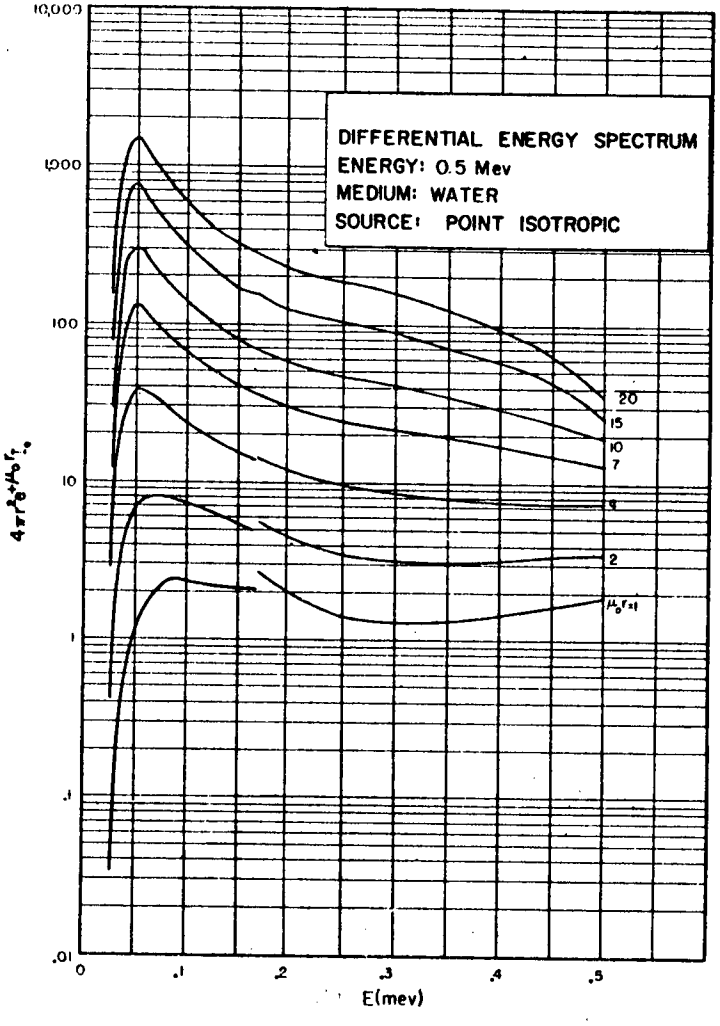

DIFFERENTIAL ENERGY SPECTRUM
ENERGY: 6.0 Mev
MEDIUM: IRON
SOURCE: POINT ISOTROPIC
$\mu_0 r = 20$
15
10
7
4
2
$\mu_0 r = 1$
E(mev)
$4\pi r^2 e^{+\mu_0 r} I_0$

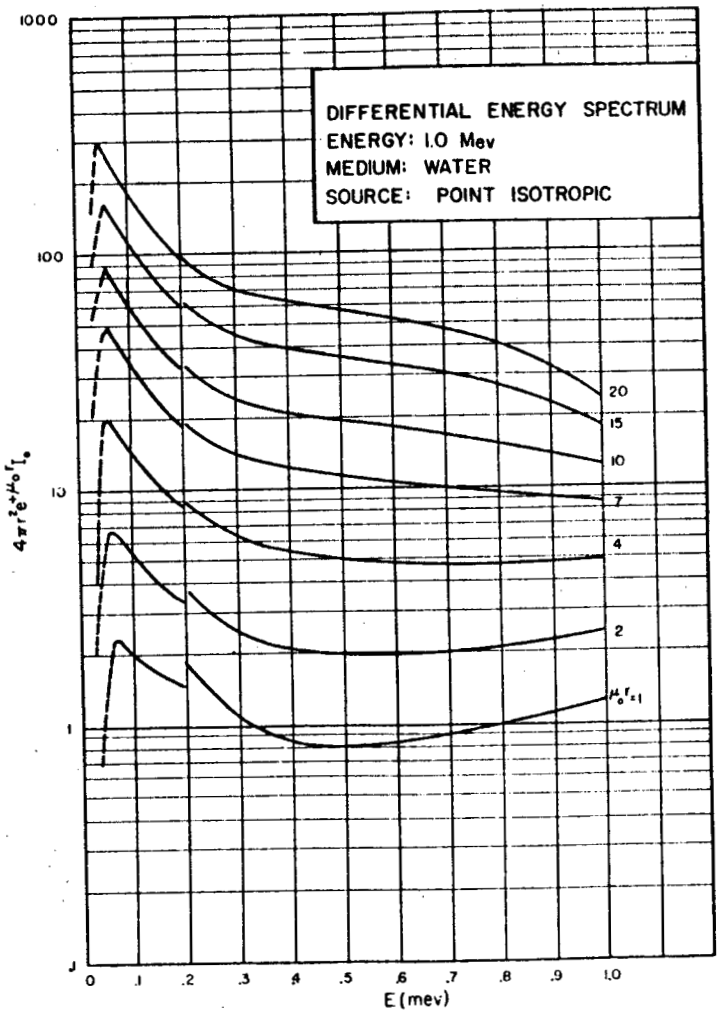

DIFFERENTIAL ENERGY SPECTRUM
ENERGY: 3.0 Mev
MEDIUM: IRON
SOURCE: POINT ISOTROPIC
20
15
10
7
4
2
$\mu_0 r = 1$
E(mev)
$4\pi r^2 e^{+\mu_0 r} I_0$

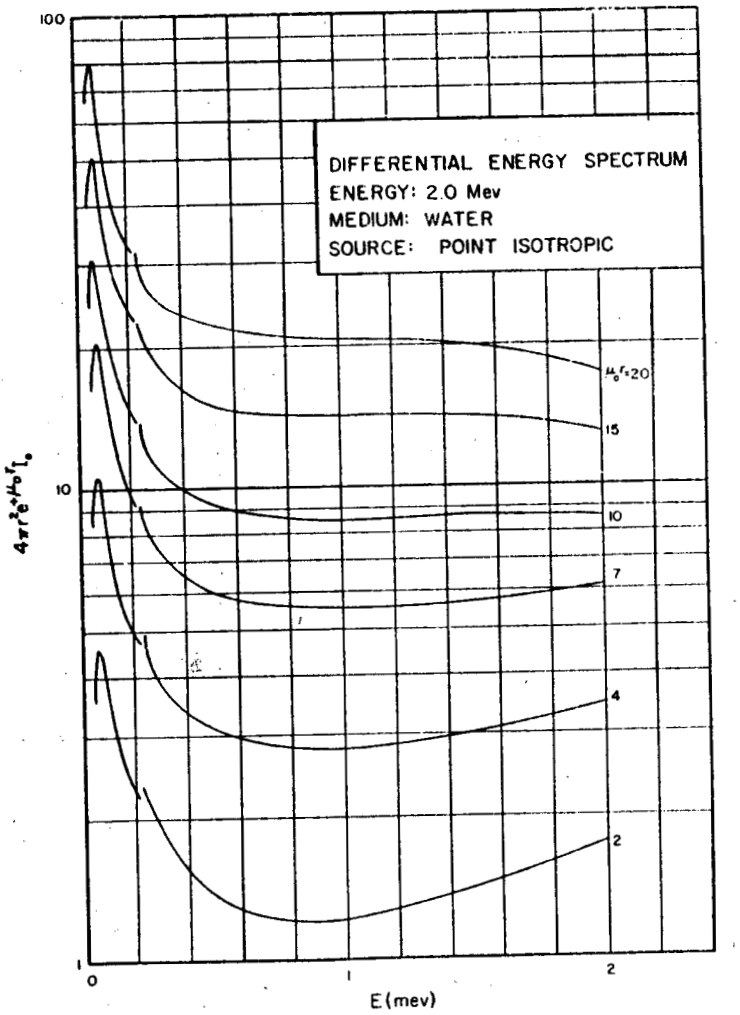

DIFFERENTIAL ENERGY SPECTRUM
ENERGY: 8.0 Mev
MEDIUM: IRON
SOURCE: POINT ISOTROPIC
100
10
1
0 1 2 3 4 5 6 7 8
E(mev)
20
15
10
7
4
2
$\mu_o r = 1$
$4\pi r^2 e^{+\mu_o r} I_o$

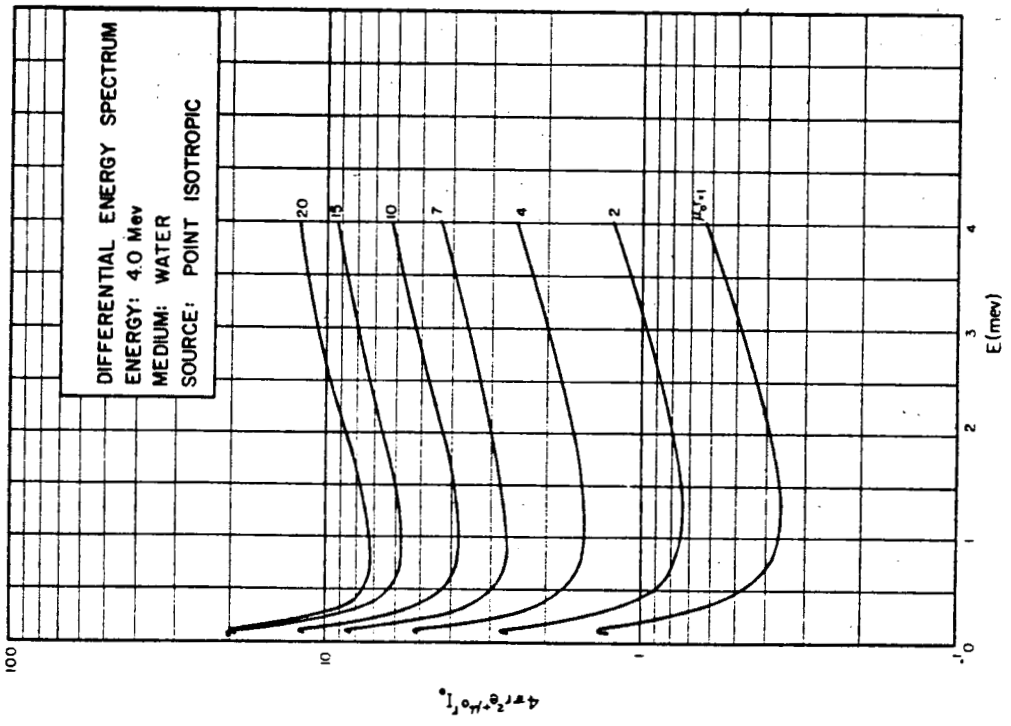

DIFFERENTIAL ENERGY SPECTRUM
ENERGY: 10.0 Mev
MEDIUM: IRON
SOURCE: POINT ISOTROPIC
100
10
1
0 1 2 3 4 5 6 7 8 9 10
E(mev)
20
15
10
7
4
2
$\mu_o r = 1$
$4\pi r^2 e^{+\mu_o r} I_o$

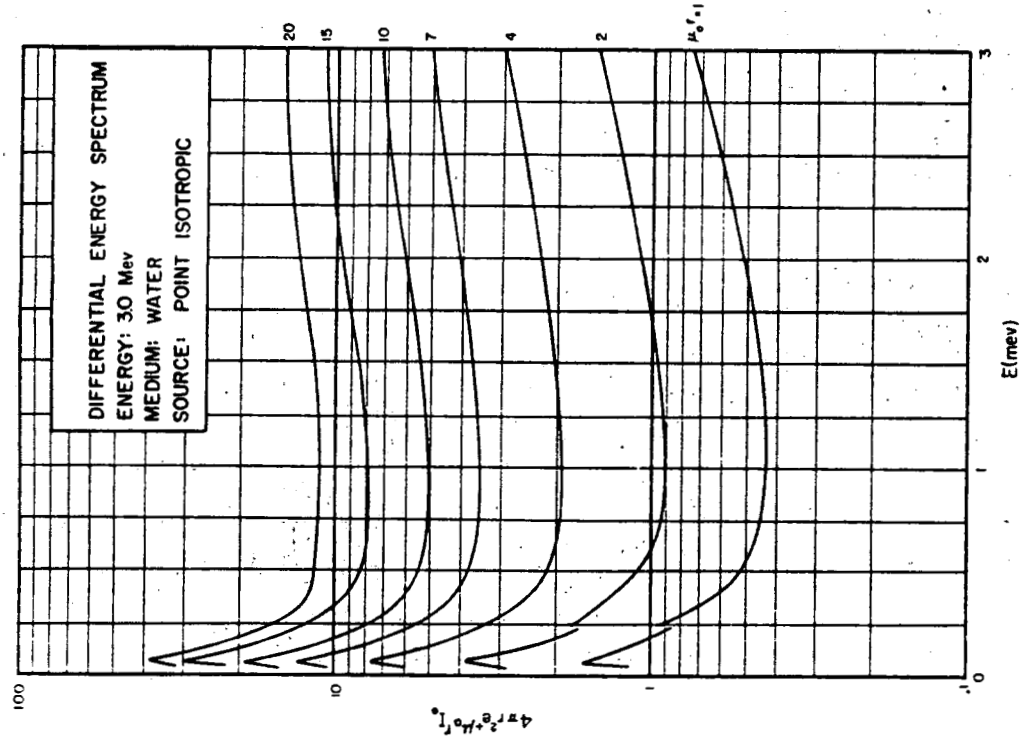

10,000
1,000
100
10
1
.1
.01
$4\pi r^2 e^{+\mu_0 r}/I_0$
$\mu_0 r = 20$
15
10
7
4
2
1
DIFFERENTIAL ENERGY SPECTRUM
ENERGY: 0.255 Mev
MEDIUM: WATER
SOURCE: POINT ISOTROPIC
.02 .04 .06 .08 .10 .12 .14 .16 .18 .20 .22 .24 .26
E(mev)

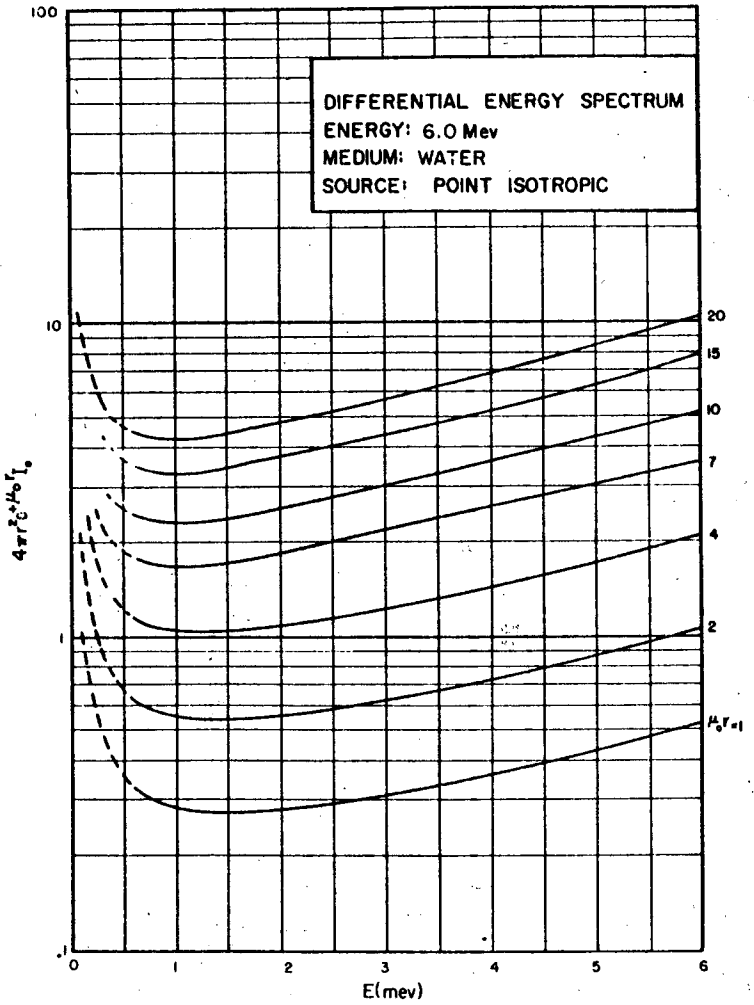

10,000
1,000
100
10
1
.1
.01
$4\pi r^2 e^{+\mu_0 r}/I_0$
DIFFERENTIAL ENERGY SPECTRUM
ENERGY: 0.5 Mev
MEDIUM: WATER
SOURCE: POINT ISOTROPIC
20
15
10
7
4
2
$\mu_0 r = 1$
0 .1 .2 .3 .4 .5
E(mev)

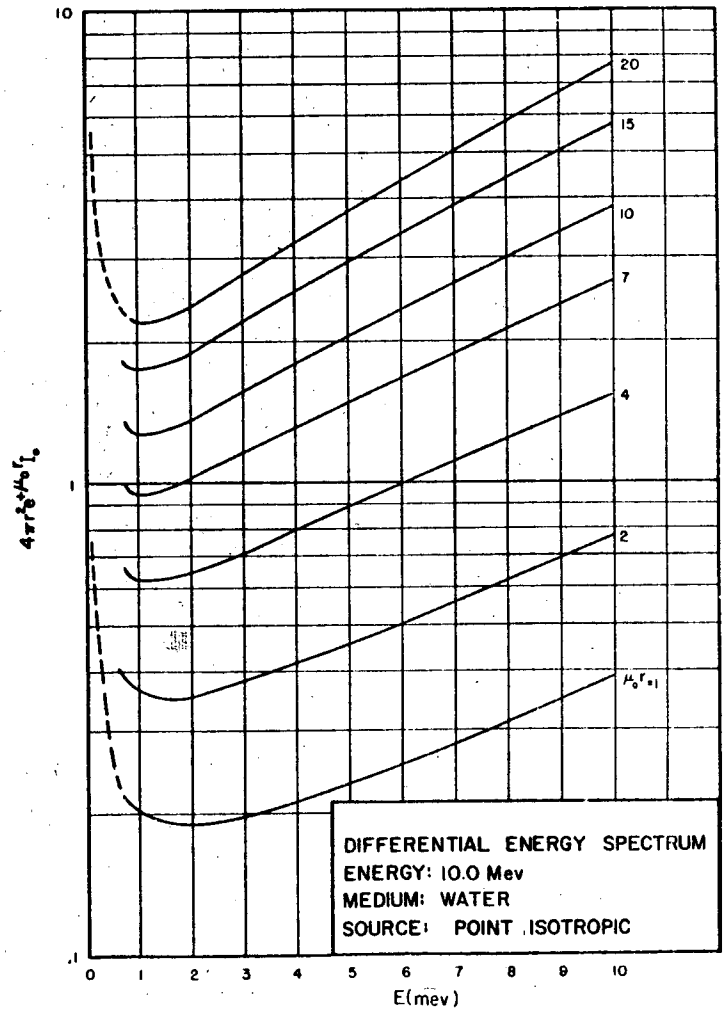

DIFFERENTIAL ENERGY SPECTRUM
ENERGY: 1.0 Mev
MEDIUM: WATER
SOURCE: POINT ISOTROPIC
1000
100
10
1
0
.1
.2
.3
.4
.5
.6
.7
.8
.9
1.0
E (mev)
20
15
10
7
4
2
μ0r=1

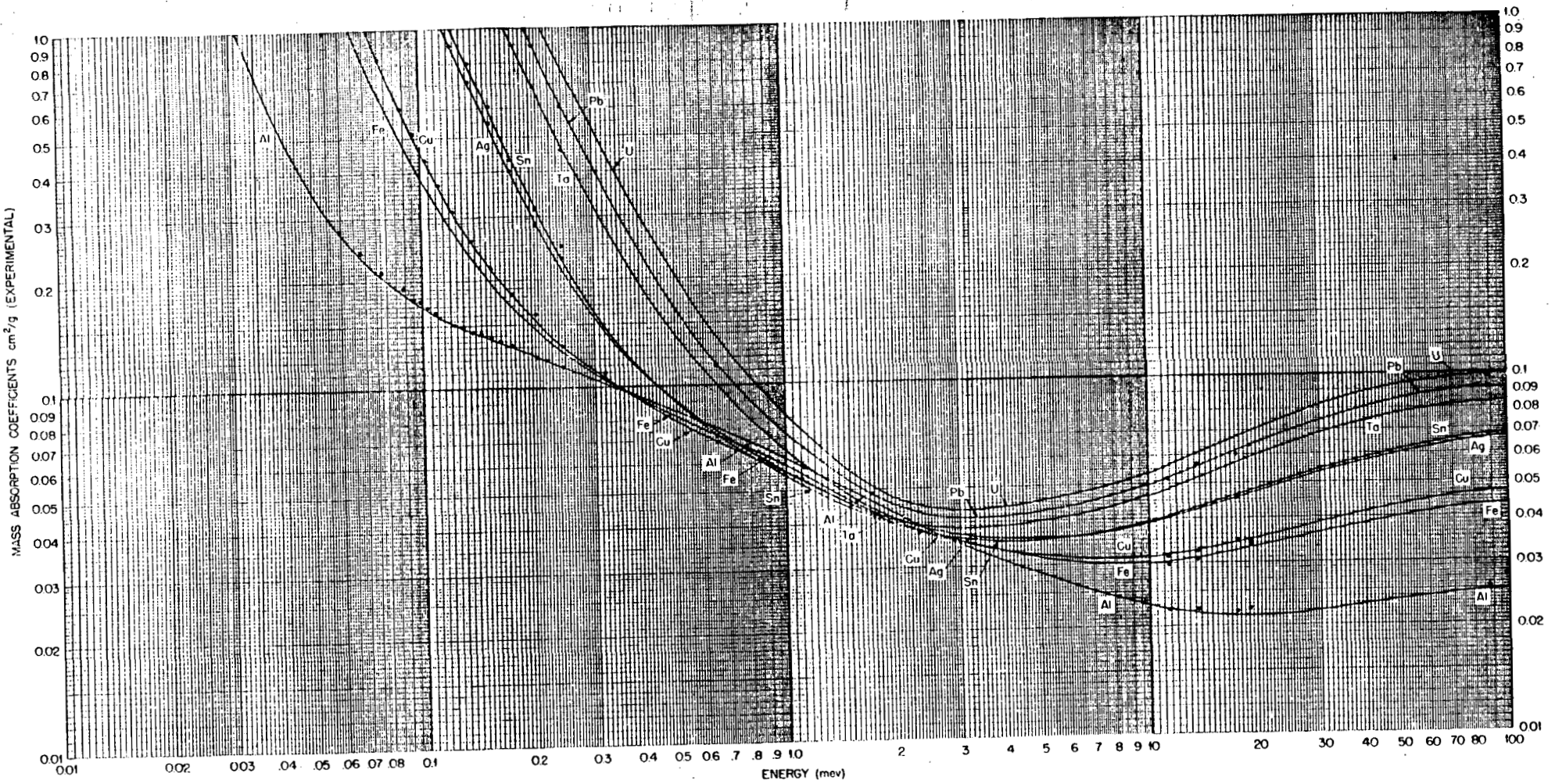

DIFFERENTIAL ENERGY SPECTRUM
ENERGY: 2.0 Mev
MEDIUM: WATER
SOURCE: POINT ISOTROPIC
100
10
1
0
1
2
E (mev)
μ0r=20
15
10
7
4
2


DIFFERENTIAL ENERGY SPECTRUM
ENERGY: 4.0 Mev
MEDIUM: WATER
SOURCE: POINT ISOTROPIC
20
15
10
7
4
2
μ₀r=1
E(mev)
4πr²e^{+μ₀r}I₀


DIFFERENTIAL ENERGY SPECTRUM
ENERGY: 3.0 Mev
MEDIUM: WATER
SOURCE: POINT ISOTROPIC
20
15
10
7
4
2
μ₀r=1
E(mev)
4πr²e^{+μ₀r}I₀


DIFFERENTIAL ENERGY SPECTRUM
ENERGY: 6.0 Mev
MEDIUM: WATER
SOURCE: POINT ISOTROPIC
100
10
1
.1
0
1
2
3
4
5
6
E(mev)
20
15
10
7
4
2
$\mu_0 r=1$

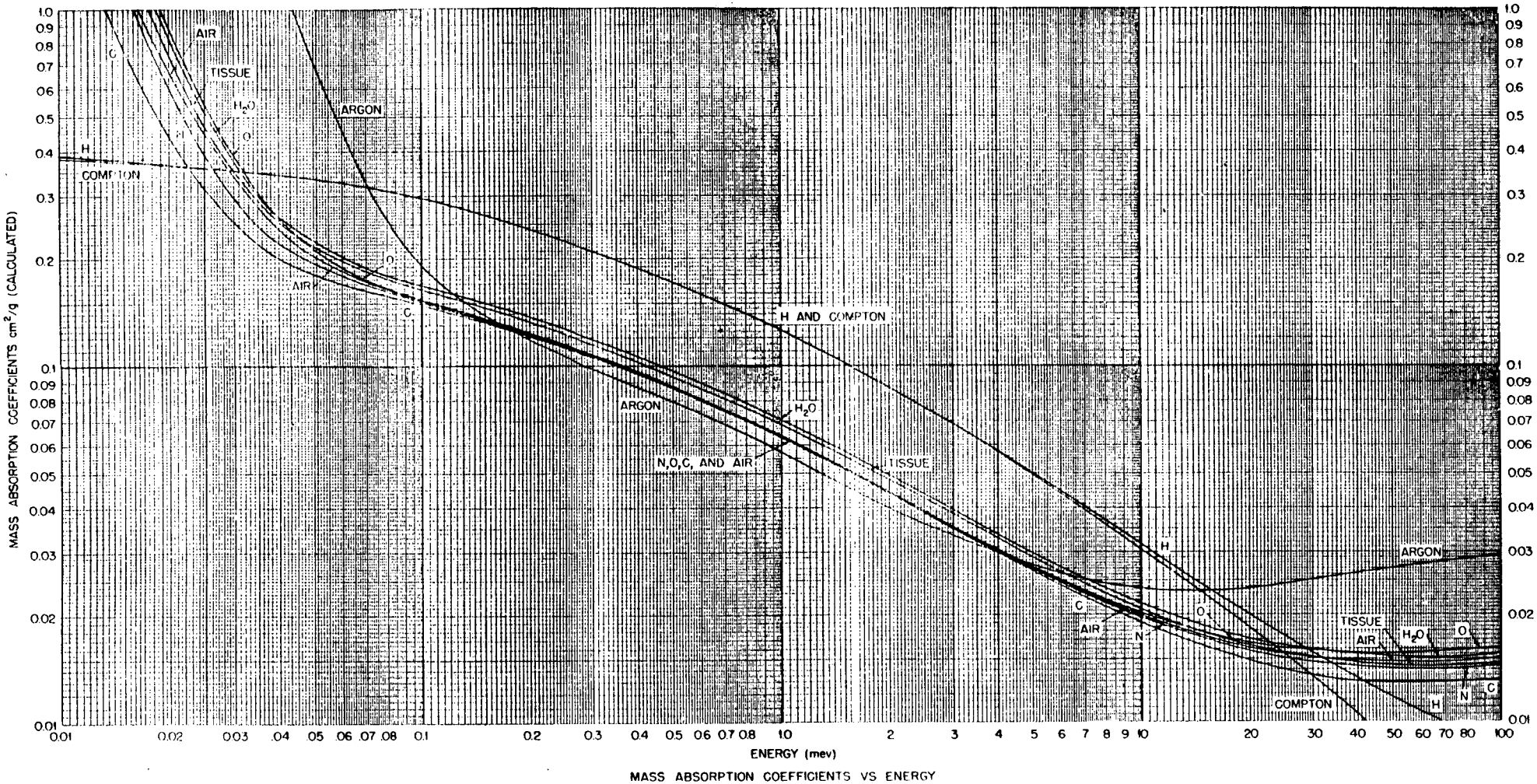

DIFFERENTIAL ENERGY SPECTRUM
ENERGY: 10.0 Mev
MEDIUM: WATER
SOURCE: POINT ISOTROPIC
10
1
.1
0
1
2
3
4
5
6
7
8
9
10
E(mev)
20
15
10
7
4
2
$\mu_0 r=1$



MASS ABSORPTION COEFFICIENTS VS ENERGY

(Macroscopic Total Cross-Section Divided by Density)

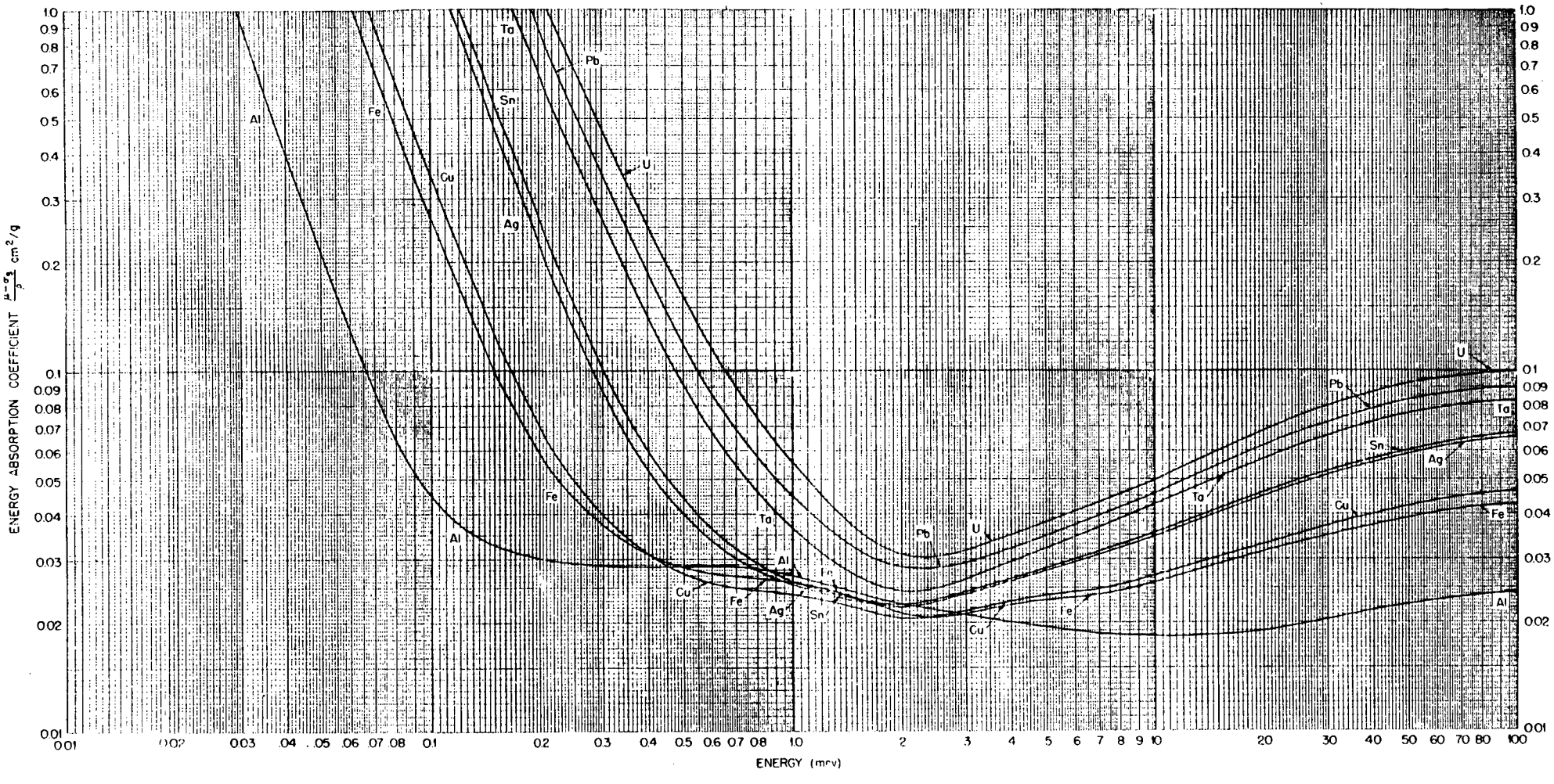
Supplement I to ORNL 421 "Absorption of γ-Rays" by Snyder and Powell



MASS ABSORPTION COEFFICIENTS VS ENERGY

(Macroscopic Total Cross-Section Divided by Density)

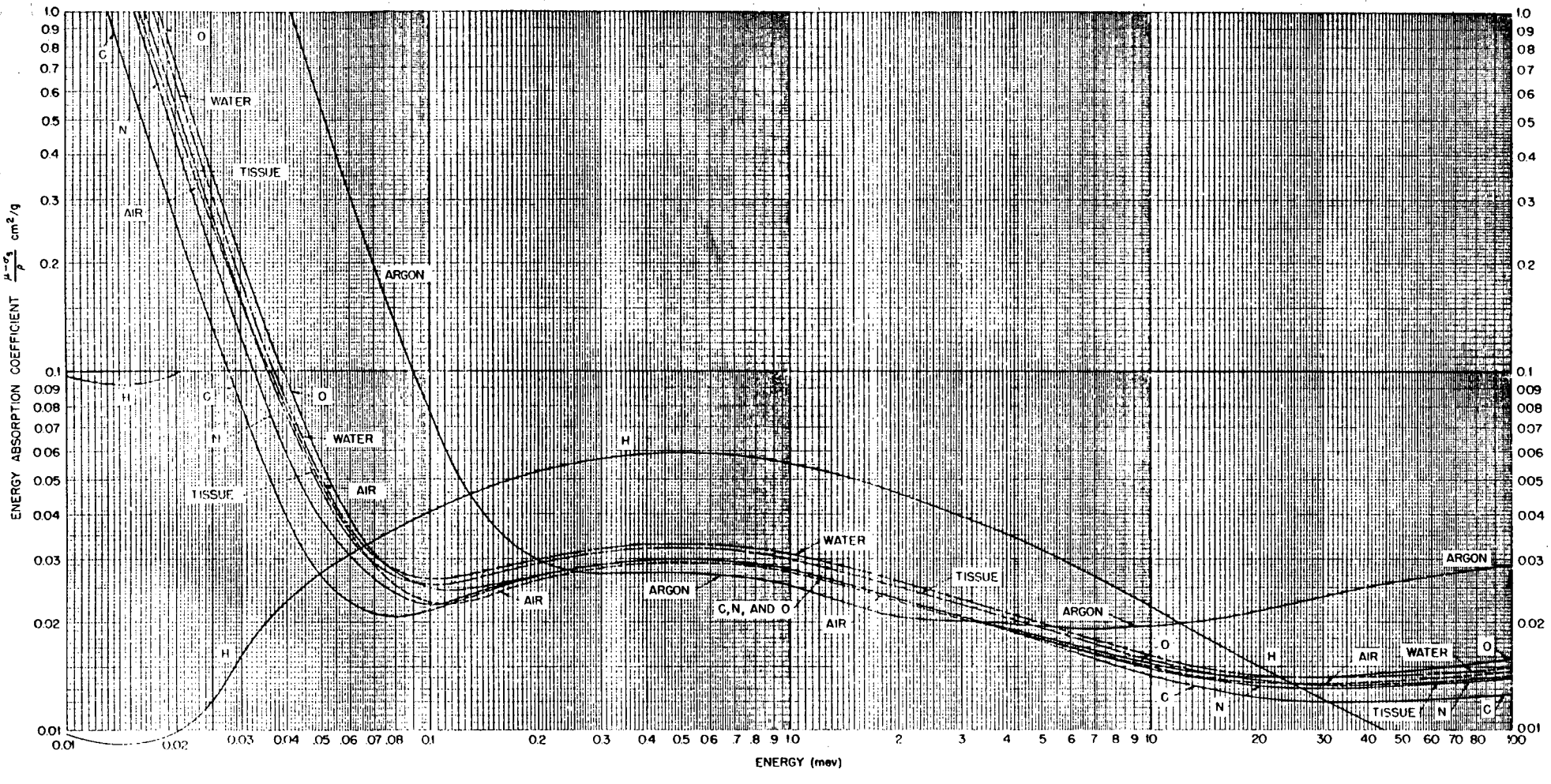
Supplement 2 to ORNL 421 "Absorption of γ-Rays" by Snyder and Powell



MASS ABSORPTION COEFFICIENTS VS ENERGY

(Macroscopic Cross-Section for Energy Absorption Divided by Density)

Supplement 3 to ORNL 421 "Absorption of γ-Rays" by Snyder and Powell.



MASS ABSORPTION COEFFICIENTS VS ENERGY

(Macroscopic Cross-Section for Energy Absorption Divided by Density)

Supplement 4 to ORNL 421 "Absorption of γ-Rays" by Snyder and Powell

Table 10.1—RADIATION DAMAGE
(A Rough Grouping of Materials and Equipment)

Nvt,* neutrons and gammas/cm^2 (see Note) ← (Damage may occur above)		→ Equivalent to 1 year at flux† of
3×10^{22}	Ductile and fluid metals (up to)	1×10^{15}
3×10^{20}	Many simple inorganic compounds (up to) Portland cement and concrete Graphite (best grades)	1×10^{13}
1×10^{20}	Springs; stainless steel and Inconel	3×10^{12}
3×10^{19}	Group 1 plastics‡ Asbestos and mineral insulators Fiberglass Glass, soft or pyrex (darkens but stronger)	1×10^{12}
1×10^{19}	Group 2 plastics‡ Cork, lab grade Unpressurized water (flux gives some decomposition)	3×10^{11}
3×10^{18}	Group 3 plastics‡ Spar varnish, aluminum paint, and black Glyptal Electronic circuitry (flux not nvt)	1×10^{11}
1×10^{18}	Wood Group 4 plastics‡ Natural rubber, no plasticizer, in air Special radiation-resistant lubricants	3×10^{10}
6×10^{17}	Bearings (in special lubricants)	2×10^{10}
3×10^{17}	Group 5 plastics‡ Permanent magnets (Alnico-V) Paper Piezoelectric crystals	1×10^{10}
1×10^{17}	Capacitors (ceramic, paper, mica) Group 6 plastics‡ Natural rubber (in helium) Group 2 elastomers§ Standard lubricants and fuels Small electric motors with standard lubricants Fission chambers Strain gauges Rectifiers (Si, Se)	3×10^{9}
3×10^{16}	Resistors Capacitors (electrolytic) Transformers, small Typical electron vacuum tubes Group 7 plastics‡ Group 3 elastomers§ Phototubes (flux not nvt) Dry-cell batteries Capacitors (oil-impregnated paper) Normal glass darkened (flux not nvt)	1×10^{9}
1×10^{16}	Rectifiers (Ge, CuO) Lead storage batteries (no effect) Capacitor (molded bakelite paper) Neoprene§	3×10^{8}

RADIATION DAMAGE — (Continued)

Nvt,* neutrons and gammas/cm^2 (see Note) ←	(Damage may occur above) →	Equivalent to 1 year at flux† of
3×10^{15}	Teflon‡	1×10^8
1×10^{15}	Explosives (typical chemical types)	3×10^7
1×10^{15} (gammas)	Food (flavor may be affected)	3×10^7
3×10^{13} (gammas)	Precipitation in untreated $ZnBr_2$ windows	1×10^6
1×10^{12} (thermal neuts.)	Food and drinking water (activation)	3×10^4

* For a roughly equivalent gamma dose, divide by 10^9 to get roentgens.
† Obtained by dividing nvt by 3×10^7 sec/year.
‡ See Table 10.2.
§ See Table 10.3.

Note:

This table is a guide to, but not a substitute for, the literally thousands of pages of literature on radiation damage. All the data are believed to be conservative. In some cases the indicated exposure caused slight damage; in others, the indicated exposure is the maximum recorded, but no damage occurred.

In general, the nvt used is the total number of thermal neutrons per square centimeter which struck the sample; in most cases, the sample also received a roughly equal number of gamma photons in the low Mev range and about one-tenth as many fast neutrons.

The effects of temperature, composition of atmosphere, particular impurities, or other factors may be very important, but they are not considered here. A few items are flux limited; most are limited in the total dose they can absorb. It is suggested that, if a reader finds an application near the limits listed in Table 10.1, he investigate further the particular application. References have not been given for each entry in the table since most entries represent an estimate from several experiments.

Several comprehensive but nonevaluating surveys of radiation damage data have been published, for example: F. E Faris et al., Report NAA-SR-241, 691 pp., Nov. 2, 1953 (Classified). N. Yoshida et al., Report NEI-4, 6 pp., Feb. 10, 1953 (Classified). E. L. Burkhard et al., Report NARF-54-IT, 712 pp., November 1954 (Classified). V. P. Calkins, Report APEX-172, 51 pp., August 1954 (Classified). E. L. Mincher, Report KAPL-731, 87 pp., Apr. 2, 1952 (Classified).

The unclassified work of Sisman and others at ORNL on organic materials is extensive and well reported [see, for example, C. D. Bopp and O. Sisman, Radiation Stability of Plastics and Elastomers, Nucleonics, 13(7): 28-33 (July 1955)].

Table 10.2—RADIATION STABILITY OF PLASTICS*

Plastic	Energy absorption, rad/10^9 nvt	Exposure for 50% decrease in most sensitive mechanical property, 10^9 rad	Nvt, thermal neutrons/cm^2 (reactor radiation)	Equivalent to 1 year at flux of
		Group 1		
Polystyrenes (amphenol, Styrons 637, 671, and 411C)	0.7	>30	$>4 \times 10^{19}$	$>1 \times 10^{12}$
		Group 2		
Triallyl cyanurate	0.7	>10	$>1.4 \times 10^{19}$	$>5 \times 10^{11}$
Polyvinyl carbazole	0.7	>10	$>1.4 \times 10^{19}$	$>5 \times 10^{11}$
Aniline formaldehyde	0.7	10	1.4×10^{19}	5×10^{11}
Plaskon alkyd (polyester)	0.4	>4	$>1 \times 10^{19}$	$>3 \times 10^{11}$
Asbestos fiber phenolic	0.4	>4	$>1 \times 10^{19}$	$>3 \times 10^{11}$
Asbestos fabric phenolic	0.4	>4	$>1 \times 10^{19}$	$>3 \times 10^{11}$
Melmac 592 (amino)	0.4	>4	$>1 \times 10^{19}$	$>3 \times 10^{11}$
Karbate (phenolic)	0.3	>3	$>1 \times 10^{19}$	$>3 \times 10^{11}$
Haveg 41 (phenolic)	0.3	3	1×10^{19}	3×10^{11}
Duralon (furan)	0.3	3	1×10^{19}	3×10^{11}
Polyvinyl formal	1	10	1×10^{19}	3×10^{11}
		Group 3		
Silicon-varnished glass cloth	0.6	4	7×10^{18}	2×10^{11}
Araldite, type B	0.7	>4	$>5 \times 10^{18}$	$>2 \times 10^{11}$
CR-39 (allyl diglycol carbonate polymer)	0.9	3	3×10^{18}	1×10^{11}
Pliotuf (butadiene-styrene, rubber blend)	0.8	2	3×10^{18}	1×10^{11}
		Group 4		
Vinyl chloride acetate polymer	2.5	5	2×10^{18}	7×10^{10}
Catalin (unfilled phenolic)	0.7	1	1.4×10^{18}	5×10^{10}
Royalite (styrene copolymer)	0.8	1	1×10^{18}	3×10^{10}
Mylar	1	1	1×10^{18}	3×10^{10}
		Group 5		
Butacite (polyvinyl butyral)	1	0.6	6×10^{17}	2×10^{10}
Polyalphamethyl styrene	0.7	0.4	6×10^{17}	2×10^{10}
Polyethylene	1	0.5	5×10^{17}	2×10^{10}
Paper-base phenolic	0.7	0.2	3×10^{17}	1×10^{10}
		Group 6		
Saran B-115 (vinyl chloride polymer)	2.5	0.5	2×10^{17}	7×10^{9}
Geon 2046 (vinyl chloride polymer)	2.5	0.4	2×10^{17}	7×10^{9}
Micarta (phenolic laminate)	0.7	0.1	1.4×10^{17}	5×10^{9}
Selectron 5038 (polyester)	0.8	0.1	1.3×10^{17}	4×10^{9}
Casein	1	0.1	1×10^{17}	3×10^{9}
Cellulose acetate	0.7	0.07	1×10^{17}	3×10^{9}

RADIATION STABILITY OF PLASTICS — (Continued)

Plastic	Energy absorption, rad/10^9 nvt	Exposure for 50% decrease in most sensitive mechanical property, 10^9 rad	Nvt, thermal neutrons/cm^2 (reactor radiation)	Equivalent to 1 year at flux of
		Group 7		
Lucite (methyl methacrylate)	0.7	0.05	7×10^{16}	2×10^9
Cellulose acetate butyrate	0.7	0.05	7×10^{16}	2×10^9
Nylon	1	0.05	5×10^{16}	2×10^9
Fluorothene	1	0.05	5×10^{16}	2×10^9
Cellulose nitrate	0.7	0.04	5×10^{16}	2×10^9
Styron 475 (high-impact polystyrene)	0.8	0.04	5×10^{16}	2×10^9
Cellulose propionate	0.7	0.04	5×10^{16}	2×10^9
Linen-fabric phenolic	0.7	0.02	3×10^{16}	1×10^9
Ethocel (ethyl cellulose)	0.7	0.02	3×10^{16}	1×10^9
		Group 8		
Teflon	1	0.003	3×10^{15}	1×10^8

• Adapted from C. D. Bopp and O. Sisman, Radiation Stability of Plastics and Elastomers, Nucleonics, 13(7): 28-33 (July 1955).

Table 10.3—RADIATION STABILITY OF ELASTOMERS*

Formulation	Energy absorption, rad/10^9 nvt	Exposure for 50% decrease in breaking elongation, 10^9 rad	Nvt, thermal neutrons/cm^2 (reactor radiation)	Equivalent to year at flux of
		Group 1		
Natural rubber (in air)	0.6	0.5	1×10^{18}	3×10^{10}
		Group 2		
Thiokol (in helium)	0.4	0.1	3×10^{17}	1×10^{10}
Thiokol ST (in air)	0.4	0.1	3×10^{17}	1×10^{10}
Hycar OR (in air)	0.6	0.1	2×10^{17}	7×10^{9}
Butyl rubber (in air)	0.6	0.1	2×10^{17}	7×10^{9}
GR-S (in air)	0.6	0.1	2×10^{17}	7×10^{9}
Hycar PA (in air)	0.6	0.1	2×10^{17}	7×10^{9}
Silastic 250 (in helium)	0.7	0.1	1.4×10^{17}	5×10^{9}
Natural rubber (in helium)	0.8	0.1	1×10^{17}	3×10^{9}
Polybutadiene (in helium)	0.8	0.1	1×10^{17}	3×10^{9}
Hycar OR-15 (in helium)	0.8	0.1	1×10^{17}	3×10^{9}
Hycar OS-10 (in helium)	0.8	0.1	1×10^{17}	3×10^{9}
Silastic 7-170 (in air)	0.7	0.06	1×10^{17}	3×10^{9}
Natural rubber with any of the following plasticizers: L. P. oil, dioctyl phthalate, dioctyl sebacate, tributoxy ethyl phosphate, TP90B, and SC	0.8	0.1	1×10^{17}	3×10^{9}
		Group 3		
Hycar PA (in helium)	0.8	0.05	6×10^{16}	2×10^{9}
Hypalon S2 (in helium)	2.5	0.1	4×10^{16}	1×10^{9}
Neoprene GN (in helium)	2.5	0.1	4×10^{16}	1×10^{9}
		Group 4		
Neoprene (in air)	2.5	0.06	2×10^{16}	7×10^{8}

* Adapted from C. D. Bopp and O. Sisman, Radiation Stability of Plastics and Elastomers, Nucleonics, 13(7): 28-33 (July 1955).

GROWTH OF A RADIOELEMENT (PRODUCED AT CONSTANT RATE)

(F = Fraction of Saturation Value = $1 - e^{-\lambda t}$)

Time in half life	F	Time in half life	F	Time in half life	F	Time in half life	F
0.01	0.0069	0.74	0.401	1.48	0.641	2.55	0.829
0.02	0.0138	0.76	0.410	1.50	0.646	2.60	0.835
0.04	0.0273	0.78	0.418	1.52	0.651	2.65	0.841
0.06	0.0407	0.80	0.426	1.54	0.656	2.70	0.846
0.08	0.0539	0.82	0.434	1.56	0.661	2.75	0.851
0.10	0.0670	0.84	0.441	1.58	0.666	2.80	0.856
0.12	0.0798	0.86	0.449	1.60	0.670	2.85	0.861
0.14	0.0925	0.88	0.457	1.62	0.675	2.90	0.866
0.16	0.105	0.90	0.464	1.64	0.679	2.95	0.871
0.18	0.117	0.92	0.471	1.66	0.684	3.00	0.875
0.20	0.129	0.94	0.479	1.68	0.688	3.10	0.883
0.22	0.141	0.96	0.486	1.70	0.692	3.20	0.891
0.24	0.153	0.98	0.493	1.72	0.696	3.30	0.898
0.26	0.165	1.00	0.500	1.74	0.701	3.40	0.905
0.28	0.176	1.02	0.507	1.76	0.705	3.50	0.912
0.30	0.188	1.04	0.514	1.78	0.709	3.60	0.918
0.32	0.199	1.06	0.520	1.80	0.713	3.70	0.923
0.34	0.210	1.08	0.527	1.82	0.717	3.80	0.928
0.36	0.221	1.10	0.533	1.84	0.721	3.90	0.933
0.38	0.232	1.12	0.540	1.86	0.725	4.00	0.938
0.40	0.242	1.14	0.546	1.88	0.728	4.25	0.947
0.42	0.253	1.16	0.553	1.90	0.732	4.50	0.956
0.44	0.263	1.18	0.559	1.92	0.736	4.75	0.963
0.46	0.273	1.20	0.565	1.94	0.739	5.00	0.969
0.48	0.283	1.22	0.571	1.96	0.743	5.25	0.974
0.50	0.293	1.24	0.577	1.98	0.747	5.50	0.978
0.52	0.303	1.26	0.582	2.00	0.750	5.75	0.981
0.54	0.312	1.28	0.588	2.05	0.759	6.00	0.984
0.56	0.322	1.30	0.594	2.10	0.767	6.50	0.989
0.58	0.331	1.32	0.599	2.15	0.775	7.00	0.992
0.60	0.340	1.34	0.605	2.20	0.782	7.50	0.994
0.62	0.349	1.36	0.610	2.25	0.790	8.00	0.996
0.64	0.358	1.38	0.616	2.30	0.797	9.00	0.998
0.66	0.367	1.40	0.621	2.35	0.804	10.00	0.999
0.68	0.376	1.42	0.626	2.40	0.811		
0.70	0.384	1.44	0.631	2.45	0.817		
0.72	0.393	1.46	0.636	2.50	0.823		

DECAY OF A RADIOELEMENT

(F = Fraction Remaining = $e^{-\lambda t}$)

Time in half life	F	Time in half life	F	Time in half life	F	Time in half life	F	Time in half life	F
0	1.000	0.86	0.551	1.72	0.304	3.45	0.0915	6.20	0.0136
0.02	0.986	0.88	0.543	1.74	0.299	3.50	0.0884	6.30	0.0127
0.04	0.973	0.90	0.535	1.76	0.295	3.55	0.0853	6.40	0.0118
0.06	0.959	0.92	0.529	1.78	0.291	3.60	0.0825	6.50	0.0111
0.08	0.946	0.94	0.521	1.80	0.287	3.65	0.0797	6.60	0.0103
0.10	0.933	0.96	0.514	1.82	0.283	3.70	0.0769	6.70	0.0096
0.12	0.920	0.98	0.507	1.84	0.279	3.75	0.0743	6.80	0.0090
0.14	0.908	1.00	0.500	1.86	0.275	3.80	0.0718	6.90	0.0084
0.16	0.895	1.02	0.493	1.88	0.272	3.85	0.0693	7.00	0.0078
0.18	0.883	1.04	0.486	1.90	0.268	3.90	0.0670	7.10	0.0073
0.20	0.871	1.06	0.480	1.92	0.264	3.95	0.0647	7.20	0.0068
0.22	0.859	1.08	0.473	1.94	0.261	4.00	0.0625	7.30	0.0063
0.24	0.847	1.10	0.467	1.96	0.257	4.05	0.0604	7.40	0.0059
0.26	0.835	1.12	0.460	1.98	0.253	4.10	0.0583	7.50	0.0055
0.28	0.824	1.14	0.454	2.00	0.250	4.15	0.0563	7.60	0.0052
0.30	0.812	1.16	0.447	2.05	0.241	4.20	0.0544	7.70	0.0048
0.32	0.801	1.18	0.441	2.10	0.233	4.25	0.0525	7.80	0.0045
0.34	0.790	1.20	0.435	2.15	0.225	4.30	0.0507	7.90	0.0042
0.36	0.779	1.22	0.429	2.20	0.218	4.35	0.0490	8.00	0.0039
0.38	0.768	1.24	0.423	2.25	0.210	4.40	0.0474	8.10	0.0036
0.40	0.758	1.26	0.418	2.30	0.203	4.45	0.0457	8.20	0.0034
0.42	0.747	1.28	0.412	2.35	0.196	4.50	0.0442	8.30	0.0032
0.44	0.737	1.30	0.406	2.40	0.189	4.55	0.0427	8.40	0.0030
0.46	0.727	1.32	0.401	2.45	0.183	4.60	0.0413	8.50	0.0028
0.48	0.717	1.34	0.395	2.50	0.177	4.65	0.0398	8.60	0.0026
0.50	0.707	1.36	0.390	2.55	0.171	4.70	0.0385	8.70	0.0024
0.52	0.697	1.38	0.384	2.60	0.165	4.75	0.0372	8.80	0.0022
0.54	0.688	1.40	0.379	2.65	0.159	4.80	0.0359	8.90	0.0021
0.56	0.678	1.42	0.374	2.70	0.154	4.85	0.0347	9.00	0.0020
0.58	0.669	1.44	0.369	2.75	0.149	4.90	0.0335	9.10	0.0018
0.60	0.660	1.46	0.364	2.80	0.144	4.95	0.0324	9.20	0.0017
0.62	0.651	1.48	0.358	2.85	0.139	5.00	0.0313	9.30	0.0016
0.64	0.642	1.50	0.354	2.90	0.134	5.10	0.0292	9.40	0.0015
0.66	0.633	1.52	0.349	2.95	0.129	5.20	0.0272	9.50	0.0014
0.68	0.624	1.54	0.344	3.00	0.125	5.30	0.0254	9.60	0.0013
0.70	0.616	1.56	0.339	3.05	0.121	5.40	0.0237	9.70	0.0012
0.72	0.607	1.58	0.334	3.10	0.117	5.50	0.0221	9.80	0.0011
0.74	0.599	1.60	0.330	3.15	0.113	5.60	0.0206	9.90	0.0010
0.76	0.590	1.62	0.325	3.20	0.109	5.70	0.0192	10.00	0.0010
0.78	0.582	1.64	0.321	3.25	0.105	5.80	0.0180		
0.80	0.574	1.66	0.316	3.30	0.102	5.90	0.0167		
0.82	0.566	1.68	0.312	3.35	0.0981	6.00	0.0156		
0.84	0.559	1.70	0.308	3.40	0.0947	6.10	0.0146		

NOMOGRAM FOR RADIOISOTOPE BUILD-UP AND DECAY

By J. R. Stehn and E. F. Clancy
Knolls Atomic Power Laboratory

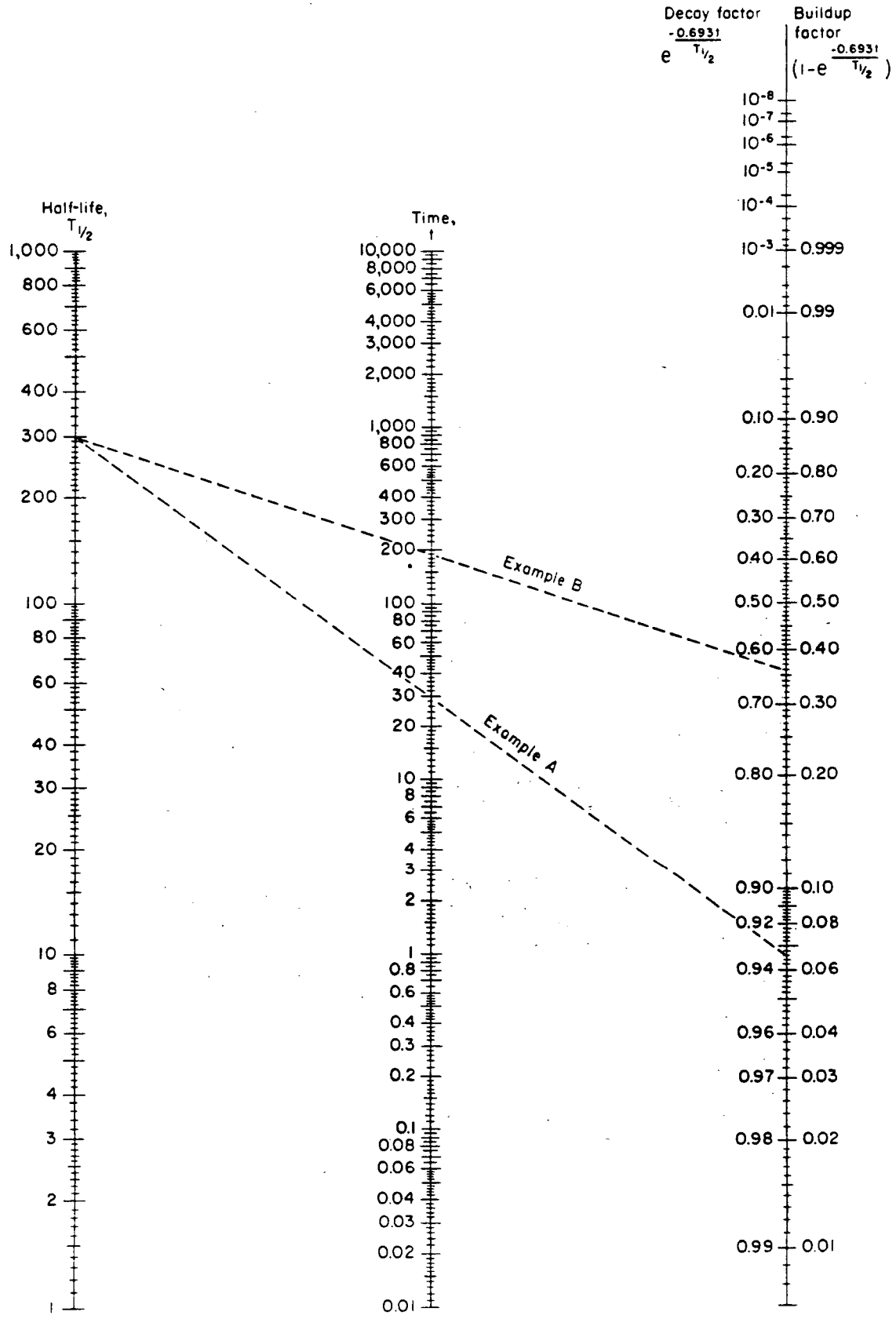
Calculations of build-up or decay of radioisotopes involve the terms $e^{-0.693t/T_{1/2}}$ or $(1 - e^{-0.693t/T_{1/2}})$ and often are inconvenient or tedious. This nomogram speeds such computations.

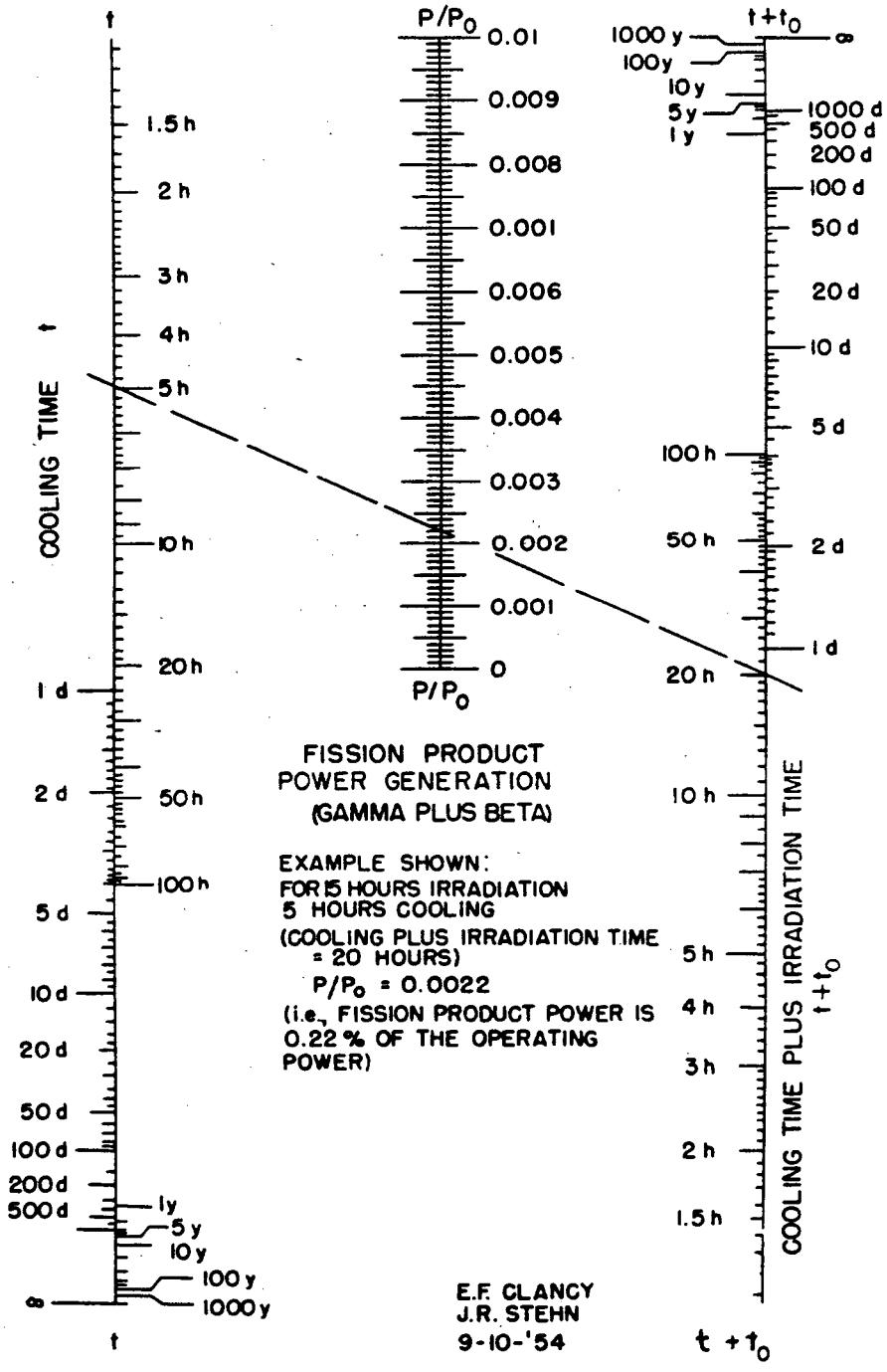
By placing a straightedge on appropriate positions on the half life and time of decay or irradiation scales, decay factors or build-up toward saturation factors for a particular isotope can be read at the straightedge intersection with the scale on the right. Be sure to state half life and time of cooling or irradiation in the same units.

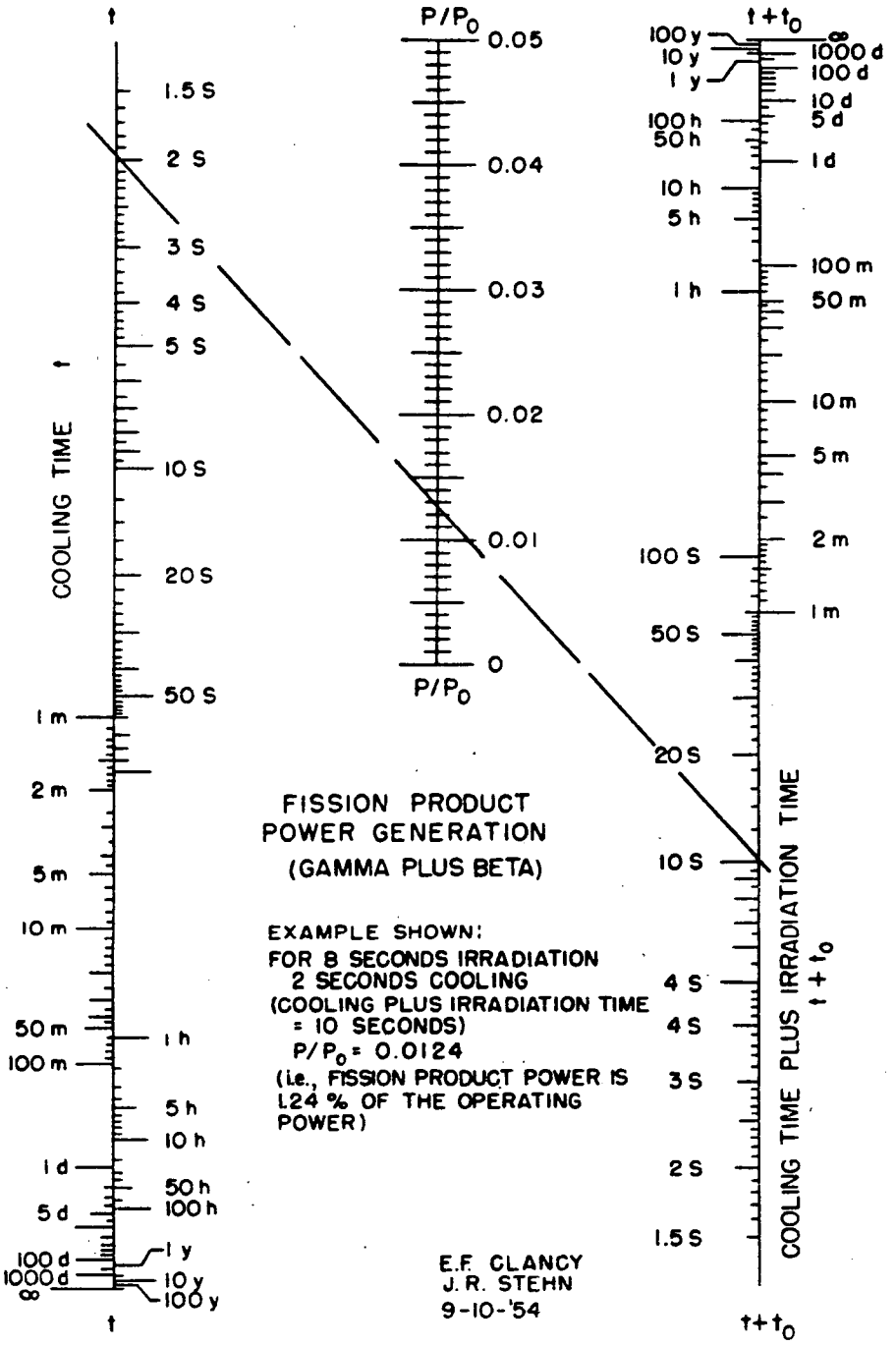
Example A: For a radioisotope whose half life is 300 days (half life scale) and whose parent is irradiated for 30 days (time scale), from the build-up factor scale it can be seen that the radioisotope achieves 0.066 (6.6%) of its saturation activity in a given neutron flux.

Example B: After the radioisotope considered in example A has been removed from the neutron flux for a period of 190 days (time scale), from the decay scale it is seen that its radioactivity has decayed to a factor of 0.64 (64%) of what it was at the time of removal.

Reprinted from "Nucleonics," Vol. 13, No. 4, p. 27, April 1955.


Decay factor
$e^{\frac{-0.693t}{T_{1/2}}}$
Buildup factor
$(1-e^{\frac{-0.693t}{T_{1/2}}})$
Half-life, $T_{1/2}$
Time, t
Example B
Example A
1,000
800
600
400
300
200
100
80
60
40
30
20
10
8
6
4
3
2
1
10,000
8,000
6,000
4,000
3,000
2,000
1,000
800
600
400
300
200
100
80
60
40
30
20
10
8
6
4
3
2
1
0.8
0.6
0.4
0.3
0.2
0.1
0.08
0.06
0.04
0.03
0.02
0.01
10^{-8}
10^{-7}
10^{-6}
10^{-5}
10^{-4}
10^{-3}
0.01
0.10
0.20
0.30
0.40
0.50
0.60
0.70
0.80
0.90
0.92
0.94
0.96
0.97
0.98
0.99
0.999
0.99
0.90
0.80
0.70
0.60
0.50
0.40
0.30
0.20
0.10
0.08
0.06
0.04
0.03
0.02
0.01


t
COOLING TIME t
1.5 h
2 h
3 h
4 h
5 h
10 h
20 h
1 d
2 d
50 h
100 h
5 d
10 d
20 d
50 d
100 d
200 d
500 d
1 y
5 y
10 y
100 y
1000 y
∞
t
P/P0
0.01
0.009
0.008
0.001
0.006
0.005
0.004
0.003
0.002
0.001
0
P/P0
t+t0
1000 y
100 y
10 y
5 y
1 y
∞
1000 d
500 d
200 d
100 d
50 d
20 d
10 d
5 d
100 h
50 h
2 d
1 d
20 h
10 h
5 h
4 h
3 h
2 h
1.5 h
COOLING TIME PLUS IRRADIATION TIME t+t0
t+t0
FISSION PRODUCT
POWER GENERATION
(GAMMA PLUS BETA)
EXAMPLE SHOWN:
FOR 15 HOURS IRRADIATION
5 HOURS COOLING
(COOLING PLUS IRRADIATION TIME
= 20 HOURS)
P/P0 = 0.0022
(i.e., FISSION PRODUCT POWER IS
0.22 % OF THE OPERATING
POWER)
E.F. CLANCY
J.R. STEHN
9-10-'54
t + t0


t
1.5 S
2 S
3 S
4 S
5 S
10 S
20 S
50 S
1 m
2 m
5 m
10 m
50 m
100 m
1 h
5 h
10 h
1 d
5 d
50 h
100 h
1 y
100 d
1000 d
∞
10 y
100 y
COOLING TIME t
P/P0
0.05
0.04
0.03
0.02
0.01
0
P/P0
t+t0
100 y
10 y
1 y
100 h
50 h
10 h
5 h
1 h
100 S
50 S
20 S
10 S
4 S
4 S
3 S
2 S
1.5 S
∞
1000 d
100 d
10 d
5 d
1 d
100 m
50 m
10 m
5 m
2 m
1 m
COOLING TIME PLUS IRRADIATION TIME t + t0
t+t0
FISSION PRODUCT
POWER GENERATION
(GAMMA PLUS BETA)
EXAMPLE SHOWN:
FOR 8 SECONDS IRRADIATION
2 SECONDS COOLING
(COOLING PLUS IRRADIATION TIME
= 10 SECONDS)
P/P0 = 0.0124
(i.e., FISSION PRODUCT POWER IS
1.24 % OF THE OPERATING
POWER)
E.F. CLANCY
J.R. STEHN
9-10-'54

VARIOUS PROPERTIES OF THE ELEMENTS

Element	Symbol	At. No. (Z)	At. Wt. (A)	At. density (N), atoms/cm³ × 10^{-22}	Density (ρ), g/cm³ at 20°C	Thermal absorption cross section (σ_a), barns/atom	Thermal absorption cross section (Σ_a), cm^{-1}	"Worst" activation products* Half life ($T^{1/2}$)	Energy (E), Mev	Gamma absorption (μ/ρ), cm²/g 0.5 Mev	1 Mev	3 Mev	6 Mev
Actinium	Ac	89	227							0.173	0.0760	0.0429	0.0465
Aluminum	Al	13	26.97	6.03	2.699	0.22	0.013	2.3min	3.01(β) / 1.8(γ)	0.0844	0.0614	0.0353	0.0266
Americium	Am	95											
Antimony	Sb	51	121.76	3.31	6.691	5	0.17	60d	1.7†(γ)	0.0928	0.0573	0.0361	0.0357
Argon	A	18	39.944	0.0025	0.00166	1		1.78h	1.3(γ)	0.0795	0.0574	0.0386	0.0267
Arsenic	As	33	74.91	4.61	5.73	4.3	0.20	27h	3.12†(β) / 1.5†(γ)	0.0824	0.0573	0.0350	0.0311
Astatine	At	85	211							0.157	0.0709	0.0409	0.0442
Barium	Ba	56	137.36	1.66	3.78	1.58	0.022	85min	2.2†(β) / 1.0†(γ)	0.0978	0.0572	0.0363	0.0367
Beryllium	Be	4	9.02	12.29	1.84	0.0085	0.001	Nothing significant		0.0772	0.0564	0.0313	0.0212
Bismuth	Bi	83	209.0	2.82	9.8	0.015	0.0004	725y	5.02(α)	0.156	0.0714	0.0417	0.0449
Boron	B	5	10.82	14.11	2.535	715	100	Nothing significant		0.0809	0.0587	0.0323	0.0277
Bromine	Br	35	79.916	2.35	3.12	6.5	0.15	18.5min / 35h	0.5(γ) / 1.0†(γ)	0.0830	0.0572	0.0350	0.0318
Cadmium	Cd	48	112.41	4.63	8.65	2500	120	43d	1.67†(β) / 0.5†(γ)	0.0912	0.0576	0.0363	0.0354
Calcium	Ca	20	40.08	2.31	1.54	0.5	0.012	152d	2.7(β)	0.0885	0.0637	0.0378	0.0302
Carbon	C	6	12.01	8.38	1.67	0.0045	0.0004	5720y	0.15(β)	0.0870	0.0635	0.0356	0.0246
Cerium	Ce	58	140.13	2.97	6.9	3	0.18	33h	1.3†(β) / 0.6†(γ)	0.103	0.0591	0.0373	0.0380
Cesium	Cs	55	132.91	0.85	1.873	26	0.22	2.3y	0.8‡(γ)	0.0978	0.0578	0.0367	0.0369
Chlorine	Cl	17	35.457	0.005	0.00295	35		38min	5†(β) / 2.5†(γ)	0.0846	0.0611	0.0357	0.0278
Chromium	Cr	24	52.01	8.01	6.92	2.5	0.20	26d	0.3†(γ)	0.0827	0.0589	0.0351	0.0293
Cobalt	Co	27	58.94	8.90	8.71	36	3.2	5.2y	1.3‡(γ)	0.0828	0.0598	0.0353	0.0472
Columbium	Cb	41	92.91	5.45	8.40	1.2	0.065	6.6min	0.4(γ)	0.0864	0.0584	0.0363	0.0343
Copper	Cu 63(69%) / 65(31%)	29	63.57	8.42	8.89	3.6	0.25	12.8h / 4.3min	1.3(γ) / 1.3(γ)	0.0834	0.0588	0.0356	0.0309
Curium	Cm	96	242										
Dysprosium	Dy	66	162.46	3.17	8.56	1200	38	2.4min	1.25†(β) / 0.76†(γ)	0.116	0.0616	0.0386	0.0403
Erbium	Er	68	167.20	3.30	9.16	5		7.5h	1.4†(β) / 0.8†(γ)	0.120	0.0626	0.0391	0.0411
Europium	Eu 151(48%) / 153(52%)	63	152.0	2.08	5.24	6000	120	9.2h / 7.5y	0.7†(γ) / 1.2(γ)	0.112	0.0613	0.0387	0.0400

Fluorine	F	9	19.00	0.005	0.00158	0.01		12s	5.1(β) / 2.2(γ)	0.0826	0.0600	0.0342	0.0245
Francium	Fr	87	223							0.164	0.0735	0.0419	0.0453
Gadolinium	Gd	64	156.9	3.05	7.94	40,000	1200	18h	0.9(β)	0.113	0.0608	0.0383	0.0397
Gallium	Ga 69(60%) / 71(40%)	31	69.72	5.10	5.90	2.8	0.11	20min / 14h	1.6(β) / 2†(γ)	0.0820	0.0575	0.0349	0.0307
Germanium	Ge	32	72.60	4.53	5.46	28	0.13	82min	1.2(β)	0.0820	0.0572	0.0347	0.0308
Gold	Au	79	197.20	5.89	19.30	95	5.6	2.7d	0.9†(β) / 0.5†(γ)	0.145	0.0687	0.0409	0.0440
Hafnium	Hf	72	178.60	3.84	11.4	13	4.0	46d	0.5‡(γ)	0.126	0.0643	0.0396	0.0420
Helium	He	2	4.003	0.0025	0.00016	0				0.0874	0.0625	0.0337	0.0247
Holmium	Ho	67	164.94	3.20	8.76	60	1.9	27h	1.8(β) / 1.2(γ)	0.118	0.0620	0.0388	0.0406
Hydrogen	H_2 (0.015%)	1	1.088	0.005	0.00008	0.33		12.4y	0.019(β)	0.173	0.126	0.0693	0.0449
Indium	In	49	114.76	3.82	7.28	190	7.3	54min	0.8(β) / 1.3(γ)	0.0922	0.0578	0.0364	0.0357
Iodine	I	53	126.92	2.34	4.94	6.1	0.16	25min	2.0(β)	0.0954	0.0579	0.0364	0.0364
Iridium	Ir 191(38.5%) / 193(65.5%)	77	193.1	6.99	22.42	440	31	70d / 19h	0.7(β) / 1.4(γ)	0.138	0.0670	0.0403	0.0431
Iron	Fe	26	55.85	8.47	7.85	2.56	0.21	45d	1.3(γ)	0.0840	0.0598	0.0359	0.0305
Krypton	Kr	36	83.7	0.0025	0.00348	0.05		78min	3.2(β) / Del.(n)	0.0817	0.0563	0.0346	0.0315
Lanthanum	La	57	138.92	2.67	8.15	8	0.21	40h	1.3‡(β) / 1.65(γ)	0.100	0.0581	0.0368	0.0373
Lead	Pb	82	207.21	3.30	11.347	0.17	0.007	3.3h	0.7(β)	0.152	0.0703	0.0413	0.0445
Lithium	Li	3	6.940	4.63	0.534	70	3.0	0.83s	13(β)	0.0756	0.0540	0.0288	0.0216
Lutetium	Lu	71	174.99	3.35	9.24	108	4.7	3.7h	1.2(β)	0.125	0.0641	0.0396	0.0420
Magnesium	Mg	12	24.32	4.31	1.741	0.05	0.013	9.6min	1.8(β) / 1.0(γ)	0.0863	0.0625	0.0362	0.0267
Manganese	Mn	25	54.93	7.89	7.2	13	1.0	2.6h	2.8†(β) / 2.1†(γ)	0.0817	0.0583	0.0348	0.0294
Mercury	Hg	80	200.61	4.07	13.546	400	16	65h	1‡(β) / 0.5‡(γ)	0.147	0.0692	0.0411	0.0441
Molybdenum	Mo 98-24% / 100-10%	42	95.95	6.40	10.2	2.6	0.17	68h / 15min	0.7(γ) / 0.9(γ)	0.0879	0.0581	0.0362	0.0343
Neodymium	Nd	60	144.27	2.91	6.96	20		11d	0.9(β) / 0.6(γ)	0.107	0.0601	0.0379	0.0389
Neon	Ne	10	20.183	0.0025	0.00084	0.04		41s	4.3(β) / 3(γ)	0.0867	0.0627	0.0357	0.0260
Neptunium	Np	93	237										
Nickel	Ni	28	58.69	9.13	8.9	4.5	0.41	2.6h	2.1(β) / 1.5(γ)	0.0866	0.0613	0.0369	0.0319
Niobium (see Columbium)													
Nitrogen	N 15 (0.365%)	7	14.008	0.005	0.00116	1.78		7.5s	10(β) / 6(γ)	0.0870	0.0636	0.0357	0.0251

VARIOUS PROPERTIES OF THE ELEMENTS—(Continued)

Element	Symbol	At. No. (Z)	At. Wt. (A)	At. density (N), atoms/cm^3 × 10^{-22}	Density (ρ), g/cm^3 at 20°C	Thermal absorption cross section (σ_a), barns/atom	Thermal absorption cross section (Σ_a), cm^{-1}	"Worst" activation products* Half life ($T^{1/2}$)	Energy (E), Mev	Gamma absorption (μ/ρ), cm^2/g 0.5 Mev	1 Mev	3 Mev	6 Mev
Osmium	Os	76	190.20	7.12	22.48	15	0.0004	32h	1(β) 1.5(γ)	0.136	0.0663	0.0402	0.0429
Oxygen	O {16(99.76%) 17(0.037%)}	8	16.00	0.005	0.00133			{7.3s 4.1s}	{6(γ) 0.9(n)}	0.0871	0.0636	0.0359	0.0255
Palladium	Pd	46	106.7	6.86	12.16	6	0.41	13.1h	1(β)	0.0901	0.0577	0.0363	0.0351
Phosphorus	P	15	30.98	4.55	2.34	0.3	0.014	14.3d	1.7(β)	0.0854	0.0617	0.0358	0.0274
Platinum	Pt	78	195.23	6.59	21.37	8	0.53	4.3d	1.5(γ)	0.142	0.0676	0.0407	0.0435
Plutonium	Pu	94	239										
Polonium	Po	84	210							0.160	0.0728	0.0420	0.0456
Potassium	K	19	39.096	1.34	0.87	2.5	0.034	12.5h	{3.5(β) 2.4(γ)}	0.0859	0.0620	0.0366	0.0289
Praseodymium	Pr	59	140.92	2.77	6.475	10	0.28	19h	2.2(β)	0.106	0.0601	0.0380	0.0388
Promethium	Pm	61	147			60				0.109	0.0607	0.0385	0.0395
Protactinium	Pa	91	230.9							0.183	0.0784	0.0443	0.0475
Radium	Ra	88	226.05	1.33	5					0.168	0.0746	0.0423	0.0458
Radon	Rn	86	222	1.19	4.4					0.161	0.0723	0.0415	0.0449
Rhenium	Re	75	186.31	6.47	20	85	5.5	93h	{1(β) 1(γ)}	0.134	0.0662	0.0402	0.0429
Rhodium	Rh	45	102.91	7.32	12.5	150	11	44s	2.5(β)	0.0902	0.0584	0.0367	0.0353
Rubidium	Rb	37	85.48	1.08	1.532	0.6	0.006	19.5d	{1.8(β) 1(γ)}	0.0835	0.0567	0.0349	0.0322
Ruthenium	Ru	44	101.7	7.23	12.2	2.5	0.22	4.4h	{1.5(β) 0.7(γ)}	0.0883	0.0577	0.0361	0.0344
Samarium	Sm	62	150.43	3.08	7.7	10,000	270	47h	{0.7(β) 0.6(γ)}	0.110	0.0606	0.0382	0.0394
Scandium	Sc	21	45.10	3.34	2.5	12	0.74	85d	{1.5(β) 1.2(γ)}	0.0826	0.0593	0.0350	0.0284
Selenium	Se	34	78.96	3.43	4.5	12	0.52	59min	1.5(β)	0.0811	0.0561	0.0343	0.0308
Silicon	Si	14	28.06	5.19	2.42	0.2	0.010	2.6h	1.8(β)	0.0873	0.0635	0.0367	0.0279
Silver	Ag {107(51.3%) 109(48.7%)}	47	107.880	5.86	10.5	60	3.5	{2.3min 24s}	{2.8(β) 1.5††‡(γ)}	0.0920	0.0586	0.0369	0.0358
Sodium	Na	11	22.997	2.54	0.9712	0.45	0.011	15h	2.76(γ)	0.0835	0.0608	0.0348	0.0255
Strontium	Sr	38	87.63	1.79	2.6	1.2	0.032	53d	1.5(β)	0.0842	0.0569	0.0351	0.0327
Sulphur	S	16	32.06	3.76	2.0	0.4	0.015	87d	2††‡(β)	0.0879	0.0636	0.0368	0.0287
Tantalum	Ta	73	180.88	5.53	16.6	20	1.1	117d	{0.5(β) 1.2(γ)}	0.128	0.0650	0.0399	0.0424
Technetium	Tc	43	99										
Tellurium	Te	52	127.61	2.95	6.25	4.5	0.12	25min	1.8(β)	0.0915	0.0560	0.0354	0.0351

Terbium	Tb	65	159.2	8.15	8.33	44	0.32	73d	{0.8(β) 0.2(β)}	0.115	0.0613	0.0386	0.0401
Thallium	Tl	81	204.39	3.49	11.86	3	0.11	4.3min	1.7(β)	0.149	0.0695	0.0410	0.0442
Thorium	Th	90	232.12	2.98	11.5					0.175	0.0762	0.0428	0.0463
Thulium	Tm	69	169.4	3.32	9.34	100	3.3	129d	1(β)	0.122	0.0632	0.0394	0.0415
Tin	Sn	50	118.7	3.70	7.3	0.6	0.022	10d	{2.3(β) 2(γ)}	0.0923	0.0573	0.0361	0.0356
Titanium	Ti	22	47.90	5.66	4.5	5.8	0.28	6min	1.6(β)	0.0818	0.0588	0.0347	0.0285
Tungsten (see Wolfram)													
Uranium	U	92	238.07	4.73	18.7	650				0.185	0.0779	0.0435	0.0471
Vanadium	V	23	50.95	7.05	5.96	4.5	0.32	3.8min	{2(β) 1.4(γ)}	0.0805	0.0577	0.0342	0.0283
Wolfram	W	74	183.92	6.32	19.3	18	1.1	24.1h	{1.3(β) 0.6(γ)}	0.131	0.0655	0.0400	0.0426
Xenon	Xe	54	131.3	0.0025	0.00546				†	0.0954	0.0571	0.0361	0.0363
Ytterbium	Yb	70	173.04	2.44	7.01	21		4.2d	{0.5(β) 0.3(γ)}	0.123	0.0633	0.0393	0.0415
Yttrium	Y	39	88.92	2.57	3.8	1.2	0.031	61h	2.3(β)	0.0859	0.0577	0.0358	0.0335
Zinc	Zn {64(49%) 68(19%)}	30	65.38	6.67	7.19	0.9	0.060	{250d 14h}	{1.2(γ) 0.9(γ)}	0.0841	0.0585	0.0357	0.0314
Zirconium	Zr	40	91.22	4.25	6.44	0.4	0.017	17h	{2(β) 0.8(γ)}	0.0864	0.0578	0.0360	0.0338

* See also C. D. Bopp and O. Sisman, How to Calculate Gamma Radiation Induced in Reactor Materials, Nucleonics, 14(1): 46-50 (January 1956).

† Predominant energy from mixed spectrum.

‡ More than one gamma per decay.

§ Predominant activity; activities from other isotopes present.